



Investigating The Mechanism of Radioresistance in SPRTN-Depleted Cells

DPhil Thesis

Supervisors:

Prof Kristijan Ramadan

Dr. Annamaria Ruggiano

Ftoon Aljarbou

Lincoln College

Department of Oncology

University of Oxford

Michaelmas Term 2024

Contents

Acknowledgement 7
Declaration 9
Abstract 10
List of Figures 12
List of Tables 15
List of Abbreviations 16
Chapter 1: Introduction 21
1.1 Radiation Therapy 21
1.1.1 Types of Radiation Therapy Based on the nature of radiation 22
1.1.1.1 Photon-Based Radiotherapy 22
1.1.1.2 Particle therapy 23
1.1.2 Types of Radiation Therapy Based on the Dose Rate 28
1.1.2.1 Mechanisms Behind the FLASH Effect 29
1.1.2.1.1 Oxygen Depletion Effect 29
1.1.2.1.2 ROS and Free Radical Effects 30
1.1.2.1.3 Immune Hypothesis 30
1.1.2.2 Damage caused by Flash radiation 31
1.1.3 Commonly Induced DNA Lesions by Conventional Ionizing Radiation 33
1.1.3.1 Base Damage: 35
1.1.3.2 AP sites (Abasic sites) 39
1.1.3.3 DNA strand breaks 41
1.1.3.4 DNA Inter-strand Crosslinks (ICLs): 44
1.1.3.5 DNA–Protein Crosslinks (DPCs): 44
1.1.3.6 Clustered DNA damage: 49
1.1.3.6.1 Impact of LET on the Formation and Complexity of DNA Damage: 50
1.1.4 DNA damage repair post Radiation: 54
1.1.4.1 Base excision repair (BER): 54
1.1.4.2 DPCs removal post radiation: 61
1.1.4.3 DSB repair 63
1.1.4.3.1 Imaging-Based Insights into LET-Dependent DNA Damage and Repair Protein Recruitment 68
1.1.4.3.2 Differential Repair Dynamics and Pathway Choice Following High-LET Radiation 69
1.1.4.3.3 Artemis, ATM, and the Essential Role of End Resection in Complex DSB Repair 70
1.1.5 Radiation-Induced Cell Death Pathways 71
1.1.5.1 Mitotic Catastrophe and Mitotic Death 72
1.1.5.2 Apoptosis 72
1.1.5.3 Senescence 73

1.1.5.4 Autophagy 74
1.1.5.5 Necrosis 74
1.1.5.6 Ferroptosis 75
1.1.6 Factors affecting Radiation response 77
1.1.6.1 Oxygen concentration: 78
1.1.6.2 Chromatin compaction 80
1.1.6.3 Cell Cycle Phase and Proliferation 81
1.1.6.4.DNA repair capacity: 82
1.2 DNA-Protein Crosslinks 86
1.2.1 Crosslinking agents: Types and mechanisms 87
1.2.1.1 Aldehydes 87
1.2.1.1.1 Formaldehyde (FA) 87
1.2.1.1.2 Malondialdehyde (MDA) 93
1.2.1.1.3 Methylglyoxal (MG) 94
1.2.1.2 Trapping of DNA-Interacting Enzymes 98
1.2.1.3 Abasic sites (AP sites) 101
1.2.1.4 Reactive Oxygen Species (ROS) 104
1.2.1.5 Chemotherapy Agents 106
1.2.1.6 ionizing radiation and Ultraviolet light 109
1.2.2 Types of DNA-Protein Crosslinks 113
1.2.3 Toxicity of DPCs 115
1.2.3.1 Effect on DNA Replication and Transcription 115
1.2.3.2 Induction of Further DNA Damage 115
1.2.4 DPCs repair pathway 117
1.2.4.1 Classification of DPC Repair Pathways based on the mechanism of crosslink resolution 117
1.2.4.1.1 Nuclease-Dependent Repair Mechanisms 117
1.2.4.1.2 Hydrolysis of The Cross-Link Between Proteins and DNA 118
1.2.4.1.3 Proteolysis-Dependent DPCs Repair 119
1.2.4.2 DPC Repair Pathways Classified by Their Association with Replication and Transcription-Dependent Mechanisms 122
1.2.4.2.1 Replication-coupled repair: 122
1.2.4.2.2 Replication-independent DPCs repair or General G repair: 132
1.2.4.2.3 Transcription-coupled DPCs repair: 136
1.3 SprT-like N-terminal domain (SPRTN) 139
1.3.1 SPRTN Domains 139
1.3.2 SPRTN Substrate Specificity 142
1.3.3 DPCs Removal by SPRTN 142
1.3.3.1 Regulation of SPRTN Activity 143

1.3.3.1.1 Post-translational Modifications 143
1.3.3.1.2 DNA Binding and DNA Structure 144
1.3.3.1.3 DNA-Dependent Autocleavage: 144
1.3.3.1.4 Interaction with other Proteins 146
1.3.3.1.5 Modification of DPCs 147
1.3.3.2 Post-Cleavage Processing 148
1.3.4 SPRTN Expression in Cancer Cells 148
1.4 DPCs Isolation Methods 151
1.4.1 Detection of DPCs Isolated by Protein-Targeted Methods 152
1.4.1.1 RADAR assay 152
1.4.1.2 Caesium chloride (CsCl) 154
1.4.1.3 STAR assay 155
1.4.1.4 PxP (Purification of Crosslinked Proteins) 156
1.4.2 DNA-Targeted Methods 161
1.4.2.1 KCl-SDS 161
1.4.2.2 ARK assay 162
1.4.2.3 Modified Comet assay 162
1.4.3 Immunodetection with Specific DPC Antibodies 167
1.5 Aim 170
Chapter 2: Materials and Methods 175
2.1 Cell culture 175
2.2 Radiation 175
2.3 siRNA treatment 176
2.4 Colony Forming Assay 177
2.5 MTT assay 177
2.6 Resazurin assay 178
2.7 Caspase 3/7 activity assay 178
2.8 RADAR Assay 179
2.9 STAR assay 179
2.10 ARK Assay (advanced recovery of K [potassium]-SDS precipitates) 180
2.11 Modified comet assay 180
2.12 Western Blot (WB) 181
2.12.1 Sample preparation 181
2.12.2 Protein Separation 181
2.12.3 Immunoblotting 182
2.12.4 Band detection 182
2.13 Immunofluorescence 184
2.14 Neutral Comet assay: 185

2.15 Alkaline Comet assay 186
2.16 Flow cytometry 186
2.17 Mnase assay 187
2.18 RNA sequencing 188
2.18.1 RNA extraction and quality assessment 188
2.18.2 RNA-seq 189
Chapter 3: DNA-Protein Crosslinks – Isolation Methods 191
3.1 Introduction 191
3.2 Results 192
3.2.1 DPCs isolation using by Protein-Targeted Methods (RADAR and STAR assay) 192
3.2.1.2 Evaluating DNA Recovery Efficiency and RNA Contamination 195
3.2.1.3 DPCs detection post-benzonase treatment (without precipitation) 195
3.2.2 DNA-targeted DPCs isolation method 200
3.2.2.1 ARK assay 200
3.2.2.2 Modified comet assay: 203
3.2.3 Detecting DPCs formed by FLASH radiotherapy RADAR assay 207
3.2.3.1 DPC Formation in Conventional RT 208
3.2.3.2 DPC Formation in FLASH-RT 211
3.2.4 DPCs formation in Hypoxia measured by RADAR 215
3.3 Discussion 219
3.3.1 Choosing the appropriate DPCs method 219
3.3.2 DPCs formation post Flash Radiation 222
3.3.2 DPCs formation under Hypoxia 224
Chapter 4: SPRTN Depletion Causes Radioresistance 226
4.1 Results 226
4.1.1 SPRTN Depletion Enhances Chemotherapy Sensitivity 226
4.1.2 SPRTN Depletion Causes Radioresistance in Most Cell lines Studied 231
4.1.3 Proteolytic Activity of SPRTN Is Required for Radiosensitivity 247
4.1.4 Caspase 3/7 Activation Is Impaired in SPRTN-Depleted Cells 251
4.2 Discussion 255
Chapter 5: DDR Signalling is Disrupted in SPRTN-Depleted Cells Post-Radiation 263
5.1 Results 263
5.1.1 SPRTN inactivation affects DDR signalling post radiation 263
5.1.2 Delayed Resolution of DSBs in SPRTN-Depleted Cells Post-Radiation 279
5.2 Discussion 304
Chapter 6: DPCs Accumulation Role in Radioresistance in SPRTN-Depleted Cells 311
6.1 Results 311
6.1.1 SPRTN depletion causes DPCs accumulation post IR 311

6.1.2 Incubating cells with scavengers rescue the radioresistnce in ΔSPRTN 317
6.1.3 Incubating cells with NAC rescues the DNA damage levels in ΔSPRTN post-IR 320
6.1.4 FA treated cells show a similar radioresistance to ΔSPRTN 324
6.2 Discussion: 329
Chapter 7: SPRTN Depletion Causes Chromatin Compaction Post-Radiation 334
7.1 Results 334
7.1.1 SPRTN depletion alters chromatin state through modulation of histone marks 334
7.1.2 Formaldehyde-induced DNA–protein crosslinks alter histone modification 337
7.1.3 SPRTN-depleted cells post-irradiation modulate chromatin markers 342
7.1.4 SPRTN Deficiency in HeLa cells Enhances Chromatin Compaction via Accumulation of Linker Histone H1.2 355
7.1.5 SPRTN Deficiency Impairs Histone H3.3 Incorporation and Chromatin Remodelling Post-Damage 358
7.1.6 MNase Digestion Confirms Enhanced Chromatin Compaction in SPRTN-Deficient Cells 360
7.1.6.1 Optimizing Mnase assay 363
7.1.6.2 MNase Analysis Reveals Chromatin Condensation in ΔSPRTN Cells After Radiation 369
7.1.7 HDAC Inhibition and Knockdown of chromatin compaction regulators Reverses Radioresistance in SPRTN-Deficient HeLa Cells 377
7.2 Discussion 389
Chapter 8 Concluding Discussion and Future Directions 398
8.1 Heterochromatin Formation in ΔSPRTN could Enable Escape from Apoptosis 399
8.2 Delayed Repair in ΔSPRTN could Prevent Complex Damage Formation 403
8.3 Future Directions and Study Improvements 410
Chapter 9: Research Projects and Contributions 417
9.1 Tirapazamine-Mediated Sensitization of NSCLC to PARP Inhibitors 417
9.2 Role of TEX264 in DNA Damage Response and Genome Stability 418
9.3 Isolation and Detection of DNA–Protein Crosslinks in Mammalian Cells 420
9.4 Deletion of USP18: Antigenicity and DNA Damage Analysis 424
References 430

Acknowledgement

I want to express my gratitude to Professor Kristijan Ramadan, my supervisor and thesis mentor, whose invaluable guidance and support have been fundamental to completing this research. His motivation, insightful feedback and encouragement have been instrumental throughout the research process. I am also profoundly thankful to my co-supervisor and laboratory colleague, Dr Annamaria Ruggiano, whose contributions and valuable advice have greatly enriched my work throughout this journey. Her willingness to share her knowledge and her collaborative spirit has made this journey both productive and enjoyable. I also thank her for helping me during the final version of the thesis writing and editing.

I appreciate the support of my second co-supervisor, Dr John Christianson, who was always there for me when I needed advice. A special thanks to our lab manager and senior scientist in the Ramadan laboratory, Dr Ignacio Torrecilla, the first person who helped me a lot in my beginnings and taught me different lab protocols. I also would like to thank all the lab members I worked with: Wei, Abhay, Sam, Shudong, John, Gwennie, Susan, and Alex. Of course, a special thanks to Pauline and Cristiano, who I started my journey with them. I really enjoyed talking with them about science and life! I want to thank the Saudi Cultural Bureau; this research was made possible through their generous support and funding. I will not forget my friend Majd Abdughani, she was such a joy to be around! Her motivation and support always gave me strength. I extend my heartfelt appreciation to my parents, for their unwavering support, love, and encouragement throughout my academic journey. Their sacrifices and belief in my abilities have inspired me constantly. To my siblings, Adi, Yazeed, Bothainah and Abdulmalik thank you for your support and always being there when I needed encouragement or a moment of respite from my studies. I am incredibly grateful to my

children, Lamar and Fahad, for their patience during this demanding period, especially when I go to the lab on weekends or at night. Having a mom who is a student is never easy! Their love and joy have been a source of strength and motivation.

Lastly, I would like to acknowledge my husband, Abdullah, for his endless patience, support, and understanding. His encouragement and belief in me have been a driving force in my academic achievements.

Declaration

This dissertation is submitted for the degree of Doctor of Philosophy in Oncology. I declare that the work presented in this thesis is my own except where explicitly stated otherwise in the text, and that this work has not been submitted for any other degree at this or any other university

Abstract

SPRTN is a DNA-dependent metalloprotease essential for the replication-coupled removal of DNA–protein crosslinks (DPCs), thereby maintaining genome integrity. Loss of SPRTN function leads to the accumulation of covalent DNA–protein adducts and is associated with altered chromatin states. While SPRTN-deficient cells are hypersensitive to classical crosslinking agents such as camptothecin, cisplatin, and other chemotherapeutics, we unexpectedly observed that they exhibit increased resistance to ionising radiation (IR). This paradox prompted us to investigate the underlying chromatin-based mechanisms that might explain their radioresistance.

In Chapter 3, we evaluated methods for DPC quantification to establish a robust platform for studying DPC dynamics. Using formaldehyde-treated wild-type cells, we compared the RADAR and STAR assays. The RADAR protocol, which employs guanidine thiocyanate to inactivate nucleases and preserve labile crosslinks, detected DPCs in a clear dose- and time-dependent manner. In contrast, the STAR assay, which lacks chaotropic agents, failed to capture the same DPC increases likely due to proteolytic degradation of DPCs during lysis. Based on these findings, RADAR was adopted for all subsequent DPC burden assessments.

SPRTN-deficient cells exhibit impaired DNA damage signalling, with neutral comet assays showing more residual double-strand breaks (DSBs) after ionizing radiation (IR) compared to wild-type cells. Despite this increased damage, γH2AX and 53BP1 foci were less intense and fewer in ΔSPRTN cells, and checkpoint activation was reduced, as indicated by lower phosphorylated CHK1 levels post-radiation. Furthermore, SPRTN deficiency induces a shift toward a repressive chromatin state, even under basal conditions. Disrupting heterochromatin, via HDAC inhibitors (panobinostat, TSA) or knockdown of heterochromatin-associated factors like H1.2,

HP1, and SUV39H1, restored radiosensitivity and DDR signalling. This suggests chromatin accessibility directly modulates DDR. Formaldehyde treatment in wild-type cells, which increased DPCs and resistance to IR, mimicked the ΔSPRTN phenotype, indicating DPC accumulation may alter chromatin configuration. Chromatin compaction hinders DDR execution by restricting repair protein recruitment, allowing ΔSPRTN cells to evade apoptosis and continue proliferating. These findings highlight the role of DPCs in shielding DNA lesions, reducing DDR activation. This has translational implications for cancers with defective DPC repair, like Ruijs-Aalfs syndrome, which may possess epigenetically compacted chromatin and intrinsic radioresistance. Therapeutically, targeting heterochromatin formation could resensitize these cells to IR. HDAC inhibition reversed radioresistance in ΔSPRTN cells. Future studies on diverse cell types and in vivo models are needed, with high-LET radiation potentially bypassing chromatin shielding.

In conclusion, our results demonstrate that SPRTN loss elicits a protective chromatin condensation that attenuates DDR signalling and suppresses apoptosis in cancer cell lines examined, particularly HeLa. This work uncovers a previously unrecognised link between DPC accumulation, chromatin architecture, and DDR efficiency, and sets the foundation for chromatin-targeted radiosensitisation strategies in DPC repair-deficient cancers. Additional experiments would further clarify this finding, supporting deeper investigation into chromatin-targeted therapies and strengthens the case for SPRTN's role in mediating radioresistance.

List of Figures

Figure 1.1 Radiotherapy uses in cancer treatment. 26
Figure 1.2. Depth–Dose Profile and Radiobiological Advantages of Particle Therapy Over X-rays 27
Figure 1.3. Direct and indirect effects of radiation on DNA 34
Figure 1.4. Radiation-induced Base modification 37
Figure 1.5. Mechanisms of Radiation-Induced DNA Base Damage and N-Glycosyl Bond Disruption 40
Figure 1.6. Mechanisms of Radiation-Induced DNA Strand Break Formation 43
Figure 1.7. Radiation-Induced DNA Damage Pathways and Tumour Microenvironment Influence 48
Figure 1.8. Comparative Effects of Low-LET and High-LET Radiation on DNA Damage and Cellular Outcomes 53
Figure 1.9. Base Excision Repair (BER) Pathway for Oxidative and Alkylation-Induced DNA Damage 59
Figure 1.10. Double-Strand Break (DSB) Repair Pathways in Eukaryotic Cells 67
Figure 1.11. Comparative Summary of Factors Modulating Radiation Response under Low and High Linear Energy Transfer (LET) Conditions 84
Figure 1.12. Different types of Enzymatic DNA-Protein Crosslinks (DPCs 100
Figure 1.13. Formation of DNA-protein crosslinks (DPCs) at abasic sites 103
Figure 1.14. Proposed mechanisms of DNA–protein crosslink (DPC) formation following ionizing radiation..... 111
Figure 1.15: Toxicity of unresolved DPC during replication and transcription 116
Figure 1.16. DNA-Protein Crosslink (DPC) repair pathways 121
Figure 1.17. Replication-dependent and post-replicative repair of DPCs. 131
Figure 1.18. Replication-independent DPCs repair 135
Figure 1.19. Transcription-coupled (TC) DNA–protein crosslink (DPC) repair. 138
Figure 1.20. SPRTN domains 141
Figure 1. 21. Some regulators of SPRNT activity 149
Figure 1.22. Expression of SPRTN in different cancer types 150
Figure 1.23: Schematic of some Protein-Targeted Methods 160
Figure 1.24. Schematic of some DNA-Targeted Methods 166
Figure 1.25: Detection of TOP1cc by immunofluorescence 169
Figure 2.1. RNA-seq correlation heatmaps for HeLa cells. 190
Figure 3.1. Schematic Representation of DPC Isolation Protocol Using RADAR and STAR Assays 194
Figure 3.2. RNA Contamination Assessment in DPC Samples Isolated Using RADAR and STAR Assays 196
Figure 3.3. Total DPC Levels Isolated by RADAR and STAR Following Benzonase Treatment 198
Figure 3.4. TCA Precipitation Enhances Detection of Crosslinked Proteins 199
Figure 3.5. Evaluation of ARK Assay Sensitivity in Detecting DPC Levels 201
Figure 3.6. Detection of DPCs Accumulation in SPRTN-Depleted Cells Using ARK Assay 202
Figure 3.7. Evaluation of DPC Levels Using Modified Comet Assay post IR and FA 205
Figure 3.8. Evaluation of DPC Levels Using Modified Comet Assay in SPRTN knockout cells 206
Figure 3.9. Kinetics of DNA-Protein Crosslink (DPC) Formation and Repair Following Radiation Exposure 210
Figure 3.10. FLASH-RT Induces a Rapid Increase in DNA-Protein Crosslink (DPC) Formation 212
Figure 3.11. Dose-Dependent Effects of FLASH-RT and Conventional RT on DNA-Protein Crosslink (DPC) Formation 213
Figure 3.12. DPC Formation and Repair Kinetics Following FLASH-RT and Conventional RT 214
Figure 3.13: Impact of Hypoxia and Reoxygenation on DPC Levels 217
Figure 4.1 Survival of SPRTN-depleted cells to DPC-inducing drugs 230
Figure 4.2 SPRTN Depletion Causes Radioresistance 234
Figure 4.3. SPRTN depletion confers radiotolerance in MCF-7 and A549 cancer cell lines following ionising radiation (IR) exposure. 238
Figure 4.4. Depletion of SPRTN via auxin-inducible degradation does not sensitise HCT116 cells to DNA-damaging agents or ionising radiation (IR). 242
Figure 4.5. SPRTN mutations in a patient-derived cell line confer resistance to ionising radiation (IR). 245

Figure 4.6 Proteolytic Activity of SPRTN Is Required for Radiosensitivity 249
Figure 4.7 SPRTN depletion attenuates caspase-3/7 activation following ionising radiation in HeLa cells. 253
Figure 4.8. Crosslinking agents in SPRTN depleted cells lead to fork collapse and cell death. 256
Figure 5.1. Attenuated γH2AX and 53BP1 foci formation in ΔSPRTN cells following ionising radiation. 267
Figure 5.2. SPRTN knockdown impairs γH2AX and 53BP1 foci formation following ionising radiation. 270
Figure 5.3. SPRTN deficiency impairs DNA damage signalling and modulates recruitment of RPA and KU70 to irradiation-induced lesions. 273
Figure 5.4. SPRTN deficiency attenuates DNA damage checkpoint activation following ionising radiation. 278
Figure 5.5. SPRTN depletion impairs DNA damage resolution following ionising radiation compared to DNA repair controls. 282
Figure 5.6 SPRTN deficiency results in persistent DNA damage following ionising radiation. 285
Figure 5.7. SPRTN-deficient cells exhibit impaired DSB resolution in unsynchronized HeLa cells following ionising radiation. 287
Figure 5.8. SPRTN depletion compromises DNA double-strand break repair in MCF-7 cells following ionising radiation. 289
Figure 5.9. SPRTN deficiency impairs DNA double-strand break (DSB) resolution following ionising radiation in a dose-dependent manner. 293
Figure 5.10. Catalytic activity of SPRTN is essential for efficient DNA damage resolution following ionising radiation. 297
Figure 5.11. SPRTN-deficient cells exhibit impaired DNA damage resolution following ionising radiation. 300
Figure 5.12. Cell cycle profiles of HeLa wild-type and ΔSPRTN cells following ionising radiation. 302
Figure 5.13. Model illustrating the paradoxical survival advantage of SPRTN-deficient cells following ionising radiation (IR). 305
Figure 6.1. Radiation-induced DNA–protein crosslinks (DPCs) are elevated in SPRTN-deficient cell. 313
Figure 6.2. SPRTN depletion results in elevated radiation-induced DPCs. 315
Figure 6.3. NAC pre-treatment partially reverses the radiation resistance phenotype of SPRTN-deficient cells. 318
Figure 6.4 | Antioxidant pre-treatment rescues DNA damage levels and DDR signalling in SPRTN-deficient cells post-irradiation. 323
Figure 6.5. Formaldehyde-induced DNA–protein crosslinks promote radioresistance and reduce apoptosis following ionising radiation. 327
Figure 6.6. Model illustrating how SPRTN deficiency or FA-induced DPCs promote radioresistance. 330
Figure 7.1. SPRTN depletion alters chromatin state through modulation of histone marks 336
Figure 7.2. SPRTN depletion and formaldehyde-induced DNA–protein crosslinks alter histone modification profiles associated with chromatin state. 338
Figure 7.3. SPRTN depletion alters the expression of chromatin remodelers CHD1, CHD2, and CHD4. 341
Figure 7.4. Histone acetylation levels are reduced in SPRTN-depleted cells post-irradiation and rescued by HDAC inhibition. 343
Figure 7.5. SPRTN deficiency reduces histone acetylation and alters nucleolar architecture following ionising radiation. 350
Figure 7.6. Kegg pathway analysis of SPRTN-depleted cells. 351
Figure 7.7. SPRTN deficiency leads to increased HP1 retention after ionising radiation. 354
Figure 7.8. SPRTN deficiency leads to elevated levels of linker histone H1.2 and enhanced chromatin compaction following ionising radiation. 356
Figure 7.9 SPRTN deficiency reduces H3.3 chromatin incorporation following ionising radiation. 359
Figure 7.10 Schematic representation of chromatin accessibility measured by micrococcal nuclease (MNase) digestion. 362
Figure 7.11. Titration of Micrococcal Nuclease (MNase) to optimise digestion of chromatin for nucleosome accessibility assessment. 366
Figure 7.12. MNase digestion assay to assess chromatin accessibility in untreated, formaldehyde-treated, and HDACi-treated cells. 368

Figure 7.13. SPRTN depletion leads to enhanced chromatin compaction after ionising radiation, as assessed by MNase digestion. 372
Figure 7.14. SPRTN deficiency promotes chromatin compaction under basal and post-irradiation conditions, as revealed by MNase digestion and densitometry profiling. 376
Figure 7.15. HDAC inhibition reverses the radioresistance phenotype of SPRTN-deficient cells. 379
Figure 7.16. Knockdown of chromatin compaction regulators restores radiosensitivity in SPRTN-deficient cells. 382
Figure 7.17. Knockdown of SUV39H1 restores radiosensitivity in SPRTN-deficient cells by reducing chromatin compaction. 385
Figure 7.18. Chromatin relaxation restores apoptotic signalling in SPRTN-deficient cells. 388
Figure 8.1. Model of the mechanism of radioresistance of SPRTN inactivated cells. 401
Figure 8.2. Proposed Impact of SPRTN level on complex DNA Double-Strand Break (DSB) Formation Following Radiation. 408
Figure 9.1. Alkaline comet assay was performed on untreated cells and compared with 50 nM CPT for 1 h treatment. 419
Figure 9.2. Schematic overview of the modified comet assay for DNA–protein crosslink(DPC)detection 422
Figure 9.3. Comparison of the RADAR and STAR assays for DNA–protein crosslink (DPC) isolation and detection. 423
Figure 9.4. Comet assay reveals altered DNA repair dynamics in USP18-deficient cells. 426
Figure 9.5. Increased DNA damage signalling in USP18-deficient cells post-irradiation. 427

List of Tables

Table 1.1 Quantitative Comparison of DNA Damage Types Induced by Low-LET (Photons) and High-LET (Carbon Ions) Radiation per Gray per Cell 52
Table 1.2. Summary of DNA Glycosylases, Their Functions, and Substrate Specificities in Base Excision Repair 56
Table 1.3 Comparison of DNA Damage Characteristics and Repair Responses Induced by High-LET and Low-LET Radiation 71
Table 1.4: Types of Aldehydes, Their Chemical Structures, Endogenous Sources, and Crosslinking Properties 98
Table 1.5. Chemotherapy Agents and DPC Formation 108
Table 1.6: Comparison of Different DPC Types 114
Table 1.7. Genes encoding for DPC proteases and their known functions 120
Table 1.8. Pathways involved in SPRTN activity and their mechanisms 147
Table 1.9. Comparison between some protein-targeted DPCs isolation methods 158
Table 1.10: Comparison between some DNA-targeted DPCs isolation methods 164
Table 2.1. Sequence of oligonucleotides used for siRNA depletions 176
Table 2.2. Primary antibodies used for western blot. 183
Table 2.3. Secondary antibodies used for western blot. 184
Table 2.4. Primary antibodies used for IF. 185
Table 7.1. List of DEGs present in HeLa SPRTN -/-/+ 348
Table 7.2 Summary of the different HDAC (histone deacetylase) classes. 377

List of Abbreviations

Abbreviation	Full name
53BP1	Tumour suppressor p53-binding protein 1
APC	Anaphase Promoting Complex
AP	Apurinic/apyrimidinic sites
ARK	Advanced recovery of K [potassium]-SDS precipitates
ATR	Ataxia-Telangiectasia Rad3-related protein
ATM	Ataxia-Telangiectasia Mutated
ATCC	American Type Culture Collection
ATP	Adenosine Triphosphate
ATG	Autophagy-related genes
Bcl-2	B-cell lymphoma 2
Bcl-xL	B-cell lymphoma-extra large
BER	Base Excision Repair
BR	Basic region
BSA	Bovine serum albumin
CAM	Camptothecin
CASP3	Caspase 3
CASP8	Caspase 8
CASP9	Caspase 9
C. elegans	Caenorhabditis elegans
CFA	Colony Forming Assay
CHK1	Checkpoint kinase 1
CHK2	Checkpoint kinase 2
CMG	CDC45–MCM2/7–GINS
CPT	Camptothecin
DAPI	4′,6-Diamidino-2-phenylindole
DBC1	Deleted in Breast Cancer 1
DDI1	DNA Damage Inducible 1 Homolog 1
DDR	DNA-damage response

DMEM	Dulbecco’s Modified Eagle’s Medium
DMSO	Dimethyl sulfoxide
DNA	Deoxyribonucleic Acid
DNA-PK	DNA-dependent protein kinase
DPC	DNA-Protein Crosslinks
DSB	Double-Strand Break
DTT	Dithiothreitol
EBRT	External Beam Radiation Therapy
EDTA	Ethylenediaminetetraacetic acid
FA	Formaldehyde
FACS	Fluorescence-activated cell sorting
FAM111A/B	FAM111 Trypsin Like Peptidase A / B
FANCJ	Fanconi anaemia complementation group J
FBS	Fetal Bovine Serum
GCN5 (KAT2A)	Lysine acetyltransferase 2A
GCNA	Germ cell nuclear acidic protein
Gy	Gray (unit of radiation dose)
GTC	Guanidine thiocyanate
H3K9ac3	Triacetylated lysine of H3
H3K9me3	Trimethylated lysine of histone H3
HCl	Hydrogen chloride
HDACi	Histone Deacetylase Inhibitors
HR	Homologous recombination
HSP70	Heat shock protein 70
ICL	Inter-Strand Crosslink
IRT	Internal Radiation Therapy
IR	Ionizing Radiation
K	Lysine
KAP1	KRAB domain–associated protein 1
kDa	Kilodalton
KEGG	Kyoto Encyclopedia of Genes and Genomes

Ku70	Component of the non-homologous end joining (NHEJ) pathway
LMPA	Low melting point agarose
mA	milliampere
MNase	Micrococcal Nuclease
MRE11	Meiotic Recombination 11
MRN	MRE11-RAD50-NBS1
MTT	3-(4, 5-dimethylthiazolyl-2)-2, 5-diphenyltetrazolium bromide
mRNA	Messenger Ribonucleic Acid
NAC	N-acetyl cysteine
NaAc	Sodium acetate
NaCl	Sodium chloride
NBS1 (NBN)	Nijmegen Breakage Syndrome Protein 1
NCD	Noncommunicable diseases
NER	Nucleotide Excision Repair
NHEJ	Non-homologous end joining
NMPA	Normal melting point agarose
NP-40	Nonidet P-40
NPL4	Nuclear Protein Localisation Protein 4
ns	Not Significant
OGG1	8-Oxoguanine DNA Glycosylase
PARP	Poly(ADP-ribose) polymerase
PBS	Phosphate buffered saline
PCNA	Proliferating Cell Nuclear Antigen
PI	Propidium iodide
PIP	PCNA-interacting protein motif
Pol δ	DNA polymerase delta
PTM	Posttranslational Modification
RADAR	Rapid Approach to DNA-Adduct Recovery
RNA	Ribonucleic Acid
RNA-seq	RNA sequencing

RPA	Replication Protein A
RJALS	Ruijs-Aalfs syndrome
RNAi	RNA interference
ROS	Reactive Oxygen Species
RPM	Revolutions per minute
RT-qPCR	Quantitative reverse transcription polymerase chain reaction
siRNA	Small interfering RNA
SDS	Sodium Dodecyl Sulphate
SPRTN	SprT-like N-terminal domain
SSA	Single-Strand Annealing
SSB	Single-Strand Break
SUV39H1	Suppressor of variegation 3-9 homolog 1
TBE	Tris/Borate/EDTA
TBS-T	Tris Buffered Saline with Tween
TDP1	Tyrosyl-DNA phosphodiesterase 1
TDP2	Tyrosyl-DNA phosphodiesterase 2
TEX264	Testis-Expressed Protein 264
Tg	5,6-thymine glycol
TLS	Translesion synthesis
TOP1	Topoisomerase I
TOP2	Topoisomerase II
TOP1cc	TOP1 cleavage complex
TOP2cc	TOP2 cleavage complex
TSA	Trichostatin A
UBZ	Ubiquitin-binding zinc finger
UFD1	Ubiquitin Fusion Degradation Protein 1
UV	Ultraviolet
V	Volt
VCP	Valosin-Containing Protein
Wss1	Weak Suppressor of Smt3-1
WT	Wild-Type

ZBD	Zinc-binding domain
γH2AX	Phosphorylated H2A Histone Family Member X
Δ	Deletion

Chapter 1: Introduction

In the 21st century, cancer without a doubt represents a significant challenge to public health and societies, in addition to the economy. It accounts for nearly one in four deaths (22.8%) globally. This illness is responsible for approximately 30% of premature deaths from Noncommunicable diseases (NCDs), affecting individuals aged 30 to 70 years, ranking among the top three causes of death in this demographic across many countries (Bray, 2021). According to the global data for 2022, there were almost 20 million newly diagnosed cases of cancer, with 10 million fatalities. Moreover, the number of new cancer cases each year is expected to rise to 35 million by 2050, marking a 77% increase from the levels observed in 2022 (Ferlay et al., 2024).

There are different approaches for cancer treatment, including surgery, chemotherapy, radiation therapy, immunotherapy, targeted therapy, hormone therapy, and stem cell transplants. Each approach can be used alone or in combination. The choice of cancer therapy depends on different factors like the type, stage, location, and genetic makeup of the tumour, in addition to the patient's health and age. These therapies aim to remove or destroy cancer cells, prevent their spread, and reduce the likelihood of recurrence, ultimately improving survival rates and quality of life for patients (Debela et al., 2021).

1.1 Radiation Therapy

Radiation therapy is received by around 50% of cancer patients during their treatment (Delaney et al., 2005). It can be used as a primary choice for therapy (curative radiotherapy) or it can be used to enhance the efficacy of other treatments, such as when it is combined with chemotherapy or administered prior to surgical intervention (neo-adjuvant radiotherapy) (Figure 25). Furthermore, it aims to diminish the likelihood of cancer recurrence following primary treatments such as surgical

procedures, referred to as adjuvant radiotherapy. In cases where a cure is unattainable, palliative radiotherapy alleviates symptoms (Dong & Gewirtz, 2022; Feeney et al., 2019; Kolářová et al., 2024).

1.1.1 Types of Radiation Therapy Based on the nature of radiation

1.1.1.1 Photon-Based Radiotherapy

Photon-based radiotherapy remains one of the most widely used and essential treatment modalities in modern oncology, with an estimated 50% of all cancer patients receiving radiotherapy as part of their treatment regimen (Baskar et al., 2012).

The therapeutic use of photons began soon after their discovery. On January 29, 1896, just after the announcement of X-rays, the first radiation treatment to a cancer patient was administrated (Lederman, 1981). This marked the beginning of photon radiotherapy in clinical oncology.

Photon radiation therapy involves the use of X-rays or gamma rays, both of which are forms of electromagnetic ionising radiation. In external beam radiotherapy, X-rays are generated by linear accelerators (linacs), while gamma rays originate from radioactive decay of unstable atomic nuclei, such as cobalt-60. Despite their differing sources, both X-rays and gamma rays interact similarly with biological tissue (Attix, 2004). Once administered, photons penetrate tissues and deposit energy along their entire path. Photon beams deposit the highest radiation dose near the entrance point and continue to release energy throughout their trajectory in the body. As a result, healthy tissues surrounding and beyond the tumour receive unintended radiation exposure (Figure 26). This non-specific energy deposition significantly increases the risk of adverse effects, including inflammation, fibrosis, or damage to surrounding organs. Meanwhile, the actual tumour may receive a comparatively lower effective dose, particularly if

shielded by overlying or adjacent tissues (Baskar et al., 2012; Niemantsverdriet et al., 2012).

A critical parameter describing the nature of radiation interaction with tissue is the linear energy transfer (LET)—the amount of energy deposited per unit length of tissue traversed. X-rays and gamma rays are considered low-LET radiation, meaning they deposit energy sparsely along their path (Wilson & Bedford, 2010) Photons, being massless and electrically neutral, interact with tissues mainly by generating secondary electrons, which in turn induce DNA damage through direct ionisation or indirectly via reactive oxygen species (ROS). These interactions compromise essential cellular structures and functions, especially within rapidly dividing tumour cells, ultimately leading to cell death. They primarily induce single-strand DNA breaks (SSBs), which are generally repairable, and less frequently double-strand breaks (DSBs) (Hada & Sutherland, 2006; Lomax et al., 2013a). This contrasts with high-LET radiation, such as carbon ions, which generate dense ionisation tracks and more complex, less reparable DNA lesions as will be mentioned in the following sections.

1.1.1.2 Particle therapy

Particle therapy is a form of external beam radiotherapy that utilises charged or uncharged particles such as neutrons, protons and carbon ion for cancer treatment.

The therapeutic application of hadron therapy, which utilizes charged particles for cancer treatment, was first proposed by physicist Robert R. Wilson in 1946. In his seminal paper, Wilson highlighted the potential advantages of using protons for radiation therapy, emphasizing their unique physical properties that allow for precise dose delivery to tumours while sparing surrounding healthy tissues (WILSON, 1946).

Following this concept, the clinical use of hadrons began with fast neutrons, the first hadrons applied in medicine shortly after their discovery in 1932 (Jones, 2020). Later, in 1994, the first carbon ion therapy centre was established at the National Institute of Radiological Sciences (NIRS) in Japan, introducing a new dimension to particle therapy with the use of heavier ions.

Fast neutron therapy provides a notable therapeutic advantage due to its high LET and its capacity to induce direct DNA damage independently of oxygen levels, making it particularly effective for treating recurrent, bulky tumours in anatomically complex regions. However, its clinical application is significantly limited by its high toxicity to surrounding healthy tissues. This drawback has contributed to the increasing reliance on photon-based radiotherapy and the expanding use of proton and carbon ion therapy, which offer more favourable toxicity profiles (Goodhead, 2019).

Advancements in particle therapy, particularly with protons and carbon ions, offer distinct advantages over conventional photon therapy. A key benefit is their dose deposition pattern characterized by the Bragg Peak, a phenomenon where charged particles deposit the majority of their energy at a specific depth, corresponding to the tumour location (Durante et al., 2017). This results in minimal energy deposition in the tissues before and beyond the tumour, thereby reducing damage to healthy tissues.

The Relative Biological Effectiveness (RBE) quantifies the efficacy of different types of radiation in producing biological effects. It is defined as the ratio of the dose required to achieve a specific biological effect using a reference radiation (typically Co-60 photons) to the dose required with the test radiation. For protons, the general RBE is approximately 1.1, indicating a slightly higher effectiveness compared to conventional photons (Paganetti et al., 2002). Heavier particles, such as carbon ions, exhibit a

higher RBE, reported to be around 2 to 3.5 in various tissues and experimental settings, due to their increased LET (Sørensen et al., 2015). Protons are typically considered low-LET radiation; however, their LET is not uniform and increases progressively along their path, peaking at the distal edge of the Bragg peak, just before the particles come to rest (H. Paganetti, 2014). Nevertheless, carbon ion radiotherapy is considered more effective than photon or proton therapy due to its significantly higher LET. Additionally, carbon ion therapy demonstrates reduced sensitivity to factors such as tumour hypoxia, inherent radiosensitivity of tumour cells, and cell cycle distribution, making it a promising option for treating various cancers (Glowa et al., 2024; Sørensen et al., 2015).

The elevated ionisation density associated with particle radiation, which is reflected by LET compared to photons, results in more concentrated energy deposition within cells, particularly in nuclear DNA. This dense ionisation pattern increases the likelihood of generating localized clusters of DNA lesions. These complex DNA damage sites may include combinations of base modifications, single-strand breaks (SSBs), double-strand breaks (DSBs), and DNA crosslinks, collectively referred to as clustered or complex DNA damage. In contrast, high-LET radiation, such as that from alpha particles or heavy ions like carbon, induces localized DNA damage with a high incidence of double-strand breaks (DSBs**)**. These complex DSBs are challenging for cellular repair mechanisms, leading to increased tumour cell death (Georgakilas et al., 2013).

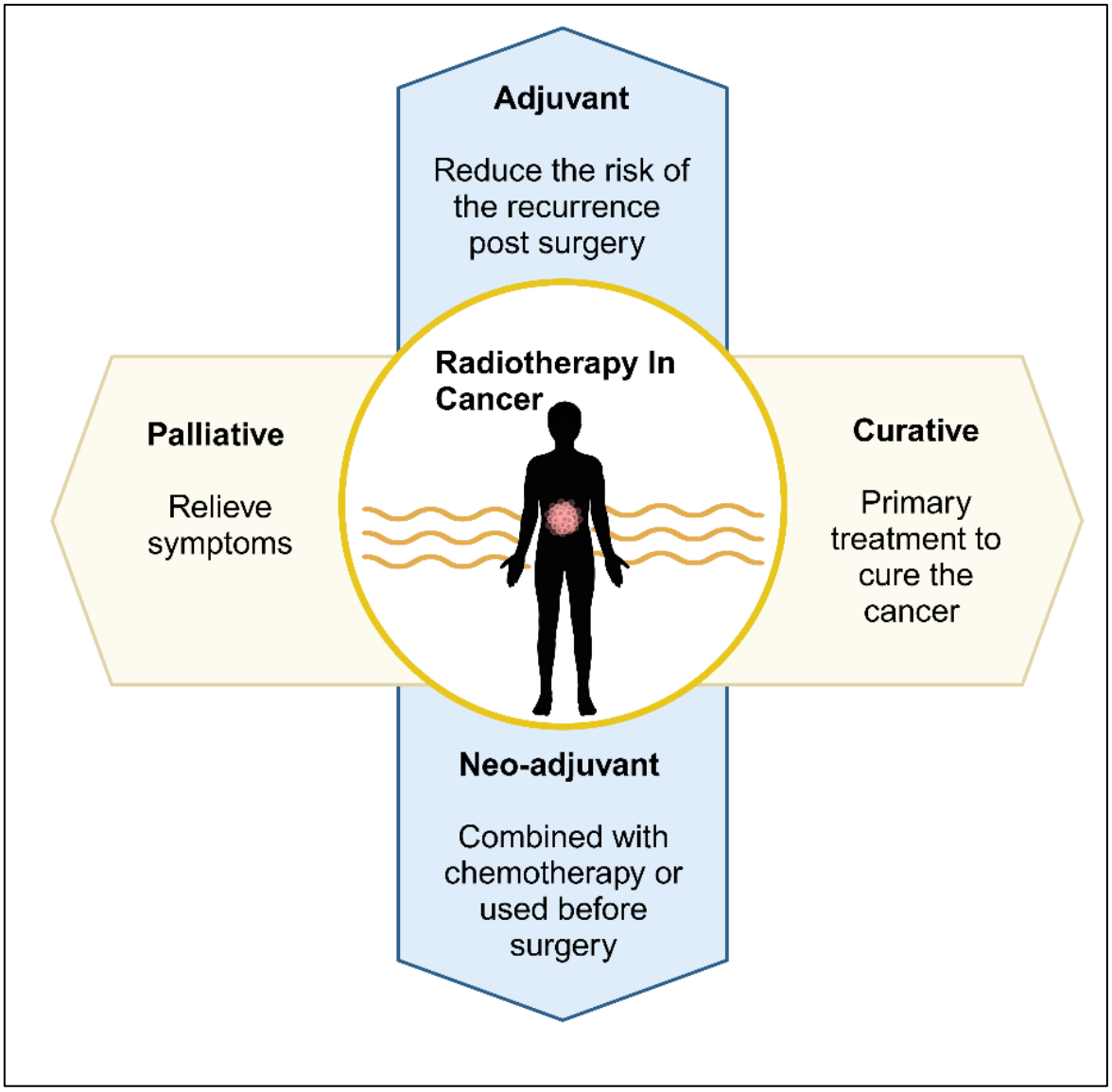


Figure 1.1 Radiotherapy uses in cancer treatment.

Different types of radiotherapy used in cancer treatment. Curative radiotherapy aims to completely eradicate the tumour. Adjuvant radiotherapy is used post-surgery to eliminate residual cancer cells, while neoadjuvant radiotherapy is administered before surgery to shrink tumours. Palliative radiotherapy focuses on symptom relief in advanced cancers. Figure created using BioRender.com.

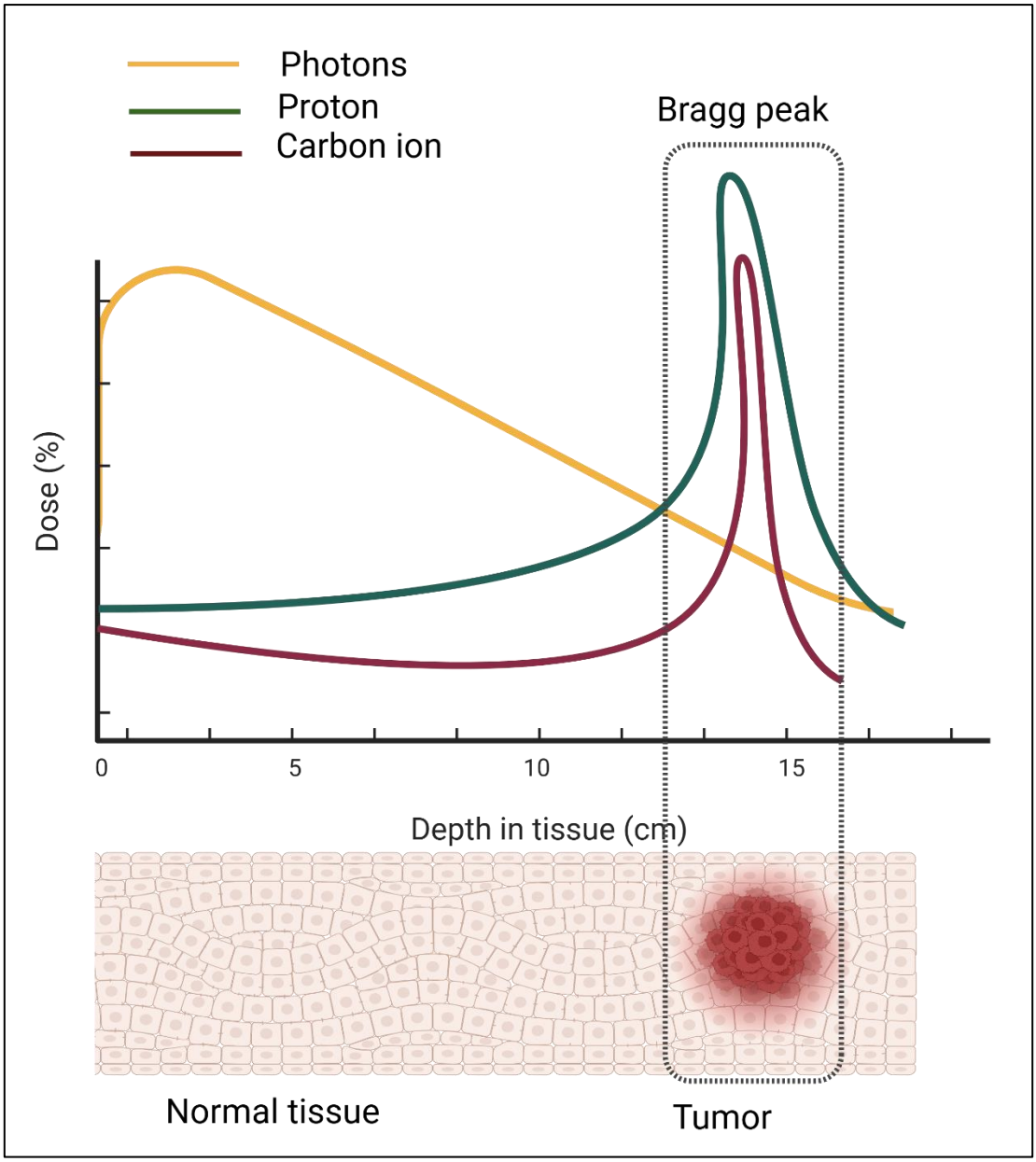


Figure 1.2. Depth–Dose Profile and Radiobiological Advantages of Particle Therapy Over X-rays

Schematic representation of the physical and biological advantages of particle therapy compared to conventional X-ray irradiation. Unlike photons, which continuously deposit energy along their path, charged particles release the majority of their energy at the end of their range, forming a sharp energy deposition peak within the tumour target. As the particles decelerate toward the end of their path, their ability to induce biological damage increases, offering enhanced therapeutic precision. This unique depth–dose distribution supports more effective tumour control while minimizing harm to surrounding healthy tissue. LET: Linear Energy Transfer, RBE: Relative Biological Effectiveness, OER: Oxygen Enhancement Ratio. *Created using BioRender.com*

1.1.2 Types of Radiation Therapy Based on the Dose Rate

Another way to classify radiation therapy is based on the dose delivery rate. Conventional radiation therapy (CONV-RT) generally delivers ionising radiation at standard dose rates between 0.01 and 0.4 Gy/s, and remains the most widely utilised approach in clinical oncology for treating various types of cancer. On the other hand, FLASH radiation therapy (FLASH-RT) involves ultra-high dose rates of ≥40 Gy/s, delivering the full dose within milliseconds. Unlike conventional radiation, FLASH-RT is a relatively new approach, first introduced in 2014 by Favaudon et al., who demonstrated its remarkable ability to minimise damage to healthy tissues while maintaining effective tumour control, a phenomenon referred to as the “FLASH effect” (Favaudon et al., 2014, 2019).

This difference in delivery rate leads to different biological responses. Numerous preclinical studies on animals have demonstrated a successful normal tissue-sparing effect associated with FLASH radiotherapy (Fouillade et al., 2020; Soto et al., 2020; Vozenin et al., 2019). However, it is important to note that several other studies have reported no significant reduction in normal tissue toxicity following irradiation at ultra-high dose rates.

Up until now, there are two clinical trials that have been published. The first peer-reviewed clinical trial of FLASH radiotherapy, published in 2019 by Bourhis et al. A patient with a 3.5 cm T-cell cutaneous lymphoma tumour received a 15 Gy dose of radiation delivered within 90 milliseconds. Within three weeks post-treatment, typically the peak of radiation-induced skin response, only mild side effects were noted, including grade 1 epithelitis and a transient grade 1 edema in adjacent tissue. Importantly, no severe toxicity was observed, a marked contrast to the significant skin reactions experienced by the patient during prior conventional radiotherapy. The

treated tumour began to shrink approximately 10 days after FLASH irradiation and achieved complete regression by day 36, with the remission still sustained at five months. The authors concluded that this first-in-human FLASH-RT was both feasible and safe, offering substantially reduced normal tissue toxicity while maintaining effective tumour control (Bourhis, Sozzi, et al., 2019).

In the second peer-reviewed clinical study, proton FLASH-RT was used for palliative treatment of painful bone metastases in 10 patients. All lesions were successfully treated without FLASH-specific delays. By 3 months post-treatment, 67% of sites had pain relief (50% with complete resolution), matching conventional 8 Gy RT benchmarks. Toxicity was mild (Grade 1), including transient skin changes and pain flares, with no unexpected or severe side effects. The study concluded that FLASH-RT was feasible, safe, and effective for symptom relief, supporting further clinical investigation (Mascia et al., 2023).

Although the exact mechanisms underlying the FLASH effect are not yet fully understood, it is hypothesised that it involves rapid oxygen depletion, reduced production of reactive oxygen species (ROS) in normal tissues, and modulation of immune responses, all of which contribute to reduced normal tissue toxicity:

1.1.2.1 Mechanisms Behind the FLASH Effect

1.1.2.1.1 Oxygen Depletion Effect

One proposed mechanism for the FLASH effect is the rapid depletion of oxygen during ultra-high dose rate (UHDR) irradiation, leading to transient hypoxia in normal tissues. This reduces radiosensitivity and spares healthy cells, while hypoxic tumours, already oxygen-deficient, gain little protection (Berry et al., 1969; C.D.Town, 1967; Michaels et al., 1978). Additionally, healthy cells may more effectively neutralize radiation-induced

byproducts like hydrogen peroxide due to superior antioxidant defences. However, recent studies challenge this theory, showing that FLASH-RT may not deplete oxygen entirely, even at high doses (López-Lázaro, 2007). Some protective effects have also been observed under normoxic conditions, suggesting that oxygen depletion alone may not fully explain the FLASH effect.

1.1.2.1.2 ROS and Free Radical Effects

FLASH-RT generates ROS, such as hydroxyl radicals and hydrogen peroxide, through the radiolysis of water (J. Ma et al., 2023). These ROS can damage DNA and proteins, but their short lifespan and limited diffusion during UHDR may restrict damage to target regions, sparing normal tissue. Normal cells may also better mitigate ROS due to stronger antioxidant systems. Experimental models, including zebrafish embryos and molecular simulations, suggest that reduced ROS generation and localized damage may underpin the differential responses between tumour and normal cells (Karsch et al., 2022).

1.1.2.1.3 Immune Hypothesis

A potential contributor to the FLASH effect is reduced immune system damage. Unlike CONV-RT, which exposes a large proportion of circulating lymphocytes to radiation over multiple fractions, FLASH-RT's ultra-short delivery time likely spares more immune cells by limiting their irradiation (Bourhis, Sozzi, et al., 2019; Durante et al., 2018) .

Supporting this, genome-wide analyses in mice have shown reduced immune activation after FLASH-RT compared to CONV-RT (Girdhani et al., 2019). Additionally, studies have reported increased T cell recruitment to the tumour microenvironment following FLASH-RT(Rama et al., 2019). Moreover, findings from

immunocompromised models where no differences in tumour response were observed suggest that immune modulation may explain the FLASH effect (Bourhis, Montay-Gruel, et al., 2019; Favaudon et al., 2019; Montay-Gruel et al., 2019). Moreover, the observation of FLASH effects in vitro and in bacterial systems where no functional immune system exists suggests that immune involvement may be secondary to other primary factors such as DNA damage response or oxidative stress regulation (DEWEY & BOAG, 1959; Ewing, 1980). Thus, although a modified immune response remains a promising avenue of investigation, more mechanistic studies are needed to determine its precise role in mediating or modulating the FLASH effect.

1.1.2.2 Damage caused by Flash radiation

In regard to DNA damage, a study demonstrated that administering high radiation doses (up to 20 Gy) at FLASH dose rates (~1000 Gy/s) resulted in significantly fewer DNA double-strand breaks (DSBs) compared to conventional dose rates. Quantification of γH2AX foci, a well-established marker of DSBs, revealed a substantially lower signal 30 minutes post-irradiation in FLASH-irradiated cells (~8-fold increase) compared to those treated at a conventional rate (~13-fold increase at 0.05 Gy/s). Furthermore, the long-term effects were also mitigated by FLASH: one month after exposure, the proportion of senescent cells (marked by SA-β-gal activity) was notably reduced in cultures treated with FLASH compared to conventional irradiation. Collectively, these findings indicate that ultra-high dose-rate exposure leads to both reduced immediate DNA damage and decreased long-term cellular toxicity in normal tissue (Buonanno et al., 2019).

A study found that the extent of DNA damage caused by Flash-RT was influenced by several factors: 1) Oxygen concentration and 2) Total dose and dose rate. In this study, Cooper et al. investigated DNA damage in ex vivo human peripheral blood

lymphocytes under varying oxygen tensions using the alkaline comet assay. Blood samples were irradiated with 20 Gy delivered either at ~2 kGy/s (FLASH) or 0.1 Gy/s (conventional). Under normoxic conditions, both dose rates produced comparable DNA damage. However, under hypoxic conditions (≤0.5% O_2), FLASH significantly reduced DNA strand breaks compared to conventional irradiation ($p < 0.01$). The protective effect of FLASH became more evident at higher doses (≥20 Gy) and dose rates (≥30 Gy/s), highlighting an oxygen-dependent mechanism that limits oxygen-mediated DNA damage(Cooper et al., 2022).

Three key plasmid-based studies have demonstrated that FLASH irradiation consistently results in reduced DNA damage compared to conventional dose rates. Perstin et al. showed that FLASH electron beams (47–93 Gy/s) caused ~45% fewer double-strand breaks (DSBs) and significantly fewer single-strand breaks (SSBs) in agarose-embedded plasmid DNA than conventional dose rates (0.17 Gy/s), indicating a clear FLASH sparing effect through reduced break induction (Perstin et al., 2022). Similarly, Wanstall et al. used ultra-high dose-rate very high energy electrons (VHEE, ~2×10^9 Gy/s) to irradiate plasmid DNA and found 16–27% fewer SSBs compared to conventional (0.08 Gy/s), even under different hydroxyl radical scavenger conditions, suggesting that radical recombination or oxygen depletion mechanisms contribute to reduced damage (Wanstall et al., 2024). Wang et al. extended this by measuring both SSBs and oxidative base lesions, reporting a ~16% reduction in SSBs and ~26% lower total break yield under FLASH (6 MeV electrons) compared to conventional exposure (Y. Wang et al., 2025). Together, these studies provide evidence that FLASH irradiation reduces both strand breaks and indirect oxidative damage in DNA, supporting the hypothesis that ultra-high dose rates alter the physicochemical environment in ways that mitigate DNA injury.

1.1.3 Commonly Induced DNA Lesions by Conventional Ionizing Radiation

Radiation therapy is one approach to inhibit the proliferation of cancer cells and is effective in killing cells by causing various types of DNA lesions (Cadet et al., 2008). Generally, radiation exerts both direct and indirect effects on cellular DNA. (Wardman, 2009). The direct effect occurs when high-energy particles or waves physically interact with the DNA, breaking its molecular structure through mechanisms such as SSBs and DSBs. These disruptions can compromise the cell's ability to replicate its DNA, leading to mutations, apoptosis, or senescence if repair processes fail. The indirect effects of IR are mediated through the radiolysis of water, a major component of cells. When IR interacts with water molecules, it generates highly reactive hydroxyl radicals and other ROS. These radicals are capable of diffusing into the DNA and surrounding cellular proteins, causing oxidative damage that further contributes to DNA lesions. The hydroxyl radicals react with nucleobases and deoxyribose residues in DNA, leading to a wide array of oxidative damage such as base modifications, strand breaks, and the formation of abasic sites. (Baskar et al., 2012).

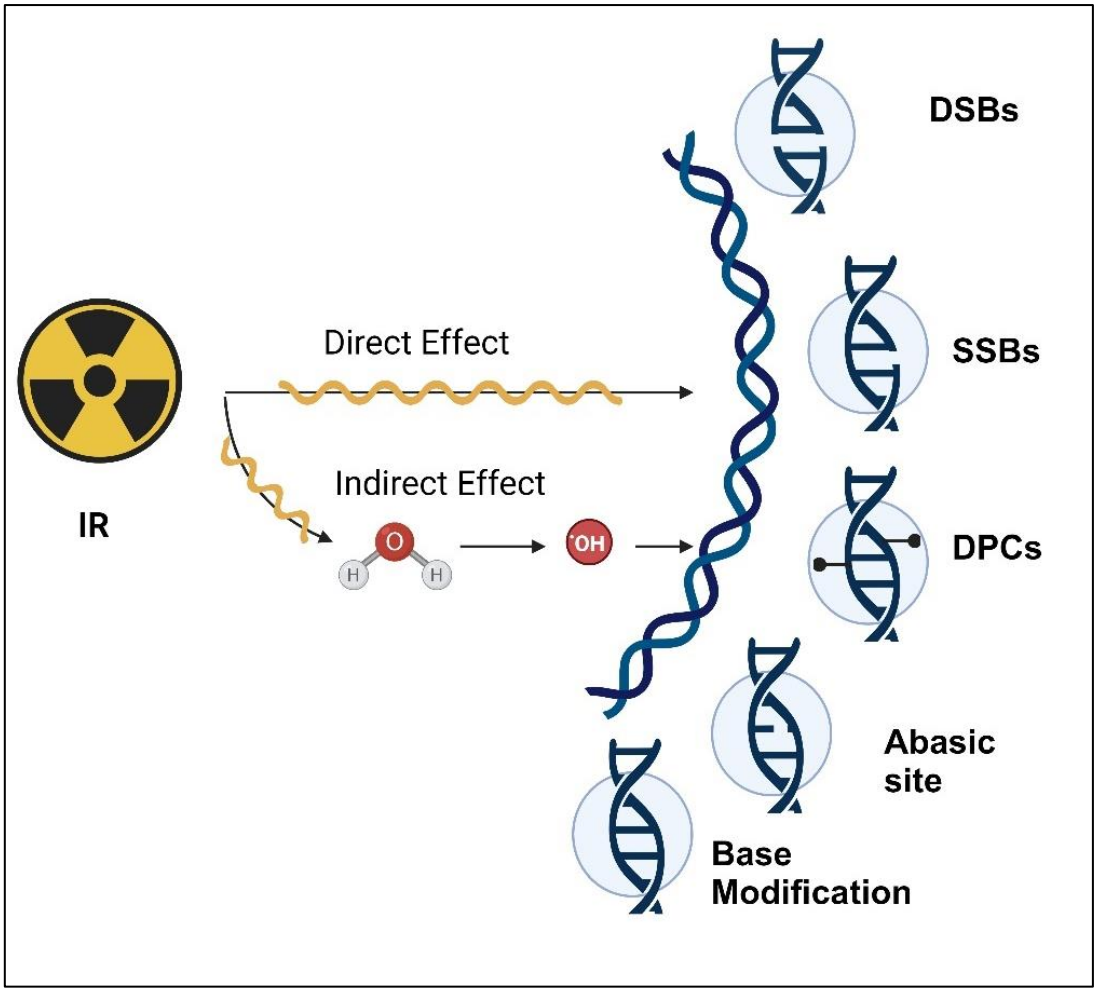


Figure 1.3. Direct and indirect effects of radiation on DNA

This figure illustrates the two primary mechanisms by which ionizing radiation damages DNA. The **direct effect** involves radiation directly interacting with DNA molecules, causing ionization and producing single-strand and double-strand breaks. This leads to structural changes in the DNA, disrupting cellular processes such as replication and transcription. The **indirect effect** occurs when radiation interacts with water molecules in the cell, generating reactive oxygen species (ROS). These ROS then attack DNA, resulting in oxidative damage, base modifications, and strand breaks. Both mechanisms contribute to the overall damage response. DSBs; Double Strand Break, SSBs; single strand break; DPCs; DNA-Protein crosslink. Created using BioRender.com.

Generally, DNA lesions caused by IR are isolated and complex damage (Hada & Sutherland, 2006; Lomax et al., 2013a):

1.1.3.1 Base Damage:

IR leads to modifications to the nitrogenous bases of DNA, such as oxidation, which can lead to incorrect base pairing during replication, increasing the mutation rate. Some of the most common base modifications caused by radiation:

1-The predominant oxidative product of thymine following exposure to ionising radiation is 5,6-dihydro-5,6-dihydroxythymine, commonly known as thymine glycol. Thymine glycol is particularly noteworthy for its ability to induce substantial distortion in the DNA double helix, thereby interfering with normal base pairing and replication (Breimer & Lindahl, 1985; Dolinnaya et al., 2013).

2-The oxidative degradation of 5-methylthymine residues, typically found in DNA as thymidine, gives rise to several modified pyrimidine bases, among which 5-hydroxymethyluracil (5-HMU) and 5-formyluracil (5-fU) are well-characterised. These lesions are primarily generated through the action of ROS, particularly ·OH, produced during ionising radiation or exposure to other oxidising agents. The oxidation of the methyl group at the 5-position of thymine initially yields 5-HMU, which may undergo further oxidation to form 5-fU (Douki et al., 1996; Wallace, 2002).

3-Guanine, which has the lowest ionisation potential of all DNA bases, is particularly susceptible to radiation-induced damage and has therefore been the focus of extensive investigation. As a result, guanine is the predominant target for one-electron oxidation and hydroxyl radical (·OH)-mediated reactions. These processes give rise to several well-characterised oxidative guanine lesions, including 2,2,4-triamino-5-(2H)-

oxazolone, 2,6-diamino-4-hydroxy-5-formamidopyrimidine (FapyGua), and 8-oxo-7,8-dihydroguanine (8-oxoGua)(Ogawa et al., 2003; Tudek et al., 1992).

4-Cytosine is particularly prone to oxidative modification, resulting in the formation of unstable intermediates that rapidly undergo further chemical transformations. One such intermediate is cytosine glycol, which is highly unstable and readily deaminates to yield uracil glycol or alternatively dehydrates to produce 5-hydroxycytosine (5-OHC). Uracil glycol itself can undergo dehydration to generate 5-hydroxyuracil (5-OHU). Collectively, 5-OHC, uracil glycol, and 5-OHU represent the principal stable products arising from free radical-induced oxidation of cytosine. These lesions are commonly observed following exposure to ionising radiation and are known to contribute to mutagenesis if not efficiently repaired (Douki et al., 1996; Wagner et al., 1992).

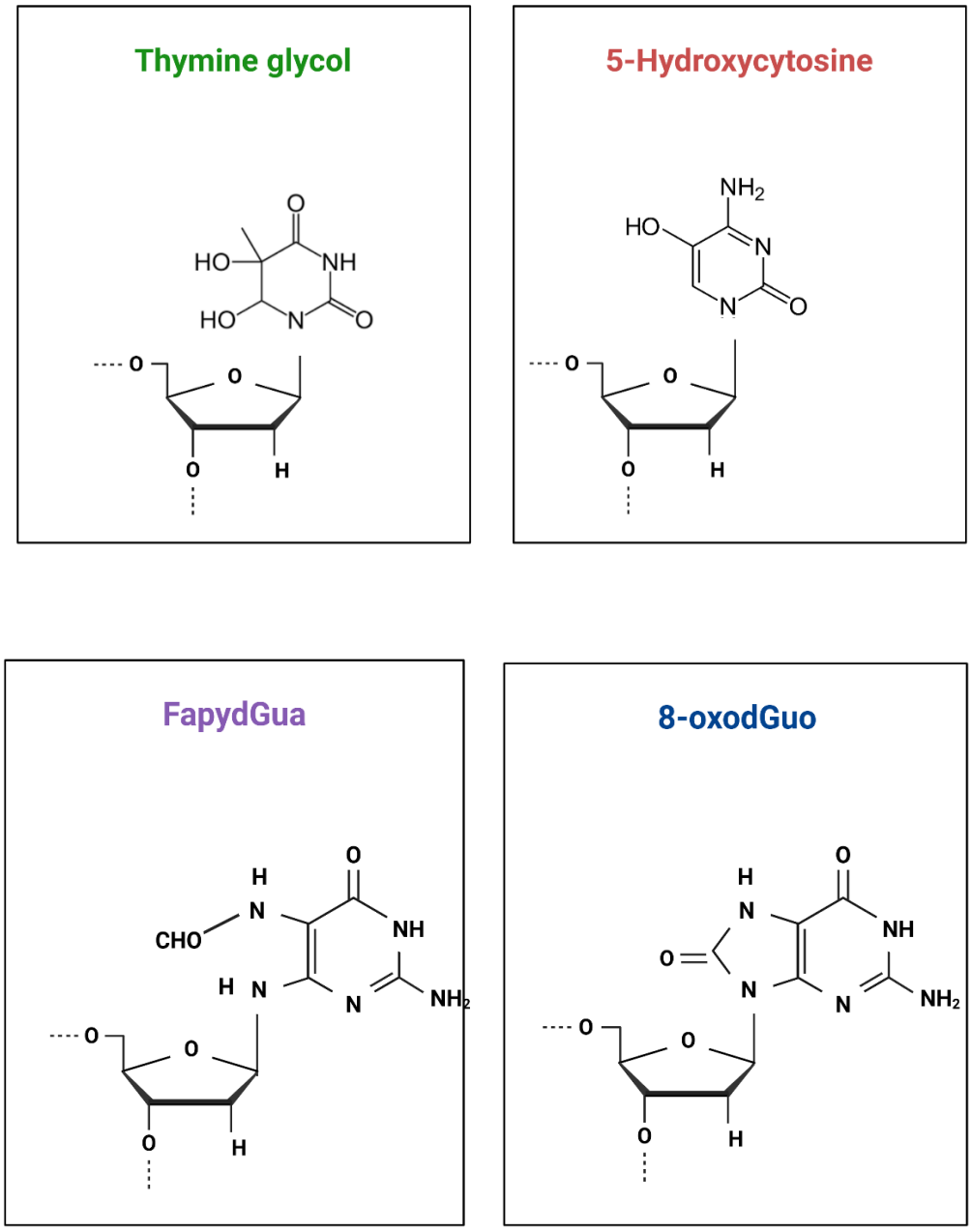


Figure 1.4. Radiation-induced Base modification

Radiation-induced oxidative stress leads to various DNA base modifications, which compromise genomic stability. This figure illustrates four prominent oxidative lesions caused by ionising radiation:

- Thymine glycol: The primary oxidation product of thymine, disrupting base pairing and distorting DNA structure.
- 5-Hydroxycytosine: An oxidative cytosine lesion that can result in mutagenesis if not repaired.
- FapyGua (2,6-diamino-4-hydroxy-5-formamidopyrimidine): A guanine oxidation product that interferes with replication fidelity.

- 8-oxoGua (8-oxo-7,8-dihydroguanine): One of the most studied oxidative lesions, known for causing G→T transversion mutations during replication.

These lesions serve as biomarkers for radiation-induced DNA damage and pose significant challenges to DNA repair mechanisms, potentially contributing to mutagenesis and carcinogenesis. Created with BioRender.com.

1.1.3.2 AP sites (Abasic sites)

IR induces the formation of highly reactive hydroxyl radicals (·OH) through the radiolysis of intracellular water, constituting a major source of DNA damage. These radicals initiate DNA lesions via multiple mechanisms, with two being particularly relevant to the formation of apurinic/apyrimidinic (AP) sites. Firstly, ·OH radicals can directly attack the N-glycosidic bond of DNA bases—especially purines—causing spontaneous cleavage and subsequent release of the nucleobase, thereby producing an AP site. Secondly, ·OH radicals can react with the 5,6-double bond of both purine and pyrimidine rings, leading to ring saturation and structural destabilisation of the adjacent N-glycosidic linkage. This alteration markedly enhances the susceptibility of the bond to hydrolytic cleavage, facilitating base loss. Beyond these direct chemical effects, IR also generates a spectrum of modified bases—including oxidised purines and pyrimidines—that are recognised as aberrant by DNA glycosylases. These lesion-specific enzymes initiate base excision repair (BER) by excising the damaged base, enzymatically generating AP sites as critical intermediates in the repair pathway. Thus, IR-induced AP site formation arises from both direct physicochemical alterations of DNA and enzymatic processing of oxidised bases, underscoring the multifaceted threat posed by ionising radiation to genome stability (Dunlap & Cerutti, 1975; RichardWagner, 2013).

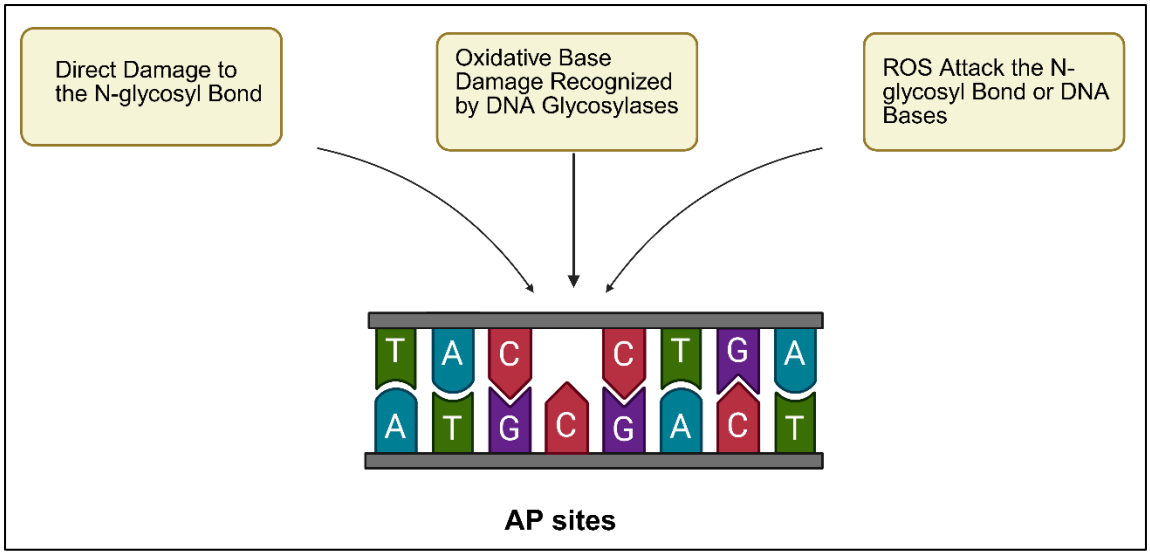


Figure 1.5. Mechanisms of Radiation-Induced DNA Base Damage and N-Glycosyl Bond Disruption

The schematic illustrates three primary pathways by which ionising radiation induces DNA base lesions and disrupts the N-glycosyl bond connecting nitrogenous bases to the sugar-phosphate backbone:

(1) Direct damage: Radiation directly cleaves the N-glycosyl bond, resulting in apurinic/apyrimidinic (AP) site formation.

(2) Oxidative base damage: Radiation-induced reactive oxygen species (ROS) oxidise DNA bases (e.g., guanine, thymine), leading to lesions such as 8-oxo-7,8-dihydroguanine (8-oxoGua), which are recognised and excised by DNA glycosylases during base excision repair (BER).

(3) ROS-mediated attack: ROS attack either the N-glycosyl bond or DNA bases, contributing to both AP site formation and base modifications. These damage types collectively initiate BER pathways to maintain genomic stability. Created with BioRender.com.

1.1.3.3 DNA strand breaks

DNA breaks represent a major form of genotoxic insult induced by IR, and they can be broadly classified into two categories: single-strand breaks (SSBs) and double-strand breaks (DSBs). Goodhead (1989) first reported radiobiology measurements estimate that low-LET radiation (e.g., X-rays or γ-rays) yields on the order of ~1000 SSBs and ~40 DSBs per cell per Gy (Goodhead, 1989). These values highlight the preponderance of SSBs over DSBs per unit dose (Tounekti et al., 2001). These breaks can form through various combinations of damage mechanisms: directly via ionisation of DNA by primary radiation or indirectly through ROS produced during radiolysis, or a combination of both. These radicals attack the deoxyribose sugar or phosphodiester backbone, resulting in the disruption of the phosphodiester bond (Juan et al., 2021). SSBs may also form as secondary consequences of oxidative base damage or as intermediates in the BER pathway, particularly after the excision of damaged bases or the processing of AP sites by specific endonucleases (Simonelli et al., 2005).

Beyond their direct impact, SSBs can compromise the repair of neighbouring lesions. The presence of an SSB or an unresolved AP site has been shown to hinder the activity of DNA glycosylases responsible for removing adjacent oxidised or mismatched bases (David-Cordonnier et al., 2002) . Similarly, the proximity of a base lesion can interfere with the accurate recognition and repair of the strand break. This reciprocal inhibition is especially problematic when lesions occur within one or two helical turns of DNA, leading to complex DNA damage, spatially clustered lesions that significantly challenge the cellular repair machinery and elevate the risk of mutagenesis or cell death.

In contrast, DSBs are less frequent but far more cytotoxic. A DSB arises when two SSBs occur on opposite strands of the DNA helix in close proximity, resulting in

disruption of the intervening base pairing and physical separation of the strands (Gulston et al., 2004). These breaks can form through various combinations of damage mechanisms: directly via ionisation of DNA by primary radiation or secondary electrons, indirectly through ROS produced during radiolysis, or a combination of both.

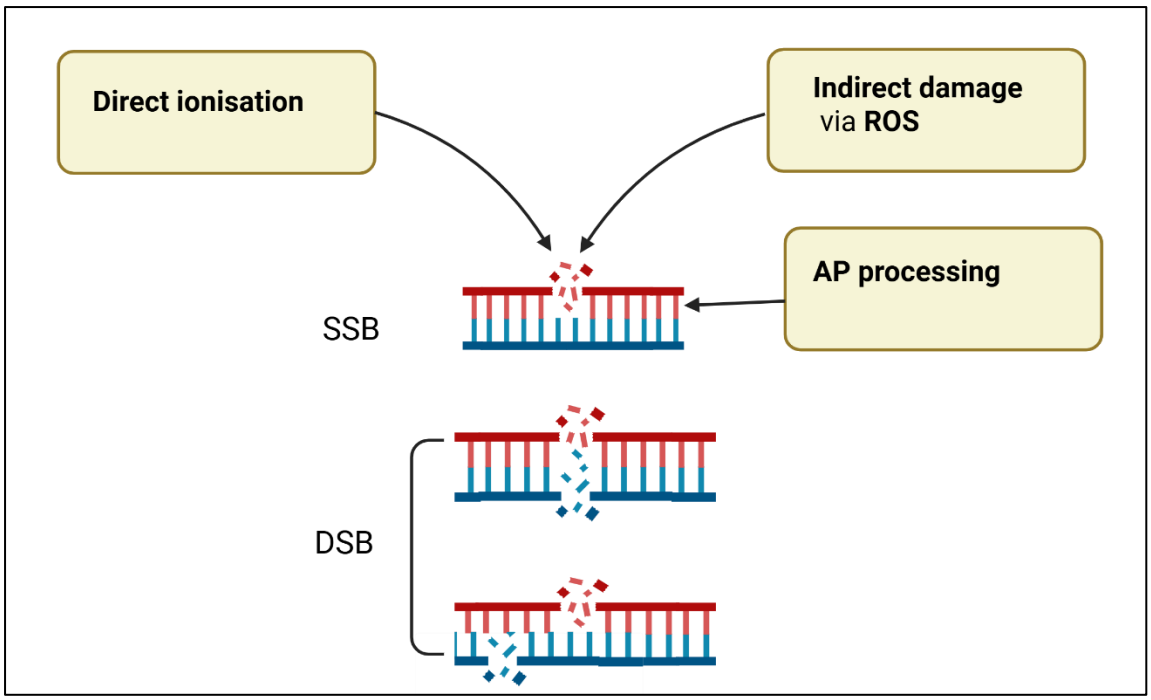


Figure 1.6. Mechanisms of Radiation-Induced DNA Strand Break Formation

The schematic outlines the primary mechanisms contributing to DNA strand breakage following exposure to ionising radiation.

(1) Direct ionisation: High-energy radiation directly ionises the DNA backbone, cleaving phosphodiester bonds and leading to strand breaks.

(2) Indirect damage via ROS: Radiation interacts with intracellular water, generating reactive oxygen species (ROS), particularly hydroxyl radicals (·OH), which attack DNA bases and sugar-phosphate linkages, resulting in strand breaks.

(3) AP site processing: Oxidative base damage or direct ionisation generates apurinic/apyrimidinic (AP) sites. These lesions, when processed by AP endonucleases during base excision repair (BER), can also lead to single-strand breaks (SSBs). If two SSBs occur on opposite strands in close proximity, they can convert into a double-strand break (DSB), a highly cytotoxic lesion. Created with BioRender.com.

1.1.3.4 DNA Inter-strand Crosslinks (ICLs):

These occur when two complementary DNA strands are covalently bonded, preventing them from separating during replication or transcription. ICLs are infrequent damage caused by IR, but biologically critical DNA lesions, often arising under specific structural conditions. One study directly demonstrated this by irradiating plasmid DNA constructs containing site-specific mismatched regions designed to mimic locally unpaired DNA. They observed that X-ray induced interstrand crosslinks only when the DNA contained short runs of 3–5 unpaired bases. The crosslinking was especially pronounced when these regions included the radiosensitizer 5-bromouracil (Dextraze et al., 2010). In contrast, no measurable ICLs were detected in fully base-paired, perfectly duplex DNA under the same irradiation conditions. Even in the absence of bromouracil, some level of crosslink formation still occurred in mismatched regions, though at lower efficiency. These findings highlight the importance of local DNA flexibility and unpairing in facilitating radiation-induced ICL formation.(Dextraze et al., 2010).

1.1.3.5 DNA–Protein Crosslinks (DPCs):

IR can also cause proteins to become covalently linked to the DNA, which could block both replication and transcription machinery. Through the direct mechanism, ionising radiation deposits energy directly onto the DNA molecule, resulting in the formation of unstable DNA radical cations that rapidly undergo decomposition. In contrast, the indirect mechanism involves the absorption of radiation by intracellular water—the primary component of cells—leading to the generation of reactive oxygen species (ROS), such as hydroxyl radicals (·OH). These highly reactive species attack DNA, producing secondary DNA radicals that are likewise unstable and prone to degradation. In addition to damaging nucleic acids, ionising radiation also targets

chromatin-associated proteins, either through direct ionisation or via oxidative damage mediated by ROS. The DNA and protein radicals produced by these processes may decompose independently or interact with surrounding biomolecules. Such interactions can result in the formation of covalent bonds between DNA and proteins, giving rise to DNA–protein crosslinks (DPCs) (Figure 1.7 A and B). These crosslinks may also arise through the recombination of adjacent radicals or through the nucleophilic attack of proteins on electrophilic apurinic/apyrimidinic (AP) sites generated by radiation.

Early investigations revealed that core histones (H2A, H2B, H3, and H4) and actin are among the primary proteins participating in radiation-induced DPC formation. For instance, experiments involving the γ-irradiation of chromatin in the presence of nitrous oxide (N_2O), which enhances hydroxyl radical (·OH) production, demonstrated the formation of cross-links between DNA and core histones. Similarly, actin was identified as a cross-linked protein in T-lymphocyte MOLT4 cells following X-ray irradiation, using SDS/PAGE analysis after DPC isolation via SDS/K^+ precipitation. Additional studies showed that matrix-attachment regions (MARs) of DNA preferentially cross-link to the nuclear matrix after γ-irradiation, suggesting that MAR–matrix protein interactions act as radiation-sensitive substrates for DPC formation. Notably, polyamines such as spermine and putrescine appear to inhibit this process by interfering with the DNA–nuclear matrix association. More recently, systematic proteomic analyses using low-dose γ-irradiation have expanded the catalogue of radiation-induced DPCs, identifying 29 proteins via SDS-PAGE and tandem mass spectrometry (MS/MS). These include nuclear matrix proteins (e.g., actin, vimentin), splicing factors (e.g., heterogeneous nuclear ribonucleoproteins—hnRNPs), chromatin-associated proteins (e.g., histones H1–H4), and stress-response proteins (e.g., HSP10, GRP78). Specific proteins such

as hnRNP A2/B1, histones H3 and H4, and GRP78 were found to be preferentially cross-linked under hypoxia. Furthermore, ionising radiation and other DNA-damaging agents generate abasic (AP) sites, which can form covalent adducts with the lysine-rich N-terminal tails of histones in reconstituted nucleosomes; the efficiency of these cross-links has been shown to depend on the spatial proximity of the AP site to the histone tail.

Covalent linkages between DNA and protein components are a defining feature of DNA–protein crosslinks (DPCs), and several base–amino acid conjugates have been characterised in experimental models of radiation-induced damage. In foundational studies, isolated nucleohistones were exposed to γ-irradiation under a nitrous oxide-enriched atmosphere to enhance hydroxyl radical formation, followed by acid hydrolysis. Gas chromatography–mass spectrometry with selected ion monitoring (GC-MS/SIM) was employed to detect and analyse the resulting cross-links. These investigations identified covalent adducts involving thymine and lysine (Thy–Lys), with evidence suggesting the existence of multiple structural isomers. Additional cross-links were observed between cytosine and tyrosine (Cyt–Tyr), and between thymine and tyrosine (Thy–Tyr); however, further research is needed to confirm whether some Thy–Tyr cross-links arise as artefacts during acid hydrolysis. Complementary studies using photooxidation of model compounds—serving as proxies for direct radiation effects—revealed additional cross-links, including those between guanine and lysine. These were observed to occur either via the ε-amino group of lysine, through various positions along the lysine side chain, or following oxidation of the primary amino group. The resulting products, including both cross-links and their precursors, were characterised using high-performance liquid chromatography coupled with tandem mass spectrometry (HPLC-ESI-MS/MS). The diversity of base–amino acid

interactions highlights the chemical complexity of DPC formation. More recently, in vivo studies have shown that ionising radiation can also induce Thy–Tyr crosslinks in mammalian tissues. Analysis of genomic DNA extracted from the liver and brain of irradiated mice revealed an increase in dT-Tyr adduct formation following exposure, with a clear dose-dependent trend observed. Notably, liver tissues exhibited a more pronounced accumulation of these adducts compared to the brain. These findings underscore the relevance of radical-mediated DPCs as biologically significant lesions that can form under physiologically relevant conditions and may persist depending on tissue type and exposure context.

Squamous carcinoma (SCCVII) tumours grown in the hind legs of mice were irradiated with either conventional X-rays (200 kVp, low-LET) or high-LET carbon-ion beams (290 MeV/u C-ions, using a spread-out Bragg peak), at doses up to 40 Gy. The study showed irradiation with X-rays DPC induction increased linearly with dose and was significantly higher in hypoxic tumours than in normoxic ones, with approximately 2.4–2.8 times greater DPC yields under hypoxia. This trend contrasted with DSB formation, which was diminished under hypoxia due to the oxygen dependence of radical-mediated DNA scission. On the other hand, Carbon-ion beams induced slightly more DPCs than X-rays, approximately 1.5-fold higher, regardless of oxygen status, indicating that high-LET radiation more efficiently generates DPCs due to dense ionization tracks that enhance recombination between DNA and proteins. Therefore, high-LET radiation, such as carbon-ion therapy, by inducing DPCs and DSBs more effectively and with less reliance on oxygen, may offer a therapeutic advantage in targeting hypoxia-associated radioresistant cancer cells.

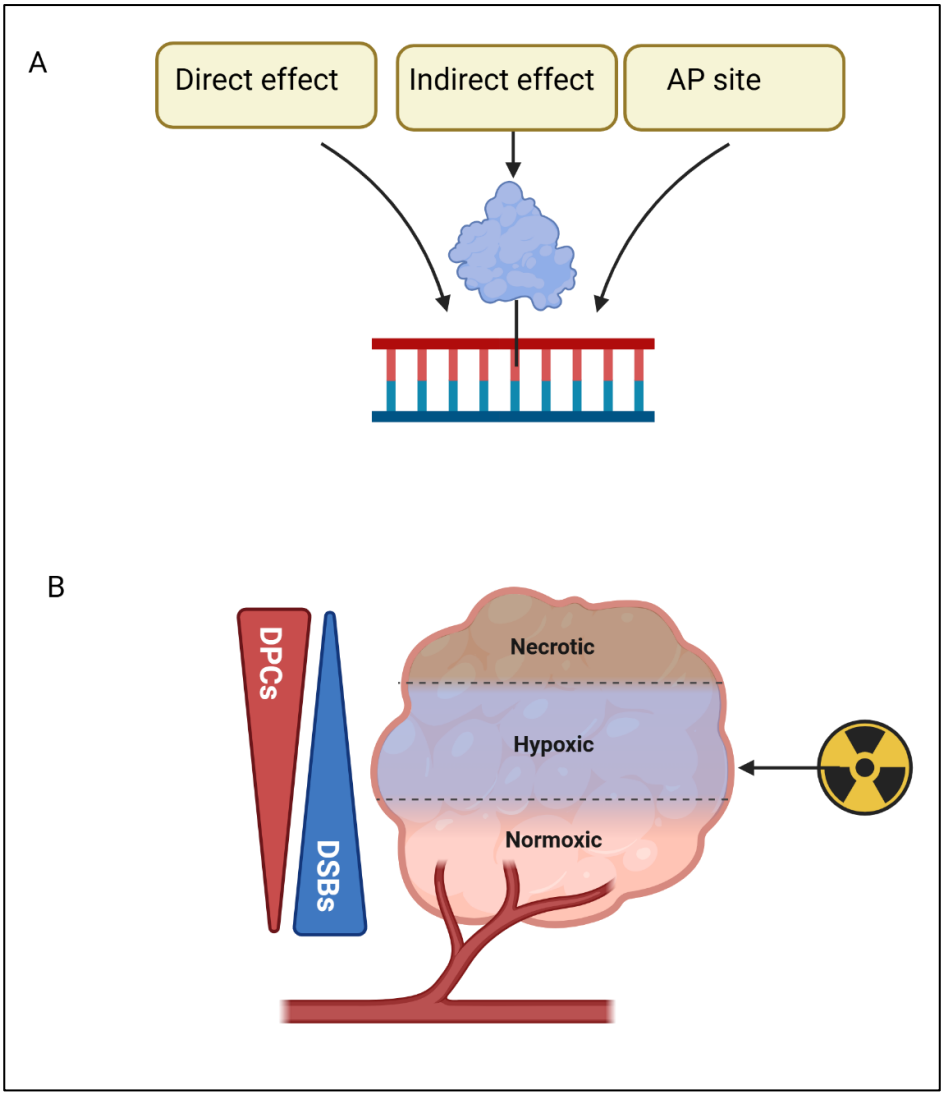


Figure 1.7. Radiation-Induced DNA Damage Pathways and Tumour Microenvironment Influence

(A): Mechanisms of DNA damage induction by ionising radiation. The direct effect refers to ionisation of DNA itself, while the indirect effect results from the generation of reactive oxygen species that cause oxidative damage. Additionally, damage at apurinic/apyrimidinic sites can exacerbate strand breakage.

(B): A depiction of a solid tumour, illustrating different microenvironmental regions: well-oxygenated (normoxic), low-oxygen (hypoxic), and anoxic (necrotic) zones. Damage induction varies by oxygenation status: strand breaks predominate in oxygen-rich zones due to ROS generation, while protein–DNA crosslinks accumulate more in hypoxic areas where direct DNA damage mechanisms prevail. DSBs, double-strand breaks; DPCs, DNA–protein crosslinks; ROS, reactive oxygen species; AP, apurinic/apyrimidinic.Created with BioRender.com.

1.1.3.6 Clustered DNA damage:

In addition to simple DNA damage that arises directly from radiation exposure and is characterized by rapid repair kinetics, clustered DNA damage presents a more challenging scenario. Clustered DNA damage is a hallmark of IR-induced damage and is significantly more difficult to repair. These lesions consist of two or more types of DNA damage, such as oxidative base damage, abasic sites, SSBs, and DSBs, all occurring within close proximity to each other, typically within 1 to 2 helical turns of the DNA double helix. Clustered DNA damage is particularly detrimental because the cell's standard repair machinery is not designed to specifically handle such complex lesions. Each individual lesion in a cluster requires a specific repair pathway; for example, BER handles oxidative base damage, SSBs are repaired by proteins of the BER pathway and DSBs require distinct repair mechanisms, which is discussed later. However, when these lesions are closely spaced, the repair machinery can interfere with itself. The repair of one lesion may obstruct or exacerbate another, leading to complications such as incomplete repair or even secondary strand breaks. As a result, clustered DNA damage often results in imprecise, delayed, or even failed repair attempts. (Eccles et al., 2011; O'Connor & Nodwell, 2005; Singleton et al., 2002). One of the most deleterious examples of clustered damage is the complex DSB, a subclass of clustered lesion where a frank double-strand break is accompanied by nearby base lesions and/or SSBs. The presence of a DSB within a cluster imposes an even greater burden on the cell's repair machinery – not only must the broken DNA ends be correctly processed and rejoined, but multiple repair pathways must act in a coordinated fashion to handle the adjacent base damage (Hada & Georgakilas, 2008). Thus, clustered DNA damage – and complex DSBs in particular – represents a critical challenge to genome integrity,

as its presence can overwhelm the cell's repair systems and drive the detrimental outcomes of ionizing radiation exposure.

1.1.3.6.1 Impact of LET on the Formation and Complexity of DNA Damage:

Although the types of DNA damage induced by radiation are broadly similar across different LET values, the proportion and frequency of each damage type vary depending on the LET. Table 1.1 shows the estimated number of different DNA lesions per cell per Gray (Gy). Gy is the SI unit of absorbed dose of ionising radiation. It quantifies the amount of radiation energy absorbed per unit mass of a material, typically biological tissue (Wyckoff et al., 1976). Low LET radiation primarily induces DNA damage through indirect mechanisms. It ionises surrounding molecules, particularly water, leading to the formation of reactive oxygen species (ROS) such as hydroxyl radicals, which subsequently interact with and damage DNA(Georgakilas et al., 2013). In contrast, high-LET radiation tends to cause DNA damage predominantly via direct interactions. Owing to its densely ionising tracks, it deposits energy along short paths that directly disrupt the DNA structure, resulting in complex and clustered lesions that are more difficult for the cell to repair. (Hada & Georgakilas, 2008).

In the case of low LET radiation, the majority of energy deposition, approximately 70%, results in the formation of isolated DNA lesions, contributing to the cell's overall oxidative stress burden(Nikjoo et al., 1999). However, a significant proportion, around 30%, gives rise to clustered damage sites, which vary in their structural and chemical complexity. In contrast, exposure to densely ionising, high-LET radiation leads to a markedly higher frequency of such complex lesions, with up to 90% of the deposited energy generating clustered damage, including DSBs (Goodhead, 1994; Hada & Georgakilas, 2008; Sutherland et al., 2001). The complexity of these clusters, typically defined by the number and proximity of individual lesions within a short DNA segment,

increases proportionally with the LET of the radiation. As LET of ionising radiation increases, the complexity and frequency of DNA damage rise significantly; however, this is not accompanied by a corresponding increase in the levels of SSBs or oxidised bases (Hada & Sutherland, 2006; Sutherland et al., 2001; Terato et al., 2008). In fact, studies using HPLC-MS/MS have demonstrated that the yield of base lesions induced by high-LET particle radiation is approximately half that produced by low-LET ^60Co γ-rays. Although proton irradiation is considered relatively low LET compared to other types of particle radiation, it exhibits a significantly higher LET than photon irradiation, particularly at and around the Bragg peak. At this point, and especially toward the distal end of the Bragg peak where LET reaches its maximum, there is an increased induction of cluster/complex DNA damage (CDD) (Wilkinson et al., 2023).

Evidence suggests that the majority of DSBs induced by low LET radiation are efficiently rejoined within 30 to 60 minutes. However, a minor subset, typically less than 20% exhibits delayed repair in mammalian cells, with some lesions persisting for over 24 hours (Botchway et al., 1997; Jakob et al., 2011; Schmid et al., 2010). As the LET of the radiation increases, the proportion of slowly repaired DSBs also rises. This delayed repair is believed to correspond to the increasing incidence of complex DNA damage, which presents a greater challenge to the cellular repair machinery, suggesting that the processing and/or repair kinetics of these breaks differ depending on the radiation quality.

Table 1.1 Quantitative Comparison of DNA Damage Types Induced by Low-LET (Photons) and High-LET (Carbon Ions) Radiation per Gray per Cell ((Hada & Georgakilas, 2008; Hada & Sutherland, 2006; Lomax et al., 2013a)

DNA Damage Type	Low-LET (Photons)	High-LET (Carbon Ions)
Double-strand breaks (DSBs)	~25–40 / Gy / cell	~ 50–70 / Gy / cell
Single-strand breaks (SSBs)	~1000 / Gy / cell	~500–800 / Gy / cell
Base damage (e.g., 8-oxo-dG)	~1000–2000 / Gy / cell	~800–1200 / Gy / cell
Clustered DNA lesions	<10 / Gy / cell	>40–100 / Gy / cel

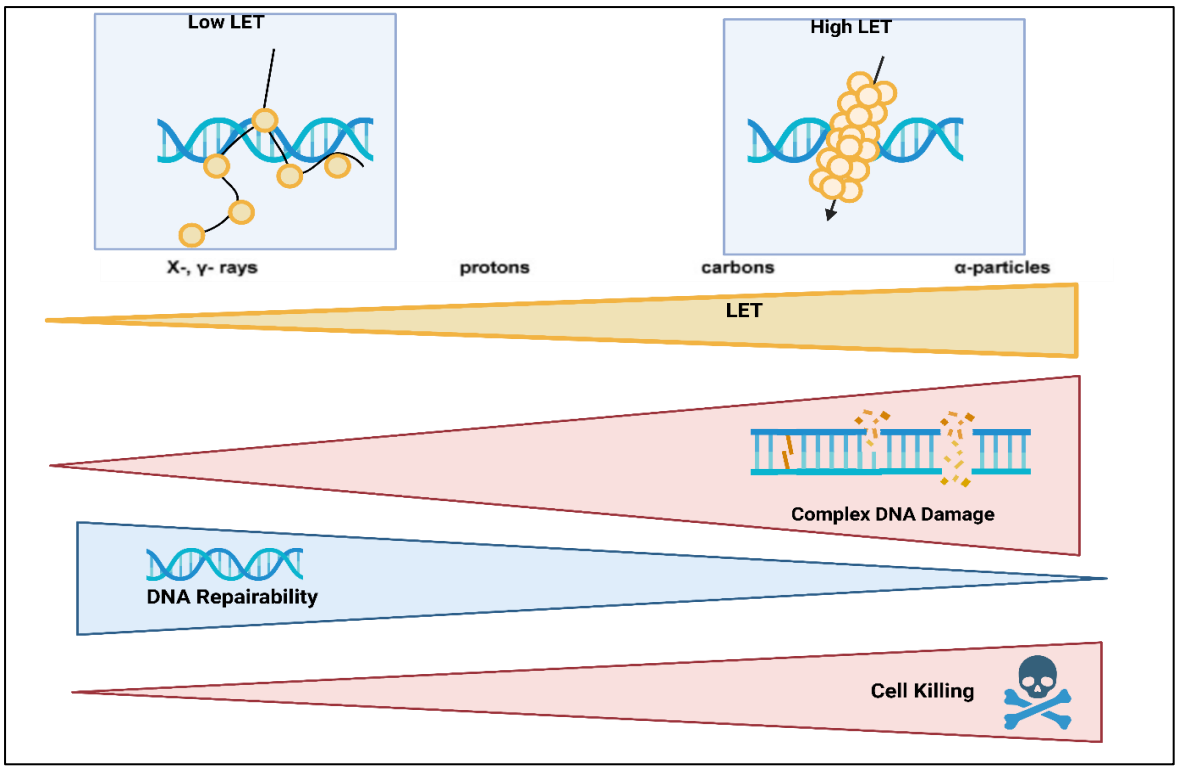


Figure 1.8. Comparative Effects of Low-LET and High-LET Radiation on DNA Damage and Cellular Outcomes

The diagram illustrates the biological effects of radiation across the linear energy transfer (LET) spectrum.

- Top Panels: Low-LET radiation (e.g., X-rays, γ-rays) induces sparsely distributed ionisations along the DNA, resulting in isolated DNA lesions. In contrast, high-LET radiation (e.g., α-particles, carbon ions) generates densely ionising tracks that lead to clustered and complex DNA damage. While both α-particles and carbon ions are classified as high-LET radiation types, their exact LET values depend on the energy and source conditions. Typically, carbon ions exhibit higher LET than α-particles at comparable biological depths due to their higher charge and mass, although this relationship can vary with energy.
- Gradient Bars (Top to Bottom):
    1. LET: Increases from low-LET (X-rays, γ-rays) to high-LET (carbon ions, α-particles).
    2. Complex DNA Damage: Increases with rising LET, as higher ionisation density leads not only to a greater frequency of clustered DNA lesions but also to an increased degree of complexity in those lesions. These complex DNA damage sites often involve multiple strand breaks and base modifications within close proximity, making them more challenging to repair accurately.
    3. DNA Repairability: Decreases with increasing LET, as clustered damage is more challenging for cellular repair mechanisms.
    4. Cell Killing: Increases with higher LET due to greater complexity and irreparability of DNA damage, resulting in enhanced cytotoxicity. LET, linear energy transfer; *Created with BioRender.com.*

1.1.4 DNA damage repair post Radiation:

1.1.4.1 Base excision repair (BER):

Base excision repair (BER) is responsible for repairing DNA lesions arising from oxidative damage, deamination, and alkylation. These types of base modifications typically induce minimal distortion to the DNA helix and are therefore specifically targeted by the BER pathway.(Krokan & Bjørås, 2013). There are around 30 proteins involved in BER and to date, at least eleven distinct DNA glycosylases have been identified in mammals, each specialising in the recognition of a subset of structurally related base lesions, often exhibiting overlapping substrate specificities (Svilar et al., 2010). The pathway begins with the recognition and excision of damaged bases by lesion-specific DNA glycosylases. Following base removal, the resulting abasic site is processed, and the gap is subsequently repaired via either short-patch repair - replacing a single nucleotide- or long-patch repair, which involves the synthesis of a longer DNA segment. In both the short-patch and long-patch sub-pathways of base excision repair (BER), the steps that follow base excision -namely strand incision, end processing, repair synthesis, and ligation are collectively referred to as the “common steps” of the pathway (Jacobs & Schär, 2012).

The process of BER is as follows: A lesion-specific DNA glycosylase excises the damaged base, which has been flipped out from the DNA helix, thereby generating an abasic (apurinic/apyrimidinic; AP) site. DNA glycosylases are classified as monofunctional or bifunctional based on their enzymatic activity. Monofunctional glycosylases possess only glycosylase activity, such as UNG, and function by excising the damaged base to generate an AP site. In contrast, bifunctional glycosylases exhibit both glycosylase and lyase activities. These enzymes cleave the DNA backbone via β-elimination (e.g., NTHL1) or β,δ-elimination (e.g., NEIL1), producing strand breaks

with chemically modified termini that require additional processing before repair can proceed(Jacobs & Schär, 2012; Svilar et al., 2010). All known mammalian glycosylases responsible for uracil removal are monofunctional. Other examples of monofunctional glycosylases include MPG and MUTYH, the latter of which excises adenine mispaired with 8-oxoG, G, or C. By contrast, most glycosylases that specialise in the removal of oxidised bases are bifunctional, such as OGG1 that recognises and excises oxidative DNA lesions, specifically 7,8-dihydro-8-oxoguanine (8-oxoG) and 2,6-diamino-4-hydroxy-5-N-methylformamidopyrimidine (Fapy), from DNA. In addition, NTHL1 and NEIL1–3 which are bifunctional (Table 1.2).

Table 1.2. Summary of DNA Glycosylases, Their Functions, and Substrate Specificities in Base Excision Repair(Krokan & Bjørås, 2013)

Glycosylase	Type	Activity	Primary Substrates	Repair Role
UNG	Monofunctional	Glycosylase	Uracil in DNA	Removes uracil from U:A and U:G
SMUG1	Monofunctional	Glycosylase	Uracil, 5-hydroxymethyluracil	Back-up for UNG, acts on oxidised bases
TDG	Monofunctional	Glycosylase	T:G mismatches	Involved in active DNA demethylation
MBD4	Monofunctional	Glycosylase	T:G mismatches	Repairs deamination of 5-methylcytosine
MPG	Monofunctional	Glycosylase	Alkylated bases (e.g., 3-meA, 7-meG)	Repairs alkylated DNA lesions
MUTYH	Monofunctional	Glycosylase	A:8-oxoG mismatches	Prevents G:C to T:A transversions
OGG1	Bifunctional	Glycosylase	8-oxoG:C pairs	Removes 8-oxoG before replication
NTHL1	Bifunctional	Glycosylase + β-lyase	Oxidised pyrimidines (e.g., thymine glycol)	Excises oxidised pyrimidines and cleaves backbone
NEIL1	Bifunctional	Glycosylase + β,δ-lyase	Oxidised purines/pyrimidines	Excises oxidised bases in transcribed regions
NEIL2	Bifunctional	Glycosylase + β,δ-lyase	Oxidised DNA base lesions	Repairs oxidative lesions in single- and double-stranded DNA
NEIL3	Bifunctional	Glycosylase + β,δ-lyase	Unusual oxidised lesions, including in telomeres	Functions in embryonic development, telomere maintenance

Monofunctional DNA glycosylases remove damaged bases by hydrolysing the N-glycosidic bond, thereby generating an intact apurinic/apyrimidinic (AP) site, which is subsequently processed by an AP endonuclease that hydrolyses the DNA backbone forming SSB. In contrast, bifunctional glycosylases possess an additional lyase activity, which enables further processing of the AP site via β- or β,δ-elimination reactions (Amanda K.McCullough, M. L. Dodson, 1999). XRCC1 and PARP1 act as sensors of SSBs formed, but they operate through distinct mechanisms. XRCC1 functions primarily as a scaffold protein, coordinating the recruitment of the various BER components. PARP1, on the other hand, is activated upon detecting SSBs and catalyse the transfer of ADP-ribose units from NAD^+ to target proteins—predominantly histones and DNA repair factors—forming poly(ADP-ribose) (PAR) chains. These chains, consisting of linear and branched ribose-ribose linkages, play a key role in signalling and protein recruitment at damage sites.

Recently, a mechanism was found to protect AP sites from being attacked by endonuclease. HMCES (5-Hydroxymethylcytosine Binding, ES Cell-Specific) is found to play a critical role at stalled replication forks, where it binds to both PCNA and ssDNA to safeguard genomic stability. Upon encountering abasic site in ssDNA, HMCES forms a covalent DPC, acting as a protective cap that shields the lesion from mutagenic repair processes. This suicide-like mechanism prevents error-prone translesion DNA synthesis and blocks the access of structure-specific endonucleases that might otherwise cleave the DNA and generate harmful DSBs. The HMCES–DPC is later resolved primarily via proteasome-mediated degradation, allowing for subsequent DNA repair steps to restore genome integrity (Mohni et al., 2019) .

In BER, removal of a damaged base typically results in a single-nucleotide gap repaired via short-patch BER (SP-BER). However, when the 5′-deoxyribose

phosphate (dRP) left by APE1 is oxidised or otherwise modified, Polβ's lyase activity is insufficient, necessitating long-patch BER (LP-BER), which involves synthesis of 2–8 nucleotides (Kubota et al., 1996). In LP-BER, DNA polymerases δ/ε perform strand-displacement synthesis, aided by PCNA and replication factor C (RFC), while FEN1 cleaves the resulting flap. LigI then completes ligation. FEN1, typically involved in Okazaki fragment processing, also removes damaged flaps during repair. Although Polβ is central to SP-BER, it can also contribute to LP-BER through interactions with FEN1 and LigI. Polβ-null cells, however, remain viable and are not hypersensitive to oxidative stress, indicating that Polδ/ε can substitute in LP-BER (Frosina et al., 1996; Klungland & Lindahl, 1997; Matsumoto, 2001).

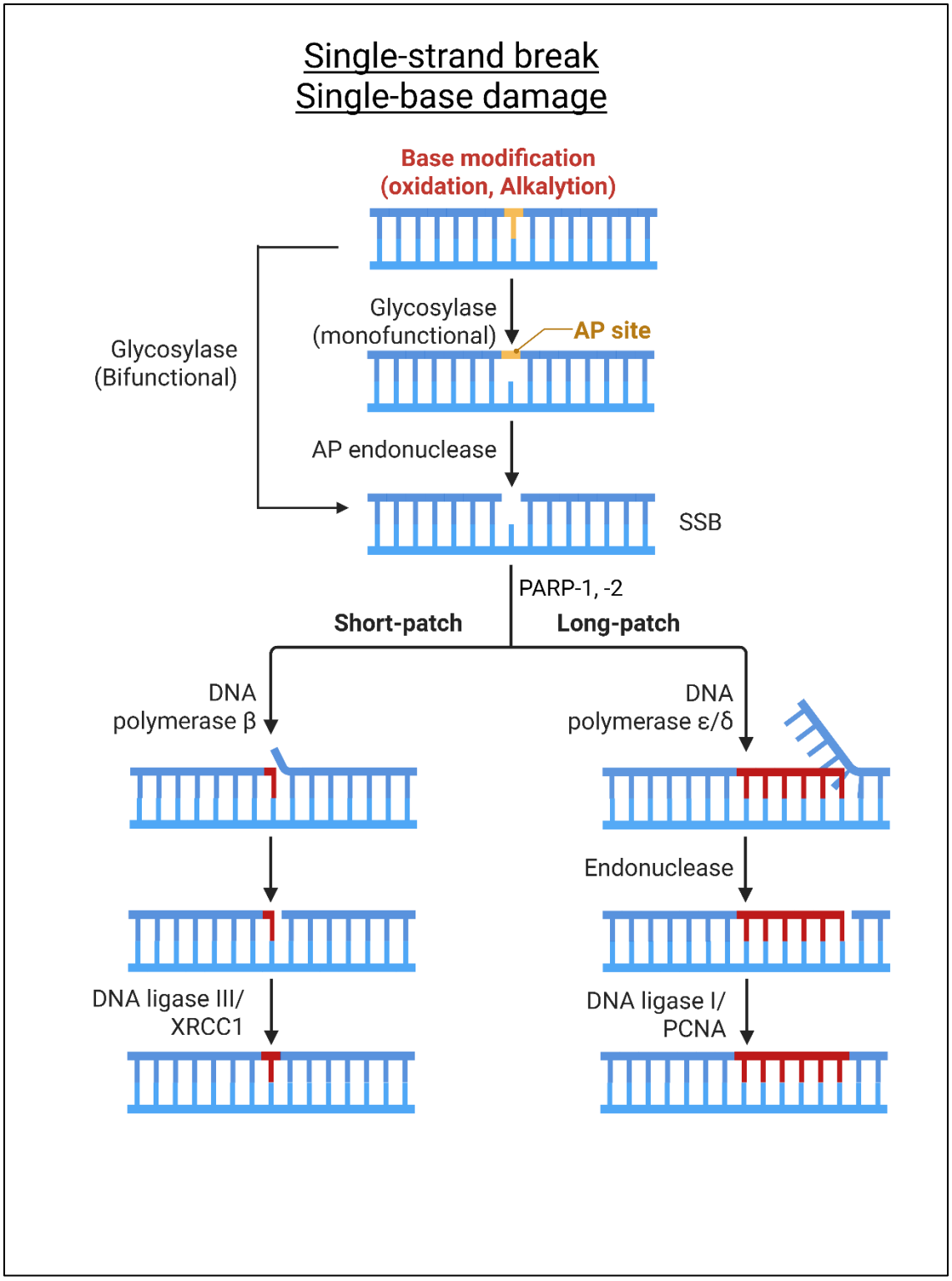


Figure 1.9. Base Excision Repair (BER) Pathway for Oxidative and Alkylation-Induced DNA Damage

This schematic illustrates the short-patch and long-patch sub-pathways of base excision repair (BER) activated in response to oxidative and alkylated base lesions. Damaged bases are first recognized and excised by mono- or bifunctional glycosylases, creating abasic (AP) sites.

These are cleaved by AP endonucleases to generate single-strand breaks (SSBs). In the short-patch pathway, DNA polymerase β inserts a single nucleotide, also it removes the 5'-dRP group prior to DNA ligation. The gap is sealed by DNA ligase III/XRCC1. In the long-patch pathway, DNA polymerase ε/δ synthesizes a short DNA strand, which is processed by endonucleases and sealed by DNA ligase I with the help of PCNA.

AP, apurinic/apyrimidinic; BER, base excision repair; SSB, single-strand break; XRCC1, X-ray repair cross-complementing protein 1; PCNA, proliferating cell nuclear antigen. *Created with BioRender.com*

1.1.4.2 DPCs removal post radiation:

Although several mechanisms involved in the repair of DNA–protein crosslinks (DPCs) are well established (as discussed in detail in Section 1.2.4 DPCs repair pathway), the specific pathways responsible for resolving DPCs induced by ionising radiation (IR) remain relatively understudied. Nakano et al. found that despite differences in the initial damage caused by high-LET irradiation and low-LET X-rays, the post-irradiation repair kinetics of DPCs were found to be remarkably slow. A study found that both DPCs and DSBs followed a biphasic pattern of removal from the genome: an initial rapid phase within the first few hours after exposure, followed by a much slower secondary phase(Nakano et al., 2015). This biphasic behavior was observed in both normoxic and hypoxic tumours, with oxygen conditions prior to irradiation having little effect on the overall repair kinetics. The half-lives associated with the slow phase differed significantly between lesion types. While the slow component of DSB repair exhibited half-lives of around 4 to 5 hours, the corresponding phase for DPCs extended to approximately 63 to 70 hours, nearly three days, indicating that a substantial portion of DPCs remain unrepaired for an extended period. The rapidly removed fraction of DPCs accounted for only about 23% to 32% of the total and had a half-life of less than one hour, whereas the majority, around 68% to 77%, were long-lived and required days for clearance. In contrast, nearly all DSBs were resolved within 18 hours post-irradiation. This highlights DPCs as persistent lesions that could present ongoing challenges to the cell's replication and transcription machinery. The authors suggest that two classes of DPCs are formed: one that is relatively easy to remove- possibly involving partial proteolysis or smaller peptide-DNA adducts- and another that is more resistant to repair, likely involving full protein cross-links that cannot be efficiently processed by conventional repair pathways such as nucleotide excision

repair. These more recalcitrant DPCs may instead require replication-coupled repair or other specialized mechanisms. Overall, the repair of DPCs was far less efficient than that of DSBs, resulting in a lasting burden of protein-DNA adducts that persist long after radiation exposure.

A very recent study showed that SPRTN plays a role in preventing the accumulation of DPCs following IR (Erber et al., 2024). SPRTN is a DNA-dependent metalloprotease that plays a central role in the repair of DPCs, particularly during replication. It functions by proteolytically processing the protein component of DPCs, facilitating their removal and enabling DNA replication and repair to proceed (the detailed mechanisms of SPRTN-mediated DPC repair and its broader implications will be explored in the following sections). In the study, they showed that in SPRTN-deficient cells, DPC levels increased significantly in a dose-dependent manner, with markedly higher accumulation compared to SPRTN-proficient controls. This suggests that without SPRTN's proteolytic activity, cells cannot efficiently resolve DPCs, leading to their persistence after damage. In contrast, SPRTN-proficient cells effectively suppressed DPC accumulation, even at high IR doses. These findings underscore SPRTN's essential function in maintaining genomic stability by resolving DPCs that would otherwise obstruct replication and transcription, particularly under oxidative stress.

In addition, exposure to radiation, especially in the context of proteasome inhibition leads to the accumulation of ubiquitinated HMCES, indicating that the proteasome plays a role in the removal of HMCES–DPCs. Additional mechanistic insights come from both in vitro experiments and Xenopus egg extract systems, where the FANCJ helicase and the SPRTN metalloprotease have been identified as key players in resolving HMCES–DPCs. In this repair pathway, FANCJ utilizes its ATPase activity to unfold the crosslinked HMCES protein, thereby allowing SPRTN to proteolytically

cleave it. This process generates short peptide–DNA adducts as intermediate repair products(Yaneva et al., 2023a). However, these residual fragments—whether originating from proteasomal degradation or SPRTN-mediated cleavage—can still impede the activity of DNA polymerases and nucleases. As a result, further processing steps are necessary to fully remove these adducts and restore genomic integrity. This multi-step resolution highlights the complexity of HMCES–DPC repair and underscores the coordinated involvement of multiple DNA damage response factors (Sugimoto et al., 2023).

1.1.4.3 DSB repair

In mammalian cells, DSBs are primarily repaired via two major pathways: non-homologous end joining (NHEJ) and homologous recombination (HR). While HR offers higher repair fidelity due to its reliance on a homologous DNA template, NHEJ serves as the predominant repair mechanism across all phases of the cell cycle, particularly for prompt DSB repair (Lieber, 2010; Van Gent et al., 2001). These pathways are not mutually exclusive, as repair events involving components of both HR and NHEJ have been observed. HR operates with greatest efficiency during the S and G2 phases of the cell cycle, when sister chromatids are available to serve as homologous templates. In contrast, during the G1 phase-when sister chromatids are absent-DSB repair can still proceed effectively via NHEJ. The following section outlines the key features of DSB repair by both HR and NHEJ.

Homologous recombination (HR) is a high-fidelity pathway for repairing DSBs and a conserved mechanism, present from yeast to mammals (Sung et al., 2000; Thompson & Schild, 1999). It utilises the undamaged sister chromatid as a template to ensure accurate restoration of the original DNA sequence. It is coordinated by the RAD52 epistasis group, which includes key proteins such as RAD50, RAD51, RAD52, RAD54,

and MRE11(Kanaar et al., 1998; Van Gent et al., 2001). The initial response to DSBs is mediated by ATM kinase and the MRN complex, composed of MRE11, RAD50, and NBS1, which facilitates damage sensing and signalling. DNA-end resection follows, generating 3′ single-stranded DNA overhangs, a step thought to involve RAD52. These overhangs are rapidly coated by RAD51, which plays a central role in homology search and strand invasion (Baumann & West, 1998; Van Dyck et al., 1999). Several accessory proteins—such as RPA, RAD54, RAD52, and RAD51 paralogues (including RAD51B, RAD51C, RAD51D, XRCC2, XRCC3, and DMC1)-support RAD51 function at various stages of HR. Subsequent DNA synthesis restores the resected strands, and recombination intermediates are resolved to complete the repair process. While BRCA1 and BRCA2 are also integral to HR, particularly in the regulation and stabilisation of RAD51 filaments, their precise molecular roles remain incompletely elucidated (Bishop et al., 1998; M. Takata et al., 2000). Unlike the RAD52 group, the BRCA proteins lack homologues in yeast, suggesting they represent a more recent evolutionary addition to the HR pathway in higher eukaryotes.

Unlike homologous recombination (HR), non-homologous end joining (NHEJ) repairs DSBs without the need for extensive sequence homology. The process is initiated by the KU heterodimer (KU70/KU80), which binds tightly to DNA ends, protecting them from degradation and serving as a scaffold for the recruitment of other repair proteins. One key component is DNA-dependent protein kinase catalytic subunit (DNA-PKcs), which binds to the KU–DNA complex to form the active DNA-PK holoenzyme. DNA-PKcs undergoes autophosphorylation and phosphorylates other proteins such as KU subunits and p53, although the biological significance of some phosphorylation targets remains uncertain (Karran, 2000; Y. Ma et al., 2004). DNA ends are often processed to make them compatible for ligation; this processing may involve Artemis, a nuclease

activated by DNA-PKcs, as well as polymerases μ and λ, and PNKP. Final ligation is carried out by DNA ligase IV in complex with XRCC4, with additional support from scaffold proteins such as XLF (Rooney et al., 2003). Although classically associated with HR, the MRN complex (MRE11, RAD50, and NBS1) has also been implicated in alternative end-joining and may support classical NHEJ in facilitating end tethering and signalling under specific conditions.

In situations where DSBs occur between regions of tandem repeats and undergo extensive 5′ to 3′ resection, the cell may employ the single-strand annealing (SSA) pathway for repair. This process involves annealing of homologous repeat sequences exposed by resection, which results in the deletion of the intervening non-homologous DNA and is therefore regarded as an error-prone mechanism (Bhargava et al., 2016). Initially, the single-stranded DNA is stabilised by replication protein A (RPA), which is subsequently replaced by RAD52 and its paralogue RAD59 (in yeast). The resulting 3′ flaps are excised by the ERCC1–XPF endonuclease complex, and the remaining nicks in the DNA backbone are sealed by DNA ligase I.

Short-range end resection by the MRN complex and CtIP can direct repair through the alternative end joining (alt-EJ) pathway, also known as microhomology-mediated end joining (MMEJ) or polymerase theta-mediated end joining (TMEJ). PARP1 binding to DNA ends prevents KU recruitment, thereby shifting repair from classical NHEJ to alt-EJ (C. Beck et al., 2014; Carvajal-Garcia et al., 2020; M. Wang et al., 2006). This error-prone mechanism uses short microhomologies (3–6 bp) for alignment, which are extended by DNA polymerase theta (POLQ). POLQ, which lacks proofreading activity, consists of helicase-like and polymerase domains and can synthesise DNA across mismatched microhomologies with low fidelity. The final ligation step is mediated by ligase I or III, often in complex with XRCC1 (Arakawa et al., 2012; Paul et al., 2013).

During this repair process, partially resected DNA ends bearing short microhomologous sequences—typically 3 to 6 base pairs—are aligned and extended by POLQ. This enzyme possesses a unique structure comprising an N-terminal helicase-like domain, a central disordered region, and a C-terminal A-family DNA polymerase domain, both terminal domains contributing to its end-joining activity. Lacking 3′ to 5′ exonuclease proofreading, POLQ exhibits low fidelity, allowing it to extend mismatched primers and perform DNA synthesis across imperfectly aligned microhomologous regions. As a result, alt-EJ is considered error-prone, frequently leading to mutations such as small insertions, deletions, and base substitutions (Hwang et al., 2020; Saito et al., 2017; Wood & Doublié, 2016). A synthetic lethal relationship between POLQ and BRCA1/2 has been identified, highlighting POLQ as a therapeutic target in BRCA-deficient cancers(Ceccaldi et al., 2015; Higgins & Boulton, 2018). Although short 3′ overhangs can also be substrates for HR or SSA, the mechanisms guiding pathway choice remain poorly understood.

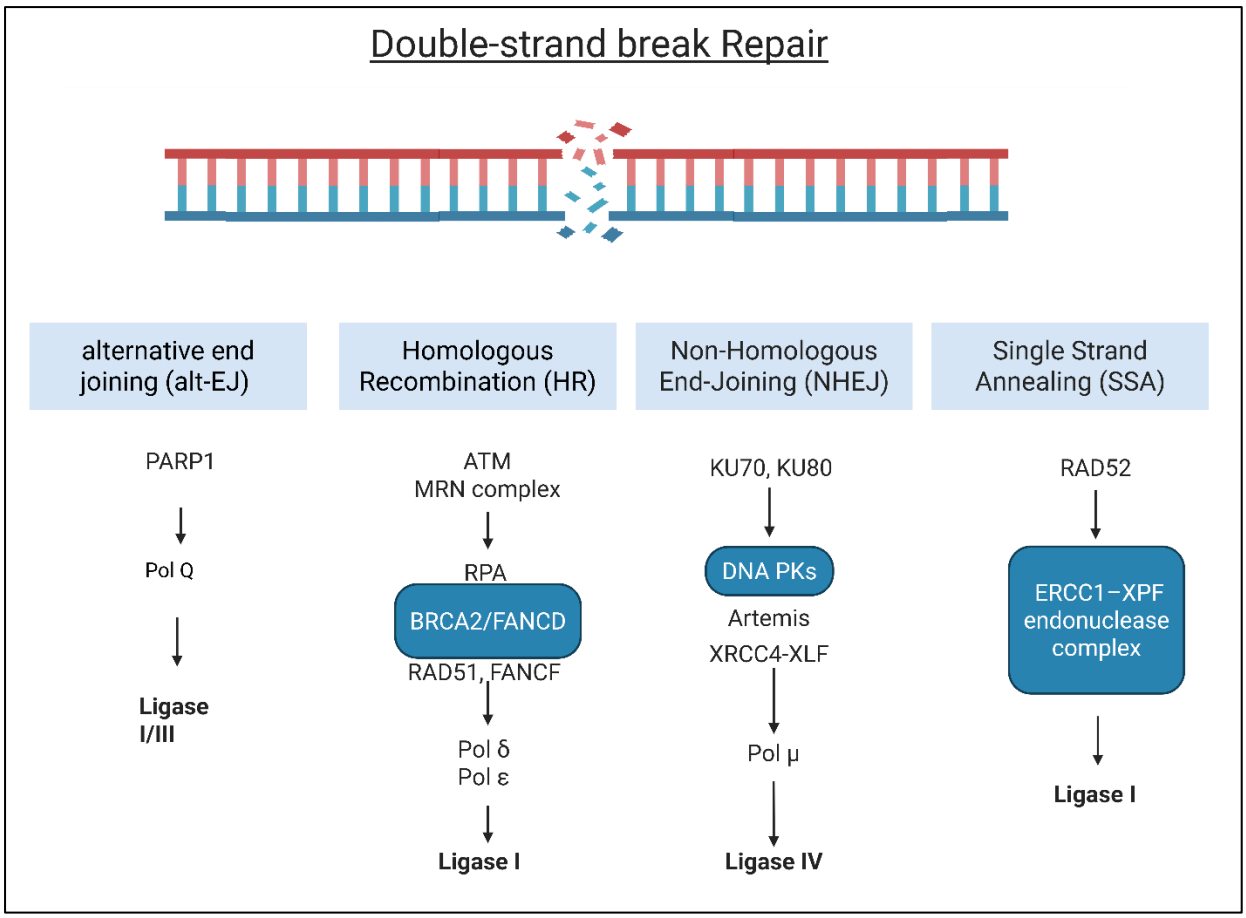


Figure 1.10. Double-Strand Break (DSB) Repair Pathways in Eukaryotic Cells

This schematic outlines the four major pathways responsible for repairing DNA double-strand breaks: alternative end joining (alt-EJ), homologous recombination (HR), non-homologous end joining (NHEJ), and single-strand annealing (SSA). Each pathway engages specific repair factors and enzymes. Alt-EJ is a backup repair mechanism initiated by PARP1 and concludes with ligation by Ligase III/I. HR is an error-free repair pathway involving the MRN complex, RPA, BRCA2/FANCD, and the RAD51 complex. NHEJ is a rapid, error-prone repair process initiated by KU70/80 and DNA-PKcs, culminating with Ligase IV. SSA operates via RAD52 and the ERCC1-XPF endonuclease complex. alt-EJ, alternative end joining; HR, homologous recombination; NHEJ, non-homologous end joining; SSA, single-strand annealing; PARP1, poly(ADP-ribose) polymerase 1; ATM, ataxia-telangiectasia mutated; MRN, MRE11-RAD50-NBS1 complex; RPA, replication protein A; BRCA2, breast cancer type 2 susceptibility protein; FANCD, Fanconi anemia group D protein; DNA-PKcs, DNA-dependent protein kinase catalytic subunit; XRCC4, X-ray repair cross-complementing protein 4; XLF, XRCC4-like factor; ERCC1, excision repair cross-complementing group 1; XPF, xeroderma pigmentosum group F-complementing protein. *Created with BioRender.com*

1.1.4.3.1 Imaging-Based Insights into LET-Dependent DNA Damage and Repair Protein Recruitment

DSBs induced by high-LET radiation, whether formed directly or through processing of complex non-DSB lesions, are substantially more resistant to repair compared to those caused by low-LET radiation. This is especially evident for lesions situated in heterochromatin, which pose a significant challenge to the repair machinery. As a result, such damage can accumulate in irradiated cells, leading either to mitotic failure and cell death or to survival with pronounced genomic instability, including mutations and chromosomal aberrations. The distinct physical characteristics of low- and high-LET IR are reflected at the cellular level through the recruitment of DNA repair and signalling proteins to sites of damage, as revealed by immunofluorescence and other imaging techniques. γ-H2AX, 53BP1, and DNA-PK form visible foci that serve as markers for DSBs and are commonly used for assessing damage localisation and repair kinetics (Asaithamby & Chen, 2011). Similarly, BER factors such as XRCC1 and OGG1 are rapidly recruited to sites of SSBs and oxidative lesions like 8-oxoG within minutes of irradiation, as observed following laser or iron particle exposure (Asaithamby & Chen, 2011; Lan et al., 2004). Notably, co-localisation of 53BP1, XRCC1, and hOGG1 foci has been reported in cells exposed to high-LET charged particles, suggesting the formation of clustered DNA lesions detectable at the single-cell level(Asaithamby et al., 2011). For instance, a study comparing DSBs induced by boron and neon ions, both with similar LET values (~135 keV/μm), demonstrated that particle type and track structure significantly influence damage complexity. Neon ions produced larger, more irregular, and persistent γ-H2AX/53BP1 foci than boron ions, with nearly half persisting 24 hours post-irradiation (Rothkamm & Löbrich, 2003). Supporting this, Lorat et al. used TEM to visualise clustered DNA damage at the

nanoscale following high-LET exposure, highlighting the utility of such methods in capturing the fine architecture of IR-induced lesions (Lorat et al., 2015). While imaging may not allow precise quantitation of clustered damage, it remains invaluable for understanding the spatiotemporal dynamics of the cellular response to radiation.

1.1.4.3.2 Differential Repair Dynamics and Pathway Choice Following High-LET Radiation

Real-time imaging studies have demonstrated that simple DSBs, such as those induced by ultra-soft X-rays or near-infrared microbeam irradiation, are repaired rapidly through the classical NHEJ pathway, involving core components like Ku70/80, XRCC4, Ligase IV, and XLF. In contrast, complex DSBs, commonly generated by high-LET radiation, are repaired with significantly slower kinetics and require additional proteins such as DNA-PKcs and ATM, with repair being further delayed in the absence of functional ATM (Reynolds et al., 2012). Although NHEJ is the predominant repair pathway for DSBs induced by low-LET radiation, its efficiency is reduced for the more intricate and clustered lesions caused by high-LET radiation. In most cases, delays in NHEJ-mediated DSB rejoining are attributed to the increased clustering of lesions caused by high-LET, which directly hinders repair efficiency. High-LET radiation has been shown to efficiently generate short DSB fragments of approximately 40 bp (Gerelchuluun et al., 2015). One hypothesis is that these short DNA fragments obstruct the binding of Ku proteins to chromosomal DSB ends, thereby impairing classical NHEJ. A study comparing DSB repair and end resection in G1 and G2 phases found that carbon ion-induced DSBs exhibited the slowest repair kinetics compared to those induced by X-rays or etoposide, irrespective of cell cycle phase. In contrast, alternative repair pathways, including PARP-dependent alt-NHEJ and MRE11-dependent HR, are less affected, as their activation is not significantly influenced by small dsDNA

fragments (Averbeck et al., 2014). Supporting this, high-LET radiation was found to be significantly more lethal to wild-type and HR-deficient (Rad54$^{-/-}$) mice compared to low-LET radiation, whereas Ku70$^{-/-}$ mice displayed no additional sensitivity to high-LET exposure. Despite the impairment of classical NHEJ, DNA-PK foci still form and co-localise with γH2AX and 53BP1 in high-LET-induced DNA damage tracks (Asaithamby & Chen, 2011).

1.1.4.3.3 Artemis, ATM, and the Essential Role of End Resection in Complex DSB Repair

Artemis, essential for V(D)J recombination, contributes to the repair of a subset (10 to 20 percent) of DSBs, especially those in heterochromatin that require ATM signalling. Artemis-deficient cells exhibit a more severe defect in repairing high-LET-induced DSBs compared to low-LET, indicating its pivotal role in processing complex lesions (Asaithamby & Chen, 2011; Moore et al., 2014). Additionally, ATM and Artemis promote HR during the G2 phase through Artemis' endonuclease activity and support NHEJ in G1, with Artemis facilitating the removal of DNA structures that hinder resection. Recent studies have shown that end resection is crucial for the repair of complex DSBs across all cell cycle phases, as evidenced by the formation of RPA, ATR, MRE11, and EXO1 foci in G1 and S/G2 cells following exposure to radiation of varying LETs (Averbeck et al., 2014). The frequency of resection correlates with lesion complexity. In S and G2 phases, resection favours HR, while in G1, it supports error-prone pathways such as alt-EJ or MMEJ. Altogether, these findings confirm that HR plays a significantly more prominent role in the repair of complex high-LET-induced DSBs, with Artemis serving as a central coordinator of pathway choice. Table 1.3 represents a comparison between High and low LET.

Table 1.3 Comparison of DNA Damage Characteristics and Repair Responses Induced by High-LET and Low-LET Radiation

Feature	High-LET Radiation	Low-LET Radiation
DSB Complexity	Generates complex clustered DSBs	Mostly simple, isolated DSBs
Repair Resistance	Substantially resistant to repair	Efficiently repaired
Heterochromatin Impact	Greater impact; lesions accumulate in heterochromatin	Less affected; heterochromatin provides a protective effect
Imaging Markers	Larger, irregular -H2AX/53BP1 foci, persistent >24h	Smaller, more uniform -H2AX/53BP1 foci, resolved quickly
Repair Protein Recruitment	Delayed recruitment of repair proteins (DNA-PKcs, ATM)	Rapid recruitment of repair proteins (Ku70/80, XRCC4)
Repair Kinetics	Slow; impaired NHEJ, reliance on HR or alt-NHEJ	Fast; classical NHEJ dominates
Dominant Repair Pathway	NHEJ impaired; HR and alt-NHEJ more active	NHEJ is the primary pathway
Role of Artemis and ATM	Artemis and ATM are crucial for repair of clustered lesions	Artemis is less critical; NHEJ repairs majority of DSBs
Fragment Size (DSBs)	Short DNA fragments (~40 bp), hindering NHEJ	Longer DNA fragments, allowing efficient NHEJ binding
End Resection Requirement	Critical for resolving complex DSBs; supports HR in G2/S, alt-EJ in G1	Less reliant; end resection mainly in HR during S/G2

1.1.5 Radiation-Induced Cell Death Pathways

One of the most critical consequences is the induction of cell death, which serves as a protective mechanism to eliminate irreparably damaged or potentially malignant cells. The mode of cell death can vary widely, ranging from tightly regulated pathways such as apoptosis and autophagy to unregulated and inflammatory processes like necrosis. Additionally, non-lethal responses such as senescence can permanently halt cell proliferation without triggering immediate cytolysis. Understanding the distinct molecular mechanisms and outcomes of these pathways is essential for improving therapeutic strategies and predicting tissue responses to radiation exposure. The

following sections provide an overview of the major cell death pathways activated in response to radiation, highlighting their defining features and regulatory mechanisms.

1.1.5.1 Mitotic Catastrophe and Mitotic Death

Mitotic catastrophe is a cell death mechanism that is triggered when cells sustain DNA damage that is beyond repair and are unable to proceed through mitosis correctly. This disruption leads to mitotic arrest, during which the cell attempts to manage the genomic damage but ultimately fails, resulting in regulated cell death (RCD). Radiation often causes such extensive DNA damage that cells with defective checkpoint mechanisms are forced into premature or aberrant mitosis. This process results in chromosome missegregation, micronuclei formation, and the eventual collapse of the mitotic spindle apparatus. Cells that undergo mitotic death may rupture and swell due to physical breakdown during mitosis or may persist temporarily before proceeding to a delayed apoptotic pathway. Mitotic catastrophe is therefore considered a gateway process that can culminate in apoptosis, necrosis, or senescence depending on the cellular context and the extent of damage (Galluzzi & Vitale, 2018; Gascoigne & Taylor, 2008)

1.1.5.2 Apoptosis

Apoptosis is a tightly regulated form of programmed cell death that plays a critical role in eliminating damaged or abnormal cells following radiation exposure. It can proceed via two major pathways: intrinsic and extrinsic. The intrinsic, or mitochondrial, pathway is activated by internal stress signals such as DNA damage, leading to the activation of p53 and the modulation of Bcl-2 family proteins. Pro-apoptotic members like PUMA, Bad, and NOXA are upregulated, while anti-apoptotic proteins such as Bcl-2 and Bcl-xL are suppressed. This shift results in mitochondrial outer membrane permeabilisation (MOMP), which facilitates the release of cytochrome c into the

cytoplasm and subsequent activation of caspase-9, followed by caspase-3 and -7. The extrinsic pathway is initiated when extracellular death ligands, such as those from the TNF family, bind to death receptors on the plasma membrane, activating caspase-8. Radiation exposure can increase the surface expression of these receptors, sensitising cells to apoptosis. Eventually, both pathways converge at the executioner caspases (3/7), leading to the systematic dismantling of the cell via DNA fragmentation, cytoskeletal breakdown, and membrane blebbing without inducing inflammation (Chakraborty et al., 2003; Eriksson & Stigbrand, 2010; Sheard et al., 2003).

1.1.5.3 Senescence

Radiation-induced senescence is a stable and typically irreversible state of growth arrest that allows damaged cells to remain metabolically active while halting their proliferation. It is primarily governed by the activation of tumour suppressor pathways involving p53 and retinoblastoma protein (pRb), which together halt progression through the G1/S checkpoint of the cell cycle. In addition to DNA damage, other radiation-associated stressors such as oxidative stress, chromatin remodelling, and persistent DDR signalling contribute to senescence induction. Unlike apoptotic cells, senescent cells do not die immediately but undergo characteristic changes, including increased cell size, senescence-associated β-galactosidase activity, and the development of a senescence-associated secretory phenotype (SASP). SASP involves the secretion of inflammatory cytokines, growth factors, and proteases, which can influence tissue remodelling and immune clearance. However, if not effectively cleared, senescent cells may contribute to tissue dysfunction and tumour promotion in the long term (Eriksson & Stigbrand, 2010; M. Li et al., 2018).

1.1.5.4 Autophagy

Autophagy is a cellular degradation process by which cells recycle cytoplasmic components and organelles through the lysosomal machinery, often as a survival mechanism under metabolic stress. Following radiation exposure, autophagy can be triggered as part of the cell's attempt to remove damaged mitochondria, misfolded proteins, and other harmful debris. This process is regulated by autophagy-related (ATG) genes and modulated by key signalling pathways such as mTOR, which is typically inhibited during cellular stress to allow autophagy induction. While autophagy generally promotes cell survival and radioresistance, excessive or dysregulated autophagy can lead to self-digestion and a form of programmed cell death known as autophagic cell death. Morphologically, this type of death is distinguished by the accumulation of autophagosomes and the absence of apoptotic or necrotic features. The outcome of autophagy—protective or destructive—depends heavily on the dose and duration of radiation, the cell type, and the intracellular energy status (Apel et al., 2008; Classen et al., 2019; Levy et al., 2017).

1.1.5.5 Necrosis

Necrosis is traditionally considered an unregulated and passive form of cell death that can occur following severe radiation damage, particularly at high doses where ATP levels are depleted, and repair mechanisms are overwhelmed. Unlike apoptosis or autophagy, necrosis is characterised by early plasma membrane rupture, uncontrolled ion fluxes, and the release of intracellular contents into the extracellular environment, often resulting in inflammation. Morphologically, necrotic cells exhibit swelling, organelle breakdown, and the loss of membrane integrity. Although often thought of as accidental cell death, recent studies suggest that certain forms of necrosis, such as

necroptosis, may involve regulated signalling cascades. In the context of radiation, necrosis is frequently observed in tissues subjected to extreme oxidative stress or hypoxia, where energy-dependent processes like apoptosis cannot proceed. The resulting inflammatory response can exacerbate tissue damage and impair regeneration, particularly in radiosensitive organs such as the gastrointestinal tract and bone marrow (Kroemer et al., 2009).

1.1.5.6 Ferroptosis

Ferroptosis is a form of regulated cell death driven by disruptions in iron homeostasis, amino acid metabolism, and ROS balance, and has emerged as a promising target in cancer therapy. Increasing evidence indicates that radiotherapy-induced ferroptosis plays a pivotal role in tumour suppression. Numerous preclinical studies have demonstrated that combining IR with small-molecule ferroptosis modulators or nanotechnology-based delivery systems can enhance therapeutic efficacy and help overcome resistance to both chemotherapy and radiotherapy.

In addition to causing direct damage to biomacromolecules such as DNA, proteins, and lipids, IR used in radiotherapy induces the production of reactive oxygen species (ROS), which play a central role in promoting lipid peroxidation and triggering ferroptosis. The involvement of ferroptosis in the cellular response to IR is supported by multiple lines of evidence. These include the detection of lipid peroxidation using ferroptosis-specific dyes (e.g., C11-BODIPY) and the elevated expression of canonical ferroptosis markers such as malondialdehyde (MDA), 4-hydroxynonenal (4-HNE), and prostaglandin-endoperoxide synthase 2 (PTGS2) in irradiated cancer cell lines and tumour tissues. Furthermore, IR-exposed cells display mitochondrial morphological changes characteristic of ferroptosis, such as condensed and shrunken mitochondria, as reported by Lang et al. (2019) (Lang et al., 2019).

The functional interplay between IR and ferroptosis is further substantiated by experiments showing that pre-treatment with iron chelators (e.g., deferoxamine) or ferroptosis inhibitors (e.g., ferrostatin-1, liproxstatin-1) confers partial protection against IR-induced cell death. This protective effect is more pronounced than that observed with inhibitors of other forms of regulated cell death (RCD), suggesting a prominent role for ferroptosis in mediating radiation-induced cytotoxicity.

IR induces ferroptosis through three major regulatory pathways (Lang et al., 2019; Lei et al., 2020; Ye et al., 2020):

1-ROS and ACSL4 Pathway:

IR leads to elevated ROS, which drives the formation of polyunsaturated fatty acid (PUFA) radicals. These radicals undergo further oxidation in the presence of molecular oxygen and iron (via the Fenton reaction), forming lipid hydroperoxides (PUFA-OOH) (Lei et al., 2020). This lipid peroxidation cascade is amplified by IR-induced upregulation of acyl-CoA synthetase long-chain family member 4 (ACSL4). ACSL4, along with lysophosphatidylcholine acyltransferase 3 (LPCAT3), promotes the incorporation of PUFAs into membrane phospholipids, rendering them highly susceptible to peroxidation.

2-GSH and GPX4 Axis:

Exposure to IR depletes intracellular glutathione (GSH), a crucial antioxidant that serves as a cofactor for glutathione peroxidase 4 (GPX4). This depletion reduces GPX4 activity and expression, thereby impairing its ability to detoxify lipid hydroperoxides. As a result, toxic lipid peroxides accumulate, enhancing ferroptotic cell death (Lei et al., 2020).

3-SLC7A11 and ATM Signalling:

IR can also suppress the expression of SLC7A11, a component of the system Xc^- cystine/glutamate antiporter, which is essential for cystine uptake and subsequent GSH biosynthesis. This suppression is mediated through the activation of ataxia telangiectasia mutated (ATM) kinase, thereby promoting ferroptosis by compromising GSH-dependent GPX4 function (Lang et al., 2019).

However, the effect of IR on SLC7A11 appears to be context-dependent. While some studies report a downregulation of SLC7A11 post-IR, facilitating ferroptosis, others observe an increase in its expression, suggesting an adaptive cellular response to restore redox balance. These discrepancies may reflect cell-type specific regulatory dynamics or differential exposure conditions (Lang et al., 2019).

1.1.6 Factors affecting Radiation response

The biological response of tumour cells to ionising radiation is governed by a complex interplay of intrinsic and extrinsic factors that significantly influence therapeutic outcomes. While physical parameters such as radiation type, dose, and energy deposition patterns determine the initial extent of DNA damage, cellular radiosensitivity is also modulated by various physiological and molecular characteristics(Lomax et al., 2013b; Sutherland et al., 2001). These include tumour oxygenation status, chromatin architecture, cell cycle phase, DNA repair proficiency, and the immune microenvironment. Together, these factors determine how effectively radiation-induced damage is detected, signalled, and repaired, thereby shaping both short-term cytotoxic responses and long-term treatment efficacy. A comprehensive understanding of these modulators is essential for optimising radiotherapy strategies, particularly in overcoming resistance observed in hypoxic, repair-proficient, or genomically unstable tumour subpopulations Figure 1.11. The following subsections explore the major

determinants of radiation response, highlighting their mechanistic contributions and clinical relevance.

1.1.6.1 Oxygen concentration:

From a clinical standpoint, one of the major challenges in radiotherapy is the presence of hypoxic regions within solid tumours, which significantly compromise treatment efficacy. Hypoxia not only triggers cellular radioprotective responses but also intrinsically enhances tumour cell resistance to radiation. This phenomenon, widely known as the “oxygen effect,” reflects the observation that cells irradiated under normoxic or hyperoxic conditions (≥20% O_2) are far more sensitive to ionising radiation than those irradiated under hypoxic or anoxic conditions. The increased radiosensitivity in oxygenated cells is primarily attributed to the oxygen-mediated “fixation of damage,” whereby oxygen reacts with radiation-induced DNA radicals—particularly hydroxyl radicals—stabilising DNA damage and preventing its repair, often resulting in lethal lesions (Carlson et al., 2006).

In poorly vascularised regions of tumours, however, the deficiency of oxygen alone contributes substantially to radioresistance, making standard low-LET photon radiotherapy less effective (Forster et al., 2019; Grimes, 2020). The degree of tumour vascularisation plays a central role in modulating this response. Well-perfused regions with high microvessel density are typically more oxygenated and hence more radiosensitive, while avascular or necrotic tumour zones remain chronically hypoxic and resistant to therapy. Moreover, tumour vasculature is often immature or abnormally structured, leading to spatial and temporal fluctuations in oxygen availability (acute hypoxia). Ionising radiation itself can damage endothelial cells, transiently worsening hypoxia during treatment. Conversely, strategies aimed at

vascular normalisation can enhance radiosensitivity by improving oxygen delivery to tumour cells.

While some clinical approaches have explored artificial tumour oxygenation to mitigate hypoxia-induced resistance, an increasingly promising alternative is the use of high-LET radiation modalities, such as protons (within the Bragg peak), carbon ions, and α-particles. Unlike low-LET radiation, which depends on ROS-mediated damage and thus oxygen availability, high-LET radiation induces densely ionising DNA lesions that are largely oxygen-independent. This property allows high-LET radiation to effectively target hypoxic tumour cells that are otherwise resistant to conventional photon-based therapies (Forster et al., 2019; Grimes, 2020).

Carbon-ion radiation therapy (CIRT), for example, has been demonstrated to be significantly less reliant on oxygen levels than standard low-LET radiotherapy (Antonovic et al., 2014). As a result, CIRT presents as an effective therapeutic option for hypoxic tumours such as melanoma, head and neck cancer, and pancreatic cancer—types that typically exhibit poor responses to traditional treatments (Strigari et al., 2018).

Nevertheless, tumour cells that have adapted to chronic hypoxia often exhibit a unique molecular phenotype characterised by altered metabolic, DNA repair, and survival pathways. These adaptations can render them more resistant not only to low-LET but also to high-LET radiation. Therefore, the combination of high-LET radiation with radiosensitising agents or molecular inhibitors targeting hypoxia-associated resistance mechanisms may be necessary to fully exploit the therapeutic potential of high-LET approaches in hypoxic tumour settings (Mistry et al., 2017).

1.1.6.2 Chromatin compaction

The structural state of chromatin, regulated by post-translational modifications (PTMs) on the N- and C-terminal tails of histones, critically influences DNA accessibility, transcription, and the cellular response to DNA damage. These modifications govern the level of chromatin compaction and, consequently, its susceptibility to damage. Heterochromatin, a tightly packed and transcriptionally inactive chromatin state, is enriched in epigenetic markers such as H3K9me3 and H3K27me3, exhibits reduced histone acetylation, and shows increased 5′-methylcytosine (Saksouk et al., 2015). In contrast, euchromatin—a more relaxed and transcriptionally active state is marked by high levels of H3K9ac, H3K4me3, and reduced DNA methylation (Karmodiya et al., 2012).

These chromatin configurations significantly influence DNA repair processes, including pathway choice, repair efficiency, and mutagenic potential, due to differences in transcriptional activity, nucleosome positioning, and chromatin accessibility. In early studies using γ-irradiation, euchromatin was found to be more prone to DSB induction and to undergo faster repair than heterochromatin, which provided relative protection against damage (Falk et al., 2008; H. Takata et al., 2013a)This protective effect is particularly evident with low-LET radiation, which predominantly causes indirect damage via free radicals. Supporting this, experimental data show that the frequency of DSBs induced by X-rays in heterochromatin is 5–50 times lower than in euchromatic regions. Furthermore, studies manipulating chromatin compaction demonstrated that the induction of complex DNA damage by low-LET radiation decreases as chromatin becomes more compact, with the highest damage levels observed in naked DNA(Magnander et al., 2009).

These findings are reinforced by previous transmission electron microscopy (TEM) studies, which showed that after low-LET exposure, single pKu70 dimers—reflecting isolated DSBs—were randomly distributed throughout the nucleus. In those studies, euchromatic DSBs were clearly repaired more rapidly than heterochromatic DSBs, and nearly all DNA lesions induced by low-LET irradiation were efficiently rejoined within 24 hours (Lorat et al., 2012; Rübe et al., 2011). In contrast, high-LET irradiation deposits energy in highly localised tracks, leading to densely clustered DNA lesions, particularly within condensed heterochromatin. The extent of clustering depends on the chromatin packing density, and results in the formation of abundant short DNA fragments in compact regions. This suggests that this increased yield of short fragments due to DSB clustering in heterochromatin is a key determinant of cellular responses to densely ionising radiation (Lorat et al., 2016) .

1.1.6.3 Cell Cycle Phase and Proliferation

Radiosensitivity varies throughout the cell cycle, particularly for low-LET radiation. Cells in the G_2/M phase are generally more sensitive, while those in the late S-phase, where DNA replication and repair are active, are more resistant. This is due to the cell's capacity to recognize and repair low-LET-induced damage during S-phase, while mitotic cells have less opportunity for repair, increasing their vulnerability. Consequently, therapeutic strategies have aimed to synchronize tumour cells into radiosensitive phases to enhance low-LET radiotherapy efficacy (Pawlik & Keyomarsi, 2004). However, for high-LET radiation, such as carbon ions or alpha particles, this dependency on the cell cycle is greatly reduced. The densely ionizing tracks of high-LET particles produce complex, clustered DNA damage that is largely irreparable, leading to G_2 arrest across all cell cycle phases and diminishing typical phase-dependent survival differences (Blakely et al., 1989).

Interestingly, some studies have highlighted exceptions to this trend. For instance, experimental exposure of cells to high-LET α-particles or neon ions has shown that cells in late S-phase can be more radiosensitive than those in G_1 or G_2, with double the number of DSBs observed. Moreover, M-phase cells, usually most radiosensitive under low-LET conditions, have been reported to be relatively resistant to α-particle exposure from ^{211}At sources, challenging conventional assumptions (Blakely et al., 1989; Claesson et al., 2011).

In addition, researchers studying the effects of high-LET ^{12}C carbon-ion radiation in HeLa cells observed significantly increased DNA damage, apoptosis, and cell killing compared to low-LET gamma rays. These effects were further amplified when PARP-1, a key DNA repair enzyme, was silenced, indicating a heightened dependency on DNA repair pathways under high-LET conditions. Both ^{12}C and γ-irradiation induced G_2/M arrest, but ^{12}C caused a stronger block, and uniquely delayed S-phase progression—an effect absent with γ-irradiation. These findings suggest that high-LET radiation not only overrides standard cell cycle-dependent responses but also sensitizes cells more profoundly to DNA repair inhibition. Thus, combining high-LET irradiation with PARP inhibitors may offer a synergistic strategy to target radioresistant cells, particularly those that evade killing under conventional radiotherapy(Ghorai et al., 2014).

1.1.6.4.DNA repair capacity:

Beyond physical and environmental influences, several intrinsic biological factors critically modulate a cell's capacity to respond to ionising radiation. One of the strongest determinants of radiosensitivity is DNA repair capacity. Cells equipped with efficient DNA damage repair pathways, particularly homologous recombination (HR) and non-homologous end joining (NHEJ), are better able to resolve radiation-induced

lesions, thereby surviving exposure and displaying greater radioresistance. Conversely, defects in key DNA repair genes such as *ATM*, *BRCA1/2*, or *DNA-PKcs* impair damage resolution and increase cellular radiosensitivity. In fact, many resistant tumour cells upregulate DNA repair pathways, and targeting these with agents like PARP inhibitors has proven to enhance radiosensitivity (Kim Daniel Y. et al., 2020). Another pivotal modulator is the p53 tumour suppressor, often dubbed the “guardian of the genome.” Wild-type p53 enables cells to arrest the cell cycle or undergo apoptosis following radiation-induced DNA damage, thereby enhancing treatment efficacy. However, tumours harbouring mutated or deleted *TP53*, which accounts for approximately 50% of cancers, are typically more resistant to radiotherapy due to impaired apoptotic signalling and reliance on error-prone repair. Additionally, the immune microenvironment plays a significant role (Al-Arafat et al., 2024). Ionising radiation can stimulate immunogenic cell death by releasing tumour antigens and damage-associated molecular patterns (DAMPs), thereby recruiting immune cells such as cytotoxic T-lymphocytes. A tumour microenvironment rich in immune effector cells and pro-inflammatory cytokines is more likely to support the clearance of irradiated cells and boost radiotherapy outcomes. Taken together, DNA repair proficiency, p53 status, and immune contexture form a network of interrelated factors that strongly influence how tumours respond to radiation therapy (Al-Arafat et al., 2024)

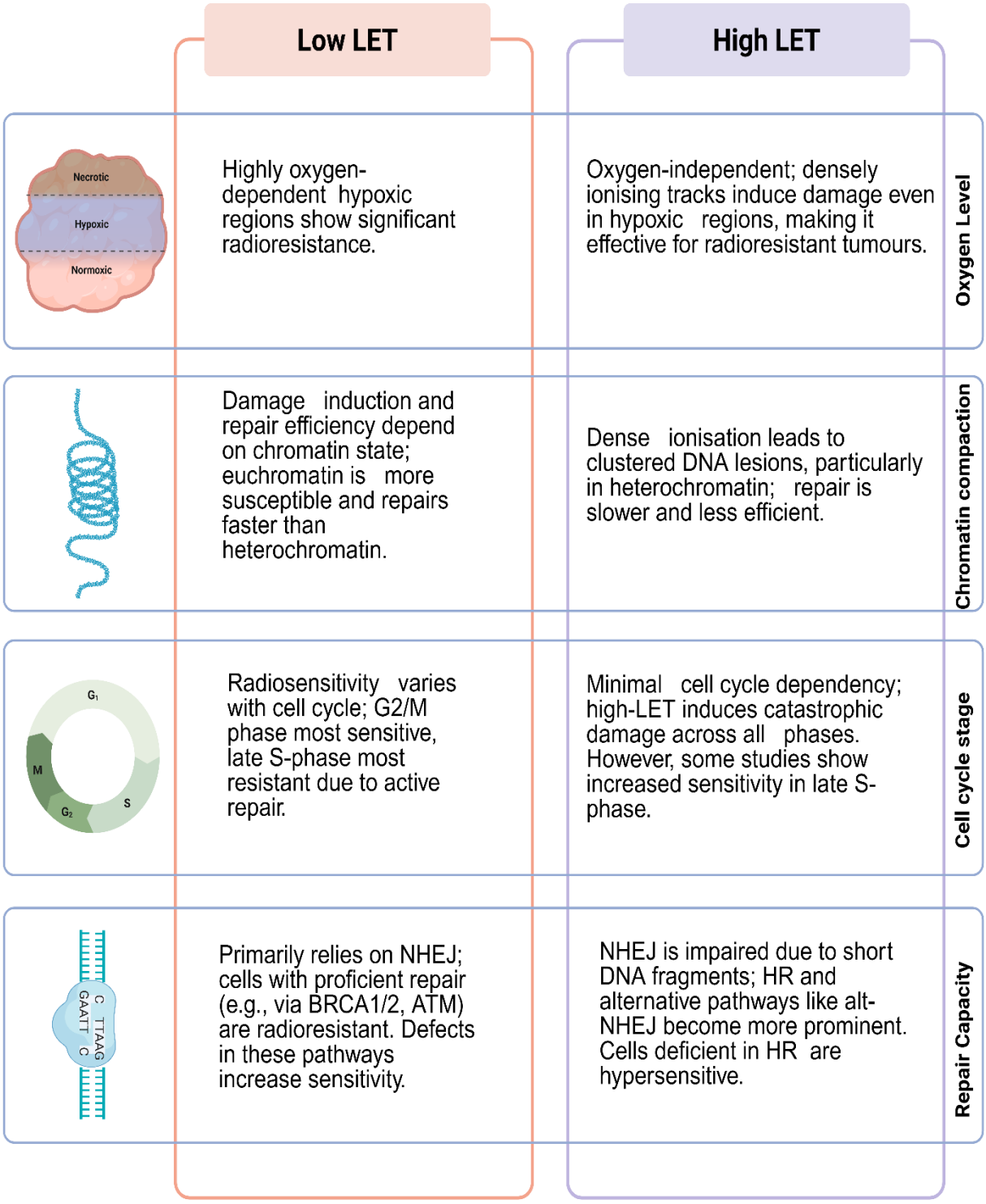


Figure 1.11. Comparative Summary of Factors Modulating Radiation Response under Low and High Linear Energy Transfer (LET) Conditions

This Figure provides an overview of key biological and environmental factors influencing the cellular response to ionising radiation under low-LET (e.g., photons) and high-LET (e.g., carbon ions, α-particles) exposures. Oxygen concentration (tumour hypoxia), chromatin

compaction, cell cycle phase, and DNA repair capacity all modulate radiosensitivity. Low-LET radiation is strongly affected by oxygen availability, chromatin state, and cell cycle phase, while high-LET radiation produces densely clustered damage, leading to less dependence on these factors. Additionally, DNA repair capacity, including homologous recombination and non-homologous end joining, significantly shapes cellular outcomes post-irradiation. LET, linear energy transfer; DSBs, double-strand breaks; G1, gap phase 1; S, synthesis phase; G2, gap phase 2; M, mitosis phase; HR, homologous recombination; NHEJ, non-homologous end joining; ROS, reactive oxygen species. *Created with BioRender.com.*

For over a decade, our lab has been dedicated to advancing the understanding of DPC biology by identifying critical factors involved in their recognition, processing, and repair. Our research focuses on uncovering how DPCs are formed, their impact on cellular function, and the mechanisms by which cells repair these complex lesions. One area of particular interest is the effect of IR, a potent inducer of various DNA lesions, including DPCs. Given the essential role of SPRTN in the proteolytic repair of DPCs, we have sought to investigate how SPRTN deficiency influences the cellular response to IR in human cell lines. This interest stems from growing evidence that IR not only induces strand breaks but also promotes the formation of covalent DNA–protein complexes, especially under oxidative stress. Understanding how SPRTN depletion compromises the cell's ability to manage DPCs under such conditions provides a crucial link between radiation exposure and DPC-induced genome instability. The following section will explore the formation, characteristics, and biological significance of DPCs, and establish how they represent a major form of IR-induced DNA damage that demands specialised repair mechanisms.

1.2 DNA-Protein Crosslinks

DNA–protein crosslinks (DPCs) are a type of DNA lesions that occur when a protein becomes covalently attached to DNA, forming a stable and irreversible bond. This type of DNA damage can interfere with critical cellular processes such as DNA replication, transcription, and repair, ultimately threatening genomic stability (Ruggiano & Ramadan, 2021a; Vaz et al., 2017a; Weickert & Stingele, 2022). DPCs were first described in a living system (bacteria) in 1962, and they form when proteins covalently and irreversibly attach to DNA upon the exposure to Ultraviolet (UV) radiation (Smith, 1962). Any protein in proximity to DNA can be crosslinked upon exposure to various crosslinking agents, either endogenous or exogenous. Endogenous crosslinking

agents originate within the cell which include reactive oxygen species, reactive nitrogen species (RNS), and aldehydes which are byproducts of normal cellular metabolism (Fielden et al., 2018; Lu et al., 2010a; Nakamura & Nakamura, 2020; Oka et al., 2024; Tretyakova et al., 2015). Exogenous crosslinking agents, on the other hand, are external factors, including ultraviolet (UV) light, ionizing radiation (IR), and certain chemotherapeutic drugs like cisplatin (Barker, Weinfeld, & Murray, 2005; Vaz et al., 2017b). Upon exposure to these agents, proteins near DNA become activated and can form radicals. When these radicals interact with DNA, they recombine to form stable covalent bonds between the DNA and protein, leading to the creation of a DPC (Nakano et al., 2015; Shoulkamy et al., 2012).

1.2.1 Crosslinking agents: Types and mechanisms

1.2.1.1 Aldehydes

Endogenous aldehydes are a significant source of DPCs and are naturally produced within cells during normal metabolic processes(Nakamura & Nakamura, 2020; Oka et al., 2024). These reactive molecules can covalently bind proteins to DNA, resulting in stable and potentially toxic crosslinks. Endogenous aldehydes such as formaldehyde and acetaldehyde are generated during cellular activities, including metabolism and oxidative stress. These types of crosslinking are general, in other words, they can crosslink any protein in close proximity to DNA (Shi et al., 2004a; Vijayraghavan & Saini, 2023). The accumulation of aldehyde-induced DPCs, if not efficiently repaired, can disrupt essential processes in the cells (Table 1.4).

1.2.1.1.1 Formaldehyde (FA)

Formaldehyde (FA) is a highly reactive one-carbon metabolite capable of forming covalent crosslinks between a wide range of biological macromolecules. Within the nucleus, FA can induce crosslinks between DNA strands (DNA–DNA) or between

DNA and adjacent proteins (DNA–protein), contributing to the formation of DNA–protein crosslinks (DPCs), as originally described by Siomin et al. (1973) (Siomin et al., 1973). In addition, FA can generate other types of crosslinks, including protein–protein and RNA-involved crosslinks (RNA–protein and RNA–DNA). More recently, FA has been shown to directly modify proteins at their N-terminal proline residues, forming a distinctive 5,5-bicyclic aminal structure, highlighting a unique biochemical interaction between FA and protein N-termini (John et al., 2023; Kamps et al., 2019). DPCs remain the most extensively studied due to their cytotoxicity and relevance in chromatin stability (Dator et al., 2022; Suryo Rahmanto et al., 2023).

Because of their high reactivity, these FA molecules released in the nucleus could cause crosslinking between DNA and adjacent proteins. FA-mediated DNA–protein cross-linking occurs between deoxyguanine (dG), deoxyadenine dA, and deoxy cytosine (dC) nucleosides of the DNA and lysine, cysteine, histidine, or tryptophan residues of the proteins (Lu et al., 2010b). This process begins with the formation of Schiff base intermediates on either proteins or DNA, which are subsequently converted into stable methylene cross-links through reactions with other biomolecules (Lu et al., 2010b).

FA -induced DNA–protein crosslinks (DPCs) and other lesions severely hinder transcriptional elongation by stalling RNA polymerase II at the site of the crosslink, triggering transcriptional stress that can activate cellular stress responses such as the unfolded protein response or p53-mediated apoptotic pathways (Suryo Rahmanto et al., 2023). Persistent transcriptional arrest may further lead to epigenetic alterations, affecting gene expression patterns. Beyond transcriptional interference, FA-induced DPCs are potent barriers to replication fork progression, causing replication stress that, if unresolved, leads to replication fork collapse and the formation of double-strand

breaks (DSBs)—a particularly cytotoxic form of DNA damage. These DSBs are repaired by non-homologous end joining (NHEJ) or homologous recombination (HR), both of which carry the risk of introducing mutations or chromosomal abnormalities (Stingele & Jentsch, 2015). Additionally, FA's ability to crosslink histones to DNA perturbs chromatin structure, disrupting nucleosome dynamics and impairing processes such as DNA repair and transcriptional regulation, thereby promoting genomic instability (Stingele et al., 2017). Persistent FA-induced DNA damage elevates mutation rates, particularly when DNA repair mechanisms are overwhelmed or compromised, as observed in conditions where aldehyde detoxification enzymes such as ADH5 and ALDH2 are deficient. This scenario contributes to bone marrow failure syndromes and cancer predisposition, including nasopharyngeal carcinoma and leukaemia (Dingler et al., 2020; Oka et al., 2024).

DPCs induced by FA have been demonstrated both in vitro and in vivo. Isotope-labelling studies show that endogenous FA continually generates DPCs in mammalian cells, even under physiological conditions, with the liver and bone marrow showing the highest accumulation (Lai et al., 2016). Endogenous formaldehyde is believed to be present in all aqueous body fluids. In humans, its half-life is estimated to range between 1 to 1.5 minutes. Studies have detected endogenous formaldehyde concentrations at approximately 0.1 mmol/L in the blood of rats, monkeys, and humans (Casanova et al., 1991; Lai et al., 2016). Additionally, formaldehyde levels in the liver and nasal mucosa of rats were found to be two to four times higher than those measured in the blood. FA is generated endogenously as a byproduct of metabolic processes, including methanol oxidation, methylamine deamination, and histone demethylation(Gerken et al., 2007; Walport et al., 2012).

Formaldehyde is generated endogenously through several metabolic processes. One primary source is oxidative demethylation of methylated macromolecules, including nucleic acids and proteins, catalysed by iron-dependent dioxygenases such as lysine-specific demethylase 1 (LSD1), which removes methyl groups from histone lysine residues, and AlkB homolog (ALKBH) enzymes, which demethylate modified DNA and RNA bases (Shi et al., 2004b). This process is integral to epigenetic regulation but releases FA as a by-product. Additionally, one-carbon (1C) metabolism, particularly within the folate cycle, contributes to FA production via methyl group transfer reactions, such as the conversion of serine to glycine by serine hydroxymethyltransferase (SHMT) (Burgos-Barragan et al., 2017). Tetrahydrofolate (THF)-dependent enzymes also indirectly promote FA formation through methylation and demethylation pathways.

Methanol oxidation provides another endogenous FA source. Methanol, derived from dietary intake (e.g., fruit pectin breakdown) or metabolism, is oxidised by alcohol dehydrogenase class I (ADH1) into FA, which is further processed into formic acid by ADH5. Amino acid catabolism, particularly of methionine, serine, and glycine, also contributes to FA release; methionine metabolism involves S-adenosylmethionine (SAM) conversion, where methyl transfer reactions produce FA as a by-product. Moreover, lipid peroxidation during oxidative stress leads to the formation of reactive aldehydes, including FA, especially under conditions like inflammation or radiation exposure(Pham et al., 2025; Reingruber & Pontel, 2018). In addition, FA is produced as a detoxification product of xenobiotics during cellular metabolism in the liver by Cytochrome P450 enzyme (WAYDHAS et al., 1978).

Environmental exposure also contributes to FA levels. Exogenous sources include vehicle exhaust, industrial activities, tobacco smoke, and certain consumer products

(Protano et al., 2022; Seifter, 2025). Additionally, substances like aspartame metabolise into methanol, which is subsequently converted into FA in the body (Troche et al., 1998). Importantly, isotope-labelling methods have distinguished between DPCs formed by endogenous and exogenous FA exposure. These studies demonstrate that endogenous FA is a significant contributor to DPC formation across multiple tissues, while exogenous FA-induced DPCs localise primarily to exposed tissues like the nasal mucosa (Lai et al., 2016).

These lesions form covalent linkages between DNA nucleobases, particularly guanine, adenine, and cytosine, and protein residues such as lysine, cysteine, histidine, or tryptophan (Tayri-Wilk et al., 2020). DPC formation follows a two-step mechanism beginning with Schiff base intermediates that subsequently convert into stable methylene crosslinks. FA-crosslinked proteins include histones and chromatin-associated factors like RNA polymerase II, leading to replication blocks and transcriptional arrest (Song & Ramadan, 2023).

The primary detoxification route involves ADH5, also known as formaldehyde dehydrogenase, which catalyses the conversion of FA into formate via S-formylglutathione intermediates. ALDH2, while primarily metabolising acetaldehyde, also mitigates aldehyde-induced toxicity. Disruption in these detoxification pathways leads to FA accumulation, as shown in studies where ADH5 and ALDH2 deficiencies promote DPC accumulation and genotoxic stress. Deficiency in these enzymes results in elevated DPC levels, increased genotoxic stress, and bone marrow failure in animal models, underscoring the essential role of aldehyde detoxification in maintaining genome integrity (Dingler et al., 2020; Oka et al., 2025).

Formaldehyde is generated endogenously through several metabolic processes. One primary source is oxidative demethylation of methylated macromolecules, including

nucleic acids and proteins, catalysed by iron-dependent dioxygenases such as lysine-specific demethylase 1 (LSD1), which removes methyl groups from histone lysine residues, and AlkB homolog (ALKBH) enzymes, which demethylate modified DNA and RNA bases (Shi et al., 2004b). This process is integral to epigenetic regulation but releases FA as a by-product. Additionally, one-carbon (1C) metabolism, particularly within the folate cycle, contributes to FA production via methyl group transfer reactions, such as the conversion of serine to glycine by serine hydroxymethyltransferase (SHMT) (Burgos-Barragan et al., 2017). Tetrahydrofolate (THF)-dependent enzymes also indirectly promote FA formation through methylation and demethylation pathways.

Methanol oxidation provides another endogenous FA source. Methanol, derived from dietary intake (e.g., fruit pectin breakdown) or metabolism, is oxidised by alcohol dehydrogenase class I (ADH1) into FA, which is further processed into formic acid by ADH5. Amino acid catabolism, particularly of methionine, serine, and glycine, also contributes to FA release; methionine metabolism involves S-adenosylmethionine (SAM) conversion, where methyl transfer reactions produce FA as a by-product. Moreover, lipid peroxidation during oxidative stress leads to the formation of reactive aldehydes, including FA, especially under conditions like inflammation or radiation exposure(Pham et al., 2025; Reingruber & Pontel, 2018). In addition, FA produced as a detoxification product of xenobiotics during cellular metabolism in the liver by Cytochrome P450 enzyme (WAYDHAS et al., 1978).

Environmental exposure also contributes to FA levels. Exogenous sources include vehicle exhaust, industrial activities, tobacco smoke, and certain consumer products (Protano et al., 2022; Seifter, 2025). Additionally, substances like aspartame metabolise into methanol, which is subsequently converted into FA in the body (Troche

et al., 1998). Importantly, isotope-labelling methods have distinguished between DPCs formed by endogenous and exogenous FA exposure. These studies demonstrate that endogenous FA is a significant contributor to DPC formation across multiple tissues, while exogenous FA-induced DPCs localise primarily to exposed tissues like the nasal mucosa (Lai et al., 2016).

1.2.1.1.2 Malondialdehyde (MDA)

Malondialdehyde (MDA) is a highly reactive, bifunctional aldehyde predominantly formed as a secondary product of lipid peroxidation, wherein reactive oxygen species (ROS) attack polyunsaturated fatty acids (PUFAs) such as arachidonic acid and docosahexaenoic acid (Ayala et al., 2014; Blouin & Saini, 2024). This oxidative degradation process results in the formation of lipid hydroperoxides, which subsequently decompose to generate MDA. In addition to non-enzymatic pathways, MDA can arise through enzymatic processes, including lipoxygenase (LOX)-mediated oxidation and cyclooxygenase (COX)-dependent prostaglandin biosynthesis, particularly during inflammation. Exogenous sources, such as the dietary intake of thermally processed oils and lipid-rich foods, can also contribute to systemic MDA burden. Under pathological conditions characterised by elevated oxidative stress such as cardiovascular disease, neurodegeneration, cancer, and diabetes MDA production is markedly increased, making it a widely recognised biomarker of lipid peroxidation and oxidative tissue damage (Niedernhofer et al., 2003).

The genotoxicity of MDA stems from its ability to form covalent adducts and crosslinks with nucleic acids and proteins. As a dialdehyde, MDA possesses two electrophilic carbonyl groups capable of reacting with nucleophilic moieties on biomolecules. DPC formation by MDA proceeds via a two-step mechanism. In the first step, MDA reacts with the ε-amino groups of lysine residues on proteins, forming Schiff bases or

Michael-type adducts. These protein-bound MDA intermediates then engage with nucleophilic sites on DNA-particularly the exocyclic amines of guanine and adenine-to establish covalent crosslinks. This mechanism has been substantiated through in vitro studies, which demonstrated that MDA-treated proteins, such as histone H1, can readily crosslink with DNA, whereas MDA-modified DNA does not effectively capture proteins in the absence of pre-formed protein adducts (Ayala et al., 2014; Blouin & Saini, 2024; Voitkun & Zhitkovich, 1999). The specificity of MDA for lysine-rich proteins reflects both the high abundance and nucleophilicity of lysine residues in chromatin-associated proteins, making them particularly vulnerable to aldehyde-induced crosslinking.

The biological consequences of MDA-induced DPCs are significant, particularly in the context of chronic inflammation, aging, and oxidative stress. Elevated levels of MDA and MDA–DNA adducts such as M1dG have been observed in human tissues and are associated with mutagenesis, genomic instability, and increased cancer risk. In neurodegenerative diseases such as Alzheimer's and Parkinson's, where oxidative stress plays a central role, the accumulation of MDA-derived adducts and crosslinks may contribute to neuronal dysfunction and progressive cell loss (Blouin & Saini, 2024). Together, these findings underscore the pathological relevance of MDA-mediated DNA–protein crosslinking and highlight its potential as a therapeutic target or biomarker in diseases driven by oxidative stress.

1.2.1.1.3 Methylglyoxal (MG)

Methylglyoxal (MG) is a highly reactive α-ketoaldehyde generated as a by-product of glycolysis, lipid peroxidation, and threonine catabolism (Vijayraghavan & Saini, 2023). The most significant source of MG in cells is glycolysis, the central metabolic pathway for glucose catabolism. MG is predominantly formed non-enzymatically from the

spontaneous degradation of two key glycolytic intermediates are Glyceraldehyde-3-phosphate (G3P) and Dihydroxyacetone phosphate (DHAP) (Kold-Christensen & Johannsen, 2020). Both G3P and DHAP contain reactive carbonyl groups and are prone to spontaneous dephosphorylation and dehydration, yielding MG. This side reaction becomes particularly pronounced under conditions of high glycolytic flux (e.g., in cancer cells or hyperglycemia), where elevated levels of G3P and DHAP accumulate. Oxidative stress, which may increase MG production due to altered redox states affecting glycolytic enzyme function.

MG is also generated enzymatically as a minor by-product of threonine catabolism in mitochondria.

Threonine dehydrogenase (TDH) converts threonine into 2-amino-3-ketobutyrate. This intermediate can non-enzymatically decompose into aminoacetone, which is subsequently oxidized (by amine oxidase) into MG and other products. Although threonine catabolism contributes less to MG production compared to glycolysis, it becomes more relevant in certain tissues, such as the liver, or under metabolic conditions where amino acid catabolism is upregulated (Hurben et al., 2024; Kold-Christensen & Johannsen, 2020; Tu et al., 2013).

MG formation from lipid peroxidation primarily occurs when fragmented lipid hydroperoxides (formed via ROS attack on lipids) decompose into smaller aldehydes. While MDA and 4-HNE are better-known products of lipid peroxidation, MG is also released in smaller but biologically relevant quantities (Blouin & Saini, 2024). Lipid peroxidation-derived MG contributes to oxidative stress-associated pathologies, such as atherosclerosis, neurodegeneration, and cancer.

It is notorious for forming covalent adducts with nucleophilic sites on both DNA and proteins, leading to the formation of DPCs. MG predominantly reacts with guanine

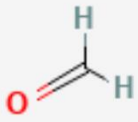
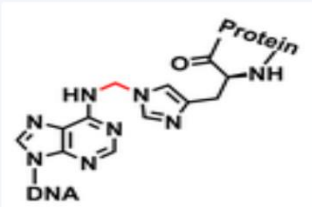
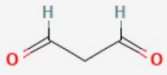
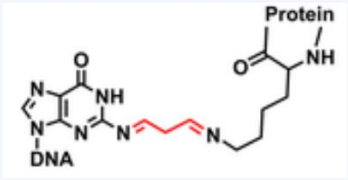
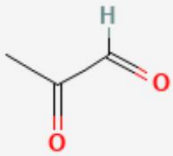
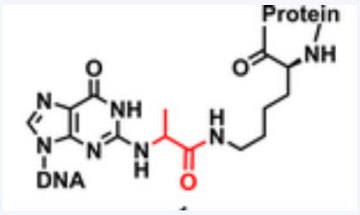
bases in DNA, forming adducts like N^2-(1-carboxyethyl)-2′-deoxyguanosine (CEdG), and with lysine, arginine, and cysteine residues in proteins, generating hydroimidazolones (MG-H1-3) and N^{ε}-(1-carboxyethyl)lysine modifications. These adducts can further interact to bridge DNA and protein molecules, creating DPCs (Brambilla et al., 1985; Hurben et al., 2024; Petrova et al., 2014a). The biochemical mechanism involves MG acting as a bifunctional electrophile, forming a Schiff base intermediate between the exocyclic amino group of guanine (typically the N^2 position) and the ε-amino group of lysine or the thiol group of cysteine. This intermediate can result in a stable covalent linkage between the DNA base and the amino acid residue. Studies have shown that the crosslink formation is enhanced by the addition of reducing agents like sodium borohydride, confirming the role of Schiff base intermediates in MG-induced DPC formation (Hurben et al., 2024; Petrova et al., 2014b).

These biochemical consequences have been substantiated through in vitro and cellular studies. For example, Murata-Kamiya and Kamiya (2001) demonstrated the formation of MG-induced DNA–polymerase crosslinks using the exonuclease-deficient Klenow fragment of *E. coli* DNA polymerase I (Murata-kamiya & Kamiya, 2001). Similarly, proteomic analyses in human cells treated with MG revealed that hundreds of proteins, including histones and metabolic enzymes like GAPDH, become covalently trapped on DNA (Hurben et al., 2024).

Beyond their molecular effects, MG-induced DPCs are implicated in various pathological conditions. Elevated levels of MG and its adducts, known collectively as advanced glycation end products (AGEs), have been detected in individuals with diabetes, cancer, and neurodegenerative diseases. MG-induced DPCs likely contribute to these pathologies by promoting genome instability and cellular

dysfunction (Thornalley et al., 2010). For instance, Thus, MG-induced DPCs may contribute to the mutagenesis and genomic instability associated with these conditions. For instance, glyoxalase I (GLO1) deficiency – which increases cellular MG – leads to higher DPC formation and DNA damage signalling. Conversely, carbonyl scavengers (e.g., aminoguanidine, glutathione precursors) can reduce MG-DPC formation in cell assays, highlighting potential therapeutic angles (Tu et al., 2013). MG's propensity to crosslink chromatin proteins also suggests potential roles in telomere maintenance defects and epigenetic dysregulation, contributing further to disease development. DPCs have been detected in Chinese hamster ovary (CHO) cells, human skin cells, and human endothelial (ECV304) cells following exposure to methylglyoxal. Moreover, MG has been found to induce stable DPCs with the exonuclease-deficient Klenow fragment (Kf−) of *E. coli* DNA polymerase I. In the same study, the extent of crosslink formation increased by approximately 50% upon the addition of sodium borohydride ($NaBH_4$), indicating that the crosslinking mechanism involves a Schiff base intermediate (Brambilla et al., 1985; Petrova et al., 2014b; Tudek et al., 1992).

Table 1.4: Types of Aldehydes, Their Chemical Structures, Endogenous Sources, and Crosslinking Properties

	Chemical Structure	Endogenous Source	Crosslinking Structure
FA		methanol oxidation, methylamine deamination, and histone demethylation	
MDA		lipid peroxidation	
MG		lipid peroxidation, the breakdown of carbohydrates threonine catabolism	

1.2.1.2 Trapping of DNA-Interacting Enzymes

DPCs can arise endogenously when DNA-interacting proteins become covalently trapped on DNA intermediates. The most widely recognized examples are Topoisomerases 1 and 2 (TOP1 and TOP2). They are essential enzymes that alleviate torsional stress in DNA by introducing temporary single-strand or double-strand breaks in the DNA respectively (J. C. Wang, 2002). This process occurs during replication and transcription, in which topoisomerases form transient covalent intermediates with the DNA through a tyrosine-phosphodiester linkage. The cross-link between TOP1 and TOP2 and DNA occurs as physiological intermediates (cleavage complexes, ccs). TOP1 forms a covalent bond between its Tyrosine residue located in the active site

and the 3’ terminus of a SSB forming the TOP1 cleavage complex (TOP1cc). Transient SSBs are produced to untwist the DNA duplex and alleviate supercoiling thereby enabling replication and transcription. Similarly, TOP2 functions to remove DNA supercoils by generating a transient DSB called a TOP2 cleavage complex (TOP2cc), where TOP2 covalently associates with the 5′ end of DSBs (Chen et al., 2013; J. C. Wang, 2002). However, if Topoisomerase encounters DNA containing damage, nicks, or a tightly supercoiled region of DNA, these intermediates can become trapped, resulting in the formation of persistence DPCs (Stantial et al., 2020). Another example is DNA polymerases, which are essential enzymes for DNA replication and repair. These enzymes can also become trapped when encountering certain types of DNA lesions, leading to the formation of DPCs. It has been found that when processing an oxidative DNA lesion, polymerase beta (Pol β) could form a covalent DNA-protein crosslink. This crosslinking appears to be irreversible and dependent on the active-site nucleophile (lysine 72) of Pol β (Demott et al., 2002). Furthermore, poly(ADP-ribose) polymerase 1 (PARP1) is covalently attached to the 3’ end of SSB as part of the DNA damage response. This attachment facilitates the recruitment of DNA repair proteins, promoting the resolution of SSBs through the BER pathway. PARP1 activation also leads to the synthesis of poly(ADP-ribose) (PAR) chains, which serve as signalling molecules to coordinate DNA repair and chromatin remodelling. However, PARP1 can become trapped on DNA when it encounters certain types of lesions, preventing its dissociation and leading to persistent protein-DNA complexes (Prasad et al., 2014). Figure 1.12 shows different types of enzymatic DPCs.

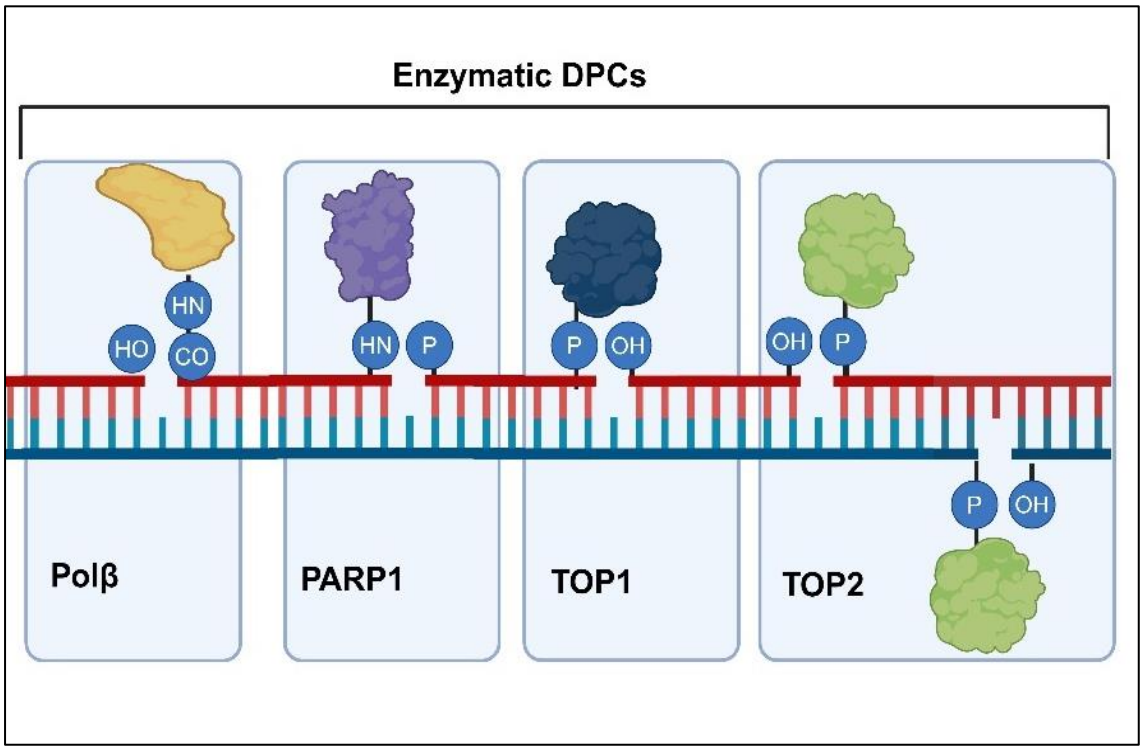


Figure 1.12. Different types of Enzymatic DNA-Protein Crosslinks (DPCs): Adaptive from (Zhang et al., 2020)

Enzymatic DPCs occur when DNA-processing enzymes, such as topoisomerases or DNA polymerases, form covalent bonds with DNA as part of their catalytic activity. These crosslinks are normally transient but can become trapped due to environmental stresses, DNA damage, or failure of repair mechanisms. Both types of DPCs pose significant obstacles to DNA replication and transcription, requiring specialized repair mechanisms, such as proteolytic degradation by enzymes like SPRTN, to resolve the crosslinks and maintain genomic integrity. Polβ; DNA polymerase β, PARP1; poly (ADP-ribose) polymerase-1, TOP1; DNA topoisomerase 1, TOP2; DNA topoisomerase 2. Created using BioRender.com.

1.2.1.3 Abasic sites (AP sites)

Abasic sites, also known as apurinic/apyrimidinic (AP) sites, are the most frequent endogenous DNA lesions with estimates of ~10,000–20,000 per human cell per day (Lindahl & Nyberg, 1972). While DNA is generally a stable biomolecule, this type of DNA lesion can form spontaneously in which the N-glycosyl bond is susceptible to hydrolysis. Under physiological conditions, spontaneous depurination occurs in duplex DNA at an approximate rate of 3×10^{-11} nucleotides per second in vitro. These sites arise when the N-glycosyl bond between a DNA base and its deoxyribose sugar is cleaved, leaving a site without a purine or pyrimidine base (Lindahl & Andersson, 1971). It can also arise as intermediates during base excision repair (BER), where DNA glycosylases generate abasic sites as an intermediate step in the repair of damaged DNA by catalysing the cleavage of the N-glycosidic bond between the modified DNA base and the sugar-phosphate backbone, resulting in the release of the base, which was previously explained in section 1.1.4.1.

The reactive nature of AP sites allows them to interact with nearby proteins, leading to the formation of DPCs. It was shown that histones could be crosslinked with the DNA when AP sites are produced approximately 1.5 helical turns from the nucleosome (Sczepanski et al., 2010). Mechanistic studies have revealed that lysine in histone tails plays a critical role in this process, in which their high reactivity with AP sites is a key factor in this interaction. Lysine forms Schiff bases with the aldehyde functional group of the AP site, resulting in DPC formation (Figure 1.13 A). One study found that among other histones, it was found that the N-terminal region of histone H4 plays a major role in both DPC formation and strand breaks. Interestingly, within nucleosome core

particles, AP sites are highly destabilised, resulting in strand scission occurring approximately 60 times more rapidly than in naked DNA (Sczepanski et al., 2010).

In addition, some repair enzymes like PARP1/2, Pol β, and KU have been identified as interacting with AP sites, resulting in the formation of DNA-protein crosslinks. One study estimated endogenous DPC levels in intact HeLa cells by analysing native AP site-Cys (S-glycosidic) linkages using LC-MS/MS. Their study identified a significant abundance of endogenous DPCs, estimated at around 250,000 per genome(Chan et al., 2019).

A novel mechanism for repairing AP sites in single-stranded DNA (ssDNA) has been recently identified. HMCES (5-hydroxymethylcytosine embryonic stem cell-specific) crosslinked with AP sites acting as a shielding protein and protecting cells against strand breaks. Specifically, the conserved catalytic SOS response-associated peptidase (SRAP) domain of HMCES plays a critical role in replication fork stability by crosslinking to AP sites in ssDNA. The formation of DNA-protein crosslinks (DPCs) is thought to initiate when the N-terminal amino group attacks the open-ring aldehyde form of the AP site, forming a Schiff base intermediate. This intermediate is subsequently stabilized into a thiazolidine ring through interaction with the sulfhydryl group of Cys2. This mechanism highlights the protective role of HMCES in genomic integrity, particularly in preventing strand breaks at sites of replication stress (Figure 1.13 B) (Mohni et al., 2019; Semlow et al., 2022).

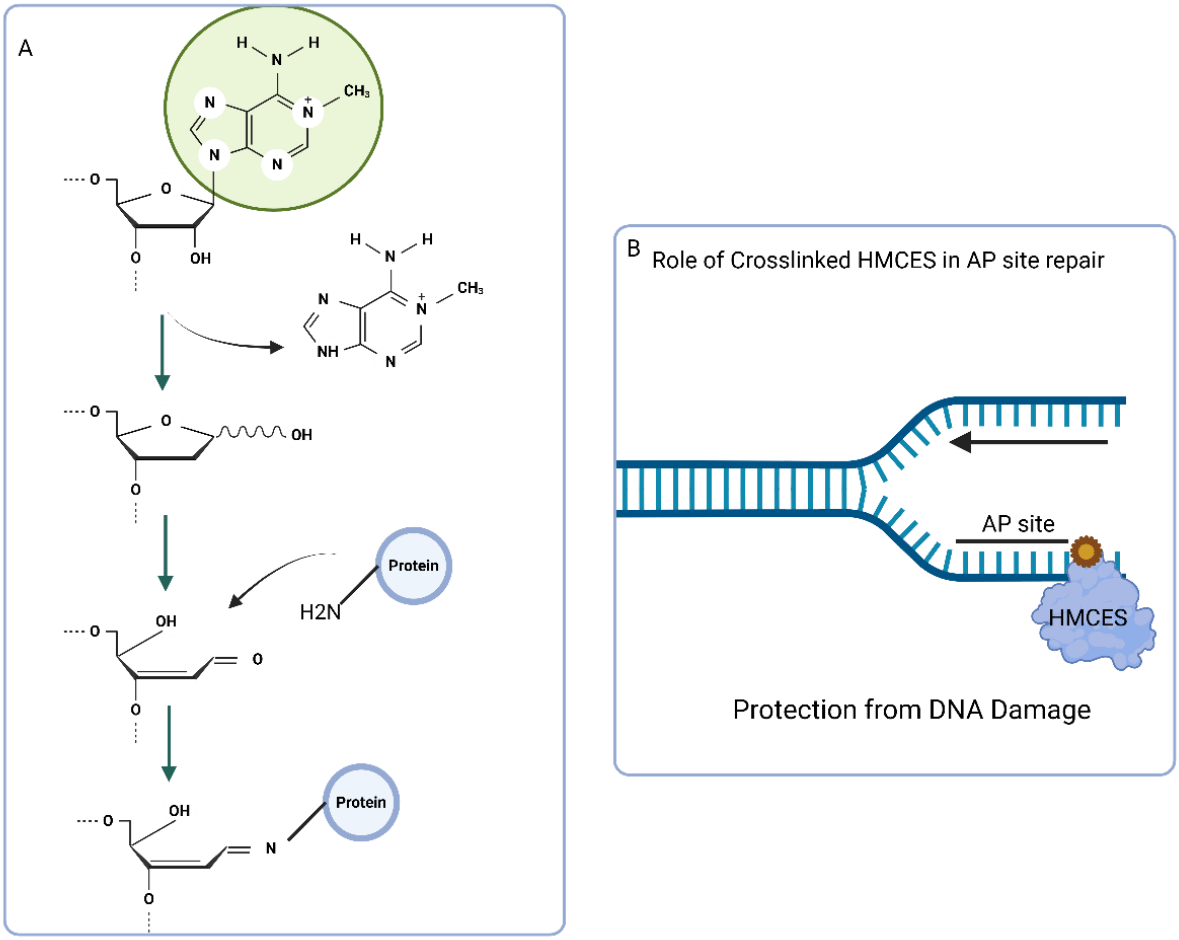


Figure 1.13. Formation of DNA-protein crosslinks (DPCs) at abasic sites

(A) Methylated DNA bases, such as 3-methyladenine, undergo spontaneous or enzymatic hydrolysis, leading to the formation of abasic (AP) sites. These sites exist in different chemical states, including the hemiacetal intermediate and the open-chain aldehyde form, which are highly reactive. The aldehyde form can covalently trap nearby proteins, leading to the formation of abasic site-derived DPCs.
(B) At stalled replication forks, HMCES (5-hydroxymethylcytosine binding, ES domain-containing protein) recognizes and covalently crosslinks to abasic sites, preventing DNA strand cleavage and promoting fork stability. This mechanism provides a protective role in preventing potentially lethal DNA damage during replication stress.

1.2.1.4 Reactive Oxygen Species (ROS)

Cellular metabolic processes, particularly aerobic respiration, contribute significantly to ROS production. The mitochondrial respiratory chain, where electron leakage leads to the formation of superoxide ($O_2^{\bullet -}$) and hydrogen peroxide (H_2O_2). Additionally, NADPH oxidase (NOX) and dual oxidase (DUOX) enzymes play a crucial role in generating superoxide and H_2O_2, especially in immune responses and redox signalling. Another important source of ROS is the peroxisomes, specialized organelles that contain oxidases, such as polyamine oxidases, which generate H_2O_2 as a byproduct. Peroxisomes also contain catalase, an enzyme responsible for detoxifying excess ROS, preventing oxidative damage. These multiple cellular sources of ROS highlight the complex regulation of oxidative stress within the cell (Murphy, 2009).

The concentration of ROS must be carefully regulated to maintain a stable redox balance, which is achieved through antioxidant defence mechanisms. However, excessive ROS production, triggered by environmental stressors or pathophysiological conditions, can overwhelm the cellular antioxidant system, leading to oxidative stress. This imbalance has been implicated in the development of various diseases, including cancer and neurodegenerative disorders. The impact of oxidative stress depends on ROS levels and their localization within the cell, influencing different biomolecules such as lipids, proteins, and nucleic acids(Beatty et al., 2000; Reczek & Chandel, 2017).

ROS are highly reactive molecules that can cause oxidative damage to various cellular components. The effect of ROS on DNA can be either through direct interactions with DNA or by modifying proteins involved in DNA maintenance and repair. Studies have

identified over 100 different oxidatively generated base lesions and modifications in in vitro experiments (Cadet et al., 1999).

One of the major consequences of ROS-induced DNA damage is the formation of DPCs. Simultaneous oxidative damage to both DNA and proteins by ROS creates favourable conditions for covalent crosslinking. Moreover, ROS can directly modify amino acid residues in proteins (e.g., cysteine, histidine, lysine, and tyrosine), increasing their reactivity toward DNA. ROS activity can lead to covalent crosslinking of tyrosine residues in proteins to DNA. In addition, ROS can oxidize deoxyribose sugars and nucleobases, leading to the generation of AP sites which, as mentioned earlier, a hotspot for DPCs formation (Grimsrud et al., 2008).

ROS-induced DPCs can involve various covalent interactions, such as crosslinks between the ε-amino group of lysine and spirodiiminodihydantoin in DNA, lysine and guanidinohydantoine in DNA, tyrosine and 8-oxoguanosine in DNA, Nε-lysine guanin-8-yl cross-links, and tyrosine-thymidine (dT-Tyr) adducts (H.Kasai, P.F.Crain, Y.Kuchino, S.Nishimura, 1986; Johansen et al., 2005; Perrier et al., 2006; Xu et al., 2008).

Mass spectrometry-based studies have identified hundreds of proteins capable of crosslinking to nuclear DNA under oxidative stress conditions. A study found that radical-induced DPCs in cardiomyocytes following ischemia-reperfusion injury in a rat model was formed. Using a highly sensitive isotope dilution nanoLC-NSI+-MS/MS assay to identify hydroxyl radical-mediated DPCs, nearly 90 proteins contribute to hydroxyl radical-induced DPC formation, including ROS scavengers, contractile proteins, and apoptosis regulators. These findings support a model in which the sudden reintroduction of oxygen to ischemic tissues triggers oxidative stress, inflammation, and DPC formation (Groehler et al., 2018).

1.2.1.5 Chemotherapy Agents

Given the toxic effects of DPCs, various physical and chemical agents induce their formation, contributing to their therapeutic effects by disrupting cellular processes, particularly in cancer treatment. Chemotherapeutic agents used in clinical practice are known to induce both enzymatic and non-enzymatic DPCs. Platinum-based compounds, such as cisplatin, carboplatin, and oxaliplatin, generate non-enzymatic DPCs through nonspecific crosslinking of chromatin-associated proteins to DNA. Other chemotherapeutic agents such as camptothecin (CPT) derivatives, such as irinotecan and topotecan induce enzymatic DPCs by either stabilising covalent DNA-protein reaction intermediates or creating pseudosubstrates that trap the enzyme on DNA.

CPT derivatives selectively trap DNA topoisomerase 1 (TOP1) by intercalating into the enzyme–DNA interface, stabilising the covalent intermediate formed during the enzyme's catalytic cycle. During the normal catalytic cycle of TOP1, transient single-strand breaks are introduced to relieve torsional strain in the DNA helix. This class of chemotherapeutic drugs functions by stabilising the TOP1-DNA cleavage complex and preventing the re-ligation of these breaks, leading to the persistence of DNA damage (Fielden et al., 2020; Hsiang et al., 1985). When replication forks collide with the trapped TOP1-DNA complexes, they generate lethal double-strand breaks. Thus, the cytotoxicity of these drugs is not due to the inhibition of TOP1 catalytic activity but rather to the trapping of the enzyme on DNA, leading to replication stress and DNA damage (J. C. Wang, 2002).

Enzyme poisons that trap TOP2 are another class of chemotherapeutic agents widely used in the treatment of various human tumours, such as bladder, testicular, prostate, stomach, and lung cancer. These agents fall into three main categories: etoposide and

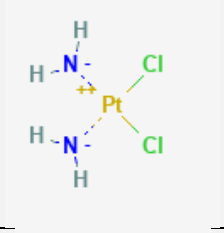
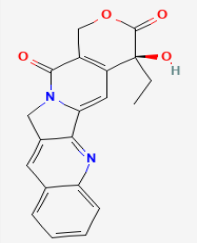
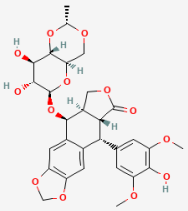
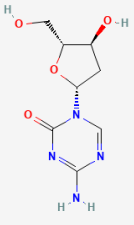
its analogue teniposide; anthracyclines such as doxorubicin, daunorubicin, epirubicin, and idarubicin; and the anthraquinone compound mitoxantrone (Hande, 1998). Similar to TOP1 trapping drugs, these drugs exert their cytotoxic effects by stabilising the transient covalent TOP2-DNA intermediate formed during the enzyme's catalytic cycle, effectively "trapping" the enzyme on DNA. Specifically, etoposide stabilises the TOP2 cleavage complexes by inhibiting the second step of the reaction—DNA re-ligation—thereby trapping the enzyme in a covalent complex with DNA.

Cellular sensitivity to these drugs is directly dependent on the expression levels of TOP1 or TOP2, as higher levels of these enzymes result in increased formation of trapped complexes and irreparable DNA damage. This mechanism classifies these agents as enzyme poisons rather than simple inhibitors, highlighting their reliance on the catalytic activity of topoisomerases to generate cytotoxic effects (W. T. Beck et al., 1993; Nitiss & Beck, 1996).

Platinum-based compounds, such as cisplatin—the first FDA-approved platinum anticancer drug—carboplatin, and oxaliplatin, are widely used to treat cancers including bladder, head and neck, lung, ovarian, and testicular cancers (Rosenberg et al., 1969). While the primary mechanism of action of platinum agents involves the formation of DNA-DNA intrastrand crosslinks, DPCs also play a role in their therapeutic effects. Cisplatin and its derivatives induce nonspecific crosslinking of chromatin-interacting proteins to DNA including histones or cytokeratins, to DNA. It was shown that it forms a ternary DNA–platinum–protein crosslink and is recognised as a significant contributors to cytotoxicity at clinically relevant doses (Chválová et al., 2007; Xun Minga, Erin D. Michaelson-Richiea, Arnold S. Groehler IVd, Peter W. Villaltab, Colin Campbellc, 2020).

Another example of chemotherapeutic agent that induces DPCs is 5-aza-dC, a cytosine analogue that becomes incorporated into DNA and functions as a pseudosubstrate for DNA (cytosine-5)-methyltransferase 1 (DNMT1), leading to the enzyme's covalent trapping. Beyond inducing DPCs, the antitumour effects of 5-aza-dC arise from its ability to inhibit DNMT1, causing a global reduction in DNA methylation (Christman, 2002). Table 1.4 show different types of chemotherapy drugs that cause DPC Formation.

Table 1.5. Chemotherapy Agents and DPC Formation

Chemotherapeutic Agent	Chemical Structure	Crosslink Structure	Target Cancer Types	Reference
Cisplatin		DNA-protein crosslinks with chromatin-associated proteins	Bladder, head and neck, lung, ovarian, testicular	(Rosenberg et al., 1969)
Camptothecin		Trapped TOP1-DNA cleavage complex	Colorectal, lung, ovarian, cervical	(Hsiang et al., 1985)
Etoposide		Trapped TOP2-DNA cleavage complex	Lung, testicular, prostate, stomach, bladder	(Hande, 1998)
5-Aza-2'-deoxycytidine (5-aza-dC)		Covalent trapping of DNMT1 enzyme to DNA	Myelodysplastic syndromes, leukemia	(Christman, 2002)

1.2.1.6 ionizing radiation and Ultraviolet light

IR is one approach to inhibit the proliferation of cancer cells and is effective in killing cells by causing various types of DNA lesions (Cadet et al., 2008). Ionizing radiation causes different types of DNA damage such as SSBs, DSBs, AP sites and DPCs through both direct and indirect mechanisms (Eriksson & Stigbrand, 2010; Lomax et al., 2013b). In the direct mechanism, radiation energy is deposited directly onto DNA, resulting in the formation of unstable DNA radical cations that subsequently decompose. In the indirect mechanism, radiation energy is absorbed by water, the primary cellular medium, generating reactive oxygen species such as hydroxyl radicals (•OH). These •OH radicals attack DNA, producing DNA radicals that are similarly unstable and prone to decomposition. Ionizing radiation also damages these chromatin-associated proteins through direct energy deposition and indirect oxidative processes. DNA and protein radicals generated by radiation can either decompose independently or react with nearby proteins or DNA, leading to the formation of covalent bonds between DNA and proteins (Figure 1.14A and 3B). Alternatively, these radicals may recombine to form covalent DPCs. In addition, proteins may react with AP sites caused by radiation forming DPCs (Barker et al., 2005; Nakano et al., 2015, 2017).

Interestingly, DPC formation is significantly enhanced when cells or tissues are exposed to radiation under hypoxic conditions. This phenomenon, known as the reverse oxygen effect, is a distinctive characteristic of radiation-induced DPCs. Studies have demonstrated that hypoxic environments lead to a higher DPC yield compared to normoxic conditions (Acta & Health, 1977; Nakano et al., 2015; Radford, 1985; Shoulkamy et al., 2012). For instance, when mouse squamous carcinoma cell

(SCC) VII tumours were irradiated with X-rays, DPC formation—detected using the FITC-labelling method—was observed to be three times greater in hypoxic tumours than in normoxic tumours (Nakano et al., 2015). The higher levels of DPCs under hypoxia could be explained by the fact that hypoxia may impair cellular mechanisms responsible for DPC repair, leading to the persistence of these lesions. Another explanation is that the reduced availability of oxygen during irradiation alters the chemical pathways leading to DPC formation, increasing their persistence (Figure 1.14C) (Nakano et al., 2017).

Ultraviolet (UV) radiation can lead to the formation of DPCs by directly interacting with DNA and proteins. When cells are exposed to UV light, particularly at a wavelength of 254 nm, the energy facilitates the creation of covalent bonds between nearby nucleic acids and proteins. These UV-induced DPCs can disrupt critical cellular functions such as replication and transcription, ultimately contributing to genomic instability. Additionally, UV irradiation has been effectively employed to crosslink single-stranded (ss) and double-stranded (ds) DNA with proteins, enabling the study of chromatin dynamics. As a result, UV-induced crosslinking, in combination with mass spectrometry (MS), represents a valuable tool for exploring functional and structural relationships in DNA–protein systems (Molnar et al., 1995; Stützer et al., 2020).

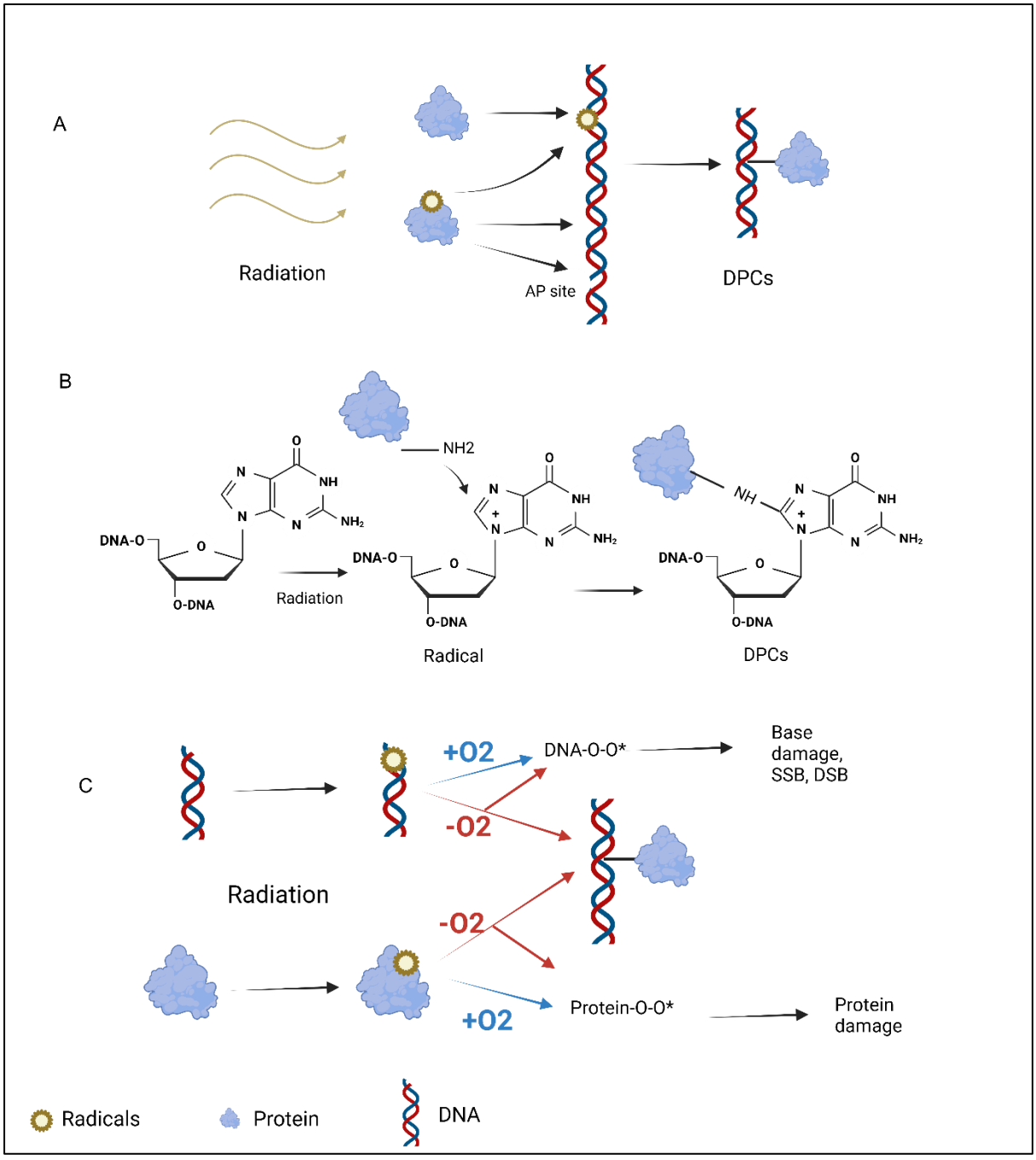


Figure 1.14. Proposed mechanisms of DNA–protein crosslink (DPC) formation following ionizing radiation.

(A) ionizing radiation affects molecules either directly or indirectly. It generates hydroxyl radicals (•OH) by radiolysis of water. These highly reactive species attack DNA, generating DNA radicals that are unstable and prone to decomposition. Simultaneously, ionizing radiation damages chromatin-associated proteins, both through direct energy deposition and indirectly via oxidative mechanisms. The resulting DNA and protein radicals can either decompose

independently or react with each other or with nearby non-radical sites, such as DNA abasic sites or amino acid side chains, leading to the formation of covalent DPCs.

(B) Radiation-induced DPC formation via base damage and reactive intermediates: Ionizing radiation induces base methylation and other forms of DNA base damage, which can lead to abasic (AP) site formation. These sites are chemically reactive and can form covalent bonds with nearby proteins, especially through nucleophilic attack by amino acid side chains. Additionally, radiation generates reactive radicals in both DNA and associated proteins. These radicals can either react directly with each other, forming covalent DPCs, or interact with non-radical counterparts (e.g., AP sites), stabilizing the crosslink. This pathway highlights how both chemical base modifications and free radical chemistry contribute to DPC generation. (C)In the presence of oxygen (blue pathway), DNA and protein radicals formed along the radiation track rapidly react with molecular oxygen to generate less reactive peroxyl radicals or hydroperoxides. These intermediates primarily undergo self-decomposition, leading to the formation of DNA and protein degradation products rather than crosslinks.
In contrast, in the absence of oxygen (red pathway), DNA and protein radicals can directly interact—either by radical addition of DNA to protein (or vice versa), or through radical recombination resulting in the formation of covalent DPCs.

1.2.2 Types of DNA-Protein Crosslinks

There is a diversity in the nature of DPCs, in terms of the size of crosslinked protein, number and nature of covalent bonds, as well as temporal distribution of crosslink occurrence. These variations determine how DPCs affect cellular processes and how they are ultimately repaired. Each of these groups poses distinct challenges to the cell's ability to maintain genomic integrity, each requiring specific mechanisms of repair and removal which will be explained in the following section.

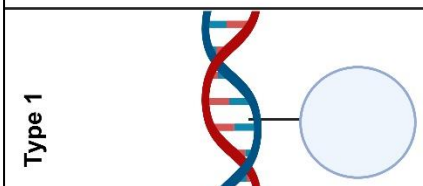
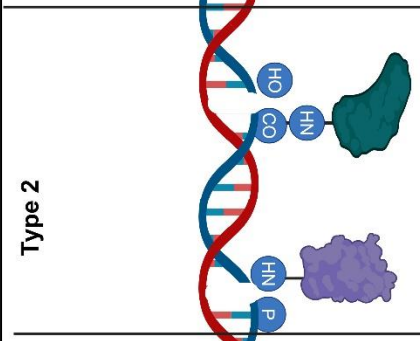
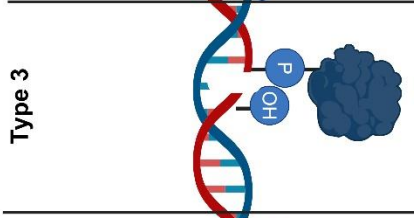
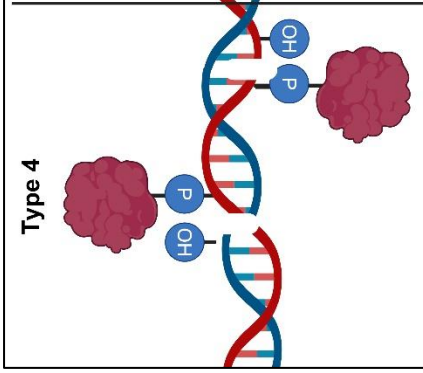
Here, DPCs are classified into four types based on cross-linking bond and flanking DNA nicks:

Type 1 DPCs consist of proteins covalently bound to an intact DNA strand. They include a wide range of proteins that can become covalently attached to DNA without being specific to a particular enzymatic activity or function. It can involve virtually any protein, regardless of its size, structure, or nature, as long as it is in close proximity to DNA. This type of DPC is likely the most frequently formed as a result of exposure to ionising radiation, UV light, aldehydes, chromate, and platinum-based compounds (Barker, Weinfeld, Zheng, et al., 2005; Chválová et al., 2007; Nakamura & Nakamura, 2020; Stützer et al., 2020).

Type 2 DPCs include enzymes that are crosslinked to the ends of SSBs and arise from abortive DNA repair processes. This primarily includes PARP 1 and DNA polymerase (Pol) β, which are covalently attached to the 3' and 5' ends of a SSB, respectively (Prasad et al., 2014; Quiñones et al., 2015). These unsuccessful repair events not only lead to the formation of stable DPCs but also interfere with further repair processes, potentially blocking replication and transcription and contributing to genomic instability.

Type 3 DPCs involve Top1 covalently linked to the 3’ end of a SSB through a tyrosinyl–phosphodiester bond. In contrast, Type 4 DPCs occur when Top2 becomes attached to the two 5’ ends of a DSB via similar tyrosinyl–phosphodiester bonds. Both Types 3 and 4 DPCs are generated when the covalent reaction intermediates of Top1 and Top2 are trapped, either by topoisomerase poisons or by adjacent DNA damage (Ledesma et al., 2009; Pommier, 2009). Table 1.6 shows a comparison between different DPCs types.

Table 1.6: Comparison of Different DPC Types

Type	Formation Mechanism	Proteins Involved
Type 1 	Exposure to ionizing radiation, UV light, aldehydes, chromate, and platinum-based compounds	Any protein in close proximity to DNA.
Type 2 	.Abortive DNA repair processes leading to stable DPC formation at SSBs.	PARP1 and DNA polymerase (Pol) Î².
Type 3 	Trapping of Top1-DNA intermediates by topoisomerase poisons or adjacent DNA damage.	Topoisomerase 1 (Top1).
Type 4 	Trapping of Top2-DNA intermediates by topoisomerase poisons or adjacent DNA damage.	Topoisomerase 2 (Top2).

1.2.3 Toxicity of DPCs

1.2.3.1 Effect on DNA Replication and Transcription

DPCs are physical blocks and DNA and RNA polymerases are unable to extend over them. Thus, they obstruct the progression of DNA polymerases during replication. This stalling of the replication fork can lead to incomplete DNA replication, ultimately causing cell cycle arrest. Moreover, this inhibition can lead to a reduction in gene expression, disrupting normal cellular functions and potentially leading to cell death (Chválová et al., 2007; Yeo et al., 2014). (Figure 1.15).

1.2.3.2 Induction of Further DNA Damage

The presence of DPCs increases the vulnerability of the DNA to further damage. When the replication fork encounters a DPC, the stalling can lead to the collapse of the fork, resulting in DSBs (Kumari et al., 2012; Lessel, Vaz, Halder, Lockhart, Marinovic-Terzic, et al., 2014). These breaks are particularly toxic and challenging to repair, contributing to genomic instability. Additionally, DPCs hinder the accessibility of DNA repair and chromatin remodelling factors with genotoxic consequences, such as chromatid breaks, chromosomal aberrations, and mutations (Barker, Weinfeld, & Murray, 2005; Halder et al., 2019).

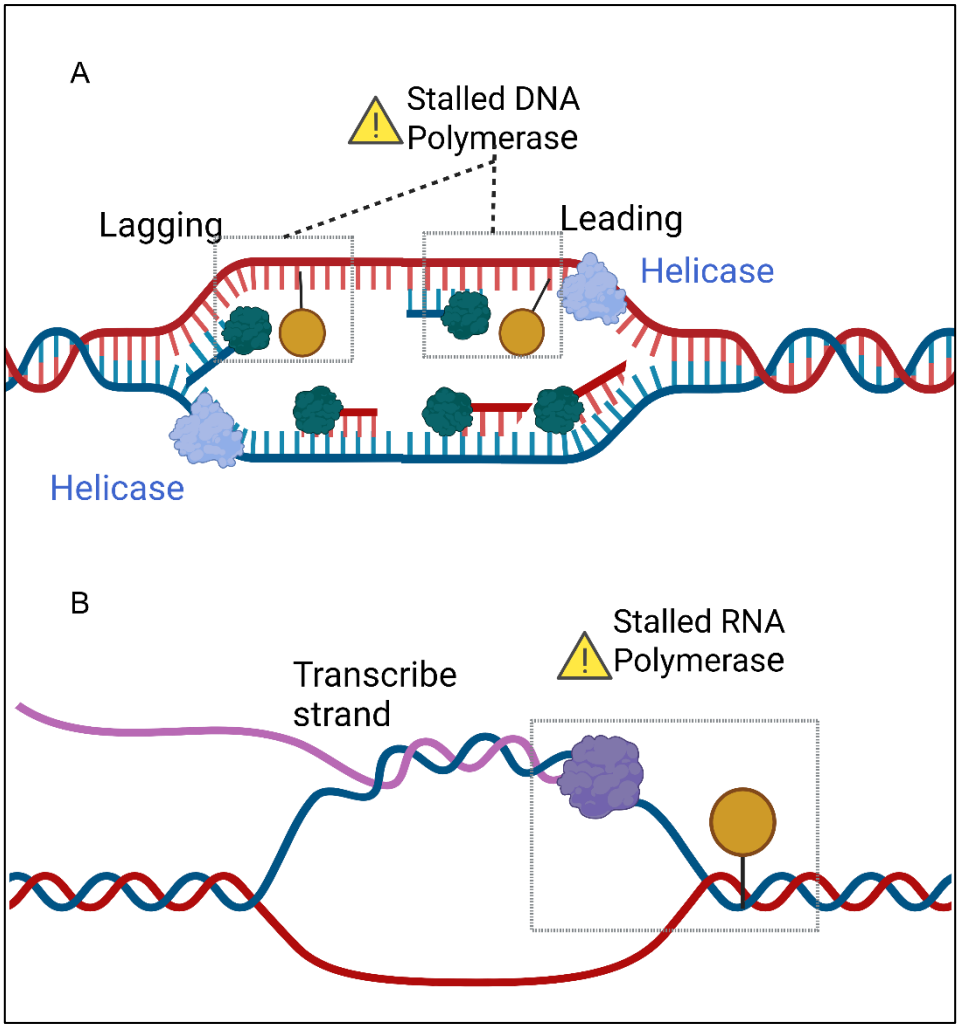


Figure 1.15: Toxicity of unresolved DPC during replication and transcription

(Adapted from (Ruggiano & Ramadan, 2021b)

A) DPCs on either the leading or lagging strand can obstruct the progression of helicases and polymerases, hindering DNA replication.
B) DPCs have the potential to block transcription; however, the mechanisms underlying transcription-dependent DPC proteolysis remain largely unexplored.

1.2.4 DPCs repair pathway

Cells utilize different pathways to repair DPCs, ensuring that both actively dividing and non-dividing cells can resolve these toxic lesions. The coordination of these repair pathways is crucial for maintaining genomic integrity, and defects in DPC repair have been linked to cancer, aging, and neurodegenerative diseases. Due to the intricate nature of DPC lesions, which involve DNA, protein, and a covalent bond linking them, their repair requires the coordinated involvement of multiple DNA repair pathways. These mechanisms vary depending on the type, size, and context of the DPC, ensuring a flexible and effective response to different forms of damage. The main stages of DPC repair include proteolysis of the crosslinked protein to produce DNA-peptide adducts, followed by either bypass or hydrolysis of these adducts. This process is then completed by repairing the resulting single- or double-strand DNA breaks to restore genomic integrity. DPCs repair pathways can be classified based on different factors. Here, they are classified based on the mechanism of crosslink resolution and based on transcription and replication dependency.

1.2.4.1 Classification of DPC Repair Pathways based on the mechanism of crosslink resolution

DPCs repair could be classified into three main pathways based on the mechanism of crosslink resolution: 1) Nuclease-dependent repair mechanisms, 2) Hydrolysis of the crosslink (bond) between protein and DNA, 3) Proteolysis-dependent repair mechanisms (Figure 1.16).

*1.*2.4.1.1 Nuclease-Dependent Repair Mechanisms

Two canonical DNA repair pathways were found to be involved in DPCs removal: nucleotide excision repair (NER) and homologous recombination (HR). They are both

dependent on nucleases that cleave the DNA flanking the DPC (Nakano et al., 2007). However, NER has a limited role in DPC repair, since it can remove small DPCs (8–10 kDa in size in mammalian cells). On the other hand, the role of HR in removing bulky DPCs requires DSB formation (Vaz et al., 2016).

1.2.4.1.2 Hydrolysis of The Cross-Link Between Proteins and DNA

The cross-link between TOP1 and TOP2 and DNA occurs as physiological intermediates (cleavage complexes, ccs). TOP1 forms a covalent bond between its Tyrosine residue located in the active site and the 3' terminus of a SSB forming the TOP1 cleavage complex (TOP1cc). Transient SSBs are produced to untwist the DNA duplex and alleviate supercoiling thereby enabling replication and transcription. Similarly, TOP2 functions to remove DNA supercoils by generating a transient DSB called a TOP2 cleavage complex (TOP2cc), where TOP2 covalently associates with the 5′ end of DSBs (J. C. Wang, 2002).

However, TOP1cc and TOP2cc could be stabilized on the DNA due to a fault or the presence of topoisomerase inhibitors such as camptothecin (CPT) and etoposide respectively (Hande, 1998; Hsiang et al., 1985). These types of cross-links are mainly repaired by a two-step pathway. First, TOP1cc/TOP2cc undergo sumoylation by small ubiquitin-related modifier (SUMO), a process facilitated by E3 SUMO-protein ligase PIAS4 (protein inhibitor of activated STAT protein 4). Then, Ring Finger Protein 4 (RNF4) identifies and binds K48-linked polyubiquitin chains to the SUMOylated TOP-DPCs. The 26S proteasome subsequently targets the ubiquitylated TOP-DPCs(Sun et al., 2020). This will expose the crosslink facilitating the access of DNA repair enzymes including Tyrosyl-DNA phosphodiesterases 1 and 2 (TDP1 and TDP2)(Lin et al., 2008; Tsuda et al., 2020). TDP1 and TDP2 will work on the hydrolysis of

crosslink bonds formed between DNA and the associated topoisomerases TOP1 and TOP2, respectively (Debéthune et al., 2002; J. C. Wang, 2002).

1.2.4.1.3 Proteolysis-Dependent DPCs Repair

Proteolysis-dependent mechanisms remove the protein component of the DPCs. One of the early mechanisms is proteosomes, which are involved in removing DPCs and their recruitment requires polyubiquitylation of DPC by the ubiquitin ligase activity of TRAF Interacting Protein (TRAIP) (Larsen et al., 2019; Quievryn & Zhitkovich, 2000). However, the inhibition of proteasome activity in egg extracts did not significantly impact DPC repair, indicating that an alternative process that operates independently of the proteasome (Duxin et al., 2014).

In 2014, researchers found a protease-dependent mechanism for DPC repair in S. cerevisiae called weak suppressor of smt3 (Wss1). The results indicated that TDP1-deficient cells are heavily reliant on Wss1 expression for their viability. The double mutant cells, ΔWss11ΔTdp1, were observed to experience cell cycle arrest, exhibit slow growth, and activate the DNA damage checkpoint (Stingele et al., 2014). A similar mechanism was suggested in higher eukaryotes, which was later characterized as one of the essential proteases, which is SPRTN (SprT-like N-terminal domain, also known as Spartan or DVC-1) (Duxin et al., 2014; Lessel, Vaz, Halder, Lockhart, Marinovic-terzic, et al., 2014; Lopez-Mosqueda et al., 2016; Vaz et al., 2016). Our lab was among the first to investigate the impact of SPRTN gene mutations on human health before discovering its role in DPCs proteolysis. Biallelic germline mutations in SPRTN were identified in three patients from two unrelated families in which these individuals presented with a novel segmental progeroid syndrome, characterised by genomic instability, early-onset hepatocellular carcinoma, and distinct progeroid features (Lessel, Vaz, Halder, Lockhart, Marinovic-terzic, et al., 2014). Alternative DPC

proteases include GCNA (Germ cell nuclear acidic protein), FAM111A and B (Family with sequence similarity 111 member A), DDI1 (DNA damage inducible 1) (Table 1.7). A detailed review was published by our lab explaining these proteases (Ruggiano & Ramadan, 2021b).

Table 1.7. Genes encoding for DPC proteases and their known functions

Name	Function	Reference
FAM111A	Interacts with PCNA. Eliminates DPCs during DNA replication through its trypsin-like protease domain. Acts specifically on PARP1-DNA complexes, induced by PARP inhibitors such as niraparib, and Top1ccs.	(Kojima et al., 2020; Welter & Machida, 2022)
FAM111B	Shares over 45% of sequence homology with FAM111B. Poorly characterized trypsin/cysteine-like protease. Protein levels increase during S-phase.The role of FAM111B in DNA repair has never been investigated.	(Arowolo et al., 2022; Kawasaki et al., 2020)
GCNA	Found in pluripotent cells and germ cells. Plays a role in repairing TOP2ccs.	(Dokshin et al., 2020)
DDI1	Ubiquitin-dependent aspartic protease. S-phase dependent repair of TOP1ccs in Saccharomyces cerevisiae. Its role in humans is under investigation.	(Yip et al., 2020)

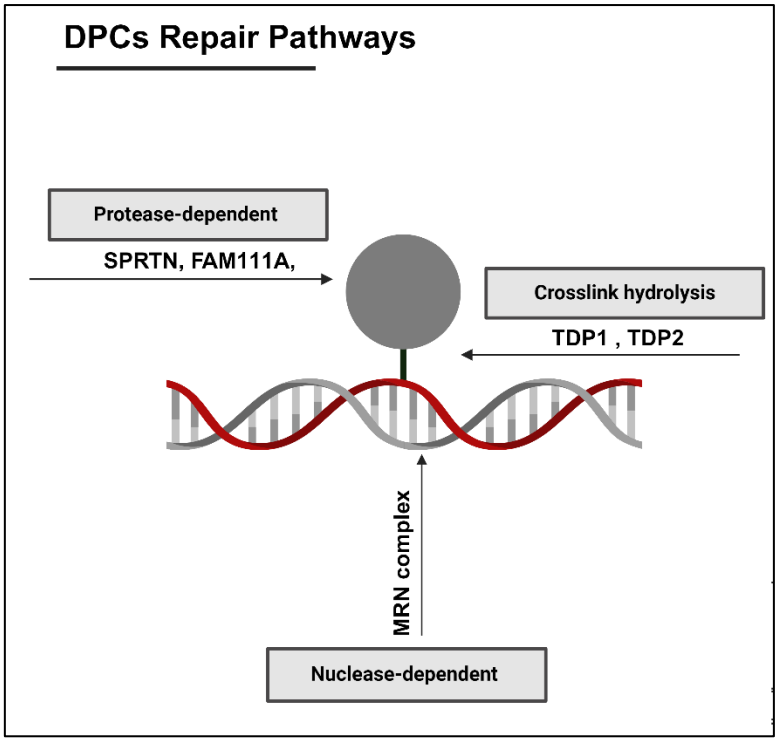


Figure 1.16. DNA-Protein Crosslink (DPC) repair pathways. Adaptive from (Fielden et al., 2018)

Three main repair pathways for DNA-protein crosslinks. Protease-dependent repair involves the proteolytic degradation of the protein component of the DPC by enzymes such as SPRTN or the proteasome, allowing DNA repair machinery access to the DNA. Crosslink hydrolysis-dependent repair involves enzymes such as TDP1 and TDP2, which hydrolyse the covalent bond between the protein and the DNA, effectively removing the crosslink. Nuclease-dependent repair involves nucleases, such as MRN complex, which cleave the DNA around the DPC, excising the crosslink and facilitating subsequent repair. SPRTN: SprT-Like N-Terminal Domain, TDP1: Tyrosyl-DNA phosphodiesterases 1, TDP2: Tyrosyl-DNA phosphodiesterases 2, MRN complex; MRE11-RAD50-NBS1. Created using BioRender.com.

1.2.4.2 DPC Repair Pathways Classified by Their Association with Replication and Transcription-Dependent Mechanisms

1.2.4.2.1 Replication-coupled repair:

Replication-coupled DPC repair is triggered when replication forks encounter protein adducts on the DNA template. The CMG (CDC45-MCM2-7-GINS) helicase, responsible for unwinding the DNA template while moving along the leading strand, is capable of bypassing protein adducts present on the lagging strand (Sparks et al., 2019). However, when DPCs obstruct the leading strand, they initially impede CMG progression. It was found that the DNA helicase RTEL1 promotes DPC bypass by generating single-stranded DNA downstream of the crosslink. In the absence of RTEL1, DPC proteolysis is impaired, indicating that CMG helicase must bypass the DPC to facilitate its degradation by DPC proteases (Sparks et al., 2019).

SPRTN serves as the primary DPC protease during the S phase. Our lab found that SPRTN knockdown cells, when synchronized, exhibit an increased accumulation of DPCs during S phase(Vaz et al., 2016). In addition, we and others found that SPRTN depletion disrupts replication progression, and this effect is further exacerbated when cells are treated with formaldehyde or CPT. The ability of full-length SPRTN, but not the catalytically inactive mutant, to rescue these defects suggests that SPRTN functions alongside the replisome, actively degrading endogenous DPCs encountered by the replication fork (Halder et al., 2019; Stingele et al., 2016a; Vaz et al., 2016; Weickert et al., 2023a). A study by our lab revealed that both ubiquitination and SUMOylation of DPCs play crucial roles in facilitating their repair by SPRTN. Ubiquitination serves as a signal for SPRTN recruitment to DPC sites, while SUMOylation suppresses homologous recombination (HR), ensuring that DPC repair proceeds through the SPRTN-mediated pathway(Ruggiano et al., 2021). In addition,

SPRTN is found to be capable of repairing unmodified DPCs, in which SPRTN-mediated degradation is triggered when a DNA polymerase stalls within a few nucleotides of the lesion on either the leading or lagging strand, independent of whether the DPC has undergone polyubiquitination (Larsen et al., 2019). The detailed mechanism of repairing DPCs by SPRTN is explained in section 1.3.

In addition to SPRTN, recent studies have identified additional proteases involved in the repair of specific types of DNA-protein crosslinks. One such enzyme, FAM111A, a protein containing a trypsin-like protease domain, has been shown to prevent replication fork stalling and facilitate DPC repair (Kojima et al., 2020; Welter & Machida, 2022) FAM111A interacts with PCNA, exhibits chymotrypsin-like protease activity, and undergoes DNA-dependent autocleavage in trans. In mammalian cells, it plays a role in the repair of TOP1-cc and PARP1-DNA crosslinks. Unlike SPRTN-deficient cells, which display significant sensitivity to DPC-inducing agents, FAM111A knockout cells exhibit only mild sensitivity to formaldehyde, suggesting that FAM111A is specifically involved in the repair of a subset of DPCs.

Moreover, there is evidence of the involvement of proteasomes in replication-coupled DPCs repair. Using Xenopus egg extracts, a study demonstrated that in addition to SPRTN, 26S proteasome is involved (Larsen et al., 2019). They showed that only the simultaneous depletion of SPRTN and inhibition of the proteasome led to a significant impairment in DPC repair, indicating that these two pathways function through distinct activation mechanisms. They found that proteasome-mediated DPC degradation, DPCs are polyubiquitinated by the ubiquitin ligase TRAIP. This modification facilitates the CMG helicase in bypassing the protein adduct and promotes its subsequent degradation by the proteasome is essential for recognizing the lesion and initiating its breakdown. It has been suggested that SPRTN may be necessary for a secondary

proteolytic cleavage event to facilitate TLS bypass of DNA-peptide crosslinks, even if the initial degradation was carried out by the proteasome (Larsen et al., 2019). On the other hand, some studies did not find a strong indication of the involvement of proteasomes in DPCs during replication. A study found that proteasome inhibition using MG132 in egg extracts did not significantly impact DPC repair during replication, suggesting that this process operates independently of the proteasome. Moreover, our lab observed a minor, though not statistically significant, defect in DPC clearance when proteasome activity was inhibited in SPRTN-depleted cells (Duxin et al., 2014). This suggests that the proteasome may assist in total DPC repair when SPRTN's capacity is exceeded. Additionally, we noted a slight delay in Topo-1cc repair following MG132 treatment, particularly when low-dose CPT was used to induce crosslinks (Ruggiano et al., 2021). Collectively, these findings indicate that while the proteasome may play a role in certain contexts, replication-coupled DPC repair can proceed through proteasome-independent mechanisms.

The proteolytic degradation during the process of DNA replication can lead to the near-total breakdown of the protein that is covalently attached to the DNA. This process results in the formation of a minor peptide-DNA adduct, which can subsequently be circumvented by the replicative CDC45–MCM2/7–GINS (CMG) helicase (Ishimi & Ide, 2013; Stingele et al., n.d.). Following this, DNA synthesis can continue over the peptide-DNA adduct, aided by a translesion synthesis polymerase such as DNA polymerase ζ (Larsen et al., 2019). Residual peptide-DNA adduct may also be eliminated post-replicative via the NER pathway (Baker et al., 2007).

In addition, homologous recombination, a canonical DNA repair pathway involves in repairing DSBs, was shown to be involved in removing DPCs, independently of or as a subsequent step of proteolytic repair. Although the exact mechanism of the involvement of HR in DPCs removal is not well characterized, certain HR-associated components have been identified as key players in DPC removal. Notably, the MRE11-RAD50-NBS1 (MRN) complex has been implicated in the removal of TOP2-ccs across multiple organisms during S-phase. The repair of antitumour agent-induced TOP-DNA crosslinks in T4 bacteriophages has been shown to depend on the MR complex (gp46/47)(Mathews, 1996; Onda et al., 2001). Similarly, in E. coli, the SbcCD complex, which is functionally equivalent to the MR complex, has been demonstrated to process protein-bound DNA ends through nucleolytic cleavage (Connelly et al., 2003). In yeast, Mre11-deficient strains exhibit heightened sensitivity to TOP inhibitors, indicating a crucial role for the MRN complex in repairing topoisomerase-mediated DNA damage (Onda et al., 2001). In vertebrate systems, biochemical studies using Xenopus egg extracts have demonstrated that the MRN complex cooperates with CtIP and BRCA1 to remove Top2-DNA covalent adducts and facilitate the subsequent resection of DSB ends(Aparicio et al., 2016). Supporting these findings, the MRN complex has also been implicated in the removal of TOP2-DNA covalent adducts in mammalian cells.

The ability of the MRN complex to process DPCs beyond TOP2-DNA cleavage complexes (TOP2-ccs) remains insufficiently characterized. The depletion of MRE11 did not lead to a global increase in DPC accumulation, suggesting that additional pathways may compensate for DPC repair. Depletion of MRE11 did not result in the accumulation of global DPCs. In yeast, the independent sensitivity of Wss1 and Rad52 to formaldehyde suggests that DPC proteolysis and HR function as separate pathways for DPC removal during the S phase (Stingele et al., 2014). While depletion of MRE11

did not lead to a global accumulation of DPCs, in vitro studies suggest that MRN's activity on DPC substrates is not strictly dependent on the specific protein being crosslinked (Deshpande et al., 2016; Sacho & Maizels, 2011; Vaz et al., 2016). Additionally, loss of the MRN complex in yeast resulted in greater sensitivity to formaldehyde compared to the loss of other HR repair factors, indicating a broader role for MRN in DPC repair beyond TOP2-ccs(de Graaf et al., 2009).

1.2.4.2.1.1 The role of autophagy in clearing DPCs

Autophagy is known to be a fundamental cellular process responsible for the degradation and recycling of cellular components through lysosomal-mediated proteolysis. It operates at a basal level in all cells and is essential for various physiological processes, including programmed cell death, development, and differentiation(Mizushima et al., 2008). Disruptions in autophagy have been implicated in a wide range of disorders, including neurodegenerative diseases, metabolic dysfunctions, infections, and cancer(Mizushima & Komatsu, 2011).

Lysosomes, which are highly acidic vesicles containing proteases, hydrolases, nucleases, and lipases, serve as the primary site for autophagic degradation. Through their enzymatic activity, lysosomes fragment cellular components into their basic building blocks, such as amino acids, nucleotides, carbohydrates, and lipids, facilitating their reuse in cellular metabolism. The specificity of autophagic degradation is achieved through selective autophagy receptors, which contain an LC3-interacting region (LIR) that links substrates to the expanding autophagic membranes. The E1-like activating enzyme ATG7 is a key regulator of this process, as it mediates the lipidation of LC3, an essential step for anchoring autophagic membranes to their targets (Mizushima et al., 2008; Mizushima & Komatsu, 2011).

The loss of autophagy has been shown to compromise DNA damage repair mechanisms and heighten cellular susceptibility to genotoxic stress, leading to increased cell death (Levine & Kroemer, 2008; Robert et al., 2011). This underscores the critical role of autophagy in preserving genomic stability. Autophagy contributes to cellular resilience by maintaining energy homeostasis, supplying essential nucleotides, and regulating the abundance of key DNA repair proteins necessary for accurate DNA replication and repair. Through these mechanisms, autophagy supports the integrity of the genome and enhances the cell's ability to respond to and recover from DNA damage.

The involvement of autophagy in DPCs clearance was shown when autophagy was inhibited using 3-methyladenine (3-MA) or chloroquine (CQ) in cells treated with DPCs inducing agents. There was a significant accumulation of DPCs, indicating that autophagy is involved in DPC clearance(Mu et al., 2016). In addition, siRNA-mediated knockdown of Atg5 and Atg7, two key autophagy-related genes, resulted in similar accumulation of DPCs, further supporting this role. The same observation was found in a mouse model, intraperitoneal injection of formaldehyde led to a significant increase in DPC levels in various organs, including the liver, lung, and spleen. Autophagy inhibition with CQ further exacerbated DPC accumulation, while autophagy induction with RAP promoted DPC clearance. However, the exact mechanism was not yet understood in this study (Mu et al., 2016).

Among the selective autophagy pathways, TEX264 (testes expressed gene 264) has emerged as a critical player in ER-phagy, contributing to approximately 50% of autophagy-dependent endoplasmic reticulum turnover under starvation conditions(An et al., 2019; Chino et al., 2019). TEX264 is a single-pass transmembrane protein embedded in the ER and nuclear envelope, possessing an LIR domain that facilitates

its role in ER remodelling and degradation through autophagy. Its function underscores the complex interplay between autophagy and cellular homeostasis, highlighting the importance of selective autophagy mechanisms in maintaining organelle integrity and responding to cellular stress (Chino et al., 2019).

Our lab was able to discover a novel mechanism of how autophagy is involved in DPCs repair, specifically Top1cc. A previous paper by Fielden et al. found that TEX264, has been identified as a key player in the degradation of topoisomerase 1 cleavage complexes (TOP1ccs) in response to clinically relevant doses of CPT. We identify TEX264 as a gyrase-inhibitory-like protein and a p97 cofactor that recruits p97 to TOP1ccs, facilitating their resolution (Fielden et al., 2020). TEX264 recognizes both unmodified and SUMO1-modified TOP1, promoting p97- and SPRTN-dependent TOP1cc repair. Importantly, TEX264 localizes to the nuclear periphery, associates with DNA replication forks, and enhances TOP1cc repair during DNA replication. Cells deficient in TEX264 exhibit an accumulation of endogenous TOP1ccs, heightened sensitivity to clinically relevant doses of TOP1 poisons, and increased DNA replication stress (Fielden et al., 2020).

Since TEX264 plays a role in two distinct cellular processes, DNA damage repair in the nucleus and ER-phagy in the endoplasmic reticulum, we were able to identify its function in coordinating the autophagy-mediated repair of TOP1cc. A recent study from our lab revealed that lysosomes play a crucial role in processing TOP1cc DNA lesions in vertebrates. We identified a selective autophagy-mediated pathway that facilitates the degradation of TOP1cc, directly influencing DNA damage repair and enhancing cell survival at clinically relevant doses of topoisomerase 1 inhibitors. Unlike traditional proteasome-mediated degradation, TOP1cc is exported from the nucleus to

lysosomes through a transient disruption of the nuclear envelope(Lascaux et al., 2024).

Mechanistically, the autophagy receptor TEX264 functions as a key sensor for TOP1cc at DNA replication forks, initiating their processing through the p97 ATPase. This process is tightly regulated by MRE11 nuclease and ATR kinase, ensuring the efficient trafficking of TOP1cc to lysosomes for degradation. Our findings highlight an evolutionarily conserved role for selective autophagy in DNA repair, demonstrating its critical function in maintaining genome stability and cellular viability. Importantly, this mechanism has significant clinical implications, particularly for colorectal cancer patients, where impaired autophagy-mediated DNA repair pathways could influence treatment responses and therapeutic outcomes. These insights pave the way for further investigation into autophagy-targeted strategies for enhancing cancer treatment efficacy (Lascaux et al., 2024). Figure 1.17 summarizes the mechanisms of DPCs replication during replication.

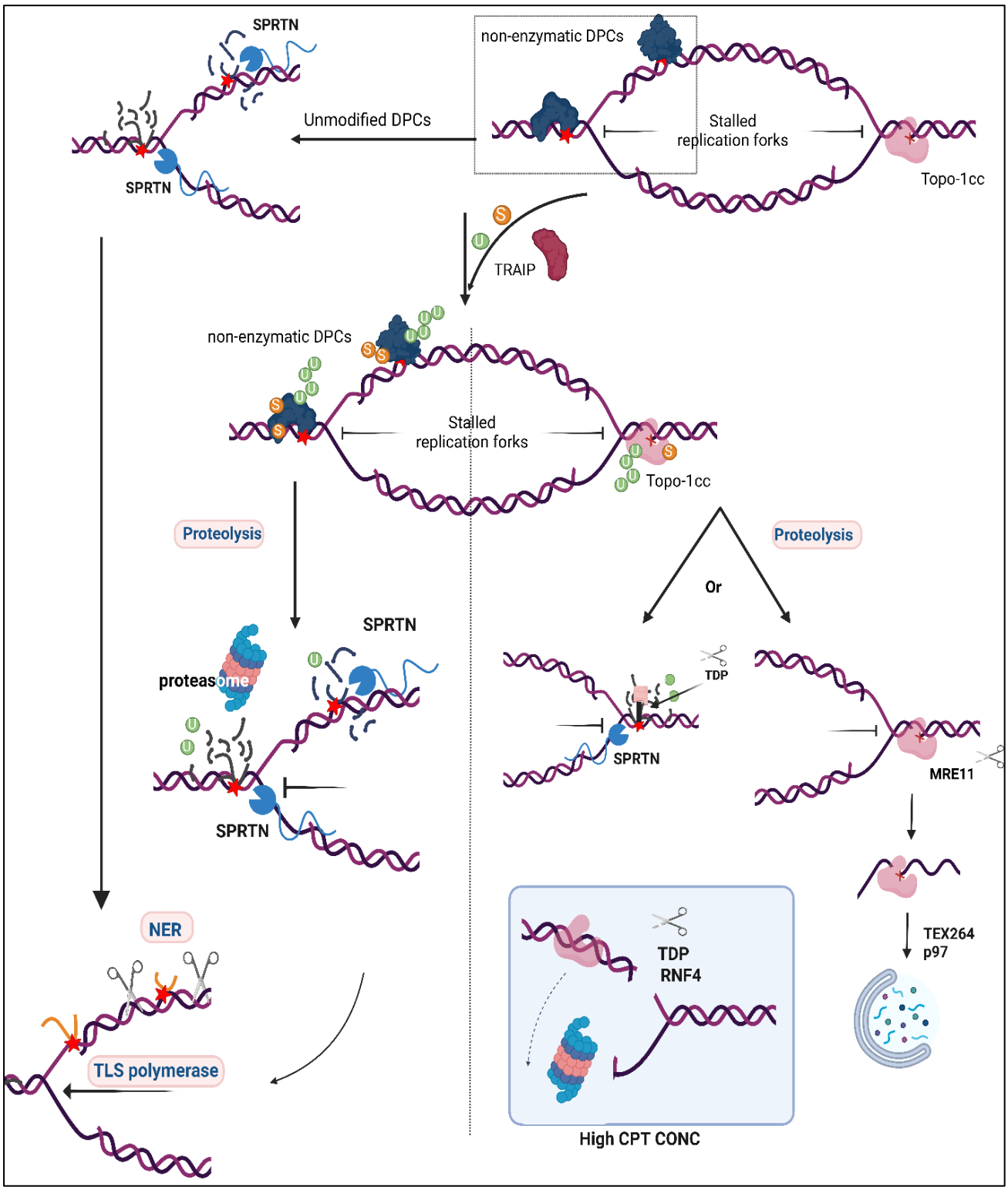

SPRTN
SPRTN
Unmodified DPCs
non-enzymatic DPCs
Stalled
replication forks
Topo-1cc
TRAIP
non-enzymatic DPCs
Stalled
replication forks
Topo-1cc
Proteolysis
Proteolysis
Or
SPRTN
proteasome
SPRTN
TDP
SPRTN
MRE11
TEX264
p97
NER
TLS polymerase
TDP
RNF4
High CPT CONC

Figure 1.17. Replication-dependent and post-replicative repair of DPCs.

DPCs encountered ahead of the replication fork can lead to persistent stalling and potential fork collapse. Both enzymatic and non-enzymatic DPCs are targeted for degradation via proteolysis. SPRTN can remove unmodified DPCs. In addition, DPCs could be modified by ubiquitylation and SUMOylation, which facilitate the recognition and recruitment of repair factors. This would help SPRTN and the 26S proteasome, which serve as the major proteolytic systems, in DPC degradation. When a protein is partially degraded ahead of the replication fork, the resulting peptide adduct can be bypassed by a TLS polymerase. In contrast, post-replicative peptide remnants are resolved by NER nucleases, a process that is limited to small crosslinked peptides in mammalian cells. TOP1cc are cleared via a proteasome-independent pathway involving their export from the nucleus to lysosomes, facilitated by a transient disruption of the nuclear envelope. Mechanistically, the autophagy receptor TEX264 functions as a sensor for TOP1cc at DNA replication forks, initiating their processing through the p97 ATPase and directing their lysosomal degradation in a manner dependent on MRE11 nuclease and ATR kinase, DPCs, DNA–protein crosslinks; SPRTN, SprT-like N-terminal domain-containing protein; TLS, translesion synthesis; NER, nucleotide excision repair; TOP1cc, topoisomerase 1 cleavage complexes; TEX264, testis expressed 264; p97, valosin-containing protein; MRE11, meiotic recombination 11 homolog; ATR, ataxia telangiectasia and Rad3-related kinase. Created using BioRender.com

1.2.4.2.2 Replication-independent DPCs repair or General G repair:

Early studies have demonstrated that the proteasome plays a crucial role in DPC proteolysis, particularly in replication-independent DPC repair. Proteolytic degradation of large DPCs by proteasomes into smaller peptide-DNA adducts facilitates their subsequent removal by nucleotide excision repair (NER) (Baker et al., 2007). This suggests that NER repair factors cannot efficiently access DNA lesions when DPCs remain too bulky, likely due to steric hindrance.

Similarly, for TDP1- or TDP2-mediated hydrolysis to process covalently trapped TOP1 or TOP2 complexes, the proteasome must first degrade the topoisomerase proteins. Supporting this, treatment of human cell lines with CPT led to a reduction in TOP1 protein levels, an effect that was blocked when cells were treated with MG132. Additionally, proteasome inhibition causes accumulation of polyubiquitinated TOP1 in CPT-treated cells, indicating that the 26S proteasome is responsible for degrading TOP1-ccs (Desai et al., 2001). Similarly, TOP2 degradation in response to etoposide treatment was found to be dependent on 26S proteasome activity, further emphasizing the role of ubiquitin-proteasome-mediated degradation in DPC resolution.

In the absence of DNA replication, DPCs are degraded via the SUMO-RNF4 pathway, ensuring their removal independently of the replication machinery. This pathway is initiated when the SUMO E3 ligase PIAS4 poly-SUMOylates the crosslinked protein, which is then recognized and poly-ubiquitylated by the E3 ubiquitin ligase RNF4, marking it for proteasomal degradation (Liu et al., 2021). SUMO-modified DNMT1 DPCs were found on mature chromatin, indicating that their modification occurs independently of DNA replication. This type of DPCs, in addition to TOP1-ccs, and TOP2-ccs undergo SUMOylation via PIAS4 SUMO ligase, followed by ubiquitination

mediated by the SUMO-targeted E3 ubiquitin ligase RNF4, leading to proteasomal degradation (Borgermann et al., 2019; Liu et al., 2021; Sun et al., 2020).

A recent study found the E3 ligase TOPORS as another regulator of SUMO-dependent DPC resolution and operating alongside RNF4. TOPORS is found to facilitate DPC repair by acting as a SUMO-targeted ubiquitin ligase (STUbL). It achieves this function through its RING domain, which provides ubiquitin ligase activity, and its SUMO-interacting motifs, enabling poly-SUMO binding, similar to the STUbL RNF4. This facilitates their processing and degradation via the p97-proteasome pathway. It is believed that TOPORS exhibits selectivity for SUMO1-modified proteins, while RNF4 appears to have a preference for SUMO2/3-modified substrates. However, these preferences are not absolute. The loss of either TOPORS or RNF4 alone leads to a reduction in STUbL-driven pathways, and simultaneous depletion of both ligases results in a severe defect in the ubiquitylation and proteolytic processing of SUMOylated proteins, ultimately leading to synthetic lethality (Liu et al., 2024).

In addition, PARP1-mediated PARylation is found to play a role in targeting DPCs for ubiquitination and subsequent proteasomal degradation. PARP1-dependent DPC resolution is essential for repairing TOP1-DNA cleavage complexes (TOP1ccs) and similar lesions flanked by DNA breaks. In the absence of PARP1-mediated PAR signaling, these lesions persist, leading to replication fork stalling and replisome disassembly upon encountering such obstacles during DNA replication (Fábián et al., 2024).

NER was found to be involved in DPCs removal outside S-phase. The role of NER in DPCs repair was first proposed when Trans-Pt(II) diamminedichloride-induced DPCs were observed to persist longer in nucleotide excision repair (NER)-deficient

xeroderma pigmentosum (XP) group A fibroblasts compared to normal cells (Seres, 1982). However, the removal of formaldehyde-derived DPCs was not significantly impacted in XP-A or XP-F cells, indicating that NER is involved in the repair of particular crosslinks (Grafstrom et al., 1984; Quievryn & Zhitkovich, 2000; Speit et al., 2000). A study by Minko et al. demonstrated that the bacterial nucleotide excision repair (NER) machinery, particularly the UvrABC nuclease complex, is capable of recognizing and cleaving DNA at sites of DPCs. Their findings suggest that NER may function as a potential repair pathway for DPCs, especially when the crosslinked proteins are relatively small. Additionally, reconstituted mammalian NER proteins efficiently removed these crosslinks, albeit with a greater variability in excision efficiency (Minko et al., 2002). Additionally, mammalian NER failed to excise even small formaldehyde-induced DPCs of 7.4 or 8.0 kDa in in vivo conditions. This finding contradicts in vitro studies using mammalian NER, which showed the ability to process similar-sized DPCs, and also differs from bacterial in vivo experiments, where larger DPCs were successfully excised. Thus, NER preferentially targets DNA–peptide cross-links (PCLs) as its primary substrates. Both mammalian and bacterial NER demonstrate the highest repair efficiency for a 1.6 kDa PCL, corresponding to a peptide of approximately 14 amino acids(Nakano et al., 2007). Therefore, DPCs can be effectively processed by NER only after proteolytic degradation, which reduces them to smaller PCLs. Figure 1.18 shows the mechanism replication replication-independent DPCs repair.

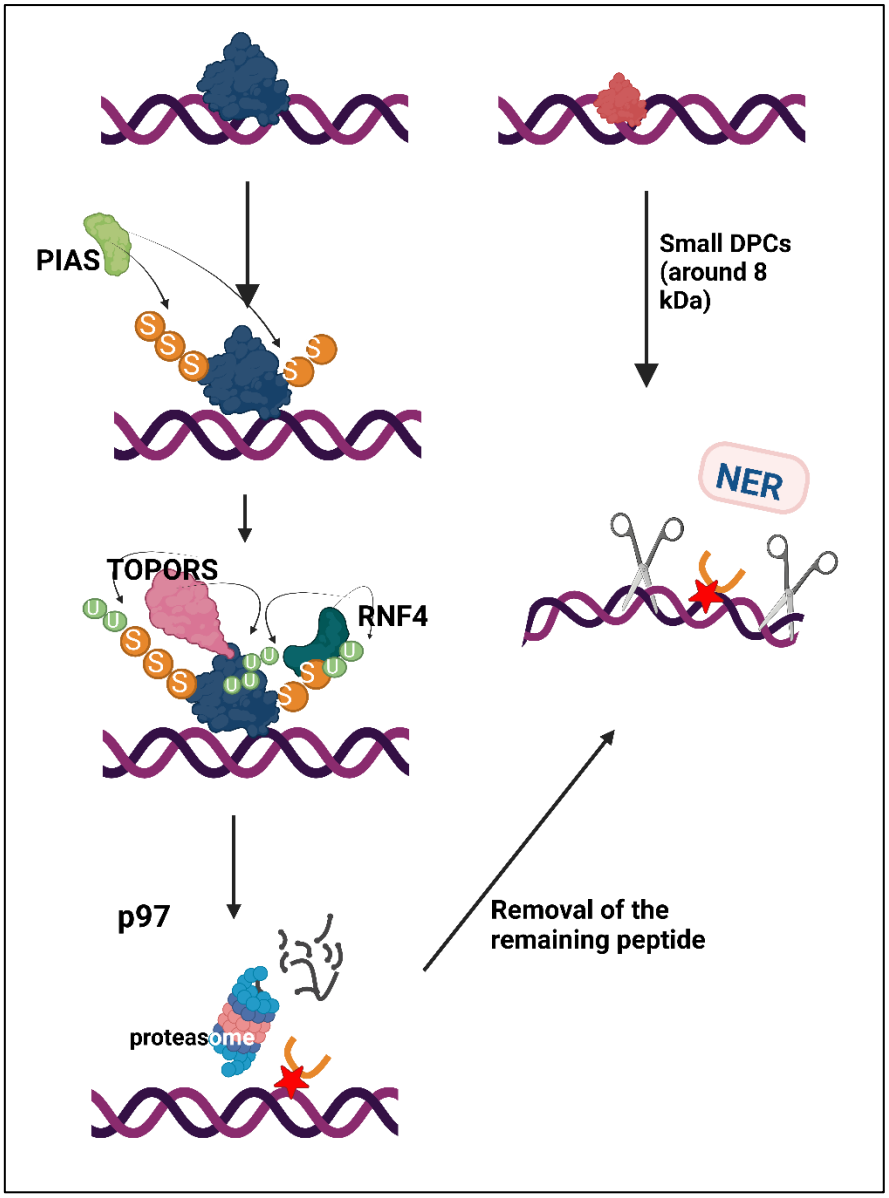


Figure 1.18. Replication-independent DPCs repair

Outside the context of DNA replication, DNA–protein crosslinks (DPCs) are marked for SUMOylation by E3 SUMO ligases such as PIAS4. This modification facilitates DPC recognition by SUMO-targeted ubiquitin ligases like RNF4, which catalyse polyubiquitination of the crosslinked protein. The resulting signal promotes proteasomal degradation of the DPC, enabling subsequent repair of the associated DNA lesions. DPCs, DNA–protein crosslinks; PIAS4, protein inhibitor of activated STAT 4; RNF4, RING finger protein 4. Created using BioRender.com

1.2.4.2.3 Transcription-coupled DPCs repair:

Evidence for the role of transcription-coupled nucleotide excision repair (TC-NER) factors in DPC tolerance comes from observations of severe aldehyde sensitivity in CSB-deficient cells, both in vitro and in vivo (Mulderrig et al., 2021; Rieckher et al., 2024). Recently, it was confirmed by several studies that TC-DPC repair pathway utilizes some components of TC-NER but functions through mechanistically distinct processes (Carnie et al., 2024; Oka et al., 2024; van Sluis et al., 2024).

A study by Oka et al. showed that a mouse model deficient in both aldehyde clearance (Adh5 and Aldh2) mechanisms and the TCR pathway experiences exacerbated AMeDS manifestations, characterized by severe hematopoietic abnormalities and systemic asthenia. These findings underscore the critical role of DPC removal in mitigating aldehyde-induced transcriptional roadblocks and offer mechanistic insights into the development of diseases linked to defective aldehyde detoxification and transcription-coupled repair (Oka et al., 2024).

In TC-DPC repair, stalled RNA polymerase II (RNAPII) recruits the Cockayne syndrome (CS) proteins CSA and CSB, which facilitate DPC ubiquitylation and proteasomal degradation. The recruitment of CSB will subsequently recruit the $CRL4^{CSA}$ complex. $CRL4^{CSA}$ facilitates the polyubiquitylation of RPB1 (the largest subunit of RNAPII) at residue K1268, a process that is likely supported by ELOF1 and UVSSA, though it is not strictly required for TC-DPC repair. The primary function of CRL4CSA in TC-DPC repair is believed to involve the ubiquitylation of the DPC itself, which, in conjunction with the ubiquitin-dependent unfoldase p97, directs the proteasomal degradation of the crosslinked protein. However, the precise molecular details of these events remain largely unresolved. Open questions include the specific role of p97 in the pathway and whether the TFIIH complex has a function in TC-DPC

repair. DPC degradation additionally requires the ubiquitin-dependent unfoldase VCP/p97 (Oka et al., 2024; van Sluis et al., 2024). The recruitment of p97 to DPC-stalled RNAPII is independent of CSB and RPB1K1268 ubiquitylation, and its chemical inhibition does not further impair TC-DPC resolution in CSB knockout cells, suggesting that p97 functions downstream of CSB in the repair process(Oka et al., 2024).

After successful DPC removal, transcription is restarted by proteasomal degradation of ATF3, an inhibitory transcription factor induced by DNA damage. Importantly, TC-DPC repair appears to function independently of SPRTN, though whether another DPC protease is involved remains unclear (Carnie et al., 2024; van Sluis et al., 2024).

Cells expressing a ubiquitylation-defective RPB1^{K1268R} variant, as well as UVSSA- and ELOF1-deficient cells, show milder defects in DPC repair, reduced sensitivity to DPC-inducing agents, and better transcriptional recovery compared to CSA or CSB-deficient cells (Carnie et al., 2024; Oka et al., 2024; van Sluis et al., 2024). This suggests that RPB1K1268 ubiquitylation plays a partial role in DPC repair, though RNAPII removal is not strictly essential for the process. Consequently, it remains unclear how or whether TFIIH can be recruited, as the steric hindrance caused by the DPC may obstruct its loading. Figure 1.19 shows the mechanism of TC-DPC repair.

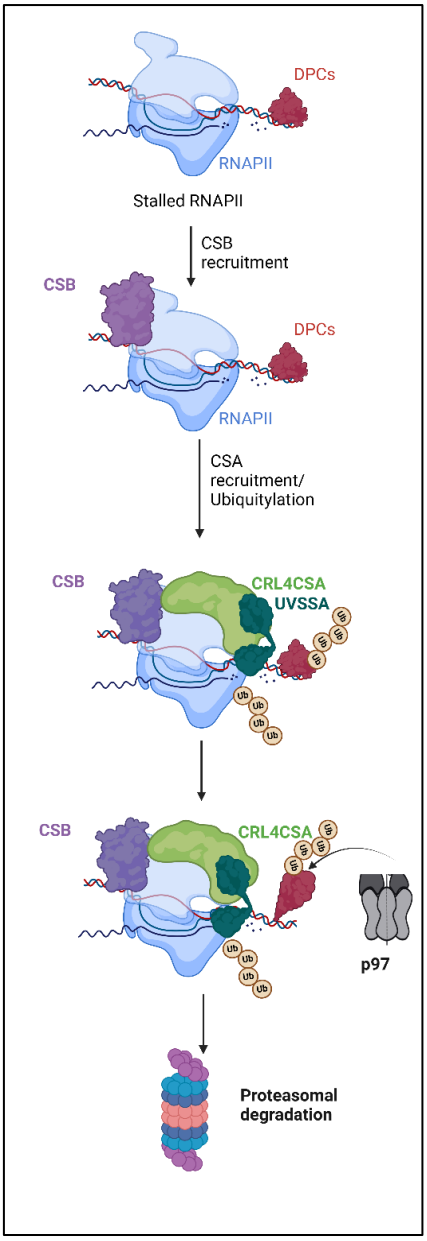


Figure 1.19. Transcription-coupled (TC) DNA–protein crosslink (DPC) repair. TC-DPC repair is initiated when RNA polymerase II (RNAPII) stalls at a DNA–protein crosslink. This stalling is recognized by Cockayne syndrome protein B (CSB), which facilitates the recruitment of the $CRL4^{CSA}$ ubiquitin ligase complex. Although polyubiquitylation of RNAPII's largest subunit RPB1 at lysine 1268—likely mediated by ELOF1 and UVSSA—occurs, this modification is not essential for DPC removal. Instead, the key role of CRL4^CSA in TC-DPC repair is thought to be the polyubiquitylation of the crosslinked protein itself, which, in coordination with the ubiquitin-dependent unfoldase p97, targets the DPC for proteasomal degradation. Despite progress in outlining this pathway, the exact mechanistic contributions of p97 and a potential role for the TFIIH complex remain to be fully defined. CSA, Cockayne syndrome protein A; CSB, Cockayne syndrome protein B; UVSSA, UV sensitivity syndrome protein A. Created using BioRender.com

1.3 SprT-like N-terminal domain (SPRTN)

SPRTN (also known as DVC1 or C1orf124) is a DNA-dependent metalloprotease. Before it was known for its role in DPCs repair, SPRTN was first identified as a protein that is involved in translesion DNA synthesis (TLS). It was found to be localized in areas of DNA damage induced by UV light within cells and is essential for cellular survival after exposure to UV radiation. It was suggested that SPRTN acts by facilitating the transition from replicative DNA polymerase to TLS polymerase, thereby ensuring effective bypass of lesions caused by UV damage (Centore et al., 2012a; Ghosal et al., 2012). Later, SPRTN was found to be involved in DPCs repair.

SPRTN has been identified as a core gene essential for cellular fitness in humans (Hart et al., 2015). The critical role of SPRTN in maintaining genome stability is evident in both human disorders and animal studies. Mutations in SPRTN, specifically monogenic and biallelic germline mutations, lead to Ruijs–Aalfs Syndrome (RJALS). This rare condition is characterized by chromosomal instability, accelerated aging, and an increased risk of hepatocellular carcinoma (Lessel et al., 2014; Ramadan et al., 2017). Similarly, in animal models, SPRTN hypomorphic mice exhibit RJALS-like symptoms, while a complete absence of SPRTN results in embryonic lethality, demonstrating its importance for development (Maskey et al., 2014). In zebrafish models, reduced SPRTN expression significantly disrupts normal embryonic development and increases the risk of embryonic death, mirroring the severe impact of SPRTN deficiencies observed in other species (Lessel et al., 2014).

1.3.1 SPRTN Domains

SPRTN is a multi-domain containing protein that was first described in 2012. The N-terminal has a metalloprotease domain similar to that of the *Escherichia coli* SprT

protein (SprT-like domain) which is mainly responsible for the proteolytic cleavage of DPCs. SprT-like domain contains two subdomains: (1) the canonical metalloprotease domain, which involves the active site, and (2) the Zn 2+ -binding subdomain which aids in substrate proteolysis and involves in DNA binding (ZBD). The C-terminal contains a p97 or VCP-binding motif (SHP-box). It also has a PCNA-interacting protein (PIP) motif as well as a ubiquitin binding zinc finger (UBZ) domain in which both together recruit SPRTN and valosin-containing protein (VCP) to DNA damage site. It also includes the basic region (BR) which is a DNA-binding element located next to SprT domain (Centore et al., 2012b; Davis et al., 2012; Juhasz et al., 2012; Mosbech et al., 2012a). SPRTN domains are shown in Figure 1.20.

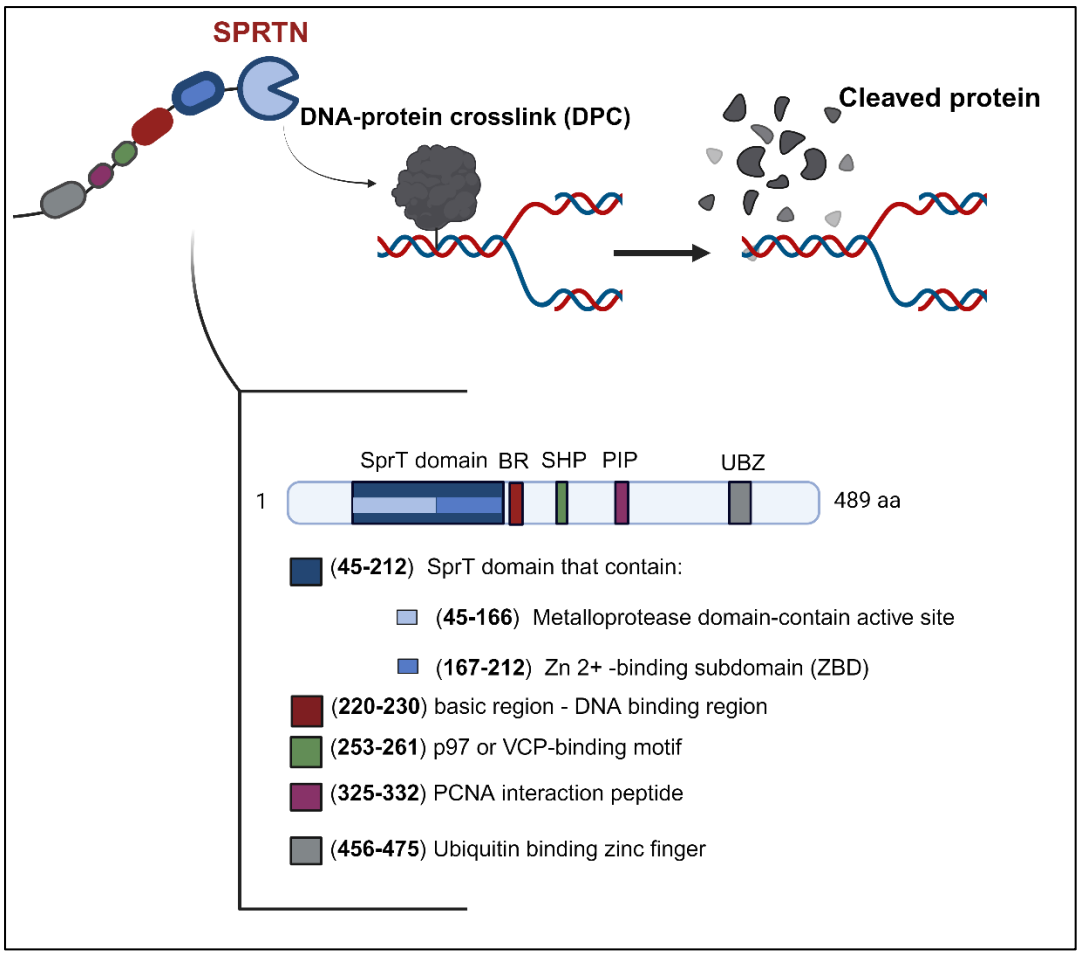


Figure 1.20. SPRTN domains

This figure illustrates the various functional domains of SPRTN. SprT domain; the zinc metalloprotease domain is responsible for the proteolytic cleavage of the protein component of DPCs. The SHP domain; AAA+ ATPase domain provides the energy necessary for substrate unfolding, facilitating access to the protease domain. The PIP box mediates SPRTN's interaction with PCNA, a key factor in DNA replication and repair. The UBZ domain allows SPRTN to recognize and bind to ubiquitinated substrates. SprT: SprT-like domain; SHP p97-interacting motif PIP: PCNA-interacting protein; UBZ: ubiquitin binding zinc finger. Created using BioRender.com.

1.3.2 SPRTN Substrate Specificity

SPRTN does not have strict sequence specificity towards DPCs; however, it preferentially cleaves DNA-binding proteins in regions rich in lysine, arginine and serine (Vaz et al., 2016). Cells deficient in SPRTN expression are sensitive to the general crosslinker formaldehyde, and to the chemotherapeutic drugs camptothecin and etoposide, which are known to induce DPCs (Stingele et al., 2016b; Vaz et al., 2016). This sensitivity indicates that SPRTN repairs most types of DPCs. Some of the known SPRTN substrates include core histones (H2A, H2B, H3, H4), linker histone H1, HMG1, HLTF, Fan1, TOP1, and TOP2 (Lopez-Mosqueda et al., 2016; Stingele et al., 2016; Vaz et al., 2016). This feature is highly significant as it emphasizes the potential of SPRTN-mediated proteolysis to engage a wide array of distinct substrates.

1.3.3 DPCs Removal by SPRTN

There are numerous factors involved in DPCs removal by SPRTN. Recent findings showed that the majority of DPCs are removed specifically during the S phase (Vaz et al., 2016). There is strong evidence that SPRTN mainly functions during the S phase, as it was shown that SPRTN is rapidly upregulated as cells enter the S-phase, this is because it is degraded by the Anaphase promoting complex-Cdh1 (APC) in the G1 phase (Mosbech et al., 2012b). Our lab and others have established that the SPRTN metalloprotease is an integral part of the DNA replication machinery and is essential for the proper progression of DNA replication (Mórocz et al., 2017; Vaz et al., 2016). Moreover, it was shown recently that SPRTN is involved in replication-independent DPC repair which requires SUMO-targeted ubiquitylation of DPCs (Weickert et al., 2023a).

1.3.3.1 Regulation of SPRTN Activity

1.3.3.1.1 Post-translational Modifications

In addition to SPRTN expression regulation during the cell cycle where it is mostly active during S-phase as mentioned earlier, there are also additional mechanisms that control its activity. The activity of SPRTN is highly regulated inside the cells to ensure it is only active when it is needed (in the presence of DPCs) as random proteolytic activity could result in DNA damage. SPRTN could be regulated by post-translational modification (PTM), such as phosphorylation, monoubiquitination and acetylation. The ubiquitin switch of SPRTN is considered the most upstream control mechanism of SPRTN activity. The monoubiquitylation of the UBZ domain of SPRTN leads to its inactivation by two mechanisms,1) by causing autocleavage to other SPRTN molecule (in *trans*). 2) by recruiting proteasome after polyubiquitination causing degradation of SPRTN (*in cis*). Upon DPC induction, SPRTN is deubiquitinated by one of the deubiquitinating enzymes; USP7, USP11 and VCPIP1. The latter was found to be phosphorylated and activated by ATM/ATR, leading to the deubiquitination of SPRTN, promoting its relocation within the chromatin (Huang et al., 2020; Perry et al., 2021; Zhao et al., 2021). Following deubiquitinating, SPRTN was shown to be acetylated and this was confirmed by DPC induction after formaldehyde (FA) treatment. The acetylation by PCAF and GCN5 is on the K230 residue that is situated in the area between the protease domain (SprT) and the SHP domain, which has DNA-binding activity of SPRTN (Huang et al., 2020). These modification on SPRTN safeguards its access to chromatin in order to repair DPCs.

Another PTM that is necessary for SPRTN is phosphorylation by CHK1 following its stimulation by SPRTN. CHK1 kinase phosphorylates SPRTN on S373, S374 and S383 of the C-terminus ultimately enhancing the recruitment of SPRTN to chromatin and its

activity toward DPC proteolysis (Halder et al., 2019) Table 1.8 summarises PTM pathways involved in SPRTN regulation activity and Figure 21 A shows the pathways involved in SPRTN regulation.

1.3.3.1.2 DNA Binding and DNA Structure

SPRTN's protease activity is strictly DNA-dependent – it will not cleave protein substrates unless they are crosslinked to DNA. In vitro, SPRTN is inactive on free proteins but becomes activated upon binding to DNA (Stingele et al., 2016a; Vaz et al., 2016). A recent publication showed that SPRTN exhibits a preference for cleaving DPCs located near the junction between single-stranded and double-stranded DNA structures. These structures are specifically identified by two unique interfaces located on the N-terminal region of SPRTN. In this study, the researchers developed a variety of DPC model templates by crosslinking Protein G to different DNA structures: ssDNA, dsDNA, and hybrids of both forms. It was determined that the most effective activator is a DNA molecule that incorporates features of both ssDNA and dsDNA. Furthermore, SPRTN exhibits peak activity when the DPC is positioned five nucleotides from the junction of dsDNA and ssDNA. This DNA structure is very similar to the dynamics of DNA replication forks and transcriptional bubbles that encounter DPCs within cellular environments in which ssDNA is produced during the progression of replication forks by the CMG helicase, which approaches and may circumvent the DPC, while the DNA polymerase lags behind. The binding of SPRTN to DNA is achieved by two essential DNA-binding domains: ZBD, which binds to the ssDNA and BR which binds dsDNA (Reinking et al., 2020).

1.3.3.1.3 DNA-Dependent Autocleavage:

The induction of DPCs by formaldehyde in cells leads to the activation of SPRTN along with an increase in its autocleavage. This was shown to be a DNA-dependent

autocleavage of SPRTN, which is an important negative regulator of its activity, limiting unnecessary proteolysis on chromatin (Stingele et al., 2016b).

Several DNA structures were found to activate SPRTN autocleavage upon binding 42-nt ssDNA, 42-nt dsDNA, and fork DNA. However, it was found that SPRTN binding to dsDNA is not activating its proteolytic activity toward DPCs unlike the binding of ssDNA and fork DNA. (F. Li et al., 2019; Stingele et al., 2016b)

However, our lab was able to show that the binding of SPRTN with ssDNA, dsDNA, and splayed DNA showed similar affinities towards DNA fragments. Furthermore, ssDNA and dsDNA were identified as the most effective stimulators of SPRTN auto-cleavage activity and dsDNA was able to activate the proteolytic activity of SPRTN (Halder et al., 2019; Vaz et al., 2016). Moreover, in a recent preprint published on bioRxiv from our lab, we developed a sensitive fluorescence-based assay to monitor SPRTN-mediated proteolysis of a physiologically relevant DPC substrate, histone H1, in vitro. Our results showed that both single-stranded and double-stranded DNA structures can activate SPRTN's proteolytic activity toward its substrate and itself. In particular, the double-stranded DNA with a 3-nucleotide overhang (20/23 nt) proved to be the most effective activator of SPRTN. Under these conditions, SPRTN cleaved both histone H1 and itself with comparable efficiency, indicating that SPRTN undergoes self-cleavage during substrate processing and does not exhibit strong substrate specificity (Song et al., 2024).

Confirming the role of DNA in autocleavage, mutations of SPRTN DNA binding domains, ZBD or BR lowered both autocleavage or substrate cleavage *in vitro*. Nuclear magnetic resonance (NMR) biochemical analysis shows that the binding of SPRTN to ssDNA activates *trans* autocleavage by bridging two SPRTN molecules,

where one is the substrate for the other *(*Figure 1.21 B). This autocleavage of SPRTN appeared to separate its protein-interacting motifs from its protease domain and is which terminates its function *in vivo* (F. Li et al., 2019).

1.3.3.1.4 Interaction with other Proteins

Several studies showed that SPRTN interacts with other accessory proteins to remove DPCs. Valosin-containing protein (VCP) also known as p97 facilitates the unfolding of tightly folded DPCs facilitating proteolysis by SPRTN. This happens with the aid of Ufd1-Npl4 adapter, which is responsible for recognizing the ubiquitylation of substrates (Kröning et al., 2022). A study found that P97 binds to SPRTN through its SHP. Moreover, our lab was able to identify gyrase inhibitory-like protein known as TEX264, as a cofactor of p97 that facilitates SPRTN recruitment to TOP1ccs, thereby enhancing the repair of TOP1cc through p97 and SPRTN. The process of proteolysis is crucial for the later cleavage of the residual peptide from DNA by Tyrosyl-DNA phosphodiesterase 1 TDP1. (Fielden et al., 2020). Another protein found to modulate SPRTN activity is FANCJ which is a helicase that promotes SPRTN activity by unfolding DPCs during replication (Figure 1.21 C) (Yaneva et al., 2023b).

Table 1.8. Pathways involved in SPRTN activity and their mechanisms

PTM	Function	Location on SPRTN	Reference
Monoubiquitination and Deubiquitination	Monoubiquitination serves to block SPRTN from accessing chromatin. The cleavage of monoubiquitin from SPRTN by a USP7, USP11 and VCPIP1 facilitates the localization of SPRTN to chromatin, enabling it to cleave DPCs.	UBZ domain	(Huang et al., 2020; Perry et al., 2021; Zhao et al., 2021)
Acetylation	SPRTN acetylation following deubiquitination by VCPIP1 is required for activation.	On K230, between the protease domain (SprT) and the SHP domain	(Huang et al., 2020)
Phosphorylation	Phosphorylation of SPRTN by CHK1 aids SPRTN association to the chromatin.	On S373, S374 and S383 of the C-terminus	(Halder et al., 2019)

1.3.3.1.5 Modification of DPCs

Labelling DPCs is critical in order to get recognized by SPRTN for degradation. During the replication process, both SUMOylation and transient ubiquitylation are essential for the repair of DPCs that depend on SPRTN (Ruggiano 2021; Hoffman, Mailand 2019). Ubiquitylation plays a vital role in facilitating SPRTN's interaction with its substrates, its localization to nuclear foci, and the overall efficiency of DPC repair. Concurrently, SUMOylation acts to inhibit homologous recombination and prevents DPC-induced DSBs (Ruggiano et al., 2021). Furthermore, the simultaneous disruption

of SPRTN-dependent proteolysis and the HR pathway results in synthetic lethality following exposure to formaldehyde, indicating that SPRTN and HR function in tandem to mitigate DPC-induced toxicity and HR is a backup mechanism for DPCs repair when SPRTN-depleted cells (Ruggiano et al., 2021).

1.3.3.2 Post-Cleavage Processing

The proteolytic degradation facilitated by SPRTN during the process of DNA replication can lead to the near-total breakdown of the protein that is covalently attached to the DNA. This process results in the formation of a minor peptide-DNA adduct, which can subsequently be circumvented by the replicative CDC45–MCM2/7–GINS (CMG) helicase (Ishimi & Ide, 2013; Stingele et al., n.d.). Following this, DNA synthesis can continue over the peptide-DNA adduct, aided by a translesion synthesis polymerase such as DNA polymerase ζ (Larsen et al., 2019). Alternatively, the residual peptide-DNA adduct may also be eliminated post-replicative via NER pathway (Baker et al., 2007).

1.3.4 SPRTN Expression in Cancer Cells

The levels of SPRTN mRNA have been found to vary across different cancer types, according to data from the publicly available Cancer Genome Atlas (TCGA) project (Weinstein et al., 2013).. The dataset was accessed through cBioPortal (https://www.cbioportal.org/). While some cancer samples exhibited elevated SPRTN mRNA levels, others showed no significant change or even lower levels. Additionally, alterations in SPRTN were analyzed based on genomic data from TCGA for the various cancer types studied (Figure 1.22). As illustrated in Figure 1.22, SPRTN gene amplification is most prevalent in breast cancer cases, whereas most other cancers do not show significant alterations in the SPRTN gene.

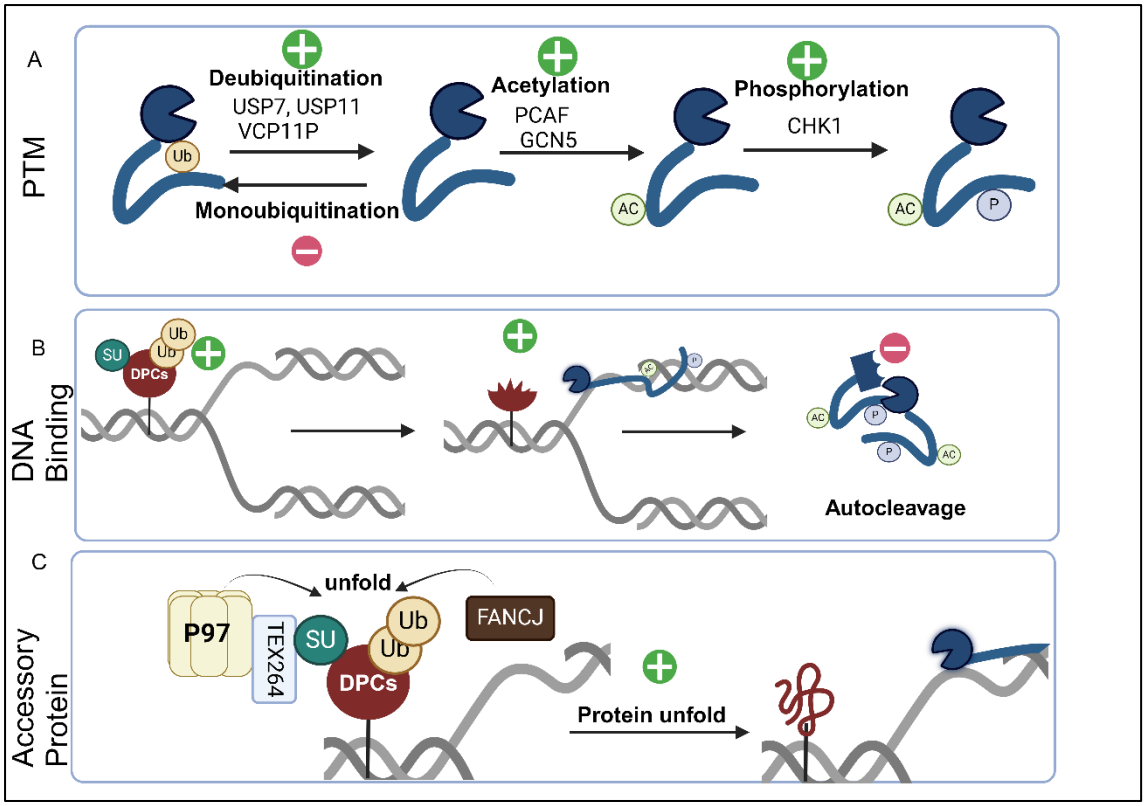


Figure 1. 21. Some regulators of SPRNT activity

This figure illustrates the different regulatory mechanisms of SPRTN. (A) Post-translational modifications (PTMs) on SPRTN that lead to its activation, including acetylation and phosphorylation, modulate SPRTN's activity, stability, and interactions with other proteins during DNA repair. (B) SPRTN regulation by DNA binding occurs when SPRTN recognizes and binds to DNA at sites of DNA-protein crosslinks (DPCs), triggering its protease activity to cleave the protein component. (C) SPRTN is further activated by its interaction with p97, a ubiquitin-selective chaperone that assists in unfolding and processing proteins, enabling SPRTN to effectively degrade the DPCs. Additionally, TEX293 and FANCJ are involved in modulating SPRTN's activity by enhancing its recruitment and activation at damage sites. Together, these pathways regulate SPRTN's function in resolving DPCs and maintaining genomic stability. Created using BioRender.com.

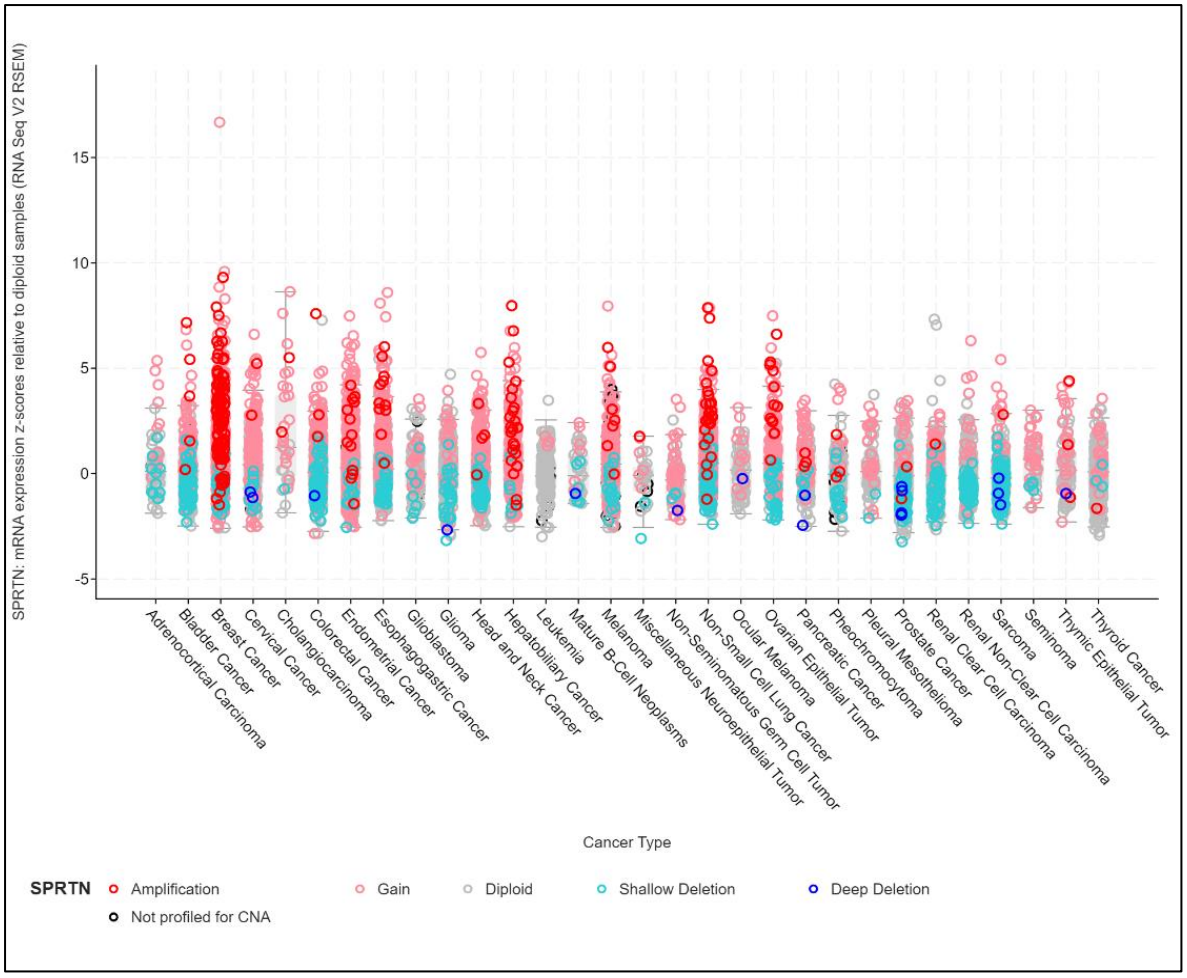


Figure 1.22. Expression of SPRTN in different cancer types

The levels of mRNA expression are shown across various cancer tissues, with mRNA expression z-scores relative to diploid samples (RNA Seq V2 RSEM). A total of 10,071 samples were analyzed. This data is publicly available from the National Cancer Institute and can be accessed through cBioPortal (https://www.cbioportal.org/).

1.4 DPCs Isolation Methods

For years, the investigation of DPC repair in mammalian cells was limited by the absence of standardized assays, particularly those capable of accurately quantifying proteins or proteolytic fragments covalently bound to DNA. However, growing interest in this field has led to the development of several biochemical methods designed to enhance DPC detection and analysis, improving our ability to study their repair mechanisms.

The complexity and heterogeneity of DPCs necessitate multiple isolation methods, as several factors influence the choice of technique. The variability in crosslink chemistry, Protein size and composition also play a role, as DPCs range from small peptides to large multi-protein complexes, demanding tailored extraction and analysis strategies. Additionally, DPC-inducing agents differ, including endogenous metabolic byproducts, environmental toxins, chemotherapy agents, and ionizing radiation, each producing structurally distinct crosslinks that require specialized isolation methods. The cellular and genomic context further influences DPC stability, as they may form in euchromatin or heterochromatin or at active replication and transcription sites, affecting their extractability. Moreover, analytical requirements dictate method selection, with different techniques optimized for mass spectrometry, immunodetection, or sequencing-based analysis. Another crucial factor is crosslink stability and reversibility, as some DPCs are irreversible, while others may revert under physiological conditions, requiring chemical stabilization or enrichment to prevent signal loss. Given these complexities, researchers employ a range of DPC isolation strategies to achieve accurate detection, quantification, and characterization, ensuring reliable analysis across diverse cellular and experimental contexts. Recently, our lab published a review article that highlights recent advancements in DPC isolation

techniques, emphasizing methods that are efficient, systematic, and cost-effective (Torrecilla et al., 2024).

DPC isolation methods can be broadly categorized based on whether they detect crosslinked proteins or DNA. It can be classified into protein-targeted approaches and DNA-targeted approaches. Additionally, the use of antibody-based techniques for identifying specific DPCs.

1.4.1 Detection of DPCs Isolated by Protein-Targeted Methods

Protein-targeted approaches isolate DNA while removing unbound proteins, allowing for the analysis of proteins that remain covalently linked to the DNA. Various isolation methods are available for DPCs extraction, with the choice depending on the factors discussed earlier. Once isolated, DPCs can be detected using specialized techniques designed to identify and quantify their presence in a given sample.

1.4.1.1 RADAR assay

The RADAR (Rapid Approach to DNA Adduct Recovery) assay was first published in May 2013 by Kiianitsa et al, (Kiianitsa & Maizels, 2013). Up till this day, it is among the most widely used biochemical methods for DPCs isolation. This technique is fast, sensitive, and requires starting material as little as 10^4 cells, yielding approximately 60 ng of DNA. In this method, the isolation process begins with lysing cells under denaturing conditions to disrupt cellular structures while preserving covalent DNA–protein interactions. High concentration of guanidine thiocyanate -Strong chaotropic agents- and SDS are used to denature proteins and dissociate non-covalent interactions, ensuring that only covalently bound proteins remain attached to DNA. Next, DNA, along with covalently attached proteins, is precipitated using alcohol-based methods (e.g., ethanol or isopropanol precipitation). Non-covalently bound

proteins are washed away, ensuring that only crosslinked proteins remain associated with the DNA. The washed pellet, containing DPCs, is resuspended in 8 mM NaOH and quantified, ensuring sample normalization. To isolate crosslinked proteins, the sample undergoes benzonase digestion, which degrades both DNA and RNA, leaving only the covalently bound proteins. The extracted DPC-associated proteins can then be analyzed using various detection methods. Total DPCs can be visualized using silver or Flamingo staining. Moreover, ELISA, slot blot, and Western blotting for targeted protein identification or mass spectrometry for an unbiased proteomic analysis of the DPC repertoire.

The RADAR assay has been widely employed to investigate chemotherapeutic agents that induce DPCs, evaluate drug efficacy, and elucidate the mechanisms of action of anti-tumour drugs. Initially, it was applied to detect DNMT1 crosslinks induced by the anti-cancer drug 5-aza-dC. Subsequently, RADAR has been used to analyze TOP1 and TOP2 adduct formation induced by CPT and etoposide and to compare the effectiveness of conventional topoisomerase-trapping agents with next-generation topoisomerase inhibitors, such as indenoisoquinolines, which exhibit improved pharmacokinetics and reduced toxicity compared to CPT (Marzi et al., 2020).

In addition to assessing drug-induced DPC formation, RADAR has been instrumental in demonstrating that exatecan induces TOP1ccs more efficiently than CPT or topotecan (Jo et al., 2022) and in revealing that CX-5461, initially identified as an RNA polymerase I inhibitor, induces TOP2B crosslinks (Pan et al., 2021). Furthermore, RADAR has provided crucial insights into the role of lipid peroxidation by-products in DPC formation within CPT-treated cells. The 4-hydroxy-2-nonenal was found to stabilize TOP1ccs with an efficacy comparable to CPT, highlighting that CPT induces covalent complex formation through both direct and indirect mechanisms (Flor et al.,

2021). More recently, using the RADAR assay, we were able to show that the inactivation of autophagy through ATG7 depletion resulted in a significant accumulation of TOP1cc, confirming the results obtained by IF using similar conditions (Lascaux et al., 2024). These findings highlight the essential role of autophagy in facilitating the clearance and repair of TOP1cc lesions.

1.4.1.2 Caesium chloride (CsCl)

Caesium chloride (CsCl) density gradient was first developed in 1976 to detect DPCs produced by irradiation of Ehrlich ascites chromatin with ultraviolet light (Julio E.Celis, 1976). It is one of the first approaches to be used for DPCs isolation. CsCl is a high-density salt that forms a linear density gradient during ultracentrifugation, with density gradually decreasing from the bottom to the top. When subjected to centrifugation, cellular components with similar densities but different molecular weights align at specific points within the gradient (Meselson et al., 1957). The covalent linkage of proteins to DNA alters the overall DNA density, resulting in a shift in its sedimentation behavior, which can be used to distinguish DPCs from unmodified DNA.

TOPccs can be efficiently detected using slot blotting with 2–20 µg of DNA, followed by immunodetection with a specific primary antibody ((Nitiss et al., 2012; Subramanian et al., 1995). Similarly, CsCl gradient fractions can be probed for other crosslinked proteins, such as DNMT1 crosslinks induced by 5-aza-dC.

Similar to the RADAR assay, the CsCl isolates can be analyzed for total DPC levels. To enhance detection, isolated proteins may be post-labelled with fluorescein isothiocyanate (FITC) for further fluorescence analysis or western blotting using anti-FITC antibodies.

1.4.1.3 STAR assay

The Superior method for True DNA–protein crosslinks Recovery (STAR) is a modified version of the RADAR assay that was developed in 2023 (Glumac et al., 2023). It was specifically designed to minimize RNA-associated protein contamination in DPC preparations, ensuring a more selective isolation of true DNA–protein crosslinks. Cells are lysed using a detergent-based buffer that does not contain guanidine thiocyanate. The resulting crude nuclear pellets are isolated through high-speed centrifugation, followed by resuspension in a guanidinium-HCl-containing buffer. DNA precipitation and subsequent sample processing are then performed following the RADAR protocol.

The STAR assay detects both enzymatic and non-enzymatic DPCs induced by various agents, including FA, ultraviolet (UV) radiation, topoisomerase inhibitors, and cisplatin. Additionally, similar to the RADAR assay, STAR assay is compatible with multiple DPC detection methods, such as gel staining, BCA assay, immunoblotting, and mass spectrometry, making it a versatile tool for comprehensive DPC analysis (Glumac et al., 2023).

The STAR assay detected formaldehyde-induced crosslinking of histone H3, a well-characterized and abundant DPCs, consistent with prior analyses. It was shown that this assay detects both enzymatic and non-enzymatic DPCs induced by various agents, including FA, UV radiation, topoisomerase inhibitors, and cisplatin. When applied to investigate DPC repair kinetics over 4 hours following exposure to 400 or 800 μM formaldehyde, the assay revealed DPC removal dynamics and SPRTN-mediated clearance, aligning with previous findings obtained using the RADAR assay (Glumac et al., 2023).

1.4.1.4 PxP (Purification of Crosslinked Proteins)

Another recent method, known as Purification of Crosslinked Proteins (PxP), used electroelution for DPCs purification instead of using precipitation-based methods. DNA extraction can be followed by immobilization on a solid matrix, such as agarose, allowing for the removal of non-crosslinked proteins via electro-elution. This technique is an adaptation of chromosome entrapment assays initially developed to study prokaryotic condensing ring interactions with DNA (Weickert et al., 2023b) .

In this method, cells are embedded in agarose plugs by mixing a cell suspension with a low-melting agarose solution and casting the mixture into plug molds. The embedded cells are then lysed within the agarose plugs using a denaturing buffer, which disrupts the cell membrane and denatures cellular proteins. To separate non-crosslinked proteins, the agarose plugs are inserted into the wells of an SDS-polyacrylamide gel electrophoresis (PAGE) gel, where electrophoresis induces electro-elution, removing non-covalently bound proteins while retaining DPCs and chromosomal DNA within the plug. Finally, plugs are retrieved, PxP samples were treated with benzonase to degrade DNA and passed through nitrocellulose columns to eliminate residual agarose, ensuring a purified preparation for subsequent analysis (Weickert et al., 2023b). However, the updated version of the protocol found that both steps were found to be unnecessary, with filtration significantly reducing PxP signals. As a result, these steps have been removed from the original protocol. DPCs can be identified using standard SDS–PAGE assays (protein staining, western blot) or mass spectrometry-based proteomics (LC–MS/MS)(Weickert et al., 2024).

PxP combined with western blotting has been successfully validated for detecting TOP1cc, histone H3, and DNMT1, which are formed in a dose-dependent manner following treatment with camptothecin (CPT), formaldehyde, and 5-aza-dC,

respectively. Notably, this approach also revealed an additional role of SPRTN in the post-replicative repair of 5-aza-dC-induced DNMT1 crosslinks. This replication-independent repair mechanism is initiated by SUMOylation of the protein adduct, followed by RNF4-dependent ubiquitylation, generating a modified DNMT1-DPC that can subsequently be resolved by either the proteasome or SPRTN (Weickert et al., 2023b). Moreover, PxP was used to HMCES–DPCs are readily detectable in S-phase synchronized cells expressing tagged HMCES–WT. Similarly, treatment with the POLα inhibitor CD437 induces HMCES–WT crosslinking, which rapidly resolves once the inhibitor is removed, likely due to the autocatalytic reversal of HMCES–DPCs (Weickert et al., 2024). Table 1.9 shows a comparison between some protein-targeted DPCs isolation methods and Figure 1.23 illustrates schematic of these methods.

Table 1.9. Comparison between some protein-targeted DPCs isolation methods

Method	Year Introduced	Principle	Advantages	Limitations	Reference
RADAR Assay	2013	Protein-targeted; isolates DNA under denaturing conditions using chaotropic agents and SDS, followed by ethanol precipitation and benzonase digestion.	Fast, sensitive, uses low cell number; compatible with Western blotting, ELISA, and MS.	May retain some RNA-associated proteins; requires benzonase digestion and denaturants.	(Kiianitsa & Maizels, 2013)
CsCl Gradient	1976	Density-based separation of DNA-protein complexes using ultracentrifugation in a CsCl gradient; crosslinks alter DNA density, aiding separation.	Can detect crosslink-induced density changes; supports fluorescence tagging and slot blot.	Time-consuming; requires ultracentrifugation and specialized equipment.	(Julio E.Celis, 1976)
STAR Assay	2023	Modified RADAR assay minimizing RNA contamination; uses detergent lysis, guanidinium buffer, and downstream benzonase treatment.	Improved specificity for DNA-protein over RNA-protein; detects enzymatic and non-enzymatic DPCs.	Still relies on precipitation steps; newer method with limited widespread validation.	(Glumac et al., 2023)
PxP Assay	2023	Protein-targeted method using agarose embedding, electrophoresis-based electro-elution to remove unbound proteins while retaining DPCs.	Highly selective purification of crosslinked proteins; effective for both replication-dependent and -independent DPCs.	More complex setup; earlier protocol steps (filtration, benzonase) later found unnecessary and removed.	(Weickert et al., 2023b)

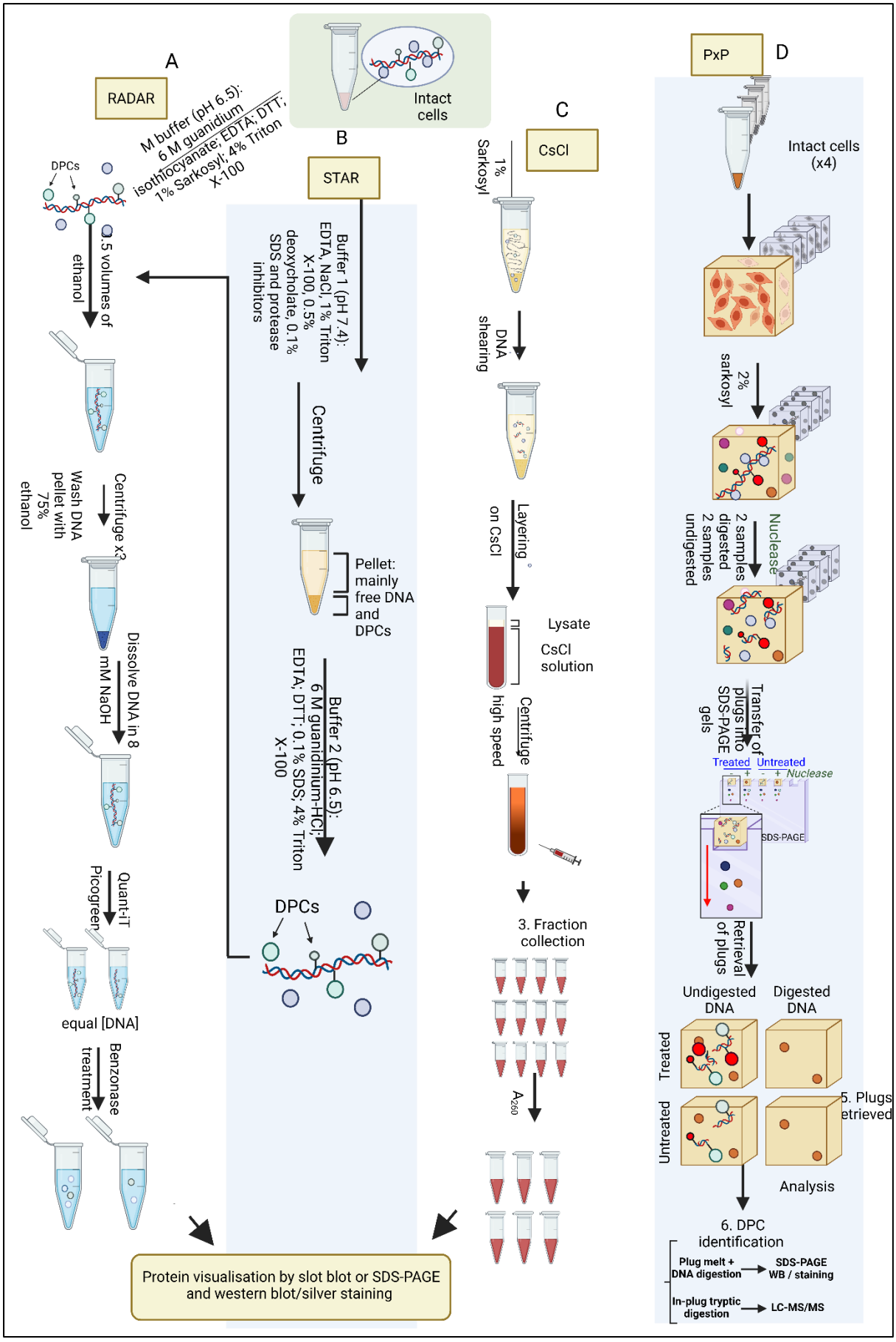

A
RADAR
M buffer (pH 6.5): 6 M guanidium isothiocyanate; EDTA; DTT; 1% Sarkosyl; 4% Triton X-100
DPCs
3.5 volumes of ethanol
Wash DNA pellet with 75% ethanol
Centrifuge x3
Dissolve DNA in 8 mM NaOH
Quant-iT Picogreen
equal [DNA]
Benzonase treatment
Intact cells
B
STAR
Buffer 1 (pH 7.4): EDTA, NaCl, 1% Triton X-100, 0.5% deoxycholate, 0.1% SDS and protease inhibitors
Centrifuge
Pellet: mainly free DNA and DPCs
Buffer 2 (pH 6.5): 6 M guanidinium-HCl; EDTA; DTT; 0.1% SDS; 4% Triton X-100
DPCs
C
CsCl
1% Sarkosyl
DNA shearing
Layering on CsCl
Lysate
CsCl solution
Centrifuge high speed
3. Fraction collection
A260
D
PxP
Intact cells (x4)
2% sarkosyl
2 samples digested
2 samples undigested
Nuclease
Transfer of plugs into SDS-PAGE gels
Treated
Untreated
Nuclease
SDS-PAGE
Retrieval of plugs
Undigested DNA
Digested DNA
Treated
Untreated
5. Plugs retrieved
Analysis
6. DPC identification
Plug melt + DNA digestion
SDS-PAGE WB / staining
In-plug tryptic digestion
LC-MS/MS
Protein visualisation by slot blot or SDS-PAGE and western blot/silver staining

Figure 1.23: Schematic of some Protein-Targeted Methods. Adapted from (Torrecilla et al., 2024)

(A) Schematic of RADAR method according to (Kiianitsa & Maizels, 2013). (B) Schematic of STAR according to (Glumac et al., 2023).(C) Schematic of CsCl gradient method (Julio E.Celis, 1976). (D) Schematic of PxP method according to (Weickert et al., 2023a).

1.4.2 DNA-Targeted Methods

DNA-targeted methods assess DPC levels by quantifying DNA rather than directly detecting crosslinked proteins. These methods isolate DPC-associated DNA either through co-precipitation with proteins (as in KCl-SDS precipitation and ARK assays) or by leveraging differences in electrophoretic mobility (as in the modified comet assay). While these approaches do not provide direct visualization of crosslinked proteins, they offer valuable insights into the genomic distribution of DPCs, making them useful for studying DPC formation and localization within the genome.

1.4.2.1 KCl-SDS

The addition of potassium chloride to sodium dodecyl sulfate (SDS) lead to the formation of an insoluble precipitate, which could be easily recovered through low-speed centrifugation. Since SDS strongly binds to proteins but not to DNA, all proteins and detergent-resistant DNA–protein complexes co-precipitated in the presence of potassium-SDS, while free DNA remained in the supernatant. The amount of SDS-precipitable DNA served as a quantitative measure of DNA–protein crosslinks (DPCs). This method has been adapted by Zhitkovich et al, to detect DPC formation in cells exposed to crosslinking agents such as chromate, cis-platinum(II) diammine dichloride, and formaldehyde, both in vitro and in vivo (Zhitkovich & Costa, 1992).

In a typical procedure, cells are lysed using a detergent-based buffer, and genomic DNA is fragmented through freeze-thaw cycles or vigorous mixing. The sample is then heated, and a salt solution is added on ice to promote the formation of insoluble DNA-protein complexes. After centrifugation, the protein-bound DNA forms a pellet, while free DNA remains in the supernatant. The pellet is then resuspended and washed multiple times through a series of temperature-controlled centrifugation steps to further purify DPC-bound DNA (Zhitkovich & Costa, 1992). To remove any remaining proteins,

enzymatic digestion is performed, and a protein-blocking agent is added to neutralize detergent effects. A final centrifugation step eliminates unwanted components, leaving a purified supernatant containing DPC-associated DNA. The concentration of DPC-bound DNA and free DNA is then quantified using fluorescent DNA detection assays. The DPC level is typically calculated as the proportion of DNA in the pellet relative to the total DNA content (pellet + supernatant), providing a quantitative measure of DNA-protein crosslink formation.

1.4.2.2 ARK assay

The ARK assay is an updated version of KCl-SDS that involves a sequential chaotropic and detergent-based method. The method involves the use of guanidine thiocyanate (GTC) for cell lysis to apply a stringent condition to eliminate noncovalent DNA-protein association, enhancing DPC isolation efficiency and improving detection sensitivity (Hu et al., 2020). Similarly to the KCl-SDS assay, the final DPC quantification is calculated as the ratio of protein-bound DNA to total DNA, providing a measure of DNA-protein crosslink formation.

The assay has been validated using genetic mutants with known DPC repair deficiencies and has demonstrated robust performance in detecting DPCs induced by common agents such as formaldehyde, camptothecin, and etoposide. Additionally, the study confirms the involvement of the Fanconi anemia pathway in DPC repair, highlighting its broader biological significance. With its high sensitivity and reliability, the ARK assay provides a tool for investigating DPC repair mechanisms.

1.4.2.3 Modified Comet assay

The comet assay is a single-cell electrophoresis-based technique primarily used to quantify DNA breaks at the individual cell level. The method involves embedding cells

in agarose on a microscope slide and exposing them to an electric field. During electrophoresis, high molecular weight DNA remains stationary, while smaller DNA fragments, typically resulting from double-strand breaks (DSBs), migrate toward the anode, forming a comet-like tail (D. Ostling. K.J. Johanson, 1984). Under alkaline conditions, the length of the comet tail reflects overall DNA damage, including DSBs, single-strand breaks (SSBs), alkali-labile sites, DNA-DNA crosslinks, and DPCs (D. Ostling. K.J. Johanson, 1984; Tice et al., 1992, 1997).

To specifically identify and quantify DPCs in samples containing both DNA-DNA and DNA-protein crosslinks (Merk & Speit, 1998, 1999). Proteinase K digestion is performed on the slides before electrophoresis. This step degrades crosslinked proteins, allowing DNA fragments previously immobilized by DPCs to migrate, thereby enhancing their detection. This Proteinase K treatment is particularly important when analyzing agents like formaldehyde, which induce both DNA-protein and DNA-DNA crosslinks. Table 1.10 shows a comparison between some protein-targeted DPCs isolation methods and Figure 1.24 illustrates schematic of these methods.

Table 1.10: Comparison between some DNA-targeted DPCs isolation methods

Method	Year	Principle	Detection Type	Advantages	Limitations	Reference
KCl-SDS Assay	1992	SDS binds proteins; addition of KCl precipitates protein-DNA complexes, while free DNA remains soluble. DPCs are quantified based on DNA in the pellet.	Bulk quantification of protein-bound DNA vs. free DNA	Simple and cost-effective; adaptable for in vivo and in vitro settings.	May retain some non-covalent associations; requires multiple centrifugation and wash steps.	(Zhitkovich & Costa, 1992)
ARK Assay	2020	Uses guanidine thiocyanate for stringent lysis to eliminate non-covalent interactions; DPCs are precipitated similarly to KCl-SDS, enhancing sensitivity.	Improved bulk quantification with higher sensitivity	High sensitivity and robustness; validated using DPC-deficient mutants; detects a wide range of DPC-inducing agents.	Still relies on precipitation and chemical denaturation; newer method with limited comparative data.	(Hu et al., 2020)
Modified Comet Assay	1998	Electrophoresis-based method; cells embedded in agarose, and Proteinase K digestion is used to release DNA previously immobilized by DPCs, enabling their quantification.	Single-cell level detection via migration shift post-protein digestion	Allows single-cell analysis; distinguishes DNA-protein crosslinks from DNA-DNA crosslinks with Proteinase K treatment.	Indirect DPC measurement; influenced by DNA breaks and crosslink types; less quantitative than bulk methods.	(Merk & Speit, 1998)

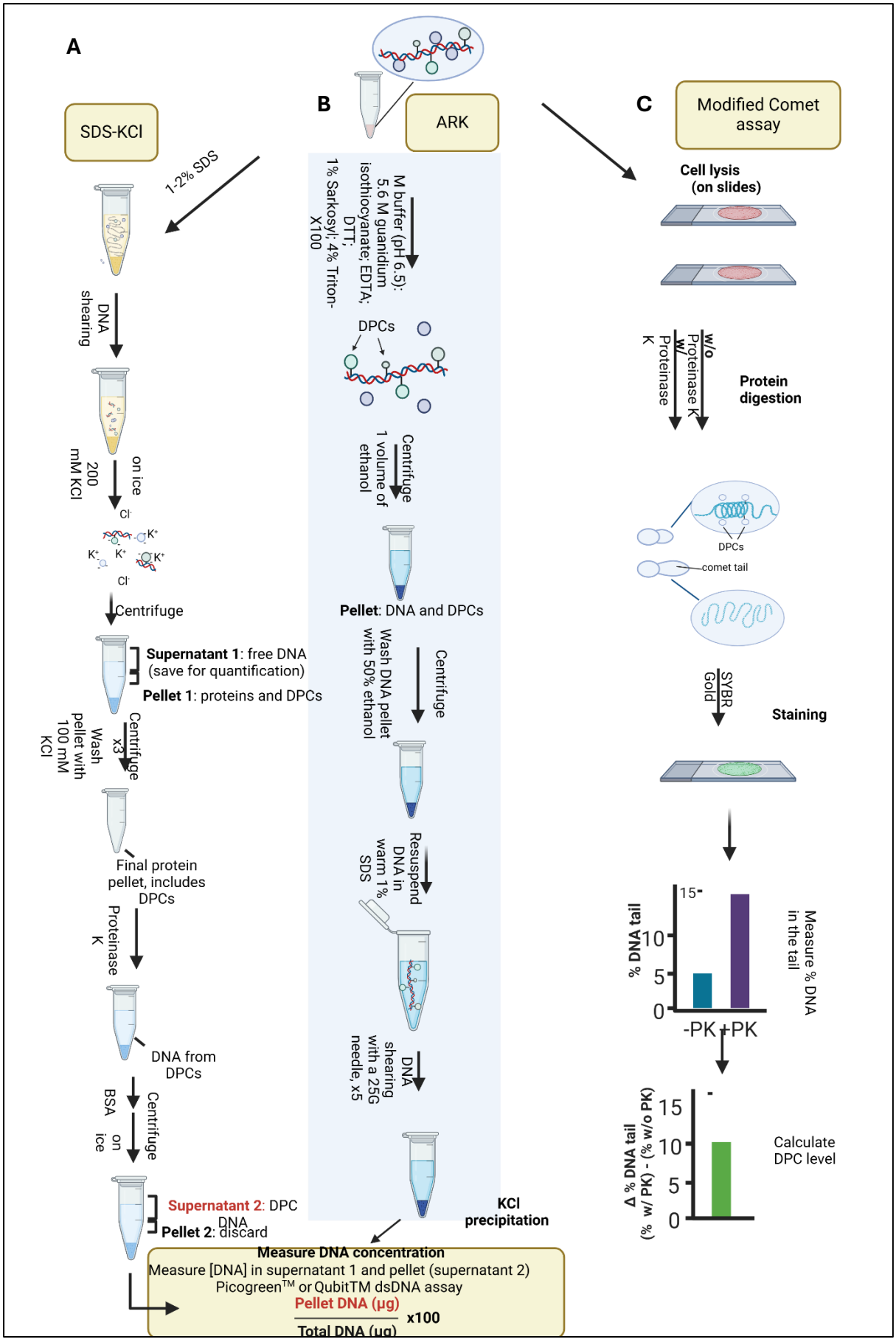

A
SDS-KCl
1-2% SDS
DNA shearing
200 mM KCl
on ice
Cl-
K+
Centrifuge
Supernatant 1: free DNA (save for quantification)
Pellet 1: proteins and DPCs
Wash pellet with 100 mM KCl
Centrifuge x3
Final protein pellet, includes DPCs
Proteinase K
DNA from DPCs
BSA
on ice
Centrifuge
Supernatant 2: DPC DNA
Pellet 2: discard
B
ARK
1% Sarkosyl; 4% Triton-X100
M buffer (pH 6.5): 5.6 M guanidium isothiocyanate; EDTA; DTT;
DPCs
Centrifuge
1 volume of ethanol
Pellet: DNA and DPCs
Wash DNA pellet with 50% ethanol
Centrifuge
Resuspend DNA in warm 1% SDS
DNA shearing with a 25G needle, x5
KCl precipitation
Measure DNA concentration
Measure [DNA] in supernatant 1 and pellet (supernatant 2)
Picogreen™ or QubitTM dsDNA assay
Pellet DNA (µg) / Total DNA (µg) x100
C
Modified Comet assay
Cell lysis (on slides)
Proteinase K
w/
w/o Proteinase K
Protein digestion
DPCs
comet tail
SYBR Gold
Staining
% DNA tail
15
10
5
0
-PK +PK
Measure % DNA in the tail
Δ % DNA tail (% w/ PK) - (% w/o PK)
15
10
5
0
Calculate DPC level

Figure 1.24. Schematic of some DNA-Targeted Methods. Adapted from (Torrecilla et al., 2024)

(A) Schematic of SDS-KCl method according to (Zhitkovich & Costa, 1992) . (B) Schematic of ARK assay according to (Hu et al., 2020).(C) Schematic of modified comet assay method (Merk & Speit, 1998).

1.4.3 Immunodetection with Specific DPC Antibodies

Another way to detect DPCs is to use an antibody designed to detect specific DPCs. One of the well-known examples is using TOP1cc antibody which allows for direct localization and co-localization analysis of TOP1 cleavage complexes without requiring cell lysis or DPC purification, enabling a more efficient and intact assessment of TOP1cc formation within cells (Patel et al., 2016).

Basically, Cells are cultured on coverslips, then subjected to treatment, fixation, permeabilization, and blocking using standard laboratory protocols. To enhance DPC accessibility, coverslips undergo a brief detergent incubation, followed by neutralization with a mild surfactant. Afterwards, they are incubated with the TOP1cc antibody, with the option of co-staining with additional primary antibodies, followed by thorough washing and incubation with fluorescently labelled secondary antibodies. Imaging is performed using a confocal microscope, and TOP1cc foci or mean fluorescence intensity is quantified for analysis (Figure 1.25) (Patel et al., 2016).

Using immunofluorescence studies using the TOP1cc antibody, the involvement of multiple key factors in TOP1cc repair has been confirmed. Our lab found that TEX264 is localized at the nuclear periphery, associates with DNA replication forks, and plays a crucial role in facilitating TOP1cc repair during DNA replication. We also found that TEX264-deficient cells exhibit an accumulation of endogenous TOP1ccs, heightened sensitivity to clinically relevant doses of TOP1 poisons, and increased DNA replication stress, highlighting its essential function in maintaining genome stability (Fielden et al., 2020). Also, using this technique, we were able to show that the autophagy receptor TEX264 functions as a TOP1cc sensor at DNA replication forks, initiating TOP1cc processing through the p97 ATPase and facilitating its lysosomal degradation in a manner dependent on MRE11 nuclease and ATR kinase activity (Lascaux et al., 2024).

In addition, Immunofluorescence studies using the TOP1cc antibody have also confirmed the involvement of several key factors in TOP1cc repair including TDP1 SPRTN, FAM111A, p97/VCP with its cofactor TEX264 (Fielden et al., 2020; Huang et al., 2020; Kojima et al., 2020; Liao et al., 2018). These studies have also reinforced that TOP1ccs undergo sequential SUMOylation and ubiquitylation, marking them for proteasomal degradation.

Another immunodetection-based method for specific DPC analysis utilizes classical DNA fibre spreading combined with PARP1 immunostaining, allowing for the direct visualization of PARP1-DPCs on DNA fibres (Prasad et al., 2014). This technique is highly versatile, providing valuable insights into the formation, localization, and distribution of PARP1-DPCs across the genome. By enabling precise detection of these crosslinks at the single-molecule level, this approach enhances our understanding of the role of PARP1-DPCs in genomic stability and DNA repair mechanisms.

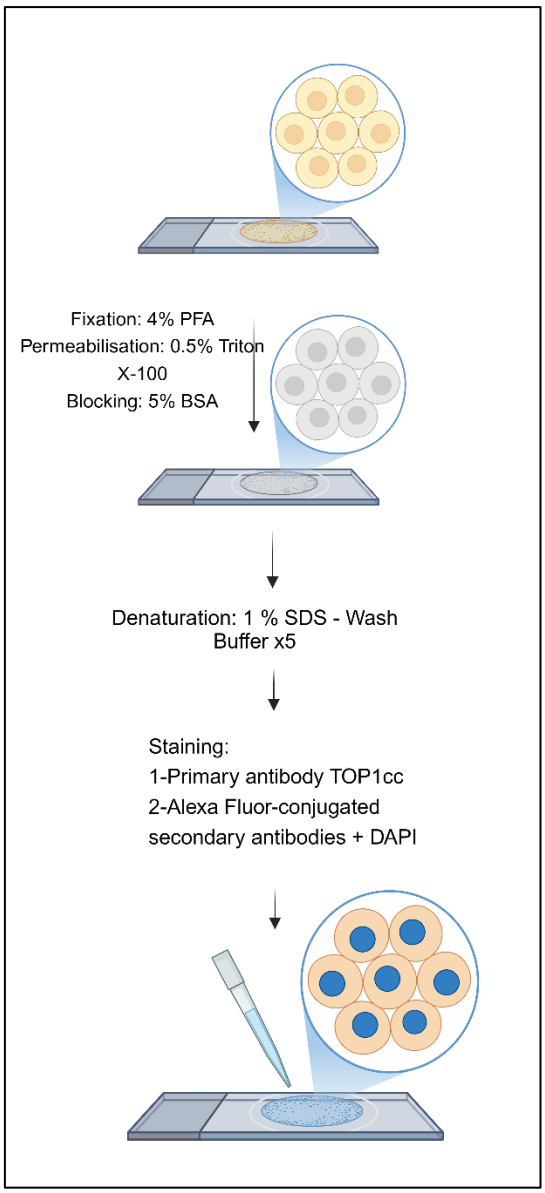


Figure 1.25: Detection of TOP1cc by immunofluorescence. Adapted from (Torrecilla et al., 2024)

Schematic of the TOP1cc immunofluorescence protocol according to (Patel et al., 2016).

These methods aim to effectively separate covalently bound DNA-protein complexes from free DNA and proteins, enabling the study of DPC formation, stability, and repair. Selecting an optimal DPC isolation and quantification technique is essential for accurately assessing the dynamics of DPCs, particularly in response to different genotoxic agents.

1.5 Aim

The field of DPC repair has seen a surge in attention in recent years since numerous chemotherapeutic agents currently employed in clinical settings demonstrate their anti-tumour effects by inducing DPCs. Thus, it is believed that targeting DPC repair proteins could enhance the effectiveness of these drugs. This observation suggests that the strategic targeting of DPC repair mechanisms like SPRTN may enhance the sensitivity of tumours to agents that induce DPCs.

Various studies have highlighted the potential role of SPRTN in modulating the effectiveness of chemotherapy (Lessel et al., 2014; Stingele et al., 2016; Vaz et al., 2016). Notably, research has established that the depletion of SPRTN enhances the cytotoxic effects of DNA crosslinking agents such as formaldehyde, camptothecin, and etoposide in HeLa cells and lymphoblastoid cells derived from patients with Ruijs-Aalfs syndrome (RJALS) (Lessel, Vaz, Halder, Lockhart, Marinovic-terzic, et al., 2014; Vaz et al., 2016). RJALS syndrome, first recognized in three individuals in 2014, is a rare genetic disorder marked by biallelic germline mutations in SPRTN, which leads to increased genomic instability, progeroid characteristics, and a heightened risk of early-onset hepatocellular carcinoma. These findings were validated in *C. elegans*, where mutant strains deficient in SPRTN exhibited heightened sensitivity to formaldehyde and cisplatin, a commonly used platinum-based chemotherapeutic agent (Stingele et al., 2016). Furthermore, the increased sensitivity to camptothecin and the elevated

levels of TOP1ccs in cells from SPRTN hypomorphic mice further underscore the involvement of SPRTN in the repair of TOP1ccs lesions caused by topoisomerase inhibitors (Maskey et al., 2017).

The primary objective of this study is to investigate the role of SPRTN in modulating cellular responses to ionising radiation, with a particular emphasis on its function in DPC repair. While DPCs are recognised as highly toxic lesions generated by various genotoxic agents, their formation and repair following IR exposure remain underexplored and frequently overlooked in the context of radiation-induced damage. Despite evidence suggesting that IR can induce DPCs either directly or through oxidative stress mechanisms, the molecular pathways governing their resolution, particularly the role of SPRTN, remain controversial and unclear.

Conflicting findings in the literature regarding SPRTN's contribution to DPC repair post-IR highlight the need for a thorough investigation. Some studies suggest a minimal role for SPRTN, whereas others propose it is crucial for maintaining genome stability under IR-induced stress. This uncertainty necessitates a systematic approach to evaluate how SPRTN depletion impacts DPC accumulation, repair kinetics, and overall radiation sensitivity, especially in proliferating human cell lines, where replication-associated repair mechanisms are vital.

In addition to observing phenotypic outcomes, this study aims to delve into the molecular mechanisms underlying these responses. Specifically, it seeks to clarify how SPRTN-mediated DPC proteolysis influences key DNA damage response pathways, checkpoint activation, and genomic integrity following IR. By elucidating these mechanisms, the research aspires to provide a mechanistic framework explaining how SPRTN modulates radiation outcomes.

Moreover, these findings may offer insights into whether SPRTN expression levels could serve as predictive biomarkers for patient responsiveness to radiotherapy or form the basis for targeted radiosensitisation strategies. Understanding these mechanisms could inform therapeutic interventions aimed at exploiting DPC repair deficiencies to enhance tumour cell killing while preserving normal tissue.

Ultimately, this work is driven by the broader goal of advancing the field of radiation biology by uncovering the molecular underpinnings of DPC repair in IR responses—an area historically neglected but increasingly recognised for its therapeutic significance.

To accurately investigate SPRTN's role in IR-induced DPC repair, it is essential to find a reliable, sensitive, and reproducible method for detecting and quantifying DPCs under IR exposure. Thus, a key secondary aim is to evaluate and compare different DPC isolation techniques, ensuring the chosen method is suitable for analysing SPRTN-dependent DPC repair.

This study will compare four distinct DPC isolation methods under identical conditions in HeLa cells:

- Protein-Targeted Methods:
    - RADAR assay: Uses guanidinium thiocyanate (GTC) to isolate covalently crosslinked DNA–protein complexes while removing non-covalently bound proteins.
    - STAR assay: A modification of the RADAR assay that minimises RNA contamination and enhances specificity.
- DNA-Targeted Methods:

- ARK assay: Utilises salt precipitation to retain DNA-bound proteins while removing free proteins.
- Modified comet assay: Employs single-cell electrophoresis, combined with Proteinase K digestion, to indirectly assess global DPC levels via DNA migration.

The goal of this methodological evaluation is to:

- Identify the most sensitive and reproducible DPC detection method.
- Select the approach best suited for studying IR-induced DPCs.

Following the identification of the most suitable DPC isolation method, its applicability was extended to assess DPC formation under specialised conditions of particular relevance to radiobiology:

FLASH Radiation: This novel radiotherapy modality delivers ultra-high dose rates and has shown promise in reducing normal tissue toxicity while preserving tumour control (Durante et al., 2018). However, its impact on DPC induction remains largely unexplored.

Hypoxic Tumour Microenvironments: Hypoxia is a hallmark of solid tumours and is known to modulate DNA repair processes, potentially influencing both the formation and resolution of DPCs (Z. Chen et al., 2023).

While these exploratory studies fall outside the primary scope of SPRTN depletion, they serve two important purposes. First, they provide an opportunity to evaluate the sensitivity, robustness, and adaptability of the selected DPC isolation method under physiologically relevant stress conditions. Second, they offer preliminary insights into how DPC dynamics may vary in response to distinct radiation modalities and

microenvironmental factors-an understanding that could inform future studies investigating SPRTN function under complex in vivo-like conditions.

By applying the chosen method to hypoxic and FLASH-irradiated cells, this work extends the utility of the methodological framework and builds a broader foundation for contextualising SPRTN's role in diverse biological settings.

Chapter 2: Materials and Methods

2.1 Cell culture

All cell lines used were grown in Dulbecco's Modified Eagle's Medium (DMEM) – High glucose [Sigma-Aldrich - D6429-500ML], supplemented with 10% Fetal Bovine Serum (FBS) [Sigma-Aldrich - F2442-500ML] and 1% Penicillin/Streptomycin [Sigma-Aldrich - P0781-100ML]. For doxycycline-inducible stable Flp-In TRex $SPRTN^{wt}$ or $SPRTN^{E112A}$ cell lines, the media was additionally supplemented with 15 µg/ml blasticidin and 100 µg/ml hygromycin. Cells were incubated at 37°C, 5% CO2. All cell lines were regularly screened for mycoplasma using a MycoAlert™ Mycoplasma Detection Kit [Lonza - LT07-318].

Human HeLa cell, MCF-7, HCT116, A and T24, were obtained from ATCC. Both the CRISPR–Cas9 SPRTN knockout cells and doxycycline (DOX) inducible stable Flp-In HeLa cell lines expressing wild-type (WT), enzymatic dead protein (E112A) were created by our lab (Vaz et al., 2016). HCT116 OsTIR1 SPRTN-AID was produced by Cristiano Peron, a previous PhD student in Ramadan Laboratory.

2.2 Radiation

For conventional radiation, cells were irradiated by Ionizing radiation (Gamma radiation) using Cesium-137 irradiator. The irradiation device used is GSR-D1 irradiator (Gamma Services, Surrey, UK) with a dose rate: 1.2 Gy/min. Cell lines were either collected or fixed at different time point post-radiation. FLASH irradiation was performed in collaboration with the Petersson Group at the Department of Oncology, University of Oxford. All irradiations were performed with a FLASH-optimized in-house developed linear accelerator (linac), delivering electrons of 6 MeV nominal energy horizontal-firing electronic linac.

2.3 siRNA treatment

Briefly, cells were dissociated into single-cell suspension by using a solution of 10% Trypsin-EDTA [Gibco – 15400-054] in Phosphate-Buffered Saline (PBS) before being transfected with the indicated siRNA and Lipofectamine RNAiMAX [Invitrogen – 13778-150] in their culture medium for 24 hours. Small interfering RNA (siRNA) transfection of cultured cells was previously diluted in 1000 µl Opti-MEM [Gibco – 31985-070] along with 10 µl Lipofectamine RNAiMAX. After 15 minutes of incubation at room temperature, the complexes were added to the cells to a final volume of 5 ml. A mechanism of expression silencing by siRNAs is explained in this overview (Birmingham et al., 2007).

siRNA against Human OGG1 (J-005147-09-0005), DNA-PK (J-005030-06-0005) siH1.2 (J-006630-06-0002) were purchased from Dharmacon (Pittsburg, PA, USA). siRNA against Histone methyltransferase [ThermoFisher – 117147]. Table 2.1 shows siRNA against SPRTN. Depletion of the target proteins was confirmed using Western blotting.

Table 2.1. Sequence of oligonucleotides used for siRNA depletions

siRNA	Target	Working	Company	Sequence
siLUC	Luciferase	20 nM	(Microsynth AG, Balgach, Switzerland)	CGUACGCGGAAUACUUCGATT
siSPRTN #1	SPRTN	50 nM		GUCAGGAAGUUCUGGUUAA
siSPRTN #2		100 nM		AGCCAAUAUAACGGUAUACCA
siSPRTN #3		20 nM		CACGAUGAGGUGGAUGAGUAU

2.4 Colony Forming Assay

Cells were trypsinized into a single-cell suspension with a 10% Trypsin-EDTA solution [Gibco – 15400-054] in PBS. Subsequently, the cells were plated in 6-well plates using DMEM – High glucose [Sigma-Aldrich - D6429-500ML] at a density ranging from 500 to 800 cells per well. A period of 24 hours was allowed for the cells to adhere to the well bottoms before the media was removed and treatment commenced for the designated duration. Following this, the cells were incubated for one week until visible colonies formed. The colonies were fixed in methanol [Fisher Chemical - M/3950/17] for 10 minutes and subsequently stained with crystal violet solution [Merck - V5265-500ML] for 30 minutes. After washing the colonies with H2O, they were allowed to dry at room temperature. Next, colony counts were performed using the automatic colony counter GelCountTM. An overview of the colony-forming assay can be found in this overview (Franken et al., 2006).

2.5 MTT assay

MTT Cell Proliferation and Cytotoxicity Assay Kit was used to determine cell viability [Elabscience - E-CK-A341].

Cells (1000 cells/ well) were plated in a 96-well plate with a final volume of 100 µl per well and left to attach to the plate overnight. The next day, cells were irradiated and left to recover for 24 hours. After that 50 µL of 1×MTT working solution (that contains (3-(4,5-dimethylthiazol-2-yl)-2,5-diphenyltetrazolium bromide) to each well and incubate for around 4 h. After incubation, the crystalline dark purple product formazan was formed then the supernatant was removed carefully followed by the addition of 150 µL DMSO to each well to dissolve the formazan format. Then absorbance was measured using POLARstar Omega plate reader (BMG Labtech, Cary, NC, USA) at

570 nm. More information about MTT assay can be found in this overview (Mosmann, 1983)

2.6 Resazurin assay

Resazurin powder [Sigma, R707-1G] was dissolved in PBS (pH 7.4) to achieve a concentration of 0.15 mg/ml. Resazurin solution was filtered using a 0.2 µm filter into a sterile dark container which was then stored at -20°C until used.

Cells (1000 cells/ well) were seeded in a 96-well plate with a final volume of 100 µl per well and left to attach to the plate overnight. The next day, cells were irradiated and left to recover for 24 hours. Then, 20 µl of the resazurin solution was added into each well and plate was incubated for a period of 4 hours at 37°C. Fluorescence was measured using a filter set with an excitation wavelength of 560 nm and an emission wavelength of 590 nm using POLARstar Omega plate reader [BMG Labtech - Cary, NC, USA). More detailed information can be here (Ansar Ahmed et al., 1994).

2.7 Caspase 3/7 activity assay

The activity of Caspase 3/7 was measured using The Apo-ONE® Homogeneous Caspase-3/7 Assay [Promega - G7791]. The protocol principle is showing in Figure 8. Briefly, cells were seeded in a 96-well plate with a final volume of 100 µl per well and left to attach to the plate overnight. Next day, cells were irradiated and left to recover for 24 hours before adding Apo-ONE® Caspase-3/7 Reagent and then incubated for 6-12 hours. Fluorescence was measured using excitation wavelength is 499nm with emission maximum at a wavelength of 521nm.

2.8 RADAR Assay

DPCs were detected using a modified rapid approach to DNA adduct recovery (RADAR) assay. In brief, 1.5 to 2 x 10^6 cells were lysed in 1 ml of M buffer (MB), containing 6 M Guanidinium thiocyanate (GTC), 10 mM Tris–HCl (pH 6.8), 20 mM EDTA, 4% Triton X100, 1% Sarkosyl and 1% dithiothreitol (DTT). DNA was precipitated by adding 1 ml of 100% ethanol and was washed three times in wash buffer (20 mM Tris–HCl pH 6.8, 150 mM NaCl and 50% ethanol) and DNA was solubilized in 1 ml of 8 mM NaOH. A small aliquot of the recovered DNA was digested with 50 µg/ml proteinase K [Invitrogen – 4333793] for 3 hours at 50°C and quantified using PicoGreen dye [Invitrogen - P11496] according to manufacturer instructions to determine DNA concentration. DNA concentration was further confirmed by slot-blot analysis followed by immunodetection with antibody against dsDNA.

2.9 STAR assay

The STAR assay protocol was followed according to (Glumac et al., 2023). Cells were lysed on ice for 15 minutes in Buffer 1 containing: 50 mM Tris–HCl (pH 7.4), 1 mM EDTA, 150 mM NaCl, 1% Triton X-100, 0.5% deoxycholate (DOC), 0.1% sodium dodecyl sulfate (SDS), and a protease inhibitor cocktail (Complete Tablets EasyPack, Roche; Cat. No. 04693116001). Lysates were centrifuged at 16,000 × g for 15 minutes, and the resulting pellet—containing DNA and other insoluble components—was resuspended in Buffer 2 composed of: 6 M guanidinium–HCl, 10 mM Tris–HCl (pH 6.5), 20 mM EDTA, 4% Triton X-100, 0.1% SDS, and 1% dithiothreitol (DTT).

DNA was subsequently isolated by ethanol precipitation using a 75% ethanol cutoff. The precipitated DNA was pelleted by centrifugation at 16,000 × g for 10 minutes, washed with 75% ethanol, and centrifuged again under the same conditions.

Supernatants were discarded, and residual ethanol was allowed to evaporate completely.

Pellets were then resuspended in Buffer 3 (16 mM NaOH) and partially neutralized by the addition of an equal volume of 40 mM Tris–HCl (pH 7.5). The samples were subsequently split for quantification of DNA and protein content.

2.10 ARK Assay (advanced recovery of K [potassium]-SDS precipitates)

ARK assay was used to determine DPCs level following the published protocol (Hu et al., 2020). Guanidine thiocyanate (GTC) was used for cell lysis to apply a stringent condition to eliminate noncovalent DNA-protein. Ethanol (50%) was used to precipitate DPCs together with free DNA and unbound proteins. Then the DNA pellet was dissolved in 1% SDS at denaturing temperature to further disrupt noncovalent DNA-protein associations. Following KCl-mediated precipitation to remove free DNA, the protein-bound DNA was released by proteinase K digestion and quantified against total genomic DNA to obtain the DPC coefficient.

2.11 Modified comet assay

Briefly, 5×10^4 cells per condition were mixed with 0.5–1% low-melting-point agarose and spread onto two microscope slides per condition. Slides were then incubated in a lysis buffer containing 1% Triton X-100 and 0.5% Sarcosyl overnight. Proteinase K (0.8% w/v) was applied to the lysis buffer of one of the two replicate slides, enabling digestion of crosslinked proteins.

Subsequently, slides were placed in an electrophoresis tank filled with Tris–acetate–EDTA buffer (TAE buffer), and electrophoresis was carried out for 25 minutes at 25 V. After electrophoresis, slides were air-dried overnight and stained with a fluorescent

DNA dye (e.g., SYBR Gold). DNA migration patterns were visualised using fluorescence microscopy.

The comet tail moment, representing the extent of DNA migration, was quantified using image analysis software such as Andor Komet and expressed as a percentage of total cellular fluorescence. DPC levels were determined by calculating the difference in tail moment between Proteinase K-treated and untreated slides, reflecting the degree of DNA–protein crosslinking.

2.12 Western Blot (WB)

Western Blot was performed using sodium dodecyl sulfate-polyacrylamide gel electrophoresis (SDS-PAGE) and immuno-blotting (Henderson & Wolf, 2003).

2.12.1 Sample preparation

First, cell were harvested and then lysed using RIPA buffer (Radioimmunoprecipitation assay) that consists of 50 mM Tris HCl,pH 7.4, 150 mM NaCl, 1X Triton, 0.5% sodium deoxycholate , 0.1 % SDS, 5 mM EDTA. Protein quantification was done for whole cell extract using DC Protein Assay Reagents [Biorad - 5000116]. Then around 60-90 µg of samples mixed to 1x Laemmli buffer (50 mM Tris-HCl pH 6.8, 2% SDS, 10% Glycerol, 0.05% bromophenol blue).

2.12.2 Protein Separation

Samples were then loaded into SDS-PAGE gels that were made as follows: each gel consists of separating and stacking buffers. Separating gel composed of 1.5 M Tris, pH 8.8, 0.4% SDS, 30% acrylamide (to a final concentration of 5 – 18%) acrylamide/ bisacrylamide solution, 0.5% ammonium persulfate and 0.06%

Tetramethylethylenediamine). For the stacking gel 0.5 M Tris, pH 6.8, 0.4% SDS, 30% acrylamide (to a final concentration of 4%). Protein separation was performed at 80 V in running buffer (1x Tris/Glycine, 0.1 %SDS).

Protein bands were then transferred from polyacrylamide gels into either a Nitrocellulose [GE Healthcare, rpn203b] or Polyvinylidene fluoride (PVDF) membrane [Bio-Rad, 1620177]. This was done in the Mini-PROTEAN Tetra Electrophoresis System (Bio-Rad) and transfer buffer (1x Tris/Glycine, 20% methanol, 0.025%).

2.12.3 Immunoblotting

Following the transfer, membranes were then washed with 1 x TBS-T (20 mM Tris, 150 mM NaCl) and then incubated with 5% milk diluted in 1x TBS-T for 1 hr at room temperature. After that, membranes were incubated with the primary antibodies against the target protein. Primary antibodies were diluted in 3% bovine serum albumin (BSA) and incubated with the membrane overnight 4˚C. Then, membranes were washed three times in 1 x TBS-T for 5 min each and then incubated with the proper Horseradish peroxidase (HRP)-conjugated secondary antibodies diluted in 2.5% milk in TBS-T) for 1 hr at room temperature. Membranes were then washed for three times in 1 x TBS-T.

2.12.4 Band detection

Membranes were incubated with enhanced chemiluminescent substrate detection reagent [Thermo Fisher – 34580 or 34094] for 5 mins. Proteins were visualised using the ChemiDoc MP system [Bio-Rad]. Quantification of western blot bands was performed on ImageLab™ software [Bio-Rad].

Table 2.2. Primary antibodies used for western blot.

Primary antibody	Working dilution	Company/ Catalogue number	Origin
β-Actin	1:2,000	Thermo Fisher Scientific/ (AM4302)	Mouse
H3	1:3,000	Abcam/ (AB1791)	Rabbit
V5	1:1,000	Novex/ (R96025)	Mouse
Vinculin	1:1,000	Santa Cruz/ (SC-73614)	Mouse
OGG1	1:1000	Novus/ (NB100-106SS)	Rabbit
DNA-PK	1:500	Abcam/ (Ab70250)	Rabbit
pCHK1 (pS317)	1:500	Cell signaling/ (2344)	Rabbit
pCHK2 (Thr68)	1:500	Cell signaling/ (2661)	Rabbit
pKAP1 (pS834)	1:500	Abcam/ (ab70369)	Rabbit
CHK1	1:1000	Abcam/ (ab32531)	Rabbit
CHK2	1:1000	Cell signaling/ (2662)	Rabbit
KAP1	1:1000	Abcam/ (ab10484)	Rabbit
H3K4AC	1:1000	(Cell Signalling)/ (26482)	Rabbit
H3K9AC	1:1000	Abcam/ (ab4441)	Rabbit
H3K9Me	1:1000	Abcam/ (ab8898)	Rabbit
H1.2	1:1000	Abcam/ (ab17677)	Rabbit

Table 2.*3*. Secondary antibodies used for western blot.

Secondary antibody	Working dilution	Company/ Catalogue number	Origin
Anti-Mouse IgG	1:10,000	Thermo Fisher/ Scientific (31430)	Goat
Anti-Rabbit IgG	1:10,000	Thermo Fisher/ Scientific (65-6120)	Goat

2.13 Immunofluorescence

Cells were seeded on glass coverslips in six-well plates. Cells were fixed in 4% formaldehyde for 15 min at room temperature. Fixed cells were washed with 1× PBS and permeabilised in 0.5% Triton X-100 prepared in PBS for 15 min at 4 °C. After blocking in 5% BSA/PBS for 1 h at room temperature, cells were incubated with primary antibodies diluted in 2.5% BSA PBS solution for 1 h at room temperature. Coverslips were then washed three times in 1× PBS and incubated with secondary antibodies and DAPI (1:500) for 1 h at room temperature. Coverslips were mounted onto slides using Fluoromount-G™ Mounting Medium [Invitrogen, 00-4958-02] and imaged using a Nikon NiE microscope. For representative Images, ImageJ was used (Schindelin et al., 2012). Analysis was carried out using Cell Profiler (Stirling et al., 2021).

Table 2.*4*. Primary antibodies used for IF.

Primary antibody	Working dilution	Company/ Catalogue number	Origin
53BP1	1:250	Cell Signalling / (4937)	Rabbit
ɣ-H2AX (Ser 139)	1:500	Millipore/ (05-636)	Mouse
H1.2	1:500	Abcam/ (ab17677)	Rabbit
H3K9Ac	1:500	Abcam/ (ab4441)	Rabbit
H3.3	1:500	Abcam/ ab176840	Rabbit
Nucleoli staining -HNRNP	1:500	Sigma-Aldrich/ (SAB4500109)	Rabbit

2.14 Neutral Comet assay:

A neutral comet assay was performed to detect total DSBs (Calini et al., 2002). Briefly, cells subjected to IR and left to recover at the indicated times. Around 800 µl of molten normal melting point agarose (NMPA) to a slide. Trypsinised cells were diluted to 2 × 10^5 cells/ml. Cells were mixed with 1 ml low melting point agarose (LMPA) (37°C). Then, 1 ml was added to NMPA-coated slide. Cells were lysed by placing the slides in coplin jars containing fresh cold lysis buffer overnight at 4°C. Slides were washed twice with cold TBE for 20 mins. Then, they were transferred to comet electrophoresis tank where electrophorese was done at 25 V for 25 mins. After the slides were allowed to air dry overnight, they were rehydrated in dH_2O for 30 mins and 1 ml SYBR Gold (1:10,000 in dH2O) [Thermo Fisher - S11494] was added to each slide for 30 mins.

2.15 Alkaline Comet assay

Alkaline Comet assay was used to detect total damage of DNA, that includes SSB, DSB, AP site and DPCs (Singh et al., 1988).

Slides for the comet assay were prepared by covering them with 1% NMPA in water and the left overnight to dry. Next day, cells were irradiated and left to recover at indicated times at 37C°, 20% O2 and 5% CO2. Cells were then tryprysnized and then immediately resuspended in 1% LMPA in PBS at 37C°. Slides were then incubated in lysis buffer (2.5 M NaCl, 100 mM EDTA, 10 mM Tris–HCl, 1% (v/v) DMSO and 1% (v/v) Triton X-100, at pH 10.5) and left overnight at 4 C°. Next, to unwind DNA slides were then incubated for 30 minutes in 4 °C electrophoresis buffer (300 mM NaOH, 1 mM EDTA, 1% (v/v) DMSO, pH > 13). Using the same buffer, electrophoresis was then performed for 25 min at 25V (300mA). Then, Tris–HCl pH 8 was added to the slides to neutralise the cells. Slides were stained with SYBR Gold (1:10,000 in dH2O) for 30 min. For both alkaline and neutral comet tail moments were measured with ImageJ software with the plugin OpenComet (Gyori et al., 2014). At least 100 cells were analysed for each sample. Statistical analysis was done by Graphpad Prism software using unpaired t-test. Data are shown as Tail% DNA, which is calculated as (the total intensity of the tail/the total intensity of the whole comet).

2.16 Flow cytometry

Trypsynised cells were washed twice with PBS and then fixed in ice-cold methanol at -20°C until use. The cells were then washed with PBS. The cells were stained with 20 µg/ml of propidium iodide (PI) diluted in PBS and 10 µg/ml RNase A for 30 minutes at 37 °C. Cells were analyzed on Bioanalysis CytoFlex flow cytometer. A minimum of

10,000 events were counted. Data analysis was performed using FlowJo™ v10.8 Software (BD Life Sciences).

2.17 Mnase assay

Mnase assay was used to what extent DNA is compacted post radiation (Chung et al., 2010). Cells were trypsenised, harvested and resuspend at ~26000 cells/ml in Buffer A (10 mM Tris-HCl pH7.5, 100 mM KCl, 3 mM MgCl2, 1mM CaCl2, 0.5 mM PSMF) followed by two washes with the same buffer. After that, cells were resuspend at ~56000 cells/ml in Buffer A + 0.6% NP-40 to allow lysis for 5 min on ice. Cells were then centrifuged for 5 min at 2000 rpm and then resuspend in 500 µl of MNase Buffer (15 mM Tris-HCl pH7.5, 15 mM NaCl, 60 mM KCl, 1 mM CaCl2, 0.25 mM PMSF) followed by two washes with the same buffer.

After that MNase was added (2U for 5 min at 30 ºC with agitation) to digest the exposed DNA. To stop the reaction, the same volume as the extract of TEES/Proteinase K was added (10 mM Tris pH7.5, 10 mM EGTA, 10 mM EDTA, 1% SDS, 50 mg/ml Proteinase K) and then incubated at 37 ºC, overnight. For DNA extraction, an equal volume of phenol/chloroform/isoamyl alcohol (25:24:1) was added to the reaction and was vortexed and then centrifuged 10 min at 10,000 rpm. Then the aqueous top layer was transferred to a new tube, then 1/10 volume of 3 M NaAc and 2 volumes of 100% ethanol were added and left for 30-60 min at -20 ºC. The mixture was centrifuged for 2 min at 10,000 rpm then it was rinsed twice with 70% ethanol. Ethanol was discarded and pellet was air dried. Finally, DNA was resuspended in TE Buffer (25-50 µl) until dissolved. Digested DNA was seperated in 2.5% agarose gel and 1:10000 GelRed for DNA staining [Millipore - SCT122]. Images were analysed using on ImageLab™ software [Bio-Rad].

2.18 RNA sequencing

RNA sequencing (RNA-seq) is a well-known method, first developed in 2008, that relies on deep-sequencing technologies to study the transcriptome of different cells(Z. Wang et al., 2009). The possibility to analyze the whole-genome transcriptome of cells under different conditions has further expanded our possibilities to understand how cells can respond and adapt to different stimuli, and a range of companies now offer support to laboratories interested in performing a transcriptomic analysis.

To perform RNA-seq, we used services provided by an external company: BGI Genomics (https://www.bgi.com/global). This Chinese genomics company was originally founded in 1999 in order to support the global efforts of the Human Genome Project, and has since specialized in DNA and RNA sequencing. Accordingly, after treating the cells as required and extracting the RNA to be sequenced, samples were shipped to BGI Genomics to perform the initial transcriptomic analysis.

The protocol was divided into two main parts:

- RNA extraction and quality assessment
- RNA-seq

2.18.1 RNA extraction and quality assessment

RNA was extracted using the GeneJET RNA Purification Kit [Thermo Scientific™-K0731]. The quality of the RNA samples was assessed with a NanoDrop™ One/OneC Microvolume UV-Vis Spectrophotometer (Thermo Fisher Scientific, ND-ONE-W). The evaluation ensured that each sample had a concentration greater than 10 ng/µl, an OD260/280 ratio above 2.0, and an OD260/230 ratio above 2.0, indicating sufficient

quality for RNA-seq. Following this assessment, samples were stored at -80°C for 48 hours until they were ready for shipment to BGI Genomics.

2.18.2 RNA-seq

The samples were analyzed under specified experimental conditions, including two different cell lines, each with or without SPRTN expression, with three independent biological replicates per condition. This resulted in a total of 12 samples, which were processed using the DNBSEQ platform, yielding an average of 4.49G data per sample.

To evaluate the consistency of gene expression among biological replicates, Pearson correlation coefficients were calculated for all gene expression comparisons between pairs of samples. The results were visualized as a heatmap in Figures 2.1, where higher correlation coefficients indicated greater similarity in gene expression levels between samples. Subsequently, principal component analysis (PCA) was performed to distill the complex gene expression data into a few key components, facilitating comparisons among samples and identifying any outliers.

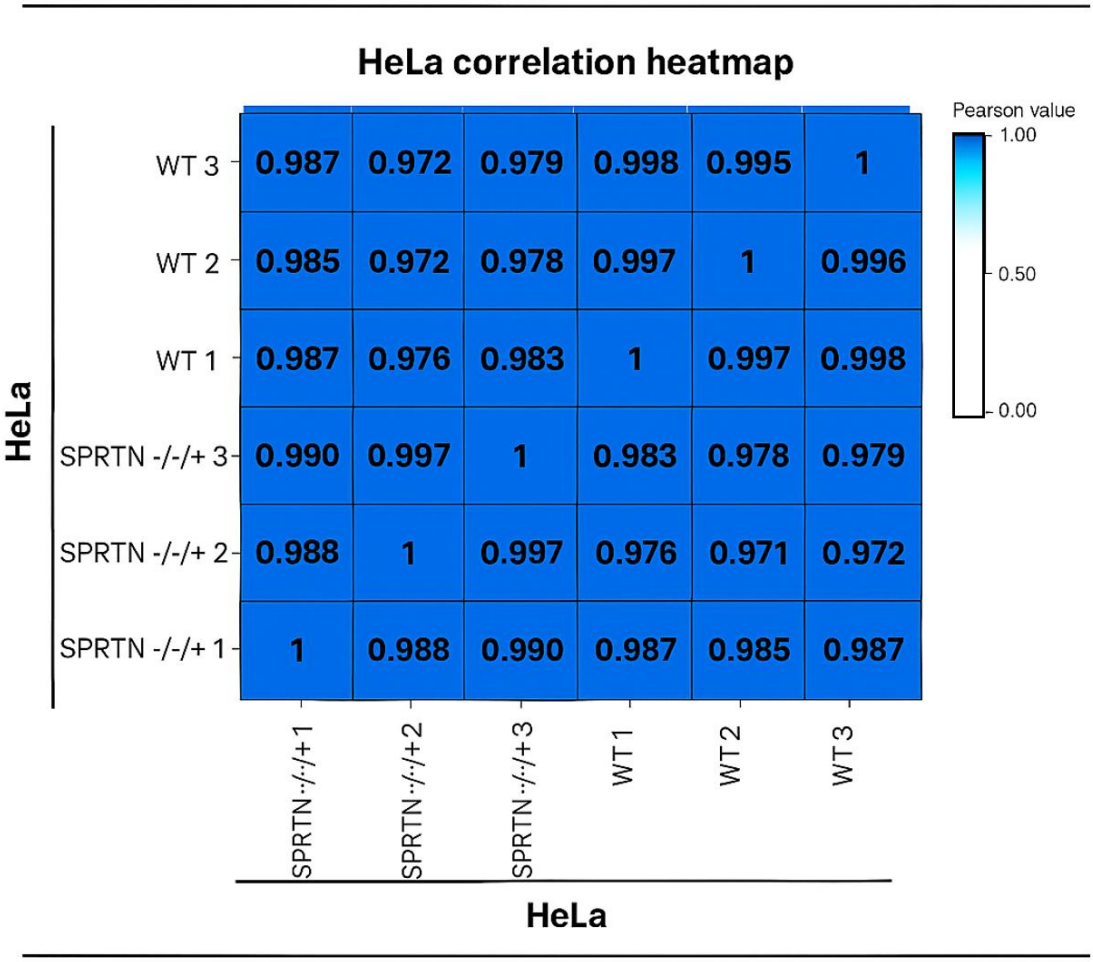


Figure 2.1. RNA-seq correlation heatmaps for HeLa cells.

Correlation heatmap of HeLa cells, with and without SPRTN depletion. This figure was prepared by Cristiano Peron, a previous PhD student in the Ramadan Laboratory

Chapter 3: DNA-Protein Crosslinks – Isolation Methods

3.1 Introduction

A critical prerequisite for elucidating the role of SPRTN in the cellular response to ionising radiation is the establishment of a reliable and biologically relevant framework for detecting and quantifying DPCs. DPCs represent a particularly deleterious form of DNA damage, characterised by covalent linkages between DNA and proteins that obstruct essential cellular processes such as replication, transcription, and repair. The accumulation and resolution of these lesions are central to understanding the functional consequences of SPRTN depletion, as SPRTN acts as a specialised protease that facilitates DPC repair. Therefore, accurately measuring DPC levels is fundamental to assessing the cellular outcomes of SPRTN loss under genotoxic stress.

To this end, the first objective of this chapter is to systematically compare and evaluate currently available DPC isolation techniques, including but not limited to the RADAR, ARK, and STAR assays. These methods differ in their chemical principles, extraction efficiencies, and compatibility with downstream applications, necessitating a rigorous assessment to determine their suitability for the specific biological context of SPRTN-deficient cells. Parameters such as sensitivity, specificity, reproducibility, background signal, and performance under radiation exposure are considered to ensure robust quantification. The overarching goal is to identify an optimal isolation strategy that enables reliable detection of both basal and radiation-induced DPCs.

3.2 Results

3.2.1 DPCs isolation using by Protein-Targeted Methods (RADAR and STAR assay)

Various methods exist for DPCs isolation and quantification, and identifying the most suitable technique is crucial for accurate DPC quantification and analysis. Since our lab is particularly interested in studying DPCs, I evaluated the four most commonly used DPC isolation methods.

One of the most well-established methods is the RADAR assay. This method was shown to effectively isolates covalently trapped DNA-protein complexes while eliminating loosely associated proteins, ensuring specificity in DPC recovery (Kiianitsa & Maizels, 2013). Using the RADAR assay, several studies conducted by our lab have extensively utilized this method to investigate DPC formation, repair mechanisms, and the effects of various genotoxic agents. Due to its sensitivity and compatibility with downstream analyses, including mass spectrometry, Western blotting, and ELISA, RADAR remains a preferred approach in DPC research. RADAR relies on guanidinium thiocyanate (GTC) to remove non-covalently bound proteins from DNA.

A recent protocol that was developed by Glumac et al. called STAR assay, which is a modified version of RADAR, specifically designed to reduce RNA-associated proteins in DPC preparations. In their study, they showed that STAR assay is more sensitive in DPCs isolation and has lower background compared to RADAR and other commercially available kits. (Glumac et al., 2023).

I wanted to test weather STAR assay would be a better method compared to RADAR to isolate DPCs. This was done by treating cells with FA, a well-characterized DPC-inducing agent, allowing a direct evaluation of their performance. Here, cells were

subjected to three experimental conditions: untreated, 0.5 mM FA, and 1 mM FA. To minimize variability and ensure a fair comparison between the two methods, an equal number of cells were used for each condition, all of which were collected from the same plate (Figure 3.1).

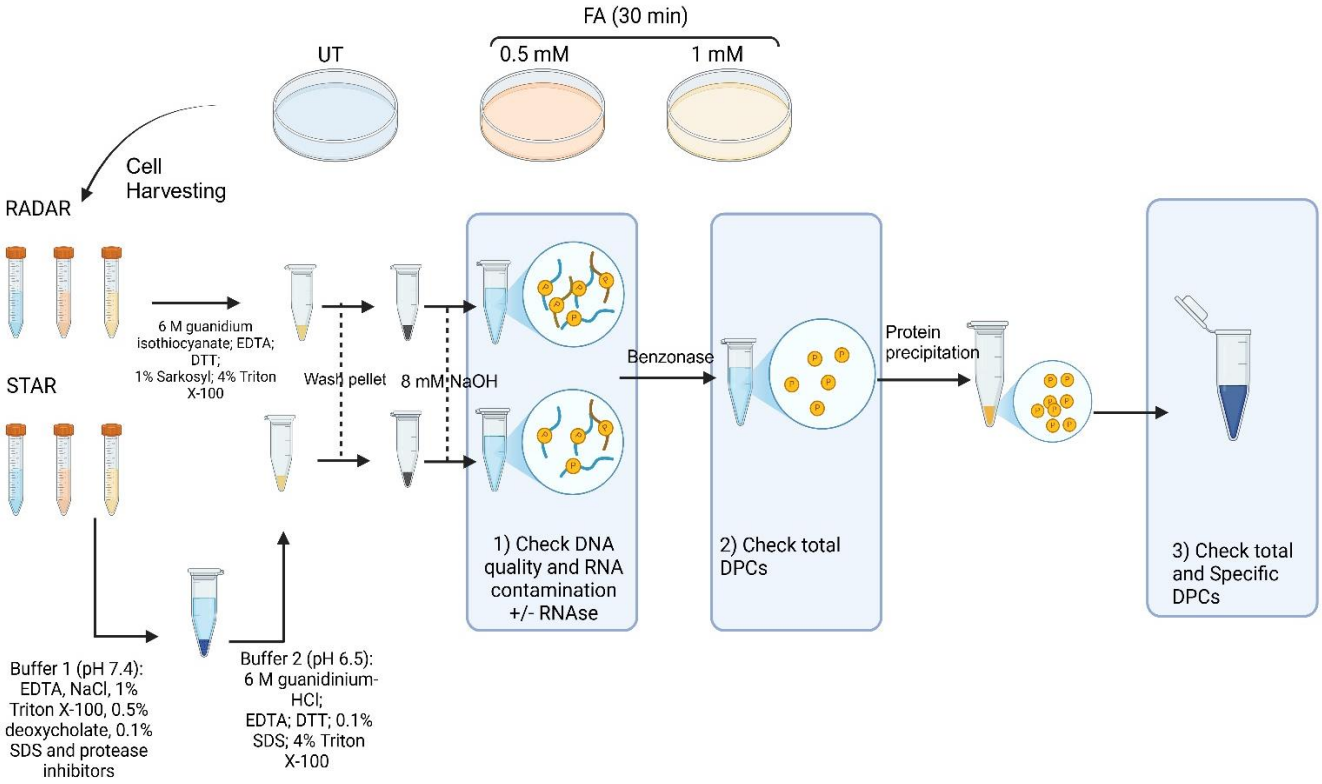


Figure 3.1. Schematic Representation of DPC Isolation Protocol Using RADAR and STAR Assays

Cells were subjected to three experimental conditions: untreated, 0.5 mM FA, and 1 mM FA. To minimize variability and ensure a fair comparison between the RADAR and STAR assays, an equal number of cells were used for each condition. All samples were collected from the same plate to control for experimental inconsistencies. Following FA treatment, cells were processed using either the RADAR or STAR protocol to isolate DPCs. The isolated DPCs were subsequently analyzed to assess the efficiency and sensitivity of each method in detecting FA-induced crosslinking. Created using Biorender.

3.2.1.2 Evaluating DNA Recovery Efficiency and RNA Contamination

To evaluate the DNA recovery efficiency of DPCs isolated using RADAR and STAR, all samples were subjected to agarose gel electrophoresis. The results demonstrated that both assays yielded comparable levels of DNA recovery. However, it is important to note that the smearing observed in DNA isolated via the RADAR assay is a consequence of the sonication step-part of the protocol- which is used to shear DNA into smaller fragments. RNA contamination appeared to be relatively higher in RADAR-extracted samples, as confirmed by RNase A digestion (Figure 3.2). This finding highlights the role of the initial lysis step followed by centrifugation in the STAR assay, which effectively removes a significant portion of RNA.

3.2.1.3 DPCs detection post-benzonase treatment (without precipitation)

Normalized samples (adjusted based on DNA concentration) from both assays were subjected to benzonase digestion to ensure complete degradation of all nucleic acids, including both DNA and RNA. The resulting protein isolate, which consists of crosslinked proteins, was subjected to SDS-PAGE, followed by Flamingo staining to detect the general DPCs level. Nevertheless, DPCs were difficult to detect at low exposure, which refers to a shorter imaging duration that limits signal amplification. At higher exposure (longer imaging time that enhances the detection of faint signals) the RADAR assay revealed a proportional increase in total DPC levels with increasing FA concentrations. In contrast, this trend was not observed in the STAR assay, where barely any detectable bands were present despite using the same amount of starting material both cells' numbers and DNA concentrations. Faint bands that were observed are likely due to the dilution of crosslinked proteins in the benzonase buffer (Figure 3.3). Thus, I decided to precipitate the protein in order to concentrate it, which could help in detecting DPCs.

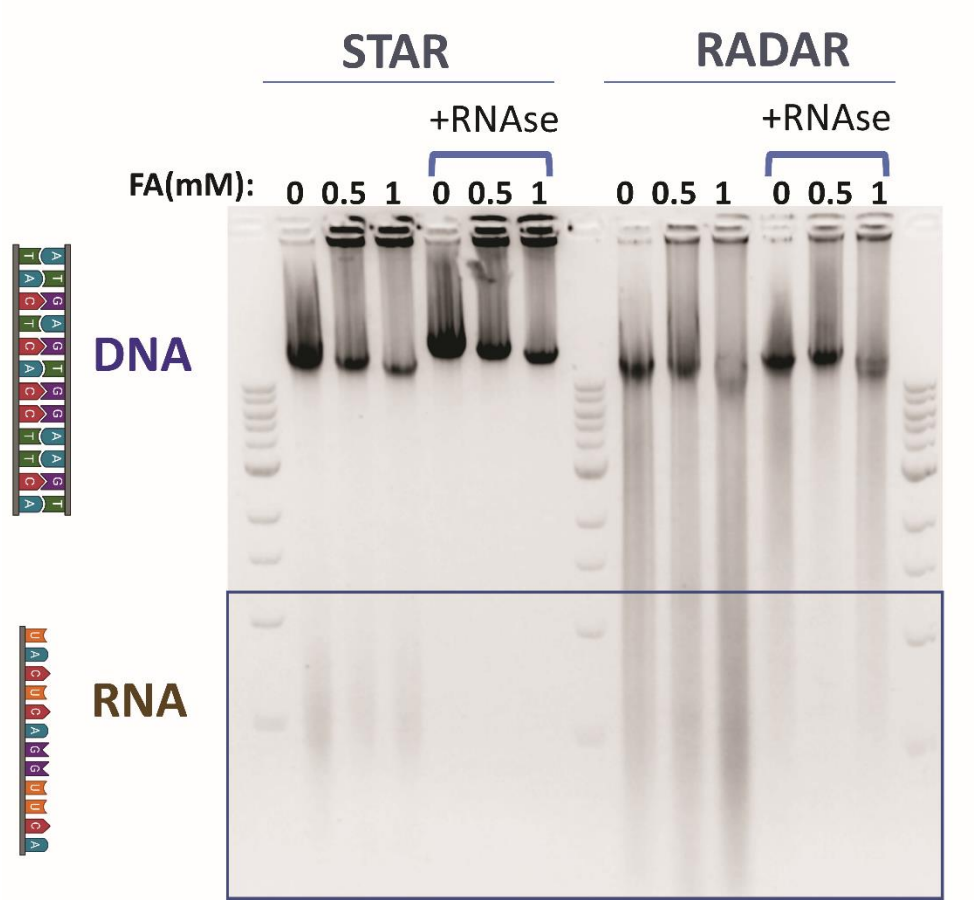


Figure 3.2. RNA Contamination Assessment in DPC Samples Isolated Using RADAR and STAR Assays

DPC samples were isolated from cells treated with 0, 0.5, and 1 mM FA using both RADAR and STAR assays. To evaluate RNA contamination, samples were processed with and without RNase A digestion. The presence of residual RNA was assessed to determine the effectiveness of each assay in eliminating RNA.

3.2.1.4 Precipitation of protein using TCA

To concentrate the samples and enhance detection sensitivity, TCA precipitation was performed, followed by centrifugation and resuspension of the proteins in a small volume of urea and 6× Laemmli buffer. The samples were then re-analyzed using SDS-PAGE. TCA treatment significantly improved the detection of crosslinked proteins in the RADAR assay. However, no substantial increase in total DPC yield was observed when using the STAR assay (Figure 3.4 A).

To further evaluate specific protein-DNA crosslinking, two proteins known to form crosslinks with DNA upon FA treatment were examined (Tayri-Wilk et al., 2020). Interestingly, the STAR assay isolates displayed little to no detectable tubulin-DNA crosslinks, suggesting that this method may have lower sensitivity for capturing specific DPCs (Figure 3.4 B).

Overall, these findings reinforce the superior sensitivity and robustness of the RADAR assay for detecting both total and specific DPCs. The use of TCA precipitation followed by SDS-PAGE substantially enhanced the detection of crosslinked proteins, highlighting the importance of sample concentration in improving assay performance. In contrast, the STAR assay consistently demonstrated lower sensitivity, with minimal improvement following TCA treatment and limited ability to detect specific protein–DNA crosslinks, such as tubulin-DNA adducts. These observations suggest that while the STAR method may be suitable for certain applications, it lacks the reliability and versatility required for comprehensive DPC analysis, particularly when evaluating protein-specific interactions or subtle changes in DPC burden. Accordingly, the RADAR assay emerges as the more appropriate method for downstream mechanistic studies, including those involving SPRTN-mediated DPC repair.

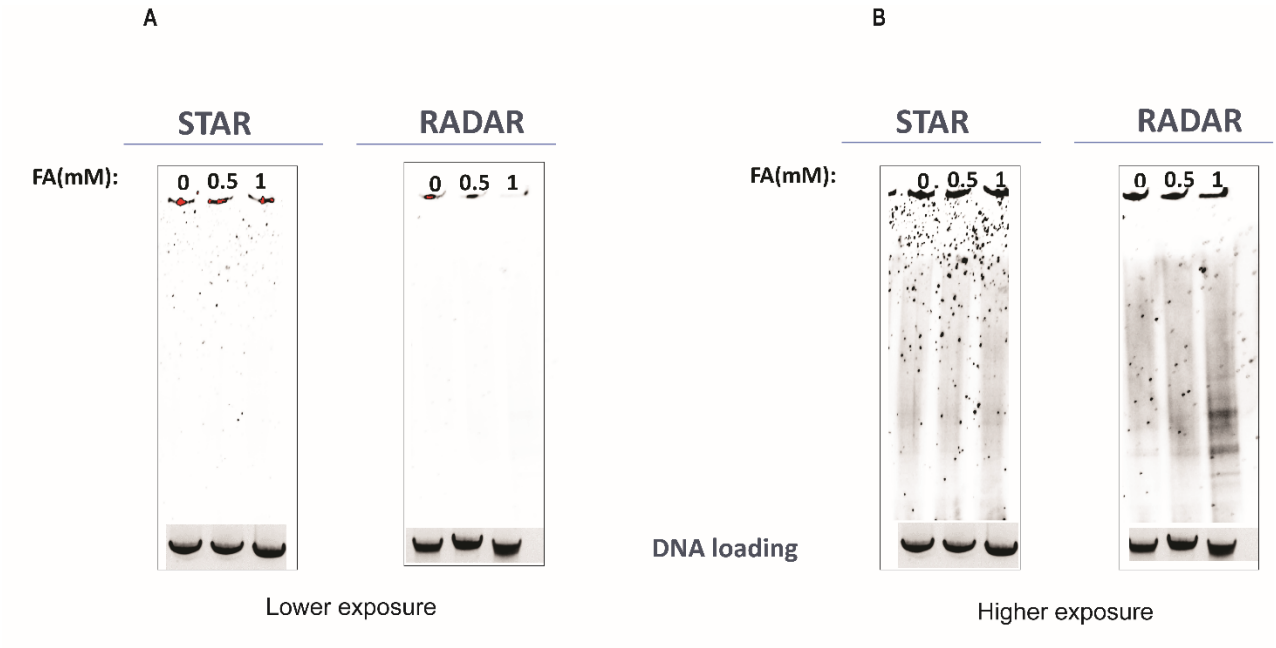


Figure 3.3. Total DPC Levels Isolated by RADAR and STAR Following Benzonase Treatment

Normalized DPC samples (adjusted based on DNA concentration) from both RADAR and STAR assays were treated with benzonase to ensure complete degradation of all nucleic acids, including DNA and RNA. The remaining protein fraction, representing crosslinked proteins, was analyzed by SDS-PAGE and visualized using Flamingo staining to assess overall DPC levels. (A) Lower exposure. (B) Higher exposure.

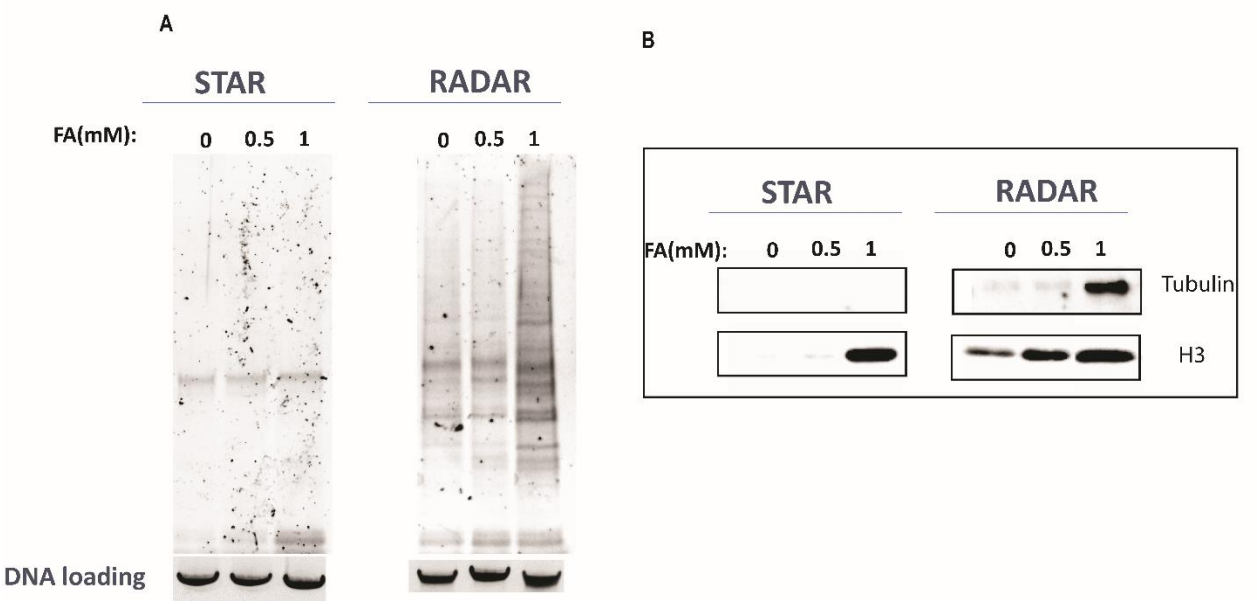


Figure 3.4. TCA Precipitation Enhances Detection of Crosslinked Proteins

DPC samples were concentrated using TCA precipitation and analyzed by SDS-PAGE. (A) Total DPC levels were assessed using Flamingo staining. (B) Western blot analysis detecting specific DPCs, including Tubulin-DNA and Histone H3-DNA crosslinks, using targeted antibodies.

3.2.2 DNA-targeted DPCs isolation method

Next, I tested the efficiency of two DNA-targeted DPCs isolation methods; ARK assay that isolate DPC-associated DNA through co-precipitation with proteins and modified comet assay which based on leveraging differences in electrophoretic mobility. These methods do not provide direct visualization of crosslinked proteins and assess DPC levels by quantifying DNA rather than directly detecting crosslinked proteins.

3.2.2.1 ARK assay

To assess the efficacy and sensitivity of the ARK assay in detecting DPC levels, I performed DPC isolation and quantification under three experimental conditions: untreated control, FA treatment, and IR exposure. FA (1 mM, 30 min) and IR (10 Gy) both used as a well-established DPC-inducing agent (Nakano et al., 2017; Vaz et al., 2016). FA-treated cells exhibited a significant increase in DPC levels, approximately four-fold higher than the untreated control, which matches the results from RADAR assay. However, IR-treated cells did not show a substantial increase in overall DPC levels, suggesting that ARK may have limitations in detecting DPCs formed under certain conditions or may not be sensitive enough to capture IR-induced DPC formation effectively (Figure 3.5).

Next, I aimed to determine whether the ARK assay could detect the accumulation of DPCs in SPRTN-depleted cells, given that SPRTN depletion is known to increase DPC levels, particularly during S-phase(Ruggiano et al., 2021; Vaz et al., 2016). To assess the impact of SPRTN depletion on DPC accumulation, both unsynchronized and synchronized HeLa cells were analyzed. In unsynchronized cells, a trend toward increased DPC levels was observed in SPRTN partial knockout cells; however, the variability between experiments prevented statistical significance (Figure 3.6). This variation may be attributed to differences in cell cycle distribution at the time of DPC

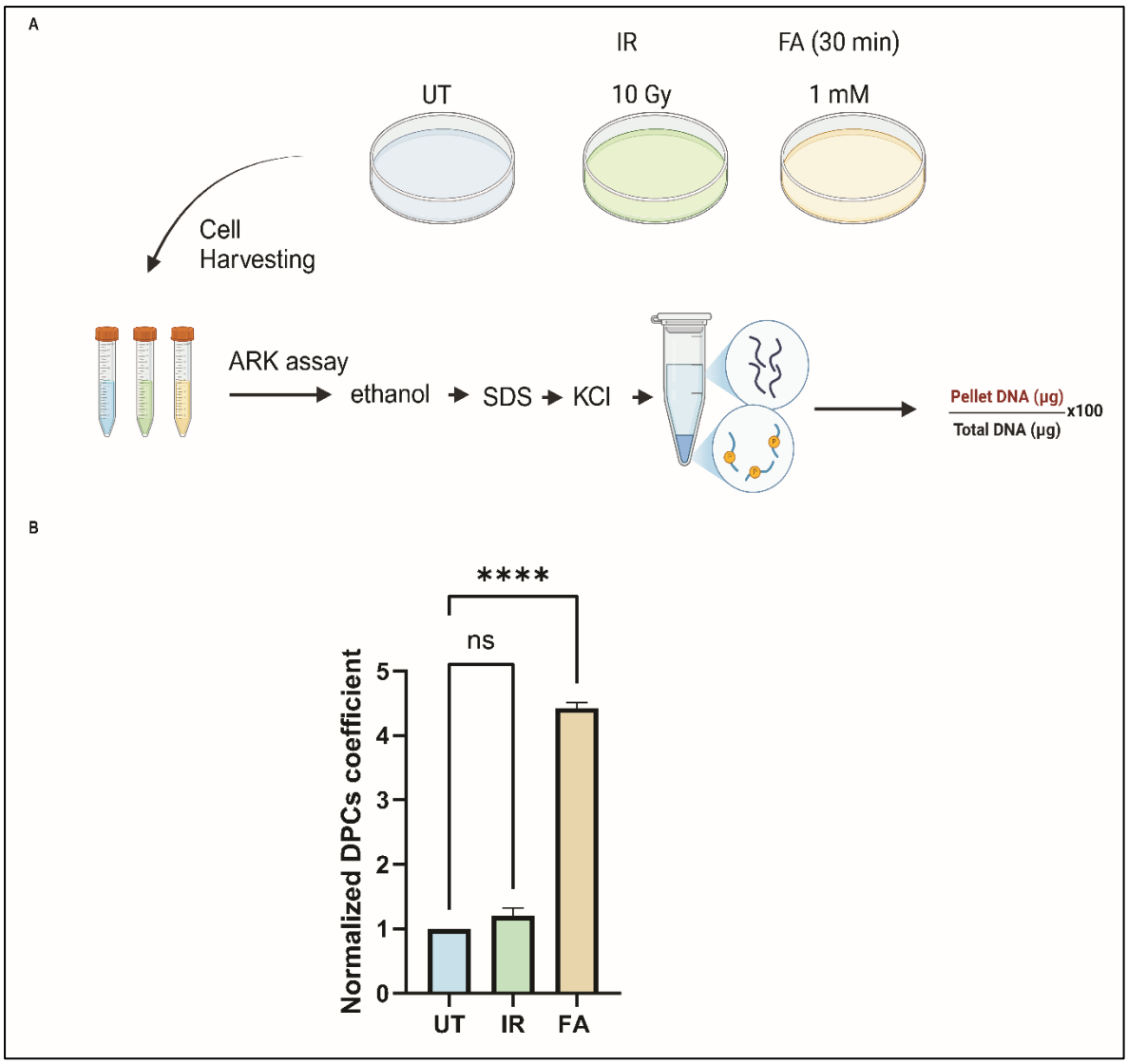


Figure 3.5. Evaluation of ARK Assay Sensitivity in Detecting DPC Levels

(A) Schematic representation of the ARK assay workflow used to assess DPC levels under three experimental conditions: untreated control, formaldehyde (FA) treatment (1 mM, 30 min), and ionizing radiation (IR) exposure (10 Gy). Created with Biorender.

(B) Normalized DPC levels detected by the ARK assay. Data are shown as normalized DPC coefficent, which is calculated as (Pellet DNA/ Total DNA). Statistical analysis was done by Graphpad Prism software using unpaired t-test. Data shown from the average of 3 independent experiments, error bars represent mean ± SD; $n = 3$. **** $p < 0.0001$, ns = not significant.

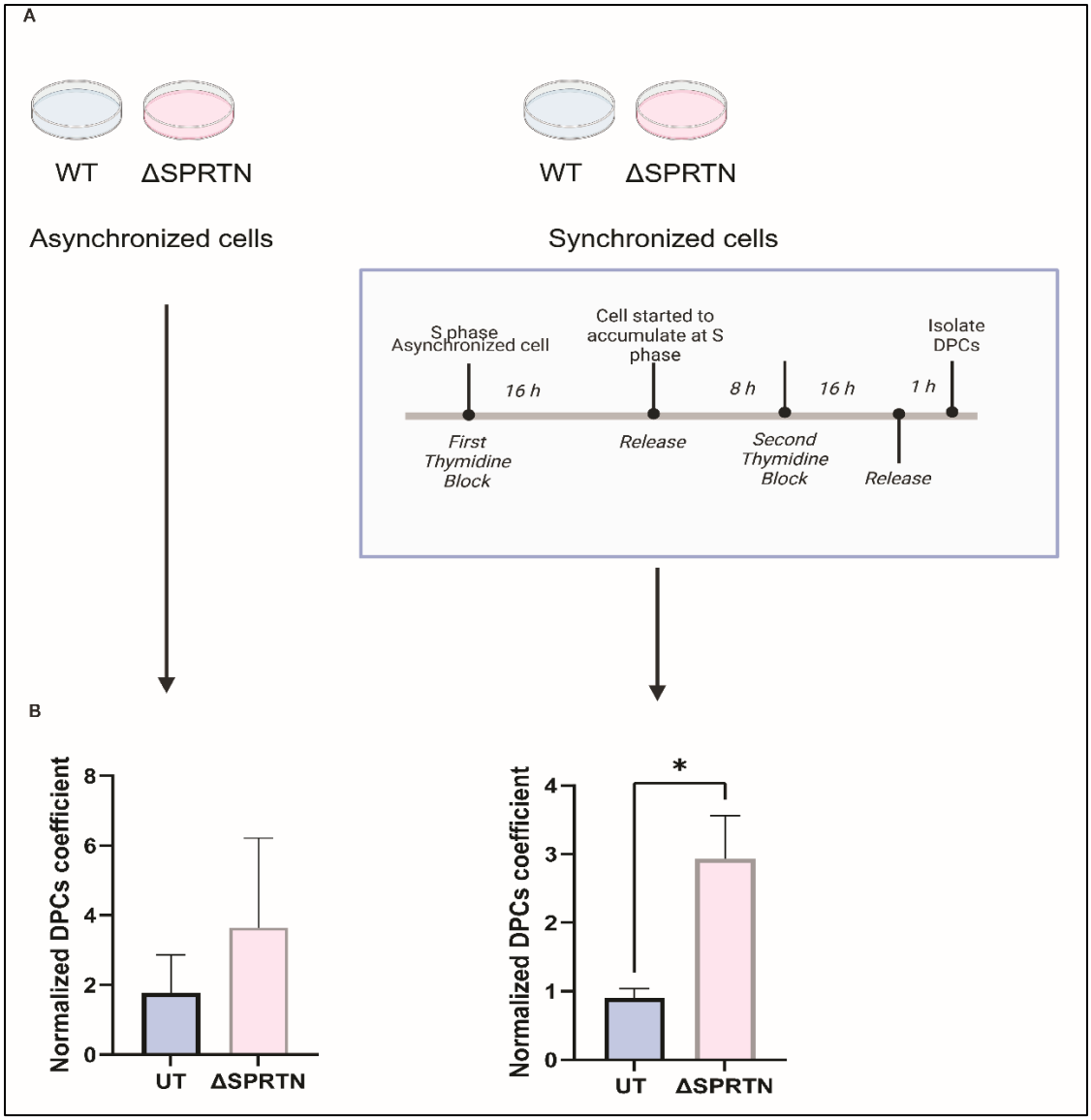


Figure 3.6. Detection of DPCs Accumulation in SPRTN-Depleted Cells Using ARK Assay

(A) Schematic representation of the experimental design to assess DPC levels in SPRTN-depleted cells. Both unsynchronized and synchronized HeLa cells were analyzed to determine whether the ARK assay could detect increased DPC accumulation following SPRTN depletion. (B) Quantification of DPC levels in SPRTN-depleted cells Data are shown as normalized DPC coefficient, which is calculated as (Pellet DNA/ Total DNA). Statistical analysis was done by Graphpad Prism software using unpaired t-test. Data shown from the average of 3 independent experiments, error bars represent mean ± SD; $n = 3$. * $p < 0.05$, ns: not significant.

isolation, as unsynchronized populations contain cells at various stages of the cell cycle. In contrast, synchronized cells displayed a statistically significant accumulation of DPCs, demonstrating the assay's capacity to detect SPRTN-dependent DPC accumulation under controlled cell cycle conditions. This underscores the importance of cell synchronization in minimizing variability and enhancing the sensitivity of DPC detection assays.

Taken these together, this suggests that while the ARK assay is capable of detecting global changes in DPC levels, its sensitivity can be influenced by type of treatment or the type of DPCs formed, and it may not be the most effective tool for detecting specific protein-linked DPCs.

3.2.2.2 Modified comet assay:

The comet assay is a widely used technique for detecting DNA damage at the single-cell level, primarily assessing strand breaks. A modified version of the comet assay has been developed to enable the detection of global DPC levels. This adaptation incorporates Proteinase K digestion prior to electrophoresis, which selectively degrades crosslinked proteins, thereby liberating DNA fragments that were previously immobilized by DPCs. This approach allows for assessment of DPC-induced genomic lesions, as it overcomes the steric hindrance imposed by covalently bound proteins, facilitating their quantification through electrophoretic mobility analysis.

Cells were subjected to different conditions, including untreated (UT), formaldehyde (FA) treatment (1 mM, 30 min), and IR (10 Gy), and the levels of tails of each condition with and without PK was measured. Both agents are known to induce DPCs.

Without PK treatment, cells exposed to IR exhibited notably longer comet tails than untreated controls, due to the presence of both DPCs and widespread DNA strand

breaks, including single-strand and double-strand lesions. In contrast, cells treated with FA showed minimal DNA migration, reflecting the formation of stable DPCs and DNA–DNA crosslinks, both of which immobilize DNA during electrophoresis (Figure 3.7 A-C).

To quantify DPCs, we calculated the difference in tail length between samples treated with and without PK (Δ tail moment), which reflects the extent of protein–DNA covalent interactions. As anticipated, FA-treated cells displayed a significant increase in Δ tail moment, confirming FA's strong crosslinking capacity. In comparison, IR-treated cells showed a lower Δ tail value than controls. This may be explained by the fact that IR generates extensive DNA fragmentation, which enhances overall DNA mobility and obscures the detection of DPCs using this approach. The presence of numerous DNA breaks likely compromises the resolution of crosslink-specific effects, making accurate quantification of DPCs more challenging in the context of IR-induced damage.

Additionally, SPRTN-depleted cells were analysed to evaluate whether this assay could effectively detect increased DPC accumulation resulting from impaired proteolytic repair. However, no detectable increase in DPC levels was observed in the absence of SPRTN, despite its well-established role in DPC resolution (Figure 3.8). This lack of signal may be attributed to the limited sensitivity of the assay employed. Unlike more advanced biochemical or proteomic techniques, this method has relatively low resolution for detecting subtle variations in DPC levels.

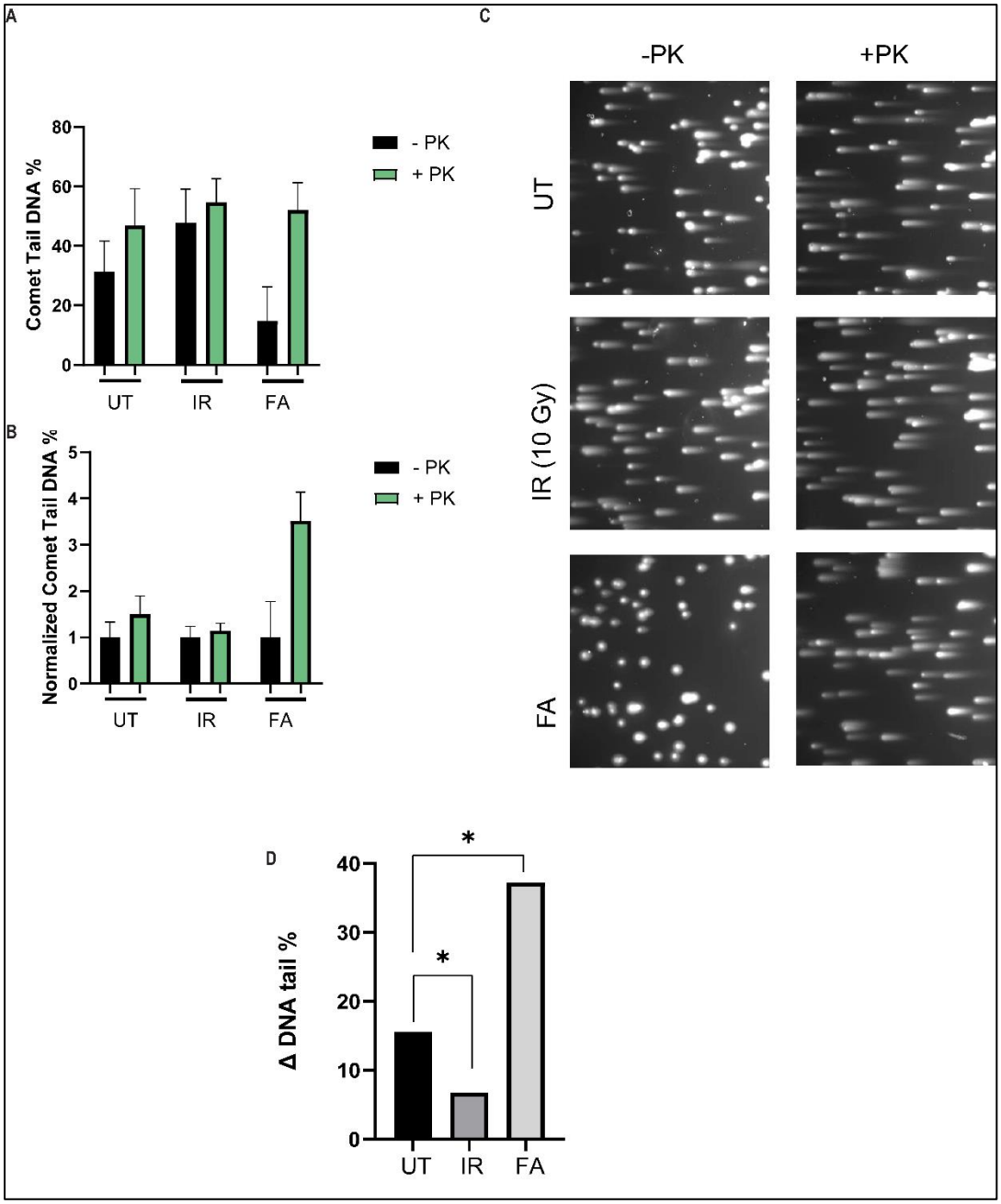


Figure 3.7. Evaluation of DPC Levels Using Modified Comet Assay post IR and FA

(A) Quantification of DNA tail % with and without Proteinase K (PK) treatment to assess DPC formation. One representative experiment of three independent replicates is shown, n ≥100 per condition.(B) Normalized DNA tail levels of (A) across different conditions.

(C) Representative comet assay images depicting tail length variations in untreated (UT), ionizing radiation-exposed (IR, 10 Gy) cells and formaldehyde-treated (FA, 1 mM, 30 min).

(D) The tail length difference with and without PK, illustrating the extent of DPC formation across experimental conditions. Statistical analysis was done by Graphpad Prism software using unpaired t-test. *p < 0.05.

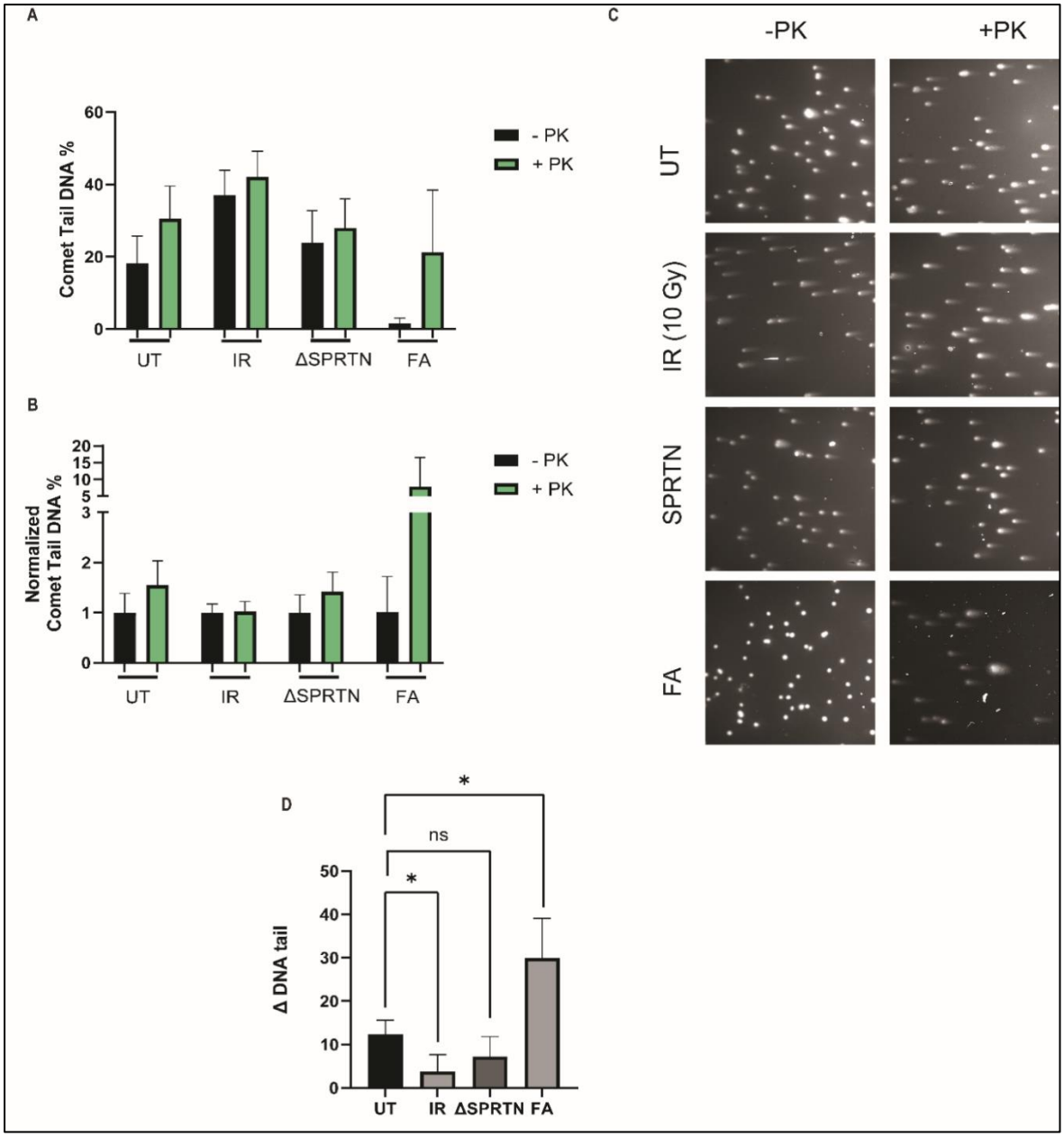


Figure 3.8. Evaluation of DPC Levels Using Modified Comet Assay in SPRTN knockout cells

(A) Quantification of DNA tail % with and without PK across different conditions. One representative experiment of three independent replicates is shown, n=100 per condition.(B) Normalized DNA tail levels of (A) across different conditions. (C) Representative comet assay images depicting tail length variations in untreated (UT), ΔSPRTN, ionizing radiation-exposed (IR, 10 Gy) cells and formaldehyde-treated (FA, 1 mM, 30 min). DNA tails are shown with and without Proteinase K (PK) treatment to assess DPC formation. The delta DNA tail length reflects the extent of DPC accumulation.(D) The tail length difference with and without PK, illustrating the extent of DPC formation across experimental conditions. Statistical analysis was done by Graphpad Prism software using unpaired t-test. Data shown from the average of 3 independent experiments, error bars represent mean ± SD; n = 3. * $p < 0.05$, ns: not significant.

Taken together, these findings demonstrate that the modified comet assay can be used to assess global DPC levels by measuring the differential DNA migration in the presence or absence of Proteinase K digestion. The significant increase in Δ tail moment observed in formaldehyde-treated cells validates the assay's ability to detect strong, chemically induced crosslinks. However, the reduced Δ tail values in ionising radiation (IR)-treated cells, despite IR's known ability to induce DPCs, suggest that extensive DNA fragmentation interferes with DPC quantification in this context. The assay's reliance on DNA mobility may limit its capacity to resolve crosslink-specific effects when strand breaks dominate the damage profile. Furthermore, the inability to detect increased DPC accumulation in SPRTN-depleted cells—despite SPRTN's critical role in crosslink proteolysis—highlights a key limitation in the assay's sensitivity. These results suggest that while the modified comet assay is effective for detecting robust crosslinking events, it lacks the resolution necessary to identify more subtle changes in DPC burden, particularly those arising from endogenous repair defects. For such applications, more sensitive biochemical or proteomic methods may be required.

3.2.3 Detecting DPCs formed by FLASH radiotherapy RADAR assay

Extensive research has established the effects of conventional radiation therapy (RT) on cells and DNA, particularly in terms of DNA damage and repair mechanisms (Lomax et al., 2013a). However, a groundbreaking development in the field of RT is FLASH-radiotherapy (FLASH-RT), which has emerged as a revolutionary approach due to its ability to deliver ultra-high dose rate (UHDR) radiation exceeding 40 Gy/s (Bourhis, Montay-Gruel, et al., 2019). Unlike conventional RT, which administers IR in multiple fractions over prolonged treatment sessions, FLASH-RT delivers the entire radiation dose within milliseconds.

This technique has garnered substantial interest due to its unique biological effects, particularly its ability to spare normal tissues while preserving strong antitumour efficacy, a phenomenon known as the FLASH effect(Fouillade et al., 2020). The underlying mechanisms driving this effect remain an area of active investigation, with hypotheses suggesting that differential oxygen consumption, transient hypoxia, and altered redox signalling contribute to its protective impact on normal tissues (Adrian et al., 2020). These potential mechanisms distinguish FLASH-RT from conventional RT, raising important questions about its influence on DNA damage, repair pathways, and cellular stress responses.

Despite promising preclinical findings, further research is essential to fully elucidate the molecular basis of the FLASH effect and to determine how FLASH-RT modulates cellular responses to radiation at the DNA and chromatin levels. Understanding these mechanisms will be crucial for optimizing treatment protocols and expanding the clinical applications of FLASH-RT, potentially revolutionizing cancer therapy by minimizing radiation-induced toxicity while maintaining high therapeutic efficacy. Thus we wanted to test DPCs levels caused by Flash-RT and if it is different from conventional radiation.

3.2.3.1 DPC Formation in Conventional RT

To determine the kinetics of DPC formation following exposure to conventional radiation therapy, I irradiated the cells and collected samples at multiple time points post-irradiation. Previous studies have demonstrated that the majority of DPCs formed after radiation exposure are rapidly processed and removed within 20 minutes to 2 hours post-IR (Chiu et al., 1984; Cress & Bowden, 1983; Nakano et al., 2017).

To detect DPC accumulation and repair dynamics over time, the samples were analysed using the RADAR assay. The results revealed a rapid induction of DPCs, with peak accumulation occurring approximately 10 minutes post-IR, indicating an immediate cellular response to radiation-induced DNA damage. Following this peak, a gradual decline in DPC levels was observed, reflecting the activation of cellular repair mechanisms responsible for resolving these lesions. In addition to FA-treated cells, siSPRTN-treated cells were included as a positive control. Previous studies have demonstrated that the RADAR assay is capable of detecting increased DPC accumulation in SPRTN-depleted cells, confirming its sensitivity in quantifying DPC formation and repair dynamics (Figure 3.9).

These findings reinforce the well-established role of conventional RT in inducing DPCs as a major form of DNA damage, emphasizing the necessity of efficient repair pathways to mitigate their cytotoxic and mutagenic effects. The ability of cells to rapidly process and remove DPCs highlights the importance of these repair mechanisms in preserving genome integrity and cellular viability after radiation exposure.

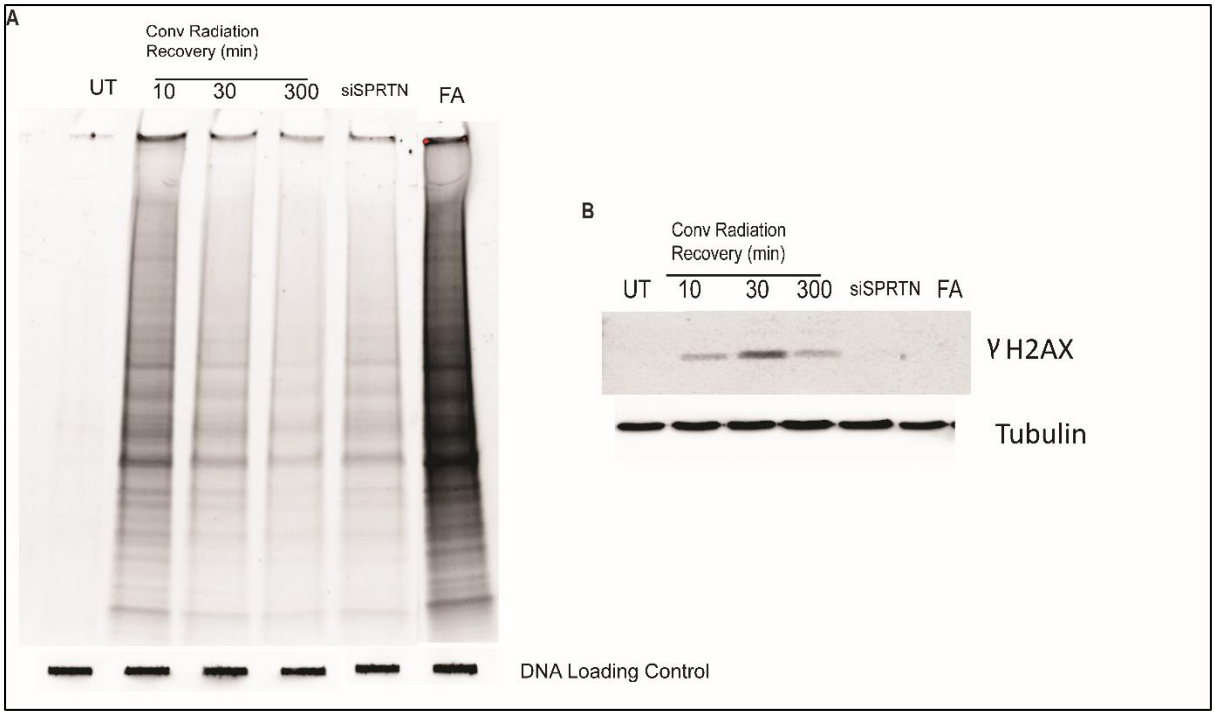


Figure 3.9. Kinetics of DNA-Protein Crosslink (DPC) Formation and Repair Following Radiation Exposure

This figure illustrates the time-dependent accumulation and resolution of DNA-protein crosslinks (DPCs) in cells following exposure to conventional radiation therapy (RT). (A) Total DPCs levels post radiation in different time point using RADAR assay. Both FA and siSPRTN were used as positive control. One representative experiment of three independent replicates is shown.

(B) Western Blot showing γH2AX levels as a marker of damage by radiation

3.2.3.2 DPC Formation in FLASH-RT

First, we wanted to test if Flash-RT causes an increase in DPCs levels. Radiation dose of 20 Gy was administered, and the total DPC levels were visualized post 10 min using RADAR, which confirmed a significant increase in DPC formation (Figure 3.10).

To evaluate the dose-dependent effects of radiation on DPC formation, DPC levels were quantified and compared between FLASH-RT and conventional RT at doses of 20 Gy and 40 Gy. Both radiation modalities demonstrated a proportional increase in DPC levels with increasing radiation dose. Particularly, despite this dose-dependent rise, the overall levels of DPC accumulation were comparable between FLASH-RT and conventional RT, suggesting that the extent of radiation-induced DPC formation is not significantly influenced by the dose delivery rate. This observation indicates that while FLASH-RT is known to induce unique biological effects, its impact on initial DPC formation is similar to that of conventional RT (Figure 3.11).

Next, I investigated DPC formation and resolution kinetics post FLASH-RT and how it might be different from conventional radiation. After cells were irradiated at 40 Gy using both radiation types, DPCs repair kinetics was followed showing similarities between FLASH-RT and conventional RT. The results indicate that DPC formation occurs rapidly post-irradiation in both treatment modalities, followed by an active repair process that restores genomic integrity over time (Figure 3.12). This data suggests that the overall pattern of DPC induction and repair is largely independent of the dose rate or radiation delivery method at least under normoxix conditions (21% O_2).

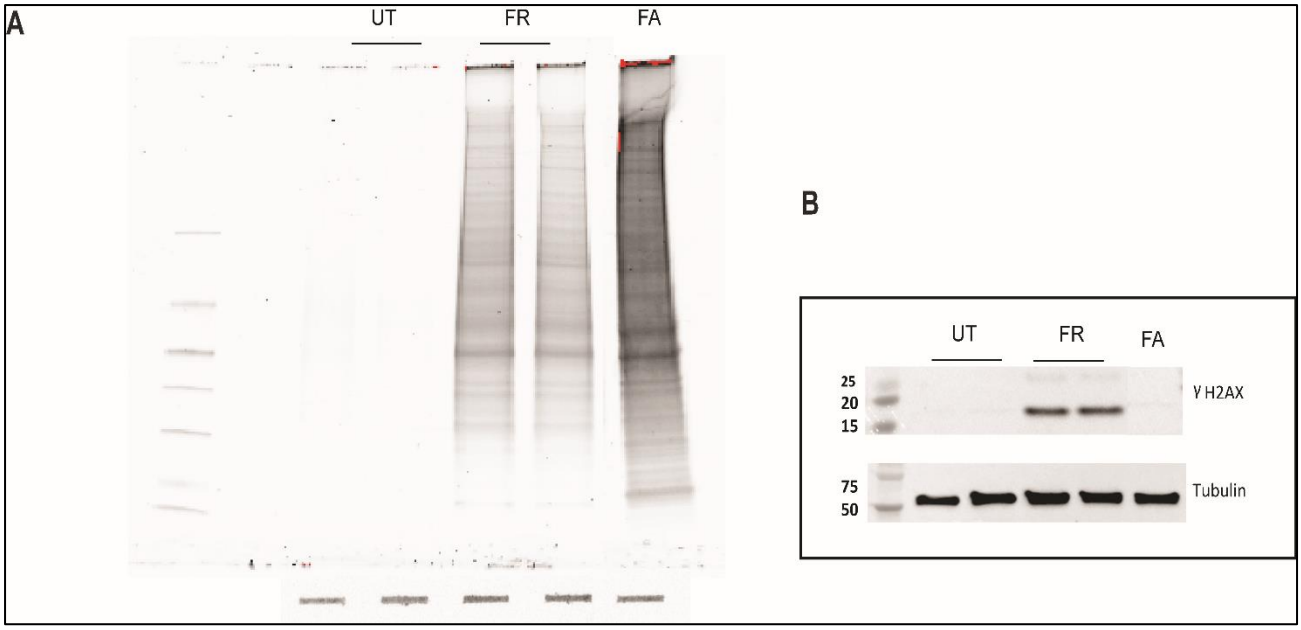


Figure 3.10. FLASH-RT Induces a Rapid Increase in DNA-Protein Crosslink (DPC) Formation

(a) A SDS-PAGE gel stained with Flamingo, showing DPC samples run in duplicate, cells were exposed to a radiation dose of 20 Gy. Total DPC levels were quantified 10 minutes post irradiation using the RADAR assay. One representative experiment of three independent replicates is shown.

(b) Western blot analysis of γH2AX, a marker of radiation-induced DNA damage, confirming cellular response to irradiation.

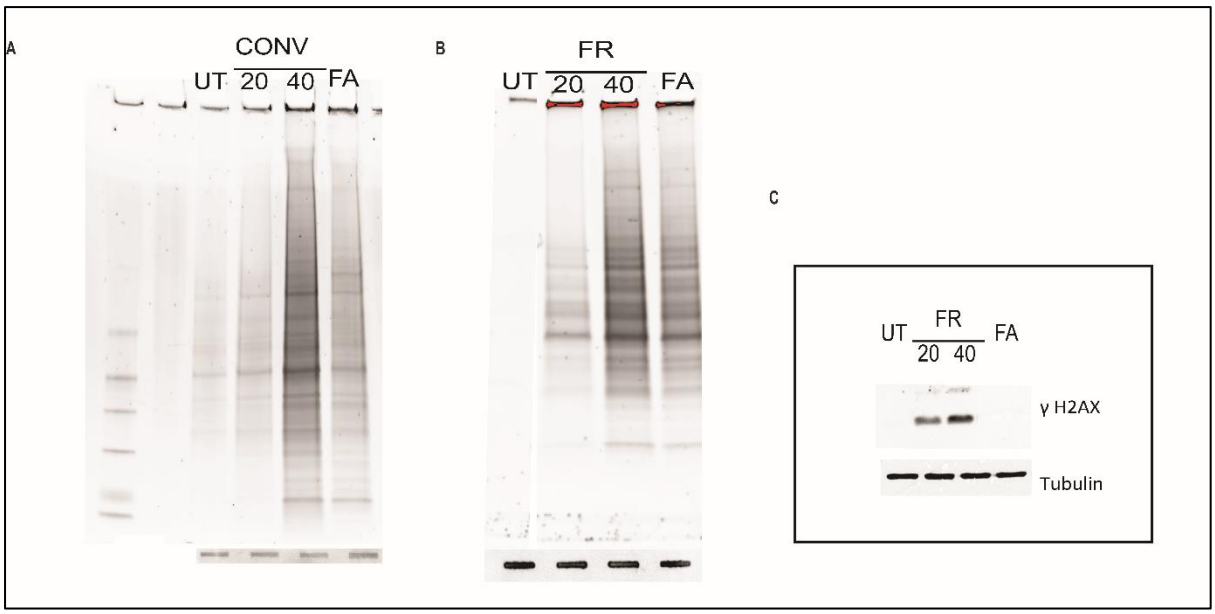


Figure 3.11. Dose-Dependent Effects of FLASH-RT and Conventional RT on DNA-Protein Crosslink (DPC) Formation

Total DPC levels compared between FLASH-RT and conventional RT at radiation doses of 20 Gy and 40 Gy to assess dose-dependent effects. The figure shows total DPCs levels (A) post conventional radiation (CONVO). (B) post FLASH radiation (FR).(C) Western blot analysis of γH2AX, a marker of radiation-induced DNA damage, confirming cellular response to irradiation. One representative experiment of two independent replicates is shown.

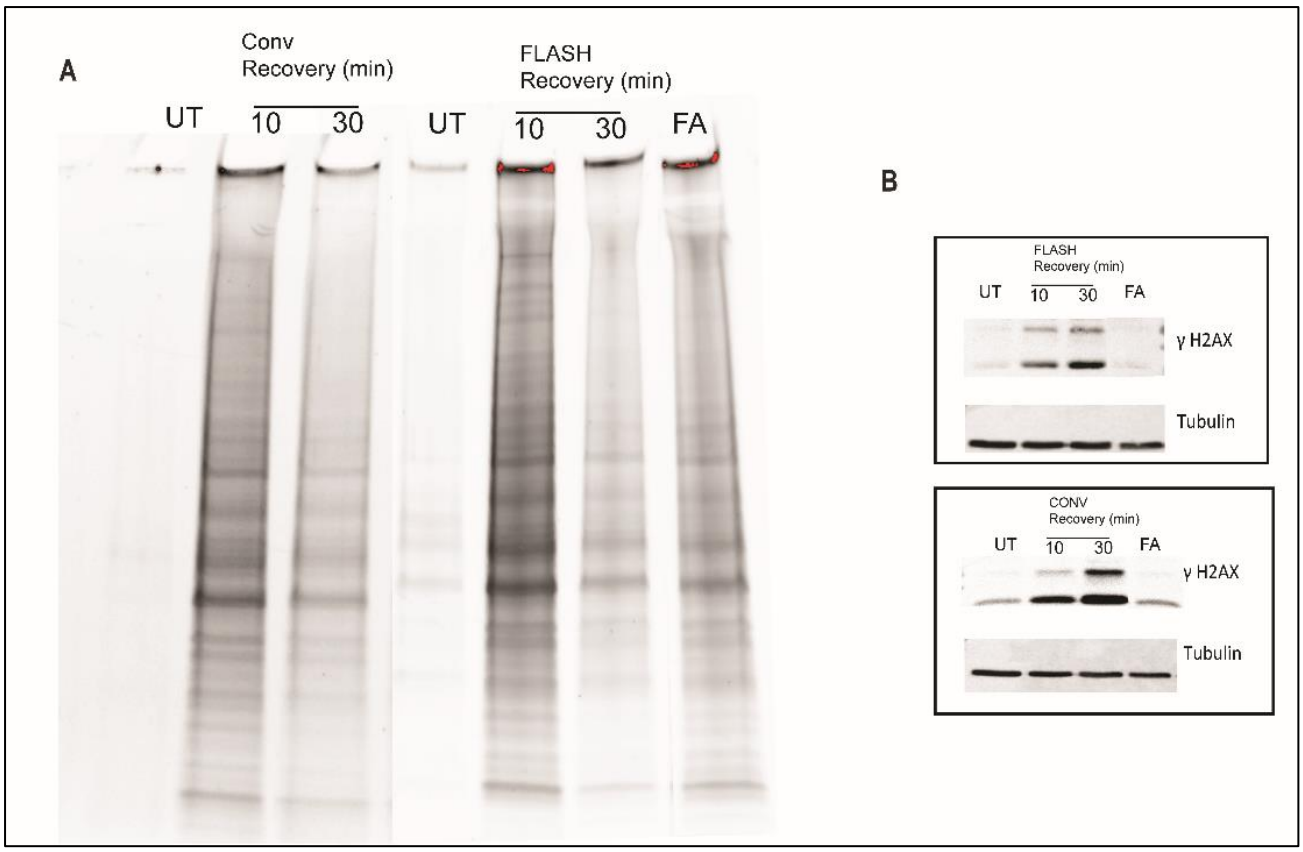


Figure 3.12. DPC Formation and Repair Kinetics Following FLASH-RT and Conventional RT

(A) Total DPC levels compared between FLASH-RT and conventional RT at cells were irradiated at 40 Gy using both radiation modalities. DPC levels were monitored post 10 and 30 min to assess repair dynamics. (B) Western blot analysis of γH2AX, a marker of radiation-induced DNA damage, confirming cellular response to irradiation. One representative experiment of three independent replicates is shown.

These findings provide an insight into the mechanisms of radiation-induced DNA damage in the context of FLASH-RT. The observation that DPC repair kinetics remain unchanged suggests that key DNA repair pathways, such as proteolysis-dependent DPC degradation, NER, and HR, function similarly under both FLASH-RT and conventional RT conditions. This reinforces the notion that while FLASH-RT exhibits unique tissue-sparing effects, the fundamental cellular processes governing DNA damage recognition and repair remain conserved under normoxia.

In addition, this study underscores the sensitivity and reliability of RADAR in detecting RT-induced DPCs and tracking their repair kinetics. Both conventional and FLASH-RT were found to induce comparable levels of DPCs, with similar repair dynamics observed across different doses. These findings suggest that while FLASH-RT is recognized for its ability to reduce NT toxicity, its impact on DPC formation remains analogous to conventional RT.

3.2.4 DPCs formation in Hypoxia measured by RADAR

Hypoxia, a condition characterized by low oxygen availability, is a common feature of both physiological and pathological conditions, including embryonic development, ischemic diseases, and solid tumours (Semenza, 2012). One of the key consequences of hypoxia is its impact on genomic stability and DNA repair pathways. Hypoxia can lead to increased levels of DNA damage through multiple mechanisms, including the generation of reactive oxygen species (ROS), alterations in replication stress, and changes in DNA repair efficiency (Bristow & Hill, 2008). ROS, which are produced in mitochondria during oxygen fluctuations, can induce a variety of DNA lesions (Tubbs & Nussenzweig, 2017).

To investigate the impact of hypoxia on DPC levels, I employed the RADAR assay, a highly sensitive method for isolating and quantifying DPCs. Two hypoxic conditions

were tested: (i) cells were incubated in a hypoxia chamber at 1% O_2 for 60 minutes, and (ii) cells were subjected to hypoxia (1% O_2 for 60 minutes) followed by reoxygenation at normoxic conditions (21% O_2) (acute hypoxia followed by rapid reoxygenation). The objective was to determine how transient hypoxia and subsequent reoxygenation influence DPC formation.

The results revealed a striking increase in DPC levels following reoxygenation. Cells that were exposed to hypoxia alone exhibited a modest elevation in DPC levels compared to normoxic controls. However, cells that underwent reoxygenation displayed a substantial accumulation of DPCs, surpassing even the levels observed in the positive control (1 mM FA) (Figure 3.13). This suggests that the reintroduction of oxygen after a hypoxic phase may exacerbate oxidative stress, leading to extensive crosslinking between proteins and DNA.

These results provide novel insights into how hypoxia and reoxygenation contribute to genomic instability by modulating DPC formation. Further investigation is required to determine whether specific repair mechanisms, such as SPRTN-mediated proteolysis or nucleotide excision repair, are differentially regulated under these conditions. Understanding these mechanisms will be crucial for elucidating the role of hypoxia-induced DPC formation in pathological contexts such as tumour progression and therapeutic resistance.

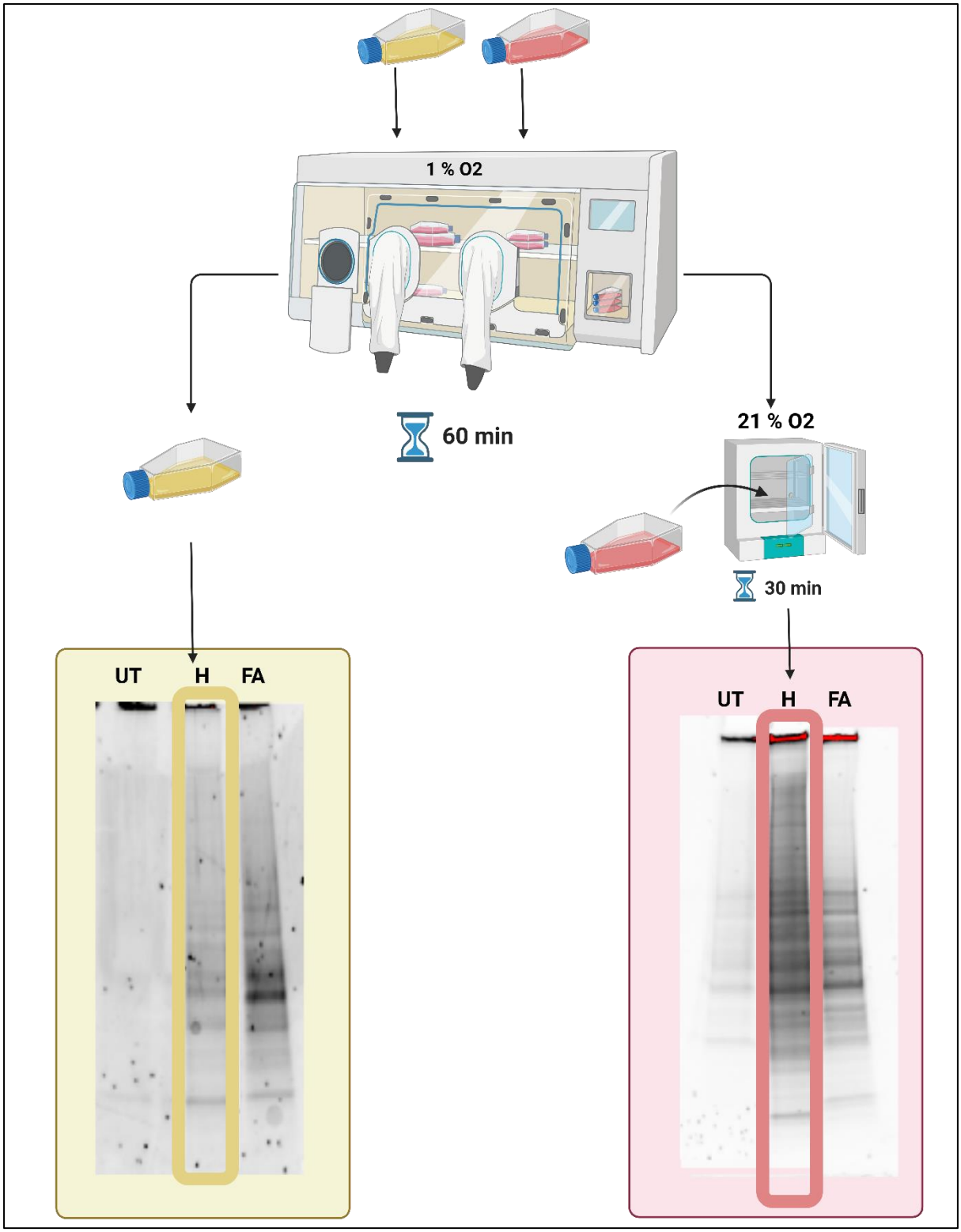


Figure 3.13: Impact of Hypoxia and Reoxygenation on DPC Levels

To assess the effects of hypoxia on DPC formation, the RADAR assay was used to isolate and quantify DPC levels under different oxygen conditions. Two hypoxic conditions were tested: (i) cells were incubated in a hypoxia chamber at 1% O_2 for 60 minutes, and (ii) cells

were subjected to acute hypoxia (1% O_2 for 60 minutes) followed by reoxygenation under normoxic conditions (21% O_2). This experiment aimed to determine how transient hypoxia and subsequent reoxygenation influence DPC formation and repair dynamics.

3.3 Discussion

3.3.1 Choosing the appropriate DPCs method

In this study, I systematically evaluated the performance and sensitivity of several DPC isolation techniques, including protein-targeted methods (RADAR and STAR) and DNA-targeted methods (ARK and the modified comet assay), under various biological conditions such as FA exposure, IR, hypoxia, and SPRTN depletion.

The accurate detection of DPCs is fundamental to investigating their biological significance and the function of DPC repair factors such as SPRTN. In this study, two established DPC isolation methods-RADAR and STAR-were comparatively evaluated using formaldehyde (FA) as a model crosslinking agent. While the RADAR assay reliably detected DPCs in a time- and dose-dependent manner, the STAR protocol failed to yield comparable results, even under conditions previously shown to induce substantial DPC accumulation at least in my own hand.

Thus, I found that RADAR was a better method in isolating DPCs based on the results shown. These findings, consistent with previous studies, confirm that DPCs isolated using the RADAR assay increase in a time- and dose-dependent manner following FA treatment. RADAR has been shown to detect elevated DPC levels at FA concentrations as low as 150 μM (Ruggiano & Ramadan, 2021b).

Following the method of STAR protocol developed by Glumac et al., no detectable increase in total DPC levels was observed, even at 1 mM FA, a concentration known to induce high levels of DPC formation in cells (Vaz et al., 2016). Although starting material and the same number of cells were used in both assays, the different in the outcome is questionable. In the STAR assay, the initial cell fractionation step utilizes

detergent-based lysis approach (RIPA buffer) without chaotropic salts, which may allow proteolytic and nucleolytic activities to persist. This could lead to the partial degradation or modification of DPCs before they can be effectively isolated, thereby impacting the accuracy and sensitivity of DPC detection potentially leading to an underestimation of their true levels (Torrecilla et al., 2024). This step introduces a time-sensitive variable, requiring rapid execution to prevent enzymatic degradation and preserve the integrity of DPCs. The necessity for precise timing and swift processing may account for the discrepancies observed in the outcomes of this study compared to the original findings. Differences in handling time and protocol execution could influence DPC recovery efficiency, potentially explaining the variation between results (Glumac et al., 2023). Unlike chaotropic agents such as GTC -which is part of RADAR lysis buffer- that denature proteins and nucleases immediately (Kiianitsa & Maizels, 2013). This raises questions about the reliability of STAR for detecting DPC formation and repair dynamics, particularly when analysing subtle changes in DPC accumulation under different experimental conditions.

One possible explanation for this inconsistency lies in the difference in cell lysis strategies. The RADAR assay employs guanidinium thiocyanate (GTC), a potent chaotropic agent that rapidly denatures proteins and inactivates nucleases and proteases upon cell lysis (Kiianitsa & Maizels, 2013). This immediate inactivation is crucial for preserving labile DNA–protein interactions. By contrast, the STAR method utilises a detergent-based RIPA buffer that lacks chaotropic salts and, therefore, does not promptly halt enzymatic activity. As a result, proteolytic or nucleolytic degradation may continue during sample processing, potentially compromising DPC stability and leading to false negatives or underestimation of crosslink levels. Moreover, the STAR

protocol introduces a time-sensitive handling step that may vary between operators, further reducing reproducibility and cross-sample consistency.

Remarkably, these findings also raise concerns about previously published studies that reported undetectable DPC accumulation with the RADAR assay at FA concentrations up to 400 μM (Glumac et al., 2023), which contradicts the results of both this and several independent investigations.

Although the STAR protocol was designed to reduce RNA contamination in isolated DPC samples, the practical advantage of this feature appears limited. RNA removal has been efficiently achieved in RADAR-based protocols through RNase treatment following lysis (Sun et al., 2020; Sun et al., 2021). Additionally, alternative methods have been described, such as selective membrane lysis with proprietary detergents (e.g., MPER, ThermoFisher) followed by high-speed centrifugation to enrich for nuclear content prior to denaturation in chaotropic agents (Kiianitsa et al., 2020). These approaches offer cleaner preparations without compromising DPC integrity and may provide a more balanced solution to RNA-associated interference.

For DNA-targeted approaches, the ARK assay proved effective in detecting global DPC accumulation, particularly following FA treatment and in synchronized SPRTN-depleted cells. However, its sensitivity appeared to vary depending on the type of crosslinking agent and the nature of the crosslinked protein, which may limit its use in detecting specific DPCs. This suggests that while the ARK assay is capable of detecting global changes in DPC levels, its sensitivity can be influenced by type of treatment or the type of DPCs formed, and it may not be the most effective tool for detecting specific protein-linked DPCs. For instance, it was shown that ARK performed as well as RADAR when detecting TOP1cc DPCs, whereas it demonstrated lower

sensitivity for DNMT1 DPCs compared to RADAR (Hu et al., 2020). This indicates that while ARK can be utilized for protein-specific DPC analysis, its effectiveness depends on the specific protein being studied.

The modified comet assay provided single-cell resolution and offered a useful readout of total DPC burden, but it lacked the sensitivity needed to detect subtle or low-abundance DPCs, such as those present in SPRTN-deficient cells under basal conditions. SPRTN is a well-established protease required for the resolution of DPCs during DNA replication and repair, and its loss is expected to result in increased DPC burden. However, no detectable elevation in DPC levels was observed. Which was also seen in previous study where an increase in DPC levels was detectable following different concentration of FA treatment; however, no such accumulation was observed in SPRTN-depleted cells (Mórocz et al., 2017).

As a result, small increases in DPC accumulation, such as those potentially occurring in SPRTN-deficient cells under basal conditions, may fall below the detection threshold. This limitation suggests that more robust crosslinking stimuli, such as higher concentrations of crosslinking agents (e.g., FA or CPT), may be required to amplify the signal. These findings underscore the importance of assay selection when studying endogenous DPC repair pathways or subtle phenotypes associated with repair factor depletion.

3.3.2 DPCs formation post Flash Radiation

Using the RADAR assay, I further investigated DPC dynamics following both conventional and FLASH-RT. Both radiation modalities induced similar DPC levels and displayed comparable repair kinetics under normoxic conditions, suggesting that the radiation dose rate does not significantly influence DPC induction or resolution under these conditions. A previous study has demonstrated that conventional and FLASH

radiation under normoxic conditions resulted in comparable levels of strand breaks and oxidative base damage, indicating that both radiation modalities induce a similar pattern of DNA lesions in the presence of sufficient oxygen. However, under hypoxic conditions (0.5% O_2), a direct comparison between conventional and FLASH irradiation revealed a significant reduction in radiation-induced strand break formation following FLASH exposure. Concurrently, there was a marked increase in oxidative base lesions, particularly in major purine oxidation products such as 7,8-dihydro-8-oxoguanine (8-oxoG), 8-oxoadenine, formamidopyrimidine-guanine (Fapy-G), and formamidopyrimidine-adenine (Fapy-A), along with other structurally altered purines (Cooper et al., 2023). This shift in damage profile suggests that FLASH irradiation induces a more anoxic pattern of DNA damage. Based on these findings, it is plausible that the levels of DPCs following FLASH irradiation under hypoxic conditions may differ from those induced by conventional irradiation. Given that FLASH induces a higher incidence of oxidative base damage which is recognized as a hotspot for DPC formation, it is likely that DPC levels post-FLASH in hypoxic conditions will be elevated compared to conventional irradiation. This hypothesis is supported by the well-established role of oxidatively modified bases, particularly 8-oxoguanine and other oxidized purines, in facilitating covalent DNA-protein interactions (Greenberg, 2014; Sczepanski et al., 2010). Investigating DPC formation under FLASH irradiation in hypoxia would provide critical insights into how different radiation modalities influence complex DNA lesions and repair mechanisms. Such studies could further elucidate the biological consequences of FLASH-induced oxidative stress in low-oxygen environments, with implications for optimizing radiotherapy strategies in hypoxic tumours. Thus, it would be particularly informative to assess DPC levels following

FLASH-RT under hypoxic conditions. Such analyses could help determine whether DPCs contribute to the unique tissue-sparing effects associated with FLASH-RT.

DPC accumulation was significantly elevated under hypoxic conditions, particularly upon reoxygenation, implicating ROS-driven mechanisms in promoting DPC formation. These findings underscore the physiological relevance of DPCs in response to IR and oxidative stress, such as that observed during ischemia-reperfusion injury. Further studies are warranted to assess DPC formation under different types of hypoxia (chronic, acute or transmitted), especially in the context of post-radiation responses. This could provide deeper insight into the mechanisms underlying tumour radio-resistance in hypoxic environments.

3.3.2 DPCs formation under Hypoxia

Cells that were exposed to hypoxia alone exhibited a modest elevation in DPC levels compared to normoxic controls, while there was an increase in DPC levels following reoxygenation. This finding aligns with previous studies indicating that reoxygenation following hypoxia induces a surge in ROS production, which can cause oxidative base damage, strand breaks, and crosslink formation (Bell & Chandel, 2007; Tubbs & Nussenzweig, 2017). One of the significant consequences of ROS-induced DNA damage is the formation of DPCs. ROS can simultaneously induce oxidative damage to both DNA and proteins, creating an environment conducive to covalent crosslinking. Additionally, ROS can directly modify amino acid residues such as cysteine, histidine, lysine, and tyrosine, increasing their reactivity toward DNA and promoting DPC formation.

One well-characterized mechanism involves ROS-mediated oxidation of tyrosine residues, which enhances their potential to form stable covalent bonds with DNA. Furthermore, ROS can oxidize deoxyribose sugars and nucleobases, generating AP

sites. These AP sites, as previously discussed, serve as hotspots for DPC formation, as they create highly reactive intermediates that can covalently link DNA with nearby proteins. A study investigating radical-induced DPCs in cardiomyocytes following ischemia-reperfusion injury in a rat model demonstrated that these lesions are formed upon reoxygenation. Utilizing a highly sensitive isotope dilution nanoLC-NSI+-MS/MS assay, researchers identified nearly 90 proteins implicated in hydroxyl radical-mediated DPC formation, including ROS scavengers, contractile proteins, and apoptosis regulators (Groehler et al., 2018). These findings support a model in which the sudden reoxygenation of ischemic tissues induces a surge in oxidative stress and inflammation, leading to the formation of DPCs. This highlights the critical role of oxygenation dynamics in modulating DPC formation and underscores the potential impact of ischemia-reperfusion injury on genomic stability and cellular function.

Taken together, these findings highlight the importance of selecting appropriate DPC assays based on the experimental objective. RADAR remains the most sensitive and versatile method for detecting both total and protein-specific DPCs based on my results. Meanwhile, ARK and the modified comet assay offer valuable complementary insights, particularly for global DPC measurements or studies requiring single-cell resolution. Understanding the strengths and limitations of each method is critical for accurately assessing DPC dynamics and furthering our understanding of genome instability and DNA repair mechanisms.

Chapter 4: SPRTN Depletion Causes Radioresistance

4.1 Results

4.1.1 SPRTN Depletion Enhances Chemotherapy Sensitivity

Previous studies by our lab and others have demonstrated that cells deficient in SPRTN expression are sensitive to general crosslinking agents such as FA and MGO. These endogenous aldehydes, as explained earlier in section 1.2.1, induce non-enzymatic DPCs by reacting with nucleophilic sites on DNA and nearby proteins. Formaldehyde is a well-studied DPC-inducing agent that covalently links amino groups in DNA bases (primarily through methylene bridges) to side-chains of lysine, cysteine, histidine or tryptophan in protein. Likewise, the glycolytic byproduct methylglyoxal (MGO) is highly reactive and forms advanced glycation end-products that link proteins (e.g. histones, GAPDH) to DNA. These studies show that SPRTN is essential for repairing these DPCs. In cultured cells, SPRTN depletion or mutation dramatically increases sensitivity to formaldehyde and MGO. For example, Vaz *et al.* reported that human SPRTN–deficient cells and Ruijs-Aalfs syndrome (RJALS) patient fibroblasts are hypersensitive to low-dose formaldehyde, exhibiting impaired fork progression and failure to eliminate DPCs (Vaz et al., 2016). Similarly, Akhter *et al.* found that reducing SPRTN expression in mouse cells caused elevated accumulation of DPCs upon MGO exposure and that RJALS patient lymphoblastoid cell lines (LCLs) are markedly more sensitive to MGO than controls. Thus, SPRTN proteolysis is a major repair pathway for aldehyde-induced DPCs, and its absence leads to sustained adducts, fork blockage and cytotoxicity (Hurben et al., 2024). This suggest that SPRTN may influence chemotherapy efficacy.

Many chemotherapeutic agents induce DPCs by trapping DNA-processing enzymes on the genome. Remarkably, the topoisomerase poisons etoposide (Topo II inhibitor) and camptothecin (Topo I inhibitor) stabilize covalent cleavage complexes (Topo–ccs) that are effectively protein–DNA crosslinks. Removal of Topo–ccs requires proteolytic degradation of the trapped enzyme followed by cleavage of the remaining peptide–DNA bond. SPRTN has been shown to perform the upstream proteolysis step. Cell viability assays demonstrate that SPRTN knockout or knockdown dramatically sensitizes cells to etoposide and camptothecin. López-Mosqueda *et al.* showed that SPRTN-null mouse embryonic fibroblasts (MEFs) are more sensitive to formaldehyde, CPT and etoposide than wild-type controls. Likewise, our lab found that SPRTN-depleted HeLa cells and RJALS LCLs display reduced survival when treated with Topo I/II poisons.

First, we systematically evaluated the sensitivity of SPRTN haploinsufficient cells to various chemotherapeutic agents that are known to induce DPCs. Specifically, we employed a colony-forming assay (CFA) to assess the long-term clonogenic survival of HeLa cells with heterozygous SPRTN deletion (HeLa SPRTN -/-/+), hereafter referred to as ΔSPRTN cells. These ΔSPRTN cells were generated in our laboratory by John Fielden using CRISPR/Cas9-mediated gene editing, producing stable cell lines with approximately 50% reduced SPRTN expression relative to wild-type HeLa controls. The use of haploinsufficient cells models a partial impairment of SPRTN function, as might occur in tumour cells with low SPRTN expression or heterozygous mutations.

Based on previous studies and given SPRTN's established role in DPC proteolysis and replication fork protection, we know that ΔSPRTN cells would exhibit increased sensitivity to chemotherapeutic agents that generate DPCs or covalent DNA adducts,

thereby challenging replication and transcriptional machinery. Cisplatin and oxaliplatin, platinum-based compounds, induce intra- and interstrand DNA crosslinks, which distort the DNA helix and obstruct replication forks. These agents also facilitate protein–DNA crosslinking, especially under conditions of oxidative stress or in the presence of chromatin-associated proteins, thus creating substrates for SPRTN-dependent repair. Camptothecin, on the other hand, stabilises topoisomerase I–DNA cleavage complexes (Topo I-cc), leading to the accumulation of covalent Topo I–DNA adducts that impede replication.

Consistent with this previous results, ΔSPRTN cells demonstrated significantly reduced survival following treatment with cisplatin, oxaliplatin, and camptothecin Figure 4.1. Cell viability decreases in a dose-dependent manner following cisplatin exposure, with ΔSPRTN cells exhibiting significantly enhanced sensitivity compared to WT. At 1 μM cisplatin, ΔSPRTN cells show a ~10-fold reduction in viability relative to WT ($p < 0.001$), and this effect becomes even more pronounced at 2 μM. Notably, no significant difference is observed at 0.5 μM, indicating a threshold concentration beyond which SPRTN deficiency critically compromises cell survival Figure 4.1 A.

Figure 4.1 B illustrates the response to oxaliplatin, a platinum-based chemotherapeutic similar to cisplatin but with distinct DNA adduct profiles. Again, ΔSPRTN cells display significantly reduced viability relative to WT at concentrations of 3 μM and higher, reinforcing the importance of SPRTN in resolving DNA lesions induced by platinum compounds. The loss of SPRTN appears to exacerbate cytotoxicity, presumably due to impaired proteolytic processing of platinum-induced DPCs.

The observed hypersensitivity of ΔSPRTN cells to camptothecin aligns with prior studies demonstrating that SPRTN-mediated proteolysis of trapped topoisomerases

is critical for resolving such lesions and maintaining replication fork stability (Vaz et al., 2016; Stingele et al., 2017). Figure 4.1 C shows camptothecin, a Topoisomerase I (Topo I) poison that stabilises covalent Topo I–DNA cleavage complexes (Topo I-ccs). ΔSPRTN cells exhibit marked hypersensitivity to camptothecin across all tested concentrations. At the lowest concentration (20 nM), viability in ΔSPRTN cells is already significantly diminished compared to WT, suggesting that SPRTN is essential for the proteolytic degradation of trapped Topo I. This role is critical in preventing replication fork stalling and collapse, key drivers of cytotoxicity in response to Topo I poisons.

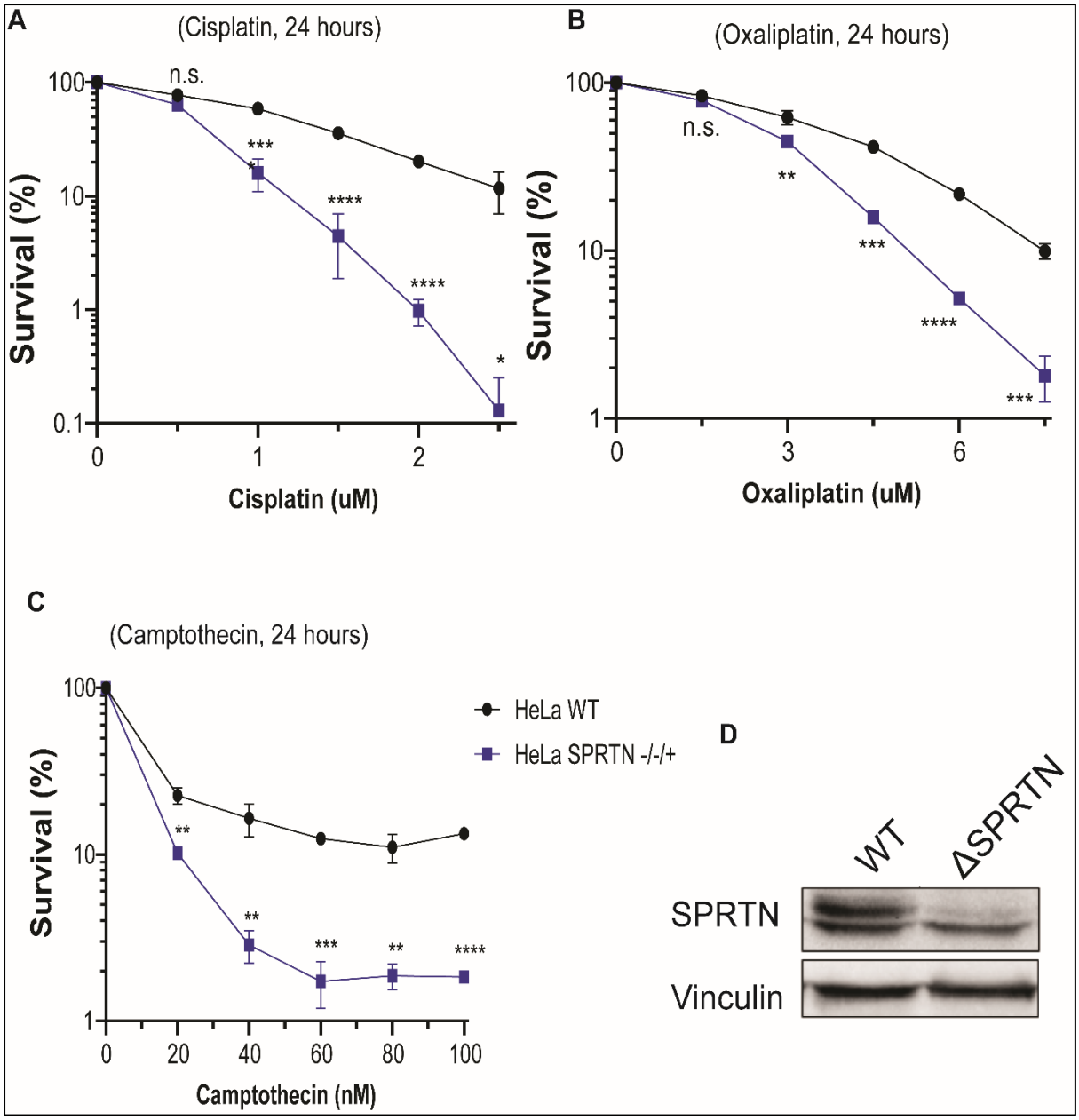


Figure 4.1 Survival of SPRTN-depleted cells to DPC-inducing drugs

Cisplatin (A), oxaliplatin (B) and camptothecin (C). Cells were incubated with the indicated concentrations for 24 h. These experiments were originally performed by Cristiano Peron, a previous PhD student in the Ramadan Laboratory. Statistical significance was calculated with t-test. (D) Western blot confirming different levels of SPRTN expression in HeLa WT and HeLa ΔSPRTN cells. Error bars represent standard deviation (SD) from biological replicates (n = 3). Statistical significance was assessed by unpaired t-test. **p < 0.01, ***p < 0.001, **** p < 0.0001 ns: not significant.

4.1.2 SPRTN Depletion Causes Radioresistance in Most Cell lines Studied

To further investigate the role of SPRTN in the cellular response to DNA damage, we extended our study to examine the effects of IR, specifically γ-radiation, which is widely recognised for inducing diverse forms of DNA lesions, including DSBs, base modifications, DPCs and to some extent complex lesions. Given SPRTN's established role in DPC repair, we hypothesised that SPRTN-deficient cells would exhibit increased sensitivity to IR due to the accumulation of unresolved DPCs, leading to impaired DNA replication and repair. To test this hypothesis, clonogenic survival assays CFA were conducted on both wild-type (WT) HeLa cells and SPRTN haploinsufficient HeLa cells (ΔSPRTN) following different doses of γ-radiation.

Contrary to expectations, ΔSPRTN cells displayed higher survival rates compared to WT cells upon exposure to ionizing radiation. This unexpected radiotolerant phenotype suggests that the loss of SPRTN does not compromise, and may even enhance, cellular resilience to IR-induced cytotoxicity. CFA was done to evaluate the sensitivity of WT HeLa cells compared to ΔSPRTN after increasing doses of γ-irradiation (0, 2, 4, 6, and 8 Gy). Consistent with the unexpected radiotolerant phenotype described in the text, ΔSPRTN cells displayed significantly higher survival rates than their WT counterparts across multiple radiation doses. At 4 Gy and 8 Gy, the ΔSPRTN cells exhibited greater clonogenic potential ($p < 0.001$), indicating enhanced resistance to IR-induced cytotoxicity (Figure 4.2 A). These data suggest that SPRTN haploinsufficiency confers a survival advantage upon radiation exposure.

To rigorously validate this observation, SPRTN depletion was independently achieved using three distinct siRNA oligonucleotides (siSPRTN #1, #2, and #3) in WT HeLa cells. Following IR exposure (4 Gy and 8 Gy), the CFA again demonstrated that

SPRTN-depleted cells exhibited significantly higher survival compared to cells transfected with non-targeting control siRNA (siLuc). This radiotolerance was reproducible across all three siRNA constructs, providing robust evidence that SPRTN depletion enhances survival in response to IR (Figure 4.2C). This confirms that the radioresistance phenotype is specifically attributable to reduced SPRTN levels.

Further corroboration of this phenotype was achieved through complementary cell viability assays. Using Resazurin cell viability assay, used to quantify the metabolic activity as a surrogate for viability of wild-type (WT) and ΔSPRTN following exposure to increasing doses of ionising radiation (IR) (0, 2, 4, and 6 Gy). DNA-PK inhibitor was used as a positive control, as it is known that the cells would be more sensitive in the absence of DNA-PK(Plumb et al., 1999).

Consistent with prior findings, ΔSPRTN cells displayed significantly higher viability at 4 and 6 Gy compared to WT cells, confirming their radioresistance phenotype (Figure 4.2 E).

Collectively, these findings reveal a counterintuitive role for SPRTN in the context of IR. Rather than sensitising cells to radiation, SPRTN deficiency appears to confer a protective effect, enhancing cell survival despite elevated DNA damage. This paradox forms the foundation for subsequent investigations into the underlying mechanisms—particularly the potential for DPC accumulation to interfere with canonical damage detection and checkpoint signalling, ultimately promoting a damage-tolerant, radioresistant phenotype.

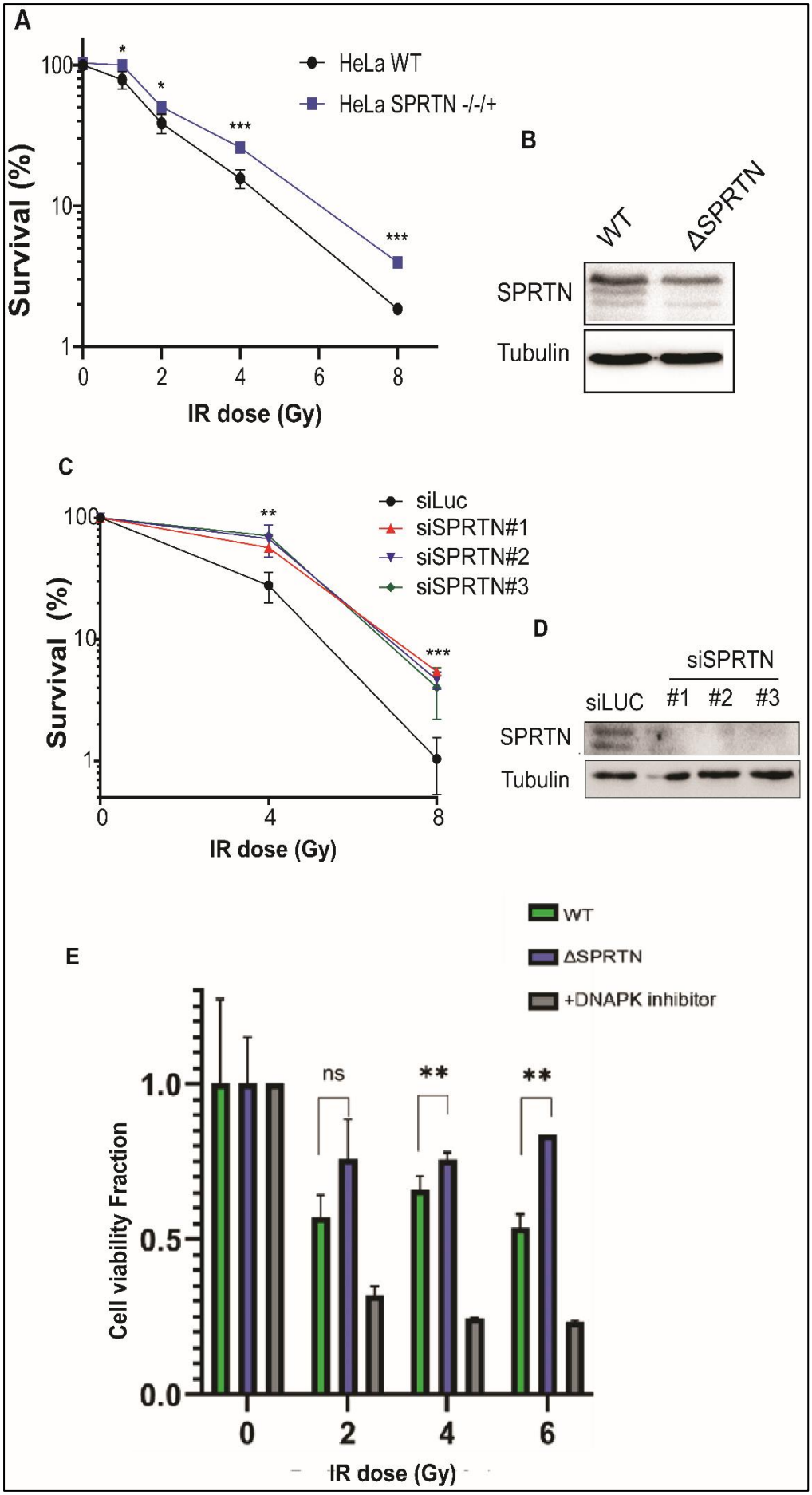

A
100
10
1
Survival (%)
0
2
4
6
8
IR dose (Gy)
*
*
***
***
HeLa WT
HeLa SPRTN -/-/+
B
WT
ΔSPRTN
SPRTN
Tubulin
C
100
10
1
Survival (%)
0
4
8
IR dose (Gy)
**
***
siLuc
siSPRTN#1
siSPRTN#2
siSPRTN#3
D
siSPRTN
siLUC
#1
#2
#3
SPRTN
Tubulin
E
WT
ΔSPRTN
+DNAPK inhibitor
1.0
0.5
0.0
Cell viability Fraction
ns
**
**
0
2
4
6
IR dose (Gy)

Figure 4.2 SPRTN Depletion Causes Radioresistance

(A) Survival assay of ΔSPRTN compared to HeLa wildtype post IR. (B) Western blot confirming different level of SPRTN expression in HeLa WT and HeLa ΔSPRTN cells. (C) Cell treated with siRNA control (siLUC) and three different siRNAs towards SPRTN after treatment with IR. (D) Western blot confirming depletion of SPRTN, the degree of SPRTN knockdown is more than 90% in all of siRNAs used as quantified by Fiji. Statistical significance was calculated with t-test. Error bars represent standard deviation (SD) from biological replicates (n = 3). Statistical significance was assessed by unpaired t-test. * $p < 0.05$, ** $p < 0.01$, *** $p < 0.001$, ns: not significant.

(C) was originally performed by Dr. Bruno Vaz, a former postdoctoral researcher in the Ramadan Laboratory.

To further investigate whether the observed radioresistant phenotype upon SPRTN depletion is cell-line specific or represents a broader biological phenomenon, we extended our analysis to include additional cancer cell lines beyond HeLa. The rationale behind this approach was to assess whether SPRTN depletion universally impacts the cellular response to IR across different genetic backgrounds and tumour types, or whether the phenotype is restricted to particular contexts.

We used MCF-7 breast cancer cell line, a well-established model that exhibits distinct molecular features compared to HeLa cells, particularly regarding its DDR profile and p53 status. These differences provide a valuable context for examining the role of SPRTN across varied genetic backgrounds. To investigate whether SPRTN depletion modulates radiosensitivity in this alternative cellular context, we utilised siRNA-mediated knockdown of SPRTN in MCF-7 cells, followed by exposure to incremental doses of ionising radiation (IR) (0, 2, 4, and 6 Gy). Due to technical limitations encountered during the optimisation phase-where alternative siRNA sequences targeting SPRTN induced excessive cytotoxicity in MCF-7 cells, I was restricted to employing a single siRNA construct (siSPRTN) for these experiments. Despite this constraint, the selected siSPRTN effectively reduced SPRTN levels without compromising baseline cell viability prior to IR exposure, allowing for a robust assessment of SPRTN's contribution to the radiation response in MCF-7 cells.

In control MCF-7 cells treated with siLuciferase (siLuc), viability decreased in a dose-dependent manner following IR exposure, consistent with expected radiosensitivity. Specifically, while control cells (siLuc) displayed the expected dose-dependent decline in viability following IR exposure, SPRTN-depleted MCF-7 cells (siSPRTN)

demonstrated significantly higher survival at 6 Gy almost ~75%. This represents an approximate 20% increase in cell survival at higher radiation doses relative to controls, a statistically significant difference ($p < 0.05$). Although this radiotolerant phenotype in MCF-7 cells was less robust than that previously observed in HeLa cells, where SPRTN depletion resulted in a much stronger resistance to IR-induced cytotoxicity across similar radiation doses, these findings suggest that SPRTN depletion confers a moderate radiotolerant phenotype in MCF-7 cells, allowing them to partially evade IR-induced cytotoxicity Figure 4.3 A.

Next, we extended our investigations to the A549 lung carcinoma cell line. This approach was taken to assess whether the radioresistant phenotype observed in HeLa and MCF-7 cells upon SPRTN depletion could be recapitulated in a third, distinct cancer model. A549 cells, which possess a robust DNA damage response (DDR) and are widely used in radiobiological studies, provide an ideal system to examine the broader relevance of SPRTN's role in modulating IR sensitivity.

For this experiment, A549 cells were transfected with either control siRNA (siLuc) or two independent siRNAs targeting SPRTN (siSPRTN#1 and siSPRTN#2). Following SPRTN knockdown, cells were exposed to escalating doses of IR (0, 4, and 8 Gy), and cell viability was assessed 24 hours post-irradiation using the Resazurin assay. As shown in the figure, in control siLuc-treated cells, IR exposure resulted in a dose-dependent decrease in cell viability, with approximately 20–30% reduction at 4 Gy and a more pronounced decline at 8 Gy. This outcome is consistent with the well-established cytotoxic effects of IR, which induces DNA damage, including double-strand breaks (DSBs), leading to reduced cell survival.

In contrast, A549 cells depleted of SPRTN exhibited a markedly different response. Across both SPRTN-targeting siRNAs, cell viability remained consistently high following IR exposure, with negligible reductions observed at either 4 or 8 Gy doses (Figure 4.3 C). This significant divergence in IR sensitivity between SPRTN-depleted and control cells underscores a consistent radioresistant phenotype in SPRTN-deficient A549 cells. Statistical analyses revealed significant differences in cell viability between siLuc-treated and siSPRTN-depleted cells at both irradiation doses, further confirming the robustness of this phenotype.

These findings are particularly intriguing, as they suggest that SPRTN depletion confers a generalised resistance to IR-induced cytotoxicity across multiple cancer cell lines, including HeLa, MCF-7, and now A549 cells. Mechanistically, this phenomenon may reflect impaired processing of DPCs or stalled replication forks induced by IR in the absence of SPRTN. Alternatively, compensatory DDR mechanisms could be activated in SPRTN-depleted cells, promoting cell survival despite the accumulation of DNA damage. Collectively, these results reinforce the notion that SPRTN plays a complex and context-dependent role in modulating cellular responses to IR, and that its depletion may paradoxically enhance cell survival following radiation exposure in certain cancer cell types.

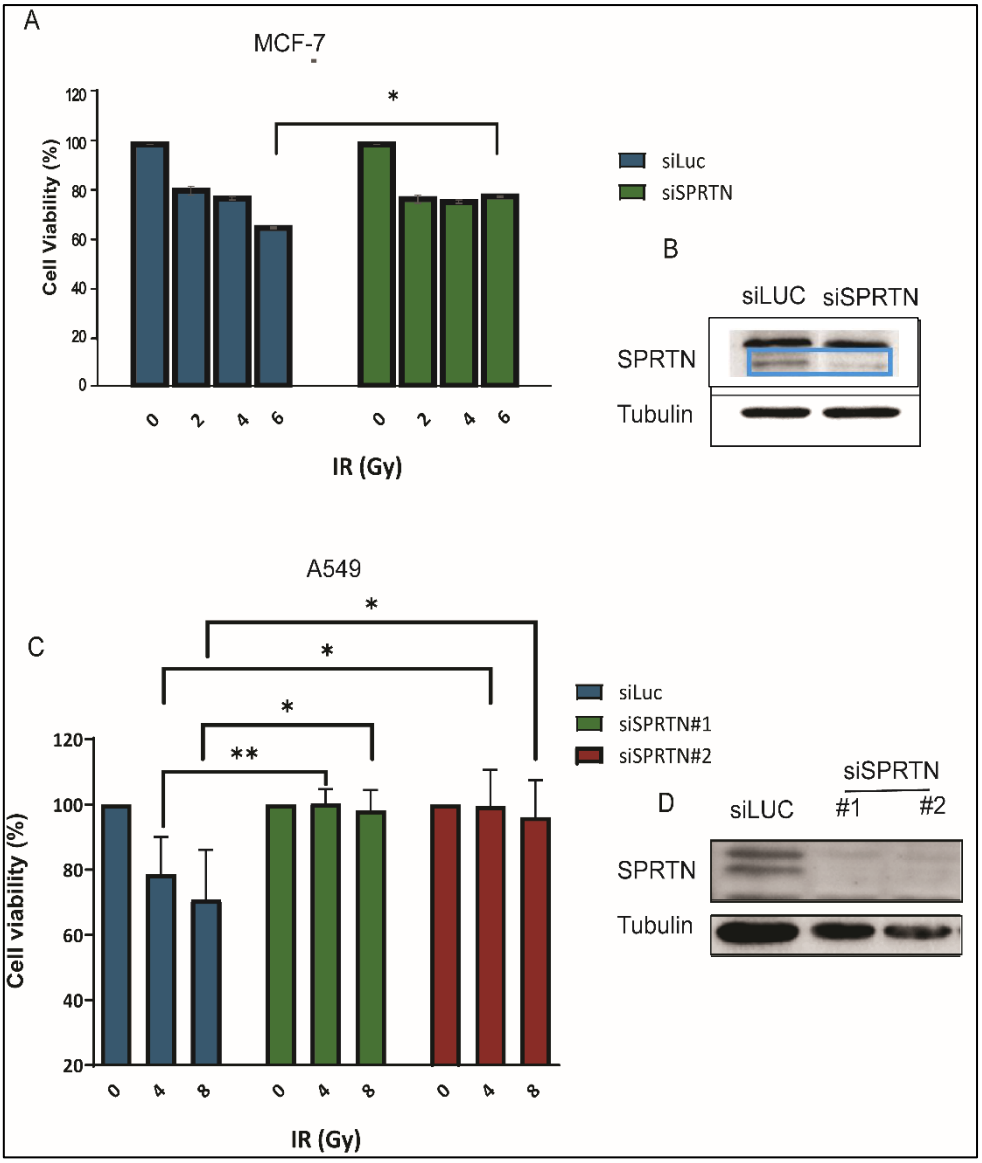


Figure 4.3. SPRTN depletion confers radiotolerance in MCF-7 and A549 cancer cell lines following ionising radiation (IR) exposure.

Cell viability was assessed in MCF-7 (A) and A549 (C) cells following siRNA-mediated knockdown of SPRTN and subsequent exposure to increasing doses of IR.

(A) MCF-7 cells were treated with either control siRNA (siLuc) or SPRTN-targeting siRNA (siSPRTN) and exposed to 0, 2, 4, or 6 Gy IR. Viability was measured 72 hours post-irradiation and normalised to the untreated control (0 Gy). SPRTN-depleted cells displayed significantly higher viability at 6 Gy relative to controls (*$p < 0.05$), suggesting moderate radiotolerance. (B) Western blot analysis confirmed effective SPRTN knockdown, with tubulin as a loading control. The degree of SPRTN knockdown is 85% as quantified by Fiji.

(C) A549 cells were transfected with siLuc, or two independent SPRTN-targeting siRNAs (siSPRTN#1 and siSPRTN#2), followed by IR exposure at 0, 4, or 8 Gy. SPRTN depletion conferred robust radiotolerance across both siRNA constructs, with significantly higher viability at 4 Gy and 8 Gy relative to controls (*$p < 0.05$, **$p < 0.01$). (D) Western blot confirmed SPRTN

knockdown for both siRNA constructs. This experiment was done by Jenny, a previous master student in Ramadan Lab. Degree of SPRTN knockdown is 95% using siSPRTN#1, and 85% using siSPRTN#2 as quantified by Fiji.

Error bars represent standard deviation (SD) from biological replicates (n = 3). Statistical significance was assessed by unpaired t-test.

Additionally, we wanted to test if SPRTN depletion in HCT116 would show a similar trend post-IR. Previously, Cristiano Peron – a previous PhD student in Ramadan lab- showed that these cells are not affected by chemotherapeutic drugs that are known to cause crosslinking (Cisplatin and Camptothecin) Figure 4.4 B and C. I have used HCT116 colon carcinoma cells that were engineered with an auxin-inducible degron (AID) system for SPRTN. In this model, the addition of auxin (AUX) triggers proteasomal degradation of SPRTN, while DMSO serves as a non-depletion control. This system allows for precise temporal control of SPRTN levels, ensuring consistency across experimental replicates Figure 4.4 A.

Following SPRTN depletion, cells were subjected to varying doses of ionising radiation (2, 4, and 6 Gy) to assess their viability using the Resazurin reduction assay, a metabolic-based assay that serves as a reliable indicator of cellular health and proliferation. As depicted in the figure, IR treatment induced a dose-dependent decrease in cell viability in both DMSO-treated and AUX-treated (SPRTN-depleted) cells. However, contrary to observations in other cell models, SPRTN depletion in HCT116 cells did not result in any significant difference in survival compared to control cells at any of the tested radiation doses.

This lack of differential viability suggests that, in HCT116 cells, SPRTN depletion does not impact the cellular response to IR-induced damage under the conditions tested.

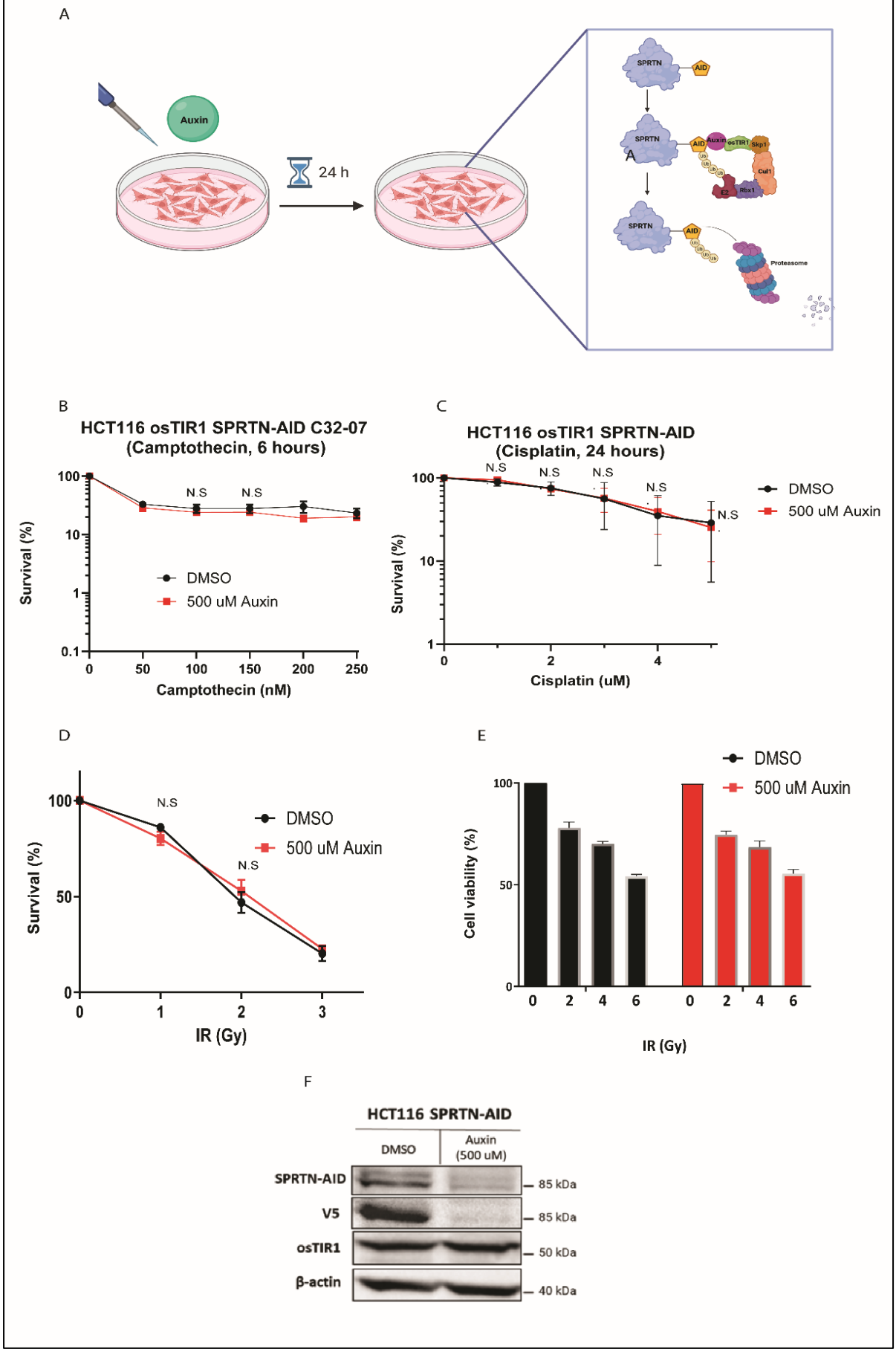

A
Auxin
24 h
SPRTN
AID
Auxin
osTIR1
Skp1
Cul1
Rbx1
E3
Proteasome
B
HCT116 osTIR1 SPRTN-AID C32-07
(Camptothecin, 6 hours)
Survival (%)
N.S
N.S
DMSO
500 uM Auxin
Camptothecin (nM)
C
HCT116 osTIR1 SPRTN-AID
(Cisplatin, 24 hours)
Survival (%)
N.S
N.S
N.S
N.S
N.S
DMSO
500 uM Auxin
Cisplatin (uM)
D
Survival (%)
N.S
N.S
DMSO
500 uM Auxin
IR (Gy)
E
Cell viability (%)
DMSO
500 uM Auxin
IR (Gy)
F
HCT116 SPRTN-AID
DMSO
Auxin
(500 uM)
SPRTN-AID
V5
osTIR1
β-actin
85 kDa
85 kDa
50 kDa
40 kDa

Figure 4.4. Depletion of SPRTN via auxin-inducible degradation does not sensitise HCT116 cells to DNA-damaging agents or ionising radiation (IR).

(A) Schematic representation of the auxin-inducible degron (AID) system. Treatment of HCT116 osTIR1 SPRTN-AID cells with auxin (500 μM) for 24 hours induces ubiquitination and proteasomal degradation of SPRTN-AID protein via the SCF complex.

(B-D) Clonogenic survival assays of HCT116 osTIR1 SPRTN-AID cells treated with either DMSO (control) or 500 μM auxin to deplete SPRTN, followed by exposure to various DNA-damaging agents:

(B) Camptothecin (0-250 nM, 6 hours). (C) Cisplatin (0-4 μM, 24 hours). (D) Ionising radiation (IR) (0-3 Gy).

Survival percentages are plotted relative to untreated controls. No significant differences (p-value >0.5) (N.S.) were observed between SPRTN-depleted and control cells across these conditions.

(E) Cell viability assay in HCT116 SPRTN-AID cells treated with DMSO or 500 μM auxin and exposed to increasing doses of IR (0, 2, 4, 6 Gy). Viability was assessed 72 hours post-irradiation. Similar to survival assays, no significant differences were detected between control and SPRTN-depleted cells.

(F) Western blot analysis confirming SPRTN depletion in HCT116 SPRTN-AID cells following auxin (500 μM) treatment. SPRTN-AID levels are reduced in auxin-treated cells compared to DMSO controls. V5 and osTIR1 were detected, and β-actin was used as a loading control.

Error bars represent standard deviation (SD) from biological replicates (n = 3). Statistical significance was determined using unpaired t-tests.

(B-D) were originally performed by Cristano Peron, a former PhD student in the Ramadan Laboratory.

Finally, to investigate whether fibroblast cell lines derived from Ruijs-Aalfs syndrome (RJALS) patients, harbouring biallelic mutations in SPRTN (SPRTN-ΔC/SPRTN^Y117C) also exhibit radioresistance, we assessed their response to ionising radiation. Our previous findings that these SPRTN-deficient cells are hypersensitive to a broad spectrum of DNA–protein crosslinking agents (Lessel, Vaz, Halder, Lockhart, Marinovic-terzic, et al., 2014). The fibroblast lines were established from patient-derived samples, providing a clinically relevant model to explore the impact of SPRTN mutations on radiation response (Figure 4.5 A, B). This figure presents data from an MTT assay evaluating the metabolic activity (as a surrogate for cell viability) of wild-type (WT) cells and RJALS patient-derived cells carrying compound heterozygous SPRTN mutations (c.717_718+2delAGGT / c.350A>G) following exposure to IR at doses of 0 Gy, 4 Gy, and 6 Gy.

The WT cells exhibited a significant, dose-dependent reduction in viability post-irradiation, with a notable decline at 4 Gy ($p < 0.001$) and an even greater decrease at 6 Gy ($p < 0.001$) relative to untreated controls (0 Gy). This trend reflects typical radiation-induced cytotoxicity in SPRTN-proficient cells.

In contrast, RJALS patient-derived cells, which harbour biallelic SPRTN mutations leading to SPRTN deficiency, displayed no significant reduction in viability at either 4 Gy or 6 Gy compared to the 0 Gy control (ns = not significant). Interestingly, a modest, non-significant increase in viability was observed at 6 Gy, suggesting a paradoxical radiotolerant phenotype in these cells. This resistance to IR-induced cytotoxicity mirrors observations in SPRTN haploinsufficient cell models (as shown in previous assays) and underscores the critical role of SPRTN-mediated DPC repair in modulating IR sensitivity.

Further, statistical comparisons between WT and RJALS cells at each radiation dose revealed a significant difference at 6 Gy ($p < 0.0001$) and 4 Gy ($p < 0.05$), confirming that SPRTN deficiency in RJALS cells confers resistance to IR-induced viability loss Figure 4.5 C.

By extending our observations across multiple cell lines, these data reinforce the hypothesis that the impact of SPRTN depletion on IR sensitivity is context-dependent and may vary according to the intrinsic DDR capacity, cell cycle profile, or tissue origin of the cells. This broader approach strengthens our overall conclusions and provides important insights into the role of SPRTN in the cellular response to IR across different cancer models.

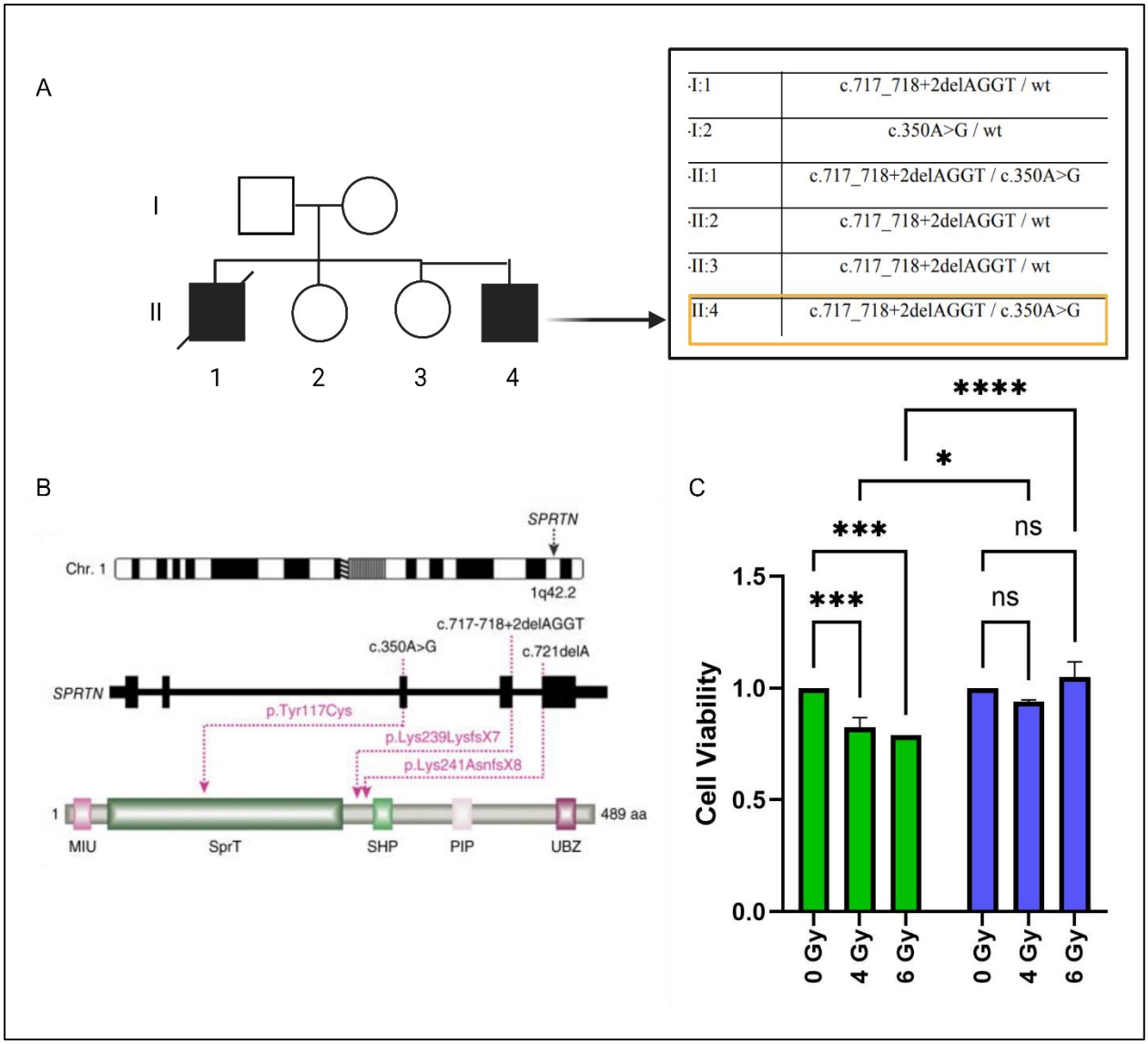


Figure 4.5. SPRTN mutations in a patient-derived cell line confer resistance to ionising radiation (IR).

(A) Pedigree chart of a family carrying compound heterozygous mutations in SPRTN. Affected individuals (solid symbols) possess both the c.717_718+2delAGGT and c.350A>G mutations. The proband (II:4), highlighted in orange, carries the compound heterozygous genotype.

(B) Genomic localisation and protein structure of SPRTN. The genomic structure is based on the longest open reading frame (ORF), comprising five coding exons represented by black rectangles. The positions of the identified mutations (c.717_718+2delAGGT and c.350A>G) are indicated at the gene level (top). The protein diagram (bottom) depicts the predicted functional domains of SPRTN, including the MIU (motif interacting with ubiquitin), SprT (metalloprotease domain), SHP (SUMO-interacting motif), PIP (PCNA-interacting peptide box), and UBZ (ubiquitin-binding zinc finger domain). The corresponding mutations are shown at the protein level, highlighting their potential functional consequences. aa, amino acids

(C) Cell viability assay using resazurin comparing fibroblasts derived from healthy controls (green bars) and patient-derived fibroblasts with SPRTN mutations (blue bars) following

exposure to IR (0, 4, and 6 Gy). Viability was assessed 24 hours post-irradiation and normalised to unirradiated controls.

Healthy fibroblasts displayed a significant reduction in viability at 4 and 6 Gy (***$p < 0.001$, ****$p < 0.0001$), indicating IR-induced cytotoxicity.

Statistical analysis was performed using unpaired t-tests. Error bars represent standard deviation (SD) from biological replicates (n = 3).

Figures (A-B) were adapted from (Lessel, Vaz, Halder, Lockhart, Marinovic-terzic, et al., 2014).

4.1.3 Proteolytic Activity of SPRTN Is Required for Radiosensitivity

To dissect the mechanistic basis underlying the radioresistant phenotype observed in SPRTN-deficient cells, we employed DOX-inducible Flp-In HeLa cell lines established in our laboratory, engineered to express either wild-type SPRTN ($SPRTN^{WT}$) or a catalytically inactive SPRTN mutant ($SPRTN^{E112A}$). This system allowed for selective depletion of endogenous SPRTN via siRNA targeting the 3′ untranslated region (3′ UTR), while concurrently inducing exogenous SPRTN expression with doxycycline (DOX). This approach ensured that the observed cellular responses to ionising radiation (IR) could be directly attributed to the presence or absence of SPRTN protease activity.

As shown in Figure 4.6, siRNA-mediated knockdown of endogenous SPRTN in $SPRTN^{WT}$ cells resulted in significantly enhanced cell viability following IR exposure (4 and 8 Gy), confirming the previously observed radioresistant phenotype. However, upon DOX induction and subsequent overexpression of exogenous $SPRTN^{WT}$, this phenotype was fully reversed. Specifically, $SPRTN^{WT}$ overexpression restored IR sensitivity, reducing cell viability to levels comparable with non-depleted controls, thus validating the functional role of SPRTN in modulating IR responses Figure 4.6 A. This restoration of IR sensitivity by $SPRTN^{WT}$ was statistically significant across multiple IR doses, indicating that SPRTN's proteolytic activity is essential for regulating cell survival under genotoxic stress conditions.

In contrast, ectopic expression of the enzymatically inactive $SPRTN^{E112A}$ mutant failed to reverse the radioresistant phenotype Figure 4.6 B. As shown in the $SPRTN^{E112A}$ panel, cells depleted of endogenous SPRTN and overexpressing $SPRTN^{E112A}$ retained high viability following IR, mirroring the SPRTN-depleted state. This demonstrates that the catalytic activity of SPRTN, and not merely its presence, is

required to mediate IR-induced cytotoxicity. The results implicate SPRTN's metalloprotease function in processing IR-induced DPCs or other lesions that interfere with DNA replication and repair.

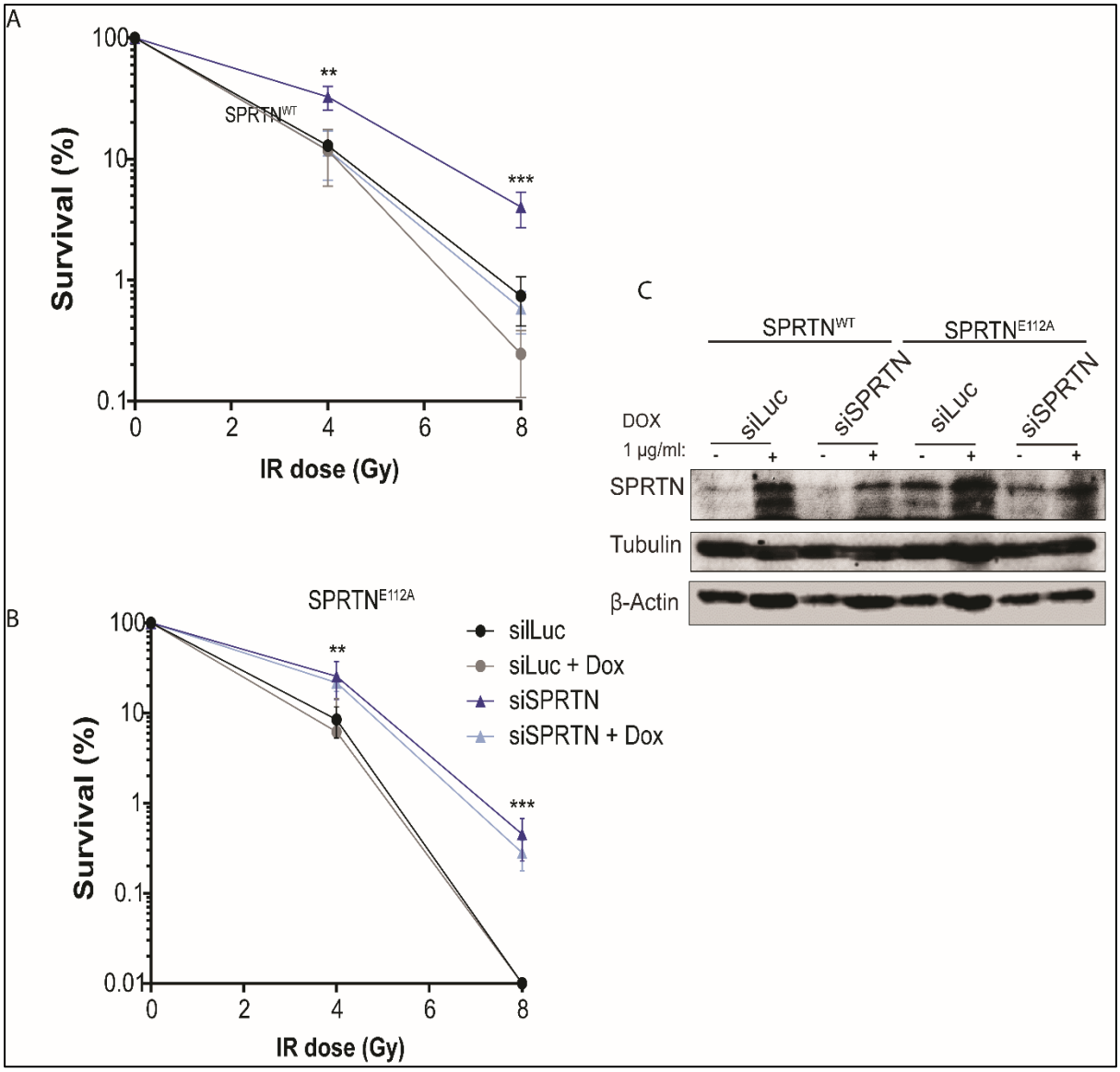


Figure 4.6 Proteolytic Activity of SPRTN Is Required for Radiosensitivity

(A-B) Clonogenic survival assays were performed to assess the role of SPRTN proteolytic activity in modulating cellular responses to ionising radiation (IR). Cells were depleted of endogenous SPRTN via siRNA-mediated knockdown (siSPRTN) and complemented with either wild-type SPRTN (SPRTN^WT) or a protease-dead mutant (SPRTN^E112A) via doxycycline-inducible expression (DOX, 1 µg/mL).

(A) In cells expressing $SPRTN^{WT}$, siSPRTN-mediated depletion conferred radioresistance compared to controls (siLuc), and this resistance was partially rescued by DOX-induced expression of SPRTN^WT (siSPRTN + DOX), restoring radiosensitivity (**p < 0.01, ***p < 0.001).

(B) In contrast, cells expressing $SPRTN^{E112A}$ exhibited no significant rescue of radiosensitivity following DOX induction (siSPRTN + DOX), indicating that SPRTN proteolytic activity is essential for the IR response.

(C) Western blot analysis confirming SPRTN depletion and doxycycline-induced expression of SPRTN^WT and SPRTN^E112A. Tubulin and β-Actin served as loading controls. The degree of SPRTN knockdown is 90%

Error bars represent standard deviation (SD) from biological replicates (n = 3). Statistical significance was determined using unpaired t-tests (**p < 0.01, ***p < 0.001).

Experiments shown in panels (A) and (B) were originally performed by Dr. Bruno Vaz, a former postdoctoral researcher in the Ramadan Laboratory.

4.1.4 Caspase 3/7 Activation Is Impaired in SPRTN-Depleted Cells

To investigate the mechanism underlying the enhanced survival of SPRTN-deficient (ΔSPRTN) cells following ionising radiation (IR), we hypothesised that this phenotype may stem from an attenuated apoptotic response. To test this, we focused on evaluating the activity of Caspase-3 and Caspase-7 (Casp-3/7), which are central executioner caspases acting at the convergence point of both the intrinsic (mitochondrial) and extrinsic (death receptor-mediated) apoptotic pathways (Clements et al., 2005; Samali et al., 1999). Caspase-3 and Caspase-7 serve as terminal effectors in the apoptotic cascade, orchestrating the dismantling of critical cellular structures such as nuclear lamins, cytoskeletal components, and poly(ADP-ribose) polymerase (PARP). Their activation leads to DNA fragmentation, membrane blebbing, and cell disassembly (Elmore, 2007). Notably, the activation of Caspase-3 is considered a point of no return in apoptosis, making it a definitive marker for cells irreversibly committed to programmed cell death. Both caspases are activated downstream of either caspase-8 (extrinsic pathway) or caspase-9 (intrinsic pathway), thus serving as a reliable integrative readout of apoptotic signalling regardless of the initiating stimulus. In the context of ionising radiation, apoptosis is primarily mediated through the intrinsic pathway. IR induces DNA double-strand breaks, leading to mitochondrial outer membrane permeabilization (MOMP), and cytochrome c release, which subsequently activates caspase-9 and ultimately caspase-3/7 (Cao et al., 2019).

To evaluate Cas-3/7 activity, we employed a fluorometric assay that utilises a profluorescent substrate cleaved specifically by active Cas-3/7 enzymes, generating a fluorescent product proportional to caspase activity. HeLa wild-type (WT) and ΔSPRTN cells were exposed to increasing doses of IR (2, 4, and 6 Gy), followed by

measurement of Cas-3/7 activity (Figure 4.7 A). As shown in Figure 4.7 B, Caspase-3/7 activity was negligible in both cell lines under untreated conditions, indicating minimal basal apoptosis. At 2 Gy, Caspase-3/7 activity in WT cells was modest (~500 RFU) and only ~1.25-fold higher than that observed in ΔSPRTN cells (~400 RFU), with no significant difference. Following 4 Gy IR, WT cells exhibited ~2000 RFU, while ΔSPRTN cells reached only ~800 RFU, representing a 2.5-fold higher caspase activity in WT cells, though this difference remained statistically non-significant. Upon exposure to 6 Gy, WT cells showed a dramatic increase in Caspase-3/7 activity (~12,000 RFU), while ΔSPRTN cells reached only ~2,000 RFU. This corresponds to a 6-fold reduction in caspase activation in ΔSPRTN cells relative to WT, a difference that was statistically significant ($*p < 0.05$).

These findings reveal a dose-dependent divergence in apoptotic commitment between WT and SPRTN-deficient cells, with the latter showing significantly attenuated Caspase-3/7 activation, particularly at higher IR doses. This suggests that SPRTN plays a critical role in facilitating executioner caspase activation and apoptosis in response to genotoxic stress.

In conclusion, our findings indicate that cells lacking SPRTN proteolytic activity exhibit resistance to ionizing radiation, and that the resistance can be, at least in part, attributed to downregulation of caspase activity.

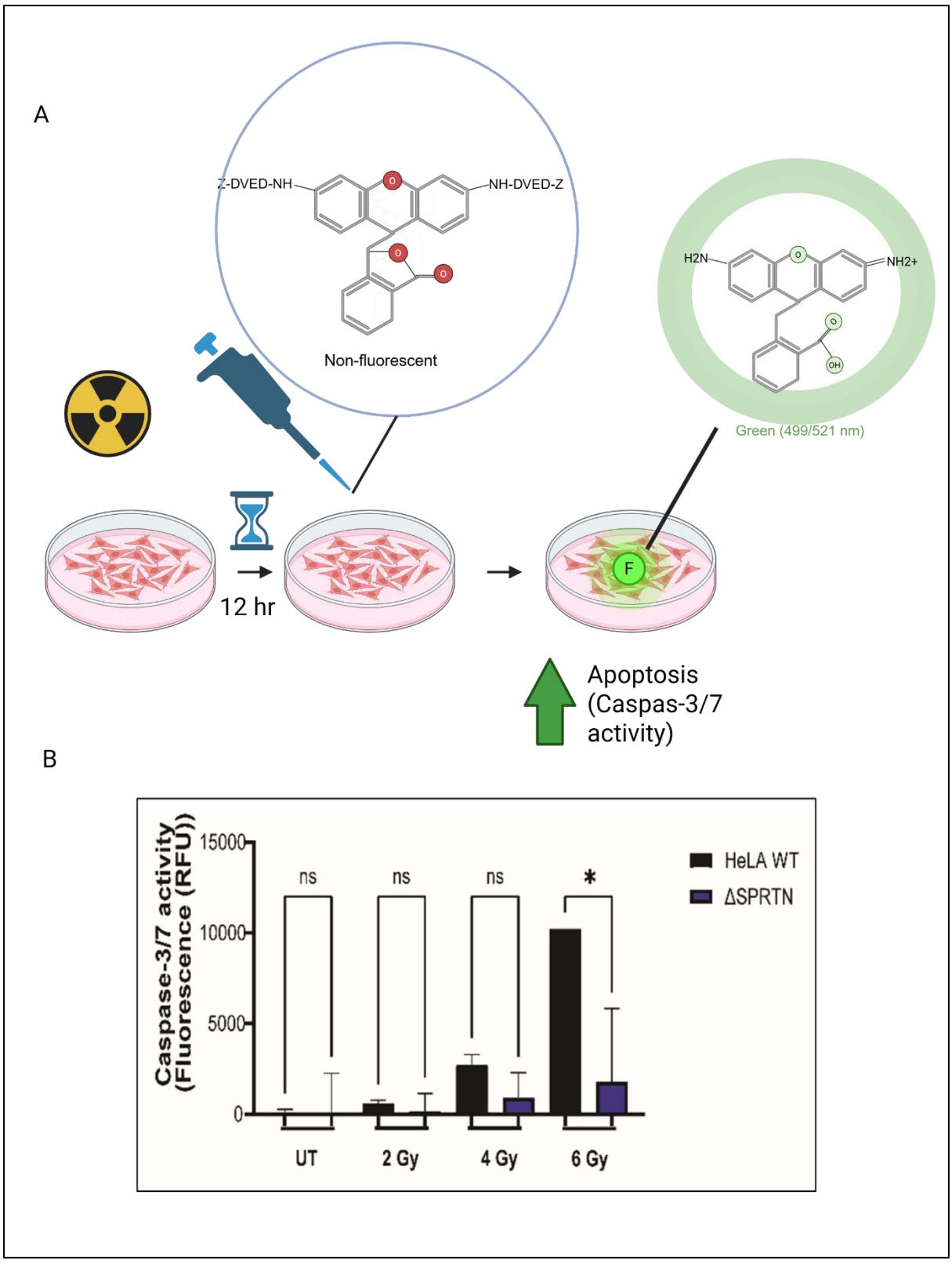


Figure 4.7 SPRTN depletion attenuates caspase-3/7 activation following ionising radiation in HeLa cells.

(A) Schematic representation (top) of the experimental workflow for assessing caspase-3/7 activation as a marker of apoptosis following IR exposure.

(B)The bar graph (bottom) presents quantification of caspase-3/7 activity, expressed as relative fluorescence units (RFU), in HeLa WT (black bars) and ΔSPRTN cells (purple bars) across IR doses. Error bars represent standard deviation (SD) from biological replicates (n = 3). Statistical significance was determined using unpaired t-tests. * $p < 0.05$, ns: not significant.

4.2 Discussion

The DNA–protein crosslink protease SPRTN plays a fundamental role in resolving DPCs, lesions that severely obstruct DNA replication and transcription. Such lesions arise from diverse genotoxic stresses, including chemotherapeutics, aldehydes, and IR. Consistent with this role, prior studies, including our own, have demonstrated that SPRTN depletion sensitises cells to DPC-inducing agents. Mechanistically, SPRTN mediates the proteolytic degradation of protein adducts in DPCs, facilitating their clearance and enabling replication fork progression. Without SPRTN, persistent DPCs stall replication forks, leading to fork collapse, double-strand break (DSB) formation, and DNA damage response (DDR) activation, culminating in reduced cell viability (Figure 4.8). This background positions SPRTN as a guardian of genomic integrity, essential for cellular resistance to DPC-inducing genotoxic insults.

Contrary to this canonical function, our study revealed an unexpected finding: SPRTN-depleted human cancer cell lines exhibited radiotolerance across multiple independent assays in most models that were studied. This finding contradicts the prevailing assumption that DPC repair deficiencies universally sensitise cells to DNA damage, particularly as IR is known to induce DPCs alongside other lesions. Instead, these data suggest that SPRTN's role in the IR response is complex and context-dependent.

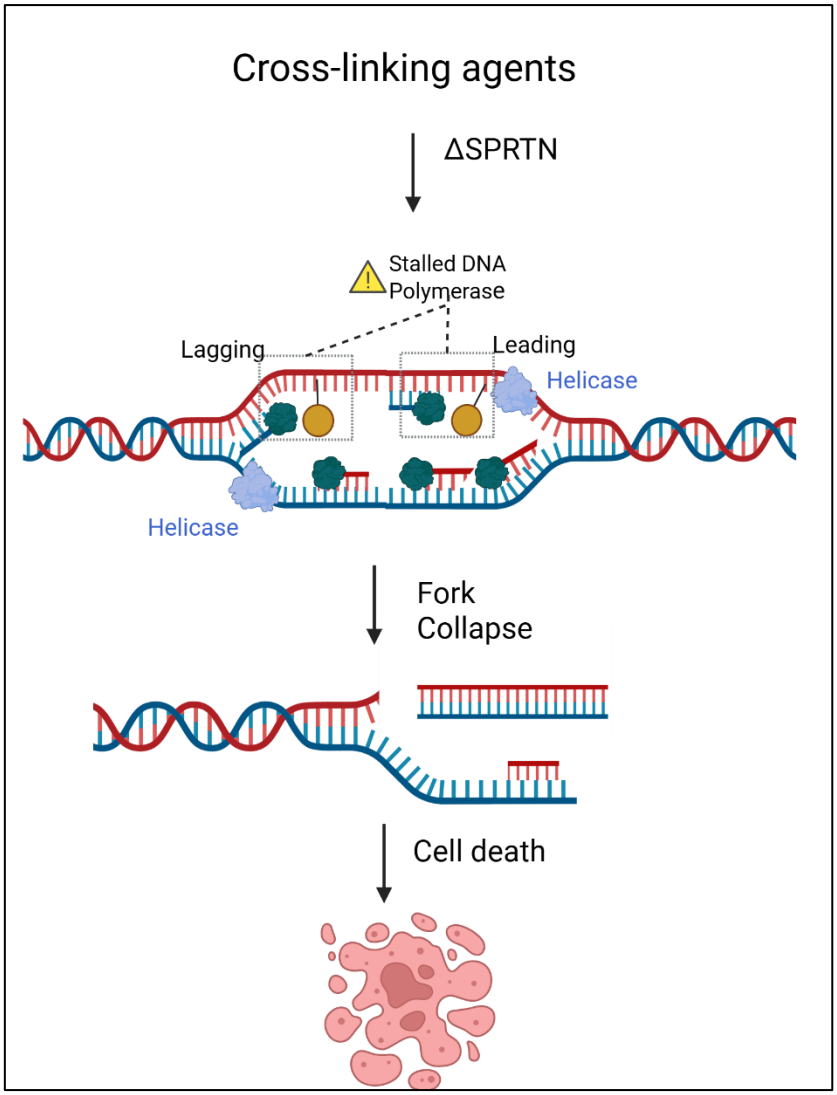


Figure 4.8. Crosslinking agents in SPRTN depleted cells lead to fork collapse and cell death.

Schematic representation of the mechanism by which DPCs induce replication stress and cytotoxicity.

During DNA replication, helicases unwind the parental DNA strands to facilitate the progression of replication forks. When a replication fork encounters a DPC (depicted as protein adducts covalently linked to the DNA), it leads to fork stalling due to the physical obstruction presented by the crosslinked proteins. Persistent fork stalling triggers replication stress and, if unresolved, results in fork collapse, characterised by the formation of a double-strand break (DSB) at the site of stalled replication. Accumulation of such replication-associated DSBs can overwhelm cellular repair mechanisms, leading to genomic instability and ultimately driving cell death. Created with Biorender.

The key to understanding this paradox lies in the diverse lesion profile induced by IR. The nature, frequency, and structural complexity of DPCs induced by IR likely differ substantially from those generated by chemotherapeutic crosslinking agents such as formaldehyde or topoisomerase inhibitors. Moreover, there are multiple factors that influence IR, chromatin context, repair capacity and cell cycle which can significantly influence both lesion accessibility and repair pathway engagement post radiation, possibly affecting SPRTN-mediated proteolysis post-IR (Hauer & Gasser, 2017; H. Takata et al., 2013b). These considerations emphasise the need to distinguish between lesion types and their repair dependencies in interpreting SPRTN's function.

However, lesion burden alone cannot fully explain the radiotolerance observed in most cell lines. DDR signalling is central to the cellular response to IR, orchestrating cell cycle arrest, repair pathway engagement, or apoptosis. The therapeutic efficacy of IR hinges on generating radiation-induced DNA damage (RIDD) that triggers apoptosis if irreparable (Huang & Zhou, 2020). Efficient activation and execution of DDR ensure that cells either repair the damage accurately or are eliminated to maintain genomic integrity. However, defects or alterations in DDR components can profoundly influence cellular sensitivity to IR. In particular, attenuation or modulation of DDR signalling can promote radioresistance by allowing cells to evade apoptosis even in the presence of unrepaired or misrepaired DNA lesions. This survival advantage, although beneficial for normal tissue repair, can be detrimental in cancer therapy, as it enables tumour cells to survive and proliferate despite therapeutic radiation (Santivasi & Xia, 2014).

Supporting evidence for a mechanistic link between SPRTN activity and radiosensitivity comes from a recent study in which overexpression of SPRTN was shown to enhance IR-induced cytotoxicity. In that work, SPRTN overexpression led to increased sensitivity to ionising radiation, which the authors attributed to its effect on

the DNA repair nuclease MRE11. Specifically, they demonstrated that SPRTN can directly cleave MRE11 in a DNA-dependent manner, generating truncated MRE11 fragments and reducing its nuclease activity. This cleavage impaired HR efficiency, leading to defective DSB repair and greater radiosensitivity. Importantly, these findings were further supported by in vitro cleavage assays, in which recombinant SPRTN, but not a protease-dead mutant (E112A), cleaved MRE11 into distinct N- and C-terminal fragments in the presence of double-stranded DNA. The study concluded that SPRTN limits the function of MRE11, and thus, overactive SPRTN can hinder DNA repair and sensitize cells to IR. These findings support the notion that SPRTN's proteolytic activity may serve as a regulatory checkpoint in the DDR, influencing radiosensitivity through modulation of DNA end resection and repair fidelity (Na et al., 2021).

In the context of our study, SPRTN depletion similarly may modulate DDR, contributing to the observed readioresistant phenotype in human cancer cell lines. Specifically, SPRTN-depleted cells exhibited reduced caspase 3/7 activation after IR, indicating a failure to fully engage apoptotic signalling pathways despite DNA damage. This dampened apoptotic response is consistent with models of radioresistance observed in other DDR-compromised contexts. To further dissect this mechanism, assessing DDR markers such as γH2AX phosphorylation and 53BP1 foci formation in SPRTN-deficient cells post-IR would clarify whether damage signalling itself is attenuated. Preliminary findings suggest SPRTN depletion impairs DDR activation, preventing full engagement of cell death pathways. Additional investigations into checkpoint kinase activity and DNA repair factor recruitment could uncover further disruptions caused by SPRTN loss.

Importantly, this radioresistance phenotype was not universal across all cell types. In the colorectal cancer cell line HCT116, SPRTN depletion neither sensitised nor

conferred resistance to IR, underscoring cell-type-specific differences in DDR engagement. Previous work by Cristiano Peron, a previous PhD student in Ramadan Lab, in HCT116 cells supports this context dependency. Although SPRTN depletion did not enhance sensitivity to DPC-inducing agents in these cells, γH2AX and 53BP1 foci confirmed elevated DNA damage accumulation. RNA-sequencing analyses revealed high basal expression of FAM111A, a DPC protease, which was upregulated upon SPRTN depletion, suggesting compensatory repair mechanisms. While FAM111A, alongside GCNA and DDI1, may partially offset SPRTN loss, their activity is insufficient to fully restore DPC repair capacity, allowing damage accumulation without compromising cell viability. This damage tolerance highlights how colorectal cancer cells exhibit resilience to SPRTN depletion, reinforcing the context-dependent nature of SPRTN's role.

Findings from C. elegans provide further insights into SPRTN's context dependency. dvc-1 mutants (SPRTN homologues) exhibit hypersensitivity to cisplatin, which induces DPCs and ICLs, but show no altered sensitivity to IR. One explanation for this context-specific engagement of SPRTN lies in its differential recruitment to chromatin in response to distinct genotoxic stresses. It has been reported that no such recruitment of unmodified SPRTN occurs following IR exposure in worms. This has been interpreted to mean that SPRTN is not broadly required for responding to IR-induced lesions in *C. elegans*. These findings likely reflect fundamental differences in how SPRTN is regulated and deployed in response to distinct types of DNA damage. This lack of chromatin association post-IR suggests that SPRTN activation in worms is damage-specific and could be linked to replication-associated lesions, making it functionally dispensable for IR-induced DNA double-strand breaks (Stingele et al., 2016b).

While our study highlights a radioresistant phenotype in mostly SPRTN-depleted human cancer cell lines tested, recent research in mouse embryonic fibroblasts (MEFs) suggests a contrasting role for SPRTN in modulating cellular responses to IR (Erber et al., 2024). Specifically, the referenced study utilised SprtnF/− MEF cells, which retain one floxed SPRTN allele, and reported increased sensitivity to IR and reactive oxygen species (ROS)-induced DPCs, as determined through clonogenic survival assay. MEF studies report SPRTN depletion sensitising cells to IR, a divergence from our findings in human cancer cells. This discrepancy likely arises from several factors, including species- and cell-type-specific differences in DNA damage response (DDR) regulation. MEFs, used in the referenced study, are non-transformed primary cells that retain intact checkpoint controls and robust DNA repair pathways, which differ substantially from transformed human cancer cell lines such as HeLa, A549, and HCT116. In human cancer cells, DNA repair mechanisms, cell cycle checkpoints, and apoptotic responses are often altered, potentially contributing to their differential tolerance to SPRTN depletion under IR stress.

A further key distinction between studies is the use of rescue experiments. In our work, we incorporated a doxycycline-inducible system to re-express wild-type SPRTN in SPRTN-depleted HeLa cells, confirming that SPRTN's proteolytic activity is essential for modulating the cellular response to IR. This critical experimental control was absent in the MEF study, making it unclear whether the observed sensitivity was due solely to SPRTN deficiency or potentially influenced by off-target effects.

Finally, methodological differences may also contribute: the MEF study primarily utilised clonogenic survival assays, which assess long-term proliferative potential, whereas our study employed short-term metabolic assays (Resazurin, MTT) alongside

colony-forming assays in human cancer models. These differences in experimental design likely influenced the observed outcomes.

In conclusion, our study challenges the prevailing assumption that DPC repair deficiencies universally sensitise cells to genotoxic agents. Instead, we demonstrate that SPRTN depletion paradoxically confers radiotolerance in certain human cancer cell lines, primarily through attenuated DDR signalling and suppressed apoptosis, as evidenced by caspase 3/7 activity assays. This context-dependent response highlights the critical influence of cellular background and repair pathway redundancies in shaping SPRTN's role in DNA damage responses. Importantly, while our findings consistently show a radiotolerant phenotype upon SPRTN depletion in the models studied, exceptions may exist, influenced by species differences, cellular context, proliferation status, and the specific DNA damage landscape. Studies in primary cells, such as MEFs, have demonstrated increased sensitivity to IR upon SPRTN loss, underscoring that SPRTN's impact is not universal but modulated by a combination of intrinsic cellular factors and genotoxic stress types. Recognising these exceptions is crucial for accurately interpreting SPRTN's function across different biological systems. These findings collectively suggest that SPRTN status could influence therapeutic responsiveness, particularly in the context of IR-based treatments. However, to fully elucidate the mechanistic basis of the observed radiotolerance, it is essential to directly assess DNA damage levels in SPRTN-deficient cells. Future experiments quantifying γH2AX phosphorylation, 53BP1 foci formation, and other damage markers will be critical for determining whether accumulated damage persists without activating canonical DDR pathways. This next phase of investigation will provide deeper insight into whether reduced damage sensing, impaired signalling cascades, or alternative tolerance mechanisms sustain the survival of SPRTN-

depleted cells. Ultimately, integrating damage quantification, repair pathway analyses, and apoptotic regulation studies will advance our understanding of SPRTN's multifaceted role in genome stability and inform its potential as a biomarker for therapeutic response.

Chapter 5: DDR Signalling is Disrupted in SPRTN-Depleted Cells Post-Radiation

5.1 Results

5.1.1 SPRTN inactivation affects DDR signalling post radiation

To further understand the paradoxical radioresistance observed in SPRTN-depleted cells in most cell lines examined, we investigated whether this phenotype could be attributed to defective DDR signalling. Among the different human cancer cell lines analysed in this study, HeLa cells consistently exhibited the strongest radiotolerant phenotype upon SPRTN depletion, making them a key model of interest for mechanistic investigation. Efficient DDR signalling is essential for the recognition, signalling, and coordinated repair of DNA lesions, particularly DSBs, which are among the most cytotoxic lesions induced by IR. Given that SPRTN is a known DPC protease involved in replication-associated repair, we hypothesised that its loss may perturb canonical DDR signalling cascades, thereby altering the cell's ability to respond appropriately to radiation-induced stress. We therefore aimed to determine whether the impaired DNA repair observed in ΔSPRTN HeLa cells could be explained by a disruption in DDR activation, which may allow damaged cells to evade apoptosis and persist, ultimately contributing to their radioresistant behaviour.

Ionising radiation induces DSBs, which rapidly trigger the activation of DNA damage response markers at lesion sites. Among these, γH2AX, formed by phosphorylation of the histone variant H2AX at serine 139, is one of the earliest and most widely used indicators of DSBs. γH2AX foci can be detected within minutes following IR, with several studies reporting peak levels between 30 minutes to 2 hours post-exposure, depending on dose and cellular context (Kinner et al., 2008). A similar recruitment pattern is observed for 53BP1, another key DSB repair factor, which colocalizes with γH2AX and displays nearly identical kinetics. 53BP1 foci also appear within the first

hour after IR and typically decline over the subsequent 12–24 hours as DNA repair progresses. Based on this well-established temporal pattern of damage marker dynamics, we focused our analyses on early post-irradiation time points (0–4 hours) to capture peak DDR activation and potential differences in foci formation kinetics between wild-type and SPRTN-deficient cells. Since previous studies have demonstrated that SPRTN plays a role in resolving DPCs, particularly during S-phase, and given that IR can induce both DPCs and DSBs, we synchronised cells at the G1/S transition to maximise the detection of SPRTN-relevant phenotypes. This synchronisation ensures that a significant proportion of the cell population is entering S-phase during or shortly after IR exposure, when SPRTN's proteolytic function is most critical for maintaining replication fork progression and genome stability.

To evaluate the activation of the DDR following IR (5 Gy), we quantified γH2AX foci formation in WT and ΔSPRTN. cells at 0 (immediately after radiation) and 4 hours post-IR, alongside untreated controls.

In WT cells, the number of γH2AX foci per nucleus increased markedly following IR. At baseline (UT), the median number of foci per cell was approximately 2. This number rose sharply to about 10 foci at 0 hours post-IR—representing an approximate 400–500% increase relative to the untreated control. By 4 hours post-IR, the median number decreased modestly to around 6 foci, indicating partial resolution of DNA lesions and initiation of repair. The increases observed at both time points were statistically significant, confirming robust DDR activation.

In contrast, ΔSPRTN cells showed a substantially attenuated response. The median number of γH2AX foci in untreated ΔSPRTN cells was approximately 3, and this value remained nearly unchanged at both 0 and 4 hours post-IR (approximately 3.5 to 4

foci), representing only a 15–30% increase relative to baseline. These differences were not statistically significant (ns), suggesting that SPRTN-deficient cells failed to properly amplify γH2AX signalling in response to IR.

When comparing across genotypes, the γH2AX foci count in WT cells at 0 hours post-IR was approximately 2.5-fold higher than in ΔSPRTN cells at the same time point. This significant disparity indicates that SPRTN plays a key role in facilitating early DDR signalling, possibly by supporting lesion recognition or signalling complex formation.

Overall, these data highlight that although ΔSPRTN cells sustain IR-induced DNA damage, they exhibit a blunted γH2AX response, suggesting defective or delayed DDR activation. This impairment may underlie the persistent DNA lesions observed and contribute to the paradoxical radioresistance phenotype.

To further evaluate the DNA damage signalling response in SPRTN-deficient cells, we quantified 53BP1 foci formation as an additional marker of DSB recognition and repair. 53BP1 is a key mediator of NHEJ and is rapidly recruited to sites of DNA damage following IR. As shown in Figure 5.1, wild-type (WT) cells exhibited a robust induction of 53BP1 foci post-IR. The median number of foci increased from approximately 7 in untreated cells to 12 immediately following IR (0 hr), and remained elevated (~11 foci) at 4 hours post-IR. These increases represent approximately a 70–80% elevation in 53BP1 recruitment and were statistically significant at both time points compared to baseline.

In contrast, ΔSPRTN cells showed no significant changes in 53BP1 foci number following IR. Median foci counts remained steady at approximately 8–9 foci per nucleus across untreated, 0 hr, and 4 hr recovery conditions, indicating a lack of dynamic 53BP1 recruitment in response to DNA damage. When comparing across

genotypes, WT cells exhibited significantly higher 53BP1 foci at 0 hr post-IR compared to ΔSPRTN cells, underscoring a defective DSB signalling response in the absence of SPRTN.

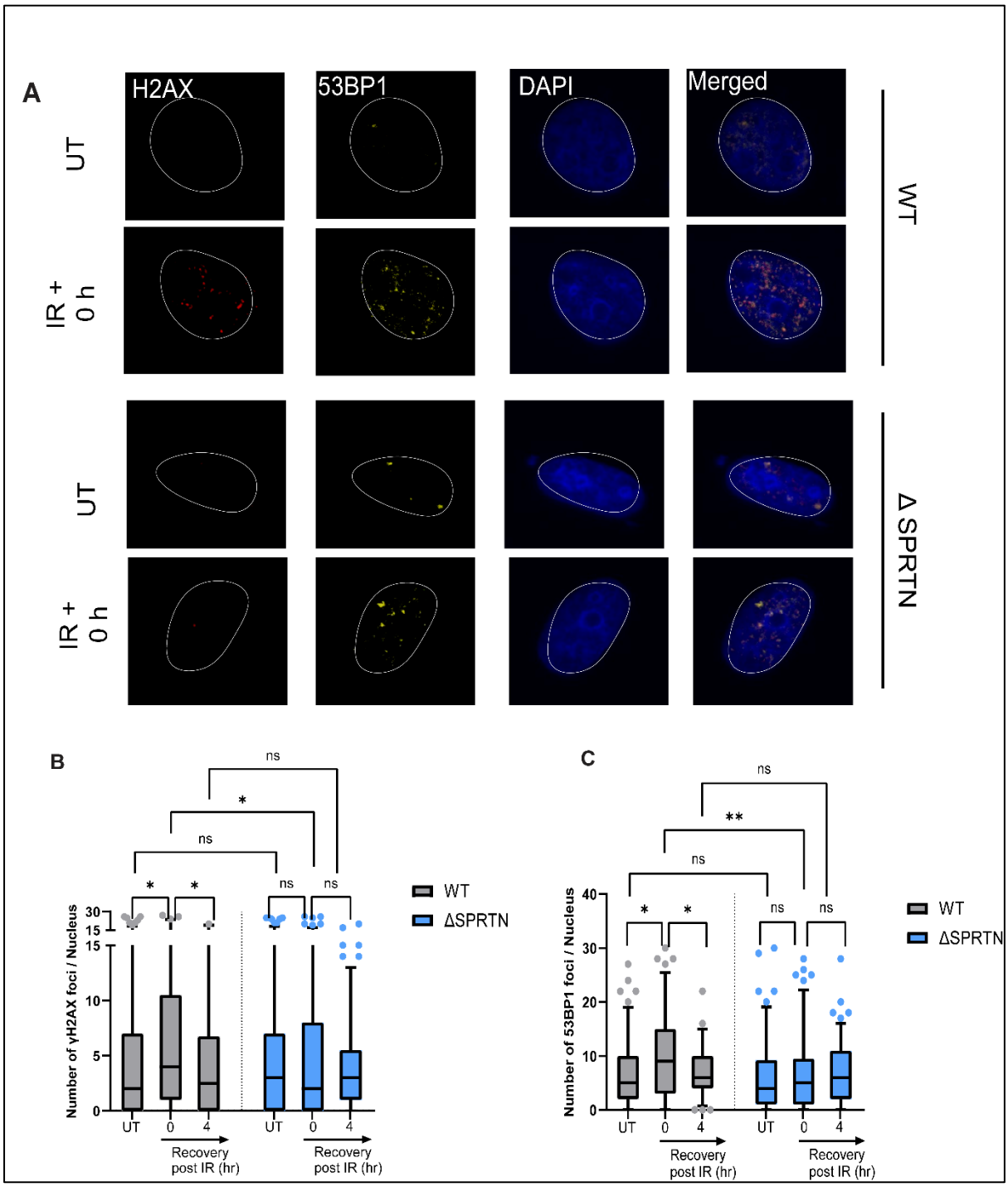


Figure 5.1. Attenuated γH2AX and 53BP1 foci formation in ΔSPRTN cells following ionising radiation.

(A) Representative immunofluorescence images of HeLa WT and ΔSPRTN cells showing γH2AX (red), 53BP1 (yellow), and DAPI (blue) staining at baseline (UT) and immediately following ionising radiation (0 h post-IR, 5 Gy). (B) Quantification of γH2AX (top) and 53BP1 (bottom) nuclear foci per nucleus in WT and ΔSPRTN cells at 0 and 4 hours post-IR. While

WT cells exhibit a transient increase in foci immediately after irradiation, followed by partial resolution, ΔSPRTN cells show no significant increase in foci formation post-IR.

Quantification of >100 cells per condition from one representative experiment is shown, and the experiment was repeated three times. Whisker box plots show median values and data within the 10–90 percentile. Statistical analysis was performed using unpaired t-test. ns: not significant, *$p < 0.05$, **$p < 0.01$.

To further confirm that the attenuated DDR phenotype observed in ΔSPRTN cells is a direct consequence of SPRTN loss, we complemented our findings with transient knockdown using siRNA. This approach allowed us to see whether acute SPRTN depletion recapitulates the impaired DDR. In siSPRTN cells, γH2AX foci formation post-IR was significantly reduced compared to siLUC controls, demonstrating impaired accumulation of this early DSB marker Figure 5.2 B. The decrease in foci number was observed consistently across conditions, with narrower distributions and statistically significant differences from controls, reinforcing that SPRTN is essential for efficient γH2AX induction. To support this observation, we also assessed 53BP1 foci. Following IR, siLUC-treated cells showed a marked increase in 53BP1 foci, as expected Figure 5.2 C. However, siSPRTN cells again showed a blunted response, with lower median foci numbers and a loss of statistical significance across multiple comparisons. This pattern mirrored that of γH2AX and further supported the hypothesis that SPRTN depletion compromises the DDR. Together, these results across two DSB markers (γH2AX and 53BP1) and two models of SPRTN loss (ΔSPRTN and siSPRTN) establish a consistent and reproducible defect in DNA damage signalling following IR.

These results further support the conclusion that SPRTN is required for effective DDR activation. The failure of ΔSPRTN cells to induce 53BP1 foci following IR, despite likely sustaining DNA damage, suggests an impaired capacity to initiate or propagate checkpoint and repair signalling pathways. This deficiency, in conjunction with the previously observed γH2AX signalling defects, highlights a broader attenuation of the DDR machinery in SPRTN-deficient cells, which may contribute to their unexpected radiotolerant phenotype

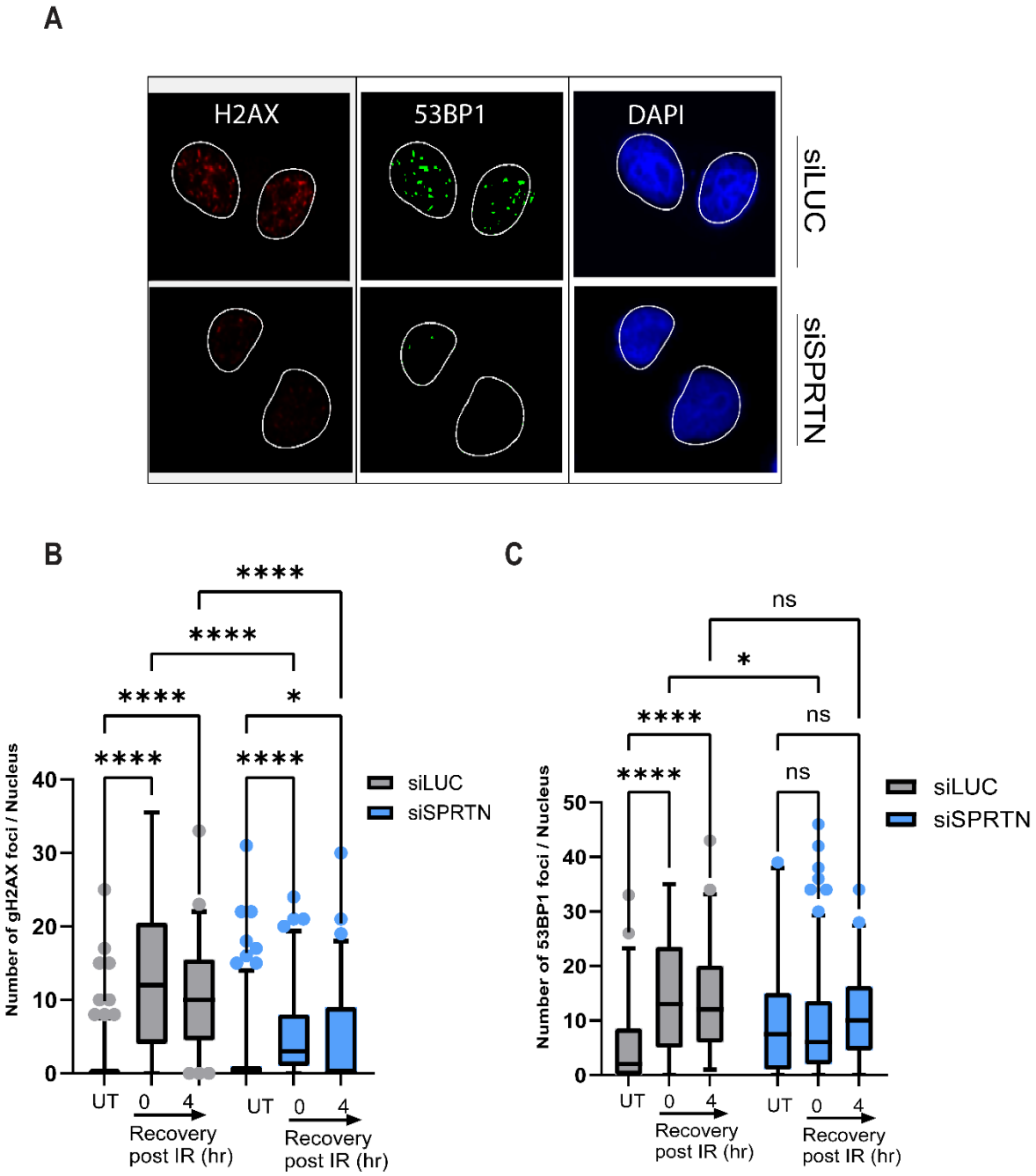


Figure 5.2. SPRTN knockdown impairs γH2AX and 53BP1 foci formation following ionising radiation.

(A) Representative immunofluorescence images (top) show staining for γH2AX (red), 53BP1 (green), and DAPI (blue) in HeLa cells transfected with siLUC (control) or siSPRTN. Merged images illustrate co-localisation of DNA damage markers.

(B,C) Quantification of nuclear foci (bottom) demonstrates that siSPRTN cells exhibit significantly fewer γH2AX and 53BP1 foci immediately and 4 hours post-IR (γ radiation) (5 Gy) compared to siLUC controls, indicating impaired recruitment of DNA damage response factors. Quantification of >100 cells per condition from one representative experiment is

shown, and the experiment was repeated two times. Whisker box plots show median values and data within the 10–90 percentile. Statistical analysis was performed using unpaired t-test. *p < 0.05, ***p < 0.001, ****p < *0.0001, ns: not significant.*

To further characterise the impact of SPRTN loss on DNA damage response dynamics, we assessed the formation of Replication Protein A (RPA) foci following IR. RPA is a crucial single-stranded DNA-binding complex that stabilises exposed ssDNA during resection and facilitates recruitment of repair factors during HR. The accumulation of RPA foci serves as a functional indicator of DNA end resection and active HR pathway engagement.

As shown in Figure 5.3 A and B, wild-type HeLa cells (WT) exhibited a robust RPA response following IR. At 1 hour post-IR, the median number of RPA foci per nucleus was significantly increased by 8 hours post-IR. This increase reflects the continued recruitment of RPA to sites of ssDNA during the repair process. Both time points showed statistically significant differences compared to each other, indicating active progression of resection over time.

In contrast, SPRTN-deficient cells (ΔSPRTN) exhibited a substantially attenuated RPA response. At 1 hour post-IR, the median RPA foci count was close to baseline (~1–2 foci per nucleus), with only a slight increase to approximately 3 foci by 8 hours. While this increase was statistically significant, it remained markedly lower than the corresponding values in WT cells. At both 1 and 8 hours post-IR, ΔSPRTN cells showed significantly fewer RPA foci compared to WT cells, indicating a persistent deficiency in ssDNA formation or in RPA recruitment.

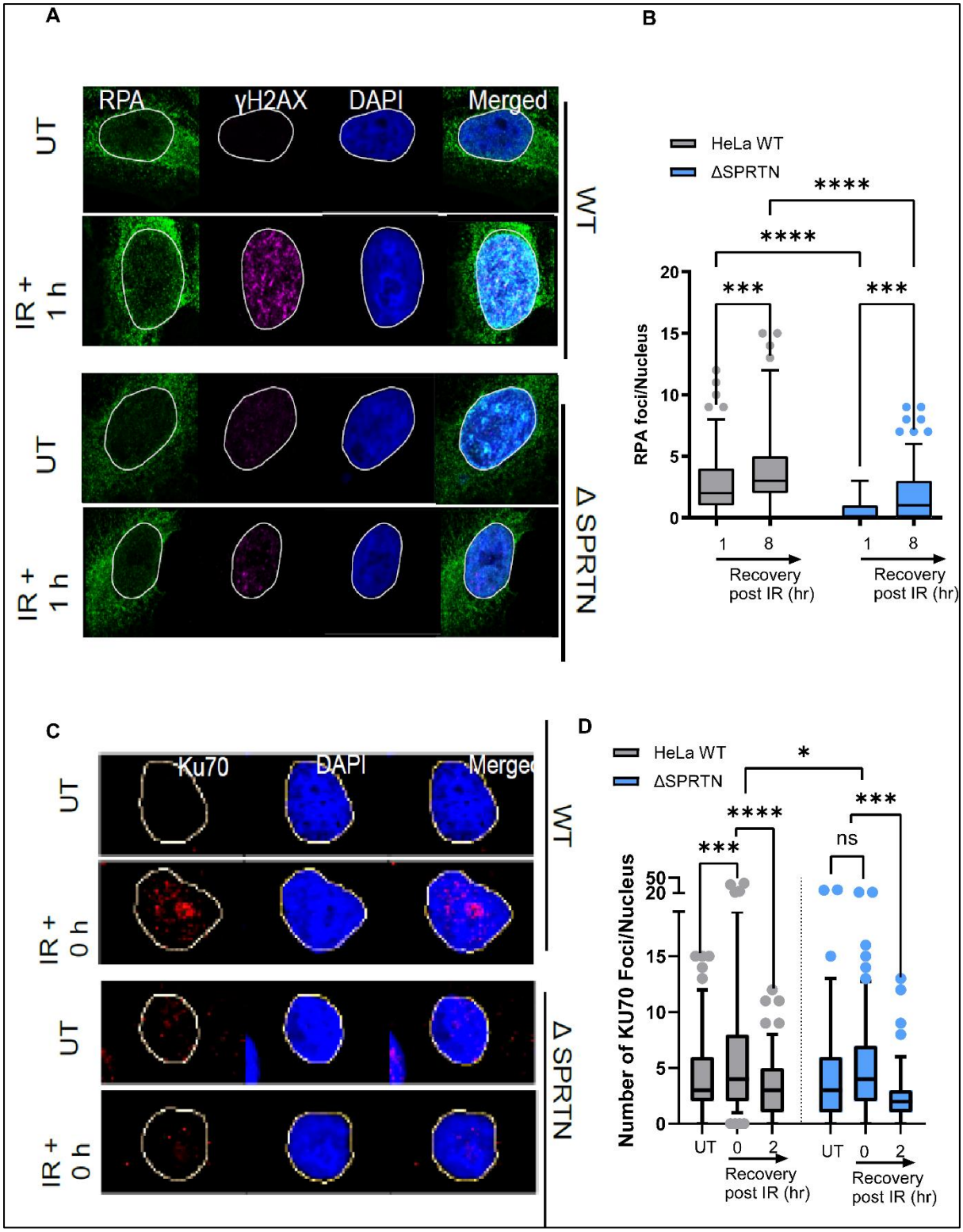


Figure 5.3. SPRTN deficiency impairs DNA damage signalling and modulates recruitment of RPA and KU70 to irradiation-induced lesions.

(A) Representative immunofluorescence images showing nuclear foci formation of RPA (green), γH2AX (magenta), and DNA (DAPI, blue) in WT and ΔSPRTN HeLa cells, either untreated (UT) or 1 hour post-irradiation (IR, 5 Gy, γ-radiation). Merged panels show co-localisation of DNA damage markers in the nucleus.

(B) Quantification of RPA foci per nucleus at 1 h and 8 h post-IR in WT and ΔSPRTN cells. ΔSPRTN cells exhibited significantly fewer RPA foci than WT at both time points, indicating compromised single-stranded DNA formation and damage signalling. Quantification of 100 cells per condition from one representative experiment is shown, and the experiment was repeated two times. Whisker box plots show median values and data within the 10–90 percentile. Statistical analysis was performed using unpaired t-test ***$p < 0.001$, ****$p < 0.0001$

(C) Representative immunofluorescence images of KU70 (red) and DAPI (blue) in WT and ΔSPRTN cells under untreated conditions and immediately (0 h) after IR.

(D) Quantification of KU70 foci per nucleus at 0 h and 2 h post-IR. WT cells showed significant induction and partial resolution of KU70 foci post-irradiation, whereas ΔSPRTN cells exhibited elevated baseline KU70 signal and defective resolution. Quantification of 100 cells per condition from one representative experiment is shown, and the experiment was repeated two times. Whisker box plots show median values and data within the 10–90 percentile. Statistical analysis was performed using unpaired t-test. *$p < 0.05$, ***$p < 0.001$, ****$p < 0.0001$, ns: not significant.

Moreover, to assess the impact of SPRTN deficiency on other DNA damage markers, we quantified the formation of Ku70 foci, a core component of the NHEJ repair machinery that is rapidly recruited to DSBs following IR. Ku70, in complex with Ku80, binds to DSB ends and initiates repair by recruiting downstream NHEJ effectors. The number of Ku70 foci per nucleus serves as an indicator of NHEJ activation and DSB engagement.

In WT HeLa cells, IR induced a significant increase in Ku70 foci. The median foci count rose slightly at 0 hours post-IR. By 2 hours post-IR, the number of foci decreased slightly, suggesting progression of repair and foci resolution. Both the immediate (0 hr) and 2-hour post-IR timepoints showed statistically significant changes compared to the untreated condition, and a significant overall decrease from 0 to 2 hours was also observed ($p < 0.05$), indicating dynamic repair activity (Figure 5.3 C and D).

In contrast, ΔSPRTN cells exhibited a slightly less Ku70 response overall compared to WT post radiation. Although the baseline number of foci (UT) was similar to WT (~3–4), there was no significant increase at 0 hours post-IR (ns). Notably, the absence of significant induction at the 0-hour timepoint and the overall lower number of foci at each stage compared to WT cells indicates a defective or delayed DSB repair in SPRTN-deficient cells.

Taken together, these results suggest that SPRTN is required for efficient Ku70 recruitment. The impaired Ku70 foci formation in ΔSPRTN cells, in combination with attenuated γH2AX, 53BP1, and RPA responses, supports the conclusion that SPRTN deficiency could lead to widespread disruption of DDR signalling.

To evaluate the impact of SPRTN deficiency on DNA damage checkpoint activation following IR, we analysed the phosphorylation status of key DDR signalling proteins in wild-type (WT) and SPRTN-deficient (ΔSPRTN) HeLa cells. Whole-cell lysates were collected at 0, 2, 4, and 8 hours post-IR (5 Gy), and western blotting was performed to detect phosphorylated and total levels of CHK2 (pThr68), CHK1 (pSer317), and KAP1 (pSer824). These proteins are direct targets of the ATM and ATR kinases and serve as indicators of DNA damage signal transduction. Histone H3 was used as a loading control, and loss of SPRTN expression in the knockout cells was confirmed.

In WT cells, a time-dependent increase in phosphorylation was observed for all three markers. CHK2 phosphorylation (pThr68) increased noticeably by 2 hours and remained elevated through 8 hours, indicating sustained ATM pathway activation in response to DSBs. KAP1 phosphorylation (pSer824), which facilitates chromatin relaxation and repair, followed a similar pattern, with a clear rise at 2 and 4 hours post-IR before tapering off slightly by 8 hours. CHK1 phosphorylation (pSer317), a marker of ATR pathway activation, was also upregulated post-IR, though to a lesser extent compared to CHK2 and KAP1.

In ΔSPRTN cells, phosphorylation of all three markers was visibly reduced relative to WT. For CHK2 (pThr68), the increase observed post-IR was present but less pronounced. Densitometric analysis at 4 hours post-IR (Figure 5.4) revealed that CHK2 phosphorylation in ΔSPRTN cells reached approximately 50–60% of that observed in WT cells. A similar reduction (50%) was noted for KAP1 (pSer824), where phosphorylation levels in ΔSPRTN cells were lower throughout the recovery period, suggesting diminished ATM activation or reduced chromatin response to damage. CHK1 phosphorylation was also reduced, with ΔSPRTN cells showing consistently

lower levels of pCHK1 relative to WT, especially at 4 hours post-IR, though total CHK1 levels remained comparable.

Together, these results indicate that SPRTN-deficient HeLa cells exhibit a quantitatively weaker DDR signalling response after IR, as shown by reduced phosphorylation of checkpoint proteins. While phosphorylation is not completely abolished, the lower levels in ΔSPRTN cells suggest that SPRTN may contribute, either directly or indirectly, to efficient activation or amplification of DDR signals. This could be through its role in facilitating DNA–protein crosslink resolution, thereby enabling proper damage sensing, or through interactions with chromatin or repair complexes that modulate kinase accessibility or activity. These findings align with other observations in SPRTN-deficient cells showing impaired foci formation of DNA damage sensors (e.g., γH2AX, 53BP1) and support the idea that checkpoint engagement is functionally attenuated in the absence of SPRTN. This attenuated signalling may play a role in the reduced apoptosis and enhanced survival observed in these cells following IR.

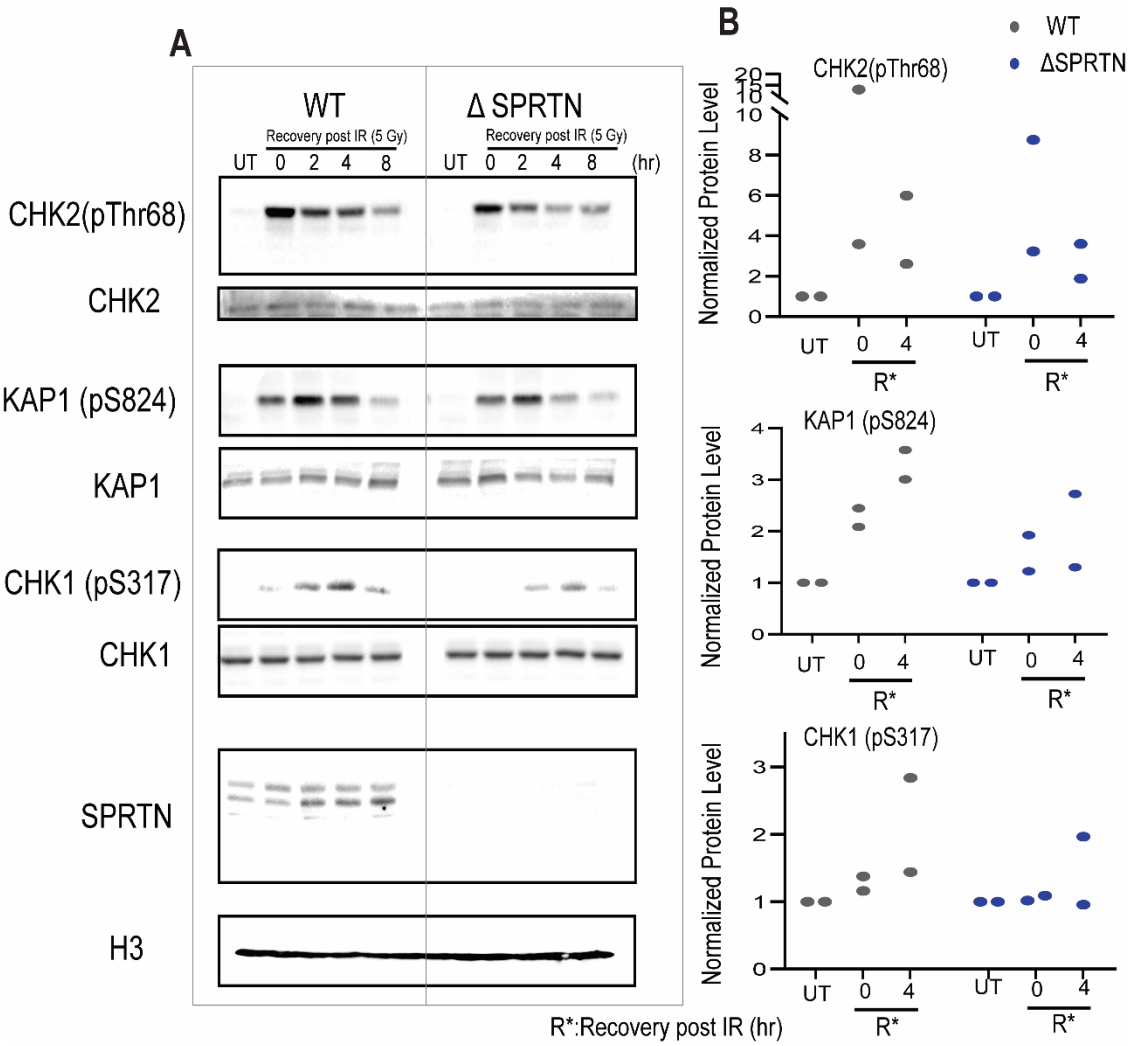


Figure 5.4. SPRTN deficiency attenuates DNA damage checkpoint activation following ionising radiation.

(A) Immunoblot analysis of DNA damage response (DDR) checkpoint proteins in wild-type (WT) and ΔSPRTN HeLa cells. Cells were either untreated (UT) or irradiated with 5 Gy and collected at 0, 2, 4, and 8 hours post-irradiation. Phosphorylation of CHK2 (pThr68), KAP1 (pSer824), and CHK1 (pSer317) was assessed as markers of ATM/ATR activation. Total levels of CHK2, KAP1, and CHK1 were also probed. SPRTN protein was absent in ΔSPRTN cells, and Histone H3 was used as a loading control. (B) Quantification of phosphorylated protein levels at 0 and 4 hours post-IR in WT and ΔSPRTN cells from two blots, normalised to untreated controls. WT cells showed a robust increase in CHK2 and KAP1 phosphorylation after IR, while ΔSPRTN cells displayed attenuated or delayed induction. CHK1 activation remained modest in both genotypes.

5.1.2 Delayed Resolution of DSBs in SPRTN-Depleted Cells Post-Radiation

Next, we examined whether SPRTN-deficient cells experience a decoupling between lesion accumulation and canonical damage response signalling. To achieve that, I directly quantified the level of DSBs and assessed their resolution following IR by performing the neutral comet assay, also known as single-cell gel electrophoresis (SCGE). While immunofluorescence-based detection of DNA damage markers such as γH2AX and 53BP1 provides insight into damage recognition and signalling, these are indirect measures that can be influenced by upstream regulatory processes. In contrast, the neutral comet assay provides a direct physical readout of DSBs by measuring DNA migration under an electric field, where fragmented DNA moves toward the anode to form a “tail” whose intensity correlates with the extent of damage. The percentage of total DNA found in the comet tail (% tail DNA) thus serves as a quantitative indicator of DSB burden within individual cells.

To evaluate the kinetics of DSB repair, we analysed % tail DNA at defined time points post-IR, allowing us to determine not only the extent of initial damage but also the efficiency of subsequent repair over time. This is particularly important given the biphasic nature of DSB repair: a fast phase dominated by NHEJ and a slower phase involving HR, which may be differentially impacted in SPRTN-deficient cells. Since previous studies have demonstrated that SPRTN plays a role in resolving DPCs particularly during S-phase, and given that IR can induce both DPCs and DSBs, we synchronised cells at the G1/S transition to maximise the detection of SPRTN-relevant phenotypes.

Cells were transfected with control siRNA (siLUC), siRNA against SPRTN (siSPRTN), or siRNA against DNA-PK (siDNAPK), a key factor in the NHEJ pathway, which served as a positive control for impaired DSB (Fabbrizi et al., 2024). In addition, cells depleted of OGG1 (siOGG1), a DNA glycosylase involved in base excision repair, were included to control for specificity, as OGG1 is not directly implicated in DSB repair. Previously, it has been shown that the inhibition of OGG1 would reduce the levels of strand cleavage causing a lower level of DSBs post radiation making its depletion a good negative control for DSBs levels post radiation (Jakob et al., 2020). All cells were synchronised at the G1/S boundary to enhance detection of SPRTN-dependent phenotypes, and samples were collected at 0h and 4h following IR exposure.

In control cells (siLUC), DNA damage increased sharply at 0h post-IR, with a median tail DNA of approximately 15%, compared to ~2% in unirradiated cells. By 4h, damage was substantially reduced, with % tail DNA returning to near-baseline levels (~5%), indicating efficient DSB repair. A similar pattern of damage induction and repair was observed in siOGG1 cells, with no significant difference from siLUC at either time point. This confirms that OGG1 depletion does not impair the resolution of IR-induced DSBs, consistent with its role outside the DSB repair pathways.

In contrast, SPRTN-depleted cells (siSPRTN) displayed a comparable level of DNA damage at 0h post-IR (~18% tail DNA), but failed to efficiently resolve this damage by 4h, retaining significantly elevated % tail DNA (~10%). This persistence of DSBs suggests that SPRTN is required for timely repair or clearance of lesions that impede standard DSB repair machinery. A similar pattern was observed in siDNAPK cells, which also showed impaired resolution of DSBs, consistent with the known role of DNA-PK in facilitating NHEJ. Importantly, damage levels at 4h in both siSPRTN and

siDNAPK cells remained significantly higher than in controls, whereas siOGG1 cells showed no such impairment.

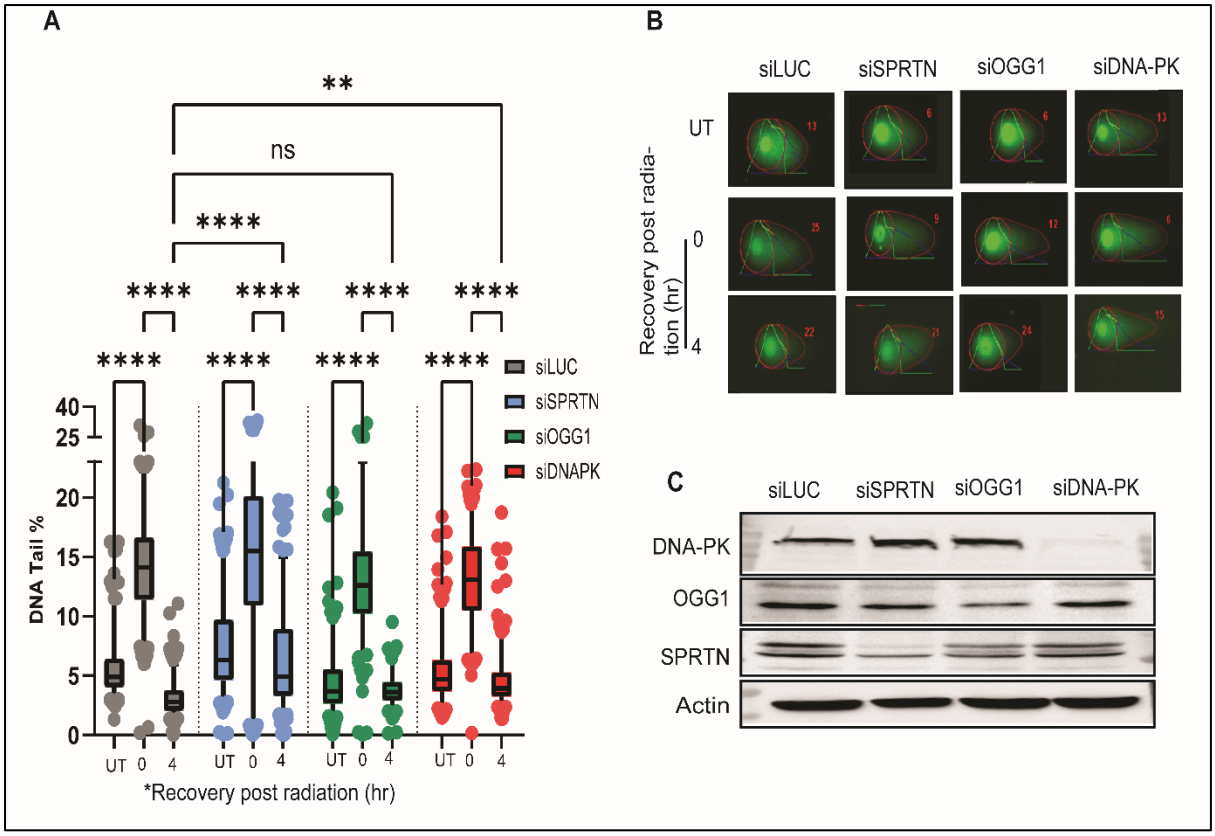


Figure 5.5. SPRTN depletion impairs DNA damage resolution following ionising radiation compared to DNA repair controls.

(A) Quantification of DNA strand breaks using the alkaline comet assay in HeLa cells transfected with control (siLUC), siRNA against SPRTN (siSPRTN), OGG1 (siOGG1), or DNA-PK (siDNA-PK). Cells were untreated (UT) or irradiated with 5 Gy and harvested at 0 and 4 hours post-irradiation. siSPRTN and siDNA-PK cells exhibited significantly higher residual DNA damage at 4 hours post-IR, whereas siOGG1 behaved similarly to control, validating the specificity of the assay for DSB repair. Quantification of 100 cells per condition from one representative experiment is shown, and the experiment was repeated three times. Whisker box plots show median values and data within the 10–90 percentile. Statistical analysis was performed using unpaired t-test. Statistical analysis: ****p < 0.0001, **p < 0.01, ns = not significant

(B) Representative comet assay micrographs showing DNA damage in each knockdown condition at baseline and recovery post-IR. Remarkably, siSPRTN and siDNA-PK cells retain longer comet tails at 4 hours, consistent with inefficient repair.

(C) Immunoblot validation of protein knockdown in each condition. Efficient depletion of SPRTN, OGG1, and DNA-PK was confirmed. Actin served as a loading control.

To independently validate our findings from siRNA-mediated SPRTN depletion, we employed an isogenic ΔSPRTN knockout HeLa cell line alongside wild-type HeLa controls to evaluate DSB levels following IR. The neutral comet assay was performed at multiple time points-0, 1, and 4 hours post-irradiation (5 Gy)-to assess the persistence and resolution of DSBs over time. The extent of DNA fragmentation was quantified using the percentage of DNA in the comet tail (% DNA tail), a direct and sensitive readout of DSBs. As a negative control, DNA from untreated cells incubated with FA was included to confirm the absence of migration under conditions where DNA remains crosslinked and highly compacted.

In wild-type HeLa cells, IR led to a marked increase in DNA tail signal immediately following exposure (median ~40%), relative to the unirradiated condition (UT; ~20%). A progressive reduction in tail signal was observed over time, with median values declining to ~25% and ~20% at 1 and 4 hours post-IR, respectively. This pattern indicates efficient DSB repair, consistent with intact DNA damage response (DDR) and repair capacity in these cells. In contrast, ΔSPRTN cells exhibited significantly elevated levels of DNA fragmentation immediately post-IR (~45% DNA tail), with a persistently high tail signal even after 4 hours of recovery (remaining above 30%), suggesting delayed or incomplete DSB repair.

Importantly, at all corresponding time points post-IR, ΔSPRTN cells showed significantly higher % DNA tail values compared to wild-type cells, particularly at the 4-hour recovery mark ($p < 0.0001$), indicating sustained DNA damage. These findings closely mirror the phenotype observed in siSPRTN knockdown cells and reinforce the conclusion that SPRTN is required for efficient resolution of IR-induced DSBs. The consistency between the knockdown and knockout systems strengthens the robustness of our interpretation and excludes the possibility of off-target siRNA effects.

As expected, the FA-treated condition demonstrated negligible DNA migration in both wild-type and ΔSPRTN cells, validating the technical integrity of the comet assay by confirming that non-fragmented DNA remains immobile. Together, this dataset substantiates that SPRTN plays a critical role in facilitating DSB repair post-irradiation, likely by promoting the clearance of DNA–protein crosslinks or other replication-blocking structures that interfere with repair machinery.

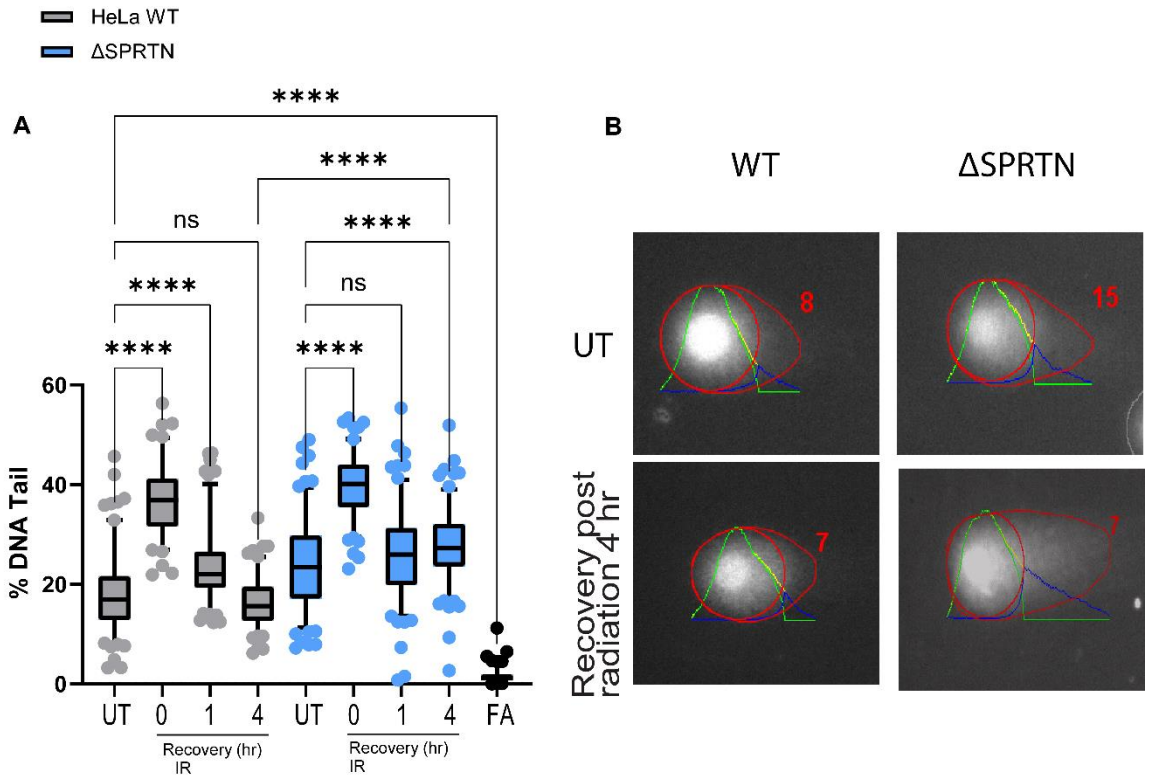


Figure 5.6 SPRTN deficiency results in persistent DNA damage following ionising radiation.

(A) Quantification of DNA strand breaks using the neutral comet assay in wild-type (WT; grey) and SPRTN-knockout (ΔSPRTN; blue) HeLa cells. Cells were either untreated (UT), irradiated with 5 Gy and harvested at 0 or 4 hours post-irradiation, or treated with formaldehyde (FA; 1 mM, 10 min) as a DPC-positive control. DNA fragmentation was quantified by % DNA in tail. WT cells showed a time-dependent decrease in DNA tail signal post-IR, indicating active repair. In contrast, ΔSPRTN cells retained significantly higher DNA tail percentages at both time points post-IR, consistent with impaired DNA damage resolution. FA treatment resulted in minimal DNA migration, validating assay specificity for strand breaks. Quantification of 100 cells per condition from one representative experiment is shown, and the experiment was repeated two times. Whisker box plots show median values and data within the 10–90 percentile. Statistical analysis was performed using unpaired t-test. Statistical analysis: ****$p < 0.0001$, **$p < 0.01$, ns = not significant

(B) Representative comet images from WT and ΔSPRTN cells at baseline (UT) and 4 hours post-irradiation. ΔSPRTN cells display longer and more intense tails post-IR compared to WT, consistent with defective repair of radiation-induced damage

To determine whether the impaired DNA damage resolution observed in ΔSPRTN cells was dependent on cell cycle synchronisation, we repeated the neutral comet assay under unsynchronised conditions. This approach allowed us to assess the robustness and cell-cycle independence of the observed phenotype in a more physiologically relevant, asynchronous population. Both wild-type (blue) and SPRTN knockout (green) cells were subjected to ionising radiation (10 Gy), and DNA tail % was measured at multiple time points post-IR, including a key recovery point at 4 hours.

As shown in Figure 5.7, unsynchronised wild-type cells exhibited the expected increase in DNA tail% immediately following IR, followed by a progressive reduction over time, indicating efficient DNA DSB repair. In contrast, ΔSPRTN cells displayed persistently higher DNA tail% at the 4-hour mark. At this later recovery stage, the difference in DNA tail% between wild-type and ΔSPRTN cells remained substantial, reflecting a significantly greater degree of residual DNA fragmentation in the SPRTN-deficient population.

With that being said, these results should be interpreted with caution. At 4 hours post-irradiation, cells showed a slightly lower DNA % tail than untreated controls, a consistent observation across replicates. This reduction may reflect radiation-induced cell-cycle redistribution rather than actual repair. HeLa cells lack a functional G1 checkpoint and tend to accumulate in G2 while slowing S phase progression following DNA damage. As S phase is associated with replication stress and elevated DNA breaks, a reduced proportion of S-phase cells could lower the overall comet signal. Although a technical artefact cannot be entirely excluded, its likelihood is minor given the reproducibility. Thus, the apparent reduction in DNA damage likely results from shifts in cell-cycle composition, underscoring the importance of considering population dynamics when analysing comet assay data in unsynchronized cells.

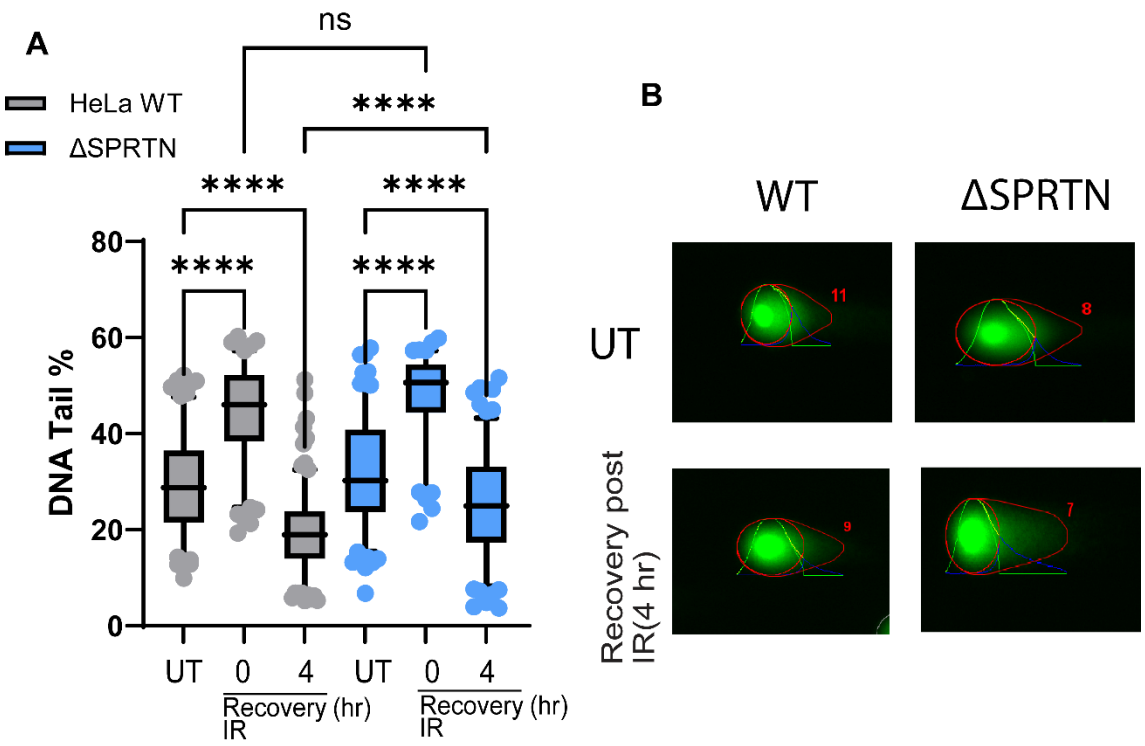


Figure 5.7. SPRTN-deficient cells exhibit impaired DSB resolution in unsynchronized HeLa cells following ionising radiation.

(A) Quantification of DNA double-strand breaks using neutral comet assay in unsynchronized HeLa wild-type (WT; grey) and SPRTN-knockout (ΔSPRTN; blue) cells. Cells were either untreated (UT) or exposed to 10 Gy ionising radiation and harvested at 0 and 4 hours post-irradiation. DNA fragmentation was assessed by DNA tail % measurements. WT cells showed a significant reduction in DNA tail% at 4 hours post-IR, indicating effective DSB repair. In contrast, ΔSPRTN cells retained significantly elevated DNA tail %, indicating impaired DSB resolution. Quantification of 100 cells per condition from one representative experiment is shown, and the experiment was repeated three times. Whisker box plots show median values and data within the 10–90 percentile. Statistical analysis was performed using unpaired t-test. Statistical analysis: ****p < 0.0001, **p < 0.01, ns = not significant

Statistical significance was determined using appropriate tests (****p < 0.0001; **p < 0.01; ns = not significant).n=100 per condition.

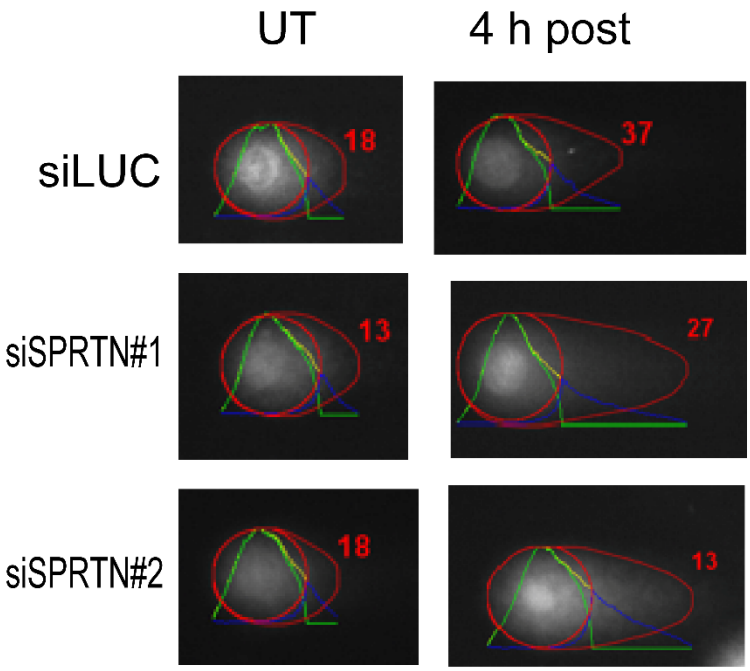
(B) Representative images of comet tails from untreated and irradiated (4 hr recovery) WT and ΔSPRTN cells. Comet images illustrate the increased tail DNA in SPRTN-deficient cells following radiation, consistent with persistent DNA breaks

To further validate the effect of SPRTN depletion on DNA damage resolution in an alternative cancer model, we performed neutral comet assays in MCF-7 breast cancer cells following exposure to ionising radiation. The extent of DNA fragmentation was quantified using the DNA tail %, which reflects both the intensity and the distance of DNA migration, offering a sensitive metric for DNA double-strand break (DSB) burden. Cells were collected at 0, 1, and 4 hours post-IR to monitor the dynamics of DSB repair over time (Figure 5.8).

Control cells transfected with non-targeting siRNA (siLuc; blue) showed a marked increase in DNA tail% immediately after IR (0 h), which gradually decreased at 1 and 4 hours, consistent with active DSB repair. In contrast, SPRTN-depleted cells—targeted with two independent siRNAs (maroon and green), exhibited elevated DNA tail % values at 4 hours, indicating increased DNA fragmentation and slower repair kinetics relative to controls.

Notably, although one of the SPRTN-targeting siRNAs (green) induced mild cytotoxicity in MCF-7 cells during transfection, sufficient viable cells were obtained for comet analysis, allowing robust measurement of damage levels. siSPRTN-treated cells showed a reduction in DNA tail % between 0 and 4 hours post-IR; however, this decrease was less pronounced compared to the reduction observed in the control group. These data suggest that SPRTN depletion compromises the resolution of IR-induced DSBs in MCF-7 cells, consistent with our findings in other cancer cell models.

A



B

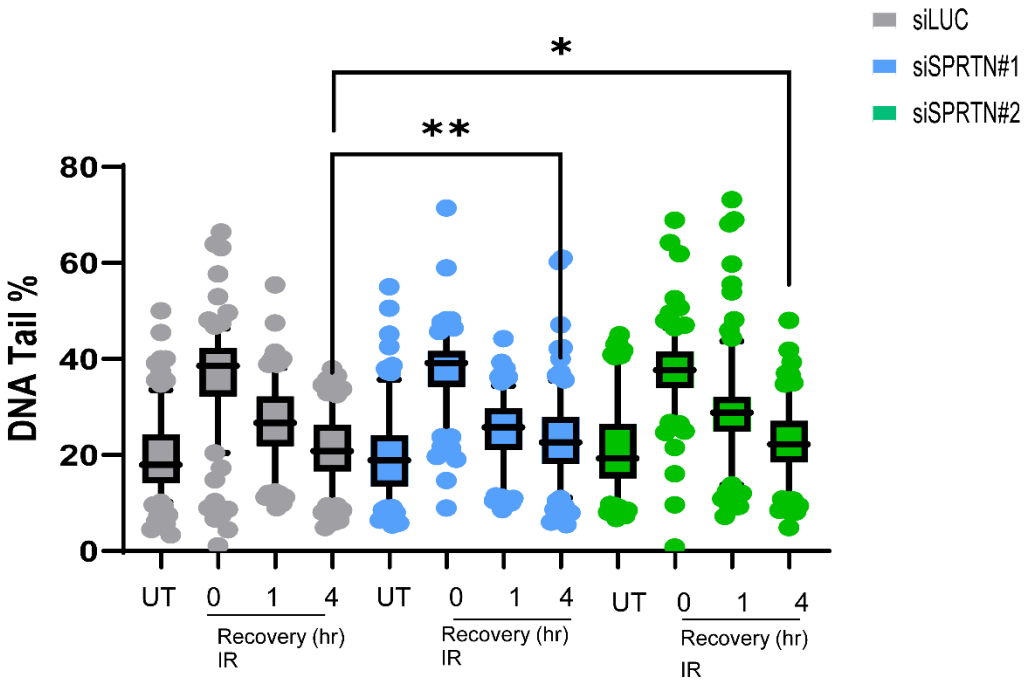


Figure 5.8. SPRTN depletion compromises DNA double-strand break repair in MCF-7 cells following ionising radiation.

(A) representative images of tails of UT and 4h post-IR

(B) Quantification of DNA damage in MCF-7 breast cancer cells transfected with control siRNA (siLUC, grey), or two independent siRNAs targeting SPRTN (siSPRTN#1 and siSPRTN#2, blue and green, respectively). Cells were exposed to 10 Gy ionising radiation and collected at 0, 1, and 4 hours post-irradiation. DNA damage was assessed using the neutral comet assay, with DNA tail %used as a measure of DNA fragmentation. SPRTN-depleted cells exhibited significantly higher DNA tail %compared to controls at all time points, indicating impaired DSB resolution. Each dot represents an individual cell; boxes represent interquartile range with median values. The consistent elevation in DNA damage across both siSPRTN conditions supports a role for SPRTN in efficient repair of IR-induced DSBs in this model. Quantification of 100 cells per condition from one representative experiment is shown, and the experiment was repeated two times. Whisker box plots show median values and data within the 10–90 percentile. Statistical analysis was performed using unpaired t-test. Statistical analysis: ****$p < 0.0001$, **$p < 0.01$, ns = not significant.

To investigate the dose-dependent effect of IR on DNA damage resolution in the absence of SPRTN, we performed neutral comet assays in wild-type and ΔSPRTN HeLa cells following increasing doses of IR (2, 4, and 6 Gy). Cells were harvested 4 hours post-irradiation to assess residual DSBs, and the extent of DNA fragmentation was quantified as % DNA tail.

As shown in Figure 5.9, wild-type cells demonstrated relatively stable levels of residual DNA damage across all IR doses. While an increase in residual DNA damage with higher IR doses might be expected, our data consistently showed relatively stable levels across all tested doses. This could suggest a dose-independent threshold of damage retention, possibly due to saturation of the damage detection assay. Further experiments would be needed to dissect these possibilities. Although DNA tail percentage increased modestly following irradiation, the extent of damage remained moderate (~10% median), indicating that DNA repair was effectively initiated and progressed within the 4-hour recovery period.

In contrast, ΔSPRTN cells exhibited a pronounced increase in DNA tail percentage at all IR doses compared to wild-type controls. Specifically, even at the lowest tested dose of 2 Gy, ΔSPRTN cells showed elevated residual damage (~13–15% median), which further increased at 4 Gy and 6 Gy. This sustained accumulation of unrepaired DNA damage suggests a critical role for SPRTN in facilitating DSB resolution across a range of genotoxic stress intensities.

Importantly, the statistical comparisons reveal that the differences between wild-type and ΔSPRTN cells at each radiation dose are highly significant, confirming that SPRTN deficiency results in impaired repair irrespective of radiation dose. These findings underscore that the elevated DNA damage observed in SPRTN-depleted cells

is not merely a threshold effect at high doses, but rather a consistent deficiency in the capacity to resolve IR-induced DSBs, even at lower levels of genotoxic insult.

Collectively, this dose–response analysis confirms that SPRTN is required for efficient repair of DSBs induced by ionising radiation and that its absence leads to persistent DNA damage, further supporting SPRTN's essential role in maintaining genome integrity under radiation-induced stress.

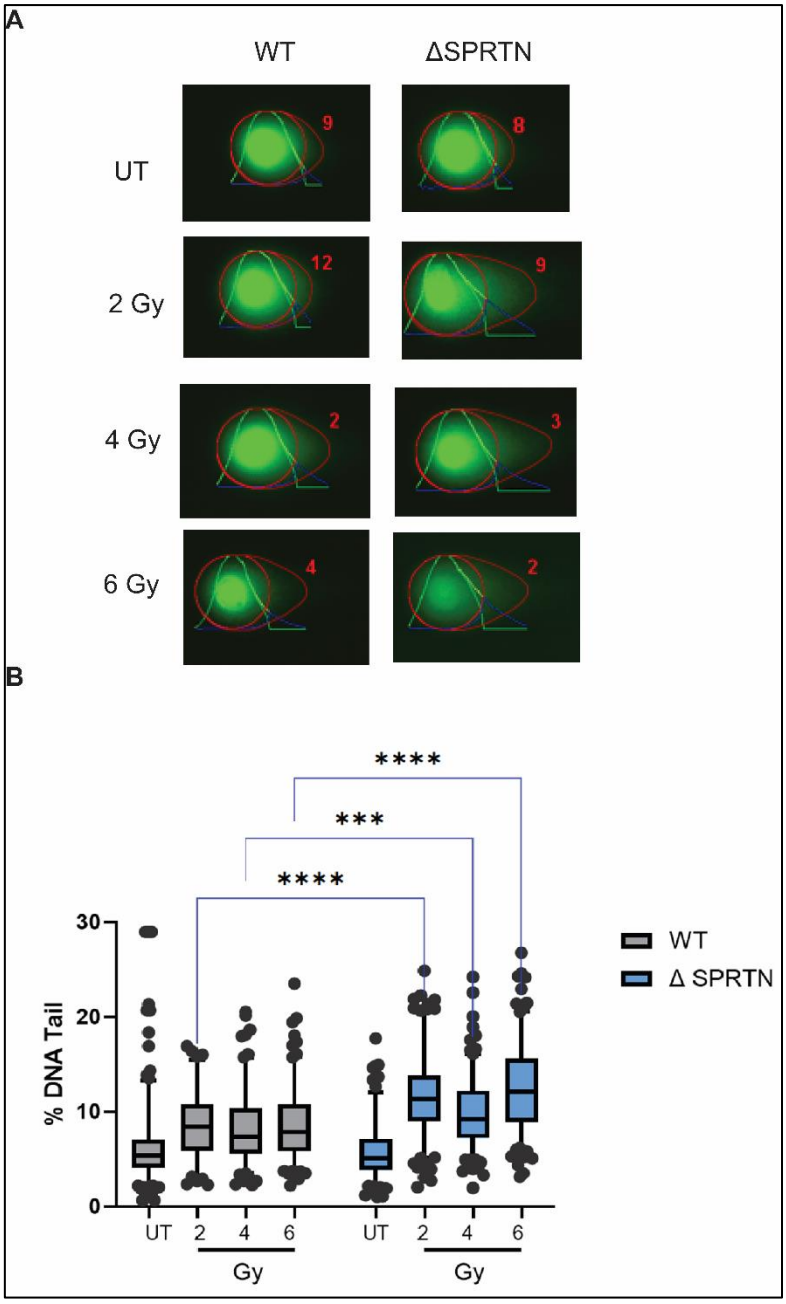


Figure 5.9. SPRTN deficiency impairs DNA double-strand break (DSB) resolution following ionising radiation in a dose-dependent manner.

(A) Representative images of tails (Ut, 2,4,6 Gy) post 4 hour IR in WT and ΔSPRTN (B) Box-and-whisker plots show the percentage of DNA in comet tails (% DNA Tail) measured by neutral comet assay 4 hours after exposure to increasing doses of ionising radiation (0, 2, 4, and 6 Gy) in HeLa wild-type and SPRTN-knockout cells. While WT cells show relatively stable levels of DNA damage across all doses, ΔSPRTN cells exhibit a dose-dependent increase in residual DNA fragmentation, with significantly higher % DNA Tail at each dose compared to WT. Quantification of 100 cells per condition from one representative experiment is shown, and the experiment was repeated three times. Whisker box plots show median values and data within the

10–90 percentile. Statistical analysis was performed using unpaired t-test. Statistical analysis: ****p < 0.0001, ***p < 0.001, ns = not significant.

To confirm the functional requirement of SPRTN protease activity in the resolution of DNA damage following IR, we conducted a rescue experiment using doxycycline (DOX)-inducible expression of either wild-type SPRTN ($SPRTN^{WT}$) or a catalytically inactive mutant ($SPRTN^{E112A}$) in SPRTN-depleted HeLa cells. The neutral comet assay was employed to quantify DNA fragmentation, and DNA tail values were normalised across conditions to account for experimental variation. Cells were analysed 4 hours after exposure to 5 Gy IR to assess DSB resolution.

In the $SPRTN^{WT}$ background (Figure 5.10, left), SPRTN knockdown using siRNA (siSPRTN) resulted in significantly elevated DNA tail signals compared to control siRNA (siLUC), indicating impaired DNA repair. However, re-expression of SPRTN^WT via DOX induction effectively restored DNA tail values to baseline levels, confirming that SPRTN activity is essential for efficient DSB resolution. In contrast, in the SPRTN^E112A background (Figure 5.10, right), re-expression of the enzymatically inactive mutant failed to rescue the DNA repair defect, as DNA tail signals remained significantly elevated in siSPRTN + DOX cells compared to controls. This result highlights the necessity of SPRTN's protease activity, rather than its structural presence alone, for resolving IR-induced DNA damage.

Complementary visual evidence was provided by neutral comet assay micrographs (panel E), where increased DNA migration (comet tail intensity) was observed in SPRTN-depleted cells following IR, particularly in the $SPRTN^{E112A}$-expressing background. In the SPRTN^WT-expressing cells, DOX-induced reconstitution reduced comet tail intensity, further substantiating the functional restoration of DNA repair capacity. These images also demonstrated the persistence of comet tails in SPRTN^E112A-rescued cells, consistent with defective DSB repair.

Together, these findings conclusively demonstrate that SPRTN's catalytic activity is required to facilitate the timely resolution of IR-induced DNA damage. The inability of the SPRTN^E112A mutant to compensate for SPRTN loss confirms that the protease function of SPRTN, rather than a scaffolding or non-enzymatic role, underlies its critical function in genome maintenance following genotoxic stress.

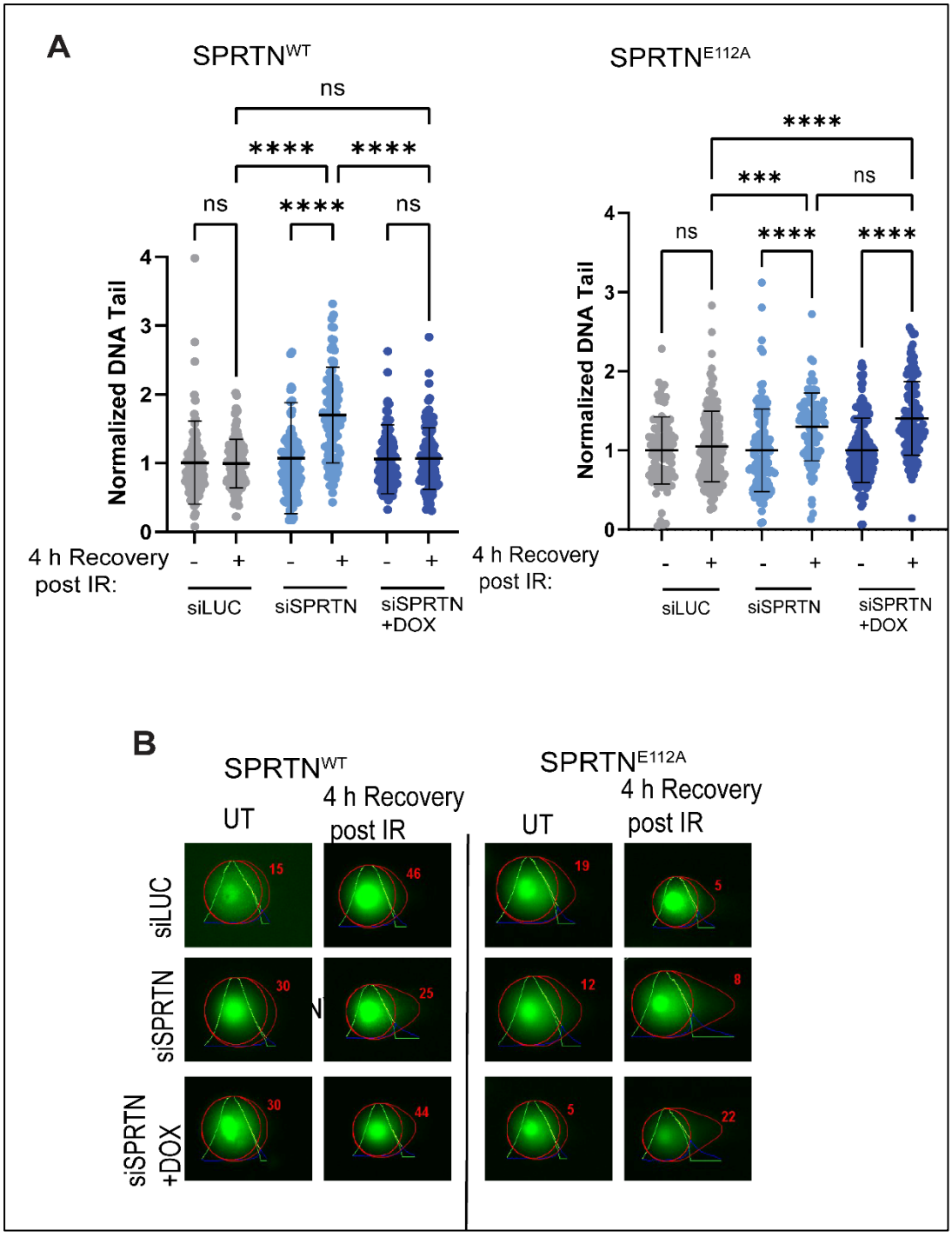


Figure 5.10. Catalytic activity of SPRTN is essential for efficient DNA damage resolution following ionising radiation.

(A) Quantification of DNA damage using the neutral comet assay in HeLa cells expressing doxycycline (DOX)-inducible SPRTN^WT (left panel) or the catalytically inactive SPRTN^{E112A} mutant (right panel). Cells were transfected with control siRNA (siLUC) or SPRTN-targeting siRNA (siSPRTN), followed by induction of exogenous SPRTN with doxycycline (+DOX),

where indicated. DNA damage was assessed 4 hours after 5 Gy ionising radiation and values were normalised to unirradiated controls. In the SPRTN^WT background, SPRTN depletion significantly increased DNA damage, which was rescued by re-expression of wild-type SPRTN (+DOX). In contrast, in the SPRTN^E112A background, re-expression failed to rescue the damage phenotype. Quantification of 100 cells per condition from one representative experiment is shown, and the experiment was repeated two times. Whisker box plots show median values and data within the 10–90 percentile. Statistical analysis was performed using unpaired t-test. Statistical analysis: ****p < 0.0001, ***p < 0.001, ns = not significant.

(B) Representative neutral comet assay images corresponding to each condition in panel A. HeLa cells expressing $SPRTN^{WT}$ (left) or $SPRTN^{E112A}$ (right) were either untreated (UT) or exposed to 5 Gy IR and recovered for 4 hours. Tail moments (in red) were quantified and are shown in the top-right corner of each image. Re-expression of SPRTN^WT reduced comet tail length post-IR, whereas SPRTN^E112A expression did not, confirming the requirement for SPRTN's protease activity in DSB resolution.

To evaluate whether SPRTN is also involved in the repair of a broader spectrum of DNA lesions beyond DSBs, we employed the alkaline comet assay. Unlike the neutral comet assay, which primarily detects DSBs, the alkaline version enables the detection of both SSBs and alkali-labile sites, providing a more comprehensive view of radiation-induced DNA damage and repair capacity.

HeLa wild-type and ΔSPRTN cells were exposed to ionising radiation and allowed to recover for 4 hours. DNA damage was assessed by measuring the percentage of DNA in the comet tail (tail DNA %), which reflects the extent of strand breakage. As shown in the quantitative graph (left), ΔSPRTN cells (blue dots) displayed significantly elevated tail DNA percentages relative to wild-type cells (grey dots) at 4 hours post-irradiation. The difference was highly statistically significant, indicating a clear impairment in DNA damage repair in the absence of SPRTN. Representative images from the comet assay (right) visually support the quantitative data. ΔSPRTN cells exhibited larger and more intense comet tails compared to their wild-type counterparts following 4 hours of recovery, consistent with an accumulation of unrepaired or misrepaired DNA lesions. Untreated cells in both genotypes showed minimal background damage, confirming the specificity of the IR-induced response. To confirm the genetic status of the cells, a Western blot (panel H) was included, verifying the absence of SPRTN protein in ΔSPRTN cells and confirming comparable loading with tubulin as a control. These results demonstrate that SPRTN deficiency leads to a substantial delay in the resolution of strand breaks, encompassing both SSBs and DSBs, following ionising radiation. The data further reinforce SPRTN’s critical function in maintaining genome integrity by promoting efficient repair across multiple types of DNA lesions.

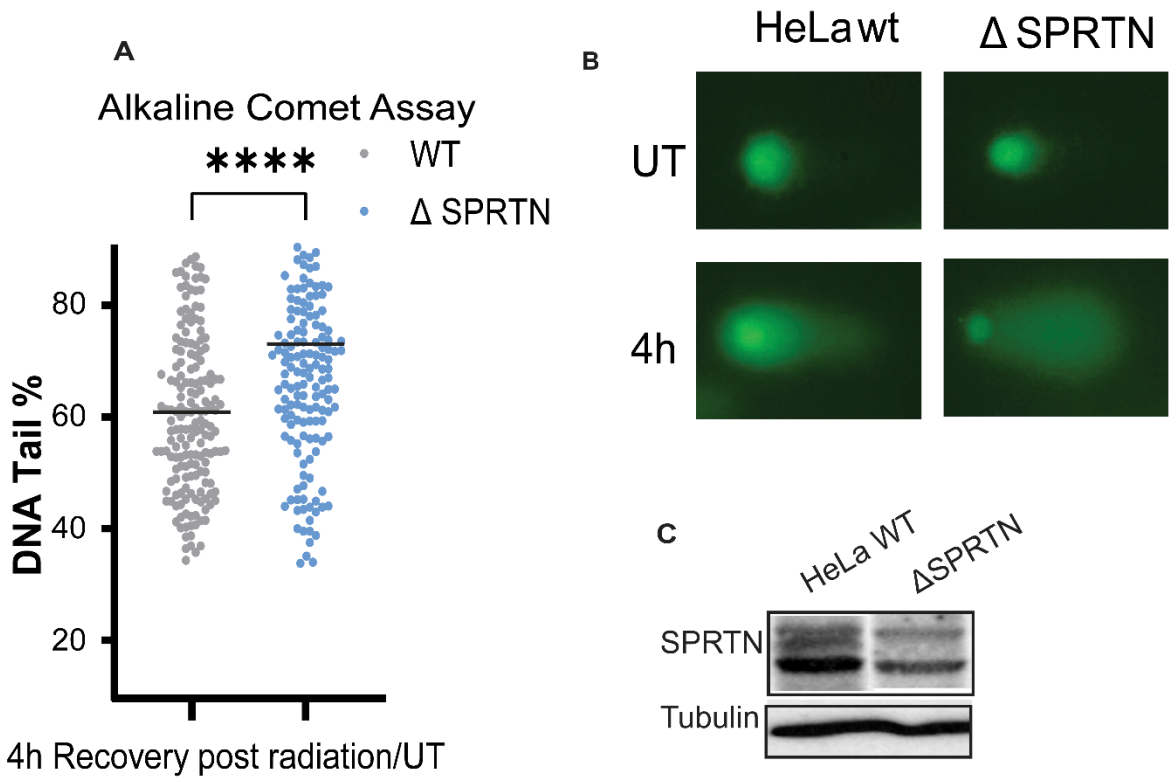


Figure 5.11. SPRTN-deficient cells exhibit impaired DNA damage resolution following ionising radiation.

(A) Quantification of DNA damage using the alkaline comet assay in HeLa wild-type (WT) and (ΔSPRTN) cells. Cells were irradiated (5 Gy) and allowed to recover for 4 hours before analysis. Data are expressed as the percentage of DNA in the comet tail (% tail DNA). ΔSPRTN cells exhibited significantly higher DNA tail values compared to WT, indicating persistent DNA strand breaks. Quantification of 100 cells per condition from one representative experiment is shown, and the experiment was repeated two times. Whisker box plots show median values and data within the 10–90 percentile. Statistical analysis was performed using unpaired t-test. Statistical analysis: ****$p < 0.0001$.

(B) Representative comet assay images of untreated (UT) and 4-hour post-irradiation samples from HeLa WT and ΔSPRTN cells. Increased comet tail formation is visible in ΔSPRTN cells at 4 hours, supporting quantitative analysis.

(C) Western blot confirming SPRTN knockout. Lysates from HeLa WT and ΔSPRTN cells were probed for SPRTN and tubulin (loading control). SPRTN protein was undetectable in ΔSPRTN cells, confirming successful deletion.

To rule out the possibility that the elevated DNA damage observed in ΔSPRTN cells was a secondary consequence of cell cycle perturbation rather than a direct defect in DNA repair, we conducted a comparative analysis of the cell cycle profiles between ΔSPRTN knockout cells and their wild-type counterparts. Cell cycle status was assessed using flow cytometry following propidium iodide staining to quantify DNA content, allowing discrimination between G1, S, and G2/M phases (Figure 5.12).

Our analysis revealed no significant differences in the distribution of cells across the various cell cycle phases between ΔSPRTN and wild-type populations under steady-state conditions. Following ionising radiation, both genotypes exhibited a comparable G2/M checkpoint arrest at 8 hours, consistent with a typical DNA damage-induced response. However, the magnitude and timing of this arrest were similar in ΔSPRTN and wild-type cells, indicating that SPRTN deficiency does not impair the activation of the G2/M checkpoint. These findings exclude cell cycle alterations as a confounding variable and support the interpretation that the increased DNA damage observed in ΔSPRTN cells post-irradiation is due to defective repair mechanisms rather than aberrant checkpoint control or cell cycle progression.

This result is particularly important given SPRTN's established role during S-phase in resolving DPCs and protecting replication fork integrity. The absence of cell cycle abnormalities strengthens the conclusion that the persistent DNA lesions in SPRTN-deficient cells are due to a failure in lesion resolution, rather than disrupted cell cycle checkpoints or replication timing. Thus, the DNA damage phenotype observed post-irradiation in ΔSPRTN cells is likely a direct consequence of SPRTN loss and the resulting inefficiency in processing IR-induced DNA lesions.

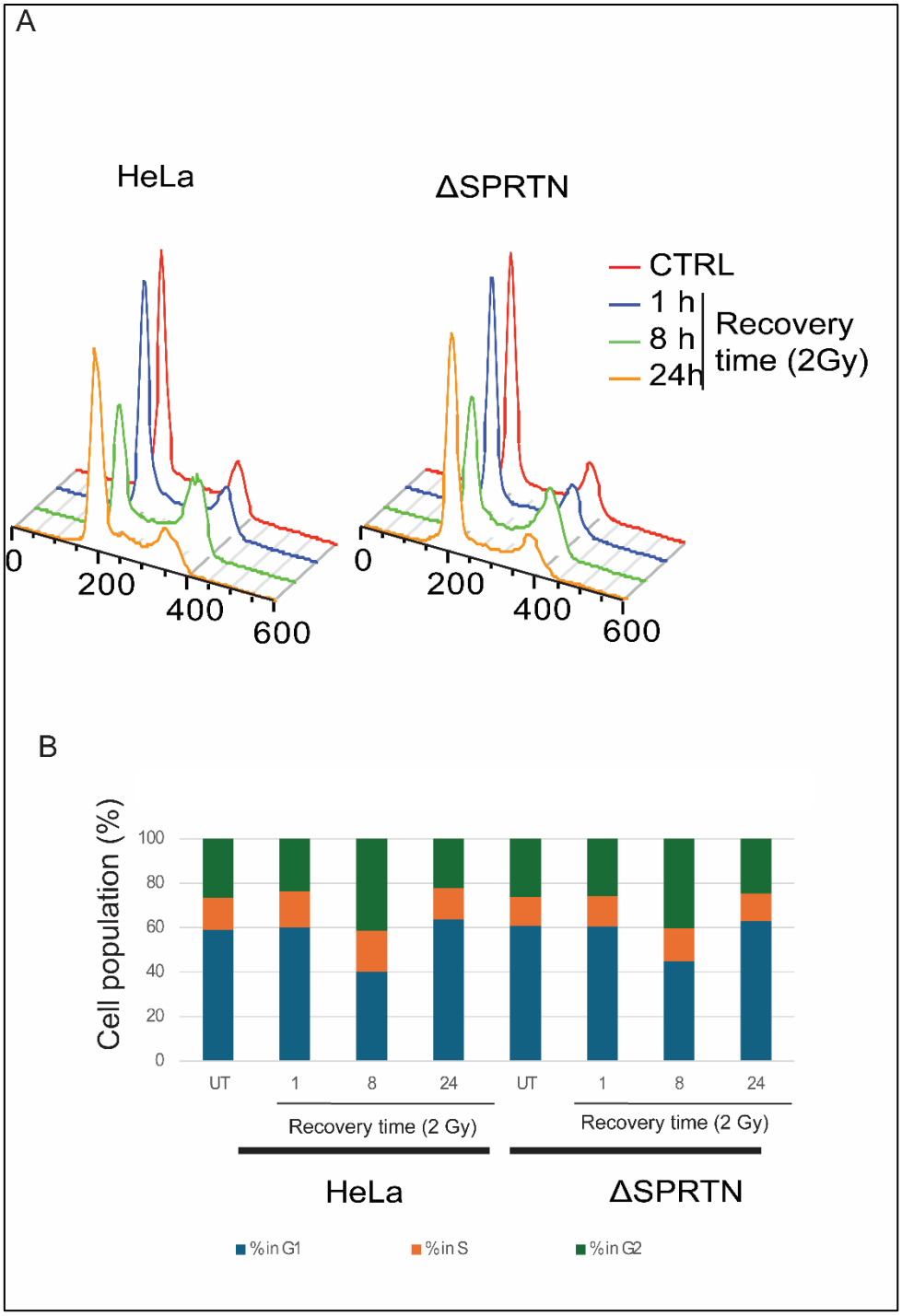


Figure 5.12. Cell cycle profiles of HeLa wild-type and ΔSPRTN cells following ionising radiation.

(A) Representative DNA content histograms generated by flow cytometry analysis of HeLa and ΔSPRTN cells at baseline (CTRL) and at 1, 8, and 24 hours following exposure to 2 Gy ionising radiation. Cells were fixed and stained with propidium iodide, and DNA content was assessed to determine cell cycle distribution. Peaks corresponding to G1, S, and G2/M

phases are shown. No marked differences in cell cycle profiles were observed between genotypes across time points.

(B) Quantification of the percentage of cells in G1, S, and G2/M phases at the indicated recovery times. Cell cycle distributions were comparable between HeLa and ΔSPRTN cells at all time points. Number of cells used is around 10,000 cells per conditions.

5.2 Discussion

The protease SPRTN plays a critical role in the resolution of DPCs, lesions that pose significant obstacles to DNA replication and transcription. Its loss has been associated with increased genomic instability and hypersensitivity to crosslinking agents, underscoring its essential function in DNA repair. Given that IR is known to induce a diverse array of DNA lesions, including DPCs, DSBs, and base damage, it was initially anticipated that SPRTN deficiency would universally sensitise cells to IR. However, our study reveals a counterintuitive phenotype in most cell lines studied: SPRTN-deficient cells exhibit enhanced survival following IR, despite harbouring increased levels of DNA damage.

In light of this, we sought to investigate the mechanisms underlying this phenotype. The contradictory phenotype observed in SPRTN-deficient cells-marked by persistent DNA damage, attenuated DDR signalling, and increased survival following ionising radiation-suggests a fundamental decoupling of DNA lesion accumulation from canonical checkpoint and apoptotic pathways (Figure 5.13).

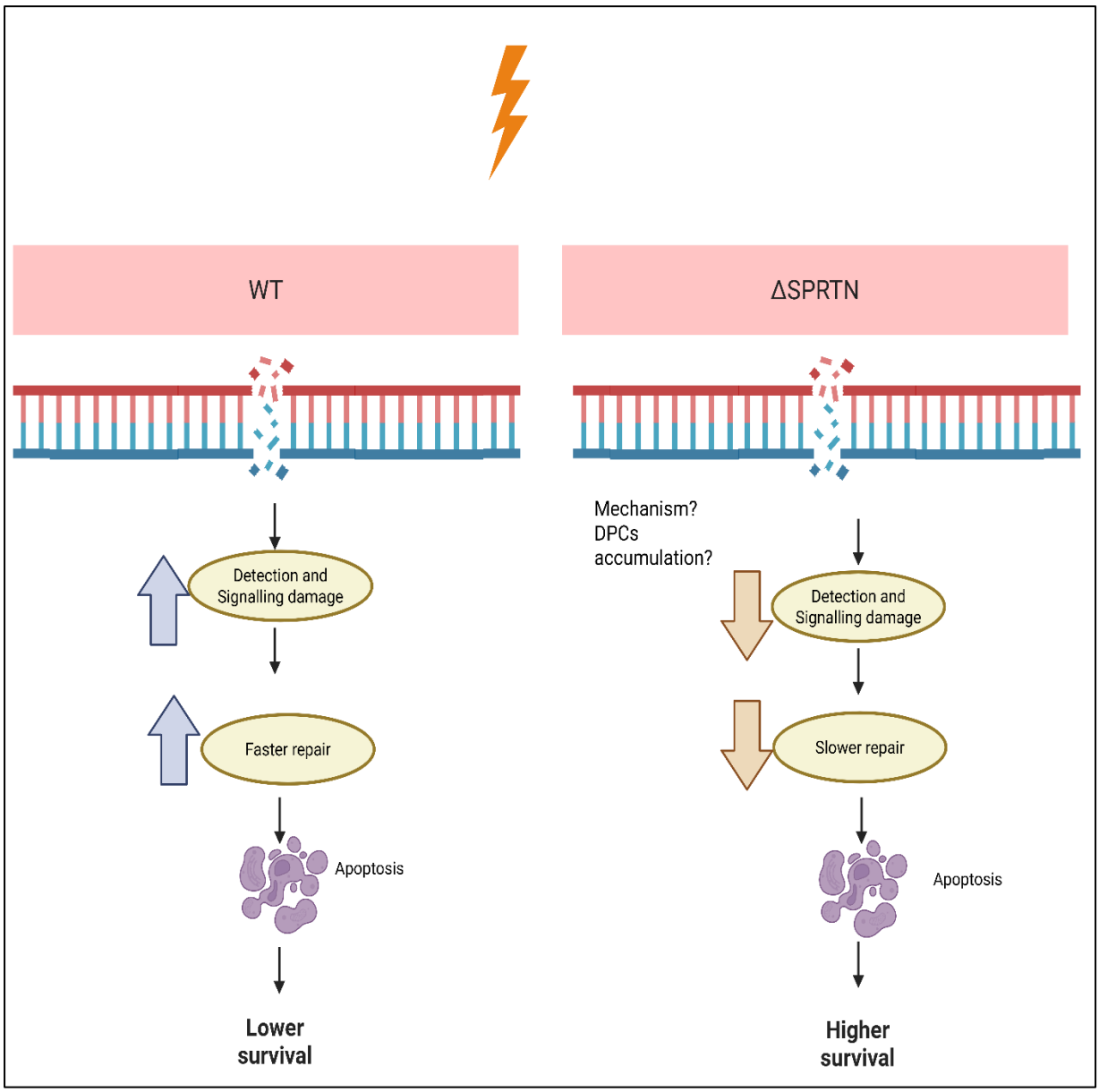


Figure 5.13. Model illustrating the paradoxical survival advantage of SPRTN-deficient cells following ionising radiation (IR).

This schematic compares the DNA damage response in wild-type (WT) versus SPRTN-deficient (ΔSPRTN) cells following exposure to ionising radiation. In WT cells (left panel), radiation induces DNA lesions, including DNA–protein crosslinks (DPCs), which are promptly detected and processed by SPRTN, enabling efficient activation of DNA damage response (DDR) signalling pathways such as ATM and ATR. This robust signalling facilitates rapid recruitment of repair machinery and promotes effective resolution of DNA damage. Consequently, while repair is efficient, the activation of checkpoint and apoptotic pathways also leads to higher rates of cell death, manifesting as lower overall survival.

In contrast, SPRTN-deficient cells (right panel) fail to efficiently resolve radiation-induced DPCs. These bulky adducts persist and interfere with lesion recognition by DDR sensors. As a result, key signalling events, such as γH2AX and 53BP1 focus formation, are attenuated, leading to reduced checkpoint engagement and impaired repair. Paradoxically, this blunted response allows cells to bypass apoptosis and survive despite harbouring significant DNA damage. The model highlights a fundamental uncoupling between DNA damage burden and cell fate in ΔSPRTN cells, offering a mechanistic explanation for their unexpected radioresistance.

One possible explanation may be the accumulation of DPCs, which are known substrates of SPRTN's protease activity. In the absence of SPRTN, unresolved DPCs can physically block access to DNA by both replicative polymerases and DDR sensors such as ATM, ATR, and associated chromatin-modifying enzymes. This attenuation in signalling is likely due to the persistence of unprocessed DPCs, which may obstruct the recruitment of DDR mediators to chromatin. Supporting this notion, recent studies demonstrated that SPRTN-mediated proteolytic digestion of DPCs is a prerequisite for ATM activation and γH2AX phosphorylation. In the absence of SPRTN, these lesions remain physically concealed, impairing DDR activation and checkpoint signalling. (Glumac et al., 2023).

Another possible key mechanism involves disruption of the ATR–CHK1 checkpoint loop: under normal conditions, SPRTN cleaves CHK1's inhibitory C-terminal domain to produce active CHK1 fragments, while CHK1 in turn phosphorylates SPRTN to promote its recruitment during replication. In the absence of SPRTN, this feedback loop is lost-CHK1 remains uncleaved and chromatin-bound, resulting in diminished ATR-CHK1 checkpoint activation, impaired cell cycle arrest, and reduced formation of early DDR markers (Halder et al., 2019). In parallel, SPRTN also regulates other repair proteins through proteolytic cleavage, most notably MRE11. SPRTN truncates MRE11 into a less active C-terminally deleted form (TR-MRE11) with reduced DNA-binding and nuclease function; thus, SPRTN overexpression sensitizes cells to IR by impairing DSB repair, whereas SPRTN-deficient cells retain full-length MRE11, potentially affecting downstream steps. (Na et al., 2021). This could affect signalling cascade and apoptosis.

The hypoxic tumour microenvironment adds another dimension to this phenotype. Under low oxygen conditions, the nature of radiation-induced DNA damage shifts away from generating canonical strand breaks and instead favours the formation of covalent DPCs (Stingele & Jentsch, 2015). This transition is largely driven by the suppression of reactive oxygen species and the classical oxygen fixation effect, which diminishes the conversion of transient DNA damage into fixed lesions. Although one might expect the accumulation of persistent DPCs to be cytotoxic, hypoxic cells frequently exhibit increased survival after irradiation.

Hypoxia also remodels the DDR in a manner that may resemblance SPRTN deficiency in the models that we studied. Specifically, severely hypoxic tumours exhibit elevated replication stress and constitutive activation of apical DDR kinases such as ATM, ATR, and DNA-PKcs-even in the absence of overt DNA breaks. However, despite this upstream activation, downstream repair effectors are frequently repressed.

This uncoupling of damage sensing from checkpoint execution contributes to a radioresistant phenotype, wherein cells accumulate DNA lesions without fully activating repair or apoptotic responses. Experimental evidence supports the idea that DDR activation is altered under hypoxia. Menegakis et al. (2021) reported that RPE-1 cells irradiated under 1% O_2 exhibited significantly fewer γH2AX and 53BP1 foci at 30 minutes post-irradiation compared to normoxic conditions, a difference that was reversed by re-oxygenating cells before IR exposure. Similarly, SPRTN-null models accumulate unrepaired DPCs and exhibit attenuated checkpoint activation, including reduced γH2AX and 53BP1 focus formation, despite high levels of DNA damage. In both contexts, checkpoint signalling is blunted, facilitating cell survival under genotoxic stress. A contributing factor to this impaired checkpoint engagement is the transcriptional repression of HR factors under hypoxic conditions. Key HR

components, including BRCA1 and RAD51, are downregulated via HIF-1α and E2F-dependent mechanisms, limiting high-fidelity repair. Thus, SPRTN deficiency may mimic aspects of the hypoxic DDR landscape, characterised by persistent DPCs, compromised repair capacity, and a paradoxical increase in radiation survival. These mechanistic overlaps offer a compelling framework to understand how SPRTN loss reshapes the cellular response to ionising radiation.

However, the presence of high DPC loads does not necessarily predict cell death. Rather, the combination of altered lesion profiles, suppressed checkpoint signalling, and reduced proteolytic activity may permit damaged cells to bypass canonical surveillance mechanisms and persist in a state of damage tolerance. Thus, radioresistance under hypoxia cannot be attributed solely to reduced DNA breakage or to the DPC burden, but likely reflects a nuanced interplay between lesion complexity, DDR modulation, and the tumour microenvironment.

Another mechanistically similar phenomenon that could explain the phenotype is seen with HMCES, a single-stranded DNA-binding protein that forms a programmed DPC at abasic sites. HMCES covalently crosslinks to AP sites in the leading/lagging strand during replication, shielding them from error-prone polymerases and endonucleases. By locking the AP site in a protein-DNA complex, HMCES prevents premature cleavage or misincorporation that would create DSBs. In HMCES-deficient cells, these AP sites instead become vulnerable to cleavage, leading to fork collapse and DSB. Crucially, HMCES knockout cells are hypersensitive to IR, indicating that masking of lesions by HMCES normally modulates replication stress signalling (Mohni et al., 2019; Semlow et al., 2022). These findings reinforce the concept that intentional lesion shielding (by HMCES) or unintended shielding (by unrepaired DPCs) may profoundly alter DDR outcomes. In SPRTN-null cells, persistent DPCs may act like HMCES-

linked AP sites – hiding the underlying DNA and forestalling the ATR/ATM checkpoints. Both situations illustrate that a bulky crosslink can paradoxically protect the lesion from being recognized, trading canonical DDR activation for an alternative survival outcome.

In conclusion, our findings reveal that SPRTN-deficient cells exhibit a paradoxical phenotype in response to ionising radiation: elevated DNA damage is accompanied by diminished DDR signalling and enhanced cellular survival. This decoupling suggests that unresolved DNA–protein crosslinks, a hallmark of SPRTN deficiency, may not only hinder repair but also impair damage recognition and checkpoint activation. In this context, persistent DPCs could act as physical and signalling barriers, preventing full engagement of canonical DDR pathways and apoptotic responses. Additional factors such as CHK1 inactivation, MRE11 stability, and hypoxia-induced modulation of repair pathways further contribute to this phenotype. The parallels drawn with HMCES-mediated lesion shielding underscore the broader relevance of crosslink-driven checkpoint evasion. Taken together, these findings support a model in which DPCs - when unresolved - act not only as cytotoxic lesions but also as modulators of damage signalling outcomes. As a next step, we aim to test directly whether the accumulation of DPCs plays a causal role in the observed radioresistance by using biochemical and genetic strategies to modulate DPC load and assess their impact on survival and DDR activation following radiation. This will clarify whether persistent DPCs has a role the radioreistance of SPRTN-deficient cells.

Chapter 6: DPCs Accumulation Role in Radioresistance in SPRTN-Depleted Cells

To explore the mechanistic basis underlying the paradoxical radioresistance observed in SPRTN-deficient cells, we focused on the enzyme's canonical role in resolving DPCs-bulky lesions that interfere with replication and transcription. Given that SPRTN is the principal replication-coupled protease responsible for DPC clearance, its loss is expected to result in the persistent accumulation of these lesions. Since our previous results indicated that SPRTN depletion leads to both increased DNA damage and attenuated DDR signalling, we hypothesised that DPC accumulation itself may be central to this phenotype. Specifically, we aimed to investigate whether the persistence of DPCs following IR contributes to checkpoint attenuation and enhanced survival.

6.1 Results

To assess whether the accumulation of DPCs contributes to the altered radiation response observed in SPRTN-deficient cells, we analysed DPC levels using two complementary biochemical approaches: the RADAR and the ARK assay. These assays allowed us to measure the presence of covalent protein–DNA adducts in genomic DNA preparations, providing insight into how SPRTN deficiency influences DPC clearance following IR.

6.1.1 SPRTN depletion causes DPCs accumulation post IR

In the RADAR assay (Figure 6.1 A), DPCs were enriched and visualised by slot blotting from genomic preparations of HeLa cells WT and ΔSPRTN, both untreated and irradiated. ΔSPRTN cells showed visibly increased retention of protein–DNA adducts following IR (10 Gy) when compared to control cells, consistent with impaired DPC

repair. A formaldehyde-treated (FA) sample served as a positive control for robust DPC induction and confirmed the specificity of the assay.

To further validate these observations, DPC levels were quantified using the ARK assay (Figure 6.1 B), which provides a normalized DPC coefficient for accurate comparison across conditions. The quantification revealed that SPRTN-depleted cells accumulated significantly more DPCs post-irradiation relative to wild-type counterparts. While irradiation modestly increased DPC levels in wild-type cells, this effect was amplified in SPRTN-deficient cells, indicating a failure to efficiently resolve these lesions in the absence of SPRTN protease activity. As expected, FA-treated cells displayed the highest DPC signal, further validating the assay's sensitivity.

Collectively, these findings demonstrate that SPRTN plays a critical role in the clearance of radiation-induced DPCs and Its absence leads to persistent DPC accumulation.

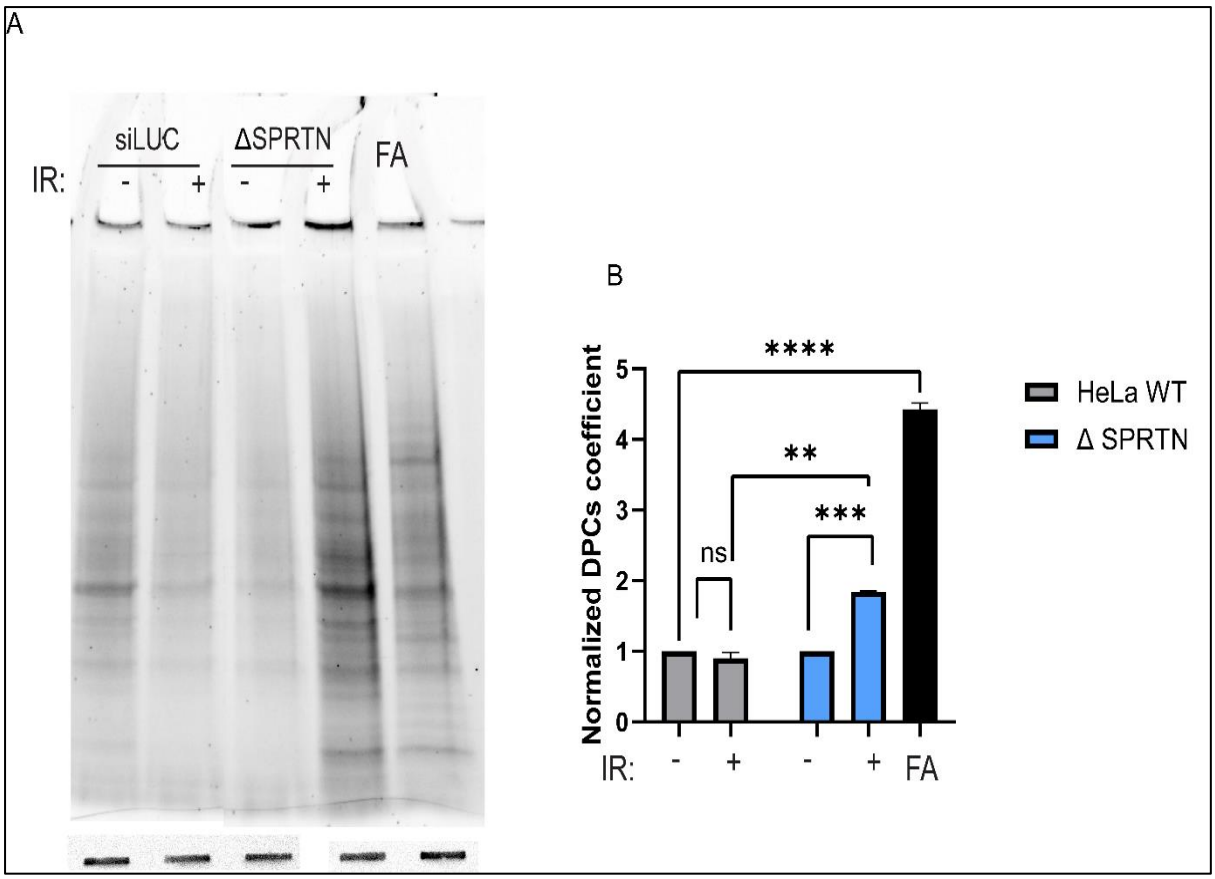


Figure 6.1. Radiation-induced DNA–protein crosslinks (DPCs) are elevated in SPRTN-deficient cell.

(A) Representative RADAR (Rapid Approach to DNA–Protein Crosslink Adduct Recovery) assay showing DPC accumulation in HeLa cells. Genomic DNA was extracted from control (siLUC), SPRTN-deficient (ΔSPRTN), and formaldehyde (FA)-treated cells following ionising radiation (10 Gy, γ-radiation) (IR, +) or no treatment (–). Samples were subjected to slot blot analysis and probed for protein–DNA adducts. Increased retention of protein-bound DNA is visible in irradiated ΔSPRTN cells relative to controls, with FA serving as a positive control for robust DPC formation. (B) Quantification of DPC levels using the ARK (Alkaline and SDS-based Recovery of DNA–Protein Crosslinks) assay. The DPC coefficient was calculated and normalised to untreated WT. Irradiation modestly increased DPC levels in WT cells, while ΔSPRTN cells showed significantly elevated DPC accumulation post-IR. FA treatment induced the highest level of DPCs, validating assay sensitivity. Data shown from the average of 3 independent experiments, error bars represent mean ± SD; $n = 3$. Statistical analysis: ****p < 0.0001, **p < 0.001, **p < 0.01, ns = not significant

To confirm that the accumulation of DPCs observed upon SPRTN depletion is reproducible and specific, we employed the RADAR (Rapid Approach to DNA–Protein Crosslink Adduct Recovery) assay using two independent siRNA oligonucleotides targeting SPRTN. As shown in Figure 6.2A and 6.2B, SPRTN knockdown with two different siRNAs (siSPRTN #1 and siSPRTN #2) in HeLa cells resulted in increased levels of DPCs following IR (10 Gy), compared to cells transfected with control siRNA (siLUC). In both experiments, genomic DNA isolated from SPRTN-depleted cells exhibited a visible retention of protein–DNA adducts, consistent with elevated DPC accumulation. These results demonstrate that general DPCs are increased in SPRTN-deficient cells following IR, further validating SPRTN's role in facilitating DPC resolution under genotoxic stress.

Moreover, in Figure 6.2C, accumulation of crosslinked histone H3 is shown post-irradiation in SPRTN-knockout cells, providing direct evidence of covalently trapped chromatin-associated proteins. This supports the interpretation that SPRTN is essential for clearing DPCs formed after radiation exposure. This confirms the increased burden of unresolved DPCs in SPRTN-deficient cells. Together, these complementary approaches establish that SPRTN is a critical regulator of DPC proteolysis following IR and that its depletion leads to persistent DPCs, potentially contributing to altered DNA damage responses and enhanced cellular survival post-irradiation

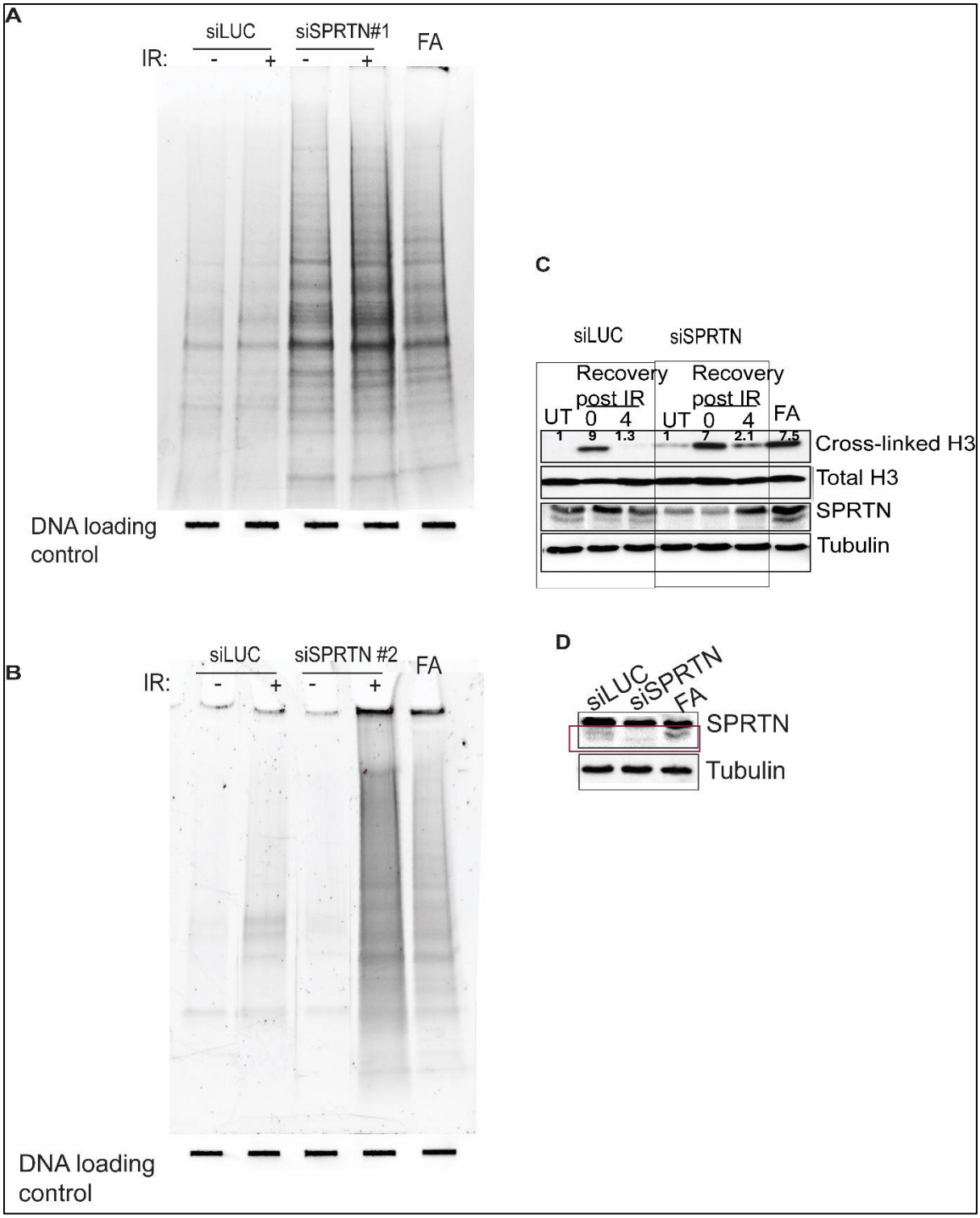


Figure 6.2. SPRTN depletion results in elevated radiation-induced DPCs. (A, B) RADAR assays were performed using two independent siRNA oligonucleotides targeting SPRTN (siSPRTN#1 and siSPRTN#2) to evaluate DPC accumulation following IR(γ-radiation). HeLa cells were transfected with either control siRNA (siLUC) or SPRTN-targeting siRNAs and treated with or without IR. Genomic DNA was extracted and slot-blotted to detect retained protein–DNA adducts. FA (formaldehyde) treatment served as a positive control for

DPC formation. Both SPRTN-depleted conditions show visibly enhanced DPC signal post-IR compared to controls.

(C) Western blot analysis for crosslinked histone H3 (H3-DPCs) confirms the accumulation of chromatin-associated DPCs in SPRTN-depleted cells. HeLa cells were irradiated and harvested at 0 or 4 hours post-IR. The crosslinked H3 signal is markedly elevated in SPRTN-deficient cells compared to controls, with FA again used as a positive control. Quantification of bands is shown under each lane, normalized to the untreated sample (set as 1.0). Band intensities were measured by densitometry.

(D) Validation of SPRTN knockdown efficiency by immunoblotting in siSPRTN-transfected cells. Tubulin was used as a loading control. These results confirm specific SPRTN depletion in siRNA-transfected cells

6.1.2 Incubating cells with scavengers rescue the radioresistnce in ΔSPRTN

To explore whether the observed radioresistance phenotype in SPRTN-deficient cells is linked to hydroxyl radical-induced DPC formation, we assessed the impact of ROS scavenging on cellular survival following IR. It is well established that the yield of DPCs in irradiated cells can be significantly reduced in the presence of hydroxyl radical scavengers such as cysteamine or dimethyl sulfoxide, implicating ROS in the formation of radiation-induced DPCs (Nakano et al., 2017). To directly test this hypothesis, both wild-type (WT) and ΔSPRTN HeLa cells were pre-treated with N-acetylcysteine (NAC), a potent ROS scavenger, for one hour prior to IR exposure, followed by CFA to assess long-term viability (Figure 6.3).

As shown in the CFA survival curve, ΔSPRTN cells, although not as strongly as previously observed, still exhibited higher survival than WT cells following increasing doses of radiation, consistent with our earlier findings, especially at 6 Gy.

The inclusion of NAC attenuated the survival advantage previously observed in ΔSPRTN cells. At 4 Gy, ΔSPRTN + NAC survival dropped to 61.8%, lower than the 84.6% observed in WT cells. This trend continued at 6 Gy, where ΔSPRTN + NAC cells showed 39% survival, compared to 55.7% in WT cells. These findings suggest that when DPC levels are chemically reduced via ROS scavenging, the survival advantage of SPRTN-deficient cells is reversed, supporting the notion that SPRTN loss confers resistance via DPC accumulation rather than broad-spectrum damage tolerance. These results suggest that scavenging radiation-induced ROS partially restores the radiosensitivity of SPRTN-deficient cells, potentially by reducing DPC formation, thereby reinforcing the hypothesis that ROS-induced DPCs contribute to the SPRTN-deficient radiotolerant phenotype.

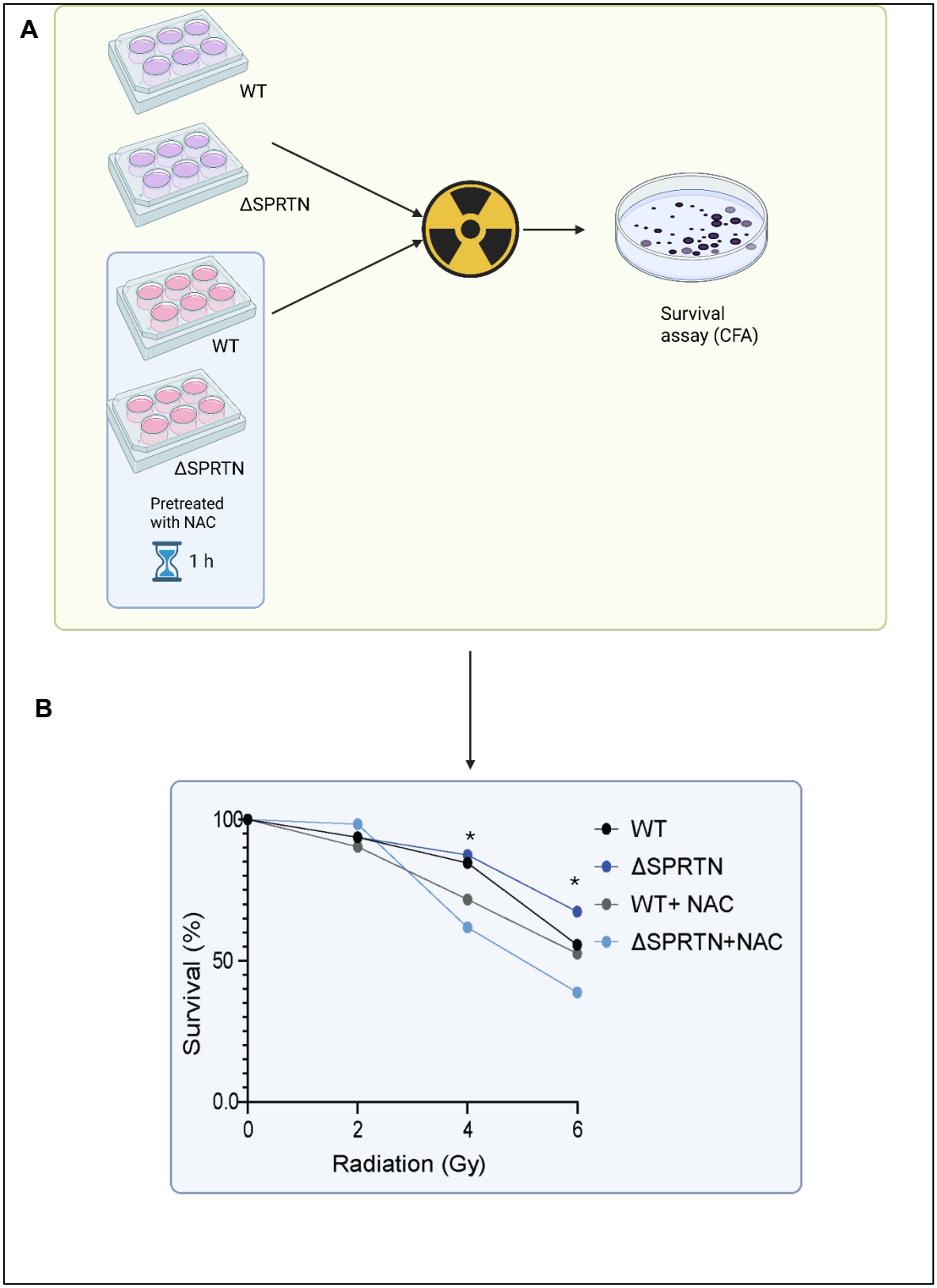


Figure 6.3. NAC pre-treatment partially reverses the radiation resistance phenotype of SPRTN-deficient cells.

(A) Schematic overview of the experimental design. Wild-type (WT) and SPRTN-deficient (ΔSPRTN) HeLa cells were pre-treated with 10 mM N-acetylcysteine (NAC) for 1 hour prior to

exposure to IR (γ-radiation). Following irradiation, cells were subjected to clonogenic survival assays (CFA) to assess long-term viability

(B) CFA survival curves of WT and ΔSPRTN cells with or without NAC pre-treatment across increasing doses of IR. ΔSPRTN cells displayed increased survival compared to WT cells, consistent with a radioresistant phenotype. Notably, NAC pre-treatment reduced the survival advantage of ΔSPRTN cells at higher radiation doses, suggesting that reactive oxygen species (ROS)-induced DPCs may contribute to the radioresistance observed in the absence of SPRTN. Data shown from the average of 3 experiments, Statistical analysis. *$p < 0.05$.

6.1.3 Incubating cells with NAC rescues the DNA damage levels in ΔSPRTN post-IR

To further evaluate the contribution of DPCs to the DNA damage response in SPRTN-deficient cells, we pre-treated cells with NAC in order to limit the formation of DPCs by ROS. We assessed DNA double-strand break signalling via γH2AX immunofluorescence and measured DNA strand break accumulation using neutral comet assays, with or without antioxidant pre-treatment.

As shown in Figure 6.4A and B, immunofluorescence staining for γH2AX was performed to assess DSB signalling in WT and ΔSPRTN. In untreated cells, both genotypes displayed low γH2AX signal. Upon exposure to IR (5 Gy), WT cells showed an increase in γH2AX foci, while ΔSPRTN cells exhibited slightly fewer foci, consistent with an attenuated DNA damage response that we observed earlier. Pre-treatment with NAC did not significantly alter the γH2AX response in WT cells but notably increased γH2AX foci in ΔSPRTN cells post-IR, suggesting partial restoration of DDR signalling.

The comet assay further confirmed these findings, as shown in Figure 6.4C and D. Neutral comet assays revealed that NAC treatment substantially reduced the comet tail DNA percentage in ΔSPRTN cells exposed to IR, bringing it down to levels comparable to WT. After IR (0h-immediately post-IR), DNA tail increased in WT and ΔSPRTN cells, with partial resolution by 4 hours in WT but sustained elevation in ΔSPRTN again conforming our previous results. NAC significantly reduced tail DNA levels in ΔSPRTN post-IR samples, indicating protection against ROS-mediated DNA strand breaks, which could be due to the accumulation of DPCs that form under oxidative stress and are not efficiently resolved in the absence of SPRTN.

Hydrogen peroxide (H_2O_2) was included as a positive control to induce ROS-mediated DNA damage. Notably, NAC pre-treatment significantly reduced γH2AX foci following H_2O_2 exposure, validating the role of ROS in driving this signalling response and confirming the efficacy of NAC as an antioxidant.

Together, these findings could provide evidence that ROS contribute to the formation of DPCs, which in turn may underlie both the suppression of DNA damage signalling and the slower repair of DNA lesions observed in SPRTN-deficient cells. These lesions may interfere with proper damage recognition and repair in the absence of SPRTN. While further work is required to confirm the precise biochemical identity of the damage, our results highlight a potential mechanistic link between oxidative stress, DPC accumulation, and impaired DNA damage responses, which may contribute to the radioresistance phenotype associated with SPRTN deficiency.

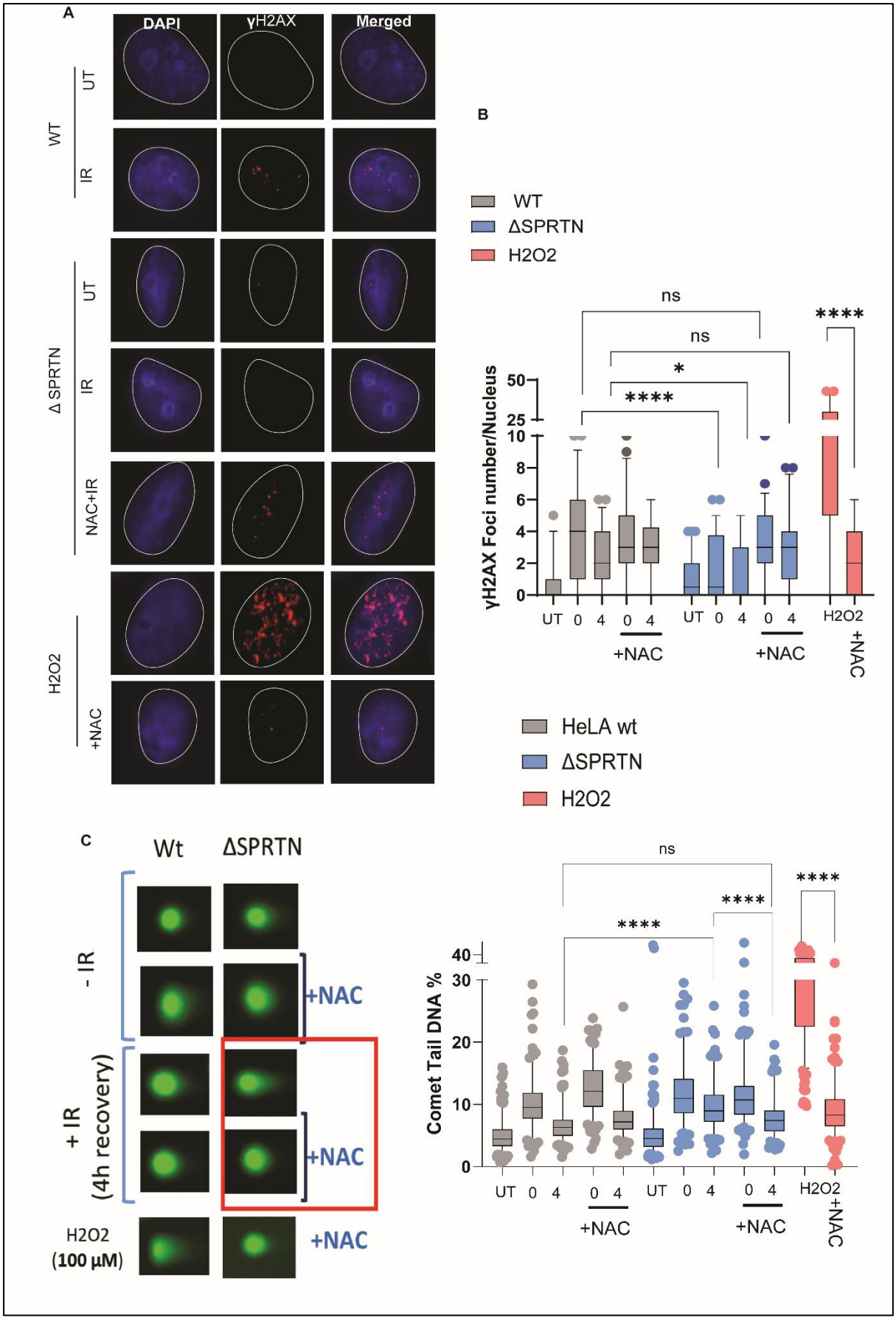

A
DAPI
γH2AX
Merged
WT
UT
IR
Δ SPRTN
UT
IR
NAC+IR
H2O2
+NAC
B
WT
ΔSPRTN
H2O2
γH2AX Foci number/Nucleus
ns
ns
*
****
****
UT 0 4 0 4 UT 0 4 0 4 H2O2
+NAC
+NAC
+NAC
HeLA wt
ΔSPRTN
H2O2
C
Wt
ΔSPRTN
- IR
+ IR
(4h recovery)
+NAC
+NAC
H2O2
(100 µM)
+NAC
Comet Tail DNA %
ns
****
****
****
UT 0 4 0 4 UT 0 4 0 4 H2O2
+NAC
+NAC
+NAC

Figure 6.4 | Antioxidant pre-treatment rescues DNA damage levels and DDR signalling in SPRTN-deficient cells post-irradiation.

(A, B) Immunofluorescence quantification of γH2AX foci per nucleus immediately post-irradiation (5 Gy, γ-radiation) demonstrates a partial restoration of DDR signalling in ΔSPRTN cells upon NAC treatment. Hydrogen peroxide (H_2O_2, 100 μM) was used as a positive control to confirm NAC efficacy in scavenging ROS. Quantification of 50 cells per condition from one representative experiment is shown, and the experiment was repeated two times. Whisker box plots show median values and data within the 10–90 percentile. Statistical analysis was performed using unpaired t-test. ns = not significant, ****p < 0.0001, *p < 0.05.

(C,D) Neutral comet assay showing reduced DNA fragmentation in WT and ΔSPRTN HeLa cells following pre-treatment with N-acetyl cysteine (NAC, 10 mM) 1 hour prior to IR (5 Gy, γ-radiation). Quantification of tail DNA (%) is shown. Hydrogen peroxide (H_2O_2, 100 μM) was used as a positive control to confirm NAC efficacy in scavenging ROS. Quantification of >100 cells per condition from one representative experiment is shown, and the experiment was repeated two times. Whisker box plots show median values and data within the 10–90 percentile. Statistical analysis was performed using unpaired t-test. ns = not significant, ****p < 0.0001.

6.1.4 FA treated cells show a similar radioresistance to ΔSPRTN

Modelling persistent DPC accumulation in a controlled system is inherently challenging due to the lack of tools that allow selective induction of DPCs without affecting other aspects of cellular physiology. Nevertheless, FA treatment represents the closest feasible model to approximate the DPC-rich state observed in SPRTN-deficient cells. We hypothesised that if DPCs are causally linked to radioresistance, then elevating DPCs in SPRTN-proficient cells should reproduce this phenotype. Formaldehyde is a potent crosslinking agent known to form covalent DNA–protein adducts that structurally resemble endogenous DPCs normally resolved by SPRTN.

We induced DPC formation in wild-type cells using low-dose FA. The dose selected (450 μM) was low enough to avoid overt cytotoxicity while still promoting DPC accumulation, thereby mimicking the biochemical context of SPRTN-deficient cells.

To test this, we performed clonogenic survival assays in four cancer cell lines, HeLa, JHH4, MCF7, and T24, with or without FA pre-treatment, followed by increasing doses of γ-irradiation. As shown in Figure 6.5 A, FA-treated cells consistently exhibited enhanced survival compared to untreated controls across all radiation doses. In HeLa, MCF7 and JHH4 cells, FA pre-treatment resulted in a pronounced rightward shift of the survival curves. T24 cells showed a more moderate effect, but the trend of increased resistance remained evident.

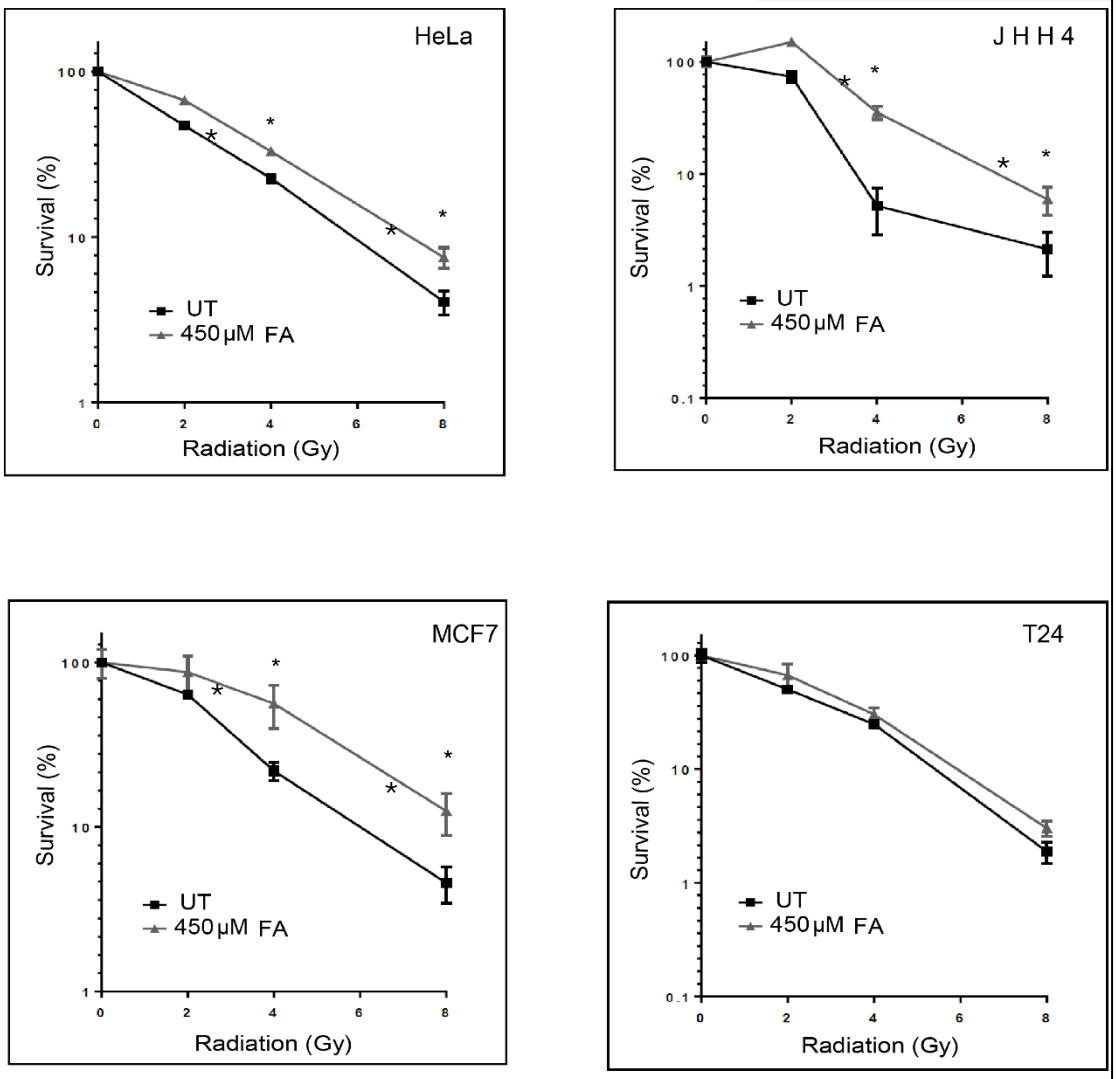
To assess whether formaldehyde-induced DPCs alter apoptotic responses to ionising radiation, we evaluated key markers of apoptosis in HeLa cells using immunoblotting. Cells were pre-treated with 450 μM FA to induce covalent protein–DNA crosslinks and subsequently exposed to ionising radiation at two doses (6 Gy and 18 Gy). As shown in Figure 6.5 B, IR exposure led to cleavage of PARP-1 in untreated cells, while caspase-3 cleavage was also observed, though at relatively modest levels. In FA-

treated cells, cleaved forms of both PARP-1 and caspase-3 were less pronounced following IR, particularly at the higher dose. These findings suggest that DPC accumulation may dampen IR-induced apoptotic signalling, potentially by interfering with the activation or progression of apoptotic pathways.

These results demonstrate that elevated DPC burden alone is sufficient to reduce IR-induced cytotoxicity, supporting the notion that unresolved DPCs interfere with canonical DNA damage signalling and apoptosis execution. The ability of FA to partially recapitulate the ΔSPRTN phenotype in otherwise DNA repair-competent cells reinforces the model in which SPRTN plays a key role in licensing full DDR engagement following radiation.

Thus, while imperfect, this model provides valuable insight into the functional consequences of DPC persistence and strengthens the mechanistic link between SPRTN activity, DPC clearance, and radiosensitivity.

A


HeLa
JHH4
MCF7
T24
Survival (%)
Radiation (Gy)
UT
450 µM FA

B

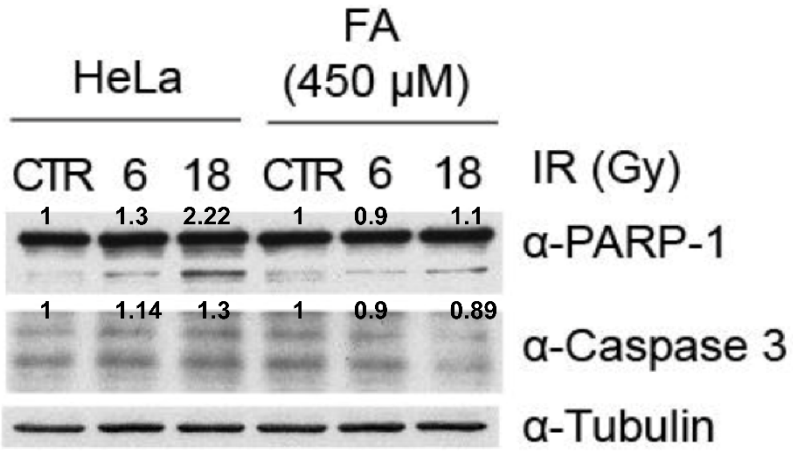

HeLa
FA (450 µM)
CTR 6 18 CTR 6 18
IR (Gy)
1 1.3 2.22 1 0.9 1.1
α-PARP-1
1 1.14 1.3 1 0.9 0.89
α-Caspase 3
α-Tubulin

Figure 6.5. Formaldehyde-induced DNA–protein crosslinks promote radioresistance and reduce apoptosis following ionising radiation.

(A) Clonogenic survival assays were performed on HeLa, JHH4, MCF7, and T24 cells either untreated (UT) or pre-treated with 450 μM formaldehyde (FA) for 1 hour prior to γ-irradiation. FA pre-treatment conferred a reproducible survival advantage in HeLa, JHH4, and MCF7 cells across all tested doses, as evidenced by a rightward shift in the survival curves. The T24 cell line showed minimal response to FA treatment. Survival is presented on a log scale to highlight differences at higher doses. Data shown from the average of 3 independent experiments, error bars represent mean ± SD; $n = 3$. Statistical analysis: *$p < 0.05$.

(B) Immunoblot analysis of apoptotic markers PARP-1 and cleaved caspase-3 in HeLa cells at 24 hours post-irradiation (10 Gy, γ-radiation), with or without FA pre-treatment. Quantification of bands is shown above each lane, normalized to the untreated sample (set as 1.0). Band intensities were measured by densitometry. This experiment was done by Bruno Vaz, a previous postdoc in Ramadan Laboratory.

In conclusion, the data presented support a model in which SPRTN loss leads to the accumulation of DPCs that may interfere with proper DNA damage recognition and signalling. These alterations could contribute to enhanced survival post-irradiation, although further studies are needed to fully define the underlying pathways and whether this response is context- or cell type-specific. DPCs could physically obstruct access to DNA and contribute to the impaired DNA damage signalling and altered checkpoint activation previously observed. These results provide support for the hypothesis that unrepaired DPCs in SPRTN-deficient cells contribute to the paradoxical radioresistance phenotype by interfering with proper damage recognition and repair coordination.

6.2 Discussion:

Given SPRTN's canonical function in replication-coupled DPC resolution, and our prior findings showing both elevated DPC levels and diminished DNA damage signalling, we hypothesised that DPCs themselves may be key contributors to the altered radiation response. Specifically, we aimed to determine whether persistent DPCs interfere with checkpoint activation or modulate survival following ionising radiation, thereby explaining the unexpected resilience of SPRTN-deficient cells.

Mechanistically, this phenotype appears to be rooted in the accumulation of unresolved DPCs and their capacity to interfere with canonical DNA damage response (DDR) signalling. Biochemical evidence from both RADAR and ARK assays confirmed increased DPC retention in SPRTN-deficient cells following IR, with covalently crosslinked histone H3 serving as a specific marker for chromatin-associated DPCs. Importantly, cells treated with the ROS scavenger N-acetylcysteine (NAC) displayed reduced DPC levels, lower DNA damage, and a partial restoration of DDR signalling — reinforcing the model in which radiation-induced DPCs are major contributors to checkpoint attenuation in SPRTN-deficient cells. Supporting this, formaldehyde-treated SPRTN-proficient cells, a model mimicking DPC accumulation, displayed improved survival after γ-irradiation, further reinforcing the notion that DPCs attenuate checkpoint engagement and apoptosis execution. The convergence of data from SPRTN knockout, siRNA depletion, ROS modulation, and FA pre-treatment all point toward a highly possible central conclusion: persistent DPCs, particularly when induced by ROS-rich low-LET radiation, blunt canonical DDR signalling and promote radioresistance.

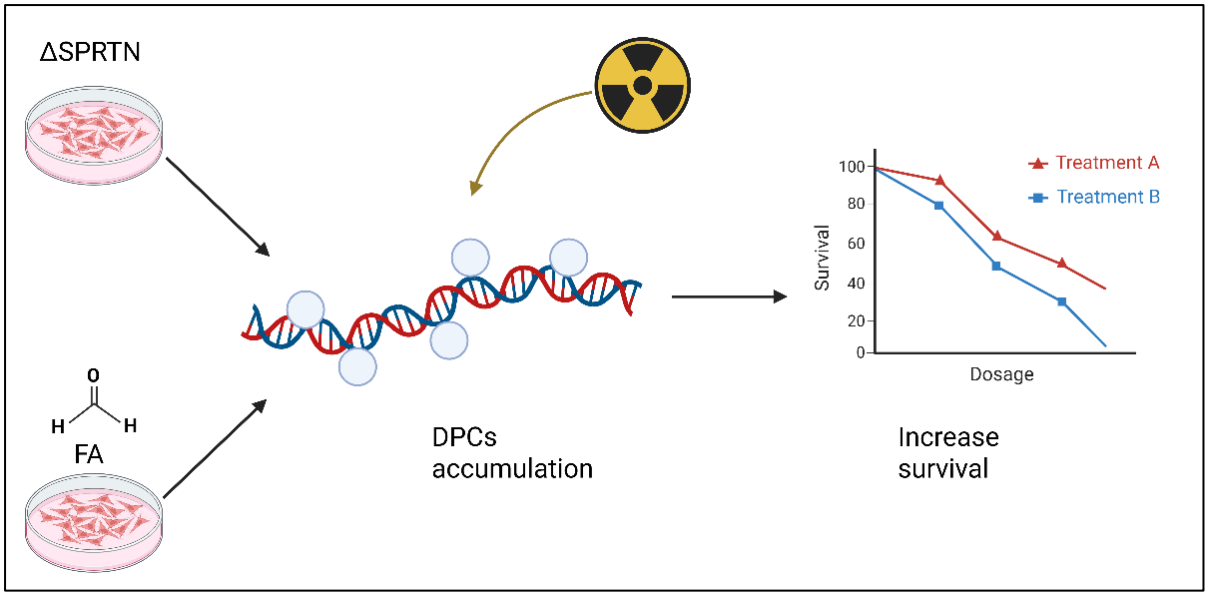


Figure 6.6. Model illustrating how SPRTN deficiency or FA-induced DPCs promote radioresistance.

This schematic represents a working model in which the loss of SPRTN (ΔSPRTN) or treatment with formaldehyde (FA) leads to the accumulation of DNA–protein crosslinks (DPCs), bulky lesions that interfere with normal chromatin dynamics and DNA damage signalling. Upon ionising radiation (IR), these unrepaired DPCs may hinder access of DNA repair machinery and dampen activation of DDR pathways, resulting in attenuated checkpoint responses. Consequently, cells exhibit increased survival despite harbouring DNA lesions. The survival curve illustrates the enhanced resistance to IR observed in DPC-accumulating conditions (Treatment A: ΔSPRTN or FA) compared to control cells (Treatment B: untreated), highlighting a potential mechanism by which DPC persistence confers radiotolerance.

One possible explanation is that persistent DPCs function not only as physical blocks to replication but also as modulators of checkpoint engagement. DPCs can obscure DNA structures required for the activation of apical damage sensors such as ATM and ATR, thereby blunting the formation of DDR markers such as γH2AX and 53BP1. Consequently, although damage accumulates, these cells fail to mount an effective checkpoint or apoptotic response.

Mechanistically, DPCs exert this suppressive effect on the DDR by physically masking DNA structures that are essential for checkpoint activation. For example, full-length crosslinked proteins occlude access to single-stranded DNA or DNA ends, which are normally required for ATR–CHK1 or ATM–γH2AX activation. As a result, despite accumulating DNA damage, SPRTN-deficient cells show reduced levels of γH2AX foci and impaired CHK1 activation post-IR, hallmarks of checkpoint attenuation.

This checkpoint attenuation in the context of DPCs creates a scenario of “silent” replication stress: damage persists, but the cell fails to appropriately signal and respond. This uncouples DNA damage accumulation from cell death pathways, enabling cells to tolerate high lesion loads and continue proliferating—albeit at the cost of genomic instability. Our NAC experiments support this interpretation: scavenging ROS (and thus reducing DPC formation) restored checkpoint markers and decreased cell survival, indicating that the DPC load is directly linked to the radioresistant phenotype.

Furthermore, modelling this effect using formaldehyde—a well-characterised DPC inducer—revealed that artificially increasing DPC levels in SPRTN-proficient cells recapitulated the SPRTN-deficient phenotype, including attenuated DDR and improved survival post-irradiation. This suggests that DPC accumulation per se, not

merely SPRTN loss, is sufficient to blunt DDR activation and promote cell survival under genotoxic stress.

DPCs could alter chromatin architecture (for example, covalent histone–DNA crosslinks fix nucleosomes). DNA-histone crosslinks (DHCs) are especially deleterious, as they tie DNA to the histone core and impede repair (Pachva et al., 2020). Recent work shows that DNA damage inherently induces a cycle of chromatin expansion and compaction, which actively regulates DDR signalling (Burgess et al., 2014). Notably, preventing normal chromatin condensation/expansion attenuates DDR: experiments blocking damage-induced compaction reduced ATM activation and γH2AX signalling. Thus, persistent DPCs might lock chromatin in an abnormal condensed state or prevent the dynamic remodelling needed for checkpoint signalling. If DPCs hold chromatin in a “closed” conformation, upstream kinases like ATM/ATR may be insufficiently activated. In other words, chromatin context provides an alternative mechanism by which DPCs modulate DDR: the lesion-induced chromatin state itself influences checkpoint activation.

Collectively, our findings support a model wherein SPRTN deficiency results in the accumulation of persistent DPCs that suppress checkpoint signalling and promote cellular survival following radiation exposure. This suppression likely arises through multiple, overlapping mechanisms: direct interference with DDR sensor access, attenuation of ATR–CHK1 signalling, chromatin compaction, and disruption of dynamic chromatin remodelling essential for full DDR activation.

Moving forward, a critical next step will be to determine whether DPC-induced chromatin condensation is a causal factor in checkpoint evasion. We aim to assess chromatin accessibility and histone modification states in SPRTN-deficient cells post-

IR. These analyses will help define whether DPCs remodel chromatin in a manner that suppresses checkpoint signalling and thereby contributes to the radioresistant phenotype. Ultimately, clarifying the intersection between DPCs, chromatin state, and DDR may reveal new therapeutic strategies that exploit chromatin modifiers or protease pathways to resensitise tumours to genotoxic therapies.

Chapter 7: SPRTN Depletion Causes Chromatin Compaction Post-Radiation

Building on the findings presented in the previous chapter, we sought to investigate whether the depletion of SPRTN influences chromatin structure. Given SPRTN's established role in DPC repair, we hypothesised that its absence may lead to alterations in chromatin organisation that could underlie the radioresistant phenotype observed in SPRTN-deficient cells. To explore this, we focused on characterising key histone modifications associated with heterochromatin and euchromatin states. By examining these chromatin marks, we aimed to delineate the epigenetic landscape of SPRTN-deficient cells and determine how such modifications may contribute to impaired DNA damage signalling and enhanced survival following ionising radiation.

7.1 Results

7.1.1 SPRTN depletion alters chromatin state through modulation of histone marks

First, we analysed several chromatin remodelling markers, focusing on key histone modifications that indicate chromatin state and accessibility: H3K9me3, H3K9ac, and H3K4me3. H3K9me3 (histone H3 lysine 9 trimethylation) is a well-established marker of constitutive heterochromatin, typically enriched in transcriptionally silent regions such as pericentromeric and telomeric domains. It promotes chromatin compaction through the recruitment of heterochromatin protein 1 (HP1), restricting DNA accessibility and repressing transcription. In contrast, H3K9ac (histone H3 lysine 9 acetylation) is associated with open chromatin and active transcription, facilitating chromatin relaxation by neutralising histone–DNA interactions. Similarly, H3K4me3 (histone H3 lysine 4 trimethylation) marks transcriptionally active promoters and supports transcription initiation and DNA repair via chromatin remodelling.

Upon SPRTN knockdown using siRNA, we observed a notable increase in H3K9me3 levels (~1.54-fold), consistent with enhanced heterochromatin formation and transcriptional repression in the absence of SPRTN (Figure 7.1). Conversely, H3K9ac levels were significantly reduced (~0.3-fold), indicating loss of euchromatin and reduced chromatin accessibility. H3K4me3 levels remained largely unchanged (~0.99-fold), suggesting that transcription initiation at active promoters may not be broadly affected by SPRTN depletion. Together, these findings suggest that SPRTN loss skews the chromatin landscape toward a more compact, transcriptionally silent state.

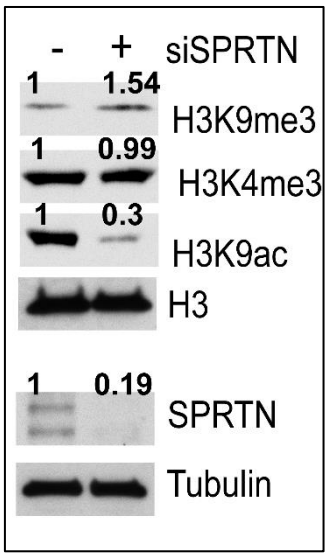


Figure 7.1. SPRTN depletion alters chromatin state through modulation of histone marks

Western blot analysis of histone modification levels in control and SPRTN-depleted cells. Quantification of bands is shown above each lane, normalized to untreated sample (set as 1.0). Band intensities were measured by densitometry. These experiments were done by Bruno Vaz, a previous postdoc in Ramadan lab.

7.1.2 Formaldehyde-induced DNA–protein crosslinks alter histone modification

To further confirm the relationship between SPRTN deficiency and chromatin organisation, again we analysed histone modification in ΔSPRTN HeLa cells. Western blotting was used to assess global levels of H3K9me3, H3K9ac, and H3K4me3. Similarly, in ΔSPRTN HeLa cells (Figure 7.2 A), loss of SPRTN led to an increase in H3K9me3, alongside a marked reduction in the euchromatin-associated marks H3K9ac. This shift was not attributable to changes in total H3 protein levels, confirming a specific alteration in histone post-translational modifications rather than a change in histone abundance.

To determine whether this chromatin remodelling phenotype could be recapitulated by DPC induction, we treated wild-type cells with low-dose formaldehyde (450 μM), a well-characterised crosslinking agent. Similar to SPRTN-deficient cells, FA treatment resulted in reduced levels of H3K9ac and H3K4me3 in HeLa, MCF7, and T24 cells (Figure 7.2 B–D). These changes were consistent across cell types, suggesting that DPC accumulation itself can drive chromatin condensation through loss of active histone marks. The decrease in H3K9ac and H3K4me3 in response to DPC-inducing conditions mirrors the chromatin signature observed in SPRTN-deficient models, further supporting the conclusion that unresolved DPCs contribute to a repressive chromatin environment. This condensed state may hinder DNA damage sensing and repair, offering a mechanistic explanation for checkpoint attenuation and increased radioresistance observed in these settings.

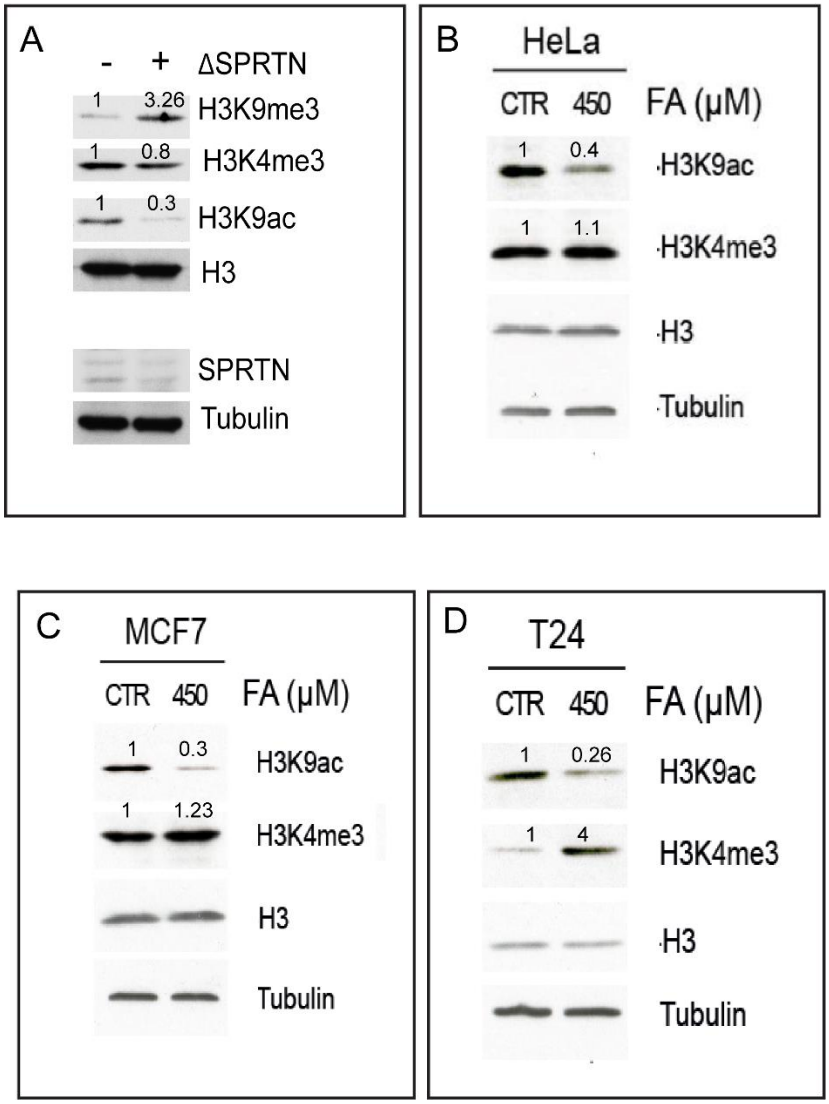


Figure 7.2. SPRTN depletion and formaldehyde-induced DNA–protein crosslinks alter histone modification profiles associated with chromatin state.

(A) Western blot analysis of histone modifications in wild-type (+) and SPRTN-deficient (ΔSPRTN) cells. SPRTN depletion led to an increase in H3K9me3 (a marker of heterochromatin) and a decrease in H3K4me3 and H3K9ac (euchromatin-associated marks), indicating a shift toward chromatin compaction. Total histone H3 was used as a loading control for histone blots, and tubulin confirmed equal protein loading and SPRTN knockdown efficiency.

(B–D) Western blot analysis of HeLa (B), MCF7 (C), and T24 (D) cell lines treated with 450 μM formaldehyde (FA) for 4 h. In all cell lines, FA treatment caused a reduction in H3K9ac and H3K4me3, consistent with a loss of euchromatin and induction of chromatin condensation.

Total histone H3 and tubulin served as controls for equal loading. Quantification of bands is shown above each lane, normalized to untreated sample (set as 1.0). Band intensities were measured by densitometry. These experiments were done by Bruno Vaz, a previous postdoc in Ramadan lab.

To further characterise the impact of SPRTN deficiency and DPC accumulation on chromatin regulation, we assessed the levels of chromatin remodelling factors of the CHD (Chromodomain Helicase DNA-binding) family, which play critical roles in maintaining chromatin accessibility and facilitating DNA repair. Western blot analysis revealed that depletion of SPRTN, either through genetic knockout (ΔSPRTN) or siRNA-mediated knockdown (siSPRTN), led to a marked reduction in CHD1, CHD3, and CHD4 protein levels compared to control cells (Figure 7.3, top and bottom panels).

Importantly, FA treatment, which induces DPCs in a SPRTN-independent manner, also resulted in a notable downregulation of CHD1, CHD3, and CHD4 across the same timeframe (450 μM, 30 min), further supporting the idea that DPC accumulation may destabilise or exclude these chromatin remodelers from chromatin (Figure 7.3, middle panel). Given the known role of CHD proteins in nucleosome remodelling and transcriptional regulation, their reduction in SPRTN-deficient and FA-treated cells suggests that DPC-induced chromatin changes extend beyond histone modification to involve structural regulators of chromatin dynamics. These results highlight a potential mechanism by which unresolved DPCs could lead to chromatin condensation and transcriptional repression, reinforcing the broader link between DPC burden and altered chromatin architecture.

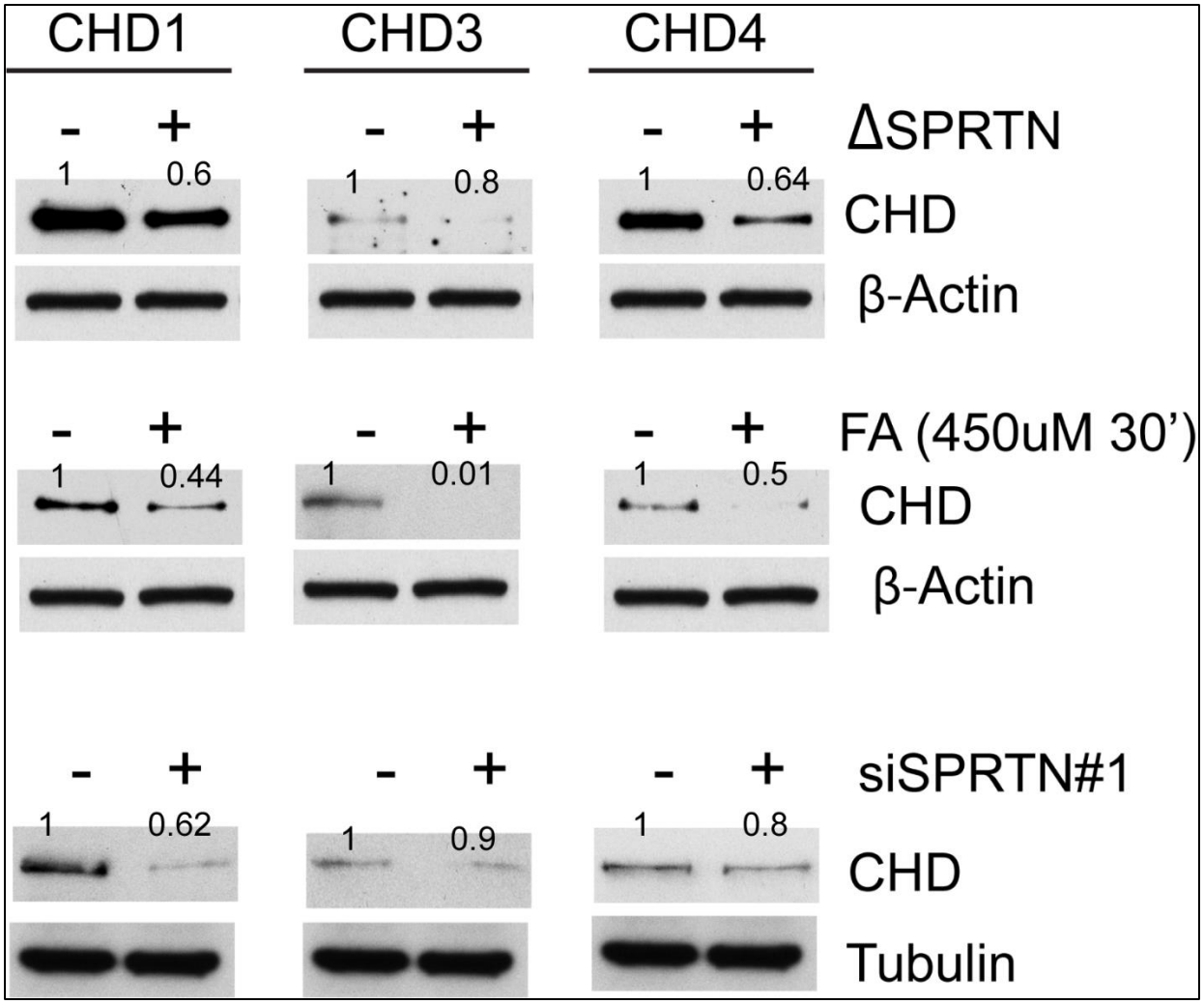


Figure 7.3. SPRTN depletion alters the expression of chromatin remodelers CHD1, CHD2, and CHD4.

Western blot analysis of CHD family remodelers in control and SPRTN-deficient cells. SPRTN loss led to reduced levels of CHD. Actin and Tubulin were used as a loading control. Quantification of bands is shown above each lane, normalized to the wild-type or untreated sample (set as 1.0). Band intensities were measured by densitometry. These experiments were done by Bruno Vaz, a previous postdoc in Ramadan lab.

7.1.3 SPRTN-depleted cells post-irradiation modulate chromatin markers

Next, we aimed to investigate the impact of ionising radiation on chromatin structure by examining the dynamics of chromatin-associated histone modifications. Given the emerging evidence that chromatin state tightly regulates the DDR, we focused on visualising changes in key epigenetic markers of heterochromatin and euchromatin following irradiation. This approach was intended to elucidate whether radiation exposure induces chromatin remodelling that may influence the cellular response to DNA damage, particularly in the context of SPRTN deficiency.

We assessed the levels of H3K9ac, a euchromatic marker associated with open, transcriptionally active chromatin. As shown in Figure 7.4, immunofluorescence staining revealed a significant reduction in H3K9ac intensity in siSPRTN cells compared to control siLUC cells, both at baseline (UT) and following radiation exposure (5 Gy, γ-radiation)(0 h and 4 h post-IR). Quantitative analysis of H3K9ac signal intensity showed a significant decrease in SPRTN-depleted cells post-irradiation relative to wild-type controls, reinforcing the notion of compromised chromatin accessibility in the absence of SPRTN in HeLa cells.

Collectively, these data suggest that SPRTN loss not only promotes basal chromatin compaction but also impairs the dynamic chromatin relaxation normally observed during DNA damage recovery. This altered chromatin landscape may hinder proper DDR activation and contribute to the persistent DNA lesions and radioresistance observed in SPRTN-deficient cells.

Treatment with a histone deacetylase inhibitor (HDACi), included as a positive control, markedly increased H3K9ac levels across both genotypes, confirming the assay's sensitivity to chromatin-modifying interventions.

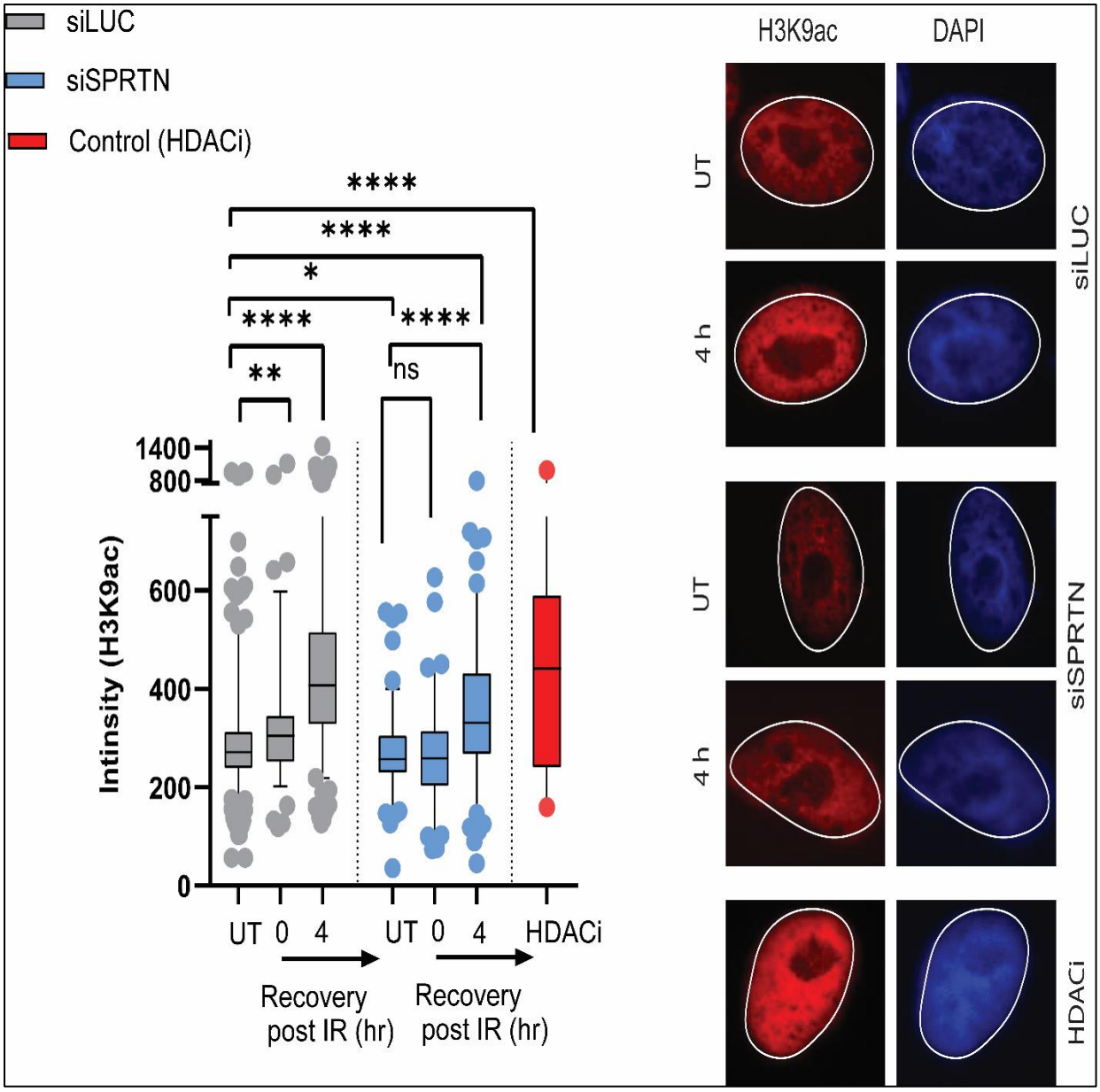


Figure 7.4. Histone acetylation levels are reduced in SPRTN-depleted cells post-irradiation and rescued by HDAC inhibition.

(Left) Quantification of H3K9ac fluorescence intensity in siLUC (control) and siSPRTN cells under unirradiated (UT), immediately post-irradiation (5 Gy, γ-radiation) (0 h), and 4 hours post-irradiation conditions. SPRTN depletion significantly decreased H3K9ac levels under all conditions compared to control. Treatment with HDAC inhibitor (HDACi, 400 nM overnight per manufacturer's protocol) was used as a positive control. Quantification of >100 cells per condition from one representative experiment is shown, and the experiment was repeated two times. Whisker box plots show median

values and data within the 10–90 percentile. Statistical analysis was performed using unpaired t-test. ****p < 0.0001. ns: not significant, * p < 0.05, ** p < 0.01, **** p < 0.0001.

(Right) Representative immunofluorescence images showing nuclear H3K9ac staining (red) and DAPI (blue) in siLUC and siSPRTN cells across treatment conditions, with HDACi treatment shown as a positive control for chromatin relaxation.

To further investigate the relationship between SPRTN deficiency, chromatin compaction, and nucleolar organisation following IR (5 Gy), we analysed histone acetylation and nucleolar morphology using immunofluorescence and quantitative image analysis. Immunofluorescence staining (Figure 7.5 A) revealed that ΔSPRTN cells exhibited a marked reduction in nuclear H3K9ac signal intensity compared to WT cells under basal conditions, indicating a shift towards a more compact chromatin state. This reduction became more pronounced following IR exposure, particularly at the 2-hour recovery timepoint. Quantitative analysis (Figure 7.5 B) confirmed a statistically significant decrease in H3K9ac intensity in ΔSPRTN cells at both 0 and 2 hours post-irradiation compared to WT cells, suggesting an impaired ability to restore euchromatin-associated histone modifications following DNA damage. This confirms that the observed chromatin compaction phenotype was not a transient artefact of siRNA-mediated knockdown, in which these knockout cells recapitulated the H3K9ac suppression observed in the siRNA experiments, validating the consistency and robustness of the phenotype.

These results were further supported by immunoblotting (Figure 7.5 C), which showed reduced H3K9ac protein levels in ΔSPRTN cells after IR. Collectively, these results confirm that SPRTN loss leads to sustained hypoacetylation of histone H3K9, indicative of persistent chromatin condensation, particularly in response to IR.

In parallel, we assessed nucleolar architecture as an indirect readout of chromatin organisation and stress adaptation. Immunofluorescence staining using a nucleolar marker revealed distinct alterations in nucleolar size and number in ΔSPRTN cells following IR (Figure 7.5 A). Quantitative analysis showed that while WT cells displayed a moderate reduction in nucleolar size after 5 Gy irradiation, ΔSPRTN cells exhibited a significant increase in nucleolar area at 2 hours post-IR (Figure 7.5 D), along with a

marked decrease in nucleolar number per nucleus (Figure 7.5 E). This shift toward fewer but enlarged nucleoli is consistent with chromatin condensation and nucleolar fusion, which are known hallmarks of stress-induced transcriptional repression. The observed nucleolar changes in ΔSPRTN cells also mirror previous reports linking DNA damage to altered nucleolar dynamics and chromatin compaction. These findings suggest that SPRTN loss affects not only global chromatin acetylation status but also impacts nucleolar organisation during the DNA damage response. Together, the results support the idea that persistent DPCs in SPRTN-deficient cells promote a condensed chromatin state, potentially interfering with the spatial and temporal regulation of damage signalling and repair.

This morphological change in SPRTN-depleted cells (fewer but larger nucleoli per nucleus) is indicative of nucleolar fusion, a phenomenon commonly associated with elevated levels of chromatin condensation and diminished ribosomal gene activity (Caragine et al., 2019). Nucleoli, being the sites of ribosomal RNA (rRNA) synthesis and ribosome assembly, are highly sensitive to changes in chromatin organisation. Under conditions of increased heterochromatin formation, the transcriptional machinery required for rRNA synthesis is sequestered or suppressed, leading to a reduction in both nucleolar number and rRNA output.

This link between chromatin state and nucleolar function is further substantiated by transcriptional profiling. RNA-seq analysis of SPRTN-depleted HeLa cells revealed a consistent downregulation of several genes involved in ribosome biogenesis, including ribosomal protein genes such as RPL11, RPL17, RPL24, and RPS16 (Figure 7.6, Table 7.1). These ribosomal protein genes are typically transcribed from euchromatic regions and are tightly co-regulated with rRNA synthesis to ensure coordinated ribosome production. The downregulation observed here suggests that chromatin

compaction extends beyond damage response loci to affect broad genomic regions, including those essential for protein biosynthesis.

Moreover, the suppression of ribosomal gene expression aligns with reports that heterochromatinisation can directly repress rRNA gene clusters by altering nucleolar organiser regions (NORs) (Ma et al., 2022). The repressive chromatin environment in SPRTN-deficient cells may thus contribute to a broader reduction in cellular biosynthetic capacity, potentially as part of a stress adaptation response. Together, these findings illustrate that the structural reorganisation of chromatin in the absence of SPRTN not only impairs DNA damage signalling and repair but also affects global transcriptional programs, particularly those related to ribosome production and nucleolar integrity.

Table 7.1. List of DEGs present in HeLa SPRTN -/-/+

This experiment was done by a previous PhD student Cristiano Peron.

List of DEGs present in HeLa SPRTN -/-/+		
Gene	**log2** (HeLa SPRTN -/-/+ / HeLa WT)	**Q- value** (HeLa SPRTN -/-/+ / HeLa WT)
'RPL11'	-0.180	0.006
'RPL17'	-0.210	0.008
'RPL24'	-0.257	3.57E-05
'RPL27'	-0.220	0.039
'RPL35A'	-0.207	0.002
'RPL5'	-0.479	9.73E-21
'RPS16'	-0.202	0.003
'RPS26'	-0.155	0.041
'RPS27A'	-0.159	0.015
'RPS28'	-0.403	1.07E-06
'RPS4X'	-0.226	0.001
'RPS5'	-0.389	9.60E-07
'RPS7'	-0.274	0.003

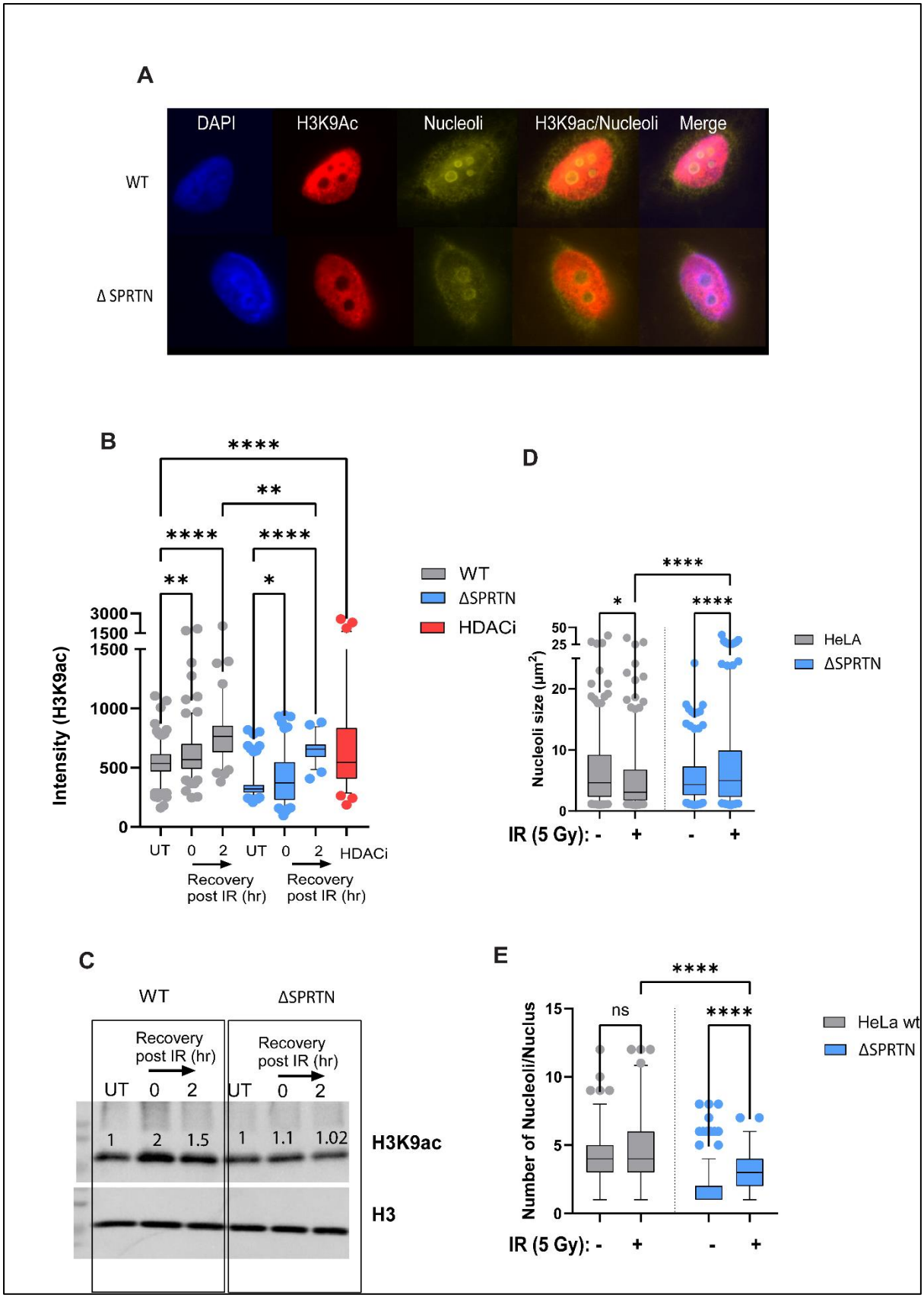

A
DAPI
H3K9Ac
Nucleoli
H3K9ac/Nucleoli
Merge
WT
Δ SPRTN
B
Intensity (H3K9ac)
3000
1500
1500
1000
500
0
UT
0
2
UT
0
2
HDACi
Recovery post IR (hr)
Recovery post IR (hr)
WT
ΔSPRTN
HDACi
D
Nucleoli size (μm²)
50
25
20
10
0
IR (5 Gy): -
+
-
+
HeLA
ΔSPRTN
C
WT
ΔSPRTN
Recovery post IR (hr)
Recovery post IR (hr)
UT
0
2
UT
0
2
1
2
1.5
1
1.1
1.02
H3K9ac
H3
E
Number of Nucleoli/Nuclus
15
10
5
0
ns
IR (5 Gy): -
+
-
+
HeLa wt
ΔSPRTN

Figure 7.5. SPRTN deficiency reduces histone acetylation and alters nucleolar architecture following ionising radiation.

(A) Representative immunofluorescence images of wild-type (WT) and SPRTN-deficient (ΔSPRTN) cells stained with DAPI (nuclei), H3K9ac (histone acetylation, red), and nucleolin (nucleoli, yellow). Merged images and overlays demonstrate reduced H3K9ac signal and altered nucleolar structure in ΔSPRTN cells compared to WT.

(B) Quantification of nuclear H3K9ac intensity in WT, ΔSPRTN, and HDAC inhibitor (HDACi)-treated cells at 0 and 2 hours post-irradiation (5 Gy). HDACi was applied overnight at 400 nM following the manufacturer's protocol. SPRTN-deficient cells showed a significant reduction in H3K9ac levels at all timepoints.

(C) Immunoblot of H3K9ac and total H3 in WT and ΔSPRTN cells, untreated or harvested at 0 and 2 hours post-irradiation. Quantification of bands is shown above each lane, normalized to the untreated sample (set as 1.0). Band intensities were measured by densitometry.

(D) Boxplot showing nucleolar size in HeLa WT and ΔSPRTN cells with and without IR (5 Gy). SPRTN-deficient cells exhibit significantly larger nucleoli post-irradiation, indicating altered nucleolar morphology.

(E) Quantification of the number of nucleoli per nucleus. SPRTN-deficient cells show fewer, enlarged nucleoli upon IR (5 Gy, γ-radiation) compared to controls. In each, quantification of 100 cells per condition from one representative experiment is shown, and the experiment was repeated two times. Whisker box plots show median values and data within the 10–90 percentile. Statistical analysis was performed using unpaired t-test.

ns: not significant, * $p < 0.05$, ** $p < 0.01$, *** $p < 0.001$, **** $p < 0.0001$.

B

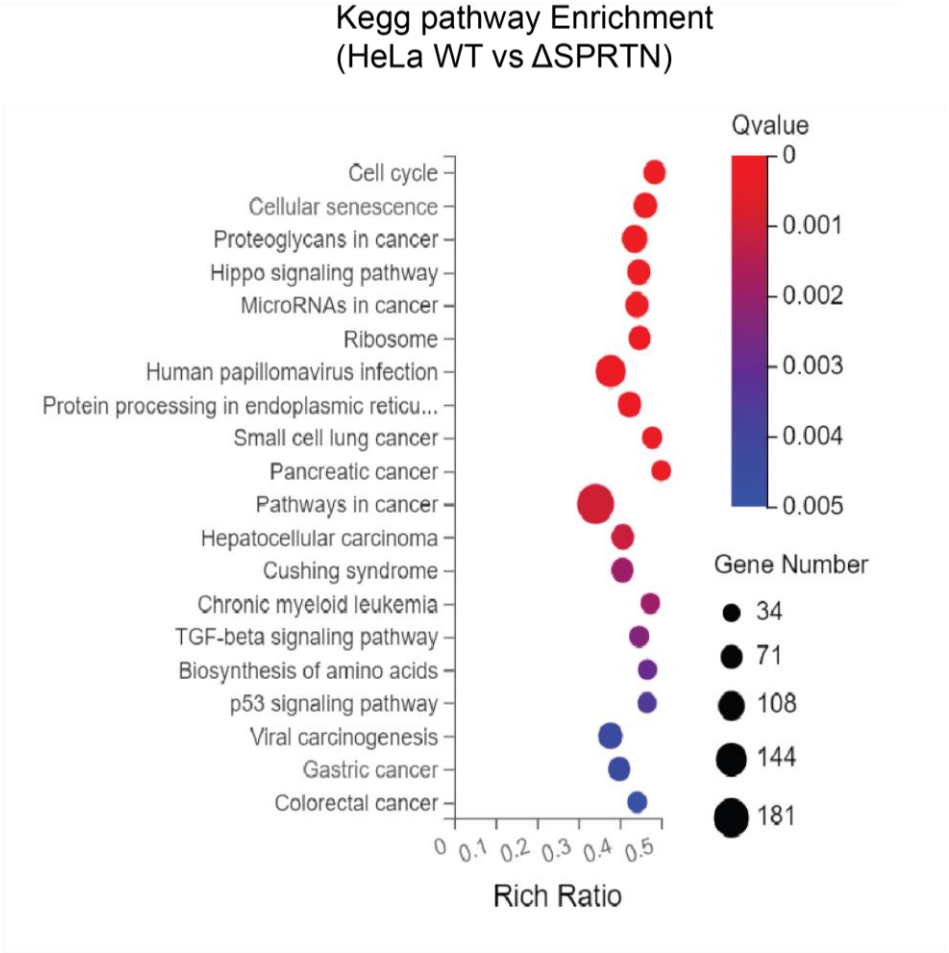


Figure 7.6. Kegg pathway analysis of SPRTN-depleted cells.

ΔSPRTN is characterised not only by the downregulation of ribosomal genes, but also by a significant downregulation of genes involved in the cell cycle when compared to HeLa WT. This experiment was done by a previous PhD student, Cristiano Peron.

To get additional insight into heterochromatin architecture following IR, we quantified HP1 foci per nucleus, an established proxy for chromatin condensation and heterochromatin integrity. As shown in Figure 7.7, untreated ΔSPRTN cells already exhibited a trend toward increased HP1 foci compared to wild-type (WT) cells, consistent with elevated basal levels of heterochromatin. This observation aligns with prior findings of increased H3K9me3 and decreased euchromatin markers in SPRTN-deficient cells, reinforcing the notion that SPRTN loss leads to a more compact chromatin state.

Upon IR exposure, a divergence in HP1 dynamics between WT and ΔSPRTN cells became more pronounced. WT cells displayed a modest elevation in HP1 foci at 2 hours post-IR, reflecting a transient chromatin compaction response known to accompany DNA damage signalling. However, this response was largely resolved by 4 hours, with HP1 foci returning toward baseline, consistent with dynamic chromatin relaxation required for efficient checkpoint resolution and repair.

In contrast, ΔSPRTN cells showed a significant and sustained increase in HP1 foci post-IR (5 Gy). At the basal level, ΔSPRTN cells exhibited significantly higher HP1 foci compared to wild-type cells ($p < 0.01$), indicating increased chromatin compaction even in the absence of DNA damage. Following ionising radiation, HP1 foci levels in ΔSPRTN cells remained elevated and were significantly higher than in wild-type cells at 2 hours post-recovery ($p < 0.01$), suggesting a further enhancement of chromatin compaction in the absence of SPRTN. By 4 hours, the difference between the two genotypes was no longer statistically significant. In contrast, wild-type cells maintained stable HP1 levels across all timepoints.

These results could provide evidence that SPRTN is not only essential for DPC clearance, but also for preserving chromatin plasticity following genotoxic stress, and that its loss leads to aberrant heterochromatin persistence that may contribute to the observed attenuation of DNA damage responses in SPRTN-deficient models.

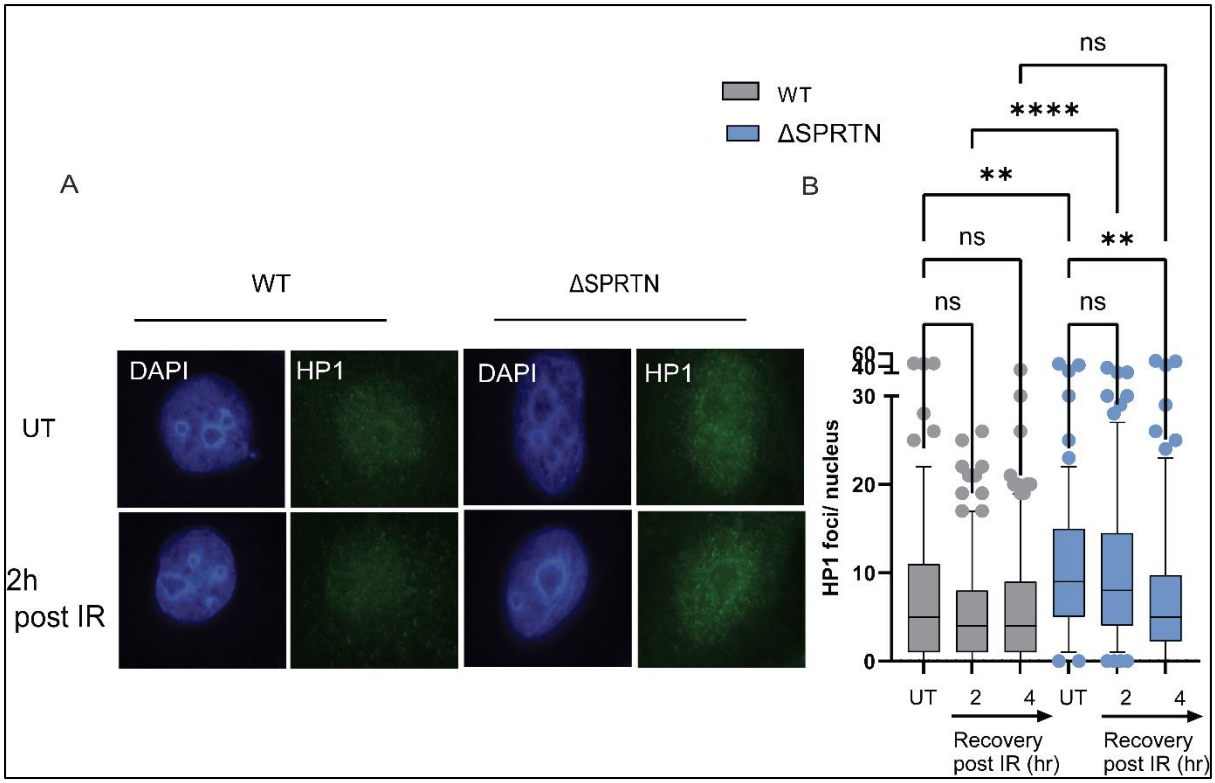


Figure 7.7. SPRTN deficiency leads to increased HP1 retention after ionising radiation.

(A) Representative immunofluorescence images showing HP1α (green) and DAPI (blue) staining in wild-type (WT) and SPRTN-deficient (ΔSPRTN) cells under untreated (UT) conditions and 2 hours after 5 Gy ionising radiation (IR). In WT cells, HP1α foci remain relatively low and unchanged after IR, while ΔSPRTN cells exhibit more intense and numerous HP1α foci post-irradiation, suggesting enhanced heterochromatin retention.

(B) Quantification of HP1α foci per nucleus across indicated timepoints post-IR (5 Gy). ΔSPRTN cells consistently show significantly higher numbers of HP1α foci compared to WT, particularly at 2 and 4 hours post-irradiation, indicating persistent or enhanced heterochromatin formation. Quantification of 100 cells per condition from one representative experiment is shown, and the experiment was repeated two times. Whisker box plots show median values and data within the 10–90 percentile. Statistical analysis was performed using unpaired t-test. ns: not significant, ** $p < 0.01$, **** $p < 0.0001$.

7.1.4 SPRTN Deficiency in HeLa cells Enhances Chromatin Compaction via Accumulation of Linker Histone H1.2

Then we looked into structural proteins involved in chromatin folding, particularly histone variants. To investigate the effect of SPRTN depletion on chromatin architecture, we examined the distribution and intensity of the linker histone H1.2, a well-established marker of chromatin compaction. Figure 7.8 A illustrates a model where elevated levels of H1.2 are associated with more compacted chromatin. As shown in Figure 7.8 B, quantitative analysis of H1.2 fluorescence intensity revealed a significant increase in ΔSPRTN cells compared to WT controls across all post-irradiation recovery timepoints (2, 4, and 6 hours). In WT cells, H1.2 levels remained relatively stable or moderately increased post-irradiation. In contrast, SPRTN-deficient cells showed consistently elevated H1.2 intensity even in the untreated condition, with further increases upon irradiation. This trend suggests a persistent and possibly exacerbated chromatin compaction in the absence of SPRTN.

The immunofluorescence images (Figure 7.8 B right panels) visually confirm the increased nuclear intensity of H1.2 staining in ΔSPRTN cells compared to WT, both under untreated conditions and 4 hours after IR. These results suggest that SPRTN deficiency promotes a more compact chromatin state, which is sustained or further intensified upon genotoxic stress.

Together, these findings indicate that SPRTN deficiency leads to persistent chromatin compaction, as evidenced by elevated levels of the linker histone H1.2. The increase in H1.2 intensity observed in ΔSPRTN cells, both at baseline and following ionising radiation, supports a model in which loss of SPRTN function promotes a structurally condensed chromatin environment.

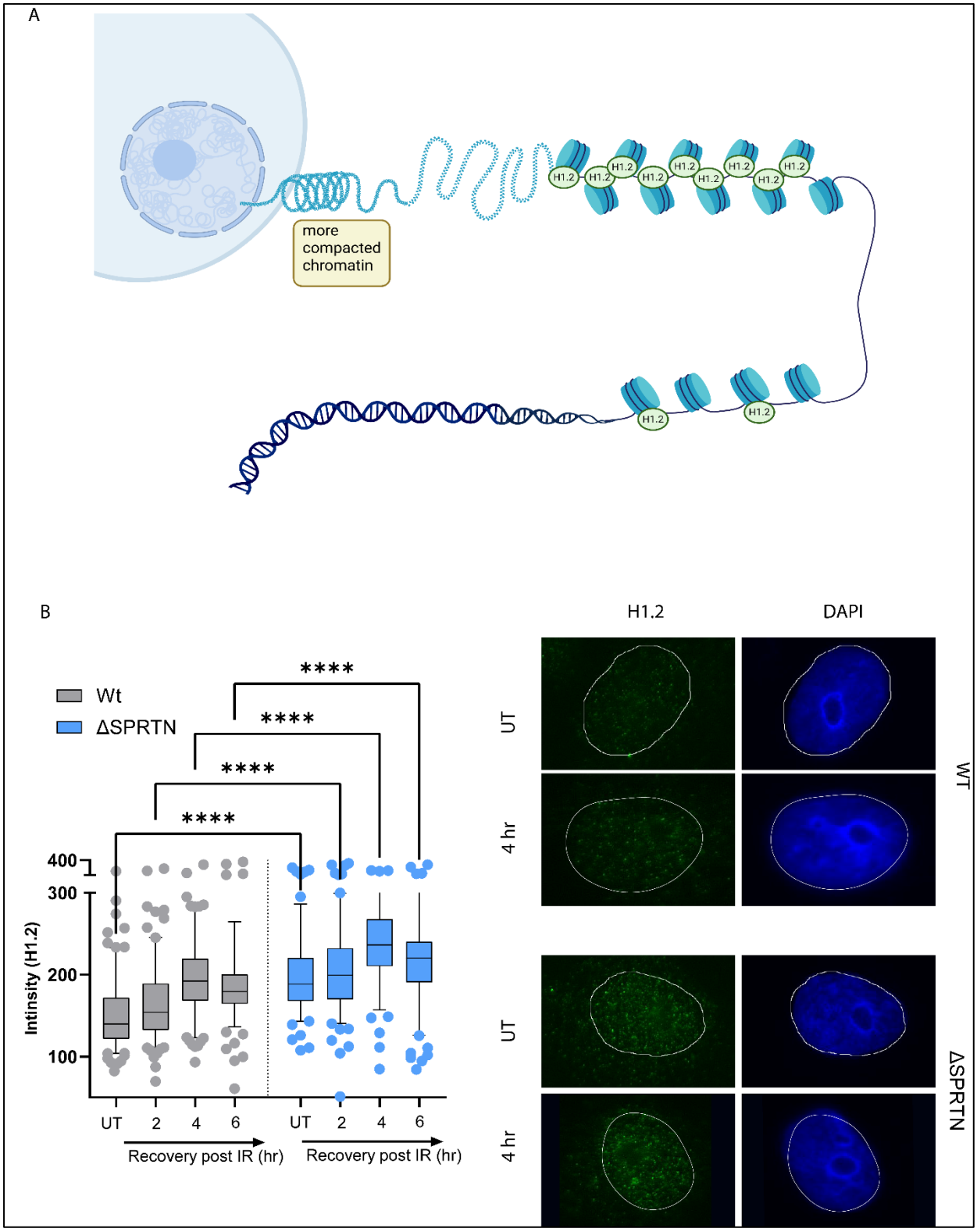


Figure 7.8. SPRTN deficiency leads to elevated levels of linker histone H1.2 and enhanced chromatin compaction following ionising radiation.

(A) Schematic representation illustrating increased deposition of linker histone H1.2 in SPRTN-deficient cells, contributing to a more compacted chromatin structure post-irradiation. Created by Biorender.

(B) Left: Quantification of nuclear H1.2 fluorescence intensity in wild-type (WT; grey) and SPRTN-deficient (ΔSPRTN; blue) cells at various recovery time points (0, 2, 4, and 6 hours) following 5 Gy ionising radiation (IR). ΔSPRTN cells show significantly higher H1.2 levels at all time points, indicating enhanced chromatin compaction. Right: Representative immunofluorescence images of H1.2 (green) and DAPI (blue) in WT and ΔSPRTN cells under untreated (UT) and 4-hour post-IR conditions. Increased nuclear H1.2 signal in ΔSPRTN cells is consistent with the observed compaction phenotype. Nuclear contours are outlined. Quantification of 100 cells per condition from one representative experiment is shown, and the experiment was repeated two times. Whisker box plots show median values and data within the 10–90 percentile. Statistical analysis was performed using unpaired t-test., **** $p < 0.0001$.

7.1.5 SPRTN Deficiency Impairs Histone H3.3 Incorporation and Chromatin Remodelling Post-Damage

To assess whether SPRTN depletion affects chromatin remodelling following DNA damage, we examined the incorporation of histone variant H3.3, which is typically associated with transcriptionally active and accessible chromatin. H3.3 serves as a dynamic chromatin marker deposited independently of DNA replication and is often enriched at actively transcribed gene loci and regulatory regions (Wirbelauer et al., 2005). Immunofluorescence staining and subsequent quantification of nuclear H3.3 levels revealed a clear reduction in signal intensity in ΔSPRTN cells compared to WT controls (Figure 7.9 A and B). This reduction was evident at baseline and persisted following exposure to IR. Specifically, WT cells demonstrated a mild but consistent increase in H3.3 nuclear intensity 2 and 4 hours after IR (5 Gy), suggesting that chromatin relaxation and transcriptional reactivation occur as part of the post-damage recovery process. In contrast, SPRTN-deficient cells failed to upregulate H3.3 incorporation following IR to matching levels of WT, maintaining significantly lower levels throughout the recovery timepoints. This blunted incorporation pattern implies that chromatin in ΔSPRTN cells remains in a more compact or less accessible state. The sustained suppression of H3.3 deposition in SPRTN-deficient cells indicates a broader defect in chromatin dynamics and remodelling capacity. These findings provide further evidence that SPRTN not only regulates DPCs repair but also it could play an essential role in maintaining chromatin plasticity under genotoxic stress.

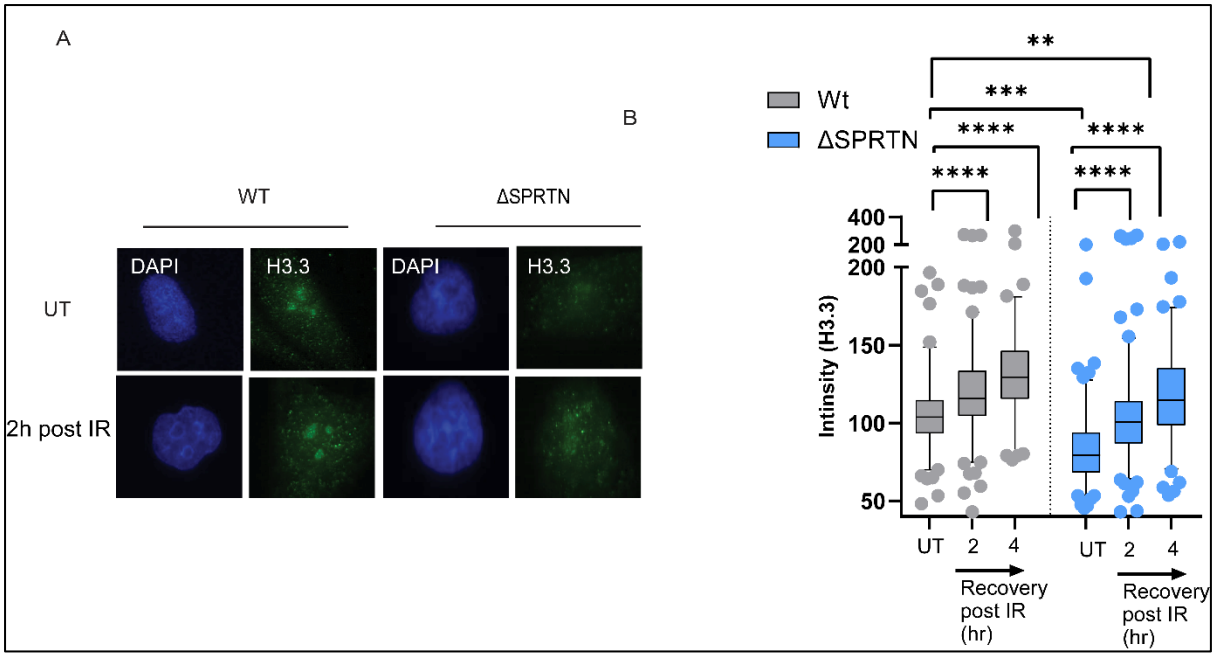


Figure 7.9 SPRTN deficiency reduces H3.3 chromatin incorporation following ionising radiation.

(A) Representative immunofluorescence images showing H3.3 (green) and DAPI (blue) in wild-type (WT) and SPRTN-deficient (ΔSPRTN) cells under untreated (UT) and 2-hour post-irradiation (5 Gy) conditions. WT cells display robust nuclear H3.3 staining, which is markedly reduced in ΔSPRTN cells, especially after irradiation.

(B) Quantification of H3.3 fluorescence intensity in WT (grey) and ΔSPRTN (blue) cells at baseline and following 2 or 4 hours of recovery after IR. Quantification of 100 cells per condition from one representative experiment is shown, and the experiment was repeated two times. Whisker box plots show median values and data within the 10–90 percentile. Statistical analysis was performed using unpaired t-test. ** $p < 0.01$, *** $p < 0.001$, **** $p < 0.0001$.

7.1.6 MNase Digestion Confirms Enhanced Chromatin Compaction in SPRTN-Deficient Cells

To further validate the hypothesis that SPRTN depletion leads to increased chromatin compaction, we performed a micrococcal nuclease (MNase) digestion assay on DNA isolated from both WT and ΔSPRTN HeLa cells following IR. While prior analyses, including elevated levels of heterochromatin-associated histone marks such as H3K9me3 and increased expression of chromatin structural components like HP1, suggested a global shift toward a more condensed chromatin architecture, these markers primarily provide indirect or qualitative insights. Therefore, the MNase assay was employed as a direct and quantitative method to assess chromatin accessibility at the nucleosomal level.

MNase preferentially cleaves the linker DNA between nucleosomes, and the resulting DNA digestion pattern reflects the degree of chromatin compaction. In less condensed chromatin, linker regions are more accessible, allowing MNase to generate a DNA ladder comprising mono-, di-, and tri-nucleosomes. In contrast, highly compacted chromatin protects linker regions from digestion, resulting in slower or incomplete digestion and an altered ladder profile (Figure 7.10).

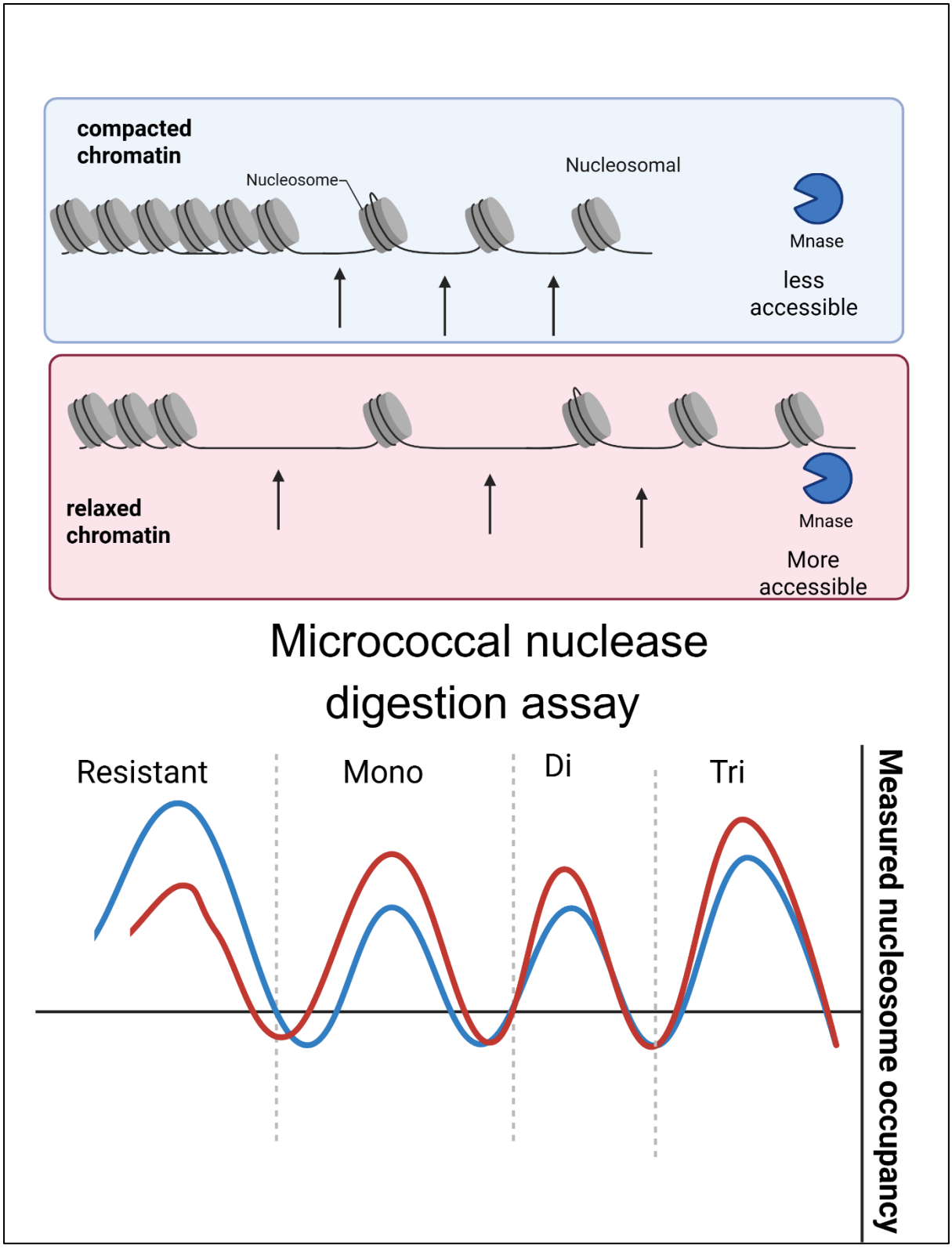

compacted chromatin
Nucleosome
Nucleosomal
Mnase
less accessible
relaxed chromatin
Mnase
More accessible
Micrococcal nuclease digestion assay
Resistant
Mono
Di
Tri
Measured nucleosome occupancy

Figure 7.10 Schematic representation of chromatin accessibility measured by micrococcal nuclease (MNase) digestion.

(Top panels): Illustrations depict differences in nucleosome organization between compacted chromatin (blue panel) and relaxed chromatin (pink panel). In compacted chromatin, nucleosomes are tightly packed, resulting in reduced accessibility to MNase and limited DNA cleavage (indicated by fewer arrows). In relaxed chromatin, nucleosomes are more spaced, increasing accessibility and allowing greater MNase cleavage at linker DNA regions.

(Bottom panel): A representative MNase digestion profile is shown. The y-axis indicates relative protection of DNA from MNase digestion, while the x-axis represents DNA fragment length or position. Blue line represents compact chromatin with lower accessibility and sharper peaks indicating positioned nucleosomes. Red line represents relaxed chromatin with higher accessibility and broader peaks due to increased linker cleavage. The dotted vertical lines denote periodic nucleosome spacing.

7.1.6.1 Optimizing Mnase assay

To establish optimal conditions for assessing chromatin accessibility using the MNase assay, we first performed a series of optimisation experiments to determine the appropriate enzyme concentration and incubation time. MNase preferentially digests accessible linker DNA between nucleosomes, and the resulting digestion pattern reflects chromatin structure and compaction state. Over-digestion may obscure informative nucleosome ladders, while insufficient digestion may fail to reveal meaningful differences in chromatin accessibility.

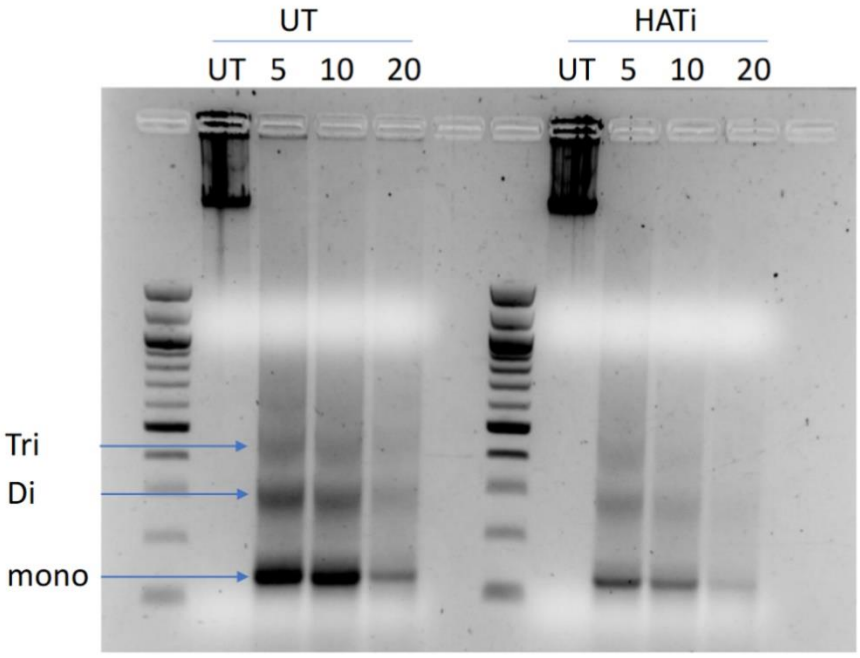
To ensure consistency and reliability in the MNase assay results, 500,000 cells were used per condition. This number was carefully standardised across all experimental groups to enable accurate comparisons of chromatin accessibility. Cells were first passed through cell strainers to eliminate aggregates and ensure a single-cell suspension, which is critical for downstream processing and uniform enzymatic digestion. Following this, automated cell counting was employed to precisely quantify viable cells, thereby reducing variability introduced by manual counting. The use of both cell strainers and automated counters was essential to guarantee that equal numbers of nuclei were subjected to MNase digestion, ensuring that observed differences in chromatin fragmentation patterns reflected true biological variation rather than inconsistencies in input material.

As an initial step, we tested MNase at relatively high concentrations of 5, 10, and 20 units per reaction for a 2-minute incubation (Figure 7.11 A). Across both UT and histone acetyltransferase inhibitor (HATi)-treated conditions, we observed extensive degradation of DNA, with a loss of the typical nucleosomal ladder pattern and predominance of mononucleosomal fragments. This over-digestion indicated that enzyme activity at these concentrations was too aggressive to resolve nucleosomal

intermediates reliably. Here, HATi was used as a control to induce a more compacted chromatin, which is expected to have less Mnase accessibility.

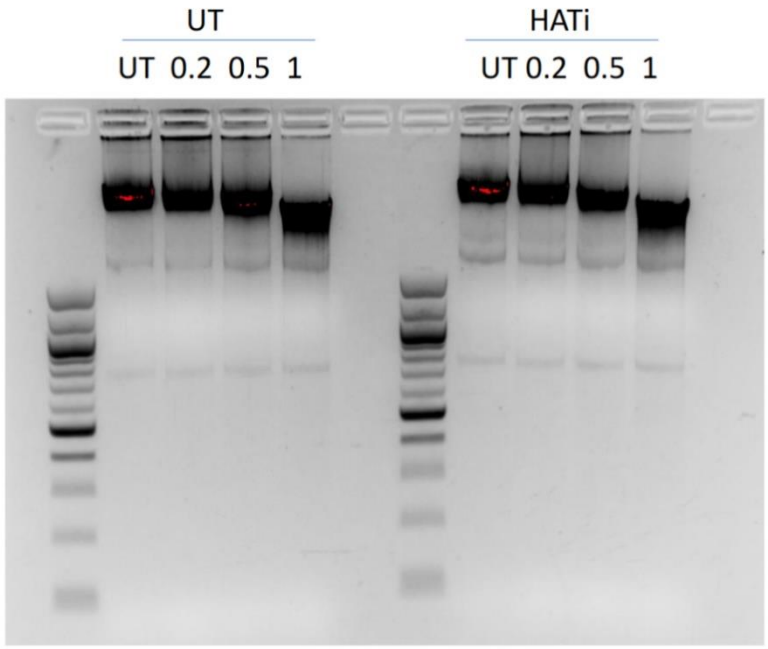
To address this, we repeated the assay using lower MNase concentrations: 0.2, 0.5, and 1 unit for the same incubation time (2 minutes) (Figure 7.11 B). However, under these milder conditions, we didn't observe the emergence of defined mono-, di-, and tri-nucleosome bands. This means that Mnase concentration and incubation time are not enough to cause digestion that preserves nucleosomal periodicity, allowing for robust assessment of chromatin accessibility.

A



Too much Mnase

B



Too low Mnase

Figure 7.11. Titration of Micrococcal Nuclease (MNase) to optimise digestion of chromatin for nucleosome accessibility assessment.

(A) MNase digestion was performed on untreated (UT) and histone acetyltransferase inhibitor (HATi)-treated cells using increasing concentrations of MNase (5, 10, and 20 U). Excess MNase leads to over-digestion, resulting in a predominant mononucleosome band and loss of dinucleosome (Di) and trinucleosome (Tri) bands, indicating reduced resolution of chromatin structure.

(B) Low MNase concentrations (0.2, 0.5, and 1 U) were tested under the same conditions. Insufficient MNase yields high-molecular-weight DNA, suggesting incomplete digestion and limited accessibility, especially in compact chromatin contexts.

Following initial enzyme titration, we selected 1 U of MNase per reaction as the optimal concentration for detecting differences in chromatin accessibility. However, preliminary digestion for 2 minutes proved insufficient to reveal well-resolved nucleosomal ladders. To refine the protocol, we next optimised the digestion duration using fixed MNase concentration (1 U) and varied incubation times (5, 8, and 12 minutes) in HeLa cells. As shown in the gel (Figure 7.12), increasing the digestion time progressively enhanced the resolution of mono-, di-, and tri-nucleosome bands.

Among the tested durations, 8 minutes produced the clearest nucleosomal pattern with minimal over-digestion, and was selected as the optimal condition for downstream analysis. The ratio of Mnase units to cell number is 1U to 500,000 cells. Formaldehyde (FA, 1 mM for 20 min) was included as a condition expected to induce chromatin compaction via DPC formation, while HDAC inhibitor (HDACi, 400 nM overnight) treatment served as a positive control for chromatin relaxation (Karagiannis & El-Osta, 2006; Leso et al., 2020).

Consistent with expectations, FA-treated cells exhibited increased resistance to MNase digestion compared to untreated controls, as indicated by the relative persistence of high-molecular-weight DNA and reduced mononucleosome signal. In contrast, HDACi-treated samples showed enhanced MNase sensitivity, reflected by more efficient generation of lower-order nucleosome bands. These results further validate that the assay is sensitive to chromatin condensation states and support the hypothesis that DPC accumulation promotes a more compact chromatin structure.

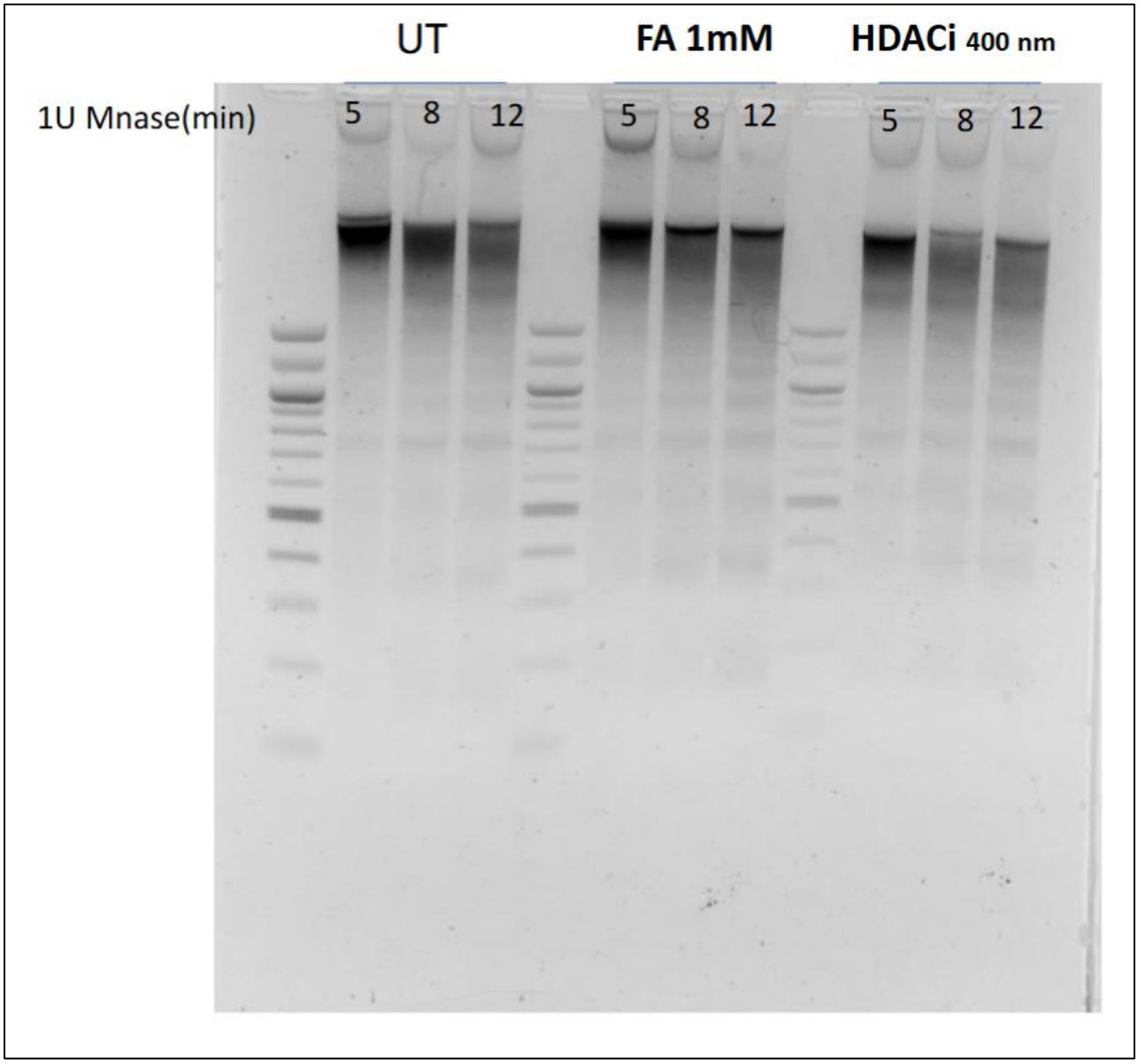


Figure 7.12. MNase digestion assay to assess chromatin accessibility in untreated, formaldehyde-treated, and HDACi-treated cells.

Chromatin was digested with 1 unit of micrococcal nuclease (MNase) for 5, 8, or 12 minutes in three experimental conditions: untreated (UT), formaldehyde-treated (FA 1 mM, 30 min), and HDAC inhibitor–treated (HDACi, 400 nM overnight). DNA fragments were resolved by agarose gel electrophoresis. In FA treated cells, chromatin displayed resistance to MNase digestion over time, as evidenced by the persistence of high-molecular-weight DNA and relatively less prominent mono-, di-, and tri-nucleosomal bands. This indicates a more compact chromatin state. In contrast, HDACi-treated samples exhibited increased digestion and more distinct nucleosome laddering, particularly at earlier time points, consistent with a relaxed chromatin conformation and increased accessibility to MNase.

7.1.6.2 MNase Analysis Reveals Chromatin Condensation in ΔSPRTN Cells After Radiation

To directly assess chromatin compaction in SPRTN-deficient cells following IR, we performed MNase digestion assays under optimised conditions (1 U MNase, 8 minutes). MNase preferentially cleaves linker DNA between nucleosomes, and the resulting ladder pattern reflects chromatin accessibility and nucleosome organisation. As shown in the MNase gel (Figure 7.13 A, untreated wild-type (WT) HeLa cells exhibited a clear nucleosomal ladder, with prominent mono-, di-, and tri-nucleosome bands, indicating a relatively open chromatin configuration that is permissive to MNase digestion.

In contrast, ΔSPRTN cells showed greater resistance to MNase digestion, particularly following irradiation (10 Gy). The chromatin in irradiated ΔSPRTN cells was notably less accessible, as evidenced by the increased retention of high-molecular-weight DNA and reduced intensity of nucleosomal bands. These observations suggest a more compact chromatin state in the absence of SPRTN, especially after IR. Conversely, treatment with HDACi, used as a positive control for chromatin relaxation, resulted in enhanced MNase sensitivity, with pronounced digestion into mono- and di-nucleosomal fragments, consistent with a more open chromatin state.

To quantitatively evaluate these differences, gel densitometry analysis was conducted (Figure 7.13 B). The grey value profile revealed distinct peak shifts and intensity reductions in ΔSPRTN samples post-irradiation. Compared to WT, the irradiated ΔSPRTN cells exhibited diminished tri- and di-nucleosome peaks and a flatter overall digestion curve, indicative of increased nucleosomal resistance and tighter chromatin packaging. In contrast, the HDACi-treated cells displayed a steeper decline in signal

across higher-order nucleosomes, confirming efficient digestion and chromatin decondensation.

Together, these data demonstrate that SPRTN loss leads to elevated chromatin compaction following IR, likely due to the accumulation of DNA–protein crosslinks that hinder normal nucleosome accessibility. The MNase assay thus provides functional validation of chromatin structural changes driven by SPRTN loss and DPC persistence.

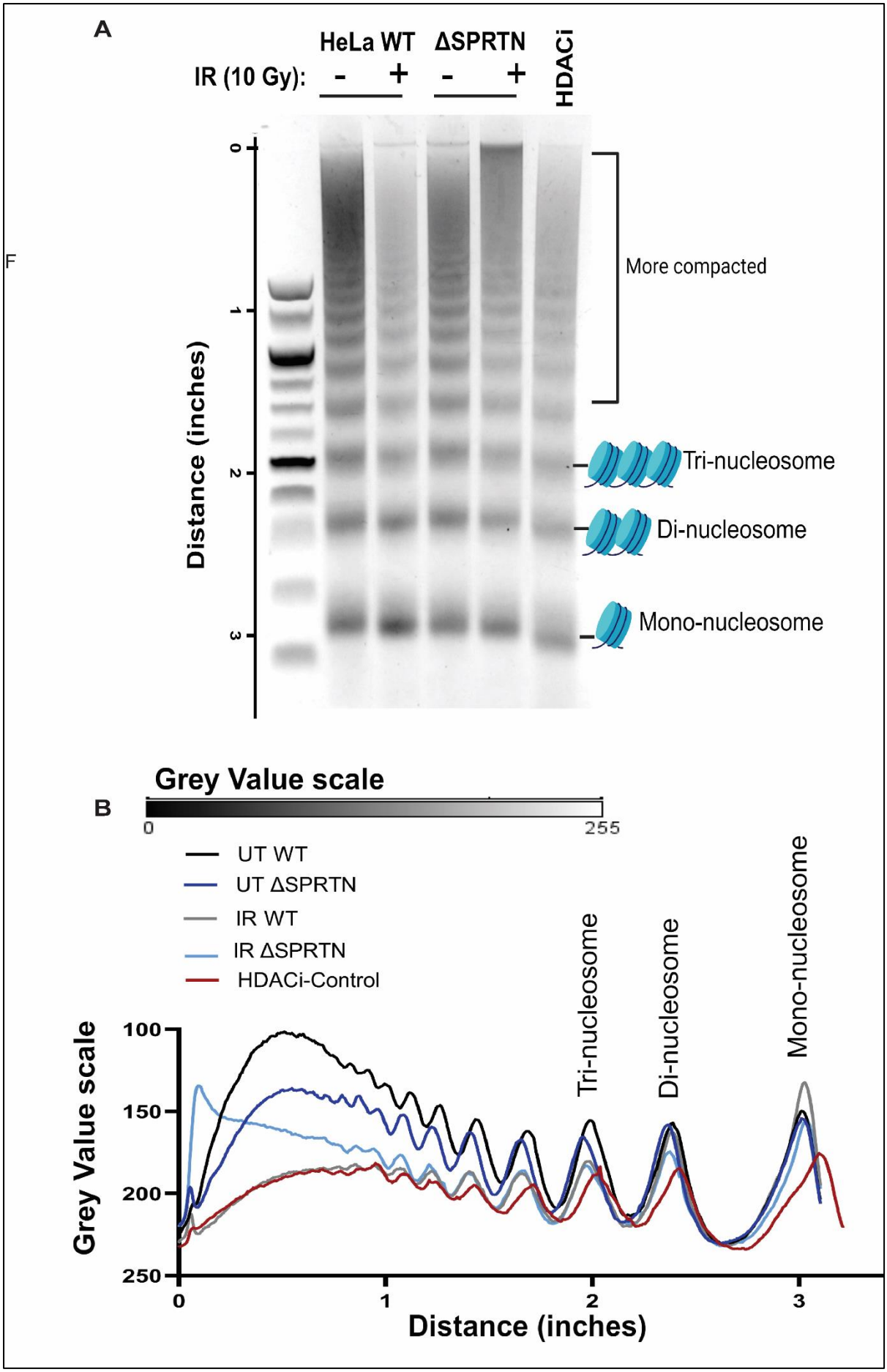

A
HeLa WT
ΔSPRTN
HDACi
IR (10 Gy):
-
+
-
+
Distance (inches)
0
1
2
3
More compacted
Tri-nucleosome
Di-nucleosome
Mono-nucleosome
B
Grey Value scale
0
255
UT WT
UT ΔSPRTN
IR WT
IR ΔSPRTN
HDACi-Control
Tri-nucleosome
Di-nucleosome
Mono-nucleosome
Grey Value scale
100
150
200
250
0
1
2
3
Distance (inches)

Figure 7.13. SPRTN depletion leads to enhanced chromatin compaction after ionising radiation, as assessed by MNase digestion.

(A) Micrococcal nuclease (MNase) digestion assay was performed on chromatin extracted from HeLa wild-type (WT) and SPRTN knockout (ΔSPRTN) cells, untreated or irradiated with 10 Gy. A control sample treated with HDAC inhibitor (HDACi, 400 nM overnight) was included to represent decondensed chromatin. Digested chromatin was resolved on an agarose gel. Compacted chromatin is indicated by stronger retention of higher-order nucleosomal bands (tri- and di-nucleosomes), whereas relaxed chromatin yields more prominent mono-nucleosome bands. ΔSPRTN cells show reduced MNase accessibility both at baseline and post-IR, indicative of a more compact chromatin state compared to WT. This effect is reversed in the HDACi-treated control, demonstrating the sensitivity of the assay to chromatin compaction status.

(B) Densitometric grey value analysis of nucleosomal bands from the MNase gel in panel A. The intensity profiles show a progressive shift toward higher nucleosomal protection in ΔSPRTN cells, especially following IR. WT cells exhibit greater mono-nucleosome release, while ΔSPRTN cells retain higher-order chromatin structures. HDACi-treated samples show enhanced mono-nucleosome release, confirming chromatin relaxation. Together, these data support that SPRTN loss results in increased chromatin compaction, which is further exacerbated by IR.

To further validate the effect of SPRTN deficiency on chromatin architecture, we used two enzyme concentrations: 2 U and 5 U of Mnase to evaluate both moderate and extensive digestion levels. The rationale for using two different units was to capture subtle differences in chromatin accessibility that might not be apparent at a single digestion intensity; 2 U was chosen to detect moderate compaction states, while 5 U provided a more stringent condition that allowed us to resolve highly protected chromatin regions.

As shown in the gel image (Figure 7.14 A), both WT and ΔSPRTN samples exhibited the expected nucleosomal laddering pattern under both enzyme concentrations. However, a marked difference was observed in the extent of digestion across timepoints. Under UT conditions, ΔSPRTN samples displayed higher resistance to MNase digestion compared to WT, especially at 5 U, indicating a more compact chromatin state. This trend was even more pronounced following IR (10 Gy) treatment, particularly at the 4-hour post-IR timepoint, where ΔSPRTN samples retained more high-molecular-weight DNA and exhibited weaker mono- and di-nucleosome bands relative to WT. These results support that chromatin compaction in ΔSPRTN cells becomes further exacerbated following radiation.

Quantitative analysis using grey value profiling (Figure 7.14 B) confirmed these findings. At both 2 U and 5 U MNase, ΔSPRTN cells showed consistently lower grey value intensities across the mono-, di-, and tri-nucleosome regions compared to WT, indicating reduced DNA accessibility and enhanced nucleosome protection. Notably, the divergence between WT and ΔSPRTN profiles was greatest at the 4-hour post-IR timepoint under 5 U digestion, highlighting that SPRTN-deficient chromatin becomes increasingly refractory to nuclease activity with time after DNA damage.

Together, these results corroborate our earlier findings from histone modification and chromatin-associated protein analyses, and provide biochemical evidence that SPRTN loss leads to persistent chromatin compaction. The MNase assay thus serves as a functional readout of nucleosome accessibility and supports the hypothesis that unresolved DPCs in SPRTN-deficient cells hinder chromatin remodelling and accessibility during DNA damage recovery.

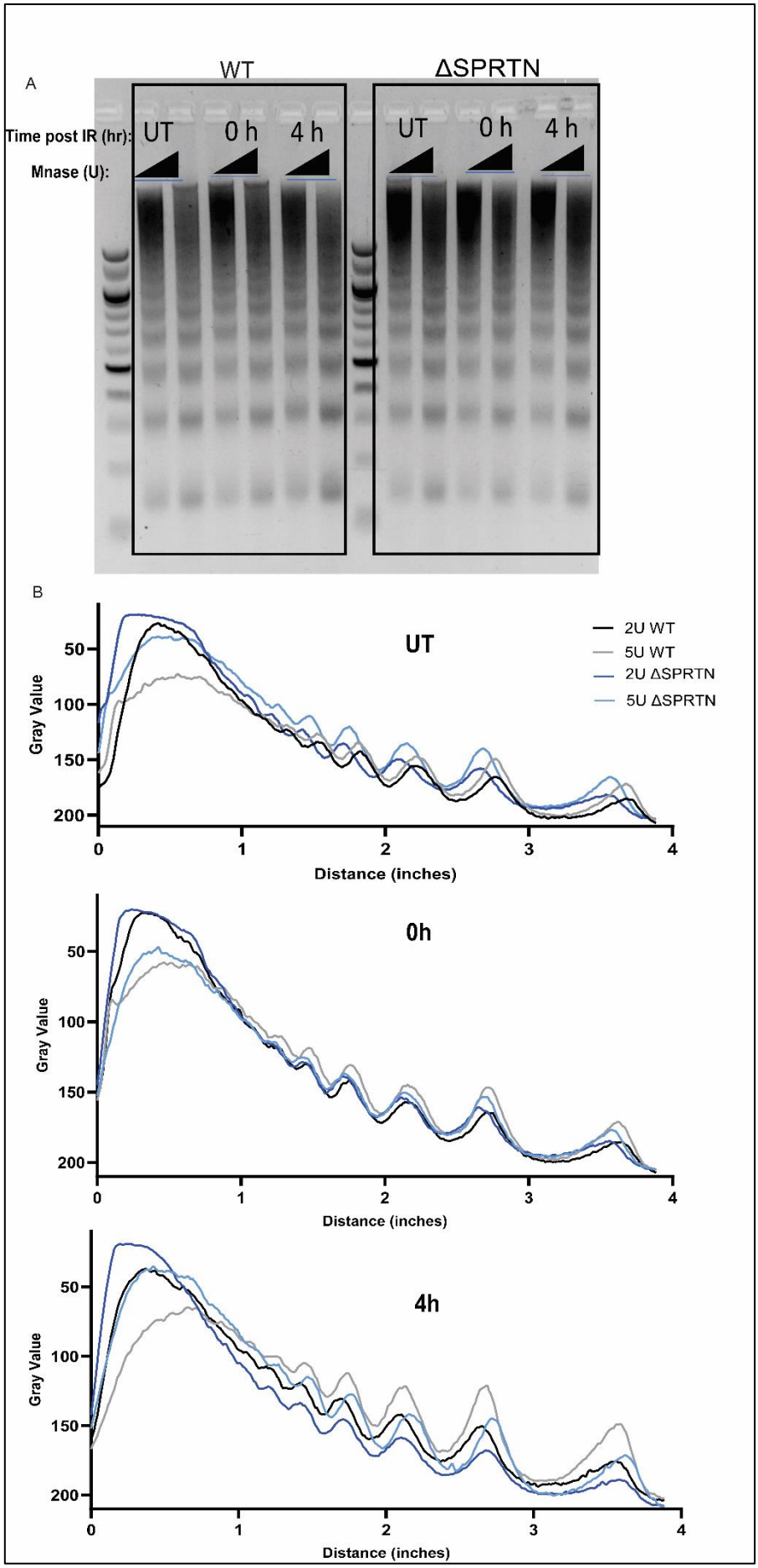

A
WT
ΔSPRTN
Time post IR (hr):
UT
0 h
4 h
UT
0 h
4 h
Mnase (U):
B
UT
2U WT
5U WT
2U ΔSPRTN
5U ΔSPRTN
Gray Value
50
100
150
200
0
1
2
3
4
Distance (inches)
0h
Gray Value
Distance (inches)
4h
Gray Value
Distance (inches)

Figure 7.14. SPRTN deficiency promotes chromatin compaction under basal and post-irradiation conditions, as revealed by MNase digestion and densitometry profiling.

(A) Micrococcal nuclease (MNase) digestion assay of chromatin isolated from wild-type (WT) and SPRTN-knockout (ΔSPRTN) HeLa cells, either untreated (UT) or harvested at 0 and 4 hours after 10 Gy ionising radiation (IR). Increasing MNase concentrations (2 U and 5 U) were applied to probe chromatin accessibility. DNA was resolved on an agarose gel, with higher-order nucleosomal bands indicating greater chromatin compaction.

(B) Densitometry profiles of MNase-digested DNA were plotted as grey value intensity across migration distance (inches). For each condition (UT, 0 h, 4 h), DNA fragmentation in WT (black and grey lines) is contrasted with ΔSPRTN (navy and blue lines). In all conditions, ΔSPRTN chromatin showed reduced MNase sensitivity, indicated by shallower curves and diminished nucleosome band resolution, consistent with increased chromatin compaction. These effects were most pronounced after IR exposure, further supporting a role for SPRTN in maintaining chromatin plasticity during the DNA damage response.

7.1.7 HDAC Inhibition and Knockdown of chromatin compaction regulators Reverses Radioresistance in SPRTN-Deficient HeLa Cells

To directly investigate whether the enhanced radioresistance observed in SPRTN-deficient cells is mediated by increased chromatin compaction, we sought to pharmacologically relax chromatin and assess its impact on radiation sensitivity using CFA. Chromatin structure is dynamically regulated by the balance between histone acetylation and deacetylation. Histone acetyltransferases (HATs) catalyse the addition of acetyl groups to lysine residues on histone tails, promoting a relaxed chromatin conformation that facilitates transcription and accessibility. In contrast, histone deacetylases (HDACs) remove these acetyl groups, leading to chromatin condensation. There are four classes of HDAC that are summarized in Table 7.1. HDAC inhibitors (HDACi) antagonise this process, increasing histone acetylation and inducing chromatin decompaction (Figure 7.15 A).

Table 7.2 Summary of the different HDAC (histone deacetylase) classes. Adapted from *(Antrobus & Parsons, 2022)*

HDAC Class	Members	Localization	Cellular targets
Class I	HDAC1, HDAC2, HDAC3, HDAC8	Mainly nuclear	Histones (H3, H4), p53, Rb, Ku70, STAT3
Class IIa	HDAC4, HDAC5, HDAC7, HDAC9	Nucleus ↔ cytoplasm shuttling	MEF2 transcription factors, Runx2, HDAC3 (as a co-repressor), SMADs
Class IIb	HDAC6, HDAC10	Mainly cytoplasmic	α-tubulin, HSP90, cortactin, peroxiredoxins, tau
Class III	SIRT1–SIRT7 (sirtuins)	Nuclear, cytoplasmic, mitochondrial	p53, FOXO, NF-κB, H3K9ac, H4K16ac, HSP70, mitochondrial proteins
Class IV	HDAC11	Nuclear and cytoplasmic	p53, cell cycle progression, glycolysis

We initially treated cells with Panobinostat, a potent pan-HDAC inhibitor that targets multiple HDAC classes (I, II, and IV). As shown in Figure 17.15 B, Panobinostat significantly sensitised ΔSPRTN cells to ionising radiation, reducing their clonogenic survival to levels lower than wild-type controls. SPRTN-deficient cells exhibit a modest survival advantage over WT, although the magnitude of radioresistance appears limited in this experiment. The ΔSPRTN+Panobinostat group trends toward lower survival, suggesting HDAC inhibition reversed the radioresistant phenotype. The limited resistance observed may reflect experimental variability. However, due to Panobinostat's broad inhibitory spectrum- which may affect cell cycle regulators and other non-chromatin-related processes- we further tested Trichostatin A (TSA), a more selective HDAC inhibitor that primarily targets class I and II HDACs, sparing class IV.

Treatment with TSA similarly restored radiosensitivity in SPRTN-deficient cells, as evidenced by the decreased survival following irradiation (Figure 17.15 C). Here, SPRTN-deficient cells demonstrate a more pronounced survival advantage at 2 and 4 Gy compared to WT cells, but then the cells are more sensitive when treated with TSA. Importantly, TSA is less likely to disrupt cell cycle progression compared to broader-spectrum inhibitors, allowing us to more specifically interrogate the role of chromatin structure in modulating the radiation response.

These results support the hypothesis that chromatin compaction contributes to the radioresistant phenotype of SPRTN-deficient cells. Pharmacologically relaxing chromatin using HDAC inhibition is sufficient to reverse this phenotype, underscoring the functional relevance of chromatin accessibility in DNA damage response signalling and cell survival.

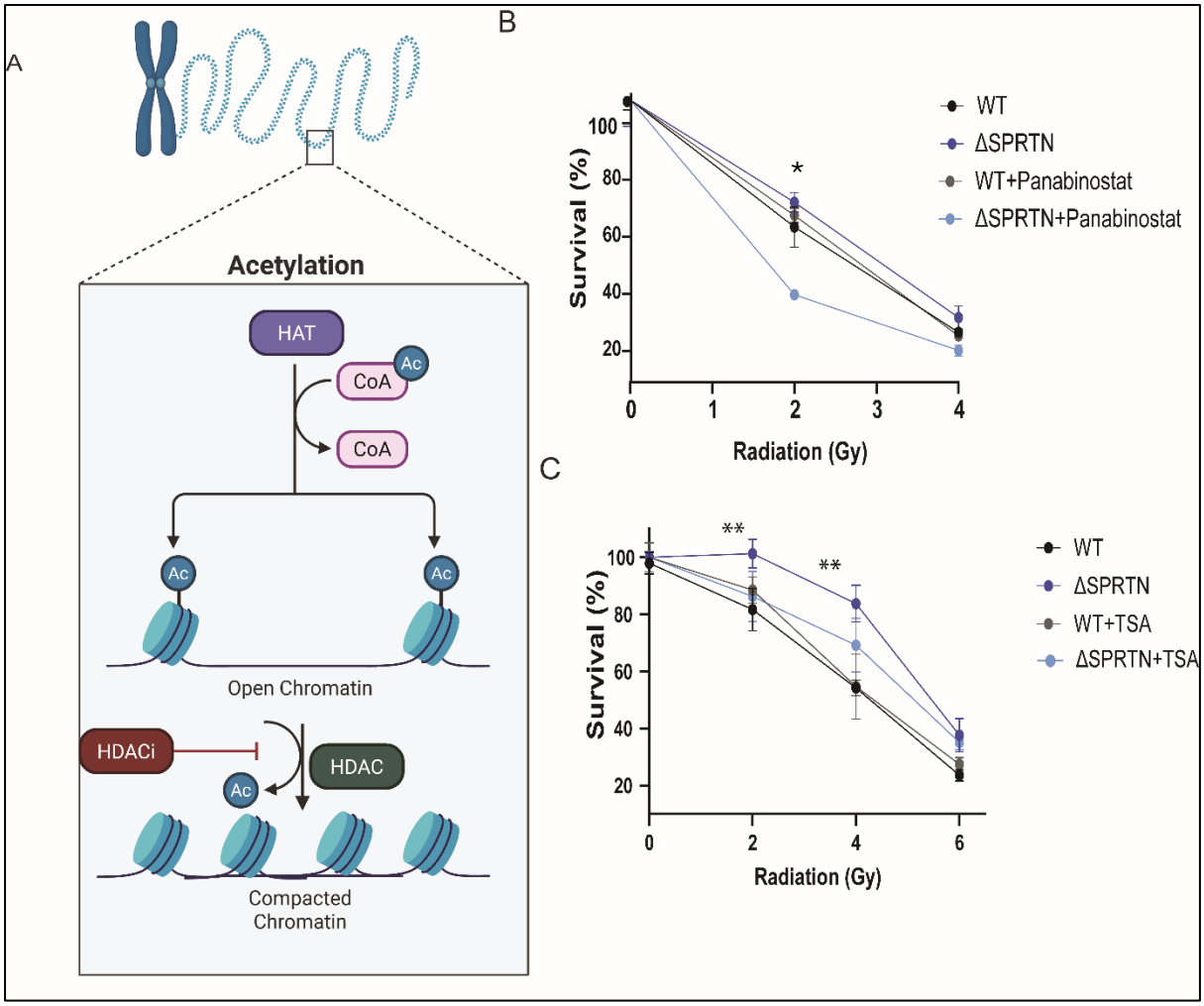


Figure 7.15. HDAC inhibition reverses the radioresistance phenotype of SPRTN-deficient cells.

(A) Schematic of histone acetylation regulation and its impact on chromatin architecture. Histone acetyltransferases (HATs) catalyse acetylation (Ac) of lysine residues on histone tails, promoting open, transcriptionally permissive chromatin. Histone deacetylases (HDACs) remove acetyl groups, resulting in chromatin compaction. HDAC inhibitors (HDACi), such as TSA and Panobinostat, prevent deacetylation and maintain open chromatin.

(B) Clonogenic survival assay showing the effect of Panobinostat treatment (10 nM) on wild-type (WT) and SPRTN-knockout (ΔSPRTN) cells exposed to increasing doses of ionising radiation (IR). ΔSPRTN cells showed enhanced sensitivity to radiation upon Panobinostat treatment, with survival levels reduced to those of WT cells.

(C) Clonogenic survival of WT and ΔSPRTN cells treated with the HDAC inhibitor trichostatin A (TSA, 100 nM) before IR. TSA treatment sensitised ΔSPRTN cells to radiation, reversing their radioresistance and reducing their survival to WT levels, particularly at 2 and 4 Gy. Data represent means ± SEM from 3 experiments. Statistical significance was calculated using unpaired t-test.* $p < 0.05$, ** $p < 0.01$.

To further dissect the contribution of chromatin compaction to the radioresistant phenotype observed in SPRTN-deficient cells, we investigated whether targeted depletion of specific chromatin-compacting factors could reverse this effect. Previous analyses revealed that histone H1.2 and heterochromatin protein 1 (HP1) were both upregulated in SPRTN-depleted cells (Figures 7.8 and 7.7), implicating them as potential mediators of chromatin structural changes. Histone H1.2, a linker histone variant, promotes higher-order chromatin folding by stabilizing the entry and exit angles of DNA on nucleosomes, thereby limiting DNA accessibility. HP1 proteins, on the other hand, bind to trimethylated H3K9 and facilitate the spreading and maintenance of heterochromatin.

To functionally assess their role, we employed siRNA-mediated knockdown of H1.2 and HP1 in both wild-type and ΔSPRTN HeLa cells and evaluated the impact on radiation sensitivity using cell viability and clonogenic survival assays. Knockdown of H1.2 significantly sensitised SPRTN-deficient cells to ionising radiation (Figure 7.16 A), suggesting that H1.2 contributes to the chromatin compaction and associated radioresistance observed in these cells. Similarly, depletion of HP1 markedly enhanced radiosensitivity in ΔSPRTN cells compared to control knockdowns (Figure 7.16 B), consistent with a model in which HP1-mediated heterochromatin formation is functionally relevant to the survival advantage conferred by SPRTN loss.

To probe the upstream regulation of heterochromatin maintenance, we next targeted SUV39H1, a histone methyltransferase responsible for the trimethylation of H3K9, the key histone mark recognized by HP1. SUV39H1-mediated H3K9me3 is a central feature of constitutive heterochromatin and is critical for compact chromatin

architecture. Knockdown of SUV39H1 led to a significant increase in radiation sensitivity in both control and SPRTN-deficient cells, with a pronounced effect in the ΔSPRTN context (Figure 7.17). These findings support a hierarchical model in which SUV39H1, by establishing H3K9me3, promotes HP1 recruitment and heterochromatin compaction, thereby facilitating the radioresistant phenotype in SPRTN-deficient cells.

Together, these experiments could provide functional evidence that chromatin compaction, mediated through specific architectural proteins and histone-modifying enzymes, underpins the radiation resistance associated with SPRTN loss at least in HeLa. Disruption of these pathways is sufficient to restore radiosensitivity, underscoring the importance of chromatin state in modulating the DNA damage response.

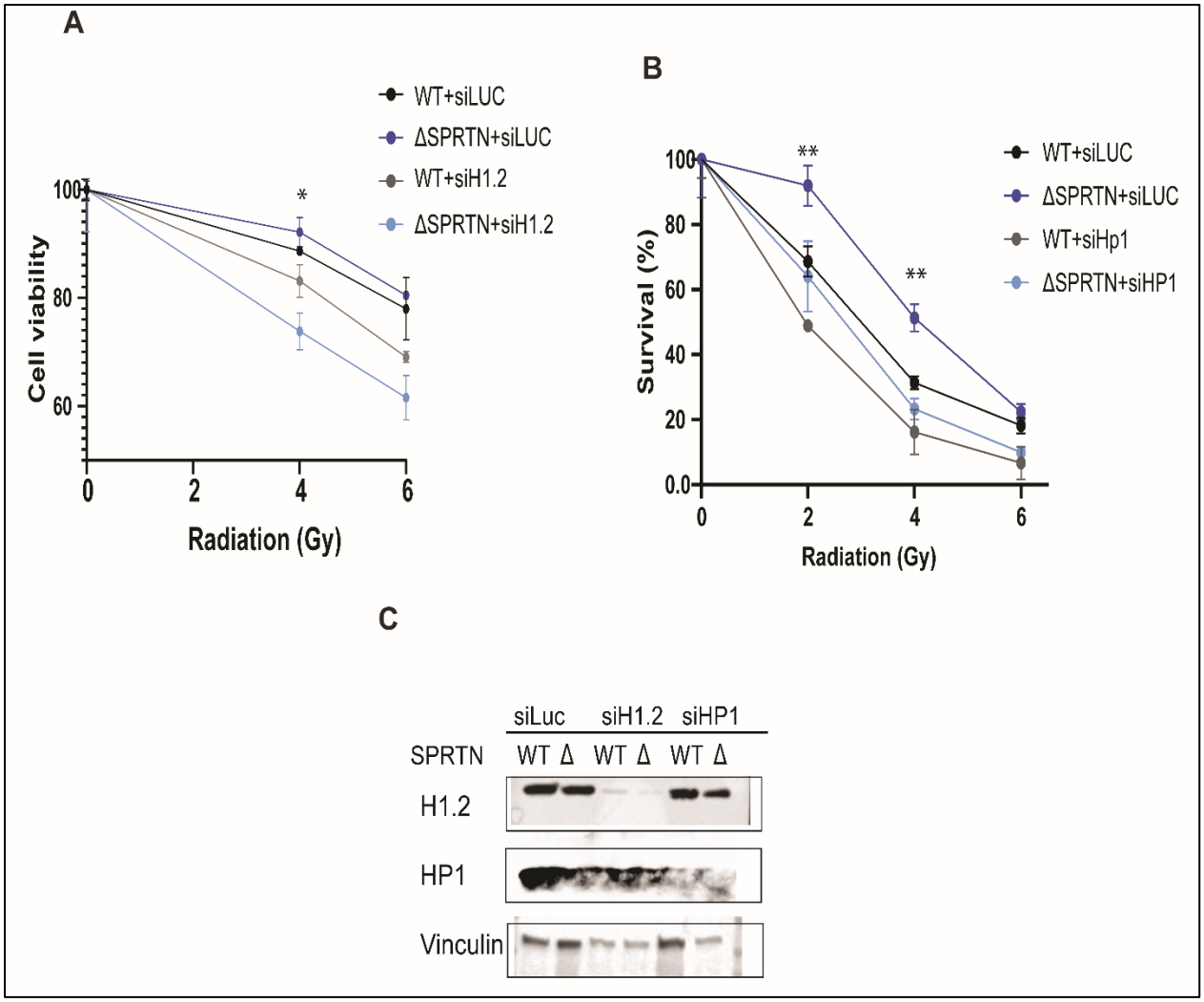


Figure 7.16. Knockdown of chromatin compaction regulators restores radiosensitivity in SPRTN-deficient cells.

(A) Cell viability following exposure to ionising radiation (0–6 Gy) in wild-type (WT) and SPRTN-deficient (ΔSPRTN) cells transfected with siRNA against H1.2 (siH1.2) or a control luciferase siRNA (siLUC). ΔSPRTN cells exhibited increased viability post-irradiation compared to WT, which was reduced upon H1.2 knockdown. * $p < 0.05$.

(B) Clonogenic survival assay in WT and ΔSPRTN cells treated with siRNA targeting HP1 (siHP1) or control (siLUC). Silencing HP1 significantly decreased survival in ΔSPRTN cells, restoring sensitivity to levels comparable with WT cells. Data represent means ± SEM from 3 experiments. Statistical significance was calculated using unpaired t-test. **$p < 0.01$.

(C) Immunoblot analysis confirming effective knockdown of HP1 and H1.2 proteins in ΔSPRTN cells. Tubulin served as a loading control.

These results support the role of H1.2 and HP1 in maintaining the compact chromatin state that underlies the radioresistant phenotype of SPRTN-deficient cells. Disruption of this compaction re-sensitises the cells to IR-induced damage.

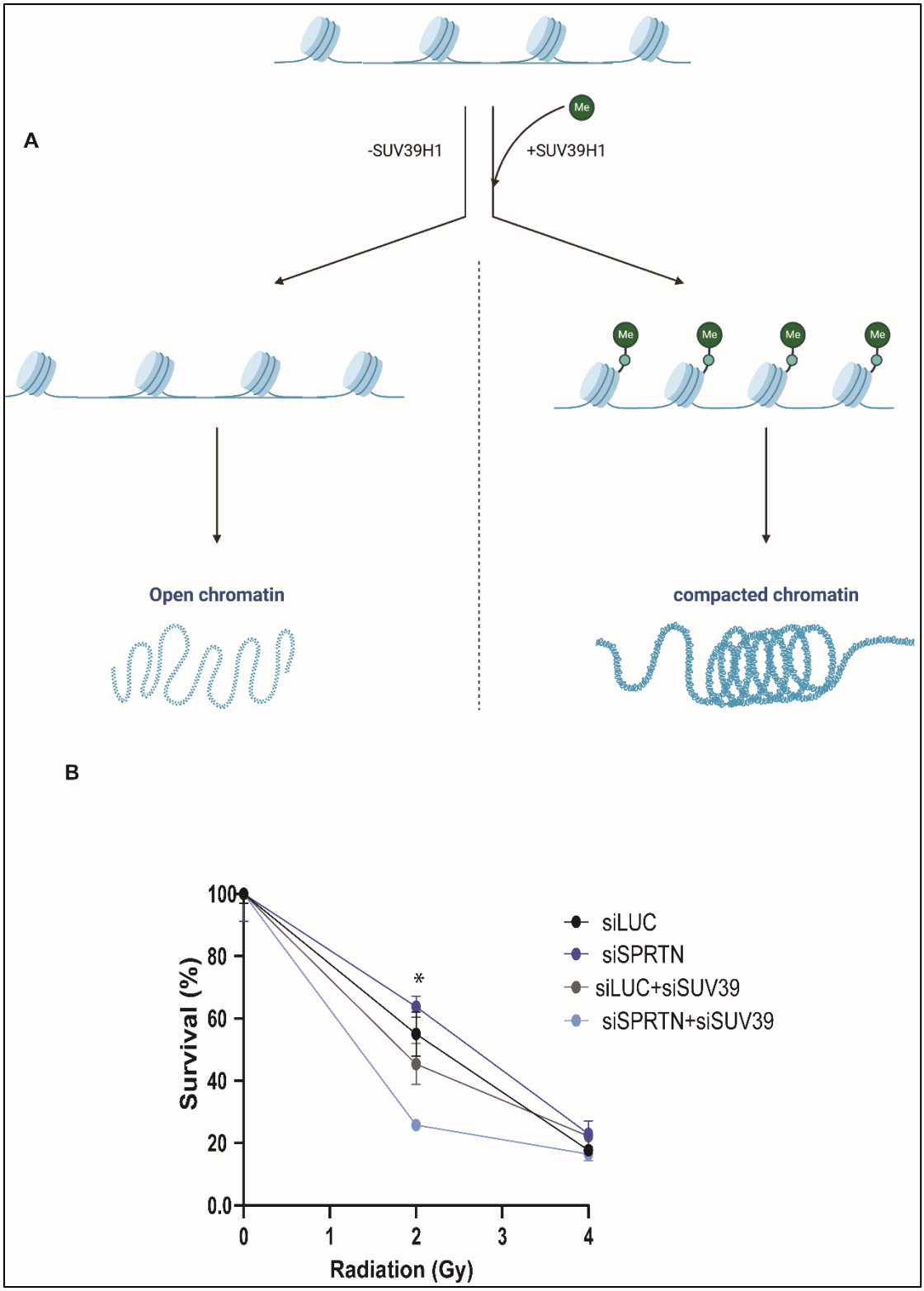

A
-SUV39H1
+SUV39H1
Me
Me
Me
Me
Me
Open chromatin
compacted chromatin
B
Survival (%)
100
80
60
40
20
0.0
0
1
2
3
4
Radiation (Gy)
*
siLUC
siSPRTN
siLUC+siSUV39
siSPRTN+siSUV39

Figure 7.17. Knockdown of SUV39H1 restores radiosensitivity in SPRTN-deficient cells by reducing chromatin compaction.

(A) Schematic model depicting the role of SUV39H1 in chromatin regulation. SUV39H1 catalyzes the trimethylation of histone H3 lysine 9 (H3K9me3), a hallmark of heterochromatin. Loss of SUV39H1 activity results in reduced H3K9me3 and more relaxed (euchromatic) chromatin, whereas active SUV39H1 promotes compact chromatin via dense H3K9me3 deposition.

(B) Clonogenic survival of cells transfected with siRNA against SPRTN (siSPRTN), SUV39H1 (siSUV39), or both, after increasing doses of ionizing radiation (IR). While SPRTN-deficient (siSPRTN) cells showed enhanced survival, co-depletion with SUV39H1 (siSPRTN+siSUV39) significantly reduced survival, indicating that SUV39H1-mediated compaction contributes to the radioresistance phenotype. Data represent means ± SEM from 3 experiments. Statistical significance was calculated using unpaired t-test. * $p < 0.05$.

To determine whether the chromatin compaction observed in SPRTN-deficient cells contributes to impaired execution of apoptosis following genotoxic stress, we quantified Caspase 3/7 activity under various conditions. Caspase 3 and Caspase 7 are crucial effector enzymes in the intrinsic apoptotic pathway, and their activation is often used as a proxy for effective apoptotic progression. Given that SPRTN-depleted cells exhibit persistent DPCs, increased heterochromatin-associated marks, and attenuated DDR signalling, we hypothesised that the radioresistant phenotype may stem from suppressed apoptotic signalling downstream of chromatin alterations.

As shown in Figure 9G, untreated ΔSPRTN cells exposed to 6 Gy of IR exhibited a marked reduction in Caspase 3/7 activity compared to wild-type (WT) controls, consistent with a defective apoptotic response. This observation is in line with our earlier findings of reduced γH2AX foci and altered checkpoint signalling in these cells. Interestingly, pharmacological treatment of ΔSPRTN cells with the histone deacetylase inhibitor (HDACi) Trichostatin A (TSA) significantly restored Caspase 3/7 activation levels post-IR. (Figure 7.18 A) The TSA treatment alone had a minimal effect in WT cells, indicating that HDAC inhibition specifically alleviates the apoptotic defect associated with SPRTN loss.

To further validate that chromatin compaction is causally linked to suppressed apoptosis, we genetically depleted H1.2, a linker histone upregulated in SPRTN-deficient cells and associated with transcriptional repression and chromatin condensation. As shown in Figure 7.18 B, knockdown of H1.2 similarly restored Caspase 3/7 activity in ΔSPRTN cells to near wild-type levels. While H1.2 depletion in WT cells led to a modest increase in caspase activity, the effect was significantly more pronounced in ΔSPRTN cells, highlighting a synergistic role of SPRTN loss and H1.2 upregulation in suppressing apoptosis.

Together, these results support the hypothesis that chromatin compaction mediated by histone deacetylation and linker histone H1.2 contributes to the radioresistance observed in SPRTN-deficient HeLa cells. Restoration of apoptotic activity through HDAC inhibition or H1.2 depletion demonstrates that chromatin architecture is a critical determinant of the cell's ability to respond to DNA damage with programmed cell death. These findings not only strengthen the mechanistic link between SPRTN, chromatin state, and DDR execution but also suggest potential therapeutic strategies to overcome radioresistance in contexts where SPRTN function is compromised.

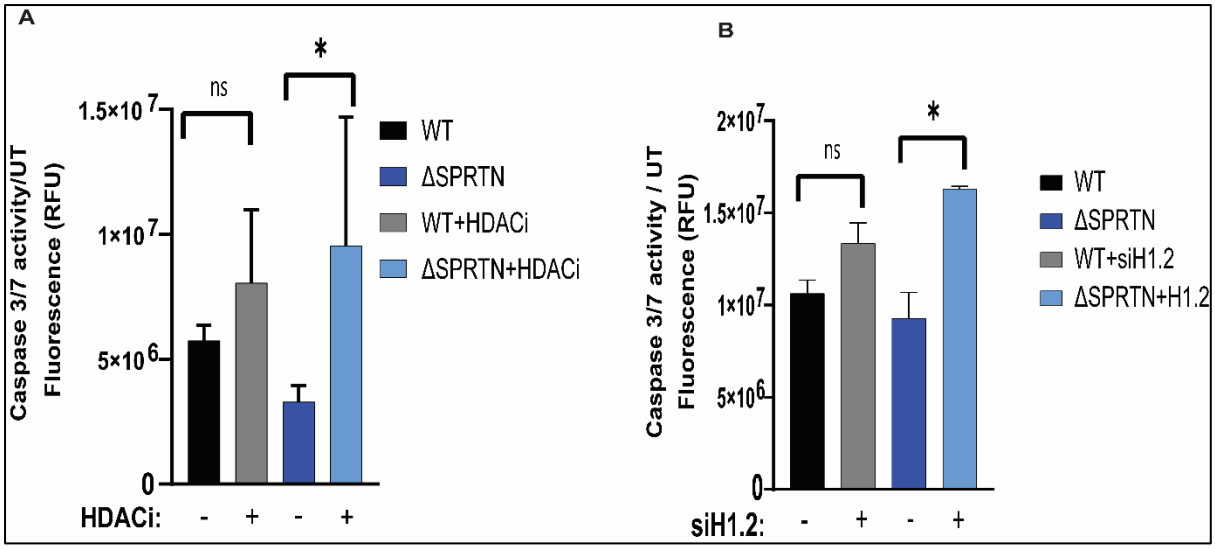


Figure 7.18. Chromatin relaxation restores apoptotic signalling in SPRTN-deficient cells.

(A) Caspase 3/7 activity measured in WT and ΔSPRTN cells following treatment with or without HDAC inhibitor (HDACi, 400 nM overnight). While SPRTN-deficient cells showed reduced caspase activity compared to WT, HDACi treatment significantly increased caspase 3/7 activation in ΔSPRTN cells, indicating restored apoptotic signalling upon chromatin decondensation.

(B) Caspase 3/7 activity in WT and ΔSPRTN cells transfected with control or H1.2-targeting siRNA. Silencing of H1.2, a linker histone that promotes chromatin compaction, significantly enhanced caspase 3/7 activity in ΔSPRTN cells, further supporting the role of chromatin compaction in suppressing apoptosis in the absence of SPRTN. Data represent means ± SEM from 3 experiments. Statistical significance was calculated using unpaired t-test: ns: not significant, * $p < 0.05$.

7.2 Discussion

Our investigation reveals that loss of the DPC protease SPRTN leads to a profound reorganisation of chromatin architecture, favouring a compact, transcriptionally repressive state. SPRTN depletion resulted in consistently elevated levels of heterochromatin markers such as H3K9me3 and linker histone H1.2, accompanied by a reduction in euchromatin-associated modifications, including H3K9ac and H3K4me3, specifically in HeLa. This phenotype was observed both under basal conditions and following exposure to IR, suggesting a defect in chromatin remodelling that is normally required during the DDR.

Functionally, this condensed chromatin state correlated with: (1) reduced DNA damage signalling despite DNA damage, (2) diminished Caspase 3/7 activity post-IR, and (3) enhanced survival in clonogenic assays. MNase digestion assays confirmed increased nucleosomal protection in SPRTN-deficient chromatin, indicating a global reduction in accessibility. In contrast, pharmacological or genetic interventions that reversed chromatin compaction, such as HDAC inhibition or knockdown of HP1, H1.2, or SUV39H1, restored radiosensitivity and checkpoint activation. Together, these findings demonstrate that SPRTN deficiency induces a functional chromatin state that attenuates DDR signalling and promotes survival following genotoxic stress in cell line studied.

7.2.1 DPCs accumulation Could Affect Chromatin structure

Interestingly, here we showed that formaldehyde-treated wild-type cells, used to mimic DPCs independently of SPRTN, partially recapitulated this phenotype. Unrepaired DPCs can have profound effects on chromatin architecture. Formaldehyde fixation provides an extreme illustration – it induces widespread DPCs that “lock” chromatin in

a rigid, condensed state. By analogy, the persistent DPCs in SPRTN-deficient cells likely tether DNA and nucleoproteins, promoting a compaction of chromatin. DNA replication, transcription, and repair all rely on the dynamic regulation of chromatin structure. This regulation is mediated by reversible, non-covalent interactions between DNA and histone proteins, which allow chromatin to transition between open (euchromatic) and closed (heterochromatic) states. This arises especially from DNA-histone crosslinks (DHCs) disrupt this plasticity by locking chromatin into a rigid conformation, thereby impairing its functional flexibility (Pachva et al., 2020).

Although more experiments are needed to confirm this conclusion, DPCs could directly interfere with histone post-translational modifications that maintain open, transcriptionally active chromatin. In particular, DPC formation is linked to a loss of active histone marks like H3K9ac and H3K4me3. Mechanistically, agents such as formaldehyde can covalently attach to lysine residues on histone tails, blocking those sites from acetylation by histone acetyltransferases (Leso et al., 2020). For example, formaldehyde-treated lung epithelial cells show a dramatic reduction in H3K14ac within minutes, an effect abolished if histones are pre-acetylated (i.e., protected) prior to DPC induction. This chemical blocking of lysines prevents normal acetylation and immediately favours chromatin compaction, since unacetylated histone tails carry positive charges that tighten DNA–histone interactions (Yoshida & Ibuki, 2014). Indeed, formaldehyde-adducted histone H3 is improperly incorporated into chromatin, leading to aberrant chromatin assembly and compaction with widespread transcriptional dysregulation. DPC agents like formaldehyde cause a pronounced deubiquitination of H2B on chromatin, which in turn would impair H3K4 methylation maintenance. Thus, as DPCs accumulate, active marks are erased or occluded: compacted chromatin can “lock in” silencing by recruiting silencer proteins that further purge activating marks.

Bidirectional feedback exists between compaction and histone modifications: once chromatin condenses and HP1/silencer complexes bind, they actively remove remaining H3K9ac/H3K4me3, which drives even further compaction (Movilla Miangolarra et al., 2024). This self-reinforcing loop ensures that regions harbouring persistent DPC lesions become heterochromatic, with low H3K9ac/H3K4me3 and enrichment of repressive marks, effectively dampening local gene activity.

Moreover, certain DNA-damaging chemotherapeutics that trap protein–DNA complexes show analogous chromatin changes. CPT, which stabilizes Topoisomerase I, DNA cleavage complexes (a form of DPC), triggers chromatin alterations that favour compaction. In yeast, for example, hypoacetylation at histone H4 lysine 16 – a key mark of open chromatin – was found to increase cellular sensitivity to CPT, whereas forcing H4K16 acetylation confers resistance. This implies that CPT-induced DPCs provoke histone deacetylation (notably H4K16ac loss) to condense chromatin, exacerbating replication stress toxicity (Puddu et al., 2017). More generally, DNA crosslinking agents often cooperate with epigenetic changes. For instance, combining cisplatin with a DNA demethylating agent or HDAC inhibitor in cancer cells was shown to suppress H3K4me3 and H3K9me3 marks, indicating that crosslink damage and chromatin-modifying treatments together push the epigenome toward a “silent” configuration (Meng et al., 2013). In summary, diverse DPC-inducing agents tend to decrease active histone marks and can increase repressive marks like H3K9me3/HP1α, especially if cells cannot properly mount chromatin-relaxing countermeasures. This has been observed in multiple cell lines and systems, underlining the generality of DPC-driven chromatin compaction

7.2.2 Chromatin compaction and radioresistance

The radioresistance phenotype that we have seen in SPRTN-depleted HeLa cells could be explained by the heterochromatin formation. Several studies have demonstrated that compact heterochromatin can enhance cancer cell survival under ionizing radiation. Dense chromatin structure is thought to act as a physical and biochemical shield that reduces DNA damage and modulates repair kinetics. For example, Storch *et al*. (2010) showed that breast cancer cells grown in 3D culture (mimicking tumour architecture) develop increased levels of heterochromatin – marked by histone H3 deacetylation and elevated HP1α – which correlated with significantly higher survival after X-ray exposure and fewer DNA DSBs compared to 2D-cultured cells (Storch et al., 2010). In these 3D cells, radiation-induced DSBs were distributed equally between euchromatin and heterochromatin, whereas in standard 2D cells, a majority of breaks occurred in euchromatin, indicating that an expanded heterochromatic compartment can reduce the effective damage load. Crucially, disrupting this compact state sensitized the cells: depletion of histone deacetylases (HDAC1/2/4) or treatment with a pan-HDAC inhibitor caused chromatin decondensation and led to higher DSB counts and radiosensitivity (Storch et al., 2010). These findings established histone deacetylation (an enzymatic driver of chromatin compaction) as a key mediator of radioresistance and suggested that heterochromatin provides a protective effect against gamma/X-ray irradiation.

Consistent with this, Wang *et al*. (2017) reported that cancer cells surviving repeated γ-ray exposures undergo heritable chromatin remodeling that enhances radioresistance. They showed that progeny of γ-irradiated cell populations exhibit markedly elevated HDAC activity and H3K9me3 levels, forming abundant heterochromatin domains (enriched in the H3K9me3-HP1α repressive mark) relative to unirradiated controls (P. Wang et al., 2017). This epigenetic shift was absent in cells

exposed to high-LET α-particle radiation, indicating an LET-dependent mechanism where low-LET X/γ-rays specifically induce heterochromatin accumulation and adaptive radioresistance. Notably, inhibiting HDACs with suberoylanilide hydroxamic acid (SAHA) reversed these effects: SAHA-treated progeny showed reduced H3K9me3 and HP1α levels alongside increased histone acetylation, and this abolished their radioresistant phenotype, equalizing radiosensitivity to control levels. Thus, HDAC-driven chromatin compaction (via H3K9 methylation and HP1α recruitment) was identified as a causal mechanism of acquired radioresistance, reversible by epigenetic therapy.

Broader correlative studies further support the link between heterochromatin and survival under irradiation. Sato *et al*. (2014) generated X-ray–resistant cancer cell subclones by repeated irradiation and found that these resistant cells harboured significantly higher numbers of HP1-stained heterochromatin foci in their nuclei. (Sato et al., 2014). Similarly, a recent transcriptomic profiling by Chan *et al*. (2024) identified upregulation of BAHD1 – a heterochromatin-promoting factor – as a signature of radioresistant prostate and head/neck cancer models, alongside global increases in H3K9me3 and H3K27me3 repressive marks (Beh et al., 2024). Strikingly, knockdown of BAHD1 in those models led to a preferential loss of H3K9me3/H3K27me3 in the radioresistant cells and reversed their radioresistance in clonogenic survival assays. BAHD1 depletion also impaired DSB repair efficiency, underscoring that the BAHD1-heterochromatin axis actively facilitates DNA damage management. In patient tumour data, high heterochromatin activity (e.g., higher H3K9/27 methylation) was associated with poorer radiotherapy outcomes. Together, these studies robustly implicate heterochromatin enrichment (via H3K9/H3K27 methylation and HP1) as an important mechanism of intrinsic and acquired radioresistance in cancer. Moreover, chromatin-

modifying enzymes like SUV39H1 (which tri-methylates H3K9 to seed HP1-binding sites) appear to play a central role in this process. Indeed, enhancing SUV39H1 stability through SIRT1-mediated deacetylation has been linked to increased genomic protection after IR exposure, whereas conversely, radiation-induced loss of SUV39H1 can provoke heterochromatin relaxation and premature senescence (Bosch-Presegué et al., 2011). These observations highlight that maintaining a compact chromatin state helps cancer cells tolerate DNA damage stress, although this same compaction must be carefully modulated (and temporarily relaxed by DDR kinases like ATM) to allow effective DNA repair when breaks do occur.

7.2.3 Chromatin compaction affects DDR:

The idea that compact chromatin impairs DDR signalling is supported by mechanistic studies in developmental and somatic systems. A recent study by Wang *et al.* (2022) demonstrated a similar effect in a transgenerational context: DSBs carried in the paternal germline (which is tightly compacted by protamines and histones) largely escaped the normal checkpoint surveillance in the early embryo (S. Wang et al., 2022). As a result, many embryos developed despite harbouring paternal DNA damage, indicating attenuated activation of damage checkpoints. However, this short-term tolerance came at a cost – the damage persisted and led to genomic instability (chromosome bridges, aneuploidy) in subsequent cell divisions. They showed that inducing chromatin relaxation, by inhibiting HDACs or by depleting heterochromatin protein 1, could rescue the checkpoint signalling and restore efficient HR repair in those compacted conditions. This aligns with our observation, when we experimentally relaxed chromatin (e.g., with a histone deacetylase inhibitor), we saw partial restoration of radiosensitivity. Therefore, the mechanistic link emerges: DPC-induced chromatin compaction in SPRTN-deficient cells acts as a physical and biochemical

barrier to DDR activation, leading to suboptimal checkpoint signalling and a bias against error-free HR repair (with repair likely shunted toward alternative, less efficient pathways or delayed altogether) (S. Wang et al., 2022). This resulted in improved offspring viability, underscoring that the heterochromatin state was directly responsible for suppressing checkpoint signalling and accurate DSB repair.

In addition, tightly compacted chromatin can impair the detection and signalling of DNA damage, as well as the efficient repair of DSBs. There is strong evidence that heterochromatin (dense, compact chromatin) poses a barrier to the DNA damage signalling cascade. In compact chromatin regions, the activation and spread of γH2AX (phosphorylated H2AX) foci are often attenuated or delayed, and recruitment of repair proteins is hindered. For instance, heterochromatic DSBs are repaired more slowly than euchromatic DSBs, and a subset of breaks requires the ATM kinase for efficient repair specifically because of the chromatin context (Goodarzi et al., 2008). Goodarzi and colleagues showed that only ~25% of IR-induced breaks depend on ATM for repair, and these were enriched in heterochromatin, implying that compacted chromatin normally resists DSB processing. ATM's role here is to phosphorylate the chromatin regulator KAP1, a factor that maintains heterochromatin; this phosphorylation event relaxes the local chromatin structure and lifts the barrier to repair in otherwise inflexible chromatin. Consistently, knockdown of KAP1 or heterochromatin-forming proteins (like HP1 or certain HDACs) can rescue the repair defect in ATM-deficient cells by artificially relaxing chromatin (Goodarzi et al., 2008). Thus, compact chromatin clearly dampens DDR signalling – full activation of checkpoints (ATM/ATR signalling and their effectors like CHK1) is harder to achieve when DNA is buried in densely packed nucleosomes. Murga et al. (2007) similarly reported that when chromatin is not properly opened, the DNA damage checkpoint is

only weakly activated, underscoring that checkpoint kinase signalling is blunted in a compacted chromatin environment (Murga et al., 2007). In SPRTN-deficient cells, we observed exactly this phenomenon despite the presence of DNA damage (from IR or replication stress); checkpoint signalling (as measured by multiple DNA damage signalling) was comparatively suppressed. One plausible explanation is that the DPC-induced chromatin compaction limits the recruitment or activation of sensor kinases at damage sites. If lesions are concealed in tight chromatin, proteins like ATM, ATR, or the MRN complex might access them less efficiently, resulting in fewer γH2AX foci and reduced downstream signalling such as CHK1 activation.

In summary, our investigation reveals that SPRTN deficiency not only compromises DPC repair but also profoundly alters the chromatin landscape, shifting it towards a compact, transcriptionally repressive state at least in HeLa cells. This chromatin reorganisation impairs both the detection and signalling of DNA damage, as well as the activation of canonical checkpoint responses. Mechanistically, we demonstrate that unresolved DPCs, either genetically induced via SPRTN loss or chemically mimicked with formaldehyde, are sufficient to promote the loss of active histone marks and enforce a heterochromatic architecture. Functionally, this results in diminished DDR activation and increased cellular survival following ionising radiation, a phenotype that is reversible upon chromatin relaxation. Our data support a model in which chromatin compaction serves as a double-edged sword, suppressing both DNA damage signalling and repair, but tipping the balance toward short-term survival under genotoxic stress. This mechanism aligns with existing cancer models of radioresistance and emphasizes the importance of chromatin state as a regulator of treatment outcomes. Taken together, our findings position SPRTN at the intersection

of DPC repair and epigenetic regulation, highlighting the critical role of chromatin architecture in modulating cellular responses to DNA damage.

Chapter 8 Concluding Discussion and Future Directions

SPRTN is a DNA-dependent metalloprotease essential for the repair of DPCs and thus for preserving genomic integrity. Cells or organisms lacking SPRTN (also known as Spartan/DVC1) exhibit hypersensitivity to classical DPC-inducing agents such as formaldehyde and cisplatin, which cause bulky protein adducts on DNA. This sensitivity aligns with SPRTN's established role in proteolytically removing protein obstacles from DNA. Paradoxically, however, we found that SPRTN-deficient cells (specifically HeLa) oppositely respond to IR – they are more radioresistant rather than radiosensitive. In other words, despite accumulating DNA damage, SPRTN-knockdown HeLa cells survived IR exposure better than their wild-type counterparts. This presents a compelling puzzle: why does loss of an important repair protease make cells less vulnerable to IR? Below, we discuss our key findings and propose explanations, integrating them with existing literature in a broader context.

In brief, multiple SPRTN-depleted cell lines that were investigated here showed attenuated DNA damage signalling in these cells: eg, IR-induced γH2AX foci were fewer and less intense, and activation of the ATR–CHK1 checkpoint pathway (as judged by CHK1 phosphorylation) was impaired in the absence of SPRTN. Although these cells showed a higher burden of DNA strand breaks, as evidenced by longer comet tails in comet assays, the activation of the DDR remained impaired. We then found that chromatin profiling revealed a globally compacted chromatin state in SPRTN-deficient cells. Heterochromatin-associated marks H3K9me3 and HP1α were elevated (along with an increase in linker histone H1.2), whereas euchromatin marks were comparatively reduced, indicating a shift toward a more repressive chromatin architecture. Functionally, this chromatin compaction appears linked to radioresistance: treating the SPRTN-deficient cells with chromatin-relaxing agents

(e.g. histone deacetylase inhibitors) or genetically reducing heterochromatin (for example, via lowering H3K9 methylation) restored their radiosensitivity to near wild-type levels. Together, these results suggest that SPRTN loss may triggers a protective mechanism via chromatin condensation, which in turn dampens DDR signalling and apoptosis after IR. We propose two, not mutually exclusive, mechanisms to explain how SPRTN-deficient cells achieve this IR resistance (specifically in HeLa): (1) enhanced heterochromatin shielding of DNA and checkpoint evasion, and (2) altered kinetics of DPC repair that prevent complex DNA damage.

8.1 Heterochromatin Formation in ΔSPRTN could Enable Escape from Apoptosis

One explanation for the improved survival of SPRTN-deficient cells is that their densely packed chromatin provides a physical shield against IR-induced damage and a roadblock to damage signalling. Heterochromatin is known to be less accessible to DNA-damaging free radicals. In fact, chromatin compaction protects DNA from radiation damage, in which tightly condensed chromatin yields significantly fewer DNA breaks upon IR compared to decondensed chromatin (Seane et al., 2024). The protective effect is attributed to both the abundance of DNA-bound proteins (which can act as radical scavengers) and the reduced water content in condensed chromatin domains, which together limit the generation and diffusion of hydroxyl radicals that cause DNA strand breaks (Seane et al., 2024). In line with this, IR-induced histone H2AX phosphorylation (γH2AX) is not uniform across the nucleus but occurs preferentially in euchromatic regions, with heterochromatic regions displaying markedly fewer γH2AX foci shortly after irradiation (Zheng et al., 2014). Notably, this is despite equal numbers of DSBs in heterochromatin, indicating that compacted DNA lesions often initially evade detection or signalling.

A key regulator of this process is the ATM kinase. Upon DNA damage, ATM phosphorylates the chromatin organizer KAP1 (TRIM28) at Ser-824, which causes local loosening of heterochromatin by reducing KAP1–HP1 binding (White et al., 2012). This relaxation is necessary to allow repair factors to access DSBs buried in heterochromatin. If chromatin fails to relax (for instance, in cells where ATM or KAP1 phosphorylation is impaired), DSBs in those regions persist unrepaired and checkpoint signalling remains attenuated. We propose that SPRTN-deficient cells, due to accumulated DPCs, experience a similar scenario of “constitutive heterochromatinization.” The unrepaired protein-DNA crosslinks could act as molecular staples that stabilize chromatin in a compact state, making it refractory to ATM-mediated relaxation. Consequently, when IR induces DSBs in these cells, the breaks reside in a chromatin context that is not readily amenable to signalling or repair. γH2AX foci and CHK1 activation are dampened, the G2/M checkpoint is compromised, and cells are less likely to undergo apoptosis or cell cycle arrest. In essence, the cells are partially blinding themselves to the damage. This allows continued cell survival in the short term, even though DNA lesions accumulate. In the context of SPRTN deficiency, the enhanced radioresistance we observe implies that, at least in the short term, the shielding effect caused by DPCs and heterochromatin outweighs the repair handicap. The compacted chromatin shields DNA ends from detection, enabling the cells to escape apoptosis triggered by extensive DNA damage. Our hypothesis aligns with prior observations that artificially increasing heterochromatin can suppress DDR signalling – for example, cells with experimentally induced heterochromatin show reduced IR-induced γH2AX and ATM signalling. Thus, SPRTN loss phenocopies this effect by promoting a heterochromatic, DDR-refractory genome state (Lorat et al., 2012; Lorković et al., 2017).

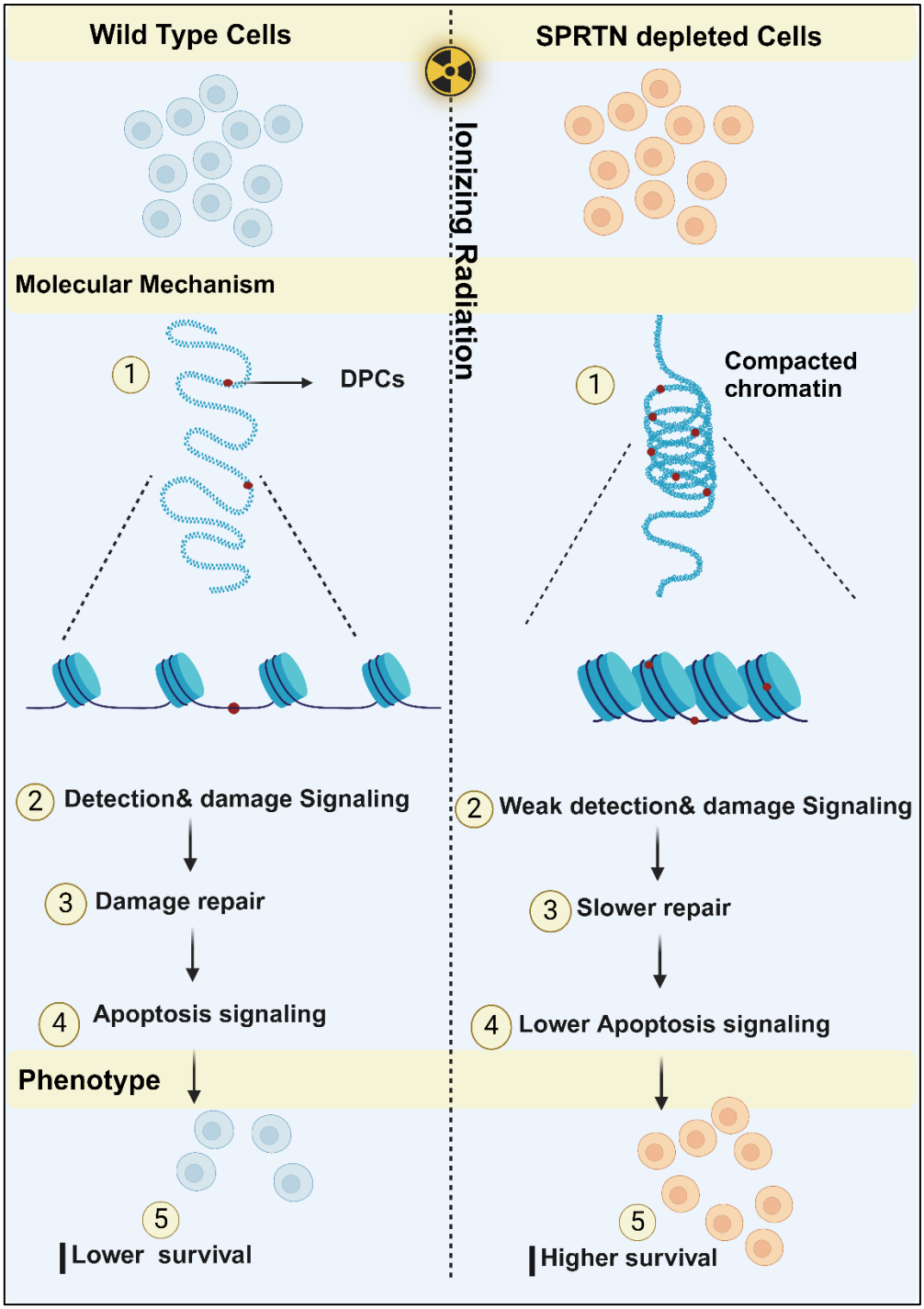


Figure 8.1. Model of the mechanism of radioresistance of SPRTN inactivated cells.

SPRTN-depleted cells are resistant to ionizing radiation due to the high chromatin compaction in these cells post-radiation. This limits the detection of DNA damage and thus the signal of apoptosis. This phenotype was rescued when relaxing the chromatin. This is mainly caused by SPRTN's function in DPC removal. Created using BioRender.com.

Interestingly, the cellular state in chronically hypoxic tumours shares striking similarities with cells lacking SPRTN. In SPRTN-deficient cells, we showed that endogenous DPCs persist, cells accumulate hallmarks of compacted chromatin and have defective damage checkpoint signalling. Analogously, hypoxic cells accumulate DPCs (especially after IR) and accumulate heterochromatin marks such as the linker histone-binding protein HP1BP3, which was identified as a hypoxia-induced "chromatin organizer." Under hypoxia, HP1BP3 mediates global chromatin condensation. Also in hypoxic cells, they are observed to develop mechanisms preventing H3K9/H3K27 demethylation and stabilizing H3K9 methyltransferases. In both contexts (SPRTN depletion and hypoxic cells), the DNA damage response is blunted: SPRTN-null cells show failure to fully activate ATR/CHK1 upon replication stress, and hypoxic cells likewise rely on an ATR-biased, incomplete DDR (Hammond et al., 2003; Casari et al., 2023). Moreover, hypoxic chromatin becomes largely inaccessible, mirroring the inaccessibility observed when DPC lesions block replisomes in SPRTN mutants. Functionally, these similarities produce parallel outcomes: SPRTN-deficient and hypoxic cells both exhibit resistance to further DNA damage. For instance, both contexts can display resistance to certain DNA-damaging drugs or altered sensitivity to radiation (since damage is shielded within dense chromatin and unrepaired adducts). This convergence implicates SPRTN and DPC clearance as critical safeguards under hypoxia.

Recent studies have shown that HDAC inhibitors (HDACi) can reverse this radioresistance. HDAC inhibitors work by increasing histone acetylation, which relaxes the chromatin structure, thereby restoring DNA repair pathways and making hypoxic tumour cells more susceptible to radiation. For instance, the use of vorinostat (an HDACi) in hypoxic glioblastoma cells has been shown to restore DDR signalling and

increase radiosensitivity by decompacting chromatin and enhancing the recruitment of DNA repair factors (Huang et al., 2016). Similarly, panobinostat, another HDACi, was found to enhance the efficiency of DNA repair and sensitize hypoxic cervical cancer cells to radiation by reversing the chromatin compaction associated with hypoxia (Wu et al., 2019). These findings suggest that HDACi can effectively overcome radioresistance in hypoxic tumours, presenting a potential therapeutic strategy for improving radiotherapy outcomes in solid tumours.

In summary, the resulting phenotype, condensed chromatin, impaired DDR signalling, and radioresistance in hypoxic tumour, closely parallels that of SPRTN-deficient cells, which further support our hypothesis (Stingele & Jentsch, 2015; Perry & Ghosal, 2022).

8.2 Delayed Repair in ΔSPRTN could Prevent Complex Damage Formation

An additional (and complementary) explanation centres on DNA repair dynamics. SPRTN-deficient cells not only have more compact chromatin but also resolve DNA damage more slowly. We observed that comet tails in these cells remained persistently long, indicating delayed repair of strand breaks. At first glance, slower DSB repair would seem detrimental; however, in a scenario with clustered DNA lesions (as is common after IR), a slow approach might avert the creation of even more deleterious damage. Ionizing radiation creates a complex mixture of lesions: single-strand breaks, abasic sites, modified bases, and DPCs in proximity. If repair enzymes immediately attempt to process all lesions, closely spaced lesions can convert into one another or aggregate into complex DSBs (Magnander et al., 2009; Singleton et al., 2002). By contrast, if certain lesions remain tethered or protected, some DSBs might be prevented or delayed.

A useful analogy comes from the recently discovered HMCES protein. Mohni *et al*. (2019) showed that HMCES shields abasic sites at replication forks by forming a reversible DNA-protein crosslink, effectively pausing their processing (Mohni et al., 2019). This “suicide” DPC prevents AP endonucleases from cleaving the DNA immediately, thereby avoiding a toxic DSB at that site. The HMCES-DPC is later removed by the proteasome, allowing repair to complete in a less hazardous context. By analogy, in SPRTN-deficient cells, unresolved DPCs might transiently cap or sequester complex lesions, such as oxidative clustered damage, preventing them from being converted into frank DSBs all at once. The DNA breaks that do form are handled in a staggered, protracted manner. While this means the cells carry unrepaired damage longer, it also means they avoid the peak of simultaneous DSBs that can overwhelm the cell’s repair capacity or create irreparable chromosomal breaks. In other words, a slower repair timeline might spare the cell from the worst-case scenario of clustered DSBs.

Conversely, having SPRTN in excess could do the opposite – removing protein-linked lesions too aggressively and generating “extra” DSBs. In support of this, Na *et al*. (2021) reported that SPRTN can cleave the DNA repair enzyme MRE11, producing a truncated form that cannot properly bind DNA or execute homologous recombination repair. This led to decreased HR efficiency and increased radiosensitivity in those cells (Na et al., 2021). One interpretation of Na *et al*.’s finding is that excessive SPRTN activity (or untimely proteolysis) can sabotage normal repair processes – effectively creating vulnerabilities rather than fixing them. Our results fit this narrative: SPRTN-deficient cells, by lacking the protease, delay the processing of DPCs and some associated lesions, which may keep complex DNA damage minimal in the immediate aftermath of IR. Only later, when/if repair finally occurs (possibly through alternate

pathways like other proteases, tyrosyl-DNA phosphodiesterases, nucleotide excision repair, or homologous recombination), are the DPCs removed and the remaining lesions resolved. This strategy is risky – prolonged damage can be mutagenic – but it might give cells a better chance to survive the initial irradiation. Thus, a balance exists: too little SPRTN impairs DPC removal and slows repair, yet grants a short-term protective effect; too much SPRTN accelerates repair at the cost of creating more lethal DSBs. The net outcome in SPRTN-deficient cells is a biased shift toward survival *now* at the expense of repair *later*.

Our findings highlight a context-dependent role of SPRTN and chromatin in DNA damage responses. SPRTN deficiency does not confer general resistance to DNA damage – on the contrary, without SPRTN, cells are exquisitely sensitive to agents like formaldehyde or cisplatin that induce DPCs as the predominant lesion. In those cases, the inability to clear DPCs leads to stalled replication forks and lethal DNA-protein entanglements. There are no concurrent DSBs that might benefit from "masking," so the cells simply accumulate damage and die. Under IR, however, DPCs are formed alongside a host of other lesions including direct DSBs. Here, the DPCs play a dual role: they are harmful lesions, yet they also modulate the damage milieu by locally suppressing DSB signalling and perhaps formation. Only in the IR scenario (or hypothetically, any scenario where DPCs and DSBs are produced together) does the protective facet of DPCs become apparent. Essentially, the DPCs created by IR act like molecular buffers that plug the breaks – at least initially – and induce a hyper-compact chromatin state that generally protects the genome (H. Takata et al., 2013a). This may explain why SPRTN-deficient cells display unexpected resistance to ionising radiation: the DPCs they fail to repair could act as a protective barrier, limiting the formation or detection of DSBs.

From a therapeutic or radiation biology perspective, this insight suggests that the type of radiation can influence the outcome for SPRTN-deficient vs. proficient cells. Low linear energy transfer (LET) radiation, like X-rays, induces a lot of diffusible radical damage, which heterochromatin can partially buffer. In contrast, high-LET radiation (such as alpha particles or heavy ions) deposits energy in a much more localized track, causing dense clusters of direct breaks. These clustered DSBs are less dependent on diffusible OH· radicals and thus are less subject to chromatin shielding (Hada & Georgakilas, 2008). We predict that high-LET irradiation would overwhelm the "protective" heterochromatin effect observed in SPRTN-deficient cells. In other words, the radioresistance conferred by SPRTN loss might be negated by heavy-ion radiation, which forces DNA damage even in tightly packed regions. This could be relevant for certain cancer treatments: tumours with SPRTN mutations might show unusual resistance to conventional X-ray/radiotherapy, yet remain sensitive to particle therapy (or to combination treatments that disrupt chromatin). Conversely, pharmacological chromatin relaxation (e.g., HDAC inhibitors) could act as radiosensitizers in SPRTN-deficient contexts by exposing their concealed DNA lesions – an idea consistent with reports that HDAC inhibitors can radiosensitize cells by opening chromatin structure.

Finally, our study underscores the delicate balance between genome protection and repair in cell lines studied, specifically HeLa. Heterochromatin and DPCs can protect DNA from immediate damage, but they also impede the repair of that damage. Over time, the lesions hidden in heterochromatin must be dealt with. If they are not, cells risk genomic instability. Indeed, SPRTN-deficient cells that survive irradiation may carry unrepaired DPCs or slowly repaired DSBs, which can lead to mutations, chromosome aberrations or mitotic errors down the line. This is reminiscent of the human syndrome caused by SPRTN mutations (RJALS), where patients exhibit

progeroid symptoms and early-onset cancer – likely due to the accumulation of DNA-protein crosslinks and secondary genomic damage over time (Lopez-Mosqueda et al., 2016).

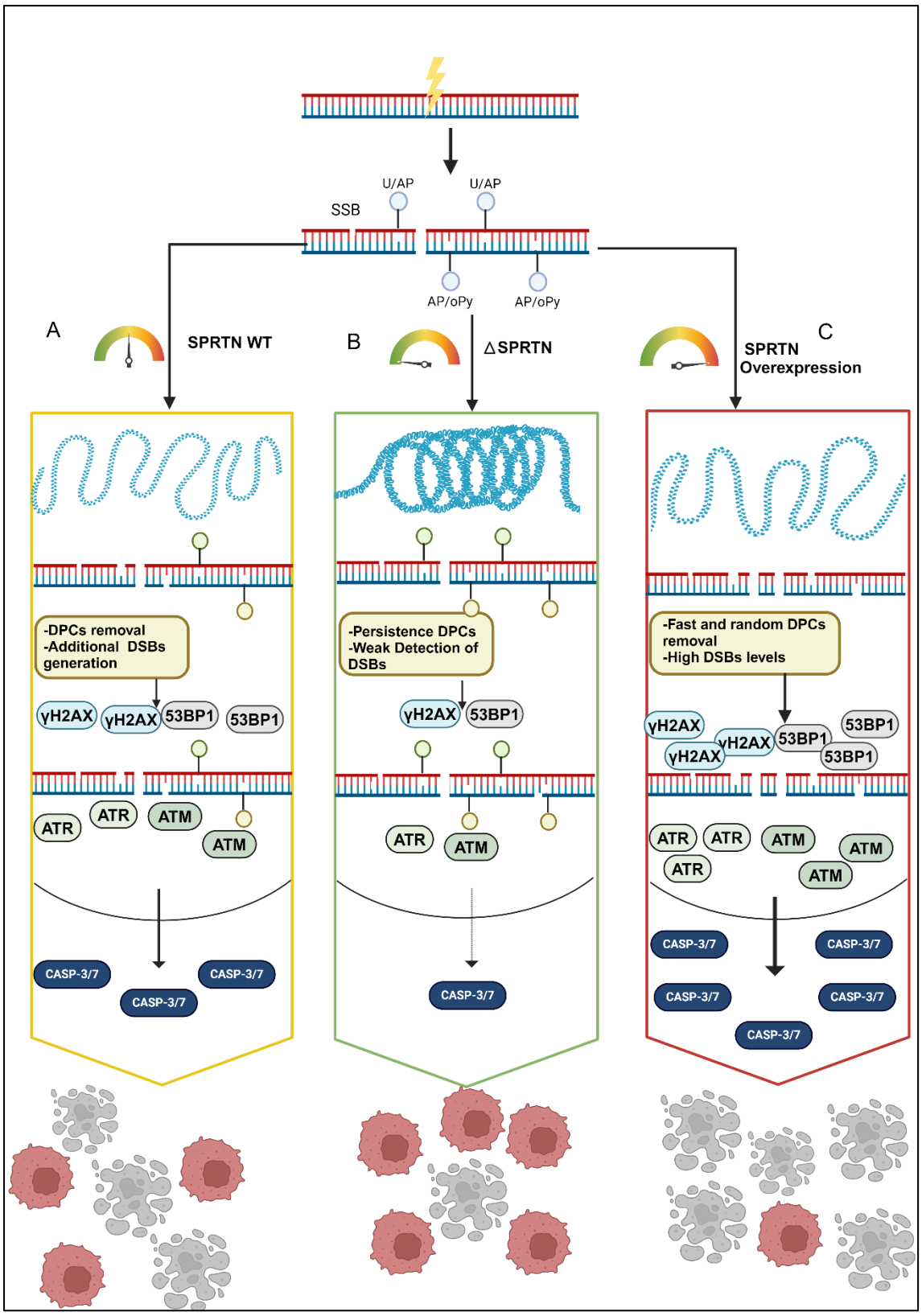


Figure 8.2. Proposed Impact of SPRTN level on complex DNA Double-Strand Break (DSB) Formation Following Radiation.

This figure illustrates the proposed mechanism by which DNA-protein crosslinks (DPCs) contribute to differential DSB formation based on SPRTN expression post-radiation. DPCs

primarily accumulate at hotspot sites such as abasic sites, which arise from radiation-induced oxidative damage. (A) In normal cells, SPRTN protease removes DPCs, enabling subsequent cleavage of clustered oxidative base damages, leading to the formation of more DSBs. (B) In contrast, SPRTN knockout cells exhibit a delay in DPC removal, reducing the formation of complex DSBs, thereby contributing to radioresistance. (C) In cells that overexpress SPRTN, they show radiosensitivity, potentially due to the accelerated DPC removal and concomitant increase in DSB formation. Created using BioRender.com.

In summary, chromatin compaction in SPRTN-deficient cells illustrates a double-edged sword; it limits DNA damage and averts cell death after IR, but at the risk of incomplete DNA repair. This nuanced behaviour highlights why the DNA damage response cannot be viewed in absolute terms of “good repair equals resistance, bad repair equals sensitivity.” Factors like SPRTN illustrate that sometimes a deficiency in repair, through unforeseen mechanisms, can tilt the balance toward cell survival under specific conditions. Understanding these mechanisms in greater detail will be important for designing better interventions, especially in cancers or genetic disorders involving DPC repair pathways.

Overall, our discussion suggests that the unusual radioresistance of SPRTN-deficient cells is a temporary reprieve granted by chromatin shielding and damage tolerance. While it allows cells to survive the initial insult of IR, it may set the stage for genomic instability later. This finding encourages further investigation into chromatin-targeted therapies and highlights the intricate interplay between DNA repair pathways and chromatin state in determining cell fate after DNA damage.

8.3 Future Directions and Study Improvements

While this study provides valuable insights into the chromatin-related consequences of SPRTN depletion and its association with cellular radioresistance, several limitations remain, and multiple promising avenues for future research have emerged. Our investigation primarily focused on HeLa cells, a model that consistently exhibited the most pronounced phenotypes in terms of chromatin compaction, impaired DNA damage signalling, and resistance to ionising radiation. This made HeLa cells an ideal foundation for mechanistic dissection. However, to better understand the broader

biological relevance and potential clinical implications of SPRTN loss, several methodological expansions and deeper mechanistic analyses are warranted.

1. Broader Cell Type Representation

HeLa cells provided a robust model for dissecting the effects of SPRTN deficiency due to their well-characterised genome and consistent chromatin response to ionising radiation. Nevertheless, cancer cell lines are inherently heterogeneous, and the chromatin environment, baseline DNA repair capacity, and redox state can vary substantially across tissues. Future studies should incorporate a panel of cancer cell lines representing different tissue origins (e.g., colorectal, breast, brain, lung), as well as non-transformed cells such as primary fibroblasts, iPSCs, and stem-like cells. Additionally, including tumour models known for therapy resistance, such as glioblastoma or triple-negative breast cancer, may help uncover whether SPRTN deficiency contributes to intrinsic or acquired resistance. Such comparative analyses will help determine whether SPRTN-related chromatin responses are universal or context-dependent and will also provide insight into tissue-specific vulnerabilities.

2. Inhibition of other DPC Proteolysis

SPRTN is a central protease in DPC repair, but the proteolytic system exhibits redundancy. Other proteases, such as FAM111A, DDI2, and the proteasome, have been implicated in processing protein-DNA adducts. To understand the compensatory mechanisms that may buffer the loss of SPRTN, future studies should systematically inhibit these alternative pathways. This would reveal whether inhibiting these enzymes exacerbates the SPRTN-deficient phenotype or if their activation could rescue certain defects. Additionally, proteomics analysis of accumulated DPCs under these

perturbations could identify protein-specific dependencies, potentially unveiling new targets for radiosensitisation or combination therapy.

3. High-LET Radiation as a Potential Bypass Mechanism

The ability of SPRTN-deficient cells to resist DNA damage caused by low-LET radiation suggests that chromatin compaction may shield the genome from widely spaced lesions typically induced by X-rays and γ-rays. However, high-LET radiation sources, such as alpha particles or carbon ions, deliver energy in dense, spatially clustered tracks that can penetrate heterochromatin and create complex, difficult-to-repair DNA lesions. Testing SPRTN-deficient cells under high-LET exposure could reveal whether their resistance extends to these more cytotoxic conditions. Experiments should include survival assays, DDR foci analysis, and chromatin accessibility measurements post-irradiation. If high-LET radiation successfully circumvents chromatin-mediated protection, this would support the use of particle therapy as a treatment strategy for tumours with SPRTN mutations or chromatin-compacted phenotypes.

4. Assessment of Long-Term Genomic Integrity

While this study focused on short-term cellular responses to IR, it remains unclear whether SPRTN deficiency leads to long-term genomic instability. This is critical, as reduced repair fidelity could predispose cells to oncogenic transformation. Longitudinal studies should examine mutation accumulation using whole-genome or exome sequencing, chromosomal aberrations via spectral karyotyping or FISH, and markers of replication stress such as RPA foci or replication fork stalling. In vitro

assays, such as the soft agar colony formation or in vivo tumour xenograft models, could be used to assess whether SPRTN-deficient cells acquire tumorigenic potential. Furthermore, these long-term studies will be essential to determine whether cells that survive radiation due to DDR attenuation retain stable genomes or become prone to malignant evolution.

5. Chromatin Relaxation and DNA Damage Signalling Restoration

One of the most striking findings of this study was the attenuation of DNA damage signalling in SPRTN-deficient cells despite the persistence of DNA lesions. This suggests that chromatin compaction acts as a physical barrier to damage recognition and repair activation. To test this model more rigorously, future work should employ chromatin-modifying agents such as histone deacetylase inhibitors (e.g., trichostatin A or valproic acid), bromodomain inhibitors (e.g., JQ1), or direct knockdown of histone H1 variants to relax chromatin. Functional assays should then quantify DNA damage signalling, including γH2AX foci kinetics, 53BP1 recruitment, and Chk1/Chk2 activation. Furthermore, chromatin accessibility profiling using ATAC-seq and CUT&RUN for DDR factors would determine whether chromatin relaxation restores accessibility to repair complexes. If successful, this would confirm that chromatin compaction, not merely DPC accumulation, is a key contributor to DDR suppression in SPRTN-deficient contexts.

6. ROS, Antioxidants, and DPC Formation Dynamics

Radiation generates reactive oxygen species that contribute to DNA base oxidation and DPC formation. While NAC was used as a general ROS scavenger in this study,

its broad antioxidant profile may obscure specific mechanisms. Future experiments should test targeted ROS modulators, such as mitochondria-targeted antioxidants (e.g., MitoQ), superoxide dismutase mimetics, or ferroptosis inhibitors. Using these tools alongside DPC quantification and chromatin structure analysis could help distinguish whether ROS-induced DPCs are a primary driver of chromatin compaction or a downstream effect. Additionally, comparing radiation modalities that differ in ROS production (e.g., proton vs. photon therapy) would clarify the role of oxidative stress in shaping the SPRTN-deficient phenotype.

7. DNA Repair Pathway Profiling

Although we observed impaired DDR signalling in SPRTN-depleted cells, it remains unclear which specific DNA repair pathways are affected. This knowledge is essential for therapeutic targeting. Reporter assays such as DR-GFP (for homologous recombination), EJ5-GFP (for non-homologous end joining), and SA-GFP (for single-strand annealing) should be used to assess functional repair efficiency. Mass spectrometry-based phosphoproteomics could also reveal pathway-specific alterations in DDR kinase signalling. Understanding whether SPRTN loss preferentially suppresses HR or NHEJ could inform synthetic lethality strategies, for example, combining SPRTN inhibition with PARP inhibitors in HR-proficient but NHEJ-defective backgrounds.

8. Genomic Localization of DPC Burden

Whether DPCs accumulate randomly or at specific genomic loci in SPRTN-deficient cells remains unknown. Technologies such as DPC-ChIP, DPC-seq, or enzymatic

mapping after crosslink enrichment (e.g., RADAR or ARK methods) should be employed to identify DPC-prone regions. Combining these maps with chromatin state annotations (e.g., H3K27me3, H3K9me3, H3K4me1) and transcriptional activity (via RNA-seq) would determine whether transcriptionally active, replication-prone, or heterochromatic domains are disproportionately affected. This could explain why certain regions remain inaccessible to DDR machinery despite persistent damage and may identify fragile chromatin regions most susceptible to collapse in the absence of SPRTN.

9. In Vitro DPC-Based Models to Establish Causality

To dissect whether DPCs alone are sufficient to induce chromatin compaction and radioresistance, SPRTN-independent DPC accumulation models should be developed. This can include exposure to crosslinking agents such as formaldehyde, cisplatin, or topoisomerase poisons (e.g., camptothecin, etoposide). By applying these agents to SPRTN-proficient cells and assessing chromatin state, DDR activation, and cell survival, it would be possible to separate the effects of DPCs from other SPRTN-dependent functions. Moreover, co-treatment with chromatin modifiers could test whether DPC-induced compaction is reversible, and whether chromatin state, rather than DPC load per se, determines cellular radiosensitivity.

10. In Vivo Models and Clinical Correlation

To translate our findings into therapeutic relevance, in vivo models are essential. Mouse models with tissue-specific or inducible SPRTN knockouts should be developed to study DPC accumulation, chromatin compaction, and IR response in

physiological settings. These models could reveal tissue-specific vulnerabilities or compensation and assess tumour development or tissue degeneration under chronic genotoxic stress. Clinically, patient datasets such as TCGA and METABRIC should be mined for SPRTN expression levels, mutations, and correlations with radiotherapy response and survival outcomes. Furthermore, analysis of patient-derived xenografts (PDXs), organoids, or tumour biopsies before and after radiation could directly test whether SPRTN-low tumours exhibit chromatin compaction, altered histone variant distribution, or differential DDR activation. Such translational studies will be critical for positioning SPRTN as a predictive biomarker and for rational design of radiosensitisation strategies in oncology.

Chapter 9: Research Projects and Contributions

This chapter summarizes several collaborative studies in which I actively participated. Each section below describes a specific project's background, my contributions, and the key outcomes relevant to my role. Where the work is ongoing or only preliminary results are available, I note this accordingly.

9.1 Tirapazamine-Mediated Sensitization of NSCLC to PARP Inhibitors

Background: Homologous recombination (HR)–proficient cancers are typically resistant to poly(ADP-ribose) polymerase inhibitors (PARPi) used in HR-deficient tumours. We hypothesized that the hypoxia-activated cytotoxin tirapazamine (TPZ) could overcome this resistance. In an AACR 2024 abstract (Jiang et al., 2024), it was shown that TPZ enhances PARPi cytotoxicity more under hypoxia than normoxia. The study examined TPZ+PARPi treatment in hypoxic 3D spheroids and mouse xenografts of HR-proficient non-small-cell lung cancer (NSCLC) cells. Results indicated that the TPZ+PARPi combination markedly inhibited growth of hypoxic spheroids and xenografts of NSCLC lines with significant hypoxic fractions, whereas well-oxygenated tumours were largely unaffected. These findings suggest that TPZ creates DNA DSBs and free radicals under hypoxia, thereby "broadening the usage of PARPi to HR-proficient cancers".

My contributions: In this project, I performed DNA damage assays (Neutral comet assay) to validate the mechanism of TPZ sensitization. Specifically, I carried out neutral comet assays to measure DNA DSB levels under various treatments. Lung cancer cells (e.g. A549) were treated with vehicle, PARPi (BMN), TPZ, or TPZ+PARPi (with or without the ferroptosis inhibitor ferrostain-1) for 24 hours under both normoxia and 2% O_2 hypoxia. I conducted the experiment. These assays allowed comparison of DNA breakage across conditions.

Key outcomes: The comet assay data confirmed that combining TPZ with PARPi significantly increases DNA damage in HR-proficient cells under hypoxia, consistent with the published results. In particular, TPZ+PARPi–treated cells showed a larger comet tail moment than either agent alone, indicating more DSBs. These results directly support the conclusion that TPZ induces DNA breaks and free radicals, helping to explain the enhanced tumour cell killing observed under hypoxia. My contribution in generating and analyzing these data was crucial for validating the study's mechanism.

9.2 Role of TEX264 in DNA Damage Response and Genome Stability

Background: TEX264 is a recently identified selective autophagy receptor for DPCs and topoisomerase 1–DNA cleavage complexes (TOP1cc). A 2024 Cell paper (Lascaux et al., 2024) demonstrated that TEX264 binds stalled TOP1 complexes at replication forks and targets them for lysosomal degradation, promoting replication fork restart and genome integrity. Loss of TEX264 is predicted to impair this nucleophagy pathway and, therefore, increase DNA damage. In this context, my project examined how depletion of TEX264 affects DNA stability in cultured cancer cells.

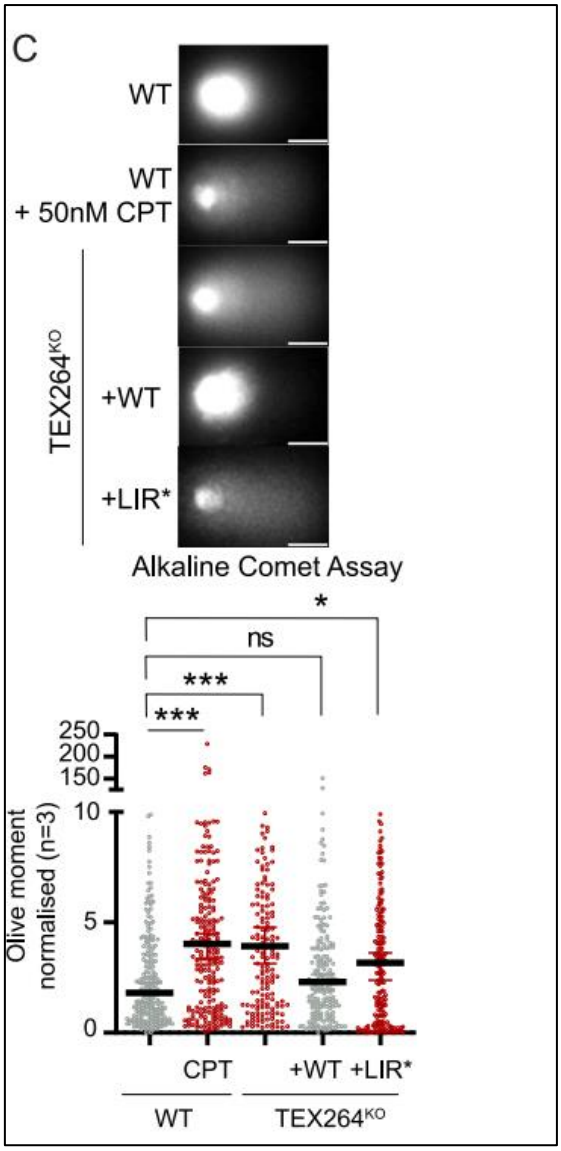


Figure 9.1. Alkaline comet assay was performed on untreated cells and compared with 50 nM CPT for 1 h treatment.

WT HeLa cells were compared with TEX264KO cells or indicated TEX264 complementation in TEX264KO background. The quantification of Olive moment normalized against WT untreated; the median is represented. Scale bar, 20 mm. One-way ANOVA

My contributions: As part of this study, I performed an alkaline comet assay (shown as supplementary Figure C in the publication) on HeLa cell lines differing in TEX264 status. I compared untreated versus camptothecin (CPT)-treated cells: wild-type (WT) HeLa, TEX264 knockout (KO), and TEX264-KO cells re-expressing TEX264. After 1 hour 50 nM CPT exposure (or untreated control), I embedded cells in agarose on slides, lysed them, and ran electrophoresis under alkaline conditions. I then quantified the DNA damage as the Olive tail moment in ≥100 cells per condition, normalizing each to WT control. Statistical analysis (one-way ANOVA) was used to compare groups.

Key outcomes: The comet assay revealed that TEX264-KO cells accumulated significantly more DNA breaks than WT cells, particularly after CPT treatment. Re-expression of TEX264 in the KO background partially rescued this effect. These findings demonstrated that depletion of TEX264 correlates with increased genomic instability and DNA damage. Indeed, the data confirmed that TEX264-deficient cells exhibit a higher Olive tail moment, supporting the published statement that “depletion of TEX264 correlates with higher genomic instability… and DNA breaks measured by alkaline comet assay. Thus, my experimental results validated the conclusion that TEX264 protects genome stability, consistent with its role in autophagic DNA repair.

9.3 Isolation and Detection of DNA–Protein Crosslinks in Mammalian Cells

Background: DPCs are covalent attachments between DNA and proteins that block replication and transcription, leading to genome instability and disease. DPCs arise from agents like formaldehyde or chemotherapy drugs (e.g. cisplatin) and must be rapidly repaired by specialized pathways. Until recently, the field lacked standardized

assays for quantifying DPCs. To address this, our group published a comprehensive methods paper in *Nucleic Acids Research* (Torrecilla et al., 2024) reviewing various DPC isolation techniques and protocols. The goal was to guide researchers in choosing suitable methods and to present reliable workflows for DPC analysis.

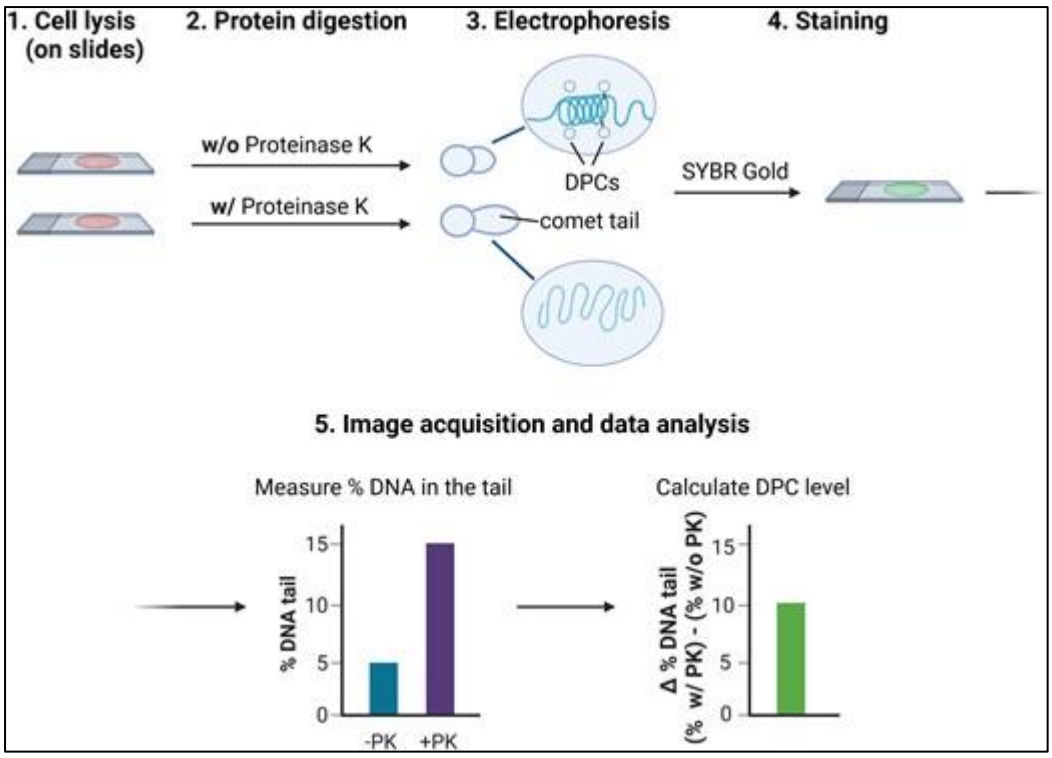


Figure 9.2. Schematic overview of the modified comet assay for DNA–protein crosslink(DPC)detection.

This figure illustrates the workflow for detecting DPCs using a modified alkaline comet assay incorporating proteinase K (PK) digestion. Cells are first lysed on slides (Step 1), followed by incubation with or without PK to digest crosslinked proteins (Step 2). During electrophoresis (Step 3), undigested DPCs restrict DNA migration, resulting in a reduced comet tail signal. Slides are then stained with SYBR Gold (Step 4) and imaged (Step 5). Quantification is performed by measuring the percentage of DNA in the tail with and without PK. The difference in % DNA tail signal (ΔPK) reflects the level of DPCs in the sample.

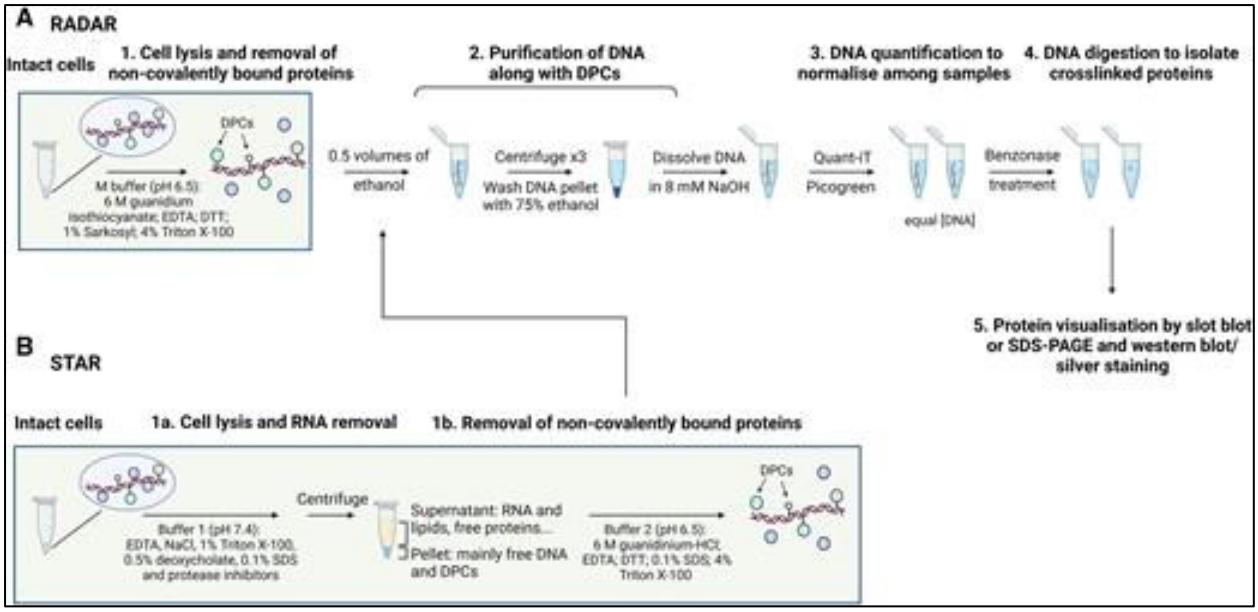


Figure 9.3. Comparison of the RADAR and STAR assays for DNA–protein crosslink (DPC) isolation and detection.
(A) The RADAR (Rapid Approach to DNA–Protein Crosslink Isolation and Detection) assay workflow includes cell lysis in a guanidinium-based buffer to remove non-covalently bound proteins, ethanol precipitation to purify DNA along with DPCs, DNA quantification using PicoGreen, enzymatic digestion with Benzonase to release crosslinked proteins, and visualisation by slot blot, SDS-PAGE, or silver staining.
(B) The STAR (Single-step Trapping of DNA–Protein Crosslinks) assay uses a sequential lysis approach with optimized buffers to separate RNA and lipids, followed by selective precipitation of DNA and covalently bound proteins. The method improves protein integrity and compatibility with downstream detection.

My contributions: For this review, I co-authored the section describing a modified comet assay designed to detect DPCs. In this assay, single cells are embedded in low-melting-point agarose on slides. I wrote text explaining that the slides are first lysed in a buffer containing 1% Triton X-100 to remove membranes and soluble proteins. Next, proteinase K is applied to digest crosslinked proteins, allowing trapped DNA fragments to migrate during electrophoresis. Without proteinase K, protein-bound DNA remains largely immobile; with it, DNA fragments resulting from DPCs form a measurable "comet" tail. I also contributed to Figure 9.2, which schematically illustrates this modified comet protocol. In the manuscript, I described how the tail length in alkaline conditions reflects the level of DNA breaks and DPCs, and how adding proteinase K distinguishes DPCs from other lesions. Also I contributed to making figures on Radar and STAR assay (Figure 9.3).

Key outcomes: The published article presents this modified comet assay as one of several validated techniques for DPC analysis. By documenting the protocol in detail (Figure 10 and accompanying text), our review provides a standardized procedure that others can use to quantify DPCs in cells. In particular, my written contribution on the modified comet assay ensures that researchers understand how to implement the assay step by step. Overall, this publication contributes a useful resource to the field, helping investigators in choosing the appropriate method in measuring DPCs more consistently

9.4 Deletion of USP18: Antigenicity and DNA Damage Analysis

Background: USP18 is a deubiquitylating enzyme that removes ISG15 modifications from proteins and is a key negative regulator of interferon signaling. Prior work

(Andersen et al., 2021) showed that USP18 deficiency in cancer cells increases antigen presentation and radiosensitivity. In other words, USP18-null tumour cells become more visible to the immune system and more susceptible to IR. However, the mechanism for their heightened radiosensitivity is not fully understood. The research led by Adán Pinto-Fernández (Career Development Fellow at Chinese Academy of Medical Sciences Oxford Institute) sought to test whether loss of USP18 leads to higher levels of DNA damage after radiation.

In addition currently I am working on a manuscript with the aim publish this data.

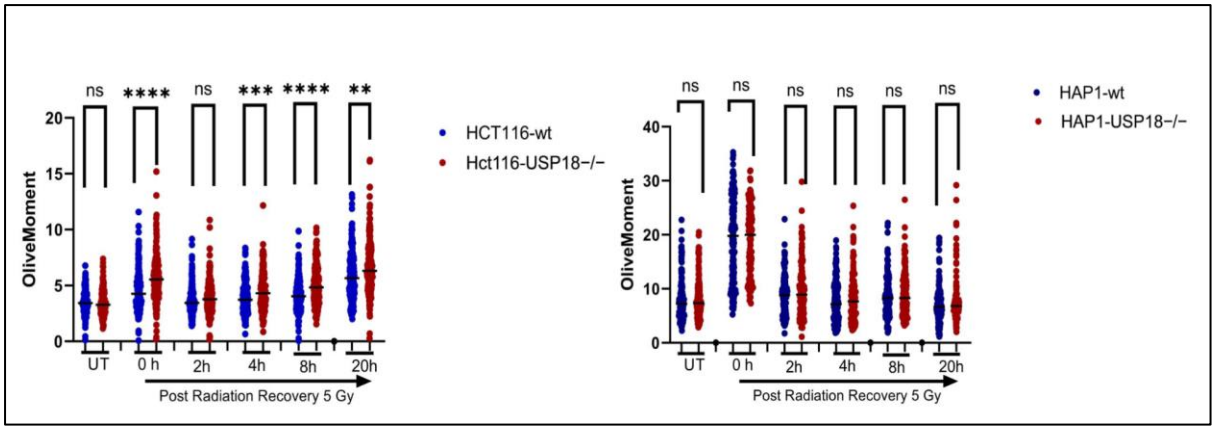


Figure 9.4. Comet assay reveals altered DNA repair dynamics in USP18-deficient cells. Representative data from alkaline comet assays showing DNA damage in HCT116 and HAP1 cells with and without USP18 after exposure to 5 Gy ionizing radiation. DNA strand breaks were quantified using Olive tail moment at various recovery time points. While USP18-deficient HCT116 cells showed delayed repair kinetics reflected in persistently high Olive moments, HAP1 USP18-KO cells did not show significant differences.I contributed to data acquisition, analysis, and interpretation in these experiments.

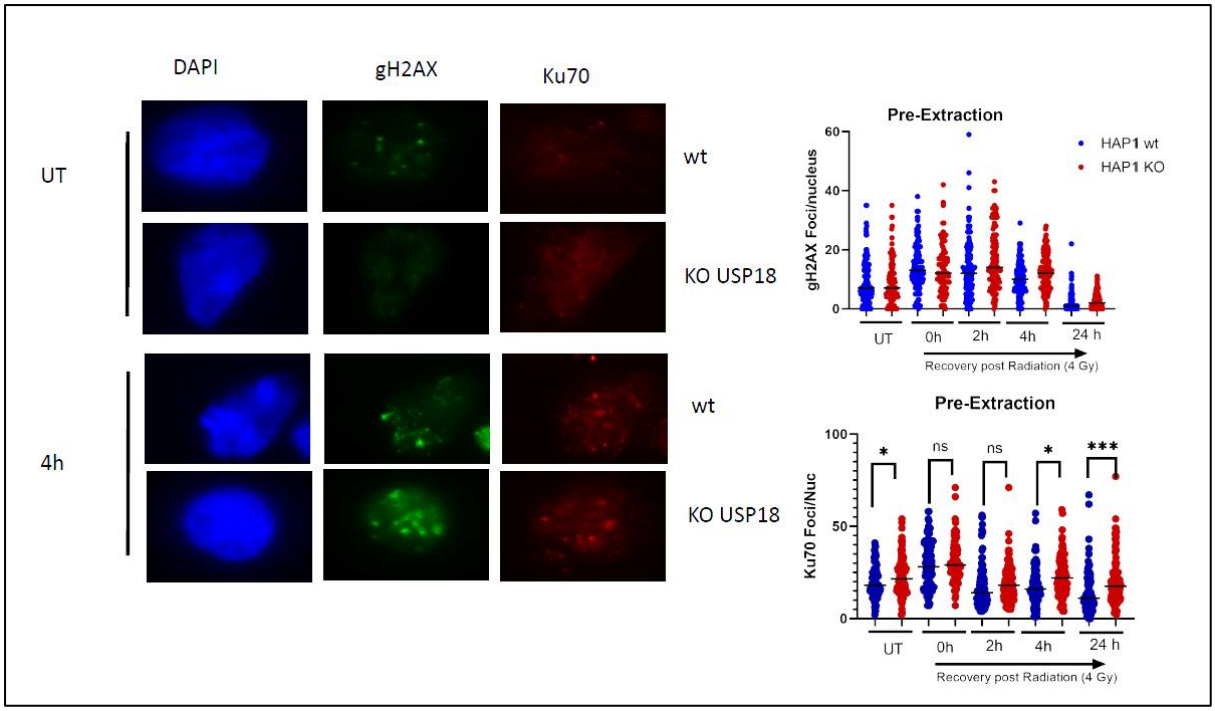


Figure 9.5. Increased DNA damage signalling in USP18-deficient cells post-irradiation.

(A) Representative immunofluorescence images of HAP1 wild-type and USP18 knockout cells stained for γH2AX and Ku70 foci pre-extraction at 0 and 4 hours post 4 Gy irradiation.

(B) Quantification of γH2AX and Ku70 foci per nucleus showed elevated levels in USP18-deficient cells compared to wild-type controls, particularly at early and late recovery time points.

I contributed to doing the experiment, foci quantification and analysis of γH2AX and Ku70 staining in this figure,

My contributions: In this ongoing project, I collaborated on experiments to quantify DNA strand breaks in USP18-deficient cells. I performed neutral comet assays on irradiated cancer cell lines with and without USP18 expression. Specifically, cells were exposed to defined doses of ionizing radiation, then embedded in agarose and processed the comet assay I measured the Olive tail moment to assess DNA breaks in USP18-null versus control cells. Additionally, I helped interpret the preliminary data and discuss potential implications.

In addition to DNA strand break quantification, I conducted immunofluorescence staining and quantitative analysis of DNA damage markers. Specifically, I assessed the formation of γH2AX and Ku70 nuclear foci post-irradiation. My analysis revealed a consistent increase in both γH2AX and Ku70 foci in USP18-deficient cells compared to controls, suggesting an elevated DNA damage response or defective repair pathway. I also contributed to preliminary data interpretation and helped contextualize the results within the broader DDR literature.

Preliminary observations: At present, the analysis is being finalized. Early data suggest that USP18-deficient cells may exhibit more DNA fragmentation after irradiation than wild-type cells. This is consistent with the hypothesis that enhanced DNA damage contributes to their radiosensitivity.

Main outcome: Our preliminary work is exploring a novel link between innate immune regulation and genome stability. While we do not yet have definitive outcomes, the ongoing assays will determine if USP18 loss potentiates radiation-induced DNA breaks. Any confirmed increase in DNA damage would help explain the radiosensitizing effect of USP18 deletion

Sources:

- Jiang Y., Estephan H., Wang Y., Aljarbou F., et al. (2024). *Tirapazamine sensitizes HR-proficient cancers by enhancing DNA damage and ferroptosis.* Proceedings of AACR Annual Meeting 2024researchgate.net.
- Lascaux P. et al. (2024). *TEX264 drives selective autophagy of DNA lesions to promote DNA repair and cell survival. Cell* 187(20), 5698–5718.e26pubmed.ncbi.nlm.nih.gov.
- Torrecilla I. et al. (2024). *Isolation and detection of DNA–protein crosslinks in mammalian cells. Nucleic Acids Research* 52(2):525–547pubmed.ncbi.nlm.nih.govpubmed.ncbi.nlm.nih.gov.
- Andersen R. et al. (2021). *Deletion of USP18 enhances tumour cell antigenicity and radiosensitivity. Br. J. Cancer* 124, 817–830nature.com.

References

Acta, B., & Health, P. (1977). *DNA CROSSLINKING INDUCED BY X-RAYS AND CHEMICAL AGENTS*. *477*, 343–355.

Adrian, G., Konradsson, E., Lempart, M., Bäck, S., Ceberg, C., & Petersson, K. (2020). The FLASH effect depends on oxygen concentration. *British Journal of Radiology*, *93*(1106). https://doi.org/10.1259/bjr.20190702

Al-Arafat, T.-, Mao, A., Katsube, T., & Wang, B. (2024). Exploring the Role of p53 in Radiosensitivity: A Key Player in Cancer Therapy. In *Radiation* (Vol. 4, Issue 4, pp. 309–324). https://doi.org/10.3390/radiation4040023

Amanda K.McCullough, M. L. Dodson, and R. S. L. (1999). INITIATION OF BASE EXCISION REPAIR:GLYCOSYLASE MECHANISMS AND STRUCTURES Amanda. *Annu. Rev. Biochem*, 1–1. https://doi.org/10.1002/9783527678679.dg00929

An, H., Ordureau, A., Paulo, J. A., Shoemaker, C. J., Denic, V., & Harper, J. W. (2019). TEX264 Is an Endoplasmic Reticulum-Resident ATG8-Interacting Protein Critical for ER Remodeling during Nutrient Stress. *Molecular Cell*, *74*(5), 891-908.e10. https://doi.org/10.1016/j.molcel.2019.03.034

Ansar Ahmed, S., Gogal, R. M., & Walsh, J. E. (1994). A new rapid and simple non-radioactive assay to monitor and determine the proliferation of lymphocytes: an alternative to [3H]thymidine incorporation assay. *Journal of Immunological Methods*, *170*(2), 211–224. https://doi.org/10.1016/0022-1759(94)90396-4

Antonovic, L., Lindblom, E., Dasu, A., Bassler, N., Furusawa, Y., & Toma-Dasu, I. (2014). Clinical oxygen enhancement ratio of tumors in carbon ion radiotherapy: the influence of local oxygenation changes. *Journal of Radiation Research*, *55*(5), 902–911. https://doi.org/10.1093/jrr/rru020

Antrobus, J., & Parsons, J. L. (2022). Histone Deacetylases and Their Potential as Targets to Enhance Tumour Radiosensitisation. In *Radiation* (Vol. 2, Issue 1, pp. 149–167). https://doi.org/10.3390/radiation2010011

Aparicio, T., Baer, R., Gottesman, M., & Gautier, J. (2016). MRN, CtIP, and BRCA1 mediate repair of topoisomerase II-DNA adducts. *Journal of Cell Biology*, *212*(4), 399–408. https://doi.org/10.1083/jcb.201504005

Apel, A., Herr, I., Schwarz, H., Rodemann, H. P., & Mayer, A. (2008). Blocked autophagy sensitizes resistant carcinoma cells to radiation therapy. *Cancer Research*, *68*(5), 1485–1494. https://doi.org/10.1158/0008-5472.CAN-07-0562

Arakawa, H., Bednar, T., Wang, M., Paul, K., Mladenov, E., Bencsik-Theilen, A. A., & Iliakis, G. (2012). Functional redundancy between DNA ligases i and III in DNA

replication in vertebrate cells. *Nucleic Acids Research*, *40*(6), 2599–2610. https://doi.org/10.1093/nar/gkr1024

Arowolo, A., Malebana, M., Sunda, F., & Rhoda, C. (2022). Proposed Cellular Function of the Human FAM111B Protein and Dysregulation in Fibrosis and Cancer. *Frontiers in Oncology*, *12*(July), 1–7. https://doi.org/10.3389/fonc.2022.932167

Asaithamby, A., & Chen, D. J. (2011). Mechanism of cluster DNA damage repair in response to high-atomic number and energy particles radiation. *Mutation Research/Fundamental and Molecular Mechanisms of Mutagenesis*, *711*(1), 87–99. https://doi.org/https://doi.org/10.1016/j.mrfmmm.2010.11.002

Asaithamby, A., Hu, B., & Chen, D. J. (2011). Unrepaired clustered DNA lesions induce chromosome breakage in human cells. *Proceedings of the National Academy of Sciences*, *108*(20), 8293–8298. https://doi.org/10.1073/pnas.1016045108

Attix, F. H. (2004). Introduction To Radiological Physics and. *John Wiley & Sons, Inc*, 607.

Averbeck, N. B., Ringel, O., Herrlitz, M., Jakob, B., Durante, M., & Taucher-Scholz, G. (2014). DNA end resection is needed for the repair of complex lesions in G1-phase human cells. *Cell Cycle*, *13*(16), 2509–2516. https://doi.org/10.4161/15384101.2015.941743

Ayala, A., Muñoz, M. F., & Argüelles, S. (2014). Lipid peroxidation: production, metabolism, and signaling mechanisms of malondialdehyde and 4-hydroxy-2-nonenal. *Oxidative Medicine and Cellular Longevity*, *2014*, 360438. https://doi.org/10.1155/2014/360438

Baker, D. J., Wuenschell, G., Xia, L., Termini, J., Bates, S. E., Riggs, A. D., & O'Connor, T. R. (2007). Nucleotide excision repair eliminates unique DNA-protein cross-links from mammalian cells. *Journal of Biological Chemistry*, *282*(31), 22592–22604. https://doi.org/10.1074/jbc.M702856200

Barker, S., Weinfeld, M., & Murray, D. (2005). DNA-protein crosslinks: Their induction, repair, and biological consequences. *Mutation Research - Reviews in Mutation Research*, *589*(2), 111–135. https://doi.org/10.1016/j.mrrev.2004.11.003

Barker, S., Weinfeld, M., Zheng, J., Li, L., & Murray, D. (2005). Identification of mammalian proteins cross-linked to DNA by ionizing radiation. *Journal of Biological Chemistry*, *280*(40), 33826–33838. https://doi.org/10.1074/jbc.M502477200

Baskar, R., Lee, K. A., Yeo, R., & Yeoh, K. W. (2012). Cancer and radiation therapy: Current advances and future directions. *International Journal of Medical Sciences*, *9*(3), 193–199. https://doi.org/10.7150/ijms.3635

Baumann, P., & West, S. C. (1998). Role of the human RAD51 protein in homologous recombination and double-stranded-break repair. *Trends in Biochemical Sciences*, *23*(7), 247–251. https://doi.org/10.1016/s0968-0004(98)01232-8

Beatty, S., Koh, H. H., Phil, M., Henson, D., & Boulton, M. (2000). The role of oxidative stress in the pathogenesis of age-related macular degeneration. *Survey of Ophthalmology*, *45*(2), 115–134. https://doi.org/10.1016/S0039-6257(00)00140-5

Beck, C., Robert, I., Reina-San-Martin, B., Schreiber, V., & Dantzer, F. (2014). Poly(ADP-ribose) polymerases in double-strand break repair: Focus on PARP1, PARP2 and PARP3. *Experimental Cell Research*, *329*(1), 18–25. https://doi.org/10.1016/j.yexcr.2014.07.003

Beck, W. T., Danks, M. K., Wolverton, J. S., Kim, R., & Chen, M. (1993). Drug resistance associated with altered DNA topoisomerase II. *Advances in Enzyme Regulation*, *33*(C), 113–116. https://doi.org/10.1016/0065-2571(93)90012-3

Beh, C. Y., Yeo, C. P. X., Hong, B. H., Tan, E. M. C., Tan, K. M., Poon, D. J. J., Chu, P. L., Susanti, D., Tai, P. L., Ryu, M., Proudfoot, J., Yeo, E. L. L., Soo, K. C., & Chua, M. L. K. (2024). Genomic and transcriptomic profiling of radioresistant prostate and head and neck cancers implicate a BAHD1-dependent modification of DNA damage at the heterochromatin. *Cell Death & Disease*, *15*(12), 929. https://doi.org/10.1038/s41419-024-07316-y

Bell, E. L., & Chandel, N. S. (2007). Mitochondrial oxygen sensing: Regulation of hypoxia-inducible factor by mitochondrial generated reactive oxygen species. *Essays in Biochemistry*, *43*, 17–27. https://doi.org/10.1042/BSE0430017

Berry, R. J., Hall, E. J., Forster, D. W., Storr, T. H., & Goodman, M. J. (1969). Survival of mammalian cells exposed to x rays at ultra-high dose-rates. *The British Journal of Radiology*, *42*(494), 102–107. https://doi.org/10.1259/0007-1285-42-494-102

Bhargava, R., Onyango, D. O., & Stark, J. M. (2016). Regulation of Single-Strand Annealing and its Role in Genome Maintenance. *Trends in Genetics*, *32*(9), 566–575. https://doi.org/https://doi.org/10.1016/j.tig.2016.06.007

Birmingham, A., Anderson, E., Sullivan, K., Reynolds, A., Boese, Q., Leake, D., Karpilow, J., & Khvorova, A. (2007). A protocol for designing siRNAs with high functionality and specificity. *Nature Protocols*, *2*(9), 2068–2078. https://doi.org/10.1038/nprot.2007.278

Bishop, D. K., Ear, U., Bhattacharyya, A., Calderone, C., Beckett, M., Weichselbaum, R. R., & Shinohara, A. (1998). Xrcc3 is required for assembly of Rad51 complexes in vivo. *The Journal of Biological Chemistry*, *273*(34), 21482–21488. https://doi.org/10.1074/jbc.273.34.21482

Blakely, E., Chang, P., Lommel, L., Bjornstad, K., Dixon, M., Tobias, C., Kumar, K., & Blakely, W. F. (1989). Cell-cycle radiation response: role of intracellular factors. *Advances in Space Research : The Official Journal of the Committee on Space Research (COSPAR)*, *9*(10), 177–186. https://doi.org/10.1016/0273-1177(89)90436-5

Blouin, T., & Saini, N. (2024). Aldehyde-induced DNA-protein crosslinks- DNA damage, repair and mutagenesis. *Frontiers in Oncology*, *14*, 1478373. https://doi.org/10.3389/fonc.2024.1478373

Borgermann, N., Ackermann, L., Schwertman, P., Hendriks, I. A., Thijssen, K., Liu, J. C., Lans, H., Nielsen, M. L., & Mailand, N. (2019). SUMO ylation promotes protective responses to DNA -protein crosslinks . *The EMBO Journal*, *38*(8), 1–17. https://doi.org/10.15252/embj.2019101496

Bosch-Presegué, L., Raurell-Vila, H., Marazuela-Duque, A., Kane-Goldsmith, N., Valle, A., Oliver, J., Serrano, L., & Vaquero, A. (2011). Stabilization of Suv39H1 by SirT1 Is Part of Oxidative Stress Response and Ensures Genome Protection. *Molecular Cell*, *42*(2), 210–223. https://doi.org/https://doi.org/10.1016/j.molcel.2011.02.034

Botchway, S. W., Stevens, D. L., Hill, M. A., Jenner, T. J., & O'Neill, P. (1997). Induction and Rejoining of DNA Double-Strand Breaks in Chinese Hamster V79-4 Cells Irradiated with Characteristic Aluminum K and Copper L Ultrasoft X Rays. *Radiation Research*, *148*(4), 317–324. https://doi.org/10.2307/3579516

Bourhis, J., Montay-Gruel, P., Gonçalves Jorge, P., Bailat, C., Petit, B., Ollivier, J., Jeanneret-Sozzi, W., Ozsahin, M., Bochud, F., Moeckli, R., Germond, J. F., & Vozenin, M. C. (2019). Clinical translation of FLASH radiotherapy: Why and how? *Radiotherapy and Oncology*, *139*, 11–17. https://doi.org/10.1016/j.radonc.2019.04.008

Bourhis, J., Sozzi, W. J., Jorge, P. G., Gaide, O., Bailat, C., Duclos, F., Patin, D., Ozsahin, M., Bochud, F., Germond, J. F., Moeckli, R., & Vozenin, M. C. (2019). Treatment of a first patient with FLASH-radiotherapy. *Radiotherapy and Oncology*, *139*, 18–22. https://doi.org/10.1016/j.radonc.2019.06.019

Brambilla, G., Sciabà, L., Faggin, P., Finollo, R., Bassi, A. M., Ferro, M., & Marinari, U. M. (1985). Methylglyoxal-induced DNA-protein cross-links and cytotoxicity in chinese hamster ovary cells. *Carcinogenesis*, *6*(5), 683–686. https://doi.org/10.1093/carcin/6.5.683

Bray, F. (2021). *The Ever- Increasing Importance of Cancer as a Leading Cause of Premature Death Worldwide*. 3029–3030. https://doi.org/10.1002/cncr.33587

Breimer, L. H., & Lindahl, T. (1985). Enzymatic excision of DNA bases damaged by exposure to ionizing radiation or oxidizing agents. *Mutation Research -*

Fundamental and Molecular Mechanisms of Mutagenesis, *150*(1–2), 85–89. https://doi.org/10.1016/0027-5107(85)90104-6

Bristow, R. G., & Hill, R. P. (2008). Hypoxia and metabolism: Hypoxia, DNA repair and genetic instability. *Nature Reviews Cancer*, *8*(3), 180–192. https://doi.org/10.1038/nrc2344

Buonanno, M., Grilj, V., & Brenner, D. J. (2019). Biological effects in normal cells exposed to FLASH dose rate protons. *Radiotherapy and Oncology : Journal of the European Society for Therapeutic Radiology and Oncology*, *139*, 51–55. https://doi.org/10.1016/j.radonc.2019.02.009

Burgess, R. C., Burman, B., Kruhlak, M. J., & Misteli, T. (2014). Activation of DNA damage response signaling by condensed chromatin. *Cell Reports*, *9*(5), 1703–1717. https://doi.org/10.1016/j.celrep.2014.10.060

Burgos-Barragan, G., Wit, N., Meiser, J., Dingler, F. A., Pietzke, M., Mulderrig, L., Pontel, L. B., Rosado, I. V, Brewer, T. F., Cordell, R. L., Monks, P. S., Chang, C. J., Vazquez, A., & Patel, K. J. (2017). Mammals divert endogenous genotoxic formaldehyde into one-carbon metabolism. *Nature*, *548*(7669), 549–554. https://doi.org/10.1038/nature23481

Cadet, J., Carell, T., Cellai, L., Chatgilialoglu, C., Gimisis, T., Miranda, M., O'Neill, P., Ravanat, J. L., & Robert, M. (2008). DNA damage and radical reactions: Mechanistic aspects, formation in cells and repair studies. *Chimia*, *62*(9), 742–749. https://doi.org/10.2533/chimia.2008.742

Cadet, J., Delatour, T., Douki, T., Gasparutto, D., Pouget, J. P., Ravanat, J. L., & Sauvaigo, S. (1999). Hydroxyl radicals and DNA base damage. *Mutation Research - Fundamental and Molecular Mechanisms of Mutagenesis*, *424*(1–2), 9–21. https://doi.org/10.1016/S0027-5107(99)00004-4

Calini, V., Urani, C., & Camatini, M. (2002). Comet assay evaluation of DNA single- and double-strand breaks induction and repair in C3H10T1/2 cells. *Cell Biology and Toxicology*, *18*(6), 369–379. https://doi.org/10.1023/A:1020811522100

Carlson, D. J., Stewart, R. D., & Semenenko, V. A. (2006). Effects of oxygen on intrinsic radiation sensitivity: A test of the relationship between aerobic and hypoxic linear-quadratic (LQ) model parameters. *Medical Physics*, *33*(9), 3105–3115. https://doi.org/https://doi.org/10.1118/1.2229427

Carnie, C. J., Acampora, A. C., Bader, A. S., Erdenebat, C., Zhao, S., Bitensky, E., van den Heuvel, D., Parnas, A., Gupta, V., D'Alessandro, G., Sczaniecka-Clift, M., Weickert, P., Aygenli, F., Götz, M. J., Cordes, J., Esain-Garcia, I., Melidis, L., Wondergem, A. P., Lam, S., … Stingele, J. (2024). Transcription-coupled repair of DNA–protein cross-

links depends on CSA and CSB. *Nature Cell Biology*, *26*(5), 797–810. https://doi.org/10.1038/s41556-024-01391-1

Carvajal-Garcia, J., Cho, J.-E., Carvajal-Garcia, P., Feng, W., Wood, R. D., Sekelsky, J., Gupta, G. P., Roberts, S. A., & Ramsden, D. A. (2020). Mechanistic basis for microhomology identification and genome scarring by polymerase theta. *Proceedings of the National Academy of Sciences*, *117*(15), 8476–8485. https://doi.org/10.1073/pnas.1921791117

Casanova, M., Morgan, K. T., Stemhagen, W. H., Everitt, J. I., Popp, J. A., & Heck, H. D. a. (1991). Covalent binding of inhaled formaldehyde to DNA in the respiratory tract of rhesus monkeys: Pharmacokinetics, rat-to-monkey interspecies scaling, and extrapolation to man. *Toxicological Sciences*, *17*(2), 409–428. https://doi.org/10.1093/toxsci/17.2.409

C.D.Town. (1967). Effect of High Dose Rates on Survival of Mammalian Cells. *Nature*, *215*, 847–848.

Ceccaldi, R., Liu, J. C., Amunugama, R., Hajdu, I., Primack, B., Petalcorin, M. I. R., O'Connor, K. W., Konstantinopoulos, P. A., Elledge, S. J., Boulton, S. J., Yusufzai, T., & D'Andrea, A. D. (2015). Homologous-recombination-deficient tumours are dependent on Polθ-mediated repair. *Nature*, *518*(7538), 258–262. https://doi.org/10.1038/nature14184

Centore, R. C., Yazinski, S. A., Tse, A., & Zou, L. (2012a). Spartan/C1orf124, a Reader of PCNA Ubiquitylation and a Regulator of UV-Induced DNA Damage Response. *Molecular Cell*, *46*(5), 625–635. https://doi.org/10.1016/j.molcel.2012.05.020

Centore, R. C., Yazinski, S. A., Tse, A., & Zou, L. (2012b). Spartan/C1orf124, a Reader of PCNA Ubiquitylation and a Regulator of UV-Induced DNA Damage Response. *Molecular Cell*, *46*(5), 625–635. https://doi.org/10.1016/j.molcel.2012.05.020

Chakraborty, M., Abrams, S. I., Camphausen, K., Liu, K., Scott, T., Coleman, C. N., & Hodge, J. W. (2003). Irradiation of Tumor Cells Up-Regulates Fas and Enhances CTL Lytic Activity and CTL Adoptive Immunotherapy. *The Journal of Immunology*, *170*(12), 6338–6347. https://doi.org/10.4049/jimmunol.170.12.6338

Chan, W., Ham, Y. H., Jin, L., Chan, H. W., Wong, Y. L., Chan, C. K., & Chung, P. Y. (2019). Quantification of a Novel DNA-Protein Cross-Link Product Formed by Reacting Apurinic/Apyrimidinic Sites in DNA with Cysteine Residues in Protein by Liquid Chromatography-Tandem Mass Spectrometry Coupled with the Stable Isotope-Dilution Method. *Analytical Chemistry*, *91*(8), 4987–4994. https://doi.org/10.1021/acs.analchem.8b04306

Chen, S. H., Chan, N. L., & Hsieh, T. S. (2013). New mechanistic and functional insights into DNA topoisomerases. *Annual Review of Biochemistry*, *82*, 139–170. https://doi.org/10.1146/annurev-biochem-061809-100002

Chino, H., Hatta, T., Natsume, T., & Mizushima, N. (2019). Intrinsically Disordered Protein TEX264 Mediates ER-phagy. *Molecular Cell*, *74*(5), 909-921.e6. https://doi.org/10.1016/j.molcel.2019.03.033

Chiu, S. M., Sokany, N. M., Friedman, L. R., & Oleinick, N. L. (1984). Differential processing of ultraviolet or ionizing radiation-induced DNA-protein Cross-links in chinese hamster cells. *International Journal of Radiation Biology*, *46*(6), 681–690. https://doi.org/10.1080/09553008414551921

Christman, J. K. (2002). 5-Azacytidine and 5-aza-2'-deoxycytidine as inhibitors of DNA methylation: Mechanistic studies and their implications for cancer therapy. *Oncogene*, *21*(35 REV. ISS. 3), 5483–5495. https://doi.org/10.1038/sj.onc.1205699

Chung, H. R., Dunkel, I., Heise, F., Linke, C., Krobitsch, S., Ehrenhofer-Murray, A. E., Sperling, S. R., & Vingron, M. (2010). The effect of micrococcal nuclease digestion on nucleosome positioning data. *PLoS ONE*, *5*(12). https://doi.org/10.1371/journal.pone.0015754

Chválová, K., Brabec, V., & Kašpárková, J. (2007). Mechanism of the formation of DNA-protein cross-links by antitumor cisplatin. *Nucleic Acids Research*, *35*(6), 1812–1821. https://doi.org/10.1093/nar/gkm032

Claesson, K., Karin, M., Helena, K., Sture, L., Ragnar, H., & and Elmroth, K. (2011). RBE of α-particles from 211At for complex DNA damage and cell survival in relation to cell cycle position. *International Journal of Radiation Biology*, *87*(4), 372–384. https://doi.org/10.3109/09553002.2011.538127

Classen, F., Kranz, P., Riffkin, H., Pompsch, M., Wolf, A., Göpelt, K., Baumann, M., Baumann, J., Brockmeier, U., & Metzen, E. (2019). Autophagy induced by ionizing radiation promotes cell death over survival in human colorectal cancer cells. *Experimental Cell Research*, *374*(1), 29–37. https://doi.org/10.1016/j.yexcr.2018.11.004

Connelly, J. C., De Leau, E. S., & Leach, D. R. F. (2003). Nucleolytic processing of a protein-bound DNA end by the E. coli SbcCD (MR) complex. *DNA Repair*, *2*(7), 795–807. https://doi.org/10.1016/S1568-7864(03)00063-6

Cooper, C. R., Jones, D. J. L., Jones, G. D. D., & Petersson, K. (2023). Comet Assay Profiling of FLASH-Induced Damage: Mechanistic Insights into the Effects of FLASH Irradiation. *International Journal of Molecular Sciences*, *24*(8), 1–15. https://doi.org/10.3390/ijms24087195

Cooper, C. R., Jones, D., Jones, G. D., & Petersson, K. (2022). FLASH irradiation induces lower levels of DNA damage ex vivo, an effect modulated by oxygen tension, dose, and dose rate. *British Journal of Radiology*, *95*(1133). https://doi.org/10.1259/bjr.20211150

Cress, A. E., & Bowden, G. T. (1983). Covalent DNA-protein crosslinking occurs after hyperthermia and radiation. *Radiation Research*, *95*(3), 610–619. https://doi.org/10.2307/3576104

D. Ostling. K.J. Johanson. (1984). MICRDELECTKOPHORETIC STUDY OF RADIATION-INDUCED DNA DAhAGES IN INDIVIDUAL MAMMALIAN CELLS. *BlOCHEMiCAL AND BIOPHYSICAL RESEARCH COMMUNiCATlONS*, *123*(1), 291–298.

Dator, R. P., Murray, K. J., Luedtke, M. W., Jacobs, F. C., Kassie, F., Nguyen, H. D., Villalta, P. W., & Balbo, S. (2022). Identification of Formaldehyde-Induced DNA-RNA Cross-Links in the A/J Mouse Lung Tumorigenesis Model. *Chemical Research in Toxicology*, *35*(11), 2025–2036. https://doi.org/10.1021/acs.chemrestox.2c00206

David-Cordonnier, M.-H., Cunniffe, S. M. T., Hickson, I. D., & O'Neill, P. (2002). Efficiency of Incision of an AP Site within Clustered DNA Damage by the Major Human AP Endonuclease. *Biochemistry*, *41*(2), 634–642. https://doi.org/10.1021/bi011682l

Davis, E. J., Lachaud, C., Appleton, P., MacArtney, T. J., Näthke, I., & Rouse, J. (2012). DVC1 (C1orf124) recruits the p97 protein segregase to sites of DNA damage. *Nature Structural and Molecular Biology*, *19*(11), 1093–1100. https://doi.org/10.1038/nsmb.2394

de Graaf, B., Clore, A., & McCullough, A. K. (2009). Cellular pathways for DNA repair and damage tolerance of formaldehyde-induced DNA-protein crosslinks. *DNA Repair*, *8*(10), 1207–1214. https://doi.org/10.1016/j.dnarep.2009.06.007

Debela, D. T., Muzazu, S. G. Y., Heraro, K. D., Ndalama, M. T., Mesele, B. W., Haile, D. C., Kitui, S. K., & Manyazewal, T. (2021). New approaches and procedures for cancer treatment: Current perspectives. *SAGE Open Medicine*, *9*. https://doi.org/10.1177/20503121211034366

Debéthune, L., Kohlhagen, G., Grandas, A., & Pommier, Y. (2002). Processing of nucleopeptides mimicking the topoisomerase I-DNA covalent complex by tyrosyl-DNA phosphodiesterase. *Nucleic Acids Research*, *30*(5), 1198–1204. https://doi.org/10.1093/nar/30.5.1198

Delaney, G., Jacob, S., Featherstone, C., & Barton, M. (2005). The role of radiotherapy in cancer treatment: Estimating optimal utilization from a review of evidence-based clinical guidelines. *Cancer*, *104*(6), 1129–1137. https://doi.org/10.1002/cncr.21324

Demott, M. S., Beyret, E., Wong, D., Bales, B. C., Hwang, J. T., Greenberg, M. M., & Demple, B. (2002). Covalent trapping of human DNA polymerase β by the oxidative DNA lesion 2-deoxyribonolactone. *Journal of Biological Chemistry*, *277*(10), 7637–7640. https://doi.org/10.1074/jbc.C100577200

Desai, S. D., Li, T. K., Rodriguez-Bauman, A., Liu, L. F., & Rubin, E. H. (2001). Ubiquitin/26s proteasome-mediated degradation of topoisomerase I as a resistance mechanism to camptothecin in tumor cells. *Cancer Research*, *61*(15), 5926–5932.

Deshpande, R. A., Lee, J. H., Arora, S., & Paull, T. T. (2016). Nbs1 Converts the Human Mre11/Rad50 Nuclease Complex into an Endo/Exonuclease Machine Specific for Protein-DNA Adducts. *Molecular Cell*, *64*(3), 593–606. https://doi.org/10.1016/j.molcel.2016.10.010

DEWEY, D. L., & BOAG, J. W. (1959). Modification of the Oxygen Effect when Bacteria are given Large Pulses of Radiation. *Nature*, *183*(4673), 1450–1451. https://doi.org/10.1038/1831450a0

Dextraze, M.-E., Gantchev, T., Girouard, S., & Hunting, D. (2010). DNA interstrand cross-links induced by ionizing radiation: An unsung lesion. *Mutation Research/Reviews in Mutation Research*, *704*(1), 101–107. https://doi.org/https://doi.org/10.1016/j.mrrev.2009.12.007

Dingler, F. A., Wang, M., Mu, A., Millington, C. L., Oberbeck, N., Watcham, S., Pontel, L. B., Kamimae-Lanning, A. N., Langevin, F., Nadler, C., Cordell, R. L., Monks, P. S., Yu, R., Wilson, N. K., Hira, A., Yoshida, K., Mori, M., Okamoto, Y., Okuno, Y., … Patel, K. J. (2020). Two Aldehyde Clearance Systems Are Essential to Prevent Lethal Formaldehyde Accumulation in Mice and Humans. *Molecular Cell*, *80*(6), 996-1012.e9. https://doi.org/https://doi.org/10.1016/j.molcel.2020.10.012

Dokshin, G. A., Davis, G. M., Sawle, A. D., Eldridge, M. D., Nicholls, P. K., Gourley, T. E., Romer, K. A., Molesworth, L. W., Tatnell, H. R., Ozturk, A. R., de Rooij, D. G., Hannon, G. J., Page, D. C., Mello, C. C., & Carmell, M. A. (2020). GCNA Interacts with Spartan and Topoisomerase II to Regulate Genome Stability. *Developmental Cell*, *52*(1), 53-68.e6. https://doi.org/10.1016/j.devcel.2019.11.006

Dolinnaya, N. G., Kubareva, E. A., Romanova, E. A., Trikin, R. M., & Oretskaya, T. S. (2013). Thymidine glycol: the effect on DNA molecular structure and enzymatic processing. *Biochimie*, *95*(2), 134–147. https://doi.org/10.1016/j.biochi.2012.09.008

Dong, P., & Gewirtz, D. A. (2022). Editorial: Risks and Benefits of Adjuvants to Cancer Therapies. In *Frontiers in Oncology* (Vol. 12). https://doi.org/10.3389/fonc.2022.913626

Douki, T., Delatour, T., Paganon, F., & Cadet, J. (1996). Measurement of Oxidative Damage at Pyrimidine Bases in γ-Irradiated DNA. *Chemical Research in Toxicology*, *9*(7), 1145–1151. https://doi.org/10.1021/tx960095b

Dunlap, B., & Cerutti, P. (1975). *APYRIMIDINIC SITES IN GAMMA-IRRADIATED DNA*. *5*(1), 4–6.

Durante, M., BräUer-Krisch, E., & Hill, M. (2018). Faster and safer? FLASH ultra-high dose rate in radiotherapy. *British Journal of Radiology*, *91*(1082), 6–9. https://doi.org/10.1259/bjr.20170628

Durante, M., Orecchia, R., & Loeffler, J. S. (2017). Charged-particle therapy in cancer: Clinical uses and future perspectives. *Nature Reviews Clinical Oncology*, *14*(8), 483–495. https://doi.org/10.1038/nrclinonc.2017.30

Duxin, J. P., Dewar, J. M., Yardimci, H., & Walter, J. C. (2014). Repair of a DNA-protein crosslink by replication-coupled proteolysis. *Cell*, *159*(2), 346–357. https://doi.org/10.1016/j.cell.2014.09.024

Eccles, L. J., O'Neill, P., & Lomax, M. E. (2011). Delayed repair of radiation induced clustered DNA damage: Friend or foe? *Mutation Research - Fundamental and Molecular Mechanisms of Mutagenesis*, *711*(1–2), 134–141. https://doi.org/10.1016/j.mrfmmm.2010.11.003

Erber, L., Groehler, A. S., Cyuzuzo, C. I., Baker-Wainwright, J., Maskey, R. S., Li, L., Machida, Y. J., & Tretyakova, N. (2024). SPRTN metalloprotease participates in repair of ROS-mediated DNA-protein crosslinks. *Scientific Reports*, *14*(1), 30919. https://doi.org/10.1038/s41598-024-81799-9

Eriksson, D., & Stigbrand, T. (2010). Radiation-induced cell death mechanisms. *Tumor Biology*, *31*(4), 363–372. https://doi.org/10.1007/s13277-010-0042-8

Ewing, D. (1980). Breaking survival curves and oxygen removal times in irradiated bacterial spores. *International Journal of Radiation Biology*, *37*(3), 321–329. https://doi.org/10.1080/09553008014550371

Fabbrizi, M. R., Doggett, T. J., Hughes, J. R., Melia, E., Dufficy, E. R., Hill, R. M., Goula, A., Phoenix, B., & Parsons, J. L. (2024). Inhibition of key DNA double strand break repair protein kinases enhances radiosensitivity of head and neck cancer cells to X-ray and proton irradiation. *Cell Death Discovery*, *10*(1), 1–10. https://doi.org/10.1038/s41420-024-02059-3

Fábián, Z., Kakulidis, E. S., Hendriks, I. A., Kühbacher, U., Larsen, N. B., Oliva-Santiago, M., Wang, J., Leng, X., Dirac-Svejstrup, A. B., Svejstrup, J. Q., Nielsen, M. L., Caldecott, K., & Duxin, J. P. (2024). PARP1-dependent DNA-protein crosslink repair. *Nature Communications*, *15*(1). https://doi.org/10.1038/s41467-024-50912-x

Falk, M., Lukášová, E., & Kozubek, S. (2008). Chromatin structure influences the sensitivity of DNA to γ-radiation. *Biochimica et Biophysica Acta (BBA) - Molecular Cell Research*, *1783*(12), 2398–2414. https://doi.org/https://doi.org/10.1016/j.bbamcr.2008.07.010

Favaudon, V., Caplier, L., Monceau, V., Pouzoulet, F., Sayarath, M., Fouillade, C., Poupon, M. F., Brito, I., Hupé, P., Bourhis, J., Hall, J., Fontaine, J. J., & Vozenin, M. C. (2014). Erratum: Ultrahigh dose-rate FLASH irradiation increases the differential response between normal and tumor tissue in mice (Science Translational Medicine DOI: 10.1126/scitranslmed.3008973). *Science Translational Medicine*, *11*(523), 1–9. https://doi.org/10.1126/scitranslmed.aba4525

Favaudon, V., Caplier, L., Monceau, V., Pouzoulet, F., Sayarath, M., Fouillade, C., Poupon, M. F., Brito, I., Hupé, P., Bourhis, J., Hall, J., Fontaine, J. J., & Vozenin, M. C. (2019). Erratum: Ultrahigh dose-rate FLASH irradiation increases the differential response between normal and tumor tissue in mice (Science Translational Medicine DOI: 10.1126/scitranslmed.3008973). *Science Translational Medicine*, *11*(523), 1–9. https://doi.org/10.1126/scitranslmed.aba4525

Feeney, G., Sehgal, R., Sheehan, M., Hogan, A., Regan, M., Joyce, M., & Kerin, M. (2019). Neoadjuvant radiotherapy for rectal cancer management. *World Journal of Gastroenterology*, *25*(33), 4850–4869. https://doi.org/10.3748/wjg.v25.i33.4850

Ferlay, J., Rebecca, M. E., & Mph, L. S. (2024). *Global cancer statistics 2022: GLOBOCAN estimates of incidence and mortality worldwide for 36 cancers in 185 countries*. *February*, 229–263. https://doi.org/10.3322/caac.21834

Fielden, J., Ruggiano, A., Popović, M., & Ramadan, K. (2018). DNA protein crosslink proteolysis repair: From yeast to premature ageing and cancer in humans. *DNA Repair*, *71*(August), 198–204. https://doi.org/10.1016/j.dnarep.2018.08.025

Fielden, J., Wiseman, K., Torrecilla, I., Li, S., Hume, S., Chiang, S. C., Ruggiano, A., Narayan Singh, A., Freire, R., Hassanieh, S., Domingo, E., Vendrell, I., Fischer, R., Kessler, B. M., Maughan, T. S., El-Khamisy, S. F., & Ramadan, K. (2020). TEX264 coordinates p97- and SPRTN-mediated resolution of topoisomerase 1-DNA adducts. *Nature Communications*, *11*(1), 1–16. https://doi.org/10.1038/s41467-020-15000-w

Flor, A., Wolfgeher, D., Li, J., Hanakahi, L. A., & Kron, S. J. (2021). Lipid-derived electrophiles mediate the effects of chemotherapeutic topoisomerase I poisons. *Cell Chemical Biology*, *28*(6), 776-787.e8. https://doi.org/10.1016/j.chembiol.2020.11.011

Forster, J. C., Marcu, L. G., & Bezak, E. (2019). Approaches to combat hypoxia in cancer therapy and the potential for in silico models in their evaluation. *Physica Medica*, *64*, 145–156. https://doi.org/https://doi.org/10.1016/j.ejmp.2019.07.006

Fouillade, C., Curras-Alonso, S., Giuranno, L., Quelennec, E., Heinrich, S., Bonnet-Boissinot, S., Beddok, A., Leboucher, S., Karakurt, H. U., Bohec, M., Baulande, S., Vooijs, M., Verrelle, P., Dutreix, M., Londoño-Vallejo, A., & Favaudon, V. (2020). FLASH irradiation spares lung progenitor cells and limits the incidence of radio-induced senescence. *Clinical Cancer Research*, *26*(6), 1497–1506. https://doi.org/10.1158/1078-0432.CCR-19-1440

Franken, N. A. P., Rodermond, H. M., Stap, J., Haveman, J., & van Bree, C. (2006). Clonogenic assay of cells in vitro. *Nature Protocols*, *1*(5), 2315–2319. https://doi.org/10.1038/nprot.2006.339

Frosina, G., Fortini, P., Rossi, O., Carrozzino, F., Raspaglio, G., Cox, L. S., Lane, D. P., Abbondandolo, A., & Dogliotti, E. (1996). Two Pathways for Base Excision Repair in Mammalian Cells (∗). *Journal of Biological Chemistry*, *271*(16), 9573–9578. https://doi.org/https://doi.org/10.1074/jbc.271.16.9573

Galluzzi, L., & Vitale, I. (2018). *Molecular mechanisms of cell death : recommendations of the Nomenclature Committee on Cell Death 2018*. 486–541. https://doi.org/10.1038/s41418-017-0012-4

Gascoigne, K. E., & Taylor, S. S. (2008). *Article Cancer Cells Display Profound Intra- and Interline Variation following Prolonged Exposure to Antimitotic Drugs*. 111–122. https://doi.org/10.1016/j.ccr.2008.07.002

Georgakilas, A. G., O'Neill, P., & Stewart, R. D. (2013). Induction and repair of clustered DNA lesions: What do we know so far? *Radiation Research*, *180*(1), 100–109. https://doi.org/10.1667/RR3041.1

Gerelchuluun, A., Manabe, E., Ishikawa, T., Sun, L., Itoh, K., Sakae, T., Suzuki, K., Hirayama, R., Asaithamby, A., Chen, D. J., & Tsuboi, K. (2015). The major DNA repair pathway after both proton and carbon-ion radiation is NHEJ, but the HR pathway is more relevant in carbon ions. *Radiation Research*, *183*(3), 345–356. https://doi.org/10.1667/RR13904.1

Gerken, T., Girard, C. A., Tung, Y. C. L., Webby, C. J., Saudek, V., Hewitson, K. S., Yeo, G. S. H., McDonough, M. A., Cunliffe, S., McNeill, L. A., Galvanovskis, J., Rorsman, P., Robins, P., Prieur, X., Coll, A. P., Ma, M., Jovanovic, Z., Farooqi, I. S., Sedgwick, B., … Schofield, C. J. (2007). The obesity-associated FTO gene encodes a 2-oxoglutarate-dependent nucleic acid demethylase. *Science*, *318*(5855), 1469–1472. https://doi.org/10.1126/science.1151710

Ghorai, A., Bhattacharyya, N. P., Sarma, A., & Ghosh, U. (2014). Radiosensitivity and Induction of Apoptosis by High LET Carbon Ion Beam and Low LET Gamma Radiation: A Comparative Study. *Scientifica*, *2014*(1), 438030. https://doi.org/https://doi.org/10.1155/2014/438030

Ghosal, G., Leung, J. W. C., Nair, B. C., Fong, K. W., & Chen, J. (2012). Proliferating Cell Nuclear Antigen (PCNA)-binding protein C1orf124 is a regulator of translesion synthesis. *Journal of Biological Chemistry*, *287*(41), 34225–34233. https://doi.org/10.1074/jbc.M112.400135

Girdhani, S., Abel, E., Katsis, A., Rodriquez, A., Senapati, S., KuVillanueva, A., Jackson, I. L., Eley, J., Vujaskovic, Z., & Parry, R. (2019). Abstract LB-280: FLASH: A novel paradigm changing tumor irradiation platform that enhances therapeutic ratio by reducing normal tissue toxicity and activating immune pathways. *Cancer Research*, *79*(13_Supplement), LB-280-LB-280. https://doi.org/10.1158/1538-7445.AM2019-LB-280

Glowa, C., Bendinger, A. L., Euler-Lange, R., Peschke, P., Brons, S., Debus, J., & Karger, C. P. (2024). Irradiation with Carbon Ions Effectively Counteracts Hypoxia-related Radioresistance in a Rat Prostate Carcinoma. *International Journal of Radiation Oncology Biology Physics*, *120*(3), 875–883. https://doi.org/10.1016/j.ijrobp.2024.05.004

Glumac, M., Polović, M., Batel, A., Gelemanović, A., Maček, B., Velić, A., & Marinović-Terzić, I. (2023). SPRTN-dependent DPC degradation precedes repair of damaged DNA: A proof of concept revealed by the STAR assay. *Nucleic Acids Research*, *51*(6), E35. https://doi.org/10.1093/nar/gkad022

Goodarzi, A. A., Noon, A. T., Deckbar, D., Ziv, Y., Shiloh, Y., Löbrich, M., & Jeggo, P. A. (2008). ATM signaling facilitates repair of DNA double-strand breaks associated with heterochromatin. *Molecular Cell*, *31*(2), 167–177. https://doi.org/10.1016/j.molcel.2008.05.017

Goodhead, D. T. (1989). The initial physical damage produced by ionizing radiations. *International Journal of Radiation Biology*, *56*(5), 623–634. https://doi.org/10.1080/09553008914551841

Goodhead, D. T. (1994). Initial events in the cellular effects of ionizing radiations: Clustered damage in DNA. *International Journal of Radiation Biology*, *65*(1), 7–17. https://doi.org/10.1080/09553009414550021

Goodhead, D. T. (2019). Neutrons are forever! Historical perspectives. *International Journal of Radiation Biology*, *95*(7), 957–984. https://doi.org/10.1080/09553002.2019.1569782

Grafstrom, R. C., Fornace, A., & Harris, C. C. (1984). *Repair of DMA Damage Caused by Formaldehyde in Human Cells*. *OCTOBER*, 4323–4327.

Greenberg, M. M. (2014). Abasic and oxidized abasic site reactivity in DNA: Enzyme inhibition, cross-linking, and nucleosome catalyzed reactions. *Accounts of Chemical Research*, *47*(2), 646–655. https://doi.org/10.1021/ar400229d

Grimes, D. R. (2020). Estimation of the oxygen enhancement ratio for charged particle radiation. *Physics in Medicine & Biology*, *65*(15), 15NT01. https://doi.org/10.1088/1361-6560/ab9371

Grimsrud, P. A., Xie, H., Griffin, T. J., & Bernlohr, D. A. (2008). *Oxidative Stress and Covalent Modification of Protein with Bioactive Aldehydes*. *283*(32), 21837–21841. https://doi.org/10.1074/jbc.R700019200

Groehler, A., Kren, S., Li, Q., Robledo-Villafane, M., Schmidt, J., Garry, M., & Tretyakova, N. (2018). Oxidative cross-linking of proteins to DNA following ischemia-reperfusion injury. *Free Radical Biology and Medicine*, *120*, 89–101. https://doi.org/10.1016/j.freeradbiomed.2018.03.010

Gulston, M., de Lara, C., Jenner, T., Davis, E., & O'Neill, P. (2004). Processing of clustered DNA damage generates additional double-strand breaks in mammalian cells post-irradiation. *Nucleic Acids Research*, *32*(4), 1602–1609. https://doi.org/10.1093/nar/gkh306

Gyori, B. M., Venkatachalam, G., Thiagarajan, P. S., Hsu, D., & Clement, M. V. (2014). OpenComet: An automated tool for comet assay image analysis. *Redox Biology*, *2*(1), 457–465. https://doi.org/10.1016/j.redox.2013.12.020

Hada, M., & Georgakilas, A. G. (2008). Formation of clustered DNA damage after high-LET irradiation: a review. *Journal of Radiation Research*, *49*(3), 203–210. https://doi.org/10.1269/jrr.07123

Hada, M., & Sutherland, B. M. (2006). Spectrum of complex DNA damages depends on the incident radiation. *Radiation Research*, *165*(2), 223–230. https://doi.org/10.1667/RR3498.1

Halder, S., Torrecilla, I., Burkhalter, M. D., Popović, M., Fielden, J., Vaz, B., Oehler, J., Pilger, D., Lessel, D., Wiseman, K., Singh, A. N., Vendrell, I., Fischer, R., Philipp, M., & Ramadan, K. (2019). SPRTN protease and checkpoint kinase 1 cross-activation loop safeguards DNA replication. *Nature Communications*, *10*(1). https://doi.org/10.1038/s41467-019-11095-y

Hande, K. R. (1998). Etoposide: Four decades of development of a topoisomerase II inhibitor. *European Journal of Cancer*, *34*(10), 1514–1521. https://doi.org/10.1016/S0959-8049(98)00228-7

Hart, T., Chandrashekhar, M., Aregger, M., Steinhart, Z., Brown, K. R., MacLeod, G., Mis, M., Zimmermann, M., Fradet-Turcotte, A., Sun, S., Mero, P., Dirks, P., Sidhu, S., Roth, F. P., Rissland, O. S., Durocher, D., Angers, S., & Moffat, J. (2015). High-Resolution CRISPR Screens Reveal Fitness Genes and Genotype-Specific Cancer Liabilities. *Cell*, *163*(6), 1515–1526. https://doi.org/10.1016/j.cell.2015.11.015

Hauer, M. H., & Gasser, S. M. (2017). Chromatin and nucleosome dynamics in DNA damage and repair. *Genes and Development*, *31*(22), 2204–2221. https://doi.org/10.1101/gad.307702.117

Higgins, G. S., & Boulton, S. J. (2018). Beyond PARP—POLu as an anticancer target. *Science*, *359*(6381), 1217–1218. https://doi.org/10.1126/science.aar5149

H.Kasai, P.F.Crain, Y.Kuchino, S.Nishimura, A. O. and H. T. (1986). Formation of 8-hydroxyguanine moiety in cellular DNA by agents producing oxygen radicals and evidence for its repair. *Carcinogeuesis*, *1390*(3), 4238–4242.

Hsiang, Y. H., Hertzberg, R., Hecht, S., & Liu, L. F. (1985). Camptothecin induces protein-linked DNA breaks via mammalian DNA topoisomerase I. *Journal of Biological Chemistry*, *260*(27), 14873–14878. https://doi.org/10.1016/s0021-9258(17)38654-4

Hu, Q., Klages-Mundt, N., Wang, R., Lynn, E., Kuma Saha, L., Zhang, H., Srivastava, M., Shen, X., Tian, Y., Kim, H., Ye, Y., Paull, T., Takeda, S., Chen, J., & Li, L. (2020). The ARK Assay Is a Sensitive and Versatile Method for the Global Detection of DNA-Protein Crosslinks. *Cell Reports*, *30*(4), 1235-1245.e4. https://doi.org/10.1016/j.celrep.2019.12.067

Huang, J., Zhou, Q., Gao, M., Nowsheen, S., Zhao, F., Kim, W., Zhu, Q., Kojima, Y., Yin, P., Zhang, Y., Guo, G., Tu, X., Deng, M., Luo, K., Qin, B., Machida, Y., & Lou, Z. (2020). Tandem Deubiquitination and Acetylation of SPRTN Promotes DNA-Protein Crosslink Repair and Protects against Aging. *Molecular Cell*, *79*(5), 824-835.e5. https://doi.org/10.1016/j.molcel.2020.06.027

Hurben, A. K., Zhang, Q., Galligan, J. J., Tretyakova, N., & Erber, L. (2024). Endogenous Cellular Metabolite Methylglyoxal Induces DNA-Protein Cross-Links in Living Cells. *ACS Chemical Biology*, *19*(6), 1291–1302. https://doi.org/10.1021/acschembio.4c00100

Hwang, T., Reh, S., Dunbayev, Y., Zhong, Y., Takata, Y., Shen, J., McBride, K. M., Murnane, J. P., Bhak, J., Lee, S., Wood, R. D., & Takata, K. I. (2020). Defining the mutation signatures of DNA polymerase θ in cancer genomes. *NAR Cancer*, *2*(3), 1–14. https://doi.org/10.1093/narcan/zcaa017

Ishimi, Y., & Ide, H. (2013). *Translocation and Stability of Replicative DNA Helicases upon Encountering DNA-Protein Cross-links * □*. *288*(7), 4649–4658. https://doi.org/10.1074/jbc.M112.419358

Jacobs, A. L., & Schär, P. (2012). DNA glycosylases: in DNA repair and beyond. *Chromosoma*, *121*(1), 1–20. https://doi.org/10.1007/s00412-011-0347-4

Jakob, B., Dubiak-Szepietowska, M., Janiel, E., Schmidt, A., Durante, M., & Taucher-Scholz, G. (2020). Differential Repair Protein Recruitment at Sites of Clustered and Isolated DNA Double-Strand Breaks Produced by High-Energy Heavy Ions. *Scientific Reports*, *10*(1), 1443. https://doi.org/10.1038/s41598-020-58084-6

Jakob, B., Splinter, J., Conrad, S., Voss, K. O., Zink, D., Durante, M., Löbrich, M., & Taucher-Scholz, G. (2011). DNA double-strand breaks in heterochromatin elicit fast repair protein recruitment, histone H2AX phosphorylation and relocation to euchromatin. *Nucleic Acids Research*, *39*(15), 6489–6499. https://doi.org/10.1093/nar/gkr230

Jo, U., Murai, Y., Agama, K. K., Sun, Y., Saha, L. K., Yang, X., Arakawa, Y., Gayle, S., Jones, K., Paralkar, V., Sundaram, R. K., Van Doorn, J., Vasquez, J. C., Bindra, R. S., Choi, W. S., & Pommier, Y. (2022). TOP1-DNA Trapping by Exatecan and Combination Therapy with ATR Inhibitor. *Molecular Cancer Therapeutics*, *21*(7), 1090–1102. https://doi.org/10.1158/1535-7163.MCT-21-1000

Johansen, M. E., Muller, J. G., Xu, X., & Burrows, C. J. (2005). Oxidatively induced DNA-protein cross-linking between single-stranded binding protein and oligodeoxynucleotides containing 8-oxo-7,8-dihydro-2'- deoxyguanosine. *Biochemistry*, *44*(15), 5660–5671. https://doi.org/10.1021/bi047580n

John, T., Pires, E., Hester, S. S., Salah, E., Hopkinson, R. J., & Schofield, C. J. (2023). Formaldehyde reacts with N-terminal proline residues to give bicyclic aminals. *Communications Chemistry*, *6*(1), 12. https://doi.org/10.1038/s42004-022-00801-5

Jones, B. (2020). Clinical Radiobiology of Fast Neutron Therapy: What Was Learnt? *Frontiers in Oncology*, *10*(September), 1–12. https://doi.org/10.3389/fonc.2020.01537

Juan, C. A., Pérez de la Lastra, J. M., Plou, F. J., & Pérez-Lebeña, E. (2021). The Chemistry of Reactive Oxygen Species (ROS) Revisited: Outlining Their Role in Biological Macromolecules (DNA, Lipids and Proteins) and Induced Pathologies. In *International Journal of Molecular Sciences* (Vol. 22, Issue 9). https://doi.org/10.3390/ijms22094642

Juhasz, S., Balogh, D., Hajdu, I., Burkovics, P., Villamil, M. A., Zhuang, Z., & Haracska, L. (2012). Characterization of human Spartan/C1orf124, an ubiquitin-PCNA

interacting regulator of DNA damage tolerance. *Nucleic Acids Research*, *40*(21), 10795–10808. https://doi.org/10.1093/nar/gks850

Julio E.Celis, M. F. (1976). On the use of ultraviolet light to study protein-DNA crosslinking. *Methods*, *12*(21), 8235–8251.

Kamps, J. J. A. G., Hopkinson, R. J., Schofield, C. J., & Claridge, T. D. W. (2019). How formaldehyde reacts with amino acids. *Communications Chemistry*, *2*(1), 126. https://doi.org/10.1038/s42004-019-0224-2

Kanaar, R., Hoeijmakers, J. H., & van Gent, D. C. (1998). Molecular mechanisms of DNA double strand break repair. *Trends in Cell Biology*, *8*(12), 483–489. https://doi.org/10.1016/s0962-8924(98)01383-x

Karagiannis, T. C., & El-Osta, A. (2006). Modulation of cellular radiation responses by histone deacetylase inhibitors. *Oncogene*, *25*(28), 3885–3893. https://doi.org/10.1038/sj.onc.1209417

Karmodiya, K., Krebs, A. R., Oulad-Abdelghani, M., Kimura, H., & Tora, L. (2012). H3K9 and H3K14 acetylation co-occur at many gene regulatory elements, while H3K14ac marks a subset of inactive inducible promoters in mouse embryonic stem cells. *BMC Genomics*, *13*(1), 424. https://doi.org/10.1186/1471-2164-13-424

Karran, P. (2000). DNA double strand break repair in mammalian cells. *Current Opinion in Genetics & Development*, *10*(2), 144–150. https://doi.org/https://doi.org/10.1016/S0959-437X(00)00069-1

Karsch, L., Pawelke, J., Brand, M., Hans, S., Hideghéty, K., Jansen, J., Lessmann, E., Löck, S., Schürer, M., Schurig, R., Seco, J., Szabó, E. R., & Beyreuther, E. (2022). Beam pulse structure and dose rate as determinants for the flash effect observed in zebrafish embryo. *Radiotherapy and Oncology*, *173*, 49–54. https://doi.org/10.1016/j.radonc.2022.05.025

Kawasaki, K., Nojima, S., Hijiki, S., Tahara, S., Ohshima, K., Matsui, T., Hori, Y., Kurashige, M., Umeda, D., Kiyokawa, H., Kido, K., Okuzaki, D., & Morii, E. (2020). FAM111B enhances proliferation of KRAS-driven lung adenocarcinoma by degrading p16. *Cancer Science*, *111*(7), 2635–2646. https://doi.org/10.1111/cas.14483

Kiianitsa, K., & Maizels, N. (2013). A rapid and sensitive assay for DNA-protein covalent complexes in living cells. *Nucleic Acids Research*, *41*(9), 1–7. https://doi.org/10.1093/nar/gkt171

Kim Daniel Y., Guo Jimmy A., Zhao Daniel, Philip Errol J., & Li Yun R. (2020). *Transcriptional Mechanisms of Radioresistance and Therapeutic Implications*. *September*, 16–23. www.appliedradiationoncology.com

Kinner, A., Wu, W., Staudt, C., & Iliakis, G. (2008). Gamma-H2AX in recognition and signaling of DNA double-strand breaks in the context of chromatin. *Nucleic Acids Research*, *36*(17), 5678–5694. https://doi.org/10.1093/nar/gkn550

Klungland, A., & Lindahl, T. (1997). Second pathway for completion of human DNA base excision-repair: reconstitution with purified proteins and requirement for DNase IV (FEN1). *The EMBO Journal*, *16*(11), 3341–3348. https://doi.org/https://doi.org/10.1093/emboj/16.11.3341

Kojima, Y., Machida, Y., Palani, S., Caulfield, T. R., Radisky, E. S., Kaufmann, S. H., & Machida, Y. J. (2020). FAM111A protects replication forks from protein obstacles via its trypsin-like domain. *Nature Communications*, *11*(1). https://doi.org/10.1038/s41467-020-15170-7

Kolářová, I., Melichar, B., Sirák, I., Vaňásek, J., Petera, J., Horáčková, K., Pohanková, D., Ďatelinka, F., Šinkorová, Z., & Vošmik, M. (2024). The Role of Adjuvant Radiotherapy in the Treatment of Breast Cancer. *Current Oncology*, *31*(3), 1207–1220. https://doi.org/10.3390/curroncol31030090

Kold-Christensen, R., & Johannsen, M. (2020). Methylglyoxal Metabolism and Aging-Related Disease: Moving from Correlation toward Causation. *Trends in Endocrinology and Metabolism: TEM*, *31*(2), 81–92. https://doi.org/10.1016/j.tem.2019.10.003

Kroemer, G., Galluzzi, L., Vandenabeele, P., Abrams, J., Alnemri, E. S., Baehrecke, E. H., Blagosklonny, M. V, El-Deiry, W. S., Golstein, P., Green, D. R., Hengartner, M., Knight, R. A., Kumar, S., Lipton, S. A., Malorni, W., Nuñez, G., Peter, M. E., Tschopp, J., Yuan, J., … Melino, G. (2009). Classification of cell death: recommendations of the Nomenclature Committee on Cell Death. *Cell Death & Differentiation*, *16*(1), 3–11. https://doi.org/10.1038/cdd.2008.150

Krokan, H. E., & Bjørås, M. (2013). Base excision repair. *Cold Spring Harbor Perspectives in Biology*, *5*(4), a012583. https://doi.org/10.1101/cshperspect.a012583

Kröning, A., van den Boom, J., Kracht, M., Kueck, A. F., & Meyer, H. (2022). Ubiquitin-directed AAA+ ATPase p97/VCP unfolds stable proteins crosslinked to DNA for proteolysis by SPRTN. *Journal of Biological Chemistry*, *298*(6), 101976. https://doi.org/10.1016/j.jbc.2022.101976

Kubota, Y., Nash, R. A., Klungland, A., Schär, P., Barnes, D. E., & Lindahl, T. (1996). Reconstitution of DNA base excision-repair with purified human proteins: interaction between DNA polymerase beta and the XRCC1 protein. *The EMBO Journal*, *15*(23), 6662–6670.

Kumari, A., Lim, Y. X., Newell, A. H., Olson, S. B., & McCullough, A. K. (2012). Formaldehyde-induced genome instability is suppressed by an XPF-dependent

pathway. *DNA Repair*, *11*(3), 236–246. https://doi.org/10.1016/j.dnarep.2011.11.001

Lai, Y., Yu, R., Hartwell, H. J., Moeller, B. C., Bodnar, W. M., & Swenberg, J. A. (2016). Measurement of endogenous versus exogenous formaldehyde-induced DNA-protein crosslinks in animal tissues by stable isotope labeling and ultrasensitive mass spectrometry. *Cancer Research*, *76*(9), 2652–2661. https://doi.org/10.1158/0008-5472.CAN-15-2527

Lan, L., Nakajima, S., Oohata, Y., Takao, M., Okano, S., Masutani, M., Wilson, S. H., & Yasui, A. (2004). In situ analysis of repair processes for oxidative DNA damage in mammalian cells. *Proceedings of the National Academy of Sciences of the United States of America*, *101*(38), 13738–13743. https://doi.org/10.1073/pnas.0406048101

Lang, X., Green, M. D., Wang, W., Yu, J., Choi, J. E., Jiang, L., Liao, P., Zhou, J., Zhang, Q., Dow, A., Saripalli, A. L., Kryczek, I., Wei, S., Szeliga, W., Vatan, L., Stone, E. M., Georgiou, G., Cieslik, M., Wahl, D. R., … Zou, W. (2019). Radiotherapy and immunotherapy promote tumoral lipid oxidation and ferroptosis via synergistic repression of SLC7A11. *Cancer Discovery*, *9*(12), 1673–1685. https://doi.org/10.1158/2159-8290.CD-19-0338

Larsen, N. B., Gao, A. O., Sparks, J. L., Gallina, I., Wu, R. A., Mann, M., Räschle, M., Walter, J. C., & Duxin, J. P. (2019). Replication-Coupled DNA-Protein Crosslink Repair by SPRTN and the Proteasome in Xenopus Egg Extracts. *Molecular Cell*, *73*(3), 574-588.e7. https://doi.org/10.1016/j.molcel.2018.11.024

Lascaux, P., Hoslett, G., Tribble, S., Trugenberger, C., Antičević, I., Otten, C., Torrecilla, I., Koukouravas, S., Zhao, Y., Yang, H., Aljarbou, F., Ruggiano, A., Song, W., Peron, C., Deangeli, G., Domingo, E., Bancroft, J., Carrique, L., Johnson, E., … Ramadan, K. (2024). TEX264 drives selective autophagy of DNA lesions to promote DNA repair and cell survival. *Cell*, 5698–5718. https://doi.org/10.1016/j.cell.2024.08.020

Lederman, M. (1981). The early history of radiotherapy: 1895-1939. *International Journal of Radiation Oncology, Biology, Physics*, *7*(5), 639–648. https://doi.org/10.1016/0360-3016(81)90379-5

Ledesma, F. C., El Khamisy, S. F., Zuma, M. C., Osborn, K., & Caldecott, K. W. (2009). A human 5'-tyrosyl DNA phosphodiesterase that repairs topoisomerase-mediated DNA damage. *Nature*, *461*(7264), 674–678. https://doi.org/10.1038/nature08444

Lei, G., Zhang, Y., Koppula, P., Liu, X., Zhang, J., Lin, S. H., Ajani, J. A., Xiao, Q., Liao, Z., Wang, H., & Gan, B. (2020). The role of ferroptosis in ionizing radiation-induced cell death and tumor suppression. *Cell Research*, *30*(2), 146–162. https://doi.org/10.1038/s41422-019-0263-3

Leso, V., Macrini, M. C., Russo, F., & Iavicoli, I. (2020). Formaldehyde Exposure and Epigenetic Effects: A Systematic Review. In *Applied Sciences* (Vol. 10, Issue 7). https://doi.org/10.3390/app10072319

Lessel, D., Vaz, B., Halder, S., Lockhart, P. J., Marinovic-terzic, I., Lopez-mosqueda, J., Philipp, M., Sim, J. C. H., Smith, K. R., Oehler, J., Cabrera, E., Freire, R., Pope, K., Nahid, A., Norris, F., Leventer, R. J., Delatycki, M. B., Barbi, G., Ameln, S. Von, … Terzic, J. (2014). *Mutations in SPRTN cause early onset hepatocellular carcinoma , genomic instability and progeroid features*. *46*(11). https://doi.org/10.1038/ng.3103

Lessel, D., Vaz, B., Halder, S., Lockhart, P. J., Marinovic-Terzic, I., Lopez-Mosqueda, J., Philipp, M., Sim, J. C. H., Smith, K. R., Oehler, J., Cabrera, E., Freire, R., Pope, K., Nahid, A., Norris, F., Leventer, R. J., Delatycki, M. B., Barbi, G., Von Ameln, S., … Kubisch, C. (2014). Mutations in SPRTN cause early onset hepatocellular carcinoma, genomic instability and progeroid features. *Nature Genetics*, *46*(11), 1239–1244. https://doi.org/10.1038/ng.3103

Levine, B., & Kroemer, G. (2008). Autophagy in the Pathogenesis of Disease. *Cell*, *132*(1), 27–42. https://doi.org/10.1016/j.cell.2007.12.018

Levy, J. M. M., Towers, C. G., & Thorburn, A. (2017). Targeting autophagy in cancer. *Nature Reviews Cancer*, *17*(9), 528–542. https://doi.org/10.1038/nrc.2017.53

Li, F., Raczynska, J. E., Chen, Z., & Yu, H. (2019). Structural Insight into DNA-Dependent Activation of Human Metalloprotease Spartan. *Cell Reports*, *26*(12), 3336-3346.e4. https://doi.org/10.1016/j.celrep.2019.02.082

Li, M., You, L., Xue, J., & Lu, Y. (2018). Ionizing radiation-induced cellular senescence in normal, non-transformed cells and the involved DNA damage response: A mini review. *Frontiers in Pharmacology*, *9*(MAY), 1–8. https://doi.org/10.3389/fphar.2018.00522

Liao, C., Beveridge, R., Hudson, J. J. R., Parker, J. D., Chiang, S. C., Ray, S., Ashour, M. E., Sudbery, I., Dickman, M. J., & El-Khamisy, S. F. (2018). UCHL3 Regulates Topoisomerase-Induced Chromosomal Break Repair by Controlling TDP1 Proteostasis. *Cell Reports*, *23*(11), 3352–3365. https://doi.org/10.1016/j.celrep.2018.05.033

Lieber, M. R. (2010). The mechanism of double-strand DNA break repair by the nonhomologous DNA end-joining pathway. *Annual Review of Biochemistry*, *79*(D), 181–211. https://doi.org/10.1146/annurev.biochem.052308.093131

Lin, C. P., Ban, Y., Lyu, Y. L., Desai, S. D., & Liu, L. F. (2008). A ubiquitin-proteasome pathway for the repair of topoisomerase I-DNA covalent complexes. *Journal of Biological Chemistry*, *283*(30), 21074–21083. https://doi.org/10.1074/jbc.M803493200

Lindahl, T., & Andersson, A. (1971). Rate of Chain Breakage at Apurinic Sites in Double-Stranded Deoxyribonucleic Acid. *Biochemistry*, *11*(19), 3618–3623.

Lindahl, T., & Nyberg, B. (1972). Rate of Depurination of Native Deoxyribonucleic Acid. *Biochemistry*, *11*(19), 3610–3618. https://doi.org/10.1021/bi00769a018

Liu, J. C. Y., Ackermann, L., Hoffmann, S., Gál, Z., Hendriks, I. A., Jain, C., Morlot, L., Tatham, M. H., McLelland, G. L., Hay, R. T., Nielsen, M. L., Brummelkamp, T., Haahr, P., & Mailand, N. (2024). Concerted SUMO-targeted ubiquitin ligase activities of TOPORS and RNF4 are essential for stress management and cell proliferation. *Nature Structural and Molecular Biology*, *31*(9), 1355–1367. https://doi.org/10.1038/s41594-024-01294-7

Liu, J. C. Y., Kühbacher, U., Larsen, N. B., Borgermann, N., Garvanska, D. H., Hendriks, I. A., Ackermann, L., Haahr, P., Gallina, I., Guérillon, C., Branigan, E., Hay, R. T., Azuma, Y., Nielsen, M. L., Duxin, J. P., & Mailand, N. (2021). Mechanism and function of DNA replication-independent DNA-protein crosslink repair via the SUMO-RNF4 pathway. *The EMBO Journal*, *40*(18), 1–21. https://doi.org/10.15252/embj.2020107413

Lomax, M. E., Folkes, L. K., & O'Neill, P. (2013a). Biological consequences of radiation-induced DNA damage: Relevance to radiotherapy. *Clinical Oncology*, *25*(10), 578–585. https://doi.org/10.1016/j.clon.2013.06.007

Lomax, M. E., Folkes, L. K., & O'Neill, P. (2013b). Biological consequences of radiation-induced DNA damage: Relevance to radiotherapy. *Clinical Oncology*, *25*(10), 578–585. https://doi.org/10.1016/j.clon.2013.06.007

López-Lázaro, M. (2007). Dual role of hydrogen peroxide in cancer: Possible relevance to cancer chemoprevention and therapy. *Cancer Letters*, *252*(1), 1–8. https://doi.org/10.1016/j.canlet.2006.10.029

Lopez-Mosqueda, J., Maddi, K., Prgomet, S., Kalayil, S., Marinovic-Terzic, I., Terzic, J., & Dikic, I. (2016). SPRTN is a mammalian DNA-binding metalloprotease that resolves DNA-protein crosslinks. *ELife*, *5*(NOVEMBER2016), 1–19. https://doi.org/10.7554/eLife.21491

Lorat, Y., Brunner, C. U., Schanz, S., Jakob, B., Taucher-Scholz, G., & Rübe, C. E. (2015). Nanoscale analysis of clustered DNA damage after high-LET irradiation by quantitative electron microscopy – The heavy burden to repair. *DNA Repair*, *28*, 93–106. https://doi.org/https://doi.org/10.1016/j.dnarep.2015.01.007

Lorat, Y., Schanz, S., Schuler, N., Wennemuth, G., Rübe, C., & Rübe, C. E. (2012). Beyond repair foci: DNA double-strand break repair in euchromatic and heterochromatic compartments analyzed by transmission electron microscopy. *PLoS ONE*, *7*(5). https://doi.org/10.1371/journal.pone.0038165

Lorat, Y., Timm, S., Jakob, B., Taucher-Scholz, G., & Rübe, C. E. (2016). Clustered double-strand breaks in heterochromatin perturb DNA repair after high linear energy transfer irradiation. *Radiotherapy and Oncology*, *121*(1), 154–161. https://doi.org/https://doi.org/10.1016/j.radonc.2016.08.028

Lorković, Z. J., Park, C., Goiser, M., Jiang, D., Kurzbauer, M. T., Schlögelhofer, P., & Berger, F. (2017). Compartmentalization of DNA Damage Response between Heterochromatin and Euchromatin Is Mediated by Distinct H2A Histone Variants. *Current Biology*, *27*(8), 1192–1199. https://doi.org/10.1016/j.cub.2017.03.002

Lu, K., Ye, W., Zhou, L., Collins, L. B., Chen, X., Gold, A., Ball, L. M., & Swenberg, J. A. (2010a). Structural characterization of formaldehyde-induced cross-links between amino acids and deoxynucleosides and their oligomers. *Journal of the American Chemical Society*, *132*(10), 3388–3399. https://doi.org/10.1021/ja908282f

Lu, K., Ye, W., Zhou, L., Collins, L. B., Chen, X., Gold, A., Ball, L. M., & Swenberg, J. A. (2010b). Structural characterization of formaldehyde-induced cross-links between amino acids and deoxynucleosides and their oligomers. *Journal of the American Chemical Society*, *132*(10), 3388–3399. https://doi.org/10.1021/ja908282f

Ma, J., Gao, H., Shen, X., Bai, X., & Tang, M. (2023). A FLASH model of radiolytic oxygen depletion and reactive oxygen species for differential tumor and normal-tissue response. *MedRxiv*. /pmc/articles/PMC10635166/%0A/pmc/articles/PMC10635166/?report=abstract%0Ahttps://www.ncbi.nlm.nih.gov/pmc/articles/PMC10635166/

Ma, Y., Lu, H., Tippin, B., Goodman, M. F., Shimazaki, N., Koiwai, O., Hsieh, C.-L., Schwarz, K., & Lieber, M. R. (2004). A Biochemically Defined System for Mammalian Nonhomologous DNA End Joining. *Molecular Cell*, *16*(5), 701–713. https://doi.org/https://doi.org/10.1016/j.molcel.2004.11.017

Magnander, K., Hultborn, R., Claesson, K., & Elmroth, K. (2009). Clustered DNA Damage in Irradiated Human Diploid Fibroblasts: Influence of Chromatin Organization. *Radiation Research*, *173*(3), 272–282. https://doi.org/10.1667/RR1891.1

Marzi, L., Sun, Y., Huang, S. Y. N., James, A., Difilippantonio, S., & Pommier, Y. (2020). The indenoisoquinoline LMP517: A novel antitumor agent targeting both TOP1 and TOP2. *Molecular Cancer Therapeutics*, *19*(8), 1589–1597. https://doi.org/10.1158/1535-7163.MCT-19-1064

Mascia, A. E., Daugherty, E. C., Zhang, Y., Lee, E., Xiao, Z., Sertorio, M., Woo, J., Backus, L. R., McDonald, J. M., McCann, C., Russell, K., Levine, L., Sharma, R. A., Khuntia, D., Bradley, J. D., Simone, C. B., Perentesis, J. P., & Breneman, J. C. (2023). Proton FLASH Radiotherapy for the Treatment of Symptomatic Bone Metastases: The

FAST-01 Nonrandomized Trial. *JAMA Oncology*, *9*(1), 62–69. https://doi.org/10.1001/jamaoncol.2022.5843

Maskey, R. S., Flatten, K. S., Sieben, C. J., Peterson, K. L., Baker, D. J., Nam, H. J., Kim, M. S., Smyrk, T. C., Kojima, Y., Machida, Y., Santiago, A., Van Deursen, J. M., Kaufmann, S. H., & Machida, Y. J. (2017). Spartan deficiency causes accumulation of Topoisomerase 1 cleavage complexes and tumorigenesis. *Nucleic Acids Research*, *45*(8), 4564–4576. https://doi.org/10.1093/nar/gkx107

Maskey, R. S., Kim, M. S., Baker, D. J., Childs, B., Malureanu, L. A., Jeganathan, K. B., Machida, Y., Van Deursen, J. M., & Machida, Y. J. (2014). Spartan deficiency causes genomic instability and progeroid phenotypes. *Nature Communications*, *5*. https://doi.org/10.1038/ncomms6744

Mathews, C. K. (1996). Bacteriophage T4 Mutants Hypersensitive to an Antitumor Agent That Induces TopoisomeraseDNA Cleavage Complexes Denise. *Encyclopedia of Life Sciences*, *1090*. https://doi.org/10.1038/npg.els.0004249

Matsumoto, Y. B. T.-P. in N. A. R. and M. B. (2001). Molecular mechanism of PCNA-dependent base excision repair. In *Base Excision Repair* (Vol. 68, pp. 129–138). Academic Press. https://doi.org/https://doi.org/10.1016/S0079-6603(01)68095-4

Meng, F., Sun, G., Zhong, M., Yu, Y., & Brewer, M. A. (2013). Anticancer efficacy of cisplatin and trichostatin A or 5-aza-2'-deoxycytidine on ovarian cancer. *British Journal of Cancer*, *108*(3), 579–586. https://doi.org/10.1038/bjc.2013.10

Merk, O., & Speit, G. (1998). Significance of formaldehyde-induced DNA-protein crosslinks for mutagenesis. *Environmental and Molecular Mutagenesis*, *32*(3), 260–268. https://doi.org/10.1002/(SICI)1098-2280(1998)32:3<260::AID-EM9>3.0.CO;2-M

Merk, O., & Speit, G. (1999). Detection of crosslinks with the comet assay in relationship to genotoxicity and cytotoxicity. *Environmental and Molecular Mutagenesis*, *33*(2), 167–172. https://doi.org/10.1002/(SICI)1098-2280(1999)33:2<167::AID-EM9>3.0.CO;2-D

Meselson, M., Stahl, F. W., & Vinograd, J. (1957). Equilibrium Sedimentation of Macromolecules in Density Gradients. *Proceedings of the National Academy of Sciences*, *43*(7), 581–588. https://doi.org/10.1073/pnas.43.7.581

Michaels, H. B., Epp, E. R., Ling, C. C., & Peterson, E. C. (1978). *Oxygen Sensitization of CHO Cells at Ultrahigh Dose Rates : Prelude to Oxygen Diffusion Studies*. *76*(3), 510–521.

Minko, I. G., Zou, Y., & Lloyd, R. S. (2002). Incision of DNA-protein crosslinks by UvrABC nuclease suggests a potential repair pathway involving nucleotide excision repair.

Proceedings of the National Academy of Sciences of the United States of America, *99*(4), 1905–1909. https://doi.org/10.1073/pnas.042700399

Mistry, I. N., Thomas, M., Calder, E. D. D., Conway, S. J., & Hammond, E. M. (2017). Clinical Advances of Hypoxia-Activated Prodrugs in Combination With Radiation Therapy. *International Journal of Radiation Oncology*Biology*Physics*, *98*(5), 1183–1196. https://doi.org/https://doi.org/10.1016/j.ijrobp.2017.03.024

Mizushima, N., & Komatsu, M. (2011). Autophagy: Renovation of cells and tissues. *Cell*, *147*(4), 728–741. https://doi.org/10.1016/j.cell.2011.10.026

Mizushima, N., Levine, B., Cuervo, A. M., & Klionsky, D. J. (2008). Autophagy fights disease through cellular self-digestion. *Nature*, *451*(7182), 1069–1075. https://doi.org/10.1038/nature06639

Mohni, K. N., Wessel, S. R., Zhao, R., Wojciechowski, A. C., Luzwick, J. W., Layden, H., Eichman, B. F., Thompson, P. S., Mehta, K. P. M., & Cortez, D. (2019). HMCES Maintains Genome Integrity by Shielding Abasic Sites in Single-Strand DNA. *Cell*, *176*(1–2), 144-153.e13. https://doi.org/10.1016/j.cell.2018.10.055

Molnar, G., O'leary, N., Pardee, A. B., & Bradley, D. W. (1995). Quantification of DNA-protein interaction by UV crosslinking. *Nucleic Acids Research*, *23*(16), 3318–3326. https://doi.org/10.1093/nar/23.16.3318

Montay-Gruel, P., Meziani, L., Yakkala, C., & Vozenin, M.-C. (2019). Expanding the therapeutic index of radiation therapy by normal tissue protection. *British Journal of Radiology*, *92*(1093), 20180008. https://doi.org/10.1259/bjr.20180008

Moore, S., Stanley, F. K. T., & Goodarzi, A. A. (2014). The repair of environmentally relevant DNA double strand breaks caused by high linear energy transfer irradiation - No simple task. *DNA Repair*, *17*, 64–73. https://doi.org/10.1016/j.dnarep.2014.01.014

Mórocz, M., Zsigmond, E., Tóth, R., Zs Enyedi, M., Pintér, L., & Haracska, L. (2017). DNA-dependent protease activity of human Spartan facilitates replication of DNA-protein crosslink-containing DNA. *Nucleic Acids Research*, *45*(6), 3172–3188. https://doi.org/10.1093/nar/gkw1315

Mosbech, A., Gibbs-Seymour, I., Kagias, K., Thorslund, T., Beli, P., Povlsen, L., Nielsen, S. V., Smedegaard, S., Sedgwick, G., Lukas, C., Hartmann-Petersen, R., Lukas, J., Choudhary, C., Pocock, R., Bekker-Jensen, S., & Mailand, N. (2012a). DVC1 (C1orf124) is a DNA damage-targeting p97 adaptor that promotes ubiquitin-dependent responses to replication blocks. *Nature Structural and Molecular Biology*, *19*(11), 1084–1092. https://doi.org/10.1038/nsmb.2395

Mosbech, A., Gibbs-Seymour, I., Kagias, K., Thorslund, T., Beli, P., Povlsen, L., Nielsen, S. V., Smedegaard, S., Sedgwick, G., Lukas, C., Hartmann-Petersen, R., Lukas, J., Choudhary, C., Pocock, R., Bekker-Jensen, S., & Mailand, N. (2012b). DVC1 (C1orf124) is a DNA damage-targeting p97 adaptor that promotes ubiquitin-dependent responses to replication blocks. *Nature Structural and Molecular Biology*, *19*(11), 1084–1092. https://doi.org/10.1038/nsmb.2395

Mosmann, T. (1983). Rapid colorimetric assay for cellular growth and survival: Application to proliferation and cytotoxicity assays. *Journal of Immunological Methods*, *65*(1–2), 55–63. https://doi.org/10.1016/0022-1759(83)90303-4

Movilla Miangolarra, A., Saxton, D. S., Yan, Z., Rine, J., & Howard, M. (2024). Two-way feedback between chromatin compaction and histone modification state explains Saccharomyces cerevisiae heterochromatin bistability. *Proceedings of the National Academy of Sciences of the United States of America*, *121*(16), e2403316121. https://doi.org/10.1073/pnas.2403316121

Mu, H., Liu, Q., Niu, H., Wang, D., Tang, J., & Duan, J. (2016). Autophagy promotes DNA-protein crosslink clearance. *Mutation Research - Genetic Toxicology and Environmental Mutagenesis*, *797*, 21–25. https://doi.org/10.1016/j.mrgentox.2015.12.001

Mulderrig, L., Garaycoechea, J. I., Tuong, Z. K., Millington, C. L., Dingler, F. A., Ferdinand, J. R., Gaul, L., Tadross, J. A., Arends, M. J., O'Rahilly, S., Crossan, G. P., Clatworthy, M. R., & Patel, K. J. (2021). Aldehyde-driven transcriptional stress triggers an anorexic DNA damage response. *Nature*, *600*(7887), 158–163. https://doi.org/10.1038/s41586-021-04133-7

Murata-kamiya, N., & Kamiya, H. (2001). DNA polymerase and the substrate DNA. *Image (Rochester, N.Y.)*, *29*(16), 3433–3438.

Murga, M., Jaco, I., Fan, Y., Soria, R., Martinez-Pastor, B., Cuadrado, M., Yang, S. M., Blasco, M. A., Skoultchi, A. I., & Fernandez-Capetillo, O. (2007). Global chromatin compaction limits the strength of the DNA damage response. *Journal of Cell Biology*, *178*(7), 1101–1108. https://doi.org/10.1083/jcb.200704140

Murphy, M. P. (2009). How mitochondria produce reactive oxygen species. *Biochemical Journal*, *417*(1), 1–13. https://doi.org/10.1042/BJ20081386

Na, J., Newman, J. A., Then, C. K., Syed, J., Vendrell, I., Torrecilla, I., Ellermann, S., Ramadan, K., Fischer, R., & Kiltie, A. E. (2021). SPRTN protease-cleaved MRE11 decreases DNA repair and radiosensitises cancer cells. *Cell Death and Disease*, *12*(2). https://doi.org/10.1038/s41419-021-03437-w

Nakamura, J., & Nakamura, M. (2020). DNA-protein crosslink formation by endogenous aldehydes and AP sites. *DNA Repair*, *88*(February), 102806. https://doi.org/10.1016/j.dnarep.2020.102806

Nakano, T., Katafuchi, A., Matsubara, M., Terato, H., Tsuboi, T., Masuda, T., Tatsumoto, T., Pil Pack, S., Makino, K., Croteau, D. L., van Houten, B., Iijima, K., Tauchi, H., & Ide, H. (2009). Homologous recombination but not nucleotide excision repair plays a pivotal role in tolerance of DNA-protein cross-links in mammalian cells. *Journal of Biological Chemistry*, *284*(40), 27065–27076. https://doi.org/10.1074/jbc.M109.019174

Nakano, T., Mitsusada, Y., Salem, A. M. H., Shoulkamy, M. I., Sugimoto, T., Hirayama, R., Uzawa, A., Furusawa, Y., & Ide, H. (2015). Induction of DNA-protein cross-links by ionizing radiation and their elimination from the genome. *Mutation Research - Fundamental and Molecular Mechanisms of Mutagenesis*, *771*, 45–50. https://doi.org/10.1016/j.mrfmmm.2014.12.003

Nakano, T., Morishita, S., Katafuchi, A., Matsubara, M., Horikawa, Y., Terato, H., Salem, A. M. H., Izumi, S., Pack, S. P., Makino, K., & Ide, H. (2007). Nucleotide Excision Repair and Homologous Recombination Systems Commit Differentially to the Repair of DNA-Protein Crosslinks. *Molecular Cell*, *28*(1), 147–158. https://doi.org/10.1016/j.molcel.2007.07.029

Nakano, T., Xu, X., Salem, A. M. H., Shoulkamy, M. I., & Ide, H. (2017). Radiation-induced DNA–protein cross-links: Mechanisms and biological significance. *Free Radical Biology and Medicine*, *107*(November), 136–145. https://doi.org/10.1016/j.freeradbiomed.2016.11.041

Niedernhofer, L. J., Daniels, J. S., Rouzer, C. A., Greene, R. E., & Marnett, L. J. (2003). Malondialdehyde, a product of lipid peroxidation, is mutagenic in human cells. *Journal of Biological Chemistry*, *278*(33), 31426–31433. https://doi.org/10.1074/jbc.M212549200

Niemantsverdriet, M., Van Goethem, M. J., Bron, R., Hogewerf, W., Brandenburg, S., Langendijk, J. A., Van Luijk, P., & Coppes, R. P. (2012). High and low LET radiation differentially induce normal tissue damage signals. *International Journal of Radiation Oncology Biology Physics*, *83*(4), 1291–1297. https://doi.org/10.1016/j.ijrobp.2011.09.057

Nikjoo, H., O'Neill, P., Terrissol, M., & Goodhead, D. T. (1999). Quantitative modelling of DNA damage using Monte Carlo track structure method. *Radiation and Environmental Biophysics*, *38*(1), 31–38. https://doi.org/10.1007/s004110050135

Nitiss, J. L., & Beck, W. T. (1996). Antitopoisomerase drug action and resistance. *European Journal of Cancer*, *32*(6), 958–966. https://doi.org/10.1016/0959-8049(96)00056-1

Nitiss, J. L., Soans, E., Rogojina, A., Seth, A., & Mishina, M. (2012). Topoisomerase assays. *Current Protocols in Pharmacology*, *SUPPL.57*, 1–27. https://doi.org/10.1002/0471141755.ph0303s57

O'Connor, T. J., & Nodwell, J. R. (2005). Pivotal roles for the receiver domain in the mechanism of action of the response regulator RamR of Streptomyces coelicolor. *Journal of Molecular Biology*, *351*(5), 1030–1047. https://doi.org/10.1016/j.jmb.2005.06.053

Ogawa, Y., Kobayashi, T., Nishioka, A., Kariya, S., Hamasato, S., Seguchi, H., & Yoshida, S. (2003). Radiation-induced oxidative DNA damage, 8-oxoguanine, in human peripheral T cells. *International Journal of Molecular Medicine*, *11*(1), 27–32.

Oka, Y., Hamada, M., Nakazawa, Y., Muramatsu, H., Okuno, Y., Higasa, K., Shimada, M., Takeshima, H., Hanada, K., Hirano, T., Kawakita, T., Sakaguchi, H., Ichimura, T., Ozono, S., Yuge, K., Watanabe, Y., Kotani, Y., Yamane, M., Kasugai, Y., … Ogi, T. (2025). Digenic mutations in ALDH2 and ADH5 impair formaldehyde clearance and cause a multisystem disorder, AMeD syndrome. *Science Advances*, *6*(51), eabd7197. https://doi.org/10.1126/sciadv.abd7197

Oka, Y., Nakazawa, Y., Shimada, M., & Ogi, T. (2024). Endogenous aldehyde-induced DNA–protein crosslinks are resolved by transcription-coupled repair. *Nature Cell Biology*, *26*(5), 784–796. https://doi.org/10.1038/s41556-024-01401-2

Onda, M., Yamaguchi, J., Hanada, K., Asami, Y., & Ikeda, H. (2001). Repair of topoisomerase-mediated DNA damage in bacteriophage T4. *Genetics*, *158*(1), 19–28. https://doi.org/10.1093/genetics/158.1.19

Pachva, M. C., Kisselev, A. F., Matkarimov, B. T., Saparbaev, M., & Groisman, R. (2020). DNA-Histone Cross-Links: Formation and Repair. *Frontiers in Cell and Developmental Biology*, *8*(December), 1–14. https://doi.org/10.3389/fcell.2020.607045

Paganetti, H. (2014). Relative biological effectiveness (RBE) values for proton beam therapy. Variations as a function of biological endpoint, dose, and linear energy transfer. *Physics in Medicine and Biology*, *59*(22), R419–R472. https://doi.org/10.1088/0031-9155/59/22/R419

Paganetti, H. P., Niemierko, A. N., Ancukiewicz, M. A., Gerweck, L. E. G., Goitein, M. G., Loeffler, J. S. L., Suit, H. D. S., & Hil, D. P. (2002). *RELATIVE BIOLOGICAL EFFECTIVENESS (RBE) VALUES FOR PROTON BEAM THERAPY*. *53*(2), 407–421.

Pan, M., Wright, W. C., Chapple, R. H., Zubair, A., Sandhu, M., Batchelder, J. E., Huddle, B. C., Low, J., Blankenship, K. B., Wang, Y., Gordon, B., Archer, P., Brady, S. W., Natarajan, S., Posgai, M. J., Schuetz, J., Miller, D., Kalathur, R., Chen, S., … Geeleher, P. (2021). The chemotherapeutic CX-5461 primarily targets TOP2B and exhibits selective activity in high-risk neuroblastoma. *Nature Communications*, *12*(1), 1–20. https://doi.org/10.1038/s41467-021-26640-x

Patel, A. G., Flatten, K. S., Peterson, K. L., Beito, T. G., Schneider, P. A., Perkins, A. L., Harki, D. A., & Kaufmann, S. H. (2016). Immunodetection of human topoisomerase I-DNA covalent complexes. *Nucleic Acids Research*, *44*(6), 2816–2826. https://doi.org/10.1093/nar/gkw109

Paul, K., Wang, M., Mladenov, E., Bencsik-Theilen, A., Bednar, T., Wu, W., Arakawa, H., & Iliakis, G. (2013). DNA Ligases I and III Cooperate in Alternative Non-Homologous End-Joining in Vertebrates. *PLOS ONE*, *8*(3), e59505. https://doi.org/10.1371/journal.pone.0059505

Pawlik, T. M., & Keyomarsi, K. (2004). Role of cell cycle in mediating sensitivity to radiotherapy. *International Journal of Radiation Oncology*Biology*Physics*, *59*(4), 928–942. https://doi.org/https://doi.org/10.1016/j.ijrobp.2004.03.005

Perrier, S., Hau, J., Gasparutto, D., Cadet, J., Favier, A., & Ravanat, J. L. (2006). Characterization of lysine-guanine cross-links upon one-electron oxidation of a guanine-containing oligonucleotide in the presence of a trilysine peptide. *Journal of the American Chemical Society*, *128*(17), 5703–5710. https://doi.org/10.1021/ja057656i

Perry, M., Biegert, M., Kollala, S. S., Mallard, H., Su, G., Kodavati, M., Kreiling, N., Holbrook, A., & Ghosal, G. (2021). USP11 mediates repair of DNA–protein cross-links by deubiquitinating SPRTN metalloprotease. *Journal of Biological Chemistry*, *296*, 100396. https://doi.org/10.1016/j.jbc.2021.100396

Perstin, A., Poirier, Y., Sawant, A., & Tambasco, M. (2022). Quantifying the DNA-damaging Effects of FLASH Irradiation With Plasmid DNA. *International Journal of Radiation Oncology, Biology, Physics*, *113*(2), 437–447. https://doi.org/10.1016/j.ijrobp.2022.01.049

Petrova, K. V., Millsap, A. D., Stec, D. F., & Rizzo, C. J. (2014a). Characterization of the deoxyguanosine-lysine cross-link of methylglyoxal. *Chemical Research in Toxicology*, *27*(6), 1019–1029. https://doi.org/10.1021/tx500068v

Petrova, K. V., Millsap, A. D., Stec, D. F., & Rizzo, C. J. (2014b). Characterization of the deoxyguanosine-lysine cross-link of methylglyoxal. *Chemical Research in Toxicology*, *27*(6), 1019–1029. https://doi.org/10.1021/tx500068v

Pham, V. N., Bruemmer, K. J., Toh, J. D. W., Ge, E. J., Tenney, L., Ward, C. C., Dingler, F. A., Millington, C. L., Garcia-Prieto, C. A., Pulos-Holmes, M. C., Ingolia, N. T., Pontel, L. B., Esteller, M., Patel, K. J., Nomura, D. K., & Chang, C. J. (2025). Formaldehyde regulates S-adenosylmethionine biosynthesis and one-carbon metabolism. *Science*, *382*(6670), eabp9201. https://doi.org/10.1126/science.abp9201

Plumb, M. A., Smith, G. C. M., Cunniffe, S. M. T., Jackson, S. P., & O'Neill, P. (1999). DNA-PK activation by ionizing radiation-induced DNA single-strand breaks. *International Journal of Radiation Biology*, *75*(5), 553–561. https://doi.org/10.1080/095530099140195

Pommier, Y. (2009). DNA topoisomerase I Inhibitors: Chemistry, biology, and interfacial inhibition. *Chemical Reviews*, *109*(7), 2894–2902. https://doi.org/10.1021/cr900097c

Prasad, R., Horton, J. K., Chastain, P. D., Gassman, N. R., Freudenthal, B. D., Hou, E. W., & Wilson, S. H. (2014). Suicidal cross-linking of PARP-1 to AP site intermediates in cells undergoing base excision repair. *Nucleic Acids Research*, *42*(10), 6337–6351. https://doi.org/10.1093/nar/gku288

Protano, C., Buomprisco, G., Cammalleri, V., Pocino, R. N., Marotta, D., Simonazzi, S., Cardoni, F., Petyx, M., Iavicoli, S., & Vitali, M. (2022). *The Carcinogenic Effects of Formaldehyde Occupational Exposure : A Systematic Review*. 1–12.

Puddu, F., Salguero, I., Herzog, M., Geisler, N. J., Costanzo, V., & Jackson, S. P. (2017). Chromatin determinants impart camptothecin sensitivity. *EMBO Reports*, *18*(6), 1000–1012. https://doi.org/10.15252/embr.201643560

Quievryn, G., & Zhitkovich, A. (2000). Loss of DNA-protein crosslinks from formaldehyde-exposed cells occurs through spontaneous hydrolysis and an active repair process linked to proteosome function. *Carcinogenesis*, *21*(8), 1573–1580. https://doi.org/10.1093/carcin/21.5.573

Quiñones, J. L., Thapar, U., Yu, K., Fang, Q., Sobol, R. W., & Demple, B. (2015). Enzyme mechanism-based, oxidative DNA-protein cross-links formed with DNA polymerase β in vivo. *Proceedings of the National Academy of Sciences of the United States of America*, *112*(28), 8602–8607. https://doi.org/10.1073/pnas.1501101112

Radford, I. R. (1985). Effect of radiomodifying agents on the ratios of x-ray-induced lesions in cellular DNA: Use in lethal lesion determination. *International Journal of Radiation Biology*, *49*(4), 621–637. https://doi.org/10.1080/09553008514552871

Rama, N., Saha, T., Shukla, S., Goda, C., Milewski, D., Mascia, A. E., Vatner, R. E., Sengupta, D., Katsis, A., Abel, E., Girdhani, S., Miyazaki, M., Rodriguez, A., Ku, A., Dua, R., Parry, R., & Kalin, T. V. (2019). Improved Tumor Control Through T-cell

Infiltration Modulated by Ultra-High Dose Rate Proton FLASH Using a Clinical Pencil Beam Scanning Proton System. *International Journal of Radiation Oncology*Biology*Physics*, *105*(1), S164–S165. https://doi.org/10.1016/J.IJROBP.2019.06.187

Ramadan, K., Halder, S., Wiseman, K., & Vaz, B. (2017). Strategic role of the ubiquitin-dependent segregase p97 (VCP or Cdc48) in DNA replication. *Chromosoma*, *126*(1), 17–32. https://doi.org/10.1007/s00412-016-0587-4

Reczek, C. R., & Chandel, N. S. (2017). The two faces of reactive oxygen species in cancer. *Annual Review of Cancer Biology*, *1*, 79–98. https://doi.org/10.1146/annurev-cancerbio-041916-065808

Reingruber, H., & Pontel, L. B. (2018). Formaldehyde metabolism and its impact on human health. *Current Opinion in Toxicology*, *9*, 28–34. https://doi.org/https://doi.org/10.1016/j.cotox.2018.07.001

Reinking, H. K., Kang, H., Jae, L. T., Go, M. J., Sattler, M., & Stingele, J. (2020). *Article DNA Structure-Specific Cleavage of DNA-Protein Crosslinks by the SPRTN Protease ll ll DNA Structure-Specific Cleavage of DNA-Protein Crosslinks by the SPRTN Protease*. 102–113. https://doi.org/10.1016/j.molcel.2020.08.003

Reynolds, P., Anderson, J. A., Harper, J. V, Hill, M. A., Botchway, S. W., Parker, A. W., & O'Neill, P. (2012). The dynamics of Ku70/80 and DNA-PKcs at DSBs induced by ionizing radiation is dependent on the complexity of damage. *Nucleic Acids Research*, *40*(21), 10821–10831. https://doi.org/10.1093/nar/gks879

RichardWagner, J. C. (2013). DNA Base Damage by Reactive Oxygen Species, Oxidizing Agents, and UV Radiation. *Cold Spring Harb Perspect Biol*, *5*, 1–18.

Rieckher, M., Gallrein, C., Alquezar-Artieda, N., Bourached-Silva, N., Vaddavalli, P. L., Mares, D., Backhaus, M., Blindauer, T., Greger, K., Wiesner, E., Pontel, L. B., & Schumacher, B. (2024). Distinct DNA repair mechanisms prevent formaldehyde toxicity during development, reproduction and aging. *Nucleic Acids Research*, *52*(14), 8271–8285. https://doi.org/10.1093/nar/gkae519

Robert, T., Vanoli, F., Chiolo, I., Shubassi, G., Bernstein, K. A., Rothstein, R., Botrugno, O. A., Parazzoli, D., Oldani, A., Minucci, S., & Foiani, M. (2011). HDACs link the DNA damage response, processing of double-strand breaks and autophagy. *Nature*, *471*(7336), 74–79. https://doi.org/10.1038/nature09803

Rooney, S., Alt, F. W., Lombard, D., Whitlow, S., Eckersdorff, M., Fleming, J., Fugmann, S., Ferguson, D. O., Schatz, D. G., & Sekiguchi, J. (2003). Defective DNA repair and increased genomic instability in Artemis-deficient murine cells. *The Journal of Experimental Medicine*, *197*(5), 553–565. https://doi.org/10.1084/jem.20021891

Rosenberg, B., VanCamp, L., Trosko, J. E., & Mansour, V. H. (1969). Platinum Compounds: a New Class of Potent Antitumour Agents. *Nature*, *222*, 385–386.

Rothkamm, K., & Löbrich, M. (2003). Evidence for a lack of DNA double-strand break repair in human cells exposed to very low x-ray doses. *Proceedings of the National Academy of Sciences of the United States of America*, *100*(9), 5057–5062. https://doi.org/10.1073/pnas.0830918100

Rübe, C. E., Lorat, Y., Schuler, N., Schanz, S., Wennemuth, G., & Rübe, C. (2011). DNA repair in the context of chromatin: New molecular insights by the nanoscale detection of DNA repair complexes using transmission electron microscopy. *DNA Repair*, *10*(4), 427–437. https://doi.org/https://doi.org/10.1016/j.dnarep.2011.01.012

Ruggiano, A., & Ramadan, K. (2021a). DNA–protein crosslink proteases in genome stability. *Communications Biology*, *4*(1), 11. https://doi.org/10.1038/s42003-020-01539-3

Ruggiano, A., & Ramadan, K. (2021b). DNA–protein crosslink proteases in genome stability. *Communications Biology*, *4*(1), 1–11. https://doi.org/10.1038/s42003-020-01539-3

Ruggiano, A., Vaz, B., Kilgas, S., Popović, M., Rodriguez-Berriguete, G., Singh, A. N., Higgins, G. S., Kiltie, A. E., & Ramadan, K. (2021). The protease SPRTN and SUMOylation coordinate DNA-protein crosslink repair to prevent genome instability. *Cell Reports*, *37*(10). https://doi.org/10.1016/j.celrep.2021.110080

Sacho, E. J., & Maizels, N. (2011). DNA repair factor MRE11/RAD50 cleaves 3'-phosphotyrosyl bonds and resects DNA to repair damage caused by topoisomerase 1 poisons. *Journal of Biological Chemistry*, *286*(52), 44945–44951. https://doi.org/10.1074/jbc.M111.299347

Saito, S., Maeda, R., & Adachi, N. (2017). Dual loss of human POLQ and LIG4 abolishes random integration. *Nature Communications*, *8*. https://doi.org/10.1038/ncomms16112

Saksouk, N., Simboeck, E., & Déjardin, J. (2015). Constitutive heterochromatin formation and transcription in mammals. *Epigenetics & Chromatin*, *8*(1), 3. https://doi.org/10.1186/1756-8935-8-3

Santivasi, W. L., & Xia, F. (2014). Ionizing Radiation-Induced DNA Damage, Response, and Repair. *Antioxidants & Redox Signaling*, *21*(2), 251–259. https://doi.org/10.1089/ars.2013.5668

Sato, K., Imai, T., Okayasu, R., & Shimokawa, T. (2014). Heterochromatin Domain Number Correlates with X-Ray and Carbon-Ion Radiation Resistance in Cancer Cells. *Radiation Research*, *182*(4), 408–419. https://doi.org/10.1667/RR13492.1

Schindelin, J., Arganda-Carreras, I., Frise, E., Kaynig, V., Longair, M., Pietzsch, T., Preibisch, S., Rueden, C., Saalfeld, S., Schmid, B., Tinevez, J. Y., White, D. J., Hartenstein, V., Eliceiri, K., Tomancak, P., & Cardona, A. (2012). Fiji: An open-source platform for biological-image analysis. *Nature Methods*, *9*(7), 676–682. https://doi.org/10.1038/nmeth.2019

Schmid, T. E., Günther, D., Wolfgang, B., Volker, H., Christoph, G., Susanne, A., Anja, M., Attila, T., Anna A., F., Michael, M., & and Röper, B. (2010). Differences in the kinetics of γ-H2AX fluorescence decay after exposure to low and high LET radiation. *International Journal of Radiation Biology*, *86*(8), 682–691. https://doi.org/10.3109/09553001003734543

Sczepanski, J. T., Wong, R. S., McKnight, J. N., Bowman, G. D., & Greenberg, M. M. (2010). Rapid DNA-protein cross-linking and strand scission by an abasic site in a nucleosome core particle. *Proceedings of the National Academy of Sciences of the United States of America*, *107*(52), 22475–22480. https://doi.org/10.1073/pnas.1012860108

Seane, E. N., Nair, S., Vandevoorde, C., & Joubert, A. (2024). Mechanistic Sequence of Histone Deacetylase Inhibitors and Radiation Treatment: An Overview. *Pharmaceuticals*, *17*(5), 1–15. https://doi.org/10.3390/ph17050602

Seifter, J. L. (2025). *Hidden Formaldehyde in E-Cigarette Aerosols*. 25–27. https://doi.org/10.1056/NEJMc1414731

Semenza, G. L. (2012). Hypoxia-inducible factors in physiology and medicine. *Cell*, *148*(3), 399–408. https://doi.org/10.1016/j.cell.2012.01.021

Semlow, D. R., MacKrell, V. A., & Walter, J. C. (2022). The HMCES DNA-protein cross-link functions as an intermediate in DNA interstrand cross-link repair. In *Nature Structural and Molecular Biology* (Vol. 29, Issue 5). Springer US. https://doi.org/10.1038/s41594-022-00764-0

Seres, A. J. F. Jr. D. S. (1982). Repair of trans - Pt (I I) diammi nedichloride D N A - protein crosslinks in normal and excision-deficient human cells. *Mutation Research*, *94*, 277–284.

Sheard, M. A., Uldrijan, S., & Vojtesek, B. (2003). Role of p53 in Regulating Constitutive and X-Radiation-Inducible CD95 Expression and Function in Carcinoma Cells. *Cancer Research*, *63*(21), 7176–7184.

Shi, Y., Lan, F., Matson, C., Mulligan, P., Whetstine, J. R., Cole, P. A., Casero, R. A., & Shi, Y. (2004a). Histone demethylation mediated by the nuclear amine oxidase homolog LSD1. *Cell*, *119*(7), 941–953. https://doi.org/10.1016/j.cell.2004.12.012

Shi, Y., Lan, F., Matson, C., Mulligan, P., Whetstine, J. R., Cole, P. A., Casero, R. A., & Shi, Y. (2004b). Histone demethylation mediated by the nuclear amine oxidase homolog LSD1. *Cell*, *119*(7), 941–953. https://doi.org/10.1016/j.cell.2004.12.012

Shoulkamy, M. I., Nakano, T., Ohshima, M., Hirayama, R., Uzawa, A., Furusawa, Y., & Ide, H. (2012). Detection of DNA-protein crosslinks (DPCs) by novel direct fluorescence labeling methods: Distinct stabilities of aldehyde and radiation-induced DPCs. *Nucleic Acids Research*, *40*(18). https://doi.org/10.1093/nar/gks601

Simonelli, V., Narciso, L., Dogliotti, E., & Fortini, P. (2005). Base excision repair intermediates are mutagenic in mammalian cells. *Nucleic Acids Research*, *33*(14), 4404–4411. https://doi.org/10.1093/nar/gki749

Singh, N. P., McCoy, M. T., Tice, R. R., & Schneider, E. L. (1988). A simple technique for quantitation of low levels of DNA damage in individual cells. *Experimental Cell Research*, *175*(1), 184–191. https://doi.org/10.1016/0014-4827(88)90265-0

Singleton, B. K., Griffin, C. S., & Thacker, J. (2002). Clustered DNA damage leads to complex genetic changes in irradiated human cells. *Cancer Research*, *62*(21), 6263–6269.

Siomin, Y. A., Simonov, V. V., & Poverenny, A. M. (1973). The reaction of formaldehyde with deoxynucleotides and DNA in the presence of amino acids and lysine-rich histone. *BBA Section Nucleic Acids And Protein Synthesis*, *331*(1), 27–32. https://doi.org/10.1016/0005-2787(73)90415-2

Smith, K. C. (1962). *Dose dependent decrease in extractability of DNA from bacteria following irradiation with ultraviolet light or with visible light plus dye*. *8*(3), 157–163.

Song, W., & Ramadan, K. (2023). Atypical K6-ubiquitin chains mobilize p97/VCP and the proteasome to resolve formaldehyde-induced RNA-protein crosslinks. *Molecular Cell*, *83*(23), 4197–4199. https://doi.org/10.1016/j.molcel.2023.11.009

Song, W., Zhao, Y., Ruggiano, A., Redfield, C., & Joseph, A. (2024). *The dual ubiquitin binding mode of SPRTN secures rapid spatiotemporal proteolysis of DNA-protein crosslinks*.

Sørensen, B. S., Horsman, M. R., Alsner, J., Overgaard, J., Durante, M., Scholz, M., Friedrich, T., & Bassler, N. (2015). Relative biological effectiveness of carbon ions for tumor control, acute skin damage and late radiation-induced fibrosis in a mouse model. *Acta Oncologica*, *54*(9), 1623–1630. https://doi.org/10.3109/0284186X.2015.1069890

Soto, L. A., Casey, K. M., Wang, J., Blaney, A., Manjappa, R., Breitkreutz, D., Skinner, L., Dutt, S., Ko, R. B., Bush, K., Yu, A. S., Melemenidis, S., Strober, S., Englemann, E., Maxim, P. G., Graves, E. E., & Loo, B. W. (2020). Flash irradiation results in reduced severe skin toxicity compared to conventional-dose-rate irradiation. *Radiation Research*, *194*(6), 618–624. https://doi.org/10.1667/RADE-20-00090

Sparks, J. L., Chistol, G., Gao, A. O., Räschle, M., Larsen, N. B., Mann, M., Duxin, J. P., & Walter, J. C. (2019). The CMG Helicase Bypasses DNA-Protein Cross-Links to Facilitate Their Repair. *Cell*, *176*(1–2), 167-181.e21. https://doi.org/10.1016/j.cell.2018.10.053

Speit, G., Schütz, P., & Merk, O. (2000). Induction and repair of formaldehyde-induced DNA-protein crosslinks in repair-deficient human cell lines. *Mutagenesis*, *15*(1), 85–90. https://doi.org/10.1093/mutage/15.1.85

Stantial, N., Rogojina, A., Gilbertson, M., Sun, Y., Miles, H., Shaltz, S., Berger, J., Nitiss, K. C., Jinks-Robertson, S., & Nitiss, J. L. (2020). Trapped topoisomerase II initiates formation of de novo duplications via the nonhomologous end-joining pathway in yeast. *Proceedings of the National Academy of Sciences of the United States of America*, *117*(43), 26876–26884. https://doi.org/10.1073/pnas.2008721117

Stingele, J., Bellelli, R., Alte, F., Hewitt, G., Sarek, G., Maslen, S. L., Tsutakawa, S. E., Borg, A., Kjær, S., Tainer, J. A., Skehel, J. M., Groll, M., & Boulton, S. J. (2016a). Mechanism and Regulation of DNA-Protein Crosslink Repair by the DNA-Dependent Metalloprotease SPRTN. *Molecular Cell*, *64*(4), 688–703. https://doi.org/10.1016/j.molcel.2016.09.031

Stingele, J., Bellelli, R., Alte, F., Hewitt, G., Sarek, G., Maslen, S. L., Tsutakawa, S. E., Borg, A., Kjær, S., Tainer, J. A., Skehel, J. M., Groll, M., & Boulton, S. J. (2016b). Mechanism and Regulation of DNA-Protein Crosslink Repair by the DNA-Dependent Metalloprotease SPRTN. *Molecular Cell*, *64*(4), 688–703. https://doi.org/10.1016/j.molcel.2016.09.031

Stingele, J., Bellelli, R., & Boulton, S. J. (2017). Mechanisms of DNA-protein crosslink repair. *Nature Reviews Molecular Cell Biology*, *18*(9), 563–573. https://doi.org/10.1038/nrm.2017.56

Stingele, J., & Jentsch, S. (2015). DNA-protein crosslink repair. *Nature Reviews Molecular Cell Biology*, *16*(8), 455–460. https://doi.org/10.1038/nrm4015

Stingele, J., Schwarz, M. S., Bloemeke, N., Wolf, P. G., & Jentsch, S. (2014). A DNA-dependent protease involved in DNA-protein crosslink repair. *Cell*, *158*(2), 327–338. https://doi.org/10.1016/j.cell.2014.04.053

Stirling, D. R., Swain-Bowden, M. J., Lucas, A. M., Carpenter, A. E., Cimini, B. A., & Goodman, A. (2021). CellProfiler 4: improvements in speed, utility and usability. *BMC Bioinformatics*, *22*(1), 1–11. https://doi.org/10.1186/s12859-021-04344-9

Storch, K., Eke, I., Borgmann, K., Krause, M., Richter, C., Becker, K., Schröck, E., & Cordes, N. (2010). Three-dimensional cell growth confers radioresistance by chromatin density modification. *Cancer Research*, *70*(10), 3925–3934. https://doi.org/10.1158/0008-5472.CAN-09-3848

Strigari, L., Torriani, F., Manganaro, L., Inaniwa, T., Dalmasso, F., Cirio, R., & Attili, A. (2018). Tumour control in ion beam radiotherapy with different ions in the presence of hypoxia: an oxygen enhancement ratio model based on the microdosimetric kinetic model. *Physics in Medicine & Biology*, *63*(6), 65012. https://doi.org/10.1088/1361-6560/aa89ae

Stützer, A., Welp, L. M., Raabe, M., Sachsenberg, T., Kappert, C., Wulf, A., Lau, A. M., David, S. S., Chernev, A., Kramer, K., Politis, A., Kohlbacher, O., Fischle, W., & Urlaub, H. (2020). Analysis of protein-DNA interactions in chromatin by UV induced cross-linking and mass spectrometry. *Nature Communications*, *11*(1), 1–12. https://doi.org/10.1038/s41467-020-19047-7

Subramanian, D., Muller, M. T., Kraut, E., Staubus, A., & Young, D. C. (1995). Analysis of Topoisomerase I/DNA Complexes in Patients Administered Topotecan. *Cancer Research*, *55*(10), 2097–2103.

Sugimoto, Y., Masuda, Y., Iwai, S., Miyake, Y., Kanao, R., & Masutani, C. (2023). Novel mechanisms for the removal of strong replication-blocking HMCES-and thiazolidine-DNA adducts in humans. *Nucleic Acids Research*, *51*(10), 4959–4981. https://doi.org/10.1093/nar/gkad246

Sun, Y., Jenkins, L. M. M., Su, Y. P., Nitiss, K. C., Nitiss, J. L., & Pommier, Y. (2020). A conserved SUMO pathway repairs topoisomerase DNA-protein cross-links by engaging ubiquitin-mediated proteasomal degradation. *Science Advances*, *6*(46), 1–17. https://doi.org/10.1126/sciadv.aba6290

Sung, P., Trujillo, K. M., & Van Komen, S. (2000). Recombination factors of Saccharomyces cerevisiae. *Mutation Research*, *451*(1–2), 257–275. https://doi.org/10.1016/s0027-5107(00)00054-3

Suryo Rahmanto, A., Blum, C. J., Scalera, C., Heidelberger, J. B., Mesitov, M., Horn-Ghetko, D., Gräf, J. F., Mikicic, I., Hobrecht, R., Orekhova, A., Ostermaier, M., Ebersberger, S., Möckel, M. M., Krapoth, N., Da Silva Fernandes, N., Mizi, A., Zhu, Y., Chen, J.-X., Choudhary, C., … Beli, P. (2023). K6-linked ubiquitylation marks formaldehyde-induced RNA-protein crosslinks for resolution. *Molecular Cell*, *83*(23), 4272-4289.e10. https://doi.org/10.1016/j.molcel.2023.10.011

Sutherland, B. M., Bennett, P. V, Schenk, H., Sidorkina, O., Laval, J., Trunk, J., Monteleone, D., & Sutherland, J. (2001). Clustered DNA damages induced by high and low LET radiation, including heavy ions. *Physica Medica : PM : An International Journal Devoted to the Applications of Physics to Medicine and Biology : Official Journal of the Italian Association of Biomedical Physics (AIFB)*, *17 Suppl 1*, 202–204.

Svilar, D., Goellner, E. M., Almeida, K. H., & Sobol, R. W. (2010). Base Excision Repair and Lesion-Dependent Subpathways for Repair of Oxidative DNA Damage. *Antioxidants & Redox Signaling*, *14*(12), 2491–2507. https://doi.org/10.1089/ars.2010.3466

Takata, H., Hanafusa, T., Mori, T., Shimura, M., Iida, Y., Ishikawa, K., Yoshikawa, K., Yoshikawa, Y., & Maeshima, K. (2013a). Chromatin Compaction Protects Genomic DNA from Radiation Damage. *PLOS ONE*, *8*(10), e75622. https://doi.org/10.1371/journal.pone.0075622

Takata, H., Hanafusa, T., Mori, T., Shimura, M., Iida, Y., Ishikawa, K., Yoshikawa, K., Yoshikawa, Y., & Maeshima, K. (2013b). Chromatin Compaction Protects Genomic DNA from Radiation Damage. *PLoS ONE*, *8*(10), 1–11. https://doi.org/10.1371/journal.pone.0075622

Takata, M., Sasaki, M. S., Sonoda, E., Fukushima, T., Morrison, C., Albala, J. S., Swagemakers, S. M., Kanaar, R., Thompson, L. H., & Takeda, S. (2000). The Rad51 paralog Rad51B promotes homologous recombinational repair. *Molecular and Cellular Biology*, *20*(17), 6476–6482. https://doi.org/10.1128/MCB.20.17.6476-6482.2000

Tayri-Wilk, T., Slavin, M., Zamel, J., Blass, A., Cohen, S., Motzik, A., Sun, X., Shalev, D. E., Ram, O., & Kalisman, N. (2020). Mass spectrometry reveals the chemistry of formaldehyde cross-linking in structured proteins. *Nature Communications*, *11*(1), 1–9. https://doi.org/10.1038/s41467-020-16935-w

Terato, H., Tanaka, R., Nakaarai, Y., Nohara, T., Doi, Y., Iwai, S., Hirayama, R., Furusawa, Y., & Ide, H. (2008). Quantitative analysis of isolated and clustered DNA damage induced by gamma-rays, carbon ion beams, and iron ion beams. *Journal of Radiation Research*, *49*(2), 133–146. https://doi.org/10.1269/jrr.07089

Thompson, L. H., & Schild, D. (1999). The contribution of homologous recombination in preserving genome integrity in mammalian cells. *Biochimie*, *81*(1–2), 87–105. https://doi.org/10.1016/s0300-9084(99)80042-x

Thornalley, P. J., Waris, S., Fleming, T., Santarius, T., Larkin, S. J., Winklhofer-Roob, B. M., Stratton, M. R., & Rabbani, N. (2010). Imidazopurinones are markers of physiological genomic damage linked to DNA instability and glyoxalase 1-

associated tumour multidrug resistance. *Nucleic Acids Research*, *38*(16), 5432–5442. https://doi.org/10.1093/nar/gkq306

Tice, R. R., Strauss, G. H. S., & Peters, W. P. (1992). High-dose combination alkylating agents with autologous bone-marrow support in patients with breast cancer: preliminary assessment of DNA damage in individual peripheral blood lymphocytes using the single cell gel electrophoresis assay. *Mutation Research/Environmental Mutagenesis and Related Subjects*, *271*(2), 101–113. https://doi.org/10.1016/0165-1161(92)91083-4

Tice, R. R., Yager, J. W., Andrews, P., & Crecelius, E. (1997). Effect of hepatic methyl donor status on urinary excretion and DNA damage in B6C3F1 mice treated with sodium arsenite. *Mutation Research - Reviews in Mutation Research*, *386*(3), 315–334. https://doi.org/10.1016/S1383-5742(97)00004-5

Torrecilla, I., Ruggiano, A., Kiianitsa, K., Aljarbou, F., Lascaux, P., Hoslett, G., Song, W., Maizels, N., & Ramadan, K. (2024). Isolation and detection of DNA–protein crosslinks in mammalian cells. *Nucleic Acids Research*, *52*(2), 525–547. https://doi.org/10.1093/nar/gkad1178

Tounekti, O., Kenani, A., Foray, N., Orlowski, S., & Mir, L. M. (2001). The ratio of single-to double-strand DNA breaks and their absolute values determine cell death pathway. *British Journal of Cancer*, *84*(9), 1272–1279. https://doi.org/10.1054/bjoc.2001.1786

Tretyakova, N. Y., Groehler, A., & Ji, S. (2015). DNA-Protein Cross-Links: Formation, Structural Identities, and Biological Outcomes. *Accounts of Chemical Research*, *48*(6), 1631–1644. https://doi.org/10.1021/acs.accounts.5b00056

Tsuda, M., Kitamasu, K., Hosokawa, S., Nakano, T., & Ide, H. (2020). Repair of trapped topoisomerase II covalent cleavage complexes: Novel proteasome-independent mechanisms. *Nucleosides, Nucleotides and Nucleic Acids*, *39*(1–3), 170–184. https://doi.org/10.1080/15257770.2019.1674332

Tu, C.-Y., Chen, Y.-F., Lii, C.-K., & Wang, T.-S. (2013). Methylglyoxal induces DNA crosslinks in ECV304 cells via a reactive oxygen species-independent protein carbonylation pathway. *Toxicology in Vitro : An International Journal Published in Association with BIBRA*, *27*(4), 1211–1219. https://doi.org/10.1016/j.tiv.2013.02.011

Tubbs, A., & Nussenzweig, A. (2017). Endogenous DNA Damage as a Source of Genomic Instability in Cancer. *Cell*, *168*(4), 644–656. https://doi.org/10.1016/j.cell.2017.01.002

Tudek, B., Boiteux, S., & Laval, J. (1992). Biological properties of imidazole ring-opened N7-methylguanine in M13mp18 phage DNA. *Nucleic Acids Research*, *20*(12), 3079–3084. https://doi.org/10.1093/nar/20.12.3079

Van Dyck, E., Stasiak, A. Z., Stasiak, A., & West, S. C. (1999). Binding of double-strand breaks in DNA by human Rad52 protein. *Nature*, *398*(6729), 728–731. https://doi.org/10.1038/19560

Van Gent, D. C., Hoeijmakers, J. H. J., & Kanaar, R. (2001). Chromosomal stability and the DNA double-stranded break connection. *Nature Reviews Genetics*, *2*(3), 196–206. https://doi.org/10.1038/35056049

van Sluis, M., Yu, Q., van der Woude, M., Gonzalo-Hansen, C., Dealy, S. C., Janssens, R. C., Somsen, H. B., Ramadhin, A. R., Dekkers, D. H. W., Wienecke, H. L., Demmers, J. J. P. G., Raams, A., Davó-Martínez, C., Llerena Schiffmacher, D. A., van Toorn, M., Häckes, D., Thijssen, K. L., Zhou, D., Lammers, J. G., … Marteijn, J. A. (2024). Transcription-coupled DNA–protein crosslink repair by CSB and CRL4CSA-mediated degradation. *Nature Cell Biology*, *26*(5), 770–783. https://doi.org/10.1038/s41556-024-01394-y

Vaz, B., Popovic, M., Newman, J. A., Fielden, J., Aitkenhead, H., Halder, S., Singh, A. N., Vendrell, I., Fischer, R., Torrecilla, I., Drobnitzky, N., Freire, R., Amor, D. J., Lockhart, P. J., Kessler, B. M., McKenna, G. W., Gileadi, O., & Ramadan, K. (2016). Metalloprotease SPRTN/DVC1 Orchestrates Replication-Coupled DNA-Protein Crosslink Repair. *Molecular Cell*, *64*(4), 704–719. https://doi.org/10.1016/j.molcel.2016.09.032

Vaz, B., Popovic, M., & Ramadan, K. (2017a). DNA-Protein Crosslink Proteolysis Repair. *Trends in Biochemical Sciences*, *42*(6), 483–495. https://doi.org/10.1016/j.tibs.2017.03.005

Vaz, B., Popovic, M., & Ramadan, K. (2017b). DNA–Protein Crosslink Proteolysis Repair. *Trends in Biochemical Sciences*, *42*(6), 483–495. https://doi.org/10.1016/j.tibs.2017.03.005

Vijayraghavan, S., & Saini, N. (2023). Aldehyde-Associated Mutagenesis–Current State of Knowledge. *Chemical Research in Toxicology*, *36*(7), 983–1001. https://doi.org/10.1021/acs.chemrestox.3c00045

Voitkun, V., & Zhitkovich, A. (1999). Analysis of DNA-protein crosslinking activity of malondialdehyde in vitro. *Mutation Research - Fundamental and Molecular Mechanisms of Mutagenesis*, *424*(1–2), 97–106. https://doi.org/10.1016/S0027-5107(99)00011-1

Vozenin, M. C., De Fornel, P., Petersson, K., Favaudon, V., Jaccard, M., Germond, J. F., Petit, B., Burki, M., Ferrand, G., Patin, D., Bouchaab, H., Ozsahin, M., Bochud, F.,

Bailat, C., Devauchelle, P., & Bourhis, J. (2019). The Advantage of FLASH Radiotherapy Confirmed in Mini-pig and Cat-cancer Patients. *Clinical Cancer Research*, *25*(1), 35–42. https://doi.org/10.1158/1078-0432.CCR-17-3375

Wagner, J. R., Hu, C. C., & Ames, B. N. (1992). Endogenous oxidative damage of deoxycytidine in DNA. *Proceedings of the National Academy of Sciences of the United States of America*, *89*(8), 3380–3384. https://doi.org/10.1073/pnas.89.8.3380

Wallace, S. S. (2002). Biological consequences of free radical-damaged DNA bases. *Free Radical Biology & Medicine*, *33*(1), 1–14. https://doi.org/10.1016/s0891-5849(02)00827-4

Walport, L. J., Hopkinson, R. J., & Schofield, C. J. (2012). Mechanisms of human histone and nucleic acid demethylases. *Current Opinion in Chemical Biology*, *16*(5–6), 525–534. https://doi.org/10.1016/j.cbpa.2012.09.015

Wang, J. C. (2002). Cellular roles of DNA topoisomerases: A molecular perspective. *Nature Reviews Molecular Cell Biology*, *3*(6), 430–440. https://doi.org/10.1038/nrm831

Wang, M., Wu, W., Wu, W., Rosidi, B., Zhang, L., Wang, H., & Iliakis, G. (2006). PARP-1 and Ku compete for repair of DNA double strand breaks by distinct NHEJ pathways. *Nucleic Acids Research*, *34*(21), 6170–6182. https://doi.org/10.1093/nar/gkl840

Wang, P., Yuan, D., Guo, F., Chen, X., Zhu, L., Zhang, H., Wang, C., & Shao, C. (2017). Chromatin remodeling modulates radiosensitivity of the daughter cells derived from cell population exposed to low- And high-LET irradiation. *Oncotarget*, *8*(32), 52823–52836. https://doi.org/10.18632/oncotarget.17275

Wang, S., Meyer, D. H., & Schumacher, B. (2022). Inheritance of paternal DNA damage by histone-mediated repair restriction. *Nature*, *613*(7943), 365–374. https://doi.org/10.1038/s41586-022-05544-w

Wang, Y., Zhang, Y., Huang, C., Fu, Q., & Huang, T. (2025). Impact of Ultra-High-Dose-Rate Irradiation on DNA: Single-Strand Breaks and Base Damage. *International Journal of Molecular Sciences*, *26*(5). https://doi.org/10.3390/ijms26051800

Wang, Z., Gerstein, M., & Snyder, M. (2009). RNA-Seq: A revolutionary tool for transcriptomics. *Nature Reviews Genetics*, *10*(1), 57–63. https://doi.org/10.1038/nrg2484

Wanstall, H. C., Korysko, P., Farabolini, W., Corsini, R., Bateman, J. J., Rieker, V., Hemming, A., Henthorn, N. T., Merchant, M. J., Santina, E., Chadwick, A. L., Robertson, C., Malyzhenkov, A., & Jones, R. M. (2024). VHEE FLASH sparing effect measured at CLEAR, CERN with DNA damage of pBR322 plasmid as a biological

endpoint. *Scientific Reports*, *14*(1), 14803. https://doi.org/10.1038/s41598-024-65055-8

Wardman, P. (2009). The importance of radiation chemistry to radiation and free radical biology (the 2008 silvanus thompson memorial lecture). *British Journal of Radiology*, *82*(974), 89–104. https://doi.org/10.1259/bjr/60186130

WAYDHAS, C., WEIGL, K., & SIES, H. (1978). The Disposition of Formaldehyde and Formate Arising from Drug N-Demethylations Dependent on Cytochrome P-450 in Hepatocytes and in Perfused Rat Liver. *European Journal of Biochemistry*, *89*(1), 143–150. https://doi.org/10.1111/j.1432-1033.1978.tb20906.x

Weickert, P., Dürauer, S., Götz, M. J., Li, H. Y., & Stingele, J. (2024). Electro-elution-based purification of covalent DNA–protein cross-links. In *Nature Protocols* (Vol. 19, Issue October). Springer US. https://doi.org/10.1038/s41596-024-01004-z

Weickert, P., Li, H. Y., Götz, M. J., Dürauer, S., Yaneva, D., Zhao, S., Cordes, J., Acampora, A. C., Forne, I., Imhof, A., & Stingele, J. (2023a). SPRTN patient variants cause global-genome DNA-protein crosslink repair defects. *Nature Communications*, *14*(1), 1–14. https://doi.org/10.1038/s41467-023-35988-1

Weickert, P., Li, H. Y., Götz, M. J., Dürauer, S., Yaneva, D., Zhao, S., Cordes, J., Acampora, A. C., Forne, I., Imhof, A., & Stingele, J. (2023b). SPRTN patient variants cause global-genome DNA-protein crosslink repair defects. *Nature Communications*, *14*(1), 1–14. https://doi.org/10.1038/s41467-023-35988-1

Weickert, P., & Stingele, J. (2022). DNA-Protein Crosslinks and Their Resolution. *Annual Review of Biochemistry*, *91*, 157–181. https://doi.org/10.1146/annurev-biochem-032620-105820

Weinstein, J. N., Collisson, E. A., Mills, G. B., Shaw, K. R. M., Ozenberger, B. A., Ellrott, K., Sander, C., Stuart, J. M., Chang, K., Creighton, C. J., Davis, C., Donehower, L., Drummond, J., Wheeler, D., Ally, A., Balasundaram, M., Birol, I., Butterfield, Y. S. N., Chu, A., … Kling, T. (2013). The cancer genome atlas pan-cancer analysis project. *Nature Genetics*, *45*(10), 1113–1120. https://doi.org/10.1038/ng.2764

Welter, A. L., & Machida, Y. J. (2022). Functions and evolution of FAM111 serine proteases. *Frontiers in Molecular Biosciences*, *9*(December), 1–11. https://doi.org/10.3389/fmolb.2022.1081166

White, D., Rafalska-Metcalf, I. U., Ivanov, A. V, Corsinotti, A., Peng, H., Lee, S.-C., Trono, D., Janicki, S. M., & Rauscher, F. J. 3rd. (2012). The ATM substrate KAP1 controls DNA repair in heterochromatin: regulation by HP1 proteins and serine 473/824 phosphorylation. *Molecular Cancer Research : MCR*, *10*(3), 401–414. https://doi.org/10.1158/1541-7786.MCR-11-0134

Wilkinson, B., Hill, M. A., & Parsons, J. L. (2023). The Cellular Response to Complex DNA Damage Induced by Ionising Radiation. In *International Journal of Molecular Sciences* (Vol. 24, Issue 5). https://doi.org/10.3390/ijms24054920

Wilson, P. F., & Bedford, J. S. (2010). Radiobiologic Principles. *Leibel and Phillips Textbook of Radiation Oncology, Third Edition*, 3–30. https://doi.org/10.1016/B978-1-4160-5897-7.00001-9

WILSON, R. R. (1946). Radiological use of fast protons. *Radiology*, *47*(5), 487–491. https://doi.org/10.1148/47.5.487

Wirbelauer, C., Bell, O., & Schübeler, D. (2005). Variant histone H3.3 is deposited at sites of nucleosomal displacement throughout transcribed genes while active histone modifications show a promoter-proximal bias. *Genes and Development*, *19*(15), 1761–1766. https://doi.org/10.1101/gad.347705

Wood, R. D., & Doublié, S. (2016). DNA polymerase θ (POLQ), double-strand break repair, and cancer. *DNA Repair*, *44*, 22–32. https://doi.org/https://doi.org/10.1016/j.dnarep.2016.05.003

Xu, X., Muller, J. G., Ye, Y., & Burrows, C. J. (2008). DNA-protein cross-links between guanine and lysine depend on the mechanism of oxidation for formation of C5 vs C8 guanosine adducts. *Journal of the American Chemical Society*, *130*(2), 703–709. https://doi.org/10.1021/ja077102a

Xun Minga, Erin D. Michaelson-Richiea, Arnold S. Groehler IVd, Peter W. Villaltab, Colin Campbellc, N. Y. T. (2020). Cross-Linking of the DNA Repair Protein O6 - Alkylguanine DNA Alkyltransferase to DNA in the Presence of Cisplatin. *DNA Repair*, *176*(1), 139–148. https://doi.org/10.1016/j.dnarep.2020.102840.Cross-Linking

Yaneva, D., Sparks, J. L., Donsbach, M., Zhao, S., Weickert, P., Bezalel-Buch, R., Stingele, J., & Walter, J. C. (2023a). The FANCJ helicase unfolds DNA-protein crosslinks to promote their repair. *Molecular Cell*, *83*(1), 43-56.e10. https://doi.org/https://doi.org/10.1016/j.molcel.2022.12.005

Yaneva, D., Sparks, J. L., Donsbach, M., Zhao, S., Weickert, P., Bezalel-Buch, R., Stingele, J., & Walter, J. C. (2023b). The FANCJ helicase unfolds DNA-protein crosslinks to promote their repair. *Molecular Cell*, *83*(1), 43-56.e10. https://doi.org/10.1016/j.molcel.2022.12.005

Ye, L. F., Chaudhary, K. R., Zandkarimi, F., Harken, A. D., Kinslow, C. J., Upadhyayula, P. S., Dovas, A., Higgins, D. M., Tan, H., Zhang, Y., Buonanno, M., Wang, T. J. C., Hei, T. K., Bruce, J. N., Canoll, P. D., Cheng, S. K., & Stockwell, B. R. (2020). Radiation-Induced Lipid Peroxidation Triggers Ferroptosis and Synergizes with Ferroptosis

Inducers. *ACS Chemical Biology*, *15*(2), 469–484. https://doi.org/10.1021/acschembio.9b00939

Yeo, J. E., Wickramaratne, S., Khatwani, S., Wang, Y. C., Vervacke, J., Distefano, M. D., & Tretyakova, N. Y. (2014). Synthesis of site-specific DNA-protein conjugates and their effects on DNA replication. *ACS Chemical Biology*, *9*(8), 1860–1868. https://doi.org/10.1021/cb5001795

Yip, M. C. J., Bodnar, N. O., & Rapoport, T. A. (2020). Ddi1 is a ubiquitin-dependent protease. *Proceedings of the National Academy of Sciences of the United States of America*, *117*(14), 7776–7781. https://doi.org/10.1073/pnas.1902298117

Yoshida, I., & Ibuki, Y. (2014). Formaldehyde-induced histone H3 phosphorylation via JNK and the expression of proto-oncogenes. *Mutation Research/Fundamental and Molecular Mechanisms of Mutagenesis*, *770*, 9–18. https://doi.org/https://doi.org/10.1016/j.mrfmmm.2014.09.003

Zhang, H., Xiong, Y., & Chen, J. (2020). DNA-protein cross-link repair: What do we know now? *Cell and Bioscience*, *10*(1), 1–10. https://doi.org/10.1186/s13578-019-0366-z

Zhao, S., Kieser, A., Li, H. Y., Reinking, H. K., Weickert, P., Euteneuer, S., Yaneva, D., Acampora, A. C., Götz, M. J., Feederle, R., & Stingele, J. (2021). A ubiquitin switch controls autocatalytic inactivation of the DNA-protein crosslink repair protease SPRTN. *Nucleic Acids Research*, *49*(2), 902–915. https://doi.org/10.1093/nar/gkaa1224

Zheng, H., Chen, L., Pledger, W. J., Fang, J., & Chen, J. (2014). p53 promotes repair of heterochromatin DNA by regulating JMJD2b and SUV39H1 expression. *Oncogene*, *33*(6), 734–744. https://doi.org/10.1038/onc.2013.6

Zhitkovich, A., & Costa, M. (1992). A simple, sensitive assay to detect dna-protein cromlinks in intact cells and in vivo. *Carcinogenesis*, *13*(8), 1485–1489. https://doi.org/10.1093/carcin/13.8.1485